NASA Conference Publication 2181

15th Aerospace Mechanisms Symposium

Proceedings of a symposium held at
George C. Marshall Space Flight Center
Marshall Space Flight Center, Alabama
May 14-15, 1981

Lockheed

NASA

NASA Conference Publication 2181

15th Aerospace Mechanisms Symposium

Proceedings of a symposium co-sponsored by
National Aeronautics and Space Administration,
California Institute of Technology, and
Lockheed Missiles and Space Company, Inc., and
held at George C. Marshall Space Flight Center,
Marshall Space Flight Center, Alabama
May 14-15, 1981

NASA
National Aeronautics
and Space Administration

Scientific and Technical
Information Branch

1981

PREFACE

The proceedings of the 15th Aerospace Mechanisms Symposium held at the George C. Marshall Space Flight Center on May 14, -15, 1981, are in this NASA Conference Publication. The symposium was co-sponsored by the National Aeronautics and Space Administration, the California Institute of Technology, and Lockheed Missiles and Space Company, Inc.

The purpose of the symposium was to provide a forum for the interchange of information among those active in the field of mechanism technology. To that end, 27 papers were presented on aeronautics and space flight, with special emphasis on actuators and aerospace applications for pointing systems, latches, connectors, and other mechanisms for large space structures. The papers were authored by engineers from a broad aerospace spectrum including the U. S. aerospace industry, NASA, and several European participants.

The efforts of the review committee, session chairmen, and speakers contributing to the technical excellence and professional character of the conference are especially appreciated.

The use of trade names or names of manufacturers in this publication does not constitute an official endorsement of such products or manufacturers, either expressed or implied, by the National Aeronautics and Space Administration.

ORGANIZING AND REVIEWING COMMITTEE

The papers presented at the symposium were selected and reviewed by the Organizing Committee. Responsibility for content and technical accuracy lies with each respective author. The committee included the following members:

General Chairman:	Charles W. Coale, Lockheed Missiles and Space Company, Inc.
Operations/Executive Chairman:	Alfred L. Rinaldo, Lockheed Missiles and Space Company, Inc.
Executive Co-Chairman:	David F. Welch, California Institute of Technology
Host Chairman:	James B. Sterrett, NASA-Marshall Space Flight Center
Committee Members:	Paul Bomke, Jet Propulsion Laboratory
	Aleck C. Bond, NASA-Johnson Space Center
	Tom F. Bonner, Jr., NASA-Langley Research Center
	H. Mervin Briscoe, European Space Technology Center
	Kenneth C. Curry, Jet Propulsion Laboratory
	Charles R. Darwin, NASA-Marshall Space Flight Center
	David F. Englebert, NASA-Ames Research Center
	Angelo Giovannetti, NASA-Ames Research Center
	Harvey H. Horiuchi, Jet Propulsion Laboratory
	Allen J. Louviere, NASA-Johnson Space Center
	Frank T. Martin, NASA-Goddard Space Flight Center
	Bowden W. Ward, NASA-Goddard Space Flight Center
	Nathan D. Watson, NASA-Langley Research Center

TABLE OF CONTENTS

DRIVE MECHANISM FOR THE SHUTTLE ORBITER/ EXTERNAL TANK PROPELLANT DISCONNECT

E. Thomas*
R. Wilders**
J. Ulanovsky**

ABSTRACT

The Space Shuttle design required development of a large, 0.43-m (17-in.) nominal diameter separable disconnect for the liquid hydrogen and liquid oxygen propellant lines at the orbiter-to-external-tank interface. The disconnect must provide for shutoff of the propellant flow area by simultaneous action of two rotary flapper valves (orbiter and external tank) prior to disconnect separation. In the case of pneumatic system failure, the rotary flapper valves are closed automatically through mechanical interlocking linkage during disconnect separation. The mechanism must meet requirements while accommodating changes in bearing clearances and linkage geometry over a wide temperature range from ambient to 20.37 K (-423°F). The mechanical design of the separable disconnect, kinematics of the drive mechanism, and the analysis and test methods used to verify proper operation and qualification for the Space Shuttle dynamic environments are presented.

INTRODUCTION

This paper describes the mechanism devised to meet the design requirements for a large, 0.43-m (17-in.) nominal diameter separable disconnect for the liquid hydrogen and liquid oxygen propellant lines of the Shuttle vehicle at the orbiter-to-external-tank interface. The disconnect must provide for shutoff of the propellant flow area by simultaneous action of two rotary flapper valves prior to orbiter/external tank structural separation. After orbiter main engine cutoff and propellant flow has ceased, the disconnect is pneumatically actuated closed. Three clamping bolts with pyrotechnic frangible nuts then are activated, separating the two sections. The orbiter side is then retracted away from the external tank section by three hydraulic actuators, which are attached between the orbiter structure and disconnect umbilical assemblies. The linkage must provide for proper positioning of the rotary flapper valves in the closed position to control leakage, and in the open position to ensure that the rotary flapper valves will not close during flow. In the open position, an open direction force is maintained on the rotary flapper valves while the mechanism is locked over center.

*Member of Technical Staff, Rockwell International Corp., North American Space Operations, Space Transportation System Development and Production Division, 12214 Lakewood Blvd., Downey, CA 90241

**Senior Project Engineer, Parker Hannifin Corp., Air and Space Products Division, 18321 Jamboree Blvd., Irvine, CA 92715

In the case of pneumatic system failure, the rotary flapper valves are closed automatically through mechanical interlocking linkage during disconnect separation. The mechanism must meet these requirements while accommodating changes in bearing clearances and linkage geometry over a wide temperature range from ambient to 20.37 K (-423°F).

The mechanical design requirements for the mechanism and the kinematics of the drive mechanism devised are described. The performance and operating parameters described are for nominal conditions only.

DISCONNECT DESCRIPTION

Installation

The orbiter-to-external-tank disconnect consists of two sections, one section mounted in the orbiter feed system umbilical assembly and the other mounted in the external tank feed system umbilical assembly (Figure 1). One pair of umbilicals is used in each of the liquid oxygen and liquid hydrogen feed lines at the orbiter-to-external-tank interface. The umbilical assemblies are held together by three clamping bolts with frangible nuts installed through the disconnect clamping ears. The disconnects are opened prior to the start of tanking and remain open until after main engine shutdown. The disconnects are then closed prior to orbiter/external tank separation.

Components

Each disconnect section contains a rotary flapper valve that is opened and closed by a pneumatic actuator mounted on the orbiter section (Figure 2). A position indicator containing redundant open and closed position indicating switches is also mounted on the orbiter section. The actuator and position indicator may be replaced without affecting disconnect adjustment. In the case of a pneumatic system failure that results in the loss of pneumatic pressure, the rotary flapper valves are closed automatically through mechanically interlocking linkage during disconnect separation.

The mechanism is bistable so that pneumatic system failure causing both sides of the actuator to be pressurized will not close the unit because of the mechanism over-center locks. In the open position, an open direction force is maintained on the rotary flapper valves by the mechanism, which is locked over center. In addition to the linkage force, the flapper shape and angle of attack in the flow stream cause the open force to increase as the flow rate increases (Figure 3). The design of the flapper linkage provides for relief of pressure buildup between the two flappers when the units are mated and closed. The relief is accomplished by allowing the flapper to lift off the seat against the spring force of the follower

arm torsion bar. The main flapper is sealed by seating a flexible Teflon-coated* metal disk, mounted on the flapper, on a narrow metal seat ring mounted in the disconnect body.

Operating Conditions

The disconnect is designed to operate in either a liquid hydrogen or liquid oxygen system. The mechanism will meet the design requirements while liquid hydrogen flows at 221.8 kg (489 lb, 49,400 gpm) per second at 3.45×10^5 Nm^2 (50 psig) or 1315.4 kg (2,900 lb, 18,156 gpm) per second of liquid oxygen at 13.79×10^5 Nm^2 (200 psig). The flappers are designed to withstand a proof pressure in the closed position of 19.72×10^5 Nm^2 (286 psig) for the orbiter section and 4.03×10^5 Nm^2 (58.5 psig) for the external tank section. In the open position with the two sections mated, the proof pressure is 26.89×10^5 Nm^2 (390 psig).

DESIGN FEATURES

The disconnect mechanism was designed to meet the following design objectives:

- Weight
- Life
- Bistability
- Locked open
- Close during separation
- Thermal relief

Weight

The use of a rotary flapper valve for main flow stream shutoff offers the following advantages to minimize weight: the flapper movement is controlled by the mechanism so that the flapper is supported around its entire periphery in the closed position; the peripheral support eliminates the need for the flapper mechanism to withstand system pressure loads and reduces the flapper weight.

Life

The use of a rotary flapper valve for main flow stream shutoff offers the following advantages for long life: it seals like a poppet valve, opens and closes without sliding contact, seats around its complete periphery separate from the sealing disk to react loads due to pressure in the closed position, minimizing seal disk wear.

*Registered trade name by E. I. DuPont.

Bistability

The mechanism is designed to maintain sufficient force on the flapper-open stops to maintain the valve in the full-open position with loss of pneumatic pressure. In case both sides of the actuator are pressurized simultaneously, the open force is sufficient to prevent valve movement that could occur due to actuator effective area unbalance.

Locked Open

The mechanism is locked over center at the actuator roller-block-to-external tank-section drive clevis. In addition, each flapper drive mechanism is locked over center.

Close During Separation

In the open position, the mechanism is designed with physical interference of the actuator roller block and drive clevis, which will cause rotation of the drive shafts when the orbiter umbilical retracts.

Thermal Relief

In the closed position, the flappers are held against the seat by a force applied by the follower arm and its torsion bar. The flapper will lift off the seat against that force when pressure rises in the trapped cavity.

Certification

The mechanism is required to meet the design objectives for a minimum life equivalent to 100 orbiter missions. To ensure that the mechanism is capable of meeting the life requirement, the certification program requires the unit to successfully complete 2,500 operating cycles at ambient temperature and 1,000 cycles at liquid hydrogen temperature as well as 48 minutes of random vibration in each of three axes, plus the environmental tests.

MECHANISM DESCRIPTION

The mechanism is driven by a pneumatic actuator mounted on the orbiter section (Figure 4). The actuator output linear motion is converted to rotary motion through two parallel links connected to the roller block assembly. The roller block assembly roller drives the external tank drive clevis, rotating the external tank torsion bar assembly. The torsion bar assembly consists of an outer hollow torsion bar and an internal solid torsion bar. The hollow torsion bar drives the external tank main closure through the drive arms. The solid torsion bar extends through the external tank section, driving the roller arm, which drives the orbiter section main closure through its drive clevis and drive arm.

The primary elements of the disconnect mechanism – the pneumatic actuator roller block and drive clevis interaction, the external tank section drive shaft torsion bar, and the drive arm and follower arm – are described in the following sections.

Roller Block Assembly

Function

The roller block assembly (Figure 5) is an integral part of the pneumatic actuator assembly. The rotary motion required to drive the disconnect mechanism open and closed pneumatically is provided by the roller block assembly. In addition to its function as the primary mechanism driving force, an over-center open lock is designed into the kinematics of the roller block and external tank section drive clevis.

Construction

The roller block assembly consists of a main structural element and the roller assembly. The main structural element is machined from a single piece of material with integral link attachment shafts and trunnion shafts. The roller assembly consists of the roller, its support shaft with spacer, shaft bearing, and a thrust bearing on each side of the roller.

Pneumatic Opening

When the pneumatic actuator is pressurized to extend the piston rod, two parallel links connected between the piston rod end and the roller block drive the roller block about Shaft A (Figure 6). The roller block output roller rotates 1.88 rad (108 deg) about Shaft A with full extension of the actuator piston rod. The roller block movement drives the clevis mounted on the external tank torsion bar through an angle of 0.72 rad (41.25 deg), opening the external tank and orbiter section flapper valves.

During the opening cycle, the drive clevis is overdriven 0.05 rad (3.0 deg) by the roller block after the flappers contact their respective open stops, winding up the external tank torsion bars. The torsion bar spring force due to the windup provides a positive open direction force and holds the flappers against the open stops. The torsion bars have an angular spring rate of 10 kgm/rad (956 in.-lb/deg) for the solid bar and 7.28 kgm/rad (740 in.-lb/deg) for the hollow bar. The torsion bars are designed to permit a twist of 0.11 rad (6.0 deg) for the solid bar and 0.14 rad (8.0 deg) for the hollow bar before sustaining a permanent set. The roller block is driven until the actuator piston bottoms in the cylinder.

When motion is complete, the roller block is over center with respect to the drive clevis 0.203×10^{-2} m (0.08 in.) (Figure 6). The torsion bar spring force on the over-center mechanism results in a tension load on the links, forcing the actuator piston against the cylinder end. With the piston bottomed out in the cylinder, rotational force on the drive

clevis in the closing direction will result in increased tension load in the links. With the mechanism in this position, the flappers are positively locked in the open position.

Pneumatic Closing

To close the flappers pneumatically, the actuator piston area is pressurized to retract the piston rod while simultaneously venting the open side of the actuator. Mechanical closing at separation is described later in this section. The first motion of the roller block is to move back over center, unlocking the mechanism. The roller block continues to rotate as the piston rod retracts, rotating the drive clevis and closing the flappers. The piston rod retracts until the piston contacts the opposite end of the cylinder. When the piston rod movement is complete, the flappers will not have reached the full closed position. The remaining flapper movement is due to force applied to the flappers by the follower arm, as discussed in the Drive Arm and Follower Arm section.

Bistable

From the open position, the force required to move the roller block back over center is equal to approximately 50 percent of the total actuator output force. The actuator output is sufficient to produce an external tank section drive shaft closing direction torque of 37.97×10^2 kgm (6300 in.-lb) at ambient temperature and 25.92×10^2 kgm (4300 in.-lb) at cryogenic temperature. The force to pull the mechanism back over center is also greater than the actuator force output when both sides of the actuator piston are pressurized. Since the mechanism is driven over center during the opening cycle, the torsion bar spring force maintains the position of the actuator piston due to the tension load. In the over-center position, the actuator may lose pressure on both sides of the piston without changing the flapper-open stop load. The result is a valve mechanism that will not unlock to allow valve closure unless the actuator piston rod is retracted, which can occur only by venting the open side of the piston and pressurizing the closed side.

Pneumatic Operating Time

When the actuator is pressurized to 51.02×10^5 Nm^2 (740 psig) by the vehicle control system, the mechanism moves the mated disconnect pair from open to closed in a total time of 1.3 sec at ambient temperature and 2.6 sec at cryogenic operating conditions. The operating time comprises two elements: (1) response – the time between control solenoid command and trip of the position switch indicating the flapper position that the valve is changing from and (2) travel – the time betwen the flapper position indicating switches.

These times for closing operation are typically 1.2 sec for response and 0.1 sec for travel at ambient temperature and 2.3 sec for response and 0.3 sec for travel at cryogenic operating temperatures. The opening time requirement of 3 ±2 sec for all operating conditions is not critical to the operation of the propellant system and is not as closely monitored as closing performance.

Mechanical Closing

The mechanism is designed so that the flappers will close during orbiter umbilical assembly retraction in case of pneumatic system failure. The force required to separate the umbilicals is provided by three hydraulic actuators, which are not part of the disconnect assemblies.

In the open position, the tip of the closing side of the clevis extends into the path through which the roller will travel during separation motion.

During separation travel, after the pyrotechnic release nuts are operated, the orbiter-side umbilical travels a nominal 0.057 m (2.25 in.) away from the external tank umbilical. The two umbilical sections are guided for the initial 0.038 m (1.5 in.) by shear pins, which are part of the disconnect orbiter section. The initial motion relieves the external tank torsion bar load. The roller block roller then translates across the clevis gap and contacts the closing surface of the clevis (Figure 6).

While the orbiter section continues to retract, the clevis is forced to rotate to clear the roller path. This motion causes the clevis to rotate 0.21 rad (12 deg) nominal before the roller clears the clevis tip, resulting in flapper rotation relative to the flow stream of 0.88 rad (50.0 deg). During this portion of the separation travel, the flapper drive arm and follower arm are driven back from the open over-center and locked position. The linkage reaches the over-center position after 0.07 rad (4.0 deg) of drive shaft rotation for the orbiter side and 0.09 rad (5.0 deg) for the external tank side. The remaining flapper closing travel is due to the follower arm force aided by flow forces on the partially closed flappers.

External Tank Drive Shaft Torsion Bar

Function

The torsion bar is located within the external tank drive shaft (Figure 7). The torsion bar provides the necessary flexibility and spring loads to accomplish the following: (1) maintain the roller block over center in the open position, (2) maintain the orbiter and external tank section flappers loaded against the open stop, and (3) absorb the tolerance differences between the open positions of the orbiter and external tank section flappers.

Construction

The torsion bar assembly consists of a solid inner bar and a hollow outer bar. The two pieces are welded together at the input end, near the drive clevis, and guided at the output end by an integral bushing. The bar has a hexagon-shaped drive at the drive clevis end that can be used to open and close the tank section manually; or, when the two sections are mated, both may be operated simultaneously.

Operation

The torsion bar is driven at the drive clevis end through the stub shaft (Figure 7). The drive clevis is splined to the stub shaft, which is in turn, splined to the input end of the torsion bar. The stub shaft has two bushings to react cantilevered loads imposed by the drive clevis. The output ends of both the hollow and solid torsion bars are splined and mated to separate details of the drive shaft assembly. The outer bar splines mate to the external tank flapper drive shaft to operate the external tank flapper mechanism. The solid bar is splined to a stub shaft that drives the roller arm assembly, providing the operating force that ultimately drives the orbiter section flapper mechanism.

Drive Arm and Follower Arm

Function

The drive arm and follower arm are connected by rotating joints to opposite sides of the flapper at its center. The drive arm transmits the drive shaft rotary motion to the flapper for opening and closing. The follower arm transmits the follower arm torsion bar spring force to the flapper to provide the initial main seal load and control thermal relief. The relationship of the drive arm and follower arm pivot points in the main housing and on the flapper controls the motion path of the flapper during opening and closing travel.

Construction

The drive arm consists of two individually machined arms welded to a spacer tube. Each arm is splined to mate with a drive tube, which is in turn splined to the external tank section torsion bar or to the orbiter section drive shaft. The follower arm consists of one machined piece splined to the follower arm torsion bar. The torsion bar has three sections splined together and arranged coaxially. The coaxial arrangement was necessary to fit a torsion bar whose length was sufficient to meet the operating requirements into the disconnect external packaging limits.

Opening Operation

To open the disconnect, the drive shaft is driven in a clockwise direction (Figure 8). The initial drive arm rotation lifts the flapper away from the main seal. The follower arm torsion bar is preloaded during the disconnect manufacturing process to apply approximately 22.7 kg (50 lb) of force to the center of the flapper. As the flapper moves toward the open position, the torsion bar load increases. Near the full-open position, the drive arm and follower arm reach an over-center position. After the over-center point is reached, the follower arm load assists the actuator to force the flapper to the full-open position. The flapper movement stops when the open stops are contacted.

The linkage is adjusted during the manufacturing process so that the flapper angle relative to the flow stream centerline in the full-open position meets the requirement for the unit being assembled (Figure 3). The individual linkage detail parts are identical for all units, and manufacturing adjustment is necessary to produce the different configurations required. The fairing configurations and flapper angles were developed to increase the flapper load on the open stops as the flow rate is increased. The variance in configuration is required because of the difference in inlet conditions for the LH_2 feed line versus the LO_2 feed line. The different internal configurations were tested in a water flow system at flow rates equivalent to 125 percent of the maximum required flow to determine the changes in open stop load. During the tests, an initial load of 77.1 kg (170 lb) without flow increased to 226.8 kg (500 lb) at full flow for the external tank oxygen unit. The test results of other units indicated a similar three-to-one load increase for the stop load between zero and full flow conditions.

Closing Operation

To close the disconnect, the drive shaft is driven in a counterclockwise direction (Figure 8). The initial movement moves the flapper off the open stops. After the linkage moves back across the over-center position, the follower arm torsion bar force assists the actuator to drive the flapper toward the closed position. During the closing cycle, the flapper rotates approximately 1.57 rad (90 deg) to a position perpendicular to the flow stream after 0.49 rad (28 deg) of drive shaft rotation. The total drive shaft rotation is 0.67 rad (38.25 deg). In this position, the flow area is reduced to 0.0042 m^2 (6.5 $in.^2$), which is the area of the annulus formed by the outer periphery of the seal disk and the inside diameter of the main body.

The closing rate after the over-center position is reached is affected by several factors: (1) valve temperature, which affects friction coefficient of the rotating surfaces, (2) the system flow rate, which determines the pressure delta across the flapper, and (3) the rate of pressure venting from the open side of the pneumatic actuator, which controls the closing rate through the roller block and drive clevis interface. The specific rate of closure is determined by the interrelationship of the above three factors. The pneumatic actuator drives the flappers fully open; but, during closing, the actuator reaches full retraction with 0.03 rad (2 deg) of drive shaft rotation still required to fully seat the flappers. The driving force for the remaining travel is provided by either Item 1 or 2 above or a combination, depending on the operating conditions.

Relief Operation

The follower arm torsion bar mechanism permits the main flapper to lift off the seat at a pressure differential of approximately 1.38×10^3 Nm^2 (0.2 psi), providing the thermal relief control.

CONCLUSION

The mechanism described has proven to be a reliable, lightweight bistable design capable of meeting the requirements. The use of the coaxial drive shaft torsion bar is an efficient method of accommodating variable open position tolerances for two separate mechanisms while maintaining mechanism preload. The flapper design and positioning in the flow stream to control the flow-induced loads allow the flapper and its operating mechanism to be a lightweight design relative to the size of the unit and the flow rate requirements. Designing the follower arm torsion bar with three concentric sections accommodates the large torsional rotation with minimal package size. Overdriving the drive clevis so that the actuator bottoms out for precise position and torsion bar load control allows the drive mechanism to lock over center. The combination of these design features has resulted in the development of a unique, successful propellant disconnect.

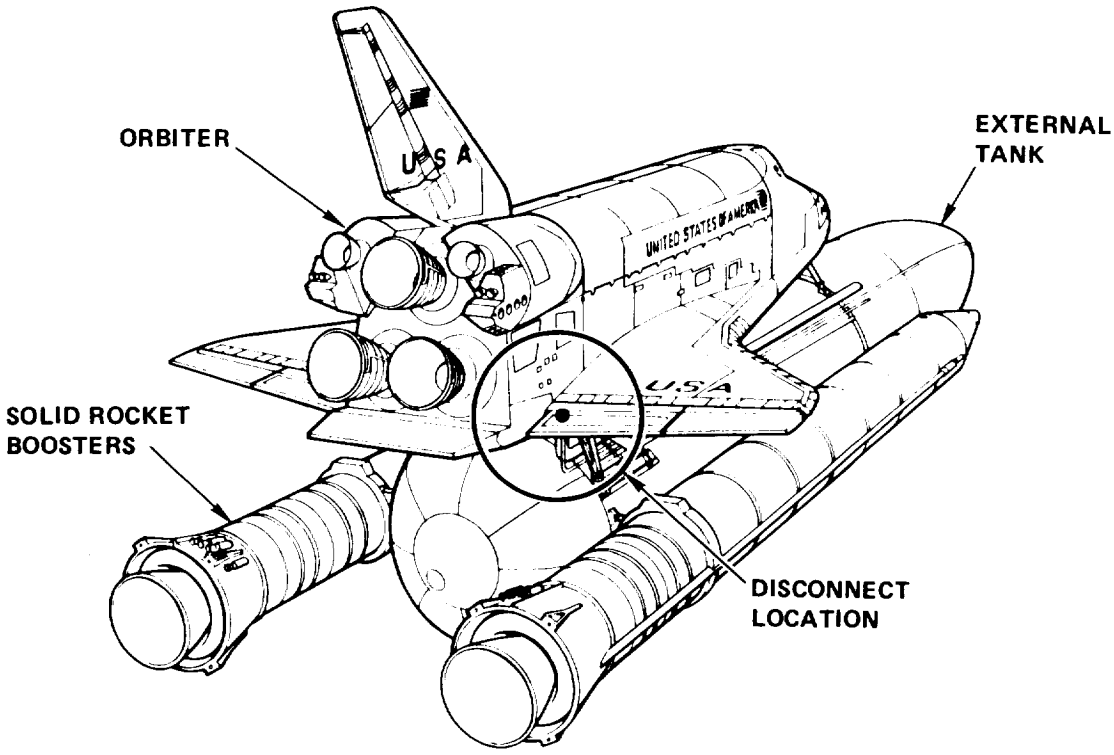

Figure 1. Orbiter/External Tank Disconnect Location

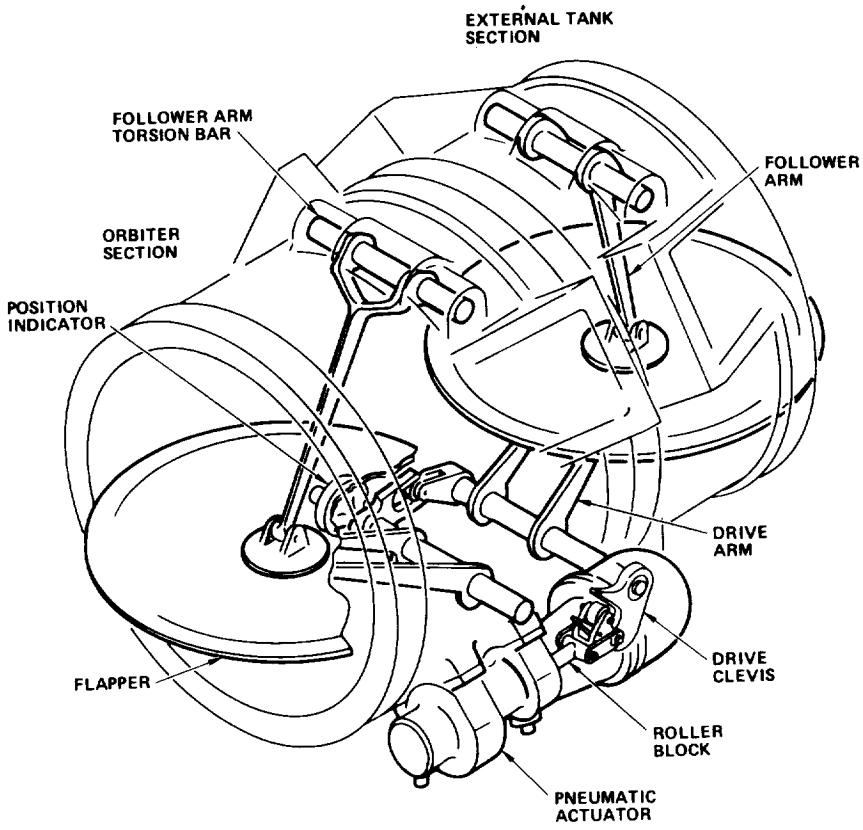

Figure 2. 0.43-Meter (17-Inch) Orbiter-to-External-Tank Disconnect

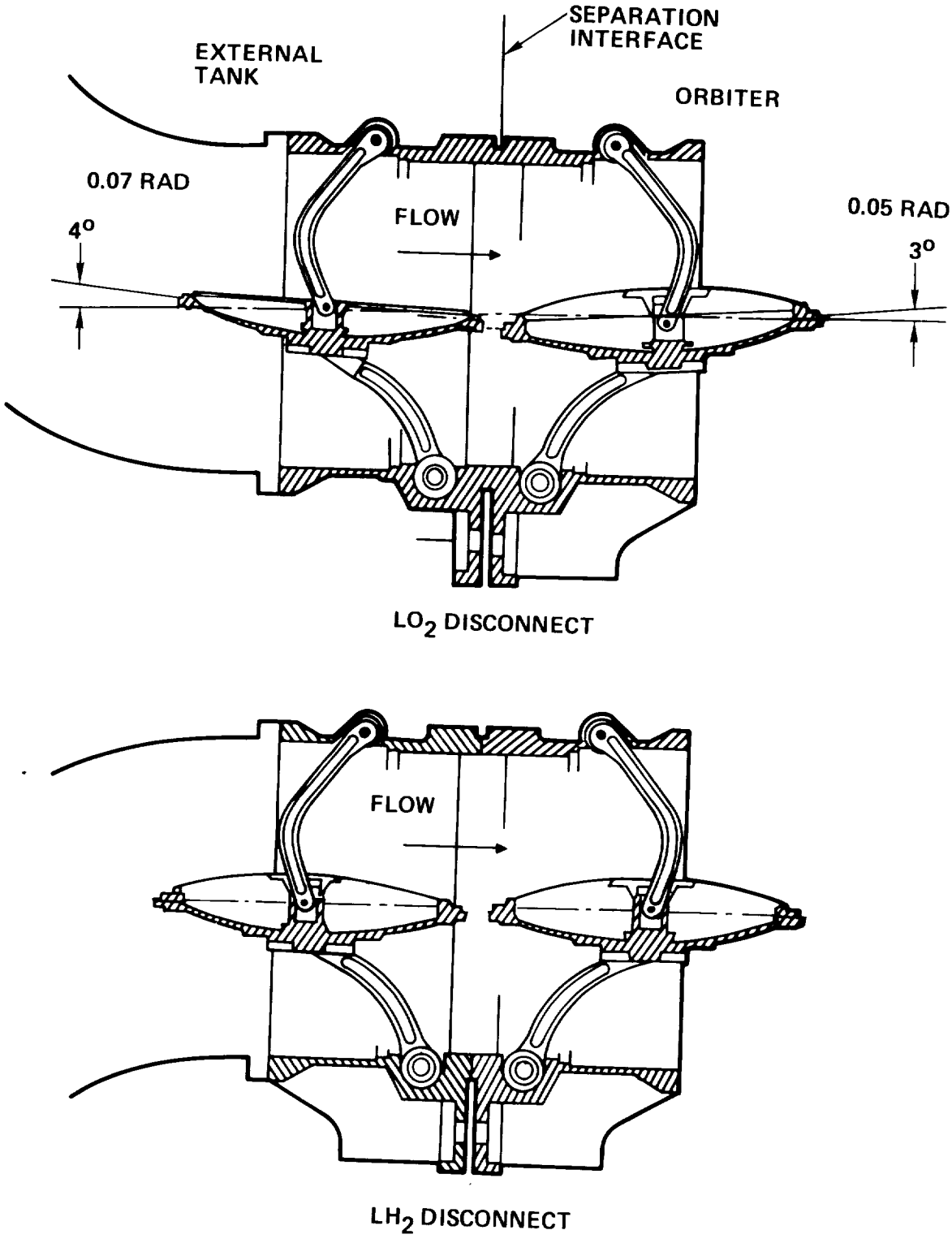

Figure 3. LO_2 and LH_2 Disconnects

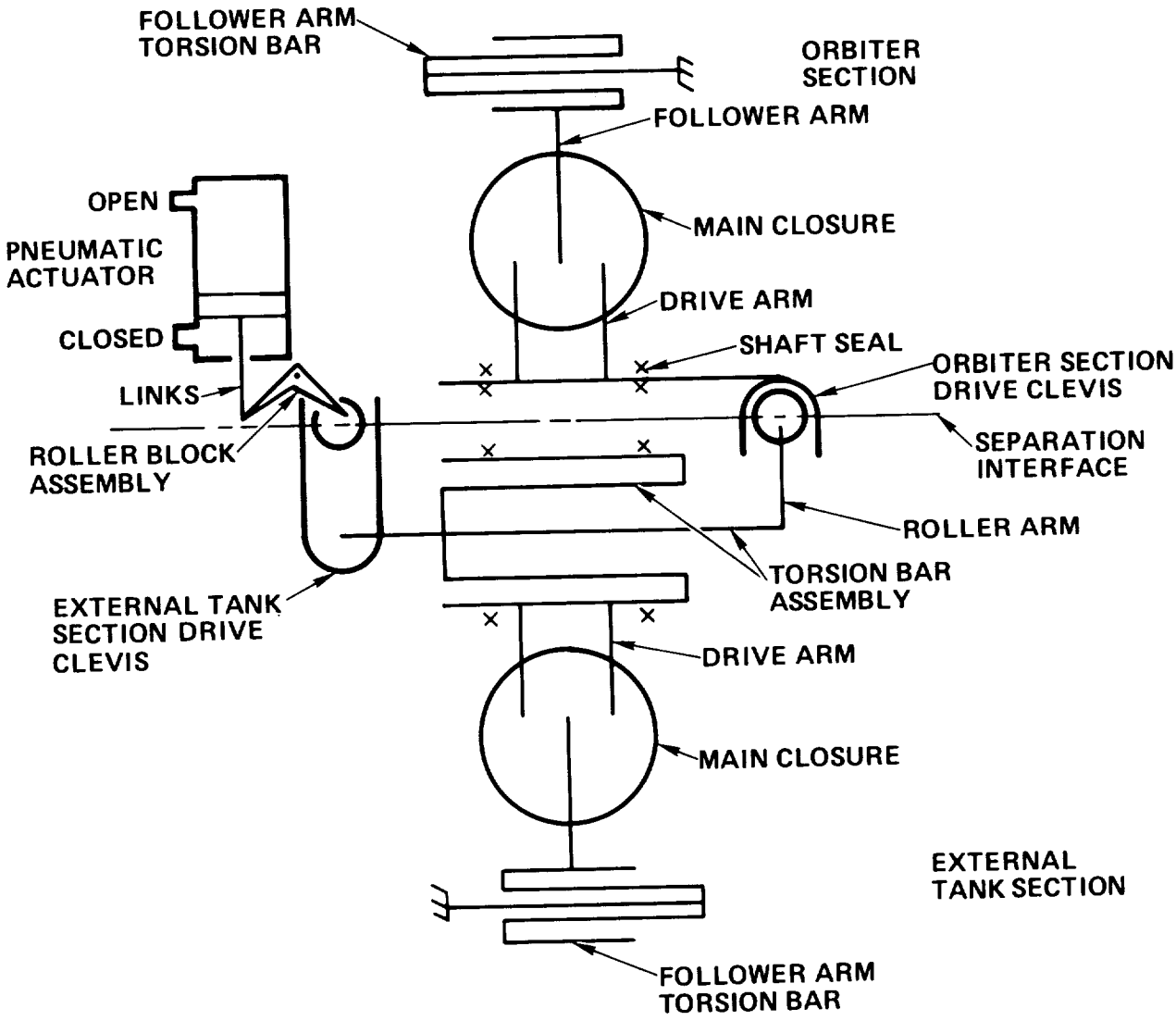

Figure 4. Linkage Schematic

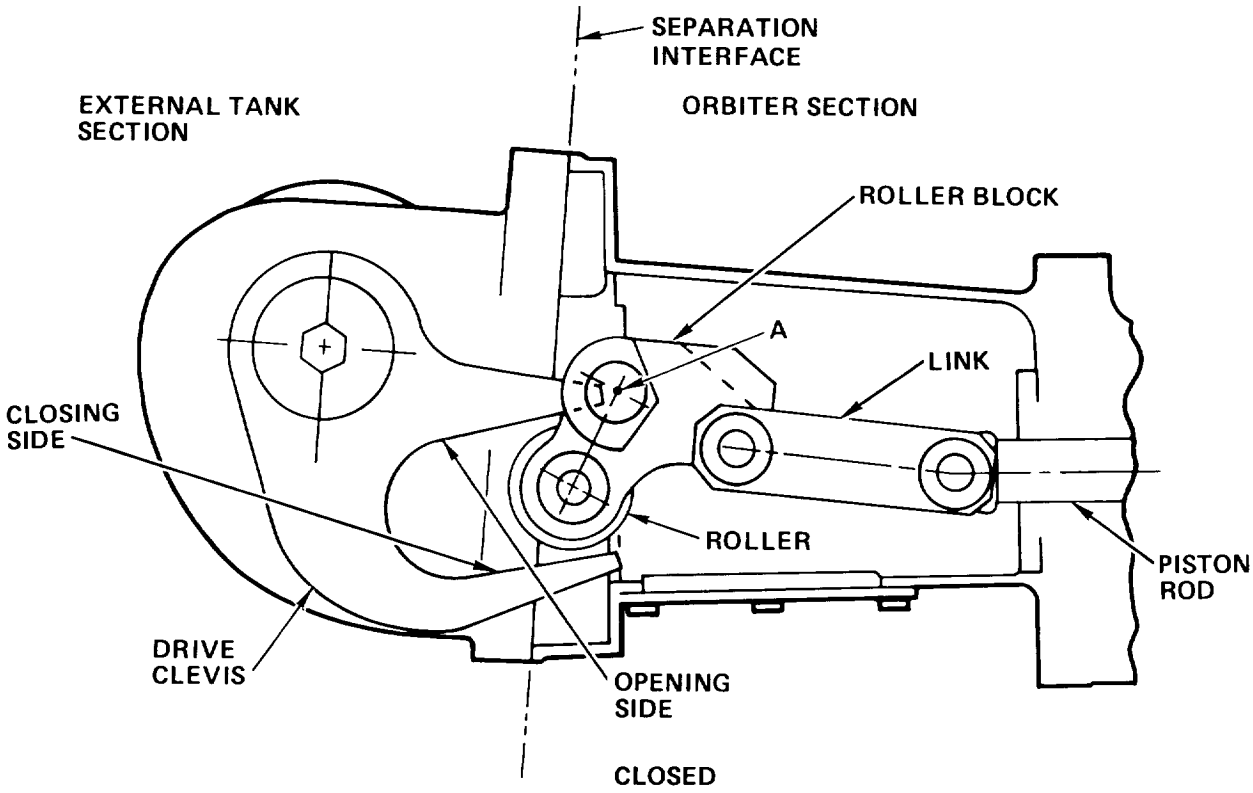

Figure 5. Roller Block Assembly

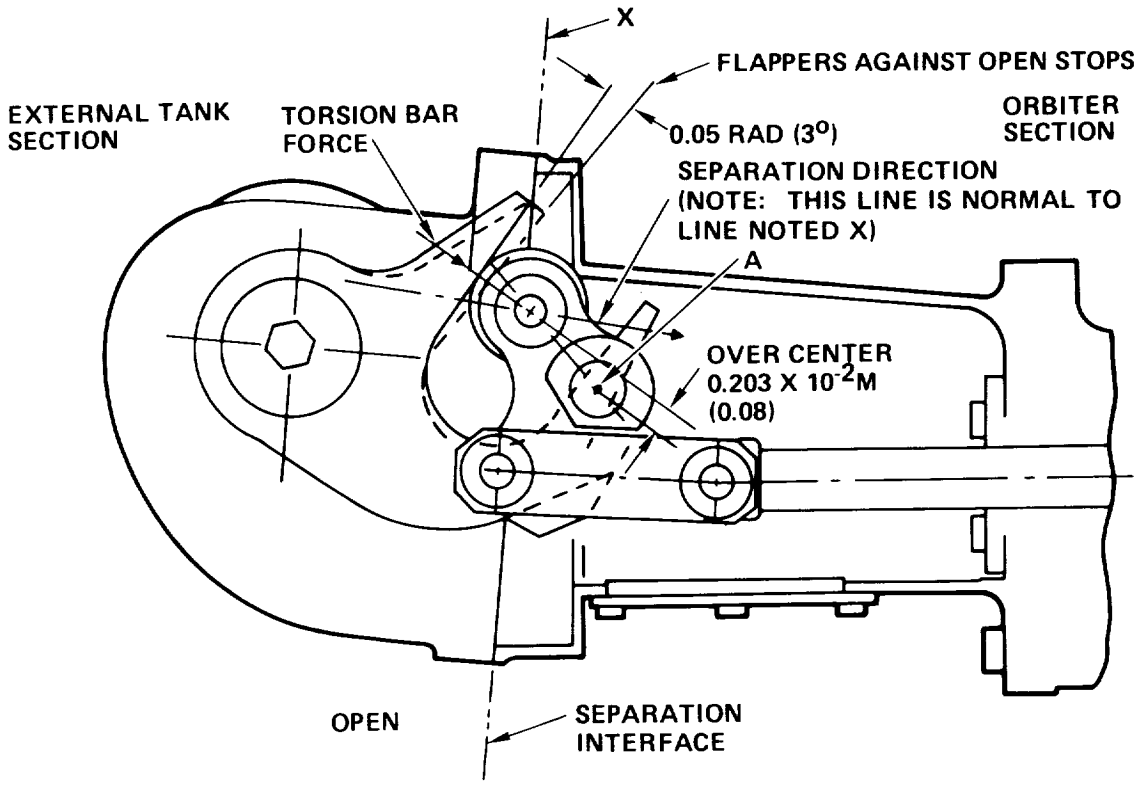

Figure 6. Pneumatic Actuation of Roller Block

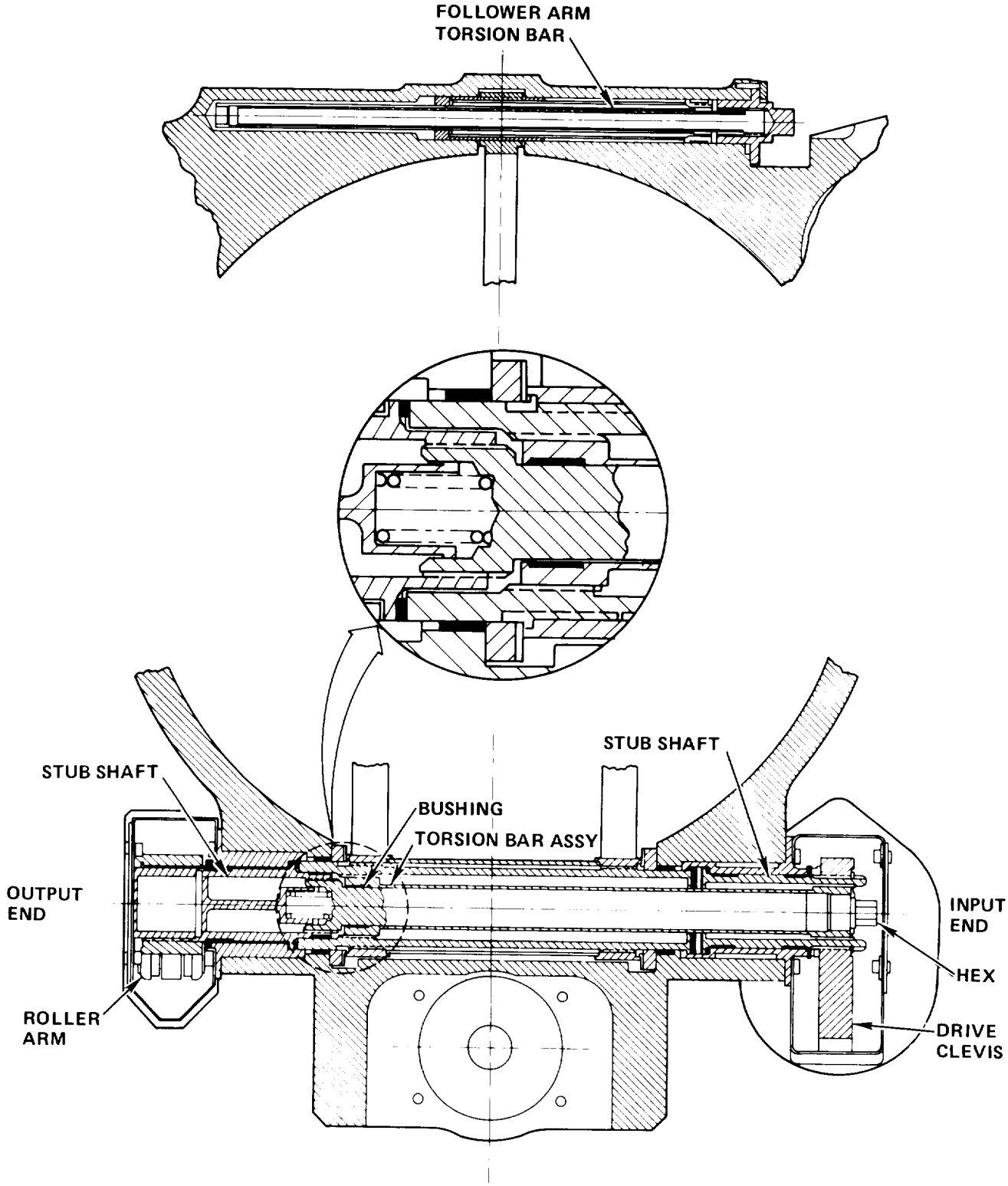

Figure 7. Disconnect – LH_2/LO_2 Orbiter-to-Tank Feed System

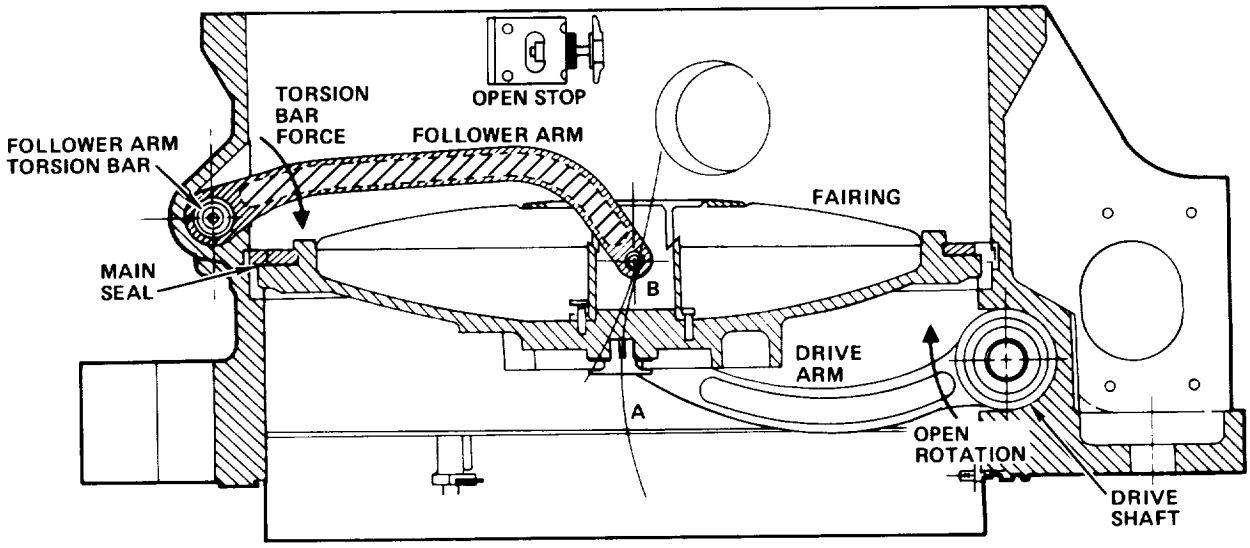

Figure 8. Opening of Disconnect – LH_2/LO_2 Orbiter-to-Tank Feed System

SPACE SHUTTLE ORBITER RUDDER/SPEEDBRAKE ACTUATION SYSTEM

Dwight Woolhouse*

ABSTRACT

A mechanical-hydraulic actuation system for control of the rudder and speedbrake aerosurfaces of the Space Shuttle orbiter has been developed to meet the strict operational requirements imposed on this flight-critical function. This paper describes the requirements, hardware configuration, development experience, and test program accomplished in the evolution of this system. This work was conducted under National Aeronautics and Space Administration (NASA) Contract NAS9-14000.

INTRODUCTION

The entry and flight-to-landing portions of a Space Shuttle mission represent a unique flight control actuation system challenge. Twenty-seven minutes of the 31-minute flyback are spent at speeds above Mach 1. Much of the entry is flown at bank angles up to 1.4 radians (80 degrees) to achieve desired crossrange and distance-to-runway guidance. These steep bank angles result in the accomplishment of a series of large S-turns, performed at hypersonic and supersonic speeds, to dissipate the high energy of the spacecraft prior to landing.

Control of the orbiter during this critical phase of the flight (Figure 1) begins with the use of reaction jet engines and transitions at Mach 10 to the use of conventional aerodynamic flight control surfaces. In operation during this high-speed, high-maneuver rate regime, the demands are great on the orbiter's aerosurface actuation systems, with regard to hinge moment and surface rate.

Because the orbiter has no active propulsion system during this portion of the flight, the requirement to achieve the proper position in the sky above the landing site the first time, and every time, is absolute. There is no opportunity to go around for a second try.

One of the orbiter's primary flight control systems is the rudder/speedbrake. To provide optimum weight and volume efficiency, these two functions have been combined through the use of a unique, split-panel rudder design, mounted at the trailing edge of the large

*Designated Subsystem Project Manager, Rockwell International, Space Transportation System Development and Production Division, Downey, CA.

vertical stabilizer (Figure 2). Actuation of both panels in the same direction provides conventional rudder (yaw) control; while actuation differentially, in a flared configuration, results in added aerodynamic drag for control of speed and pitch.

Actuation of the rudder/speedbrake panels is accomplished by a hydromechanical system responding to quadredundant avionic command inputs. The overall schematic representation of this system is shown in Figure 3. It consists of a power conversion and control component, the power drive unit (PDU), four geared rotary actuators, and ten torque transmitting driveshafts.

DESIGN REQUIREMENTS

The operational requirements imposed on the subsystem are summarized below:

- Hinge moment/rate:
  - Rudder

Stall-hinge moment	7.91×10^{11} dyn-cm (0.7×10^{6} in. lb)
Rate at load	0.24 rad/s (14°/s) at 5.65×10^{11} dyn-cm (0.5×10^{6} in. lb)
Maximum travel	±0.47 rad (±27°)

  - Speedbrake

Stall-hinge moment	2.03×10^{12} dyn-cm (1.8×10^{6} in. lb)
Rate at load	0.11 rad/s (6.1°/s) at 1.98×10^{12} dyn-cm (1.75×10^{6} in. lb)
Maximum travel	1.72 rad (98.6°)

- Full-hinge moment and rate are required following one hydraulic system failure; full-hinge moment and half rate are required following two hydraulic system failures.
- Performance is required through 100 orbiter missions and over 10 years.
- Operation is required in both 1-g and weightless conditions.
- The system must withstand the severe vibro-acoustic environment associated with the Shuttle's ascent to orbit, with consideration for its installed location in the tail near the main engines' exhaust plumes.
- Provision must be made for thermal conditioning of the hydraulic fluid while in orbit to prevent under or overtemperatures due to exposure to the extremes of space.
- Operation is required with full system performance at temperatures from 0°C (35°F) to 135°C (275°F).

- Full system operational capability is required following the loss of two avionic command input channels.

HARDWARE CONFIGURATION

Power Drive Unit (PDU)

The PDU (Figures 4 and 5) combines elements of avionics, hydraulics, and mechanics to act as the control center of the rudder/speedbrake actuation system.

Input commands are quadredundant, coming to the PDU from four different avionic sources. These four commands act on four separate electrohydraulic servovalves within the PDU. Pressures from the servovalve second stages act on areas of a single structural power spool valve, causing it to move from its null position. This movement opens ports that supply hydraulic pressure to the three hydraulic motors providing rotary power to the PDU gearbox.

Should a servovalve output to the power valve be significantly different from the other three (due to failure of the valve, or its associated avionics, for instance), the second-stage differential pressure of that servovalve will rise as it force-fights the three opposing good servovalves. This rise in pressure (Figure 6) is monitored by second-stage pressure transducers, and, when a level is attained indicative of a failed channel, a solenoid valve is commanded to open, bypassing the recalcitrant channel. The PDU, meanwhile, continues operating normally in response to the commands of the three good channels. Should a second servovalve failure occur, a similar two-versus-one vote would result in its bypass. In this way, the PDU is tolerant of two avionic failures while maintaining full performance.

During early development testing of the PDU, it was found that channel failure and isolation, while the PDU was operating at a high output rate, could result in very high internal pressure pulses as a result of compression of the fluid in manifolds and lines between the power valve and the motor. Measurements indicated that pressures up to 5,480 N/cm^2 (8,000 psig) were being generated. This problem was resolved by making several system modifications, including avionic command filtering, elimination of a power valve positioning linkage, and strengthening of pressure passages within the PDU.

The PDU is supplied hydraulic power at 2,050 N/cm^2 (3,000 psig) from all three of the orbiter's flight hydraulic systems. Pressure to operate all of the four servovalves is obtained from the output of a switching valve module, which ensures that, as long as one of the three hydraulic systems is active, the servovalves all receive pressure. If the primary hydraulic system fails, the switching valve will shift instantaneously to the first backup system. Similarly, if that system fails, another switching valve shift will supply the servovalves from the remaining third hydraulic system.

In contrast to the servovalves' hydraulic supply philosophy, the power supplied to the motors is on a system-by-system basis. If a hydraulic system is lost, the corresponding PDU motor output will also be lost. This reflects the results of studies performed early in the Shuttle program on the probabilities of avionic versus mechanical failures and the desire to guard against a failure that might affect more than one hydraulic system.

The PDU has three hydraulic motors for each of its functions: rudder and speedbrake. Each motor is a conventional swash-plate-type and delivers 2.3×10^8 dyn-cm (208 in. lb) at 7,000 rpm. The motor outputs are combined by speed summing differentials and the resultant rudder and speedbrake rotary inputs transmitted to the gear reduction section of the PDU.

Each motor is equipped with a pressure-released mechanical brake so that, should a hydraulic system fail and result in the loss of a motor's output, the brake will set, preventing spillage of the torque from the other two motors at the motor producing no torque.

The gear reduction mixer accepts input torque from the rudder and speedbrake summing differentials and produces PDU output shaft rotation for transmission to the surface actuators. Successful development of the mixer greatly reduces system complexity and weight, and it permits simultaneous rudder and speedbrake operation.

Mechanical position stops for the system and avionic position feedback readouts for monitoring of the surface position are located within the PDU and are splined to the geartrain near the PDU outputs. In keeping with the quadredundancy of the avionic system, there are four independent position readouts for both rudder and speedbrake functions.

Lubrication of the entire PDU geartrain is accomplished with a combination of Braycote* 3L-38RP grease and the MIL-H-83282 hydraulic fluid used in the orbiter hydraulic system. The Braycote grease has been extensively tested and exhibits excellent properties at the high and low temperatures imposed on this system, as well as outstanding stability at low pressure. The PDU geartrain is assembled using the Braycote grease, and, after closure of the gearbox, it is partially filled with hydraulic fluid for splash lubrication. Disassembly and inspection of the geartrain following qualification load and life tests simulating four times the required 100 mission duty cycles has shown very little gear wear and provided additional confidence in this lubricant combination.

The channel self-test features of the PDU (using majority voting) and its ability to isolate bad control channels and to switch hydraulic power supplies (following multiple failures) combine to give the unit a unique depth of redundancy when compared to aircraft flight control actuation systems.

*Registered trade name by Bray Oil Co.

Rotary Actuators

The four surface-geared rotary actuators (Figures 7 and 8) are fixed to the vertical stabilizer's aft spar and act as power hinges for the movable rudder/speedbrake panels. Each actuator is a 474-to-1 planetary-type gear reduction system that transmits the PDU-developed torque to the surfaces. Each actuator is dual in function, being connected to both left and right panels and actuating both.

The actuators are fabricated with large movable and fixed ring gears that carry very high loads for their size. Ring gear diameter of the upper two actuators is 22.3 cm (8.8 in.) and of the lower two actuators is 28.9 cm (11.4 in.). Maximum load capacities corresponding for these two gear sizes are 4.33×10^{11} dyn-cm (383,000 in. lb) and 8.27×10^{11} dyn-cm (732,000 in. lb).

During early program testing with the rotary actuators, a problem was experienced with root cracking of the highly stressed planetary gears in the actuators. This test problem triggered an improvement in gear material processing (addition of a grit-blast operation to remove some gear carbide oxide surface and additional surface shot peening to increase precompression) and modification of the tooth profile to provide better load distribution in the loaded (deflected) case.

Lubrication of the actuators is accomplished with the same Braycote 3L-38RP grease used in the PDU. Inspection of the test units after completion of life testing has verified the adequacy of this lubricant selection.

Power Transmission Shafting

To transmit the torque between the PDU and the rotary actuators, drive shafts are used. These are conventional aluminum tubes riveted to steel coupling ends. Crown splines are used to account for misalignments imposed by the system installation (as when the upper actuators are smaller in diameter than the lower) and for in-flight deflection due to the high airloads imposed on the orbiter's tail, which cause structural deflection.

TEST PROGRAM

The test program associated with the rudder/speedbrake actuation system is summarized in Figure 9. The orbiter's development program has dictated that qualification of the system be completely accomplished in support of the spacecraft's atmospheric flight tests conducted in 1977 and then repeated recently to prepare for the first orbital flight in 1981. By splitting the qualification testing into two phases, it was possible to tailor the test requirements to match more closely the mission requirements and to incorporate design improvements into the test hardware to ensure duplication of flight configurations.

Life testing, conducted during qualification tests, has subjected the subsystem components to four times the anticipated number of mission duty cycles to be encountered during the orbiter's life. Successful completion of the life test is used, in conjunction with other design factors, to verify that safe-life capability of the hardware exists. Each mission duty cycle (Figure 10) imposed on the components subjects them to the loading and rates required by a representative orbiter flight. Included in the regime are high-hinge moment full speedbrake deployment (encountered in the early phases of entry), rudder oscillations (simulating positioning of the orbiter for final approach), and high-hinge moment rudder cycling associated with transonic flight. A series of buffet loads, imposed at several points throughout the test, provides greater duplication of the actual flight environment and induces additional cyclic loads on the system gearteeth to ensure accurate mission simulation.

CONCLUSION

The design of a crew safety-critical hydromechanical flight control actuation system employing multiple levels of redundancy, where appropriate, and safe-life design concepts for primary load carrying components has been developed in response to a demanding set of environmental and operational requirements.

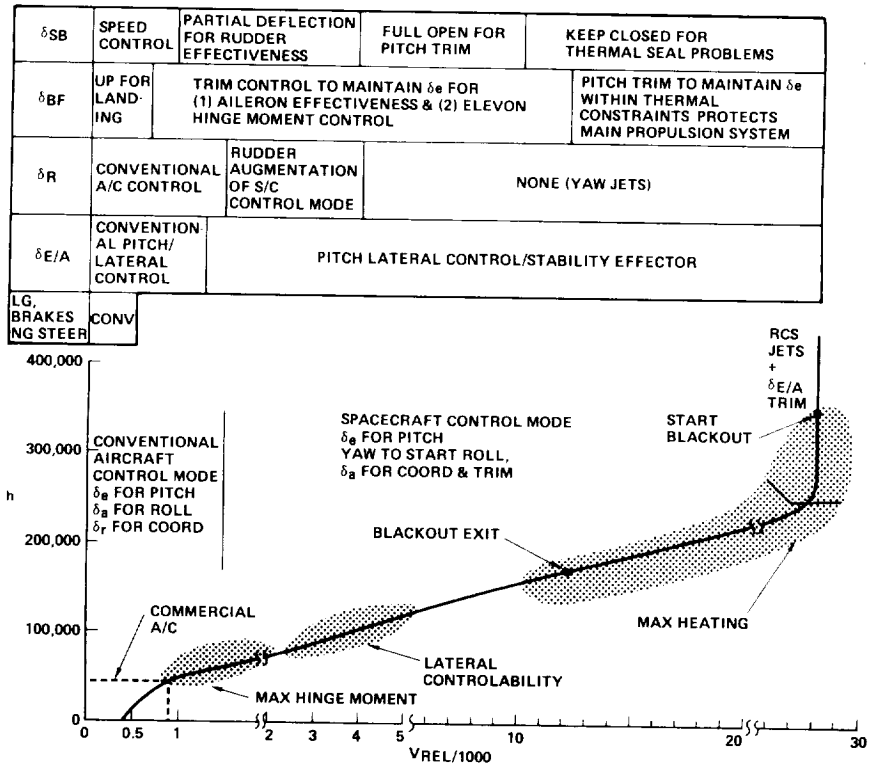

Figure 1. Orbiter Entry Summary

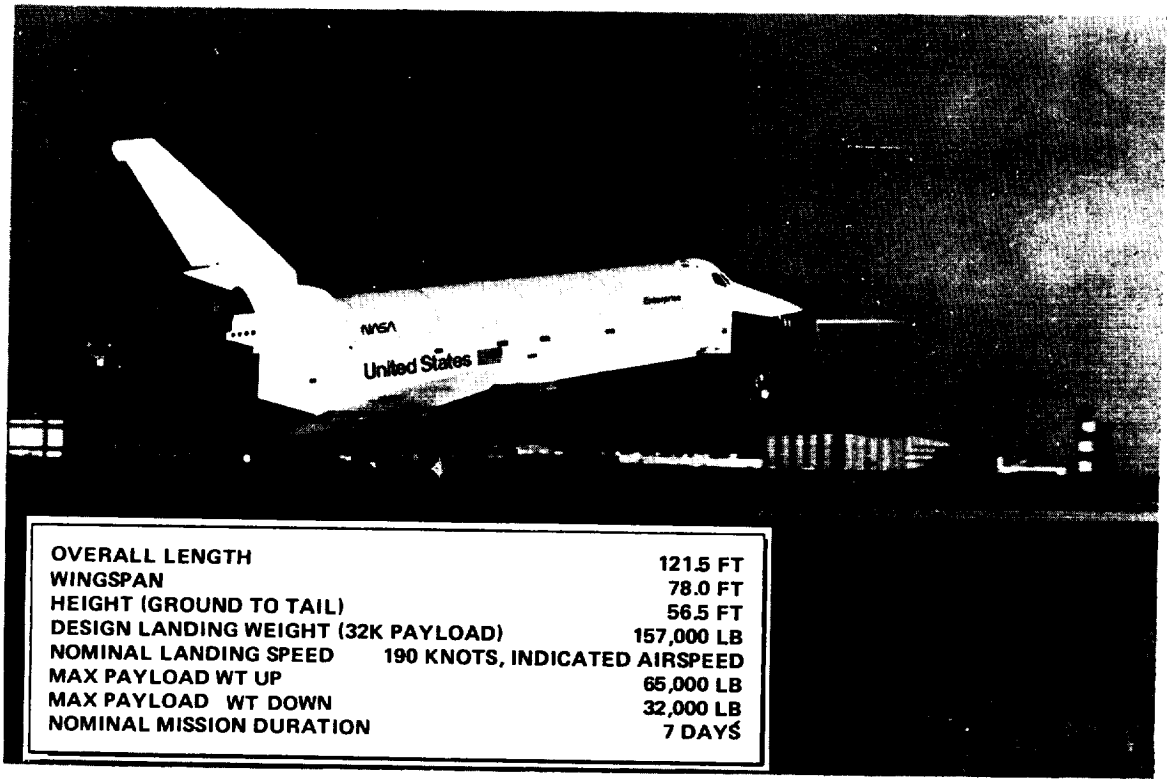

Figure 2. Orbiter Rudder/Speedbrake

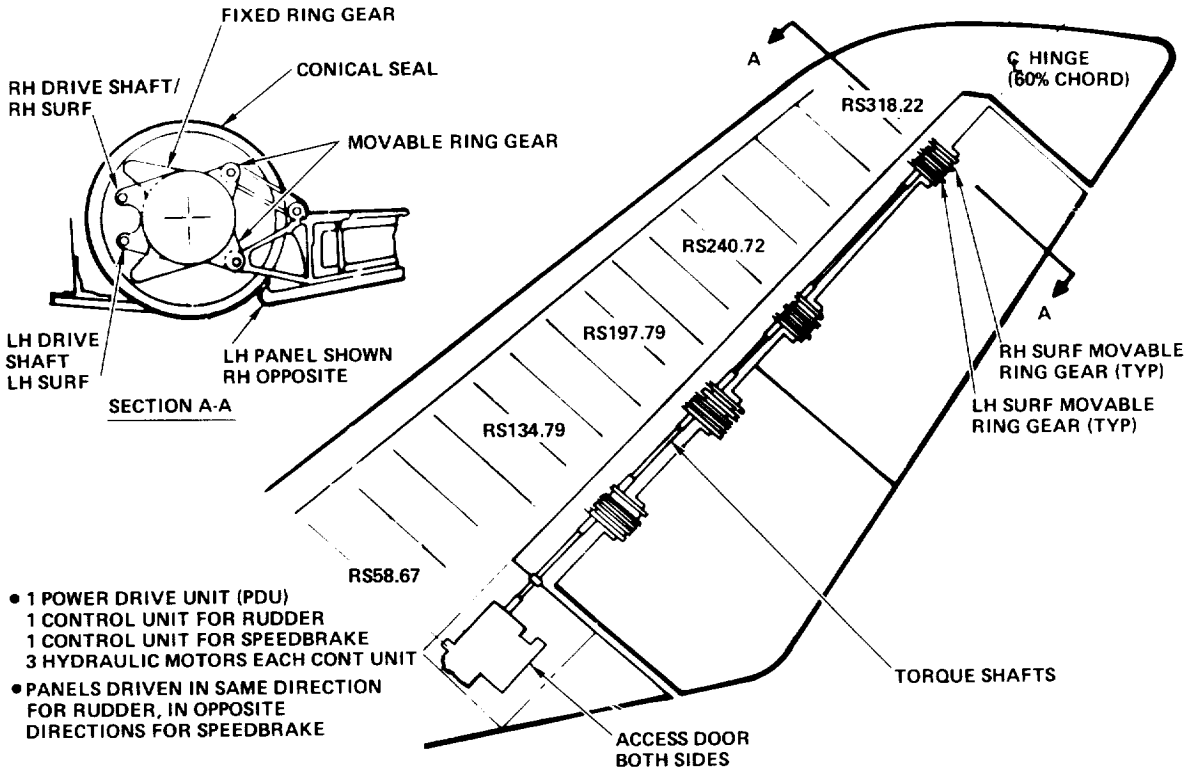

Figure 3. Rudder/Speedbrake Actuation System

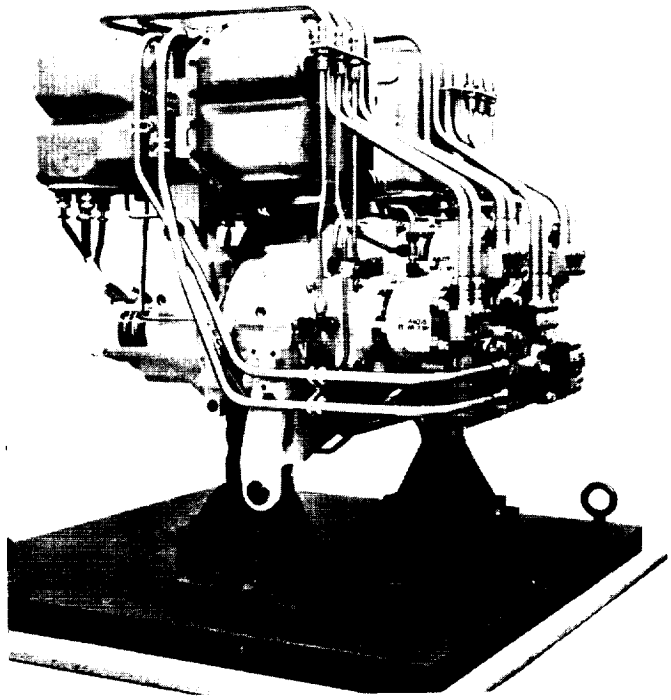

Figure 4. Power Drive Unit

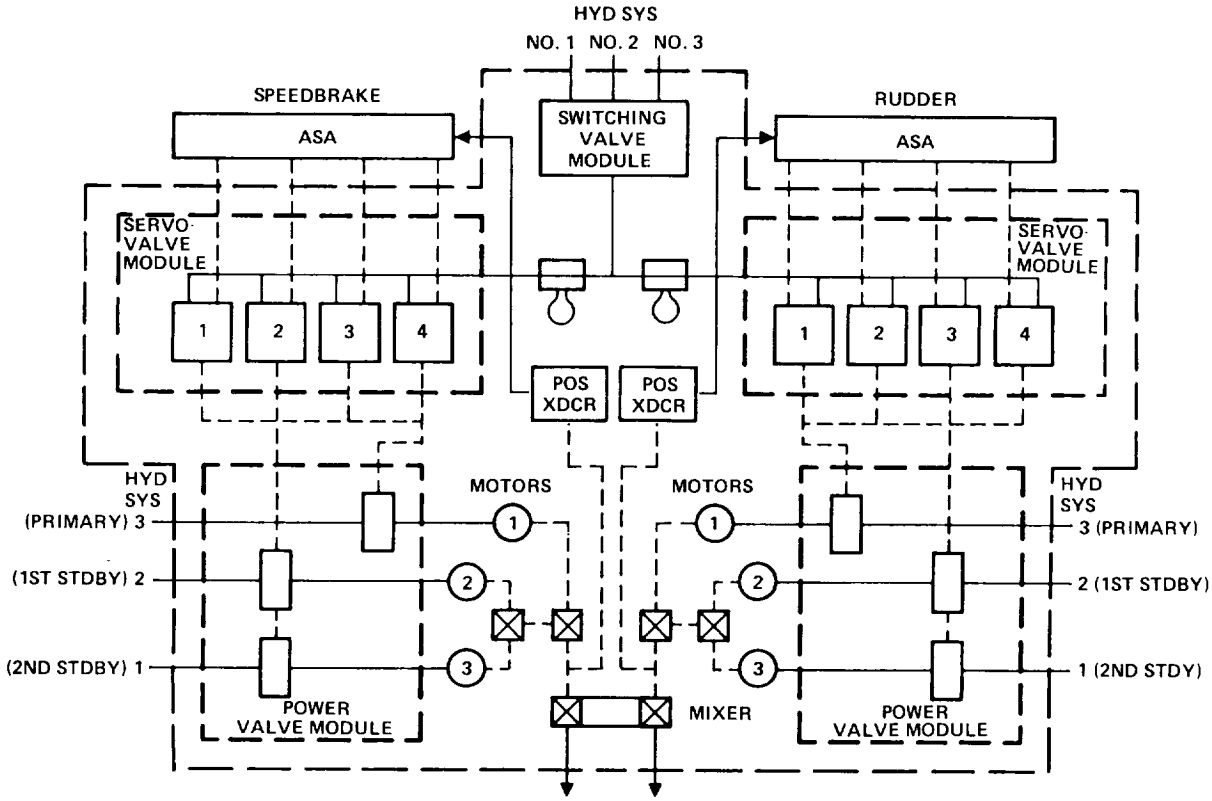

Figure 5. Power Drive Unit Schematic

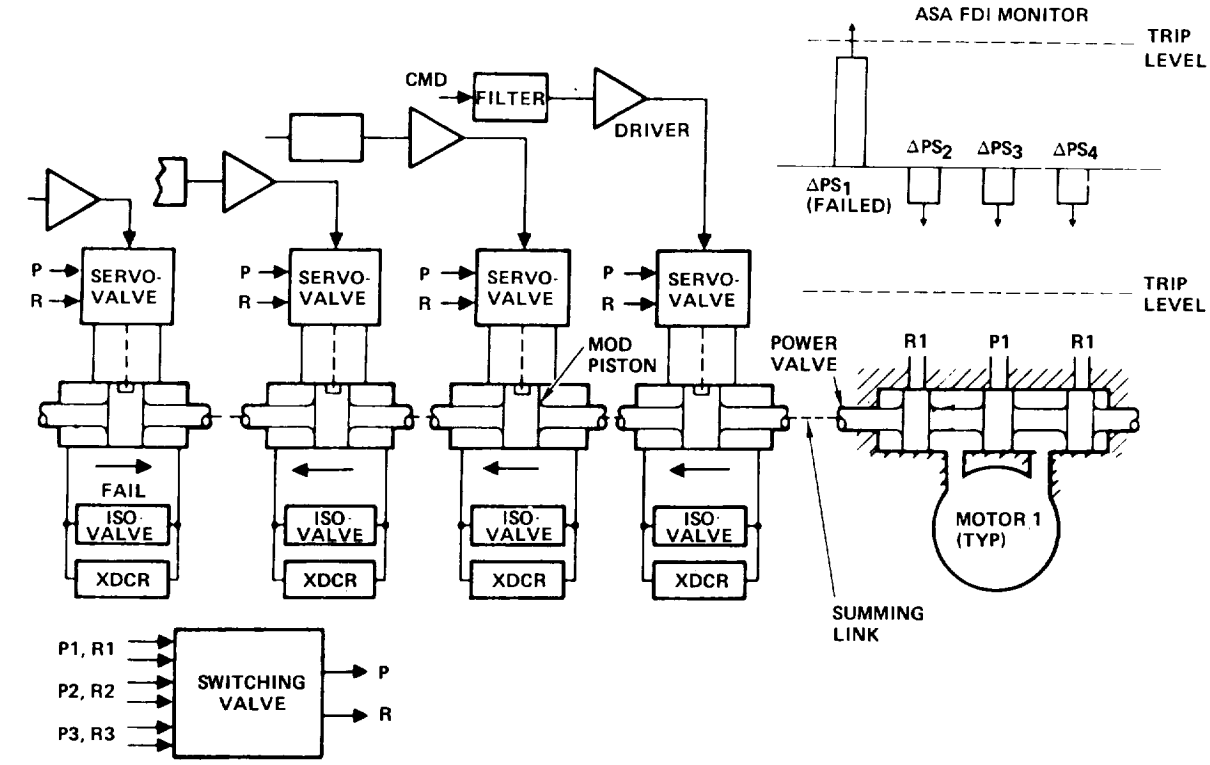

Figure 6. Channel Fault Detection

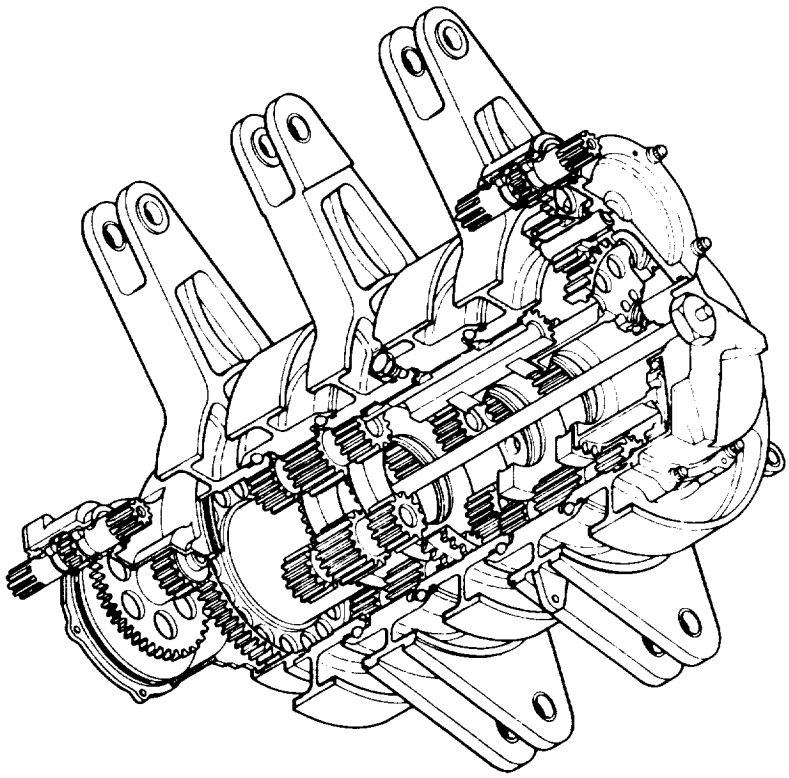

Figure 7. Rotary Actuator

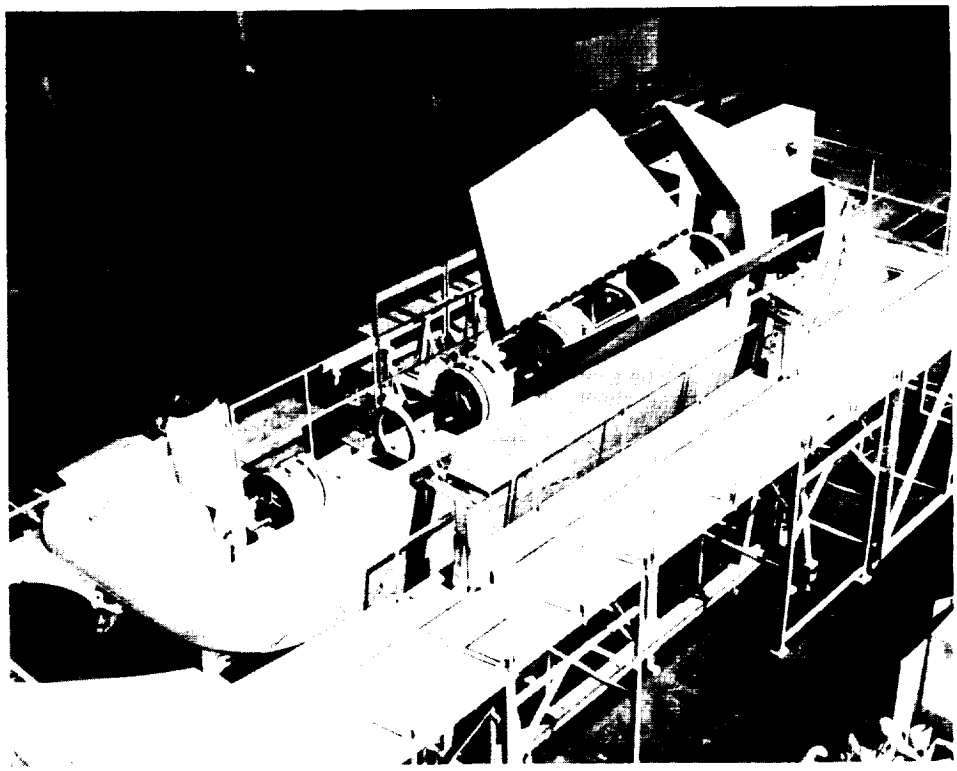

Figure 8. Rotary Actuator Installation

	ACTUATOR	PDU
• QUALIFICATION	• THERMAL VACUUM • HUMIDITY • HIGH/LOW TEMP • HANDLING SHOCK • DESIGN SHOCK • RANDOM VIBRATION • LIMIT LOAD • ULT LOAD • STIFFNESS • LIFE (FATIGUE) • BONDING	• THERMAL VACUUM • HUMIDITY • HIGH/LOW TEMP • BURST • HANDLING SHOCK • DESIGN SHOCK • RANDOM VIBRATION • LIMIT LOAD • ULT LOAD • LIFE (FATIGUE) • STIFFNESS • BONDING • PERFORMANCE • EXPLOSIVE ATMOSPHERE
• ACCEPTANCE	• OPERATING LOAD & RATE • FREE PLAY	• OPERATING TORQUE & RATE • FREE PLAY • PROOF • INSULATION RESISTANCE & DIELECTRIC • STATIC & DYNAMIC LEAKAGE • PERFORMANCE

Figure 9. Rudder/Speedbrake Actuation Test Program

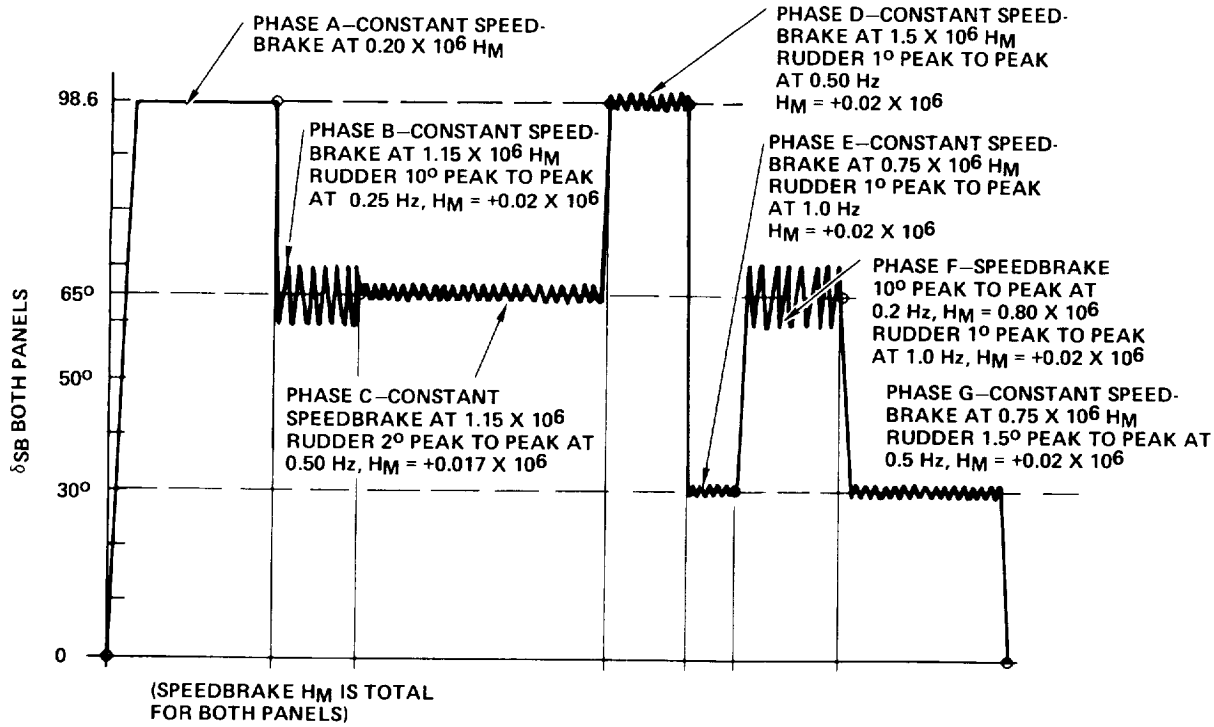

Figure 10. Test Mission Duty Cycle

PAYLOAD RETENTION LATCHES FOR THE SHUTTLE ORBITER

Robert D. Renken and Richard P. Maxwell*

ABSTRACT

Two latches were designed to mount payloads in the Shuttle Orbiter bay. Multiple retention latches attach a payload to the sill longerons and another latch device attaches it to the keel. Requirements for each actuator are defined and drive mechanisms are described. Other design aspects discussed include: switch mechanisms, motors, gearboxes, redundancy provisions, structural materials and lubricants. A preliminary dry lubricant test program is also reviewed and results presented.

INTRODUCTION

A Payload Retention Latch Actuator (PRLA) and an Active Keel Payload Retention Latch Actuator (AKA) were designed to hold payloads in the Shuttle Orbiter. The PRLA latches payloads to the longerons on each side of the Orbiter while the AKA latches payloads to the keel. The two devices, though similar, have unique drive mechanisms which were dictated by envelope and operational constraints. Both latches have switches which indicate when a payload is present and whether the latch is open or closed. It is necessary to use a variety of lubricants because of the various types of mechanisms in the latches and the harsh Shuttle payload bay environment. Bray grease, Vitrolube and Fibriloid were selected after extensive testing. The loads imposed by the payloads and envelope restrictions were accommodated by a compact design and the use of Inconel 718 and Carpenter Custom 455 stainless steel.

ORBITER PAYLOAD MOUNTING

The latches are designed to accommodate a range of payload sizes up to a length of 18.29 meters (60 feet), a diameter of 4.57 meters (15 feet), and a mass of 29,480 kilograms (65,000 pounds). Each payload is equipped with two, three, or four trunnions to interface with the PRLAs and one trunnion to interface with the AKA. Figure 1 depicts a mission in which two payloads are mounted. The forward payload, A, is shown using a five-point mount, the aft payload, B, a three-point mount. The payload trunnions are required to slip in the $\pm Y$ direction at the latch interface and also to nutate through a 0.10

*Ball Aerospace Systems Division, Boulder, Colorado

radian (6 degrees) half-cone angle. The latches themselves are designed to slip in the ±X direction at the Orbiter bridge fitting interface or to be fixed to these fittings by pins or stops. In Figure 1, the two aft PRLAs on payload A, and both PRLAs and the AKA on payload B, are fixed in the X axis to their bridge fittings. The remaining PRLAs and the AKA on payload A are free to slip. The fixed actuators can carry loads in the ±X direction. In addition, the PRLAs can carry loads in the ±Z direction while the AKAs carry loads in the ±Y direction. In this manner the latches allow in-flight deflections of both the Orbiter and the payloads without significantly loading either structure.

REQUIREMENTS

Payload Retention Latch Actuator

The loads required for the PRLA are divided into two categories: (1) loads when closed, and (2) pull-in loads or loads during operation. When closed, the PRLA is required to withstand operational limit loads of 538,200 newtons (121,000 pounds) in any direction and crash loads of up to 1.045×10^6 newtons (235,000 pounds). During operation, the PRLA is required to pull in a trunnion from 5.08 centimeters (2.00 inches) with a load that varies from zero to 66,700 newtons (zero to 15,000 pounds) as shown in Figure 2. Each PRLA is mounted on an Orbiter sill longeron bridge fitting. The top of the bridge fitting is a tee-shaped rail. The PRLA has the mating slot which extends over its entire length. This interface can be free to slip or pinned to lock the PRLA in place. The payload trunnion is 8.26 centimeters (3.25 inches) in diameter and must be able to nutate through a 0.10 radian (6 degrees) half-cone angle.

Active Keel Actuator

The AKA loads are also divided into two categories. When closed, the AKA is required to withstand limit loads of 458,200 newtons (103,000 pounds) along the ±Y axis and 30,250 newtons (6,800 pounds) along the ±X axis. The AKA is required to pull in a trunnion against a ±Y axis load of 4,450 newtons (1,000 pounds). The AKA interface differs from the PRLA in that the tee-shaped rail is built into the AKA and the Orbiter keel bridge fitting contains the mating slot. Motion can be prevented by open and closed stops or the interface can be left free to slip. The payload trunnion is 7.62 centimeters (3.00 inches) in diameter and must be able to nutate through a 0.10 radian (6 degrees) half-cone angle.

General Requirements for Both Latches

Since both latches operate in the Orbiter payload bay, there are a number of common requirements:

- Temperature: -73.3 degrees Celsius to +135 degrees Celsius (-100 degrees Fahrenheit to +275 degrees Fahrenheit) for PRLA.

  -73.3 degrees Celsius to +176.7 degrees Celsius (-100 degrees Fahrenheit to +350 degrees Fahrenheit) for AKA.

- Humidity: Zero to 100 percent including salt spray.

- Friction: The design goal for the trunnion and bridge interfaces is 0.1 maximum coefficient of friction.

- Electrical: Motors to operate on 400 hertz three-phase 115-volt power. Switches on 28-volt direct current.

- Outgassing: Materials to meet requirements of NASA.

- Switches: To define whether the actuator is open, closed, and if a trunnion is present.

- Stress Margin: Actuator must withstand ultimate loads 1.4 times limit loads without opening.

- Redundancy: All moving parts and electrical circuits must be fully redundant with the exception of rolling element bearings which may not be if L_{10} life is 17 times anticipated life.

PAYLOAD RETENTION LATCH ACTUATOR

The PRLA is shown in Figure 3. It is built around and supported by one predominant structural part: the frame. The frame has a tee-slot which ininterfaces with the bridge fitting. It also supports one-half of the spherical bearing which interfaces with the payload. The other half of this spherical bearing is contained by the claw. The claw is rotated into position to lock the trunnion in place by a linkage as shown in Figure 4. There are four links besides the claw and frame. The mechanism may be described as a double four-bar linkage. The claw, frame, driven link and compression link comprise one four-bar. The frame, crank, drive link and driven link comprise another. The crank is the driving link for the entire mechanism. The double four-bar was selected because both sets of links lock on center in the closed position and the mechanical advantage of the linkage approximates the required load stroke curve shown in Figure 2. The kinematics is also illustrated in Figure 2 by the curve labeled "Force Available." This is the nominal capability of the actuator at room temperature with a gearbox output torque of 1,277 newton-meters (11,300 inch-pounds) and a coefficient of friction of 0.20. The gearbox is bolted and pinned to the frame and provides the output torque required to drive the actuator. The mass of the PRLA is 50.3 kilograms (111 pounds).

A cross-sectional view through the gearbox is shown in Figure 5. All of the gears are cut with standard cutters. Ratios for each mesh, pressure angle, and overall ratio are shown in Table I. The gearbox is not designed with a torque-limiting device because the operation of a torque limiter is somewhat unpredictable over the required temperature range and it is a potential single-point failure. Because of this, the gears and bearings are sized to carry the loads produced when the crank hits its mechanical stops and the motor is traveling at its no-load speed. Compliance is purposely designed into the mechanism so the loads resulting from stopping the motor inertia are relatively small. The maximum loads were determined by solving the differential equation of motion of the resulting inertia/spring system.

The open and closed limit switches are actuated by a cam machined into the crank. There is also a trunnion eject device in the form of a spring-loaded arm designed to push the trunnion out of the spherical bearing when the actuator is open. This eject arm also rotates a cam which actuates the ready-to-latch switches. The payload trunnion can be pulled into the latch by the actuator as soon as it is 5.08 centimeters (2.00 inches) away from its final latched position. When it is 2.08 centimeters (0.82 inch) away, the ready-to-latch switch is tripped, and when it is 0.25 centimeter (0.10 inch) away, the 62.3 newton (14-pound) eject springs are engaged. The frame has built-in guides to guide the trunnion from 20.3 centimeters (8 inches) away. There are also optional extended guides that may be used to guide the trunnion from 55.9 or 61.0 centimeters (22.00 or 24.00 inches) away. The entire actuator may slide on the Orbiter bridge fitting on the tee slot. If the actuator is to be fixed, the frame is pinned to the bridge fitting after it is in position. Total travel for the floating PRLA is limited by a spring-loaded snubber, called a positioning device. The positioning device is pinned to the bridge fitting adjacent to the PRLA and it limits the PRLA travel to ±3.18 centimeters (±1.25 inches). At this point the high spring force limits any further travel.

ACTIVE KEEL ACTUATOR

The AKA is shown in Figure 6 and a drawing of its mechanism is shown in Figure 7. The static and dynamic latches are its primary structural elements. The AKA is opened and closed like a vice by the ball screw. The ball screw nut is attached to the spring link which drives the dynamic latch and the overcenter linkage. The spring link gets its name from the fact that it is designed to provide compliance to the gearbox/linkage system so that excessive loads are not experienced if the mechanism jams or if the switches fail to shut off the motors. The spring link also drives the overcenter links to their locked position. As the actuator is closed, the guides on the static and dynamic latches scissor together to pull the trunnion into the spherical bearings. The force available for the normal actuator is shown in Figure 8. The AKA ball screw is driven by a conventional spur gearbox with ratios and cutter pressure angles as indicated in Table II. The gears, bearings and ball screw are sized to carry the loads produced when the linkage hits its mechanical stops and the motors are traveling at their no-load

speeds. As the overcenter links lock, they actuate the closed limit switches. The open limit switches are actuated by the dynamic latch. There are also switches which are tripped when a trunnion is present in the spherical half bearing in the static latch. The AKA is designed so that stops may be bolted to the keel bridge rails to fix its position when it is opened and when it is closed. The mass of the AKA is 38.5 kilograms (85 pounds).

MOTOR/BRAKE CHARACTERISTICS

Each latch has a gearbox which is driven by two alternating current motors that are coupled together by a spur-gear differential. These motors normally operate on three-phase, 400 hertz power at 115 volts, and have a no-load speed of 8,000 rpm. Each motor products a minimum peak or breakdown torque of 0.136 newton-meter (1.2 inch-pounds) when operated on three phases and a minimum stall torque of 0.090 newton-meter (0.8 inch-pound) when operated on two phases. The motors are designed to drive either of the latches if one motor is operating on three phases and the other on two phases.

As shown in Figure 9, each motor is equipped with a fail-safe disc brake that is spring-loaded to the locked position. The brake is wired in series with the three motor phases and is electrically released by the application of either two- or three-phase power to the motor. If two-phase power is supplied to a single motor/brake on a latch, that motor can produce enough torque to prevent backdriving by the other motor powered on three phases. A brake will hold 0.158 newton-meter (1.4 inch-pounds) under static conditions, including 100 percent relative humidity, and 0.102 newton-meter (0.9 inch-pound) in a vibration environment.

SWITCH MECHANISMS

Switch mechanisms were designed to reliably operate customer-supplied switches. In addition, the mechanisms safeguard the switches from overtravel and allow for switch adjustment after the latches are assembled. The switches themselves provide Latch Open, Latch Closed and Trunnion Present indications. A pair of switches is operated for each of these indications. A typical switch mechanism is shown in Figure 10. It is comprised of a housing and two spring-loaded levers, a cam follower arm and a trip arm. The switches are actuated when the cam follower arm is engaged lifting the trip arm. The switches are protected from overtravel by a stop which physically prevents the trip arm from depressing the switch too far. One trip arm and one cam follower arm operate both switches.

The switch adjustment screws are readily accessible from the outside of the latch. In order to prevent damage to the switch mechanisms should a latch continue to operate after its switch trips, the cams that operate the switches are equipped with dwells.

REDUNDANCY PROVISIONS

Redundancy has been incorporated into both latch designs in several ways in order to minimize the chances of a single failure making a latch inoperative. As mentioned above, two motors are provided on each latch and either is capable of operating the latch if the brake on the nonfunctioning motor is engaged. To insure that it is engaged, two sliding surfaces are provided where sliding is required so that if one surface becomes inoperative the other allows the brake to work. Six springs are used to actuate the brake. Any five of the springs will provide enough force for the brake to have sufficient holding capability. If a spring should break, any stray pieces could only keep the brake friction surfaces from disengaging, not engaging.

All pinned joints, such as latch and switch linkage hinges, are either bushed so rotation can occur at either the inside diameter or the outside diameter of the bushing, or designed so that the hinge pin is free to rotate in either part of the joint. All ball bearings and roller bearings are designed to have an L_{10} life at least 17 times greater than the required life of the latch.

For each of the three switch mechanisms, a pair of switches is operated to provide redundancy for the appropriate indications. Also, each switch trip arm is supplied with two springs. Either of the springs is capable of operating the switches if the other should experience a failure.

Two electrical connectors are used to provide power-supply redundancy. Each is connected to one motor and one switch from each of the three pairs of switches. Lead wires are routed so that any bundle can be cut without losing the latch's operating capability.

All structural elements such as the latch frames, linkages and gears are specifically excluded from redundancy requirements. These parts will be tested extensively during qualification and have received thorough stress and fracture analysis.

MATERIALS USED IN THE LATCHES

Materials can be divided into two broad categories, metals and lubricants. The structural parts of both latches are fabricated from Inconel 718. Inconel 718 is precipitation-hardened to 1,241 megapascals (180,000 psi) minimum ultimate tensile strength. It was chosen particularly because of its strength, fracture toughness at low temperatures, corrosion-resistance and non-magnetic properties. Carpenter Custom 455, a corrosion-resistant steel, was selected for the gears. Its relative ease of fabrication for a steel with a minimum ultimate tensile strength of 1,241 megapascals (180,000 psi), its toughness and its wear resistance added to its desirability. The thermal

properties of both metals match well enough to use Custom 455 gears in an Inconel gearbox on the PRLA.

A variety of lubricants are used with the latches. Gears, roller bearings and ball bearings are lubricated with Bray 3L-38RP grease. This grease was selected because of its low temperature characteristics and low outgassing rate. The gearboxes are sealed, with the exception of the output shaft which is shielded. The AKA ball screw is the only exposed element that is grease-lubricated. The links, link pins, guides, tee slots and half bearing spherical surfaces are lubricated with Vitrolube. This is a dry lubricant composed of moly-disulfide and graphite which is fused into a glass binder at 524 degrees Celsius (975 degrees Fahrenheit) and covered with a topcoat composed of moly-disulfide, graphite and enhanced by Teflon. This lubricant performs well in vacuum with contact stresses of up to 689 megapascals (100,000 psi). The inside diameters of the half bearings are lubricated with Fibriloid, a fabric impregnated with Teflon and bonded to a surface. To achieve the lowest possible coefficient of friction, the mating payload trunnion is lubricated with a thin coat of Bray 815Z oil. Switch mechanism parts are lubricated with a bonded moly-disulfide.

LUBRICANT DEVELOPMENT TESTS

An extensive lubricant search was conducted early in development.[1] Original requirements specified a coefficient of friction of 0.1 or less between the tee slot and mating rails and between the payload trunnion and half bearing. During this phase of the program, tests were conducted using pins and discs as shown in Figure 11. The pins and discs could be made from Titanium, Inconel 718 or Custom 455. They were coated with various lubricants. Two discs were loaded between two pins to obtain the desired contact pressure. The discs were moved laterally between the pins. The test setup was placed inside a vacuum chamber and operated from -73.3 degrees Celsius to +176.7 degrees Celsius (-100 degrees Fahrenheit to +350 degrees Fahrenheit) at atmospheric pressures of normal ambient to less than 0.67 millipascal (5×10^{-6} torr). Lubricant combinations tested are shown in Table III. Contact pressure was varied from 13.8 to 680 megapascals (2,000 to 100,000 psi). All of the lubricants tested failed to give the required coefficient of friction for all test conditions. Vitrolube on Vitrolube combinations gave the best results, however, and efforts late in the program were devoted to enhancing this lubricant. A topcoat including Teflon-5 was developed for the Vitrolube. With the topcoat, the 0.1 coefficient of friction was met at all temperatures and contact pressures in a vacuum. The required coefficient of friction was met in a nitrogen atmosphere except at contact pressures below 34.5 megapascals (5,000 psi) and over the temperature ranges of -62.2 degrees Celsius to +4.4 degrees Celsius (-80 degrees Fahrenheit to +40 degrees Fahrenheit).

CONCLUSION

The latch designs described in this paper proved to be extremely challenging because of the limited envelope and the high loads specified. These factors, along with the environment, led to the use of state-of-the-art materials and lubricants. These constraints also led to a relatively heavy design. The resulting latches are built to be extremely reliable over a broad spectrum of environments. Their design life is for a minimum of 100 missions over a ten-year period with at least 2,000 actuations. The latches will accommodate all of the payloads presently envisioned for the Orbiter and can be used well into the future. The test program to qualify these designs will be starting in the near future.

ACKNOWLEDGEMENT

The authors wish to acknowledge the fine assistance of Gloria Bucco, our technical writer, who was able to take the information given her and transform it into this paper. We also thank the Ball Aerospace Publications Department, without whose aid this paper would not have been possible.

REFERENCE

1. David M. Frost, Kent Roller, Steve Des Palmes; Shuttle Actuator Development Friction Tests - Final Report; Contract M9H3XMN-483157D.

TABLE I

PRLA GEARBOX

MESH NUMBER	RATIO	CUTTER PRESSURE ANGLE–DEGREES
1	11.5625:1	20
2	11.9231:1	25
3	8.5385:1	25
PLANETARY	5.3333:1	25
OVERALL RATIO: 6278:1		

TABLE II

AKA GEARBOX

MESH NUMBER	RATIO	CUTTER PRESSURE ANGLE–DEGREES
1	11.5625:1	20
2	6.7200:1	20
OVERALL RATIO: 77.7:1		

TABLE III

FRICTION COEFFICIENT SAMPLE INVESTIGATIONS

PIN COATINGS	TIBON CHROME	TIODIZE	DISC COATINGS		TEFLON CARBON	BARE TITANIUM	BARE 455
			VITROLUBE TI/455	SPUTTERED MoS_2			
SPUTTERED TEFLON	X	X			X		
SPUTTERED MoS_2	X	X		X	X		
TEFLON/CARBON	X	X					
KAHRLON	X						
FIBRILOID	X						
FIBERGLIDE	X						X
KAHR x 1550	X					X	X
VITROLUBE		X	X				

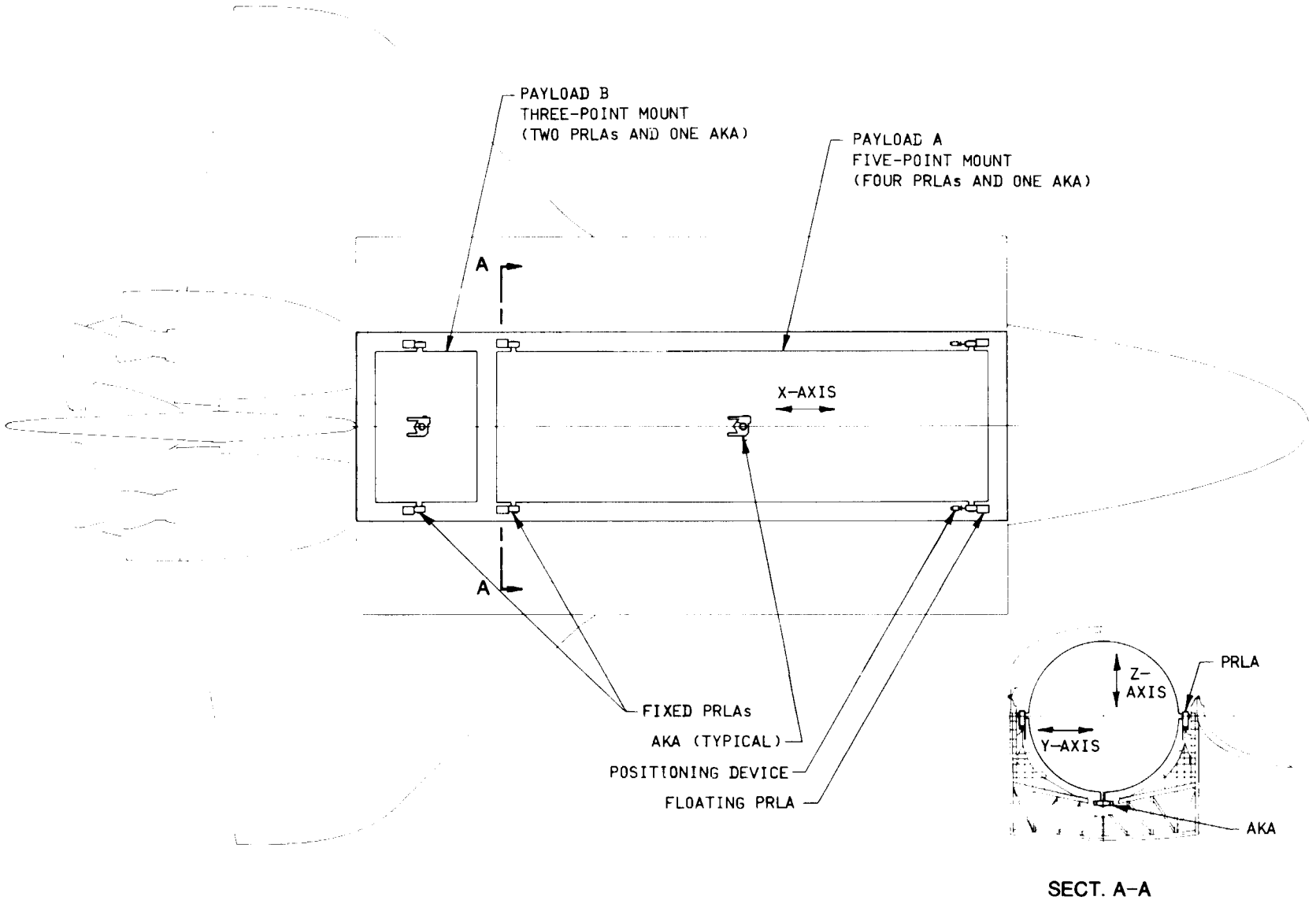

Figure 1. Shuttle Payload Arrangement

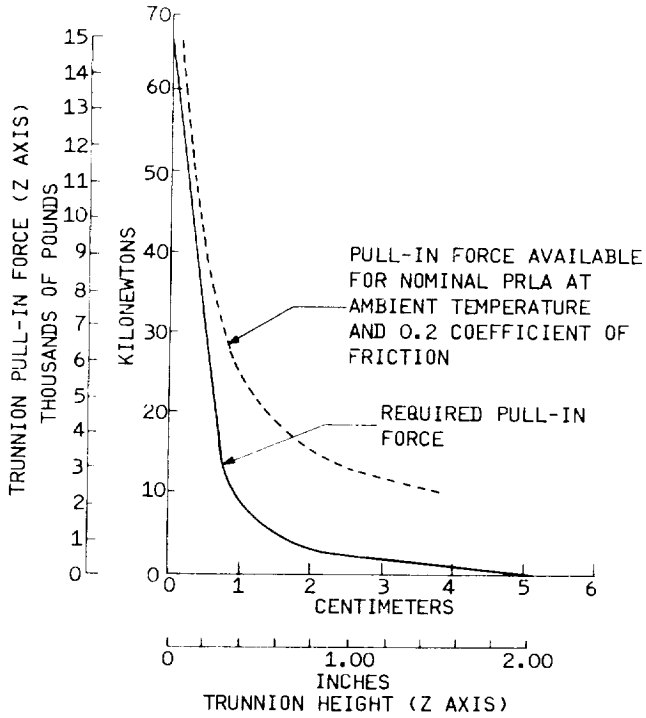

Figure 2. PRLA Pull-in Loads

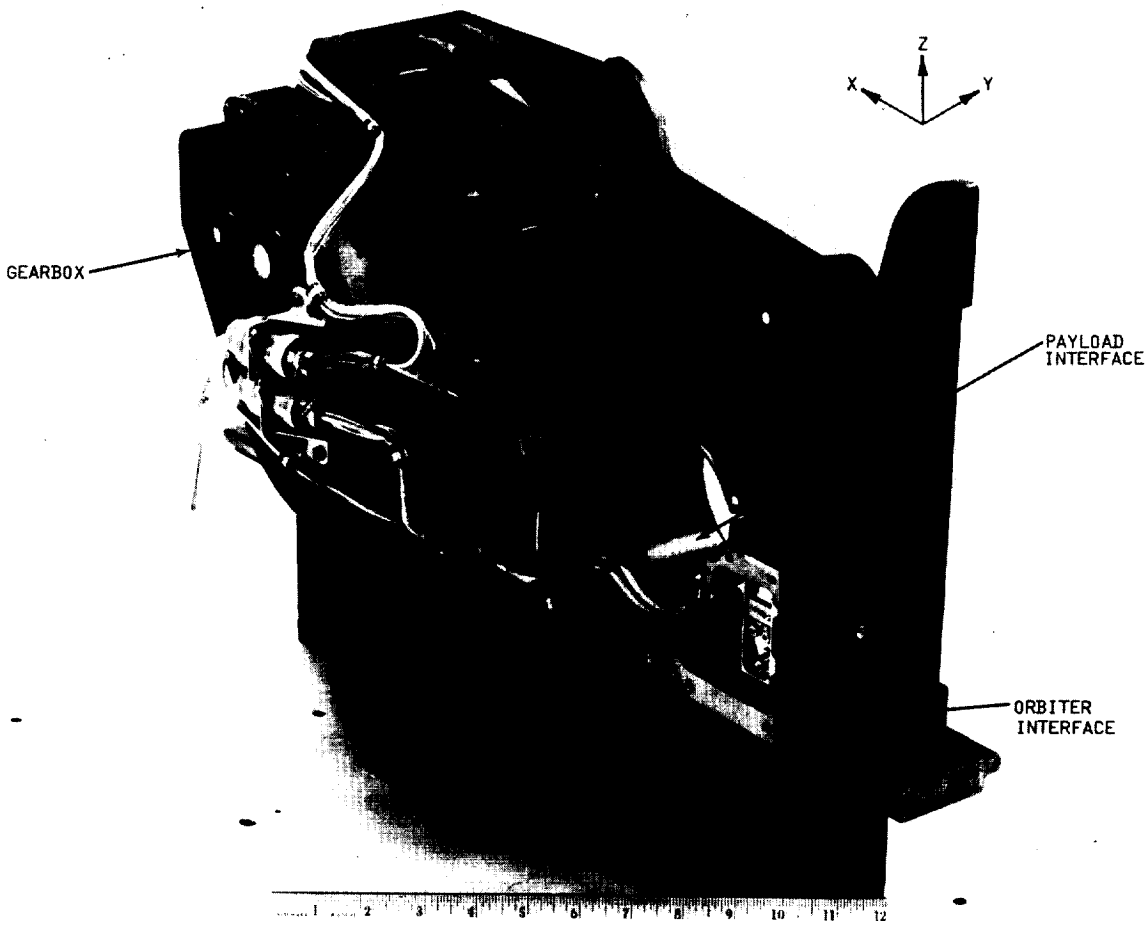

Figure 3. PRLA Photograph

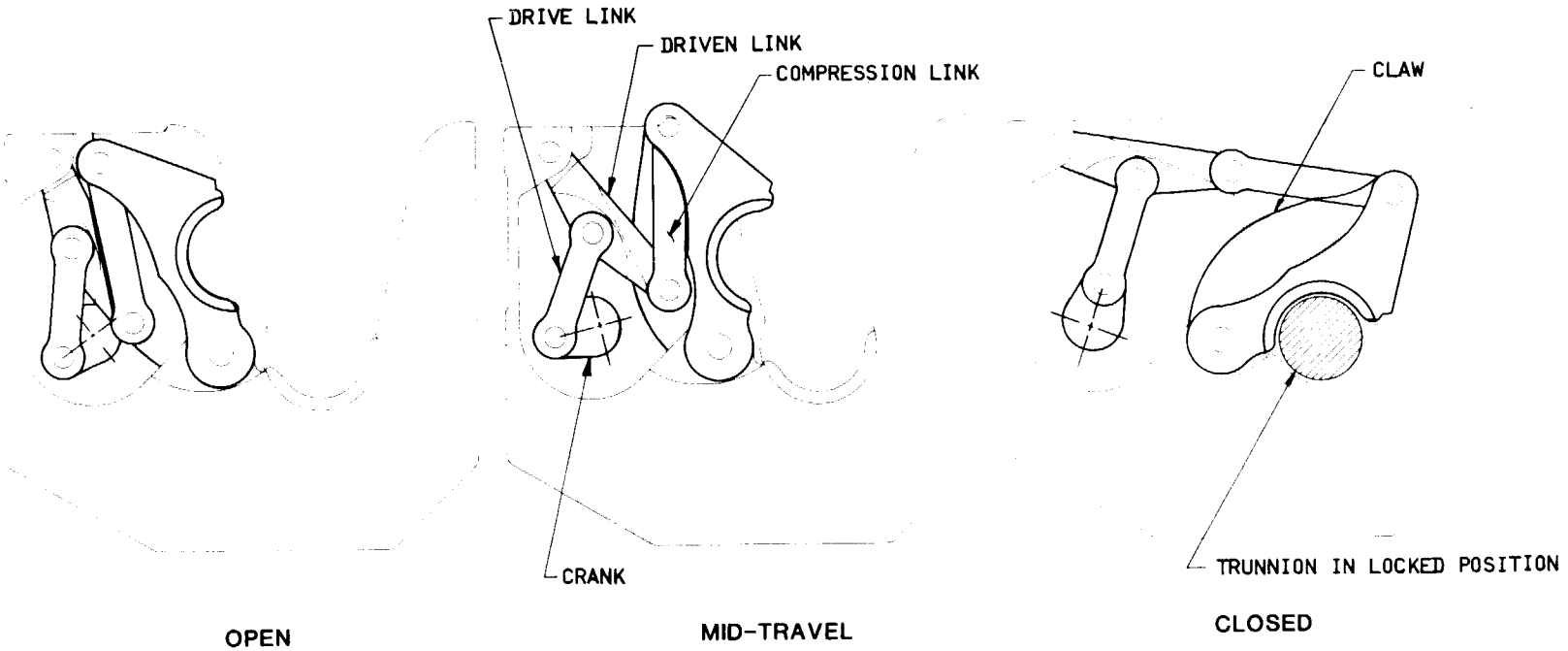

Figure 4. PRLA Linkage

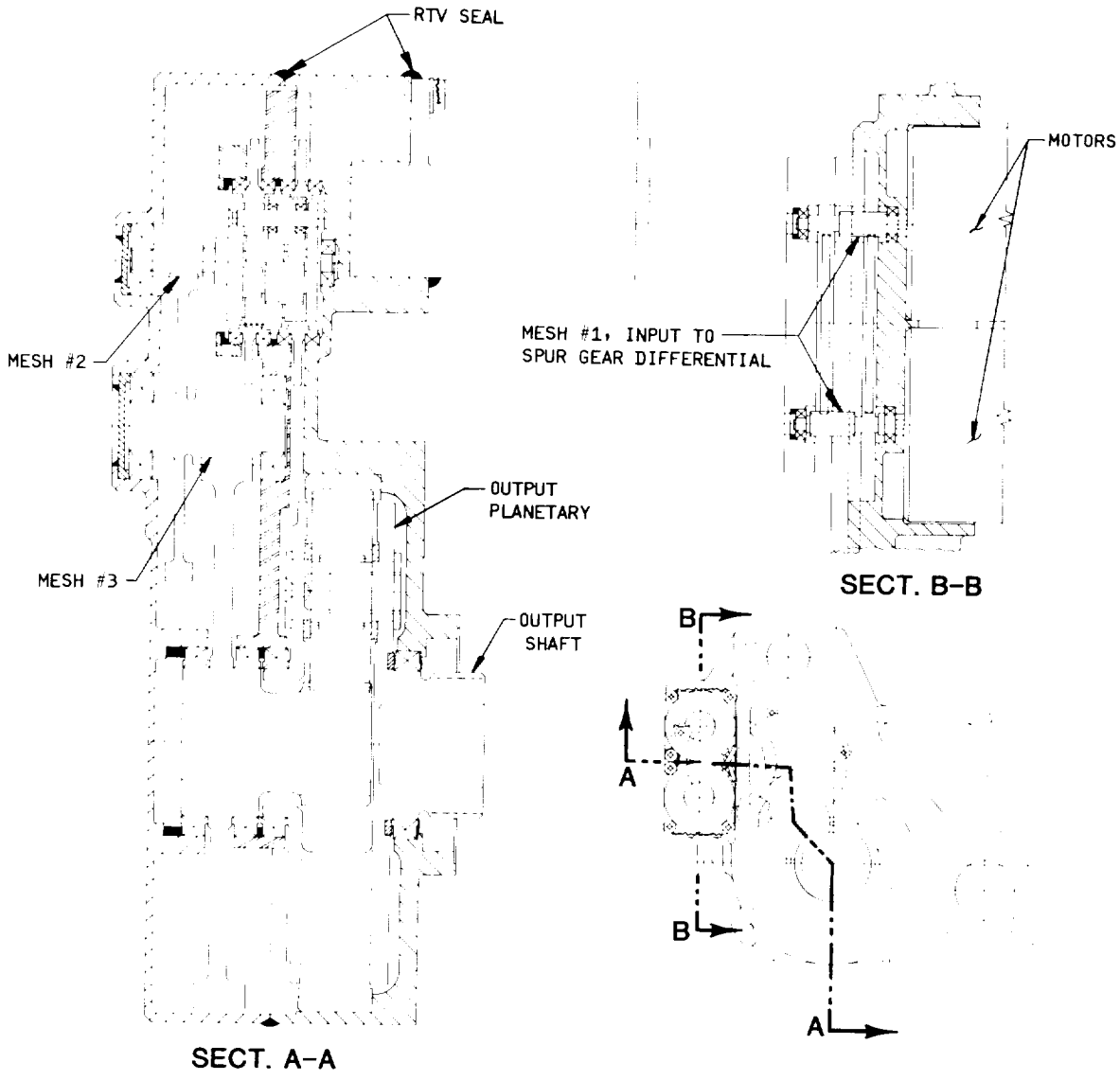

Figure 5. PRLA Gearbox Cross Section

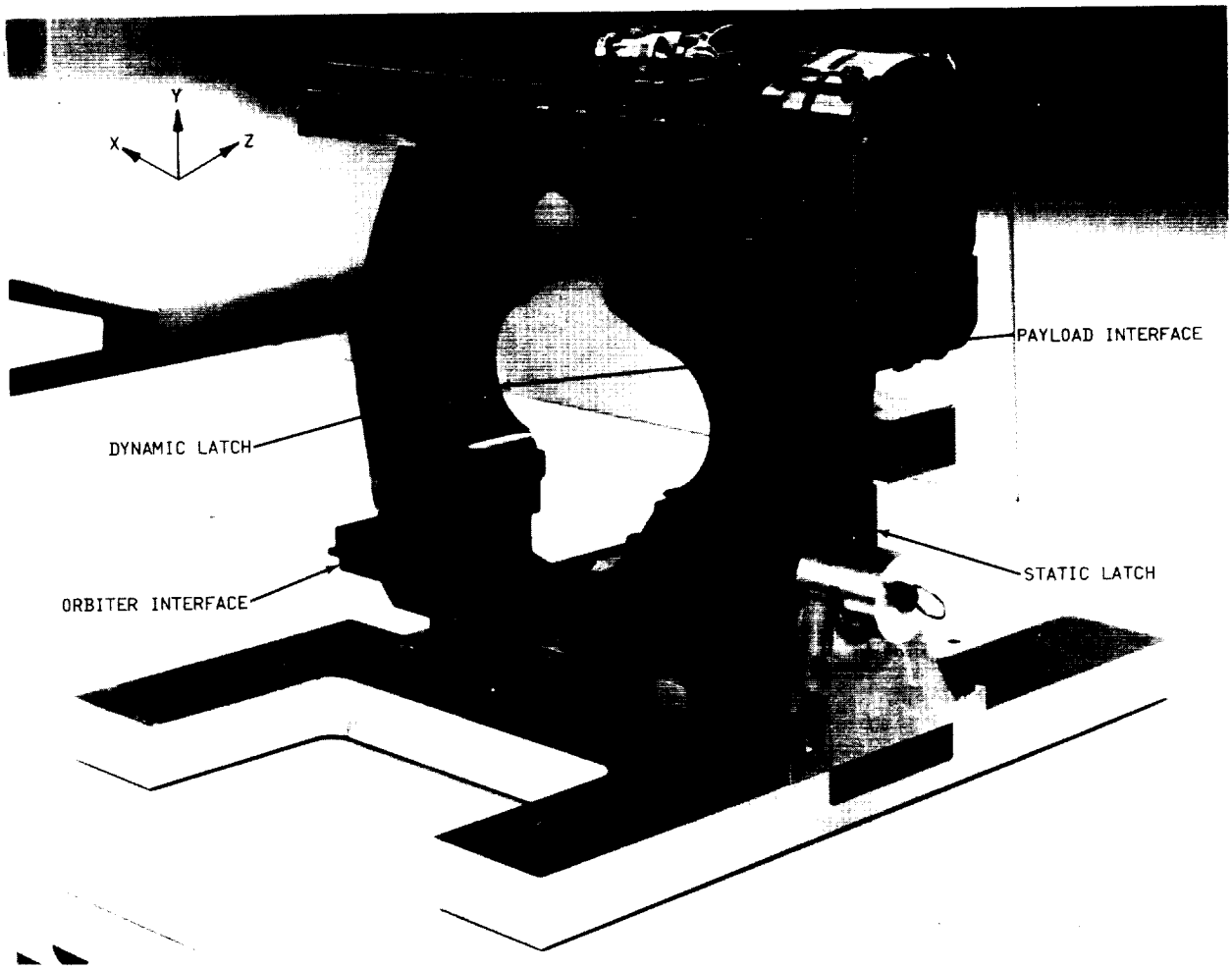

Figure 6. AKA Photograph

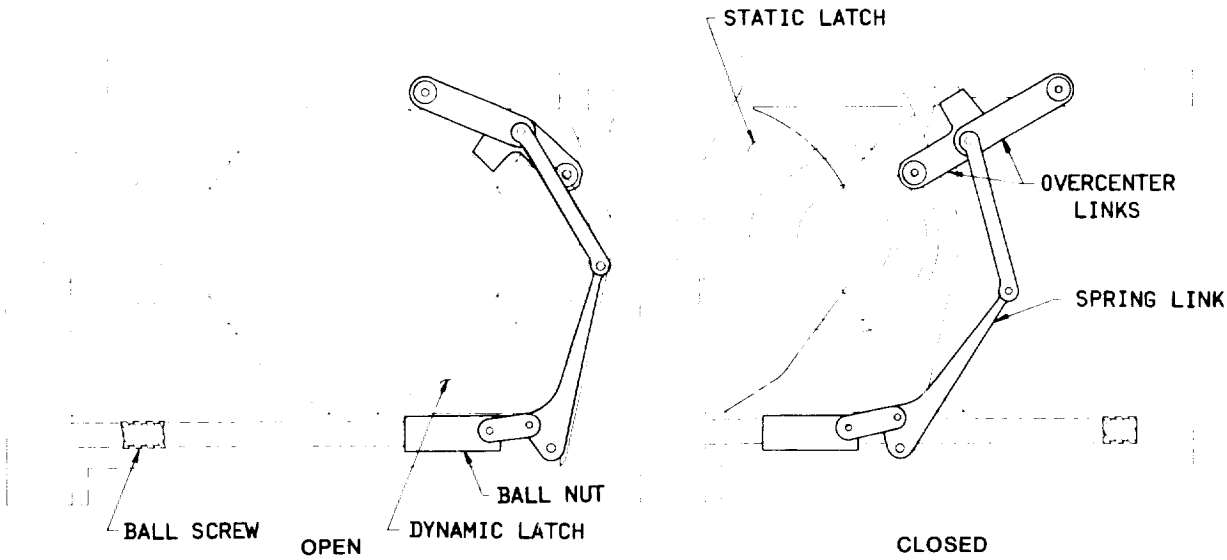

Figure 7. AKA Linkage

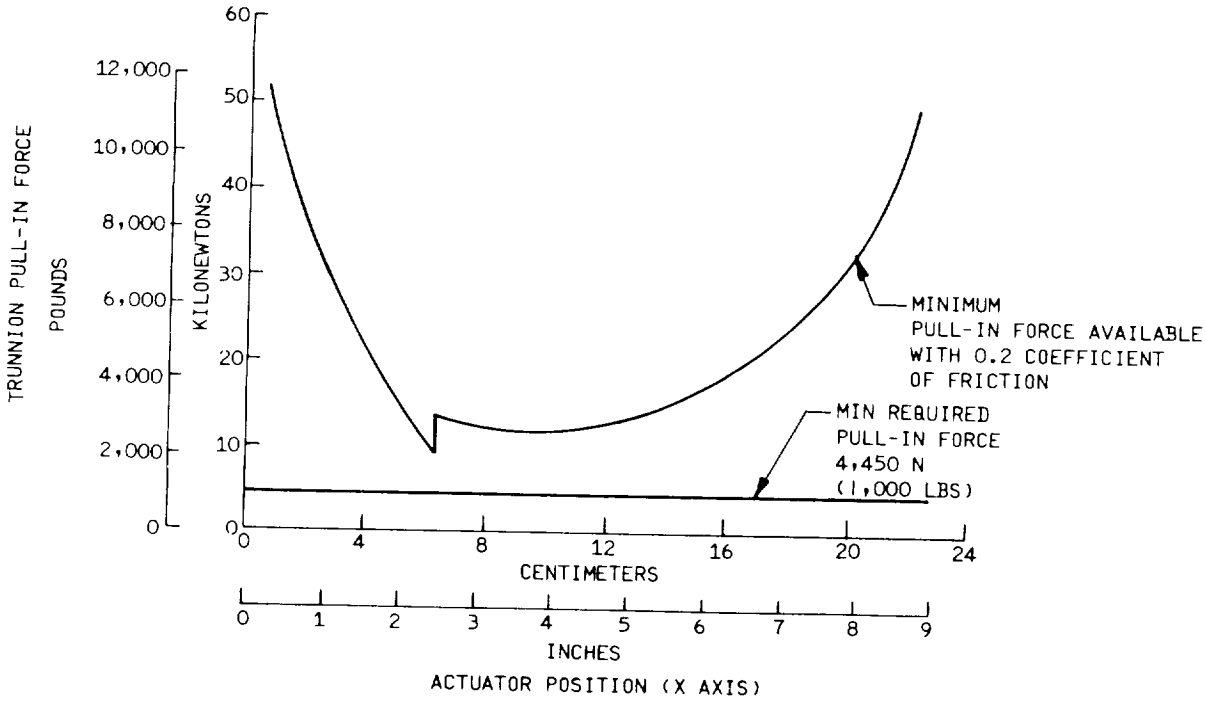

Figure 8. AKA Force Available

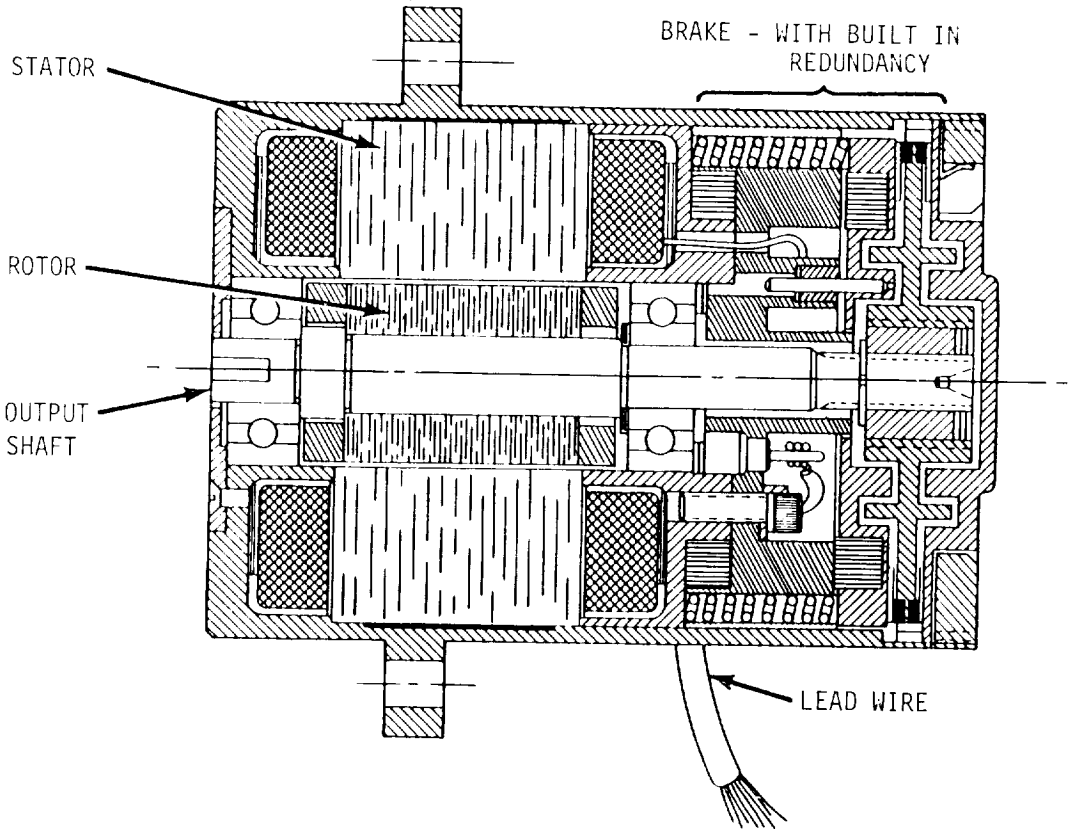

Figure 9. Motor/Brake Cross Section

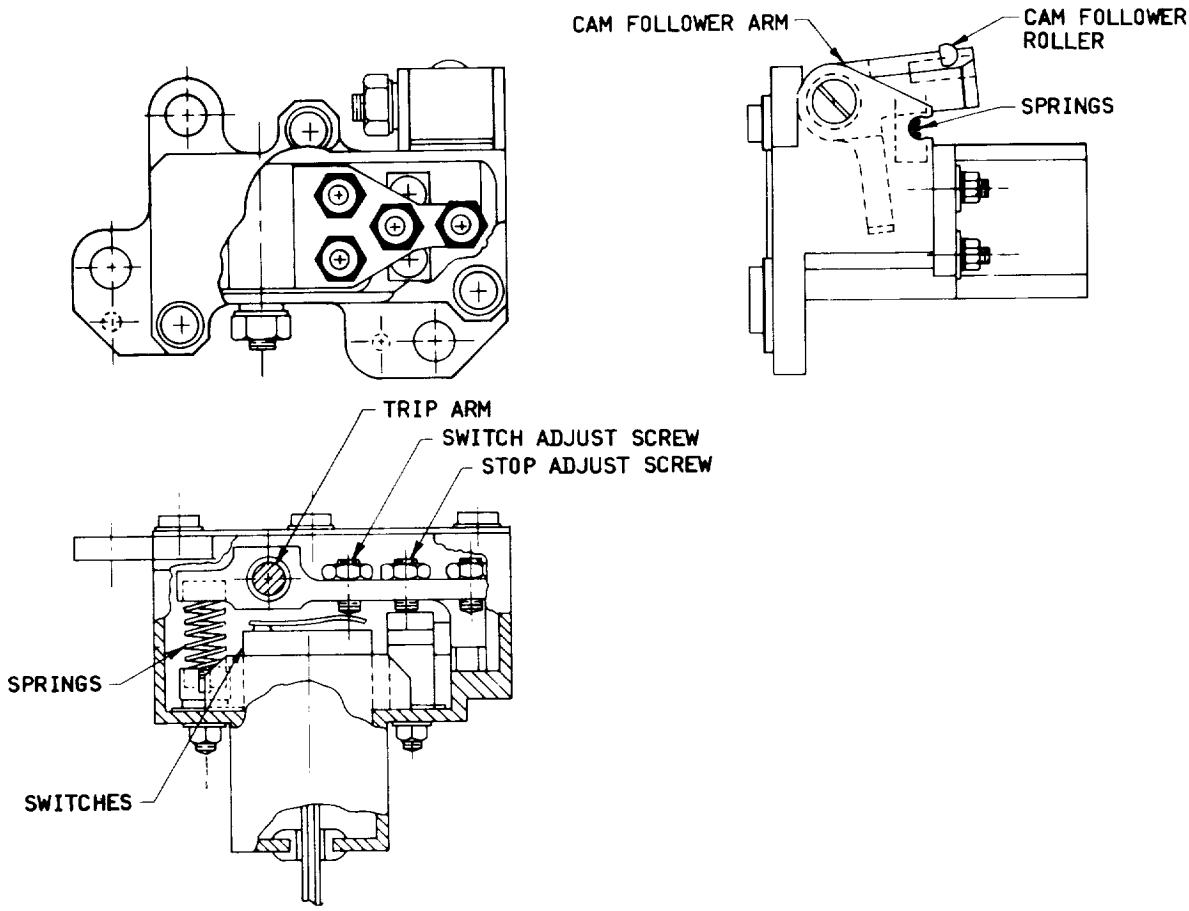

Figure 10. Switch Mechanisms

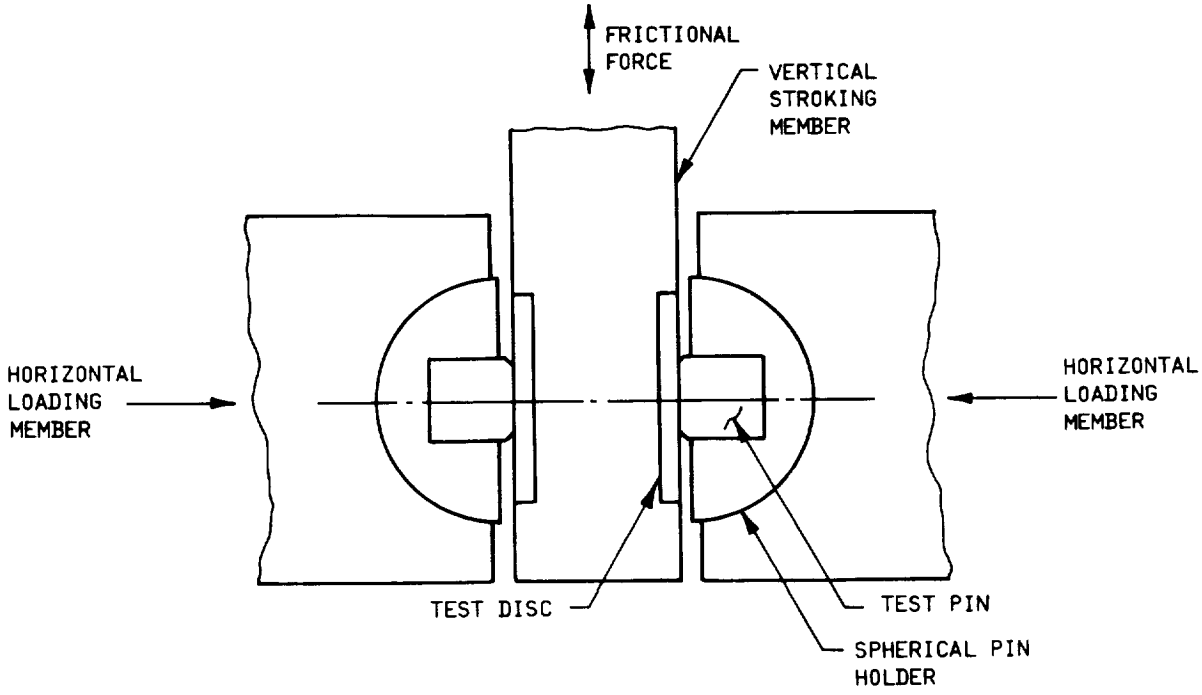

Figure 11. Pin and Disc Test Set Up

SPACE SHUTTLE SLIDEWIRE EMERGENCY EGRESS SYSTEM

Glenn B. Jeffcoat/Emile S. Stephan

NASA - John F. Kennedy Space Center

ABSTRACT

The Slidewire Emergency Egress System is designed to provide a fast and safe egress means for the Shuttle flight crew, passengers and ground closeout crew in the event of imminent danger while the space vehicle is still on the Launch Pad. Egress is from the 195' level of the Fixed Service Structure (FSS) to a ground landing area 1200' away from the launch site (Figure 1). The slidewire design is such that the flight crew and passengers can be evacuated to a safe area within two (2) minutes with winds as high as 34-knots from any direction.

INTRODUCTION

In the pre-Shuttle era, all manned space flight programs at Kennedy Space Center (KSC) have had an emergency egress system. Emergency egress for the Saturn V Apollo program utilized a nine-man cab on a single wire that required personnel to be mustered at the embarkation zone. The Space Shuttle Emergency Egress System at KSC is composed of six (6) egress platforms, five (5) slidewires, five (5) multi-man baskets (1 basket per wire), individual basket release devices, personnel safety net on the tower below the embarkation area, a deceleration system and landing zone, arresting safety nets, (a secondary stopping device in case the deceleration system fails) and protective bunkers. Each basket is secured in the embarkation area by a piece of Nomex webbing and is released manually from the basket by operating a rotating guillotine type cutter which severs the webbing and releases the basket. Each multiman basket is suspended from a 3/4" diameter slidewire by two trolleys (Figure 2). Each slidewire is preloaded to approximately 4,000 lbs. tension to provide the required catenary to obtain the proper basket acceleration necessary for the system to operate in 34-knot winds from any direction. A series of development tests determined the correct tension in the wire. The egress baskets are arrested in the landing zone by a deceleration system which limits the egressing personnel to forces of a maximum of $\pm$ 2 g's (Figure 3). The deceleration system is composed of a catch-net which has attached drag chains. A computer program was developed to predict and analyze all load conditions including varying wind directions and speeds plus varying egress basket loads (one, two or three men in basket). After the basket is arrested in the landing area, personnel exit the basket over the side and walk/run into protected bunkers (Figure 4). The basket also contains a quick-release exit system for easy removal of injured or incapacitated personnel (Figure 5).

TESTING

In the early phase of testing the Shuttle slidewire system a determination was made to use hardware that had been manrated from the Apollo program if possible. One of the objectives of the slidewire system was that once the egressing personnel release the basket from the tower they have nothing to do until the basket stopped in the landing zone. There they egress the basket and go to the bunker area. The first system to be used for the egress system was a basket construction using Nomex webbing attached to an aluminum ring five feet in diameter. This configuration was quickly discarded because of the difficulty to egress from the basket (Figure 6). An improved egress flat-bottom basket was the next tested (Figure 7). The basket was suspended by cables from a modified LC-34 slider (Figure 8), the braking action used an expendable bolt that rubbed on the underside of the cable. The location of the bolt was altered to increase or decrease braking action. A backup spacer was used in later tests to prevent brake bolt slippage or bending. The weight of this basket was made light for ease of handling and installing on the slidewire cable. When testing in headwinds over 15 knots, without brake bolt, the basket with a 400 pound load would not make it to the landing zone. Operational wind for the Shuttle vehicle is 34 knots. Therefore,this concept had to be abandoned because of the large drag force (frontal area).

The system was again modified to a two-man basket (5 baskets), two feet wide by five feet long. The weight of this basket was 500 pounds as compared to 110 pounds for the one-man basket. It was intended that this basket would have enough stored potential energy to reach the landing zone with a headwind of 34 knots. By using the two-man basket, it eliminated the slider that was used in earlier tests. Instead, the design went to two ball bearing trolleys to support the two-man basket on the slidewire. (These ball bearings had been manrated on the Apollo Saturn V program). Also, for braking, each slidewire is provided with a separate drag chain deceleration system located at the landing zone area to stop the basket after traversing the slidewire.

Prototype testing was conducted March through May 1979. Testing included 22 egress basket runs in winds from 26 knot-tailwinds to 14-knot headwinds with loads from 0 to 620 lbs. Each slidewire has been proofloaded to 15,000 lbs. which is approximately 1.7 times the maximum tension encountered if three men in a basket traversed the wire. Validation testing was conducted in March 1980 on the actual hardware comprising the egress system including all of the 5 slidewires, basket assemblies and release devices. Each basket traversed its slidewire twice with weights from 0 to 620 lbs. Each release device was tested at least two times with slidewire #1 release device being testing three additional times by a man in the basket. The release system and basket assemblies were proofloaded to two times their maximum operating load. (Basket was secured to embarkation area and not allowed to traverse the wire). Manned egress tests were performed and timed from the Orbiter Access Arm (OAA) to the time of basket release for one man, two men and three men (including an incapacitated man).

Test results indicate that all design criteria have been met. Safety and reliability have been demonstrated by the fact that 30 runs have been accomplished without problems and the deceleration system performed as designed. The maximum recorded g-loads were ± 1.6. The release devices, front compartment/rear compartment, divider nets and rear egress flaps all functioned without failure. Egress time from the OAA to basket release for two men was 14 seconds while basket run times varied from 20 to 28 seconds (for the realm of operational conditions). When the basket comes to its final stopped position in the landing area, it is 53" above the ground with one person aboard, 32" above the ground with two people aboard, and 18" above the ground with three people aboard. The rear net of the basket can be lowered in five seconds by pulling two quick release pins. The time to walk from the rear of the basket in the stopped position to the door of the bunker has been demonstrated to be twenty seconds. In summary, the total egress varies from 59 to 67 seconds which is well within the program requirement of 120 seconds.

MATH MODELS

Two math models were developed, one for the descent on the wire and the other for the arresting system. Several field tests were made and the same inputs were used to make computer runs. The errors for stopping distance and time were well within 10% which gave the math model credibility. More computer runs were made to cover all the cases as to wind speed and direction. These were not correlated with actual tests because one cannot order a 34 knot head-wind for example.

A wire suspended between two supports assumes a shape called a catenary. When a load is placed on the wire at some point, it causes discontinuity at that point and the system becomes two catenaries; one on either side of the load. If stretch is taken into account, the wire becomes non-homogeneous so it becomes obvious that the classical catenary formulae become inadequate and cumbersome to work. Therefore we used the FINITE ELEMENT approach, together with NUMERICAL METHODS (Refs. 2 & 3).

Figure 9 shows an unloaded wire attached at two points (high and low). The span, the difference in elevation of the attach points, and the weight of the wire per foot are given. Also in this case the tension at the high point is equal to 4000 lbs. The configuration of the wire and its total weight is not known. The total wire weight remains constant whether the wire is loaded or not so this is the parameter that we converge on for the dynamic computer runs. Consider a fictitious simply supported beam of the same span (Figure 10) and load it with the wire as a continuous variable load. Calculate the bending moments at equidistant points along the beam. Divide each one of these moments by "H", which is the horizontal component of "T", you will get the deviation of the wire from the diagonal (the deltas in Figure 9). (Ref. 1). However, we do not know "H" because we do not know alpha. Therefore, to get things started we assume that the wire runs along the diagonal and alpha and "H" are

calculated (Figure 11). Here we would like to introduce the idea of density. At a point on the wire where the slope is zero the density is one. Otherwise the density is equal to $\sqrt{(\text{SLOPE})^2+1}$ (Figure 12).

Load the fictitious beam, figure the moments and divide by "H" to get the deviations and calculate the deflections (distances from the horizontal). Using a numerical approach, figure the slopes then the densities. Given those we can now calculate the total weight of the wire (as a first iteration). Since we now have a different slope at the support, we can calculate a new "H" (see Figure 9) . Load the fictitious beam again and iterate until we converge on a total weight (whatever it may be).

After knowing the densities and hence the continuous variable load, change that load into a set of equivalent concentrated loads (Figure 13, Ref. 2). So when we have a real concentrated load we simply add that load to the equivalent concentrated load at the point in question, and proceed as before. Recall that we always converge on the calculated total weight, except that now we do it by manipulating "H". "T" will change depending on where the concentrated load is located. It will reach its maximum when the load is somewhere close to mid span.

THE DYNAMIC RUNS

As in the case of the static case, the span is divided into a large number of equal spaces, hence the wire itself is divided into the same number of unequal finite elements. The load is placed near the top. All the forces acting on the load (basket) are considered, namely, gravity, wind, air resistance and friction. These forces are resolved into two components, one along the tangent of the catenary ahead and the other normal to it. To begin with the vertical component was used to determine the configuration of the two catenaries. In subsequent iterations the normal component was used.

The tangential force is the force that drives the basket down the wire. We let it travel along the tangent for a small increment of time, and calculate its acceleration, velocity, horizontal distance from the high support, the tension there and the deflection (distance from the horizontal).

At time zero plus Δt, the basket has moved a certain distance; therefore, the shapes of the catenaries are altered. The process was repeated and iterated until the basket stopped short of the arresting net (due to high head wind), or until it hit the arresting net. From that point on, a second computer program takes over and figures the time, the distance traveled and the G forces (using the conservation of momentum approach). As the chains on the ground are put in motion one link at a time, giving the basket a rather gentle braking action, the moving mass is being increased as more links are put in motion thus decreasing the velocity (MV = constant). What really stops the

basket is the weight of the chain plus the friction force produced by dragging the chains on the sand (MV = FT).

OPERATIONAL CRITERIA

The system is designed to provide egress from the Shuttle vehicle via the OAA located on the 195' level of the FSS to a safe area in 2 minutes should an emergency egress become necessary (Figure 1).

The evacuees would move to the Shuttle vehicle access hatch. Once the hatch is open, they move into the White Room of the OAA, move across the OAA, go around the south side of the FSS to the embarkation zone on the FSS, get into the emergency egress basket, release the basket from the FSS, move down the slidewire to the landing area, and exit the basket at the landing zone and go to the bunker.

Conclusions: The Emergency Egress Slidewire System is operationally supporting the space vehicle at KSC and is an excellent means of safe and rapid egress to a remote area. Let's all hope that the need for this system never materializes.

REFERENCES

Ref. 1 - Norris & Wilbur, "Elementary Structural Analysis", Chapter 10

Ref. 2 - N.M. Newmark, "Numerical Procedure for Computing Deflections, Moments and Buckling Loads". Paper No. 2202 in the Transactions of the American Society of Civil Engineers. Vol. 108, 1943, p. 1161

Ref. 3 - E. Stephan, "Numerical Procedures Applied to Non-Prismatic Members". Master's Thesis 1965. University of Cincinnati

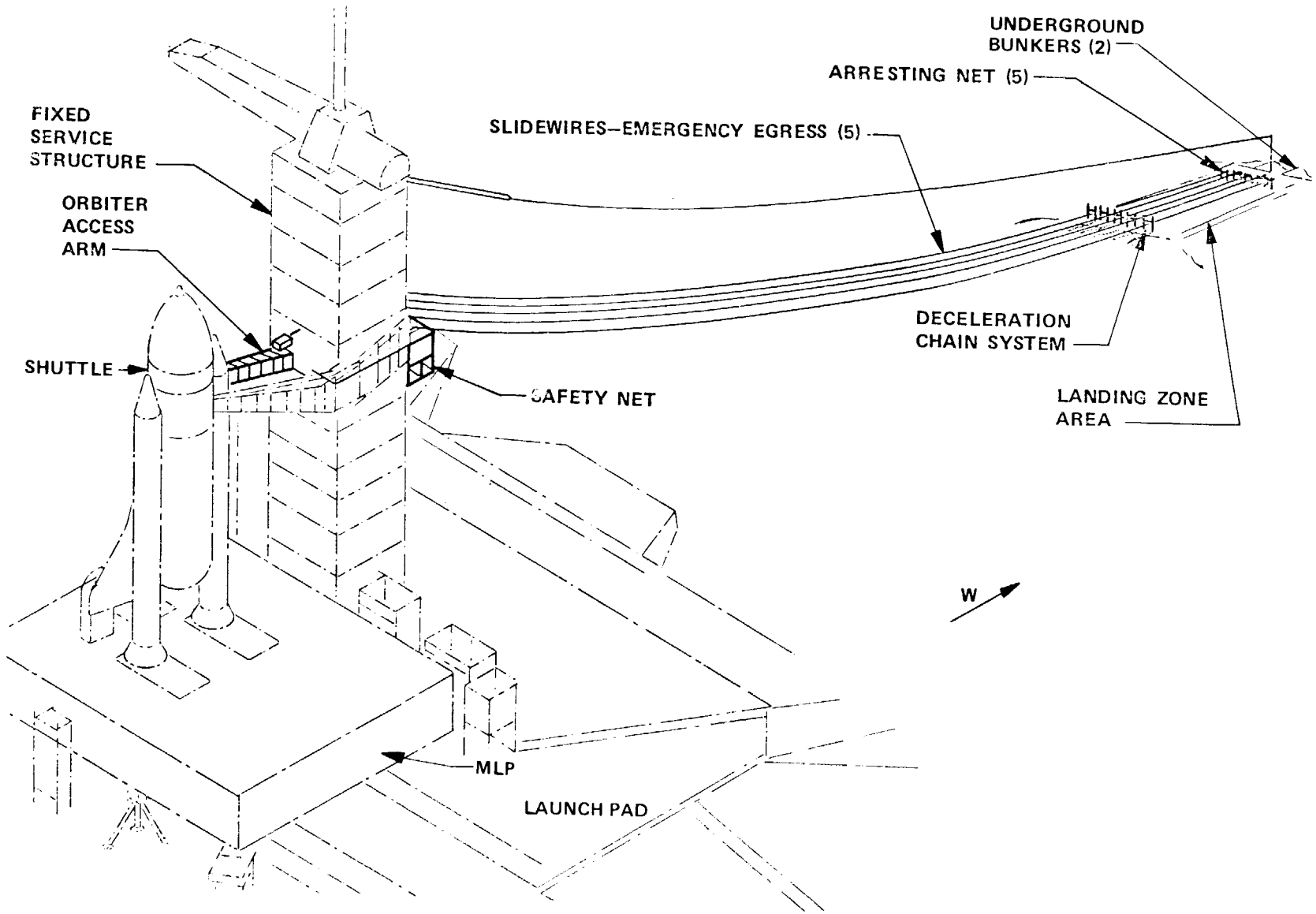

Figure 1. Emergency Egress System, Launch Pad - Complex 39A

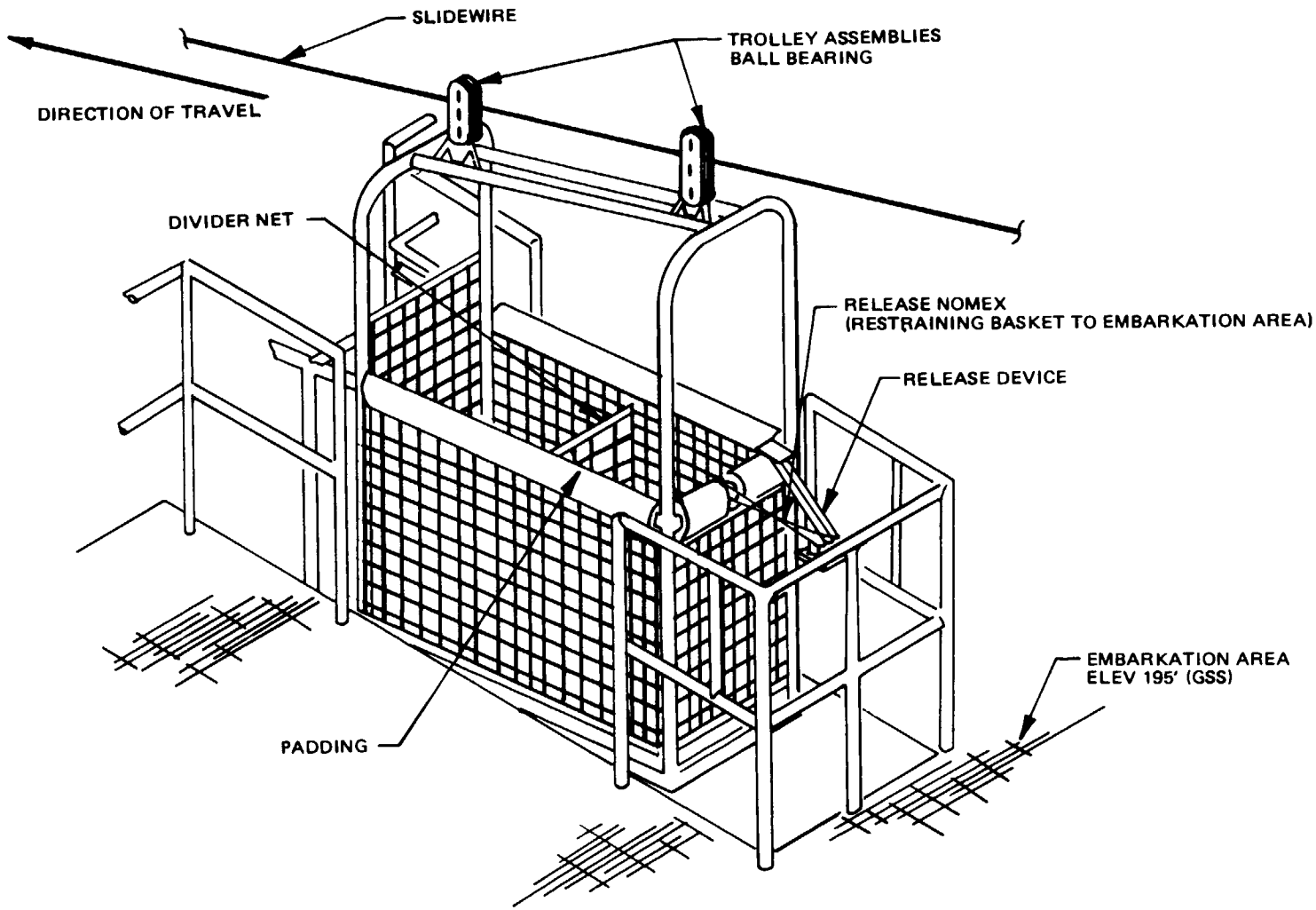

Figure 2. Slidewire Emergency Egress Baskets at the Embarkation Area

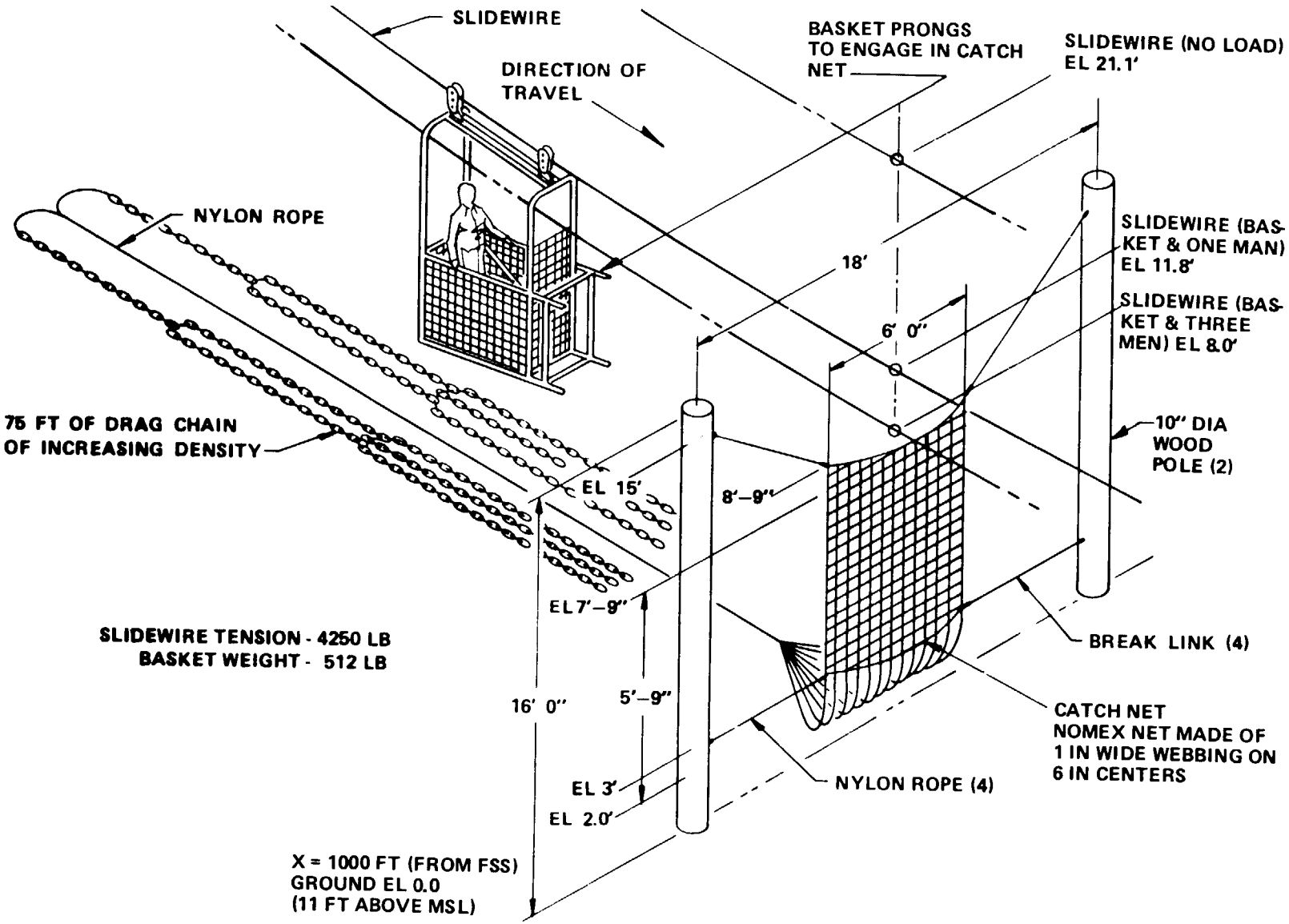

Figure 3. Slidewire Emergency Egress Deceleration System

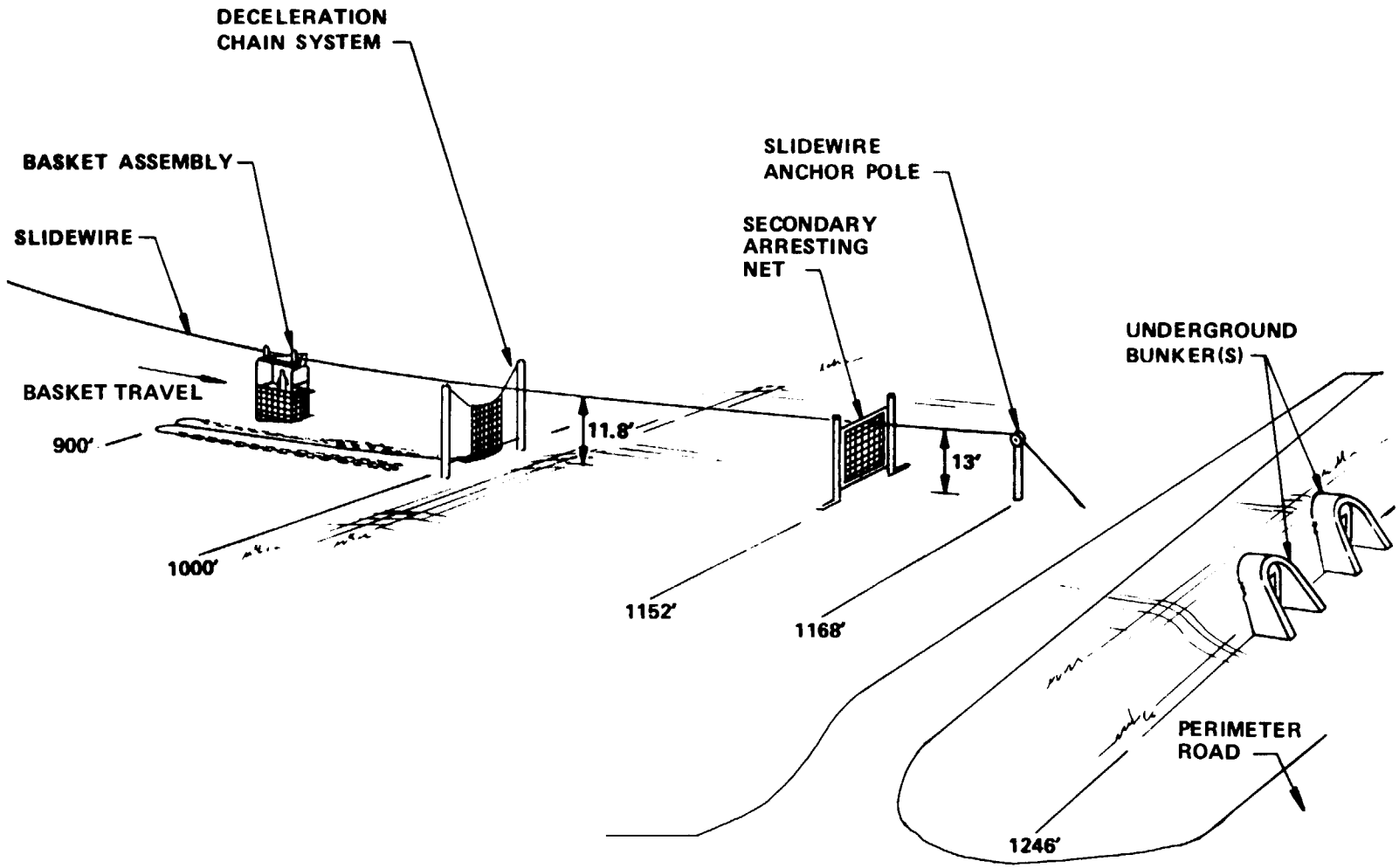

Figure 4. Slidewire Emergency Egress Landing Zone

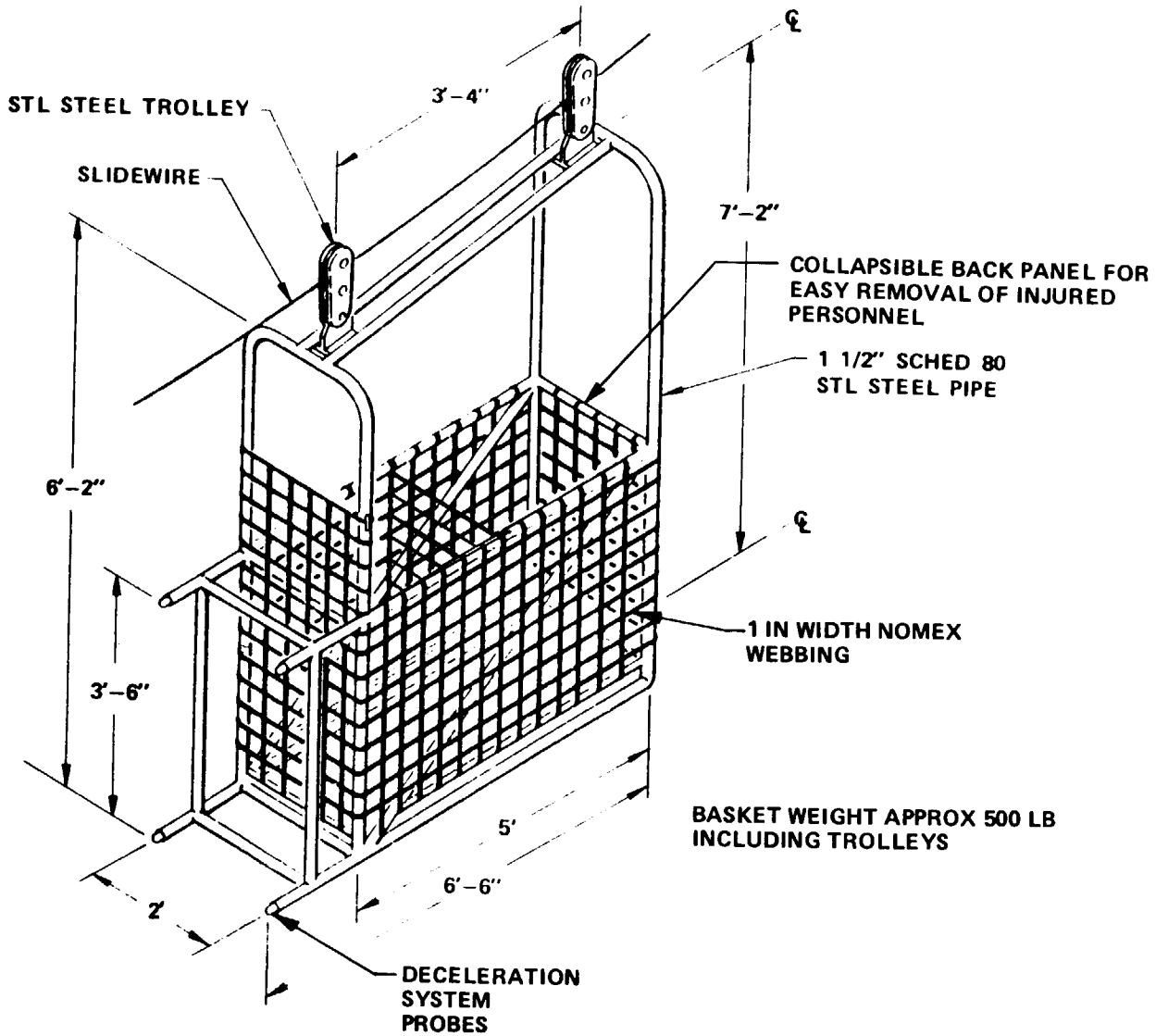

Figure 5. Slidewire Emergency Egress Basket

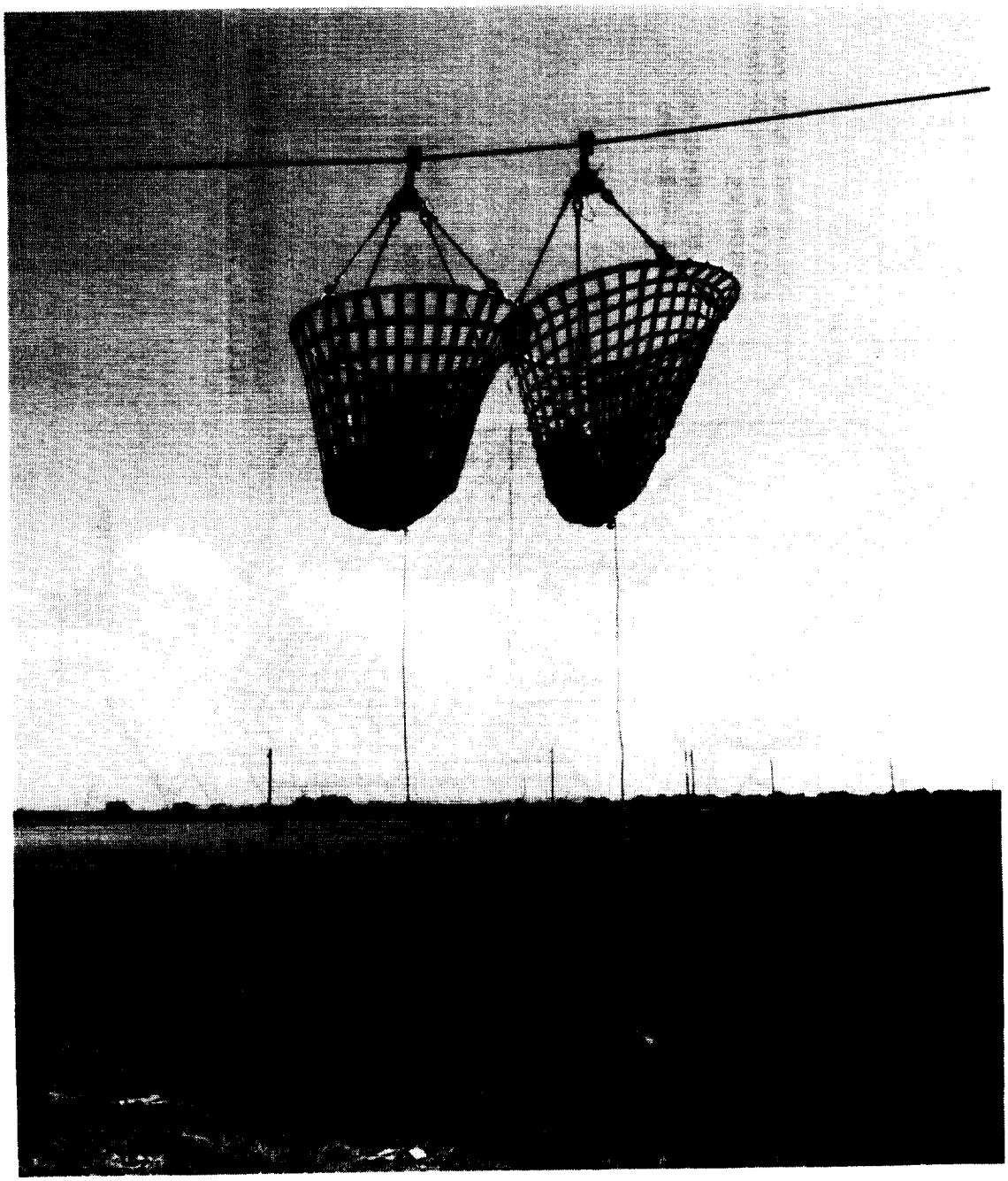

Figure 6.

Figure 7.

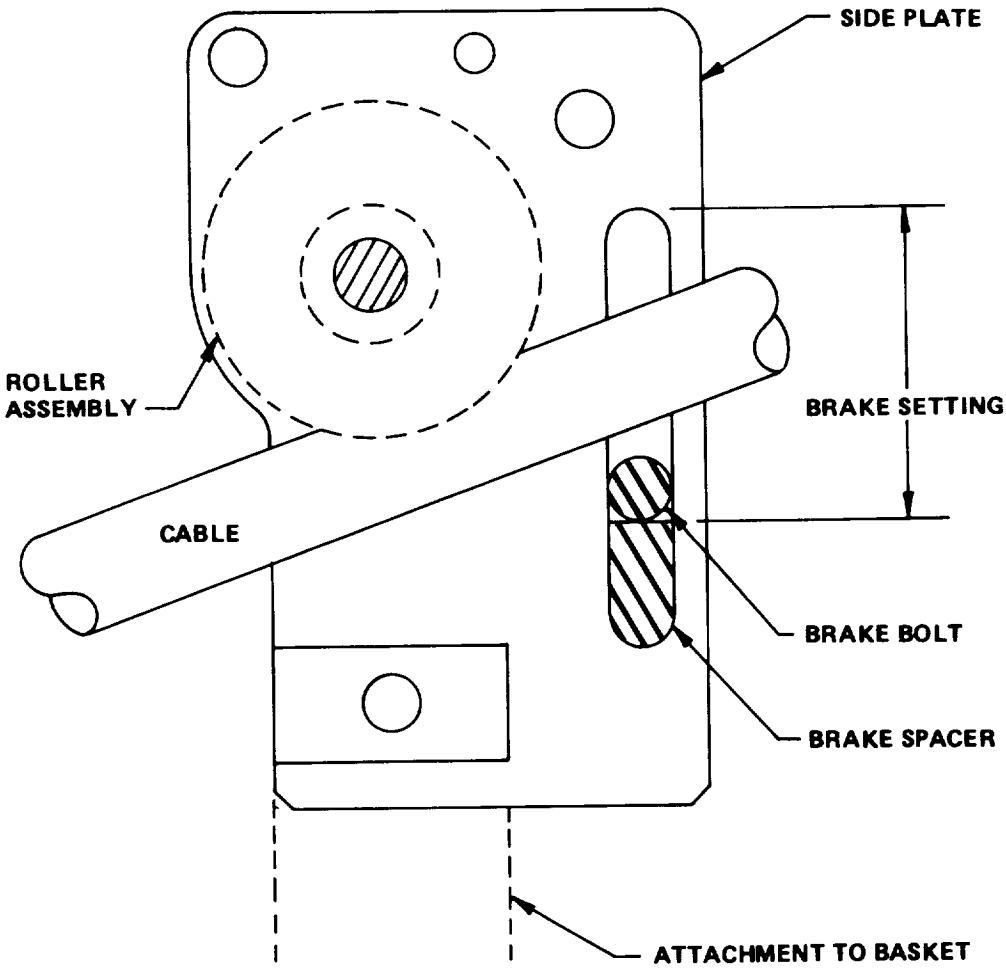

Figure 8. Sketch of Slider and Brake Assembly

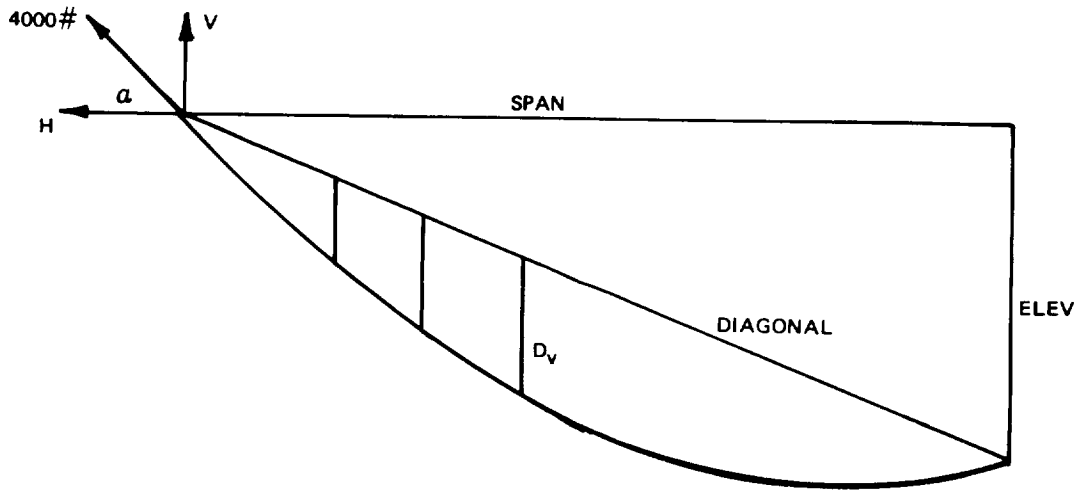

Figure 9

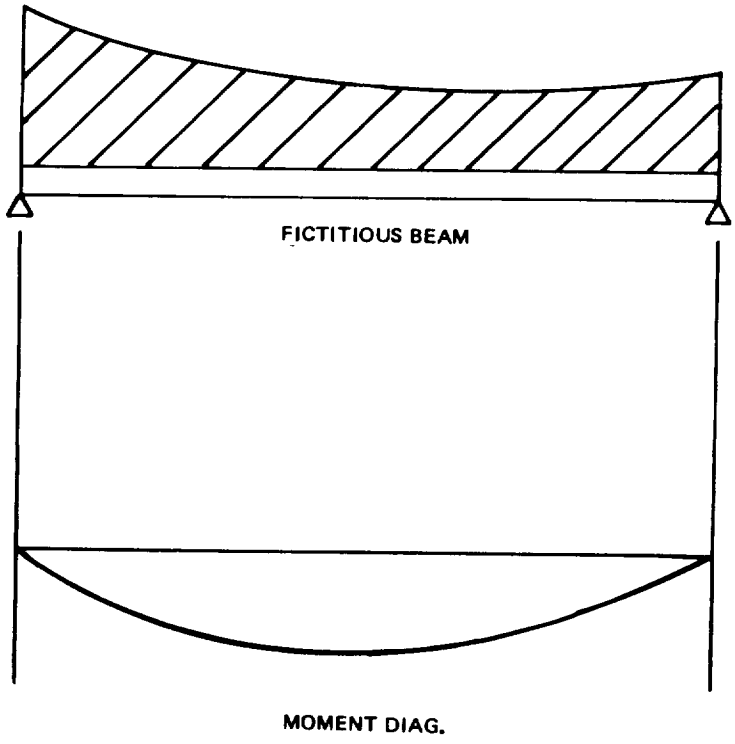

Figure 10

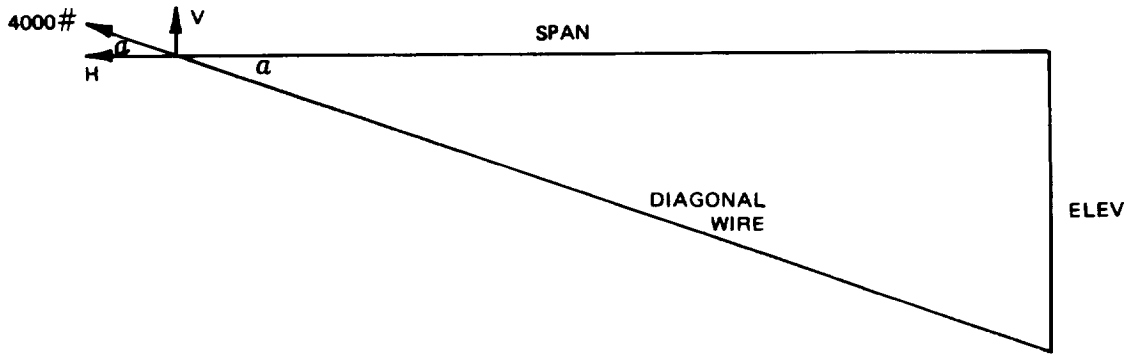

Figure 11

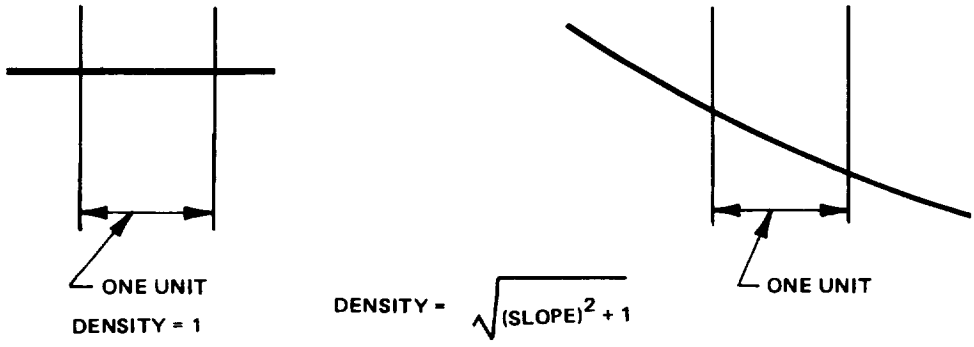

Figure 12

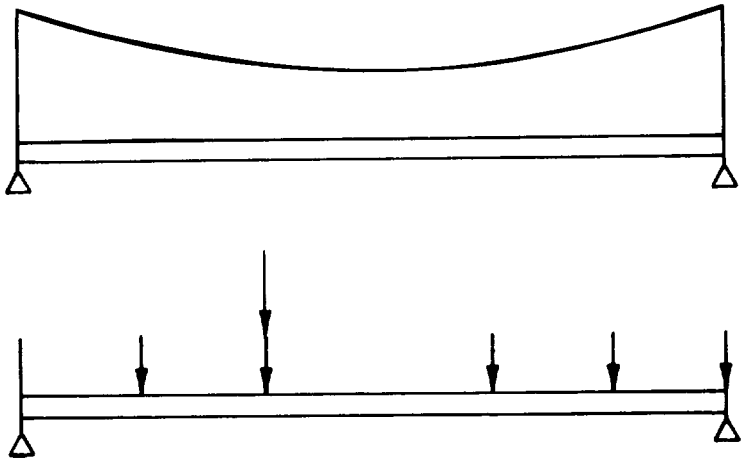

Figure 13

MULTI-CHANNEL CHOPPER SYSTEM

FOR A

TOTAL OZONE MAPPING SPECTROMETER

Arlin J. Krueger
NASA/Goddard Space Flight Center
Greenbelt, Md. 20771

August O. Weilbach
Helvart Associates
Fullerton, California

ABSTRACT

A Multi-channel chopper system designed and built to stringent NASA specifications is providing an excellent performance for a TOTAL OZONE MAPPING SPECTROMETER (TOMS). State of the art machining technology, suitable material selection and a unique way to hold and position the slit-plate resulted in the instrument's better-than-expected performance. A shutter method used for internal calibration allows compensation for the occurrence of an unlikely wavelength shift during testing, launch or during the orbiting life of the instrument. TOMS is part of a payload on NIMBUS 7 launched on October 24, 1978.

INTRODUCTION

The Nimbus 7 satellite carries a new research instrument designed to globally map the ozone content of the atmosphere. This instrument, the Total Ozone Mapping Spectrometer (TOMS) (Heath et al., 1975) is a UV spectrometer which required new design considerations to meet the experiment goals.

Chopper systems are a common feature in a great number of optical systems and instruments. It is less common for choppers to act also as optical channel selectors and for calibration as is the case in this instrument. In the design of the Total Ozone Mapping Spectrometer,we are dealing with a fixed multiple channel exit-slit array that has to provide and maintain an accurate and repeatable output for 6 preselected wavelengths at a 10 nm bandwidth each. The chopper system is the sequencer for a single Ebert monochromator with f:5 250mm focal length optics. TOMS has two major subsections; one is the monochromator, the other supports the scanner assembly, the chopper assembly and the exit optics. Electronically, the pre-amp is attached directly to the photomultiplier; an auxiliary

electronic subassembly containing primarily the high-voltage power supply is fastened to the monochromator housing, Fig. 1. All other electronics including the logic unit, motor power module and interface to spacecraft power is contained in a separate unit and located in one of the spacecraft bays.

Instrument size, configuration and interface requirements impose the need to resolve some auxiliary but not less important difficulties. Problems such as perfect synchronization of chopper and scanner sequence had to be resolved. The TOMS housing and all other major supporting and enclosing parts are made of magnesium. Maintaining a weight budget was an important consideration. Above all, instrument tolerance to environmental testing, under vibration and thermal vacuum, became of prime concern and substantially affected all design aspects. Ball-bearing preloads and proper ball-bearing lubrication, as always, had to be carefully evaluated. This paper highlights the difficulties and eventual solutions to design and manufacture of a chopper system that answered all the demanding performance requirements.

The total instrument system was built around and based on the computer generated ray trace shown in Fig. 2. The optical diagram shown in Fig. 3 describes the orientation and location of all major subcomponents.

SLIT-PLATE & CHOPPER INTERFACE

The electro-optical design and performance of TOMS required implementation of the sequential display and measurement of each one of six selected wavelengths onto a common photomultiplier (PMT). Proper processing of the signal output depends, among other factors, on wavelength accuracy and repeatability and uniform chopper speed. The input through the scanning optics has to be precisely synchronized with the chopping frequency. Speed control is achieved by a tachometer track as part of an encoder disc attached to a brushless DC drive motor. Synchronization is obtained by a Phase Reference Pulse generator (PRP) assembly. Accuracy and stability of both the entrance and especially the exit energy is achieved by most accurate and stable slit and chopper apertures and exact registration between both of them.

Because of the difference in thermal coefficient of expansion, the combined error budget, including allowance of component fabrication and assembly tolerances, indicated the need for fabrication tolerances of down to .005mm. Dispersion provided through the single monochromator system with fixed mounted quartz optical elements has inherent stability. The instrument housing, though, is subject to expansion and contraction depending at which temperature level the system is working. Fortunately, the monochromator sensitivity to axial changes is negligible. Equivalent motion across the slit plane or radially to the chopper wheel, on the other hand, would make it impossible to maintain specified wavelength accuracy. This problem was resolved by the selection of a low expanding metal, INVAR 36, used both for the slit-plate and the chopper wheel. The manufacturing problems and their eventual solution are discussed below.

The method for mounting the slit plate to be motion-independent of its mounting plate by use of a "floating" retaining method is shown in Figures 4 & 5. Looking at the longitudinal or central axis as a fixed line, the logical way was to support from this location. A protrusion on the slit and grating-mounting plate fitted the center support hole of the slit plate. The mounting plate is inserted in its pre-aligned clocking position by means of a pin on its periphery. In line with the entrance and exit slit axis, a pin with a straight protrusion and fitting a slot in the same location on the slit plate, provided a repeatable clocking position for the latter. The slit plate thickness is only .11mm, and point contact from a small pin diameter is only marginally reliable. Therefore, the line contact provides a relatively large surface, and reliability and repeatability of the horizontal axis alignment is thus assured.

In order to retain the slit plate flat against its mount, six shoulder retainers under constant load from Belleville washers are pulling the plate against the surface without impairing possible small motion or disturbing the accurate alignment. Again it is a "floating" mounting method. The slit plate itself had a slight curved preform that will provide a pre-load in the opposite direction. In order to obtain specified instrument accuracy in relation to the 6 exit wavelengths, the entrance and exit apertures had to be at the proper location of the entrance beam and match the exact locations of the exit beam array.

It must be mentioned that all dimensional values for the optical system were determined by computer-generated ray tracing (see Fig. 2). No adjustments of any kind were provided for any of the optical components. Matching machined and lapped surfaces provided front support for the collimating mirror and the grating. The method places increased responsibility on the machinist and inspector but eliminates time and frustration for the assembler. The alignment was verified as follows: Behind the slit plate is a shallow recess that will accommodate a narrow piece of photographic film, see Fig. 4. This film strip can be inserted from the outside of the monochromator assembly. Without a PMT in place, the slit pattern is exposed to the film by front exposure. Subsequently, light entering and dispersed within the monochromator will provide a pattern at the focal plane, which is the slit plane in the back of the film. The two exposures will be checked and measured under magnification. Any deviation will be corrected by a lapping operation of the grating support surface. The location and uniformity of the energy onto the PMT sensing surface is checked by a similar approach. It is a relatively simple but powerful method to check instrument performance during the assembly and test stages of the program. In addition, a method for detecting possible wavelength shifts, once the spacecraft is launched and operational, is required. The calibration method is described as part of the next paragraph.

THE CHOPPER WHEEL. CONFIGURATION AND INTERFACE

Both the slit-plate and the chopper-wheel are, as previously mentioned, made of INVAR 36, a low expansion metal. The metal's advantage is its ability to maintain dimensional stability within substantial thermal variations of the environment. Its disadvantages are: high specific weight, difficulties to apply an approved black finish, and its susceptibility to distorting-stress build-up under machining operations.

To reduce the weight of the chopper wheel and to maintain a thin chopper surface around the many apertures, appearing as in a random distribution, the backside of the blade was reinforced with a web of ribs, see Fig. 6. These ribs, of course, had to have sufficient clearance for the apertures and blend-in to the wheel-hub to give stiffness and stability to the rather large diameter disk. The need for removal of substantial amounts of metal between the ribs by conventional milling methods resulted immediately in unacceptable distortions resulting in both bending and wobble of the front surface. Stabilizing procedures and several attempts to relieve stress did not result in sufficient improvement. It was originally decided to produce the many apertures by Electrical Discharge Machining (EDM) processes. It is well established that chem-milling (unsuitable for this part) and EDM will not induce stresses such as produced through tool pressure, localized heating and friction during milling or turning operations. Subsequent to rough machining,all further material and detail removal was done by EDM. Apertures, radial distances and angular separation were achieved to tolerances as close as .005mm (.0002"). Wobble on the front surface was held to better than .01mm (.0004"). These tolerances were necessary to provide the specified resolution for the TOTAL OZONE MAPPING SPECTROMETER. Figure 6 shows the various functions of the aperture pattern.

- The entrance aperture is the only uniform pattern but it has an aperture gap permitting reset of the electronic signal cycle.
- The exit slits are sequentially placed but always on axis with the entrance slit.
- A single offset round aperture is controlling the Phase Reference Pulse generator (PRP).
- A pattern of narrow radial apertures permits internal instrument wavelength calibration over a range of ±20nm.

Figure 7 describes the method to achieve the wavelength calibration. A mercury pencil lamp, activated as part of a programmed sequence or activated by ground command, provides monochromator illumination through the separate and single long slit in the slit plate. As the calibration of the chopper sequentially selects a square portion of the elongated calibration aperture, a shift in dispersion at the exit slit array will be recognized by an increased or decreased output of the mercury lamp output in relation to

the calibration slit array of the chopper-wheel. In other words, what appears as an increased energy input at the right hand chopper calibration aperture will result in a shift to the left or higher wavelength output at the exit slit array. This difference can be programmed as a correction to the computer reading. It must be pointed out that, up to this time of the TOMS instrument life, no such shift has occurred. The same applies to two other sensors launched as part of the NIMBUS series of weather research satellites. This stability in performance presents an indirect proof of the inherent stability provided with fixed mounted optics technique. Needless to say, during the assembly or test period of the instrument, replacement of a mirror or other optical element can be done with expediency. Only verification with the photographic film at the slit plane is needed.

Earlier it was pointed out that difficulties in applying a black finish to both the chopper wheel and to the slit plate were encountered. The problem was resolved by plating the parts with a controlled thickness of copper, then in turn converting the copper layer surface to a black oxide finish. The temperatures involved in these processes did not affect instability or create distortion of the parts. Obviously plating build-up had to be taken into consideration in the pre-plating dimensioning of all critical tolerances.

CHOPPER DRIVE SHAFT ASSEMBLY

Interface requirements and optical packaging problems necessitated considerable spacial separation between the chopper-drive motor and the chopper-wheel. The total length of the drive shaft exceeded 13 cm (5¼"). This became of concern in relation to the bearing pre-load under changes of the thermal environment and also under induced external vibration during test and at launch. Both conditions could adversely affect the critical synchronous chopper speed, and relative to pre-load, the life of the duplexed ball-bearings. Figure 8 describes the final configuration of the drive shaft assembly. The motor chopper is a brushless DC unit of approximately 5cm (2") dia. with a 6mm shaft extending about one-third of the required distance to the chopper wheel. Motor rotor and shaft support was provided by a pair of duplexed bearings. No axial play was permissible neither for the motor shaft nor for the chopper wheel. The pre-loaded bearings lubricated by grease-plating, provided precise no-play radial control. With the main instrument housing made of magnesium and the shaft and bearing metals of stainless steel, it was obvious that differential expansion would be substantial. At the extreme operational temperatures (0-35 deg. C) it will amount to approximately .18mm (.006") and thus far exceed permissible increases of the ball-bearing pre-load. The chopper as shown in the assembly, Figure 8, has its own shaft with the length extending towards the motor and has a bored hole matching the shaft diameter within a slip-fit tolerance. Connection of the two shafts was achieved by means of a welded metal bellows. This resulted in excellent low-torque coupling while at the same time permitting considerable axial displacement of the two shafts within negligible wind-up.

There was an obvious need for a lubricating layer between the interfacing diameters of the two shafts. A very small amount of Krytox* oil applied to the motor shaft was the solution. Tests with a Dry Lub approach proved to be negative. The Molybdenum Disulfide particles had a tendency to accumulate in a spotty manner and increase friction between the two parts to an unacceptable amount.

Attachment of the chopper wheel to the drive shaft became a contest of ideas. Among those that surfaced were keyways, set screws, dowel-pins, etc. In the final design, a tapered-pin connected a split flange extending from the wheel-hub to the drive shaft. A retaining ring functioned as a clamp around the split flange by uniformly clamping around the shaft diameter, and at the same time securing the taper pin. Because of the critical role within the instrument assembly, the total assembly of shaft, coupling and wheel attachment was modeled up and subjected to vibration testing. The results of this test sequence indicated the need for snubbing the periphery of the chopper as shown in Figure 8, since excursions at the resonant frequency of the wheel exceeded the available space between the housing and the chopper rim. Snubbing techniques in most cases provide a sensible precautionary method and usually are easy to implement. In this particular case, 3 equally distributed VESPEL* pins inserted on both sides of the enclosure surfaces gave the necessary protection. Snubbing space was held to between .075 to .15mm (.003 - .006 inches).

TOMS POST-LAUNCH PERFORMANCE

The Nimbus 7 spacecraft, containing the TOMS instrument and seven other remote sensing instruments was launched into a sun-synchronous polar orbit on October 24, 1978. Orbital parameters were very close to the nominal planned values. The TOMS subsystem was activated during Orbit 100, on October 31, 1978, after a 7-day outgassing period. Following a very brief period (seconds) of disturbed data, attributed to corona in the high voltage system, the performance has been completely satisfactory.

The observed wavelength calibration is highly stable. Any changes are less than the 0.003 nm uncertainty in the calibration. Photometric stability has also been excellent after a 5.2 percent change in response which took place in the first 2 days after turn on.

At the present time, more than 2 years after launch, the instrument still continues to function flawlessly in its normal 50 percent duty cycle of operations.

The TOMS instrument has provided the first high resolution measurements of global total ozone. The results correspond closely to ground-truth data. Because of the very large volume of data (180,000 soundings per day), the

*Registered Trademark of the Du Pont Co., Wilmington, Delaware

results have been displayed in computer-generated false color world maps. These pictures have revealed that total ozone can serve as a tracer for meteorological processes and therefore may aid in weather forecasting, particularly for the airlines for whom information about jet stream location, clear-air turbulence, and high ozone concentrations is important for safety and fuel economy. This application will be tested in the spring of 1981 when the TOMS data will be processed and delivered to the airlines in near real-time.

The greatest limitation to the present system, and its use for meteorological purposes, is the polar orbit of the satellite. Each point in the atmosphere is viewed one or two times per day but important weather features move rapidly during a day. A TOMS instrument on a geostationary satellite above the equator would allow very frequent measurements of the entire disc of the earth. The ultimate utility of TOMS then would be available for following the development of upper air troughs and ridges.

CONCLUSION

The TOMS instrument design has required state-of-the-art technology to produce the very precise and stable device required for UV earth radiance measurements of total ozone. By careful selection of materials and the use of unique mechanical design methods, this instrument has functioned flawlessly and has produced the most precise and detailed ozone data set ever collected.

REFERENCES

Heath, D. F., A. J. Krueger, H. A. Roeder and B. D. Henderson, "The Solar Backscatter Ultraviolet and Total Ozone Mapping Spectrometer (SBUV/TOMS) for Nimbus G," Opt. Engr., 14, 323-331, 1975.

"Charmilles Technology" (EDM Technology), Charmilles, Geneva, Switzerland.

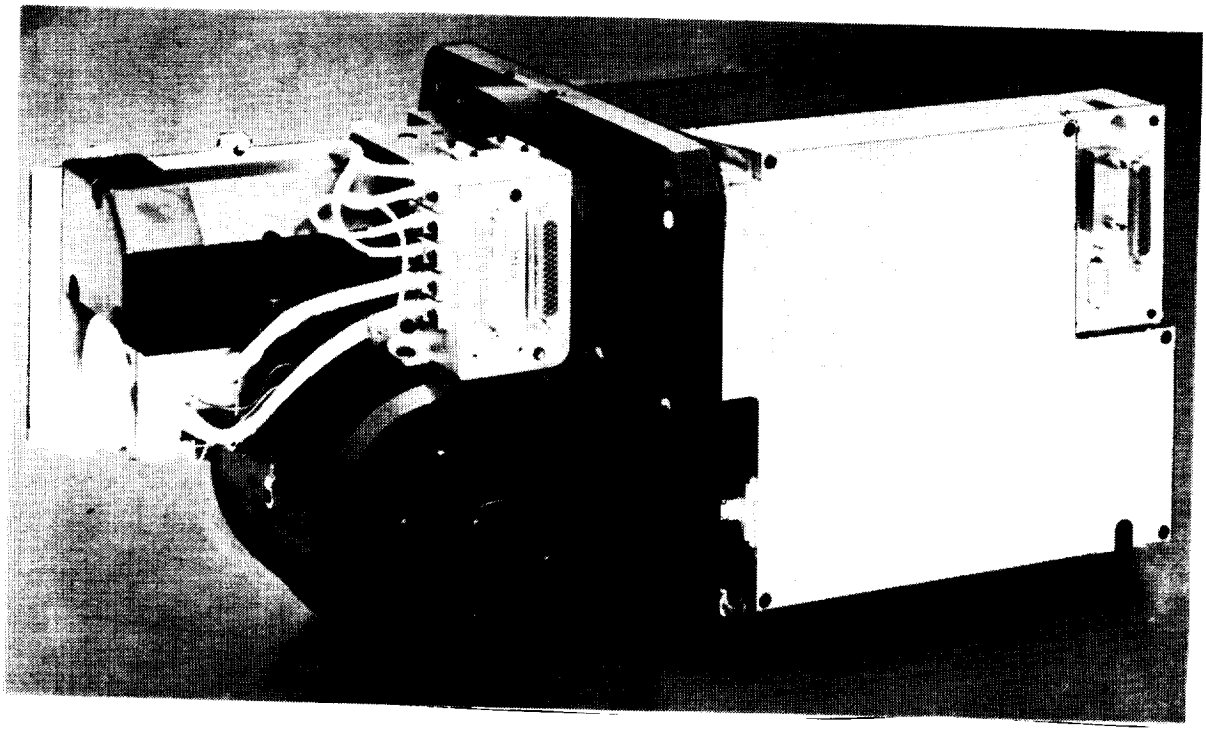

Figure 1. Total Ozone Mapping Spectrometer (TOMS)

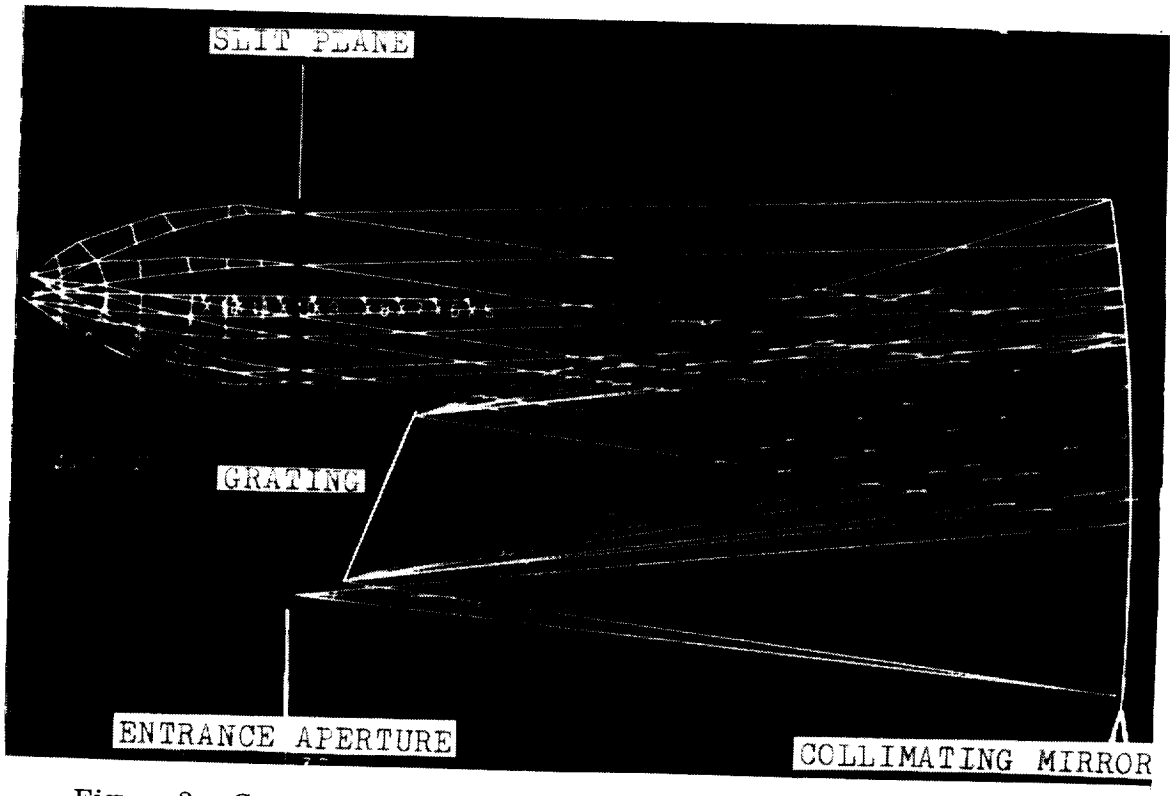

Figure 2. Computer-Generated Ray Trace for the TOMS Optical System

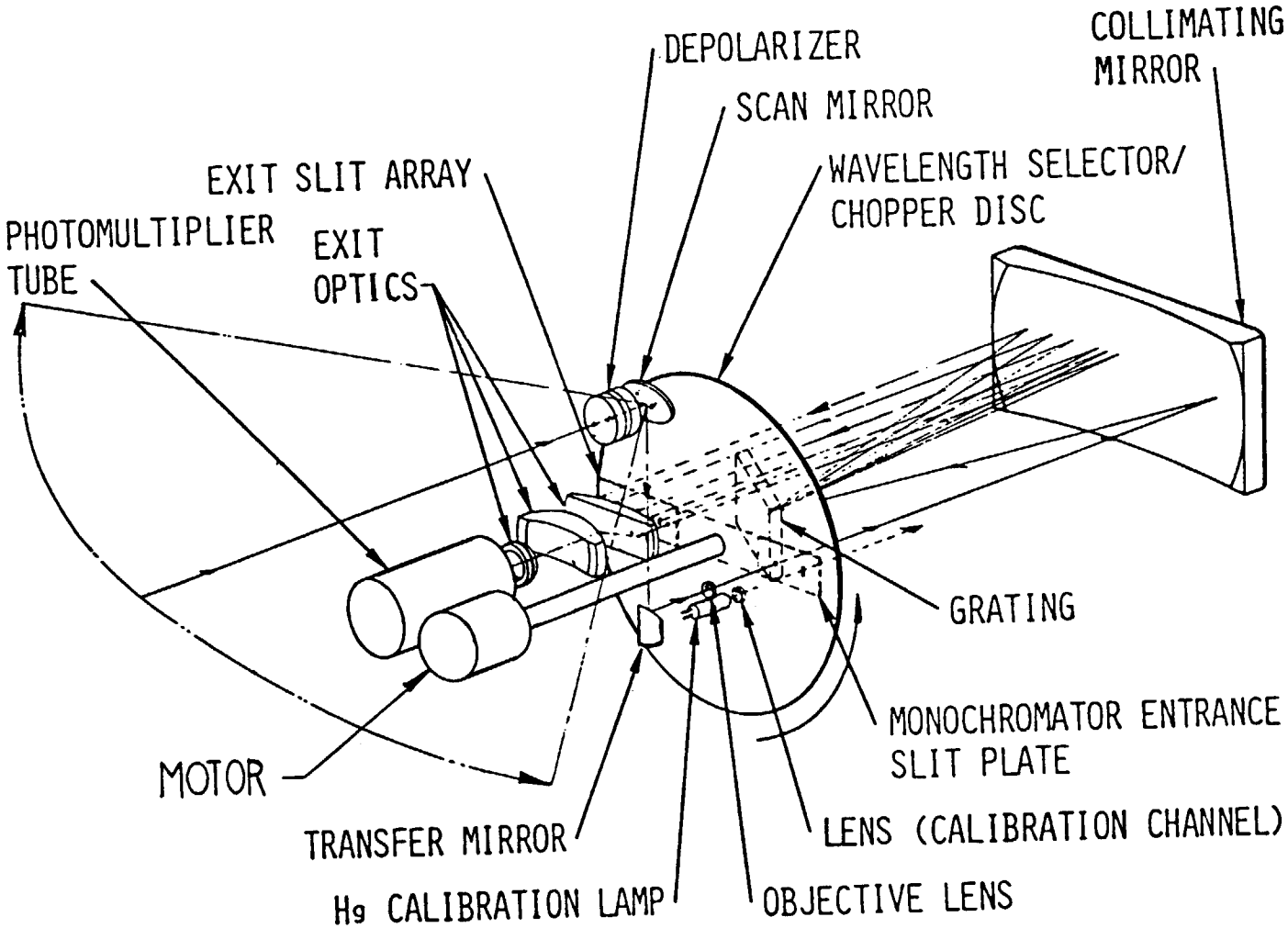

Figure 3. TOMS Optics Diagram

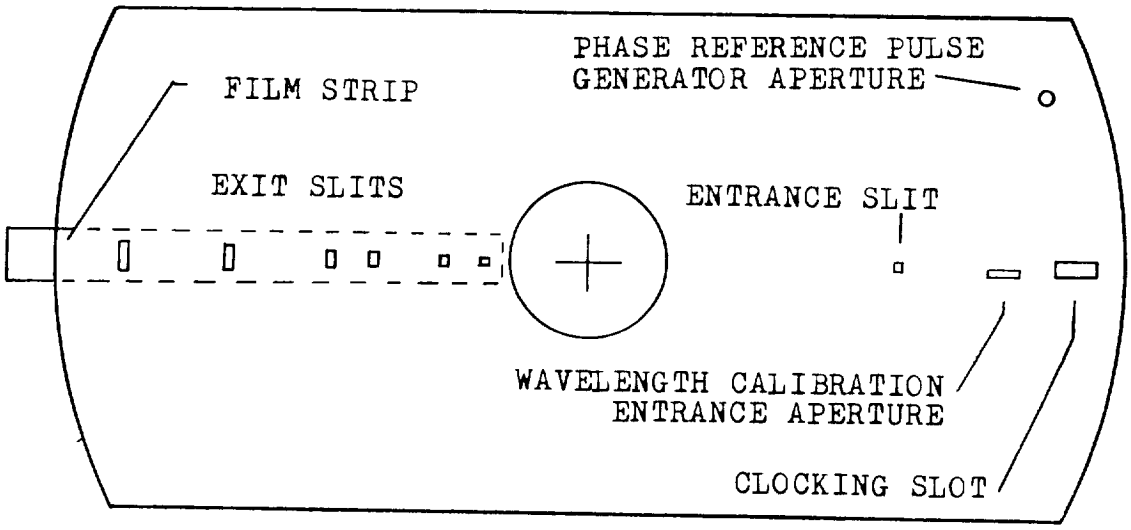

Figure 4. Floating Slit-Plate

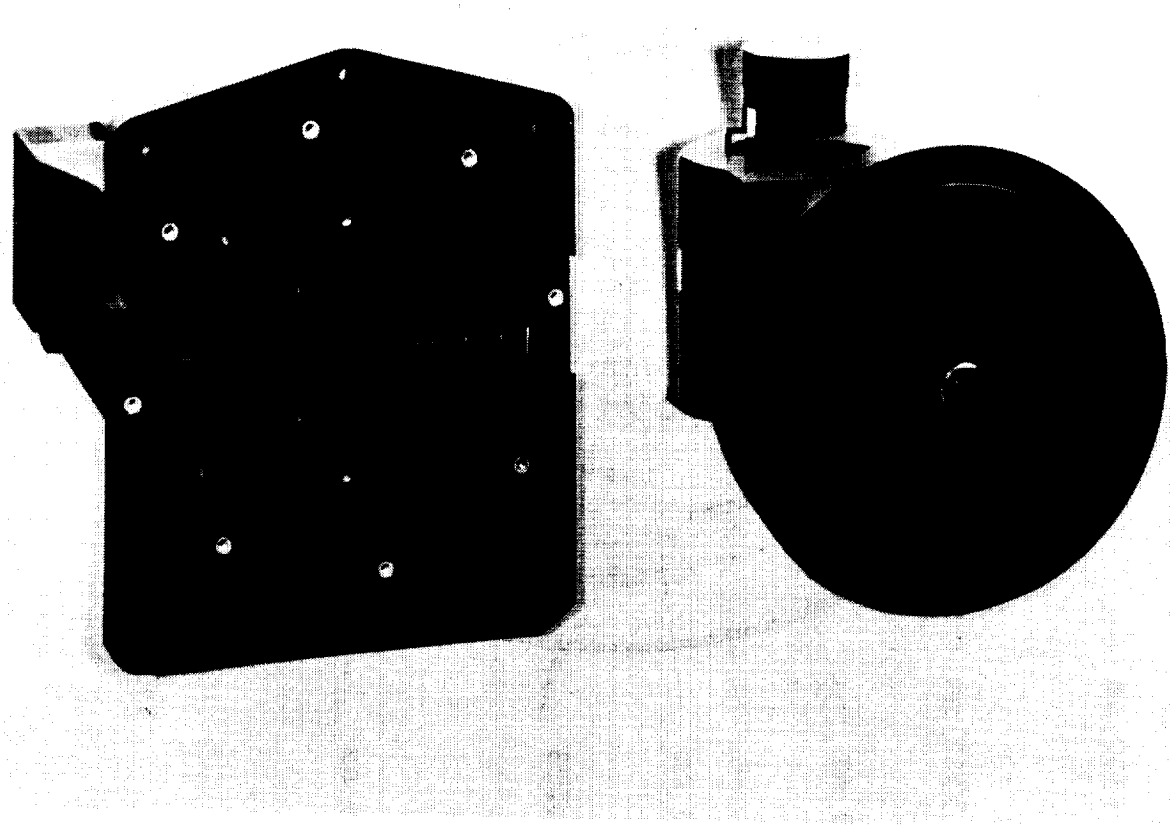

Figure 5. Slit-Plate Installed in Monochromator Housing and Chopper-Wheel Installed in Scanner and Detectorhead Assembly

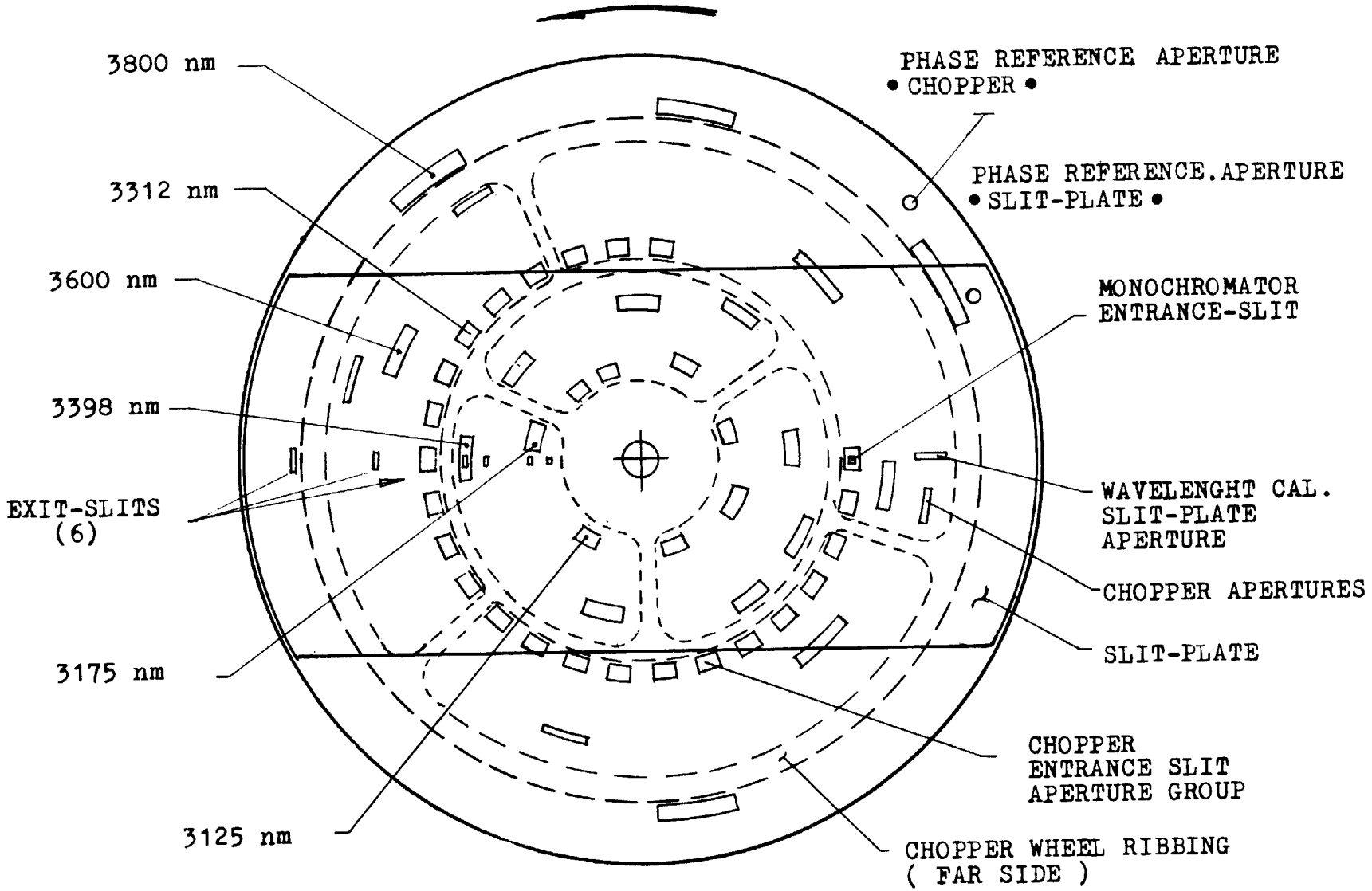

Figure 6. Wavelength Selector Chopper with Super-Imposed Slit-Plate

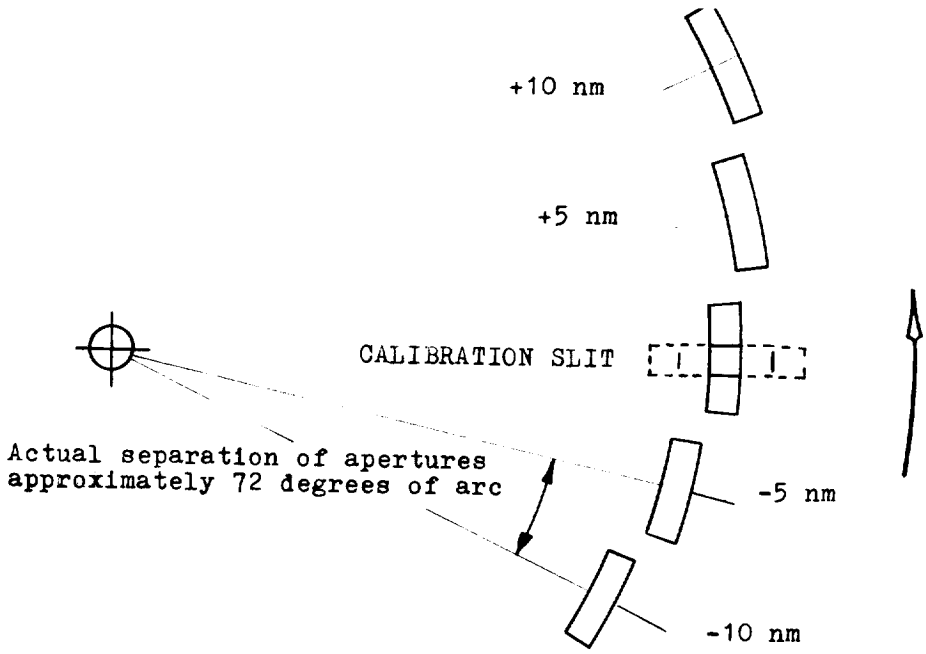

Figure 7. Calibration Apertures

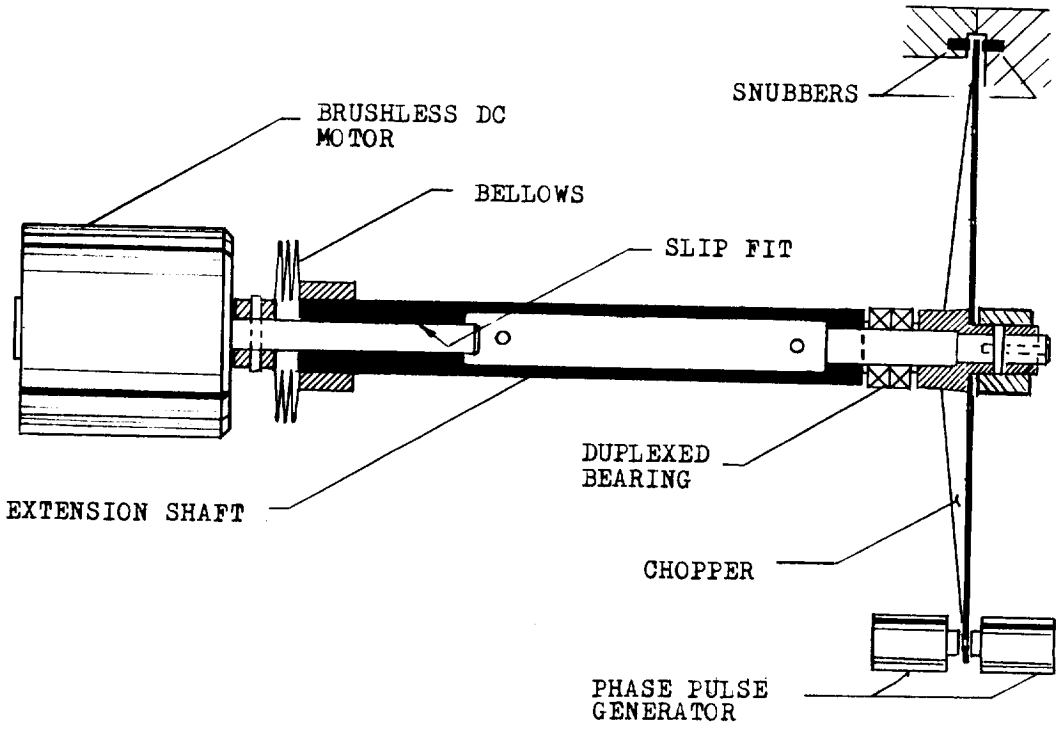

Figure 8. Chopper and Chopper Drive Assembly

A SYSTEMS APPROACH TO MECHANISMS FOR A WHITE LIGHT CORONAGRAPH/X-RAY XUV TELESCOPE

Richard Mastronardi and Richard E. Cabral
American Science and Engineering, Inc.
Cambridge, Massachusetts

ABSTRACT

A combined instrument package containing nine mechanisms has been designed and developed for the NASA/ESA International Solar Polar Mission (ISPM). This complement of instruments, commonly called the CXX, is the only imaging system on either the NASA or ESA Spacecraft and consists of a White Light Coronagraph mounted parallel to a combined X-ray and Extreme Ultra-Violet (XUV) Telescope. The nature of this mission and the anticipated spacecraft environments impose unique requirements on the CXX in general and the mechanisms in particular. This paper focuses on requirements for and implementation of mechanisms in the CXX Instrument.

INTRODUCTION

The design and fabrication of instrumentation for space experimentation is typically demanding and costly. The International Solar Polar Mission (ISPM), however, places especially difficult constraints of size, weight, power longevity and radiation resistance on its scientific instrumentation. The scientific objectives for the White Light Coronagraph/X-ray Extreme Ultra-Violet (XUV) Telescope (CXX) on ISPM place additional cleanliness demands on the design of mechansims. These constraints command a review of traditional engineering techniques for mechanism design in general and redundant and fail-safe mechanisms in particular.

This paper demonstrates, through example, that by considering the system as a whole, a complex instrument with nine separate mechanisms can be designed and fabricated satisfying demanding constraints. One of the mechanisms has no back-up features, two of the mechanisms provide redundancy, two provide a fail-safe mode and four provide both redundancy and failsafe back-up systems. This was accomplished using one stepper gearmotor design, one direct drive redundant stepper motor and two sizes of pyrotechnics.

A systems approach and a matrix of mechanism requirements are used to minimize the number of types of motors and pyrotechnics needed to achieve the objectives of all nine mechanisms. The result is a lightweight, low power tightly packaged complement of high-reliability mechanisms.

REQUIREMENTS

The International Solar Polar Mission (ISPM) is a cooperative effort by NASA and the European Space Agency to study the sun and the interplanetary medium. The two spacecraft which make up the mission will be launched simultaneously into earth orbit by the Space Shuttle. Each spacecraft will be boosted out of the earth's gravitational field by an inertial upper stage and cruise towards a Jupiter rendezvous. The two spacecraft will use the Jovian gravitational field to change their momentum from a direction which is in the ecliptic plane to one which is perpendicular to the ecliptic plane (Figure 1). One spacecraft will pass to the north of Jupiter and thus swing into an orbit to the south of the ecliptic plane, while the other spacecraft will pass to the south of Jupiter and orbit to the north of the ecliptic plane. The orbits will bring the spacecraft first over one pole of the sun, through the ecliptic plane and over the other pole. These spacecraft, the first to leave the ecliptic, will show a view of the sun and the interplanetary medium different from any we've ever had before.

The White Light Coronagraph/X-Ray XUV Telescope (CXX) on ISPM (Figures 2 and 3) is intended to observe the solar atmosphere over a wide range of solar altitudes from the chromosphere (in XUV) through the low corona (in both X-rays and XUV) to the outer corona (in white light).

The launch environment, mission profile and scientific objectives have each contributed to the stringent requirements on mechanism designs. Since approximately five years pass between launch and achieving the prime science position above the Sun's polar region, high emphasis has been placed on long term reliability of all instrumentation. Mechanisms such as the X-ray XUV Telescope (XXT) Filter Wheel and Shutter will be actuated on a regular basis for the entire mission. The filter wheel will be rotated approximately 10,000 times over that period while the XXT Shutter Mechanism (which has the same type drive system) is expected to experience close to 1 million cycles during its life. Because the spacecraft is being powered by a Radioisotope Thermoelectric Generator, power is severely limited. The power budget for mechanisms in the CXX Instrument is 2.68 watts maximum at 28 volts d.c. The need for the spacecraft to achieve proper trajectory out of the earth's gravitational field and toward Jupiter, has limited weight. The CXX Instrument will weigh approximately 13.6 KG. Other requirements include limited packaging volume, no generation of particulate contamination, no outgassing of hydrocarbons, survival of the Jovian radiation environment, survival of amplified vibrational environments during launch (approximately 60 g's) and the need to meet minimum speed, torque, and inertia requirements for the mechanisms.

Due to these stringent requirements of the mission and the importance of the science, each mechanism was assessed to establish the needs for redundancy and failsafe modes of operation. Since, for example, the XXT 15-position filter wheel contained a large portion of the X-ray and XUV science, it was decided that this mechanism should contain both a back-up drive capability (redundancy) and a one-time release to a preferred position (failsafe). Similar considerations led to the same design requirements for the White Light

Coronagraph (WLC) 10 position filter wheel and each of the two focal plane shutter mechanisms. Mechansims of less scientific importance required only redundancy or failsafe or no back-up system at all.

With each mechanism having its own set of demanding requirements and ground rules, it seemed unlikely that commonality could be achieved in power plant selection and more desirably, the mechanism designs. Much commonality, however, was achieved through establishing a requirements matrix and finding their common denominators.

THE SYSTEM APPROACH

After reviewing the requirements for each of the nine mechanisms, it appeared that each had unique factors driving its design. The first efforts in their design concentrated on each mechanism as an entity unto itself. Commonality of drive train components was a strong consideration for minimizing costs. Initially one motor was selected with a number of different ratio gear boxes. Several failsafe clutches were selected. Attempts at driving two mechanisms with the same gearmotor were also tried. The complications of designing redundant and failsafe mechanisms that were reliable, lightweight, low power and small, each with conflicting requirements, seemed almost overwhelming. Using traditional techniques for providing fully redundant and failsafe systems involved complicated schemes of gear passes, clutches, and other load transferring devices. Although these were shown to work in breadboard models, they were prone to many single-point failure modes and therefore were possibly unreliable.

It was at this point, that an extensive matrix of mechanism requirements was formulated. Some of the matrix is given in Table 1. The intent was to take a fresh unconstrained view of the requirements and their restrictions. Some requirements were modified to achieve commonality without affecting the scientific objectives. Additionally, we no longer restricted ourselves to standard motors. A departure from tradition was taken and a fully redundant direct drive stepper motor was developed with the help of Schaeffer Magnetics Inc., Chatsworth, California. The motor requirements were generated out of the commonality of the CXX mechanisms in the matrix. Because this point of change in philosophy was relatively far downstream in development of the entire instrument, the motor was configured with the intent of complementing existing work and minimizing impact.

The redundant motor design did not totally eliminate the need for gearmotors, but it did achieve commonality in all critical mechanisms leaving gearmotors to drive only non-redundant mechanisms. It also eliminated the need for clutches and facilitated the use of pyrotechnics for failsafe releases.

In the end, four different devices were needed to provide motion in all nine mechanisms. These devices are shown in Figure 4. The small pyrotechnic is used in five locations as the failsafe release pin-puller. The larger pyro-

technic is used in both the XXT door and cooler cover redundant one-time release latches. The size 8, 90°, 160:1 stepper gearmotor is used in the WLC door mechanism. Two of these motors are also used to independently drive the D4 internal occulting disc vertical and horizontal motions. The 4° redundant direct drive stepper motor developed on this program is used in five locations. The A1 - A3 Aperture Mechanism, the WLC and XXT Filter heels and Shutters all use this device. In fact, the last four mechanisms use virtually the same mechanism design throughout.

MECHANISM DESCRIPTIONS

The XXT Door shown in Figure 5 and the cooler cover door (CCD) use virtually the same design for the one-time release to an open position. They each have spring loaded hinges, supported on redundant bearing pairs, with a latch release by pin-pulling pyrotechnics. Two pyrotechnics located in series provide redundancy.

Figure 6 shows the WLC Door Mechanism. A gearmotor direct drives the door open or closed. In the event of motor failure, a pin-pulling pyrotechnic can release the spring loaded door to a fully open position. The hinge shaft is supported on redundant bearing pairs.

The A1 - A3 Aperture Mechanism is shown in Figure 7. The redundant stepper motor drives the redundant bearing supported shaft through a metal bellows coupling. Each aperture wheel is pinned to the hollow shaft. Precision repositioning is achieved by a mechanical detent that is preloaded by the magnetic detent of the stepper motor.

The D4 Internal Occulting Disc Mechanism, shown in Figures 7 and 8, provide $\pm$ 0.13 mm motion for the disc in both the horizontal and vertical directions. Preloaded eccentric circular cams cause small increments of motion (0.0025 mm), as desired for adjustments, by rotation of two independent stepper gearmotors.

Figures 9 and 10 show the differences between the traditionally designed redundant and failsafe XXT Filter Wheel and the same device using the redundant stepper motor. The most obvious difference is the fewer number of parts and the simplicity of the redundant motor design. A comparison of these designs is given in Table 2.

The XXT and WLC Filter Wheels and Shutters use identical mechanisms for their motion. Primary and redundant activations are provided by the motor. If both windings of the motor fail, a pin-pulling pyrotechnic can be used to release the spring loaded mechanism, thus allowing it to rotate to a preferred position at a mechanical stop. The motor shaft is supported on redundant bearing pairs.

CONCLUSION

Formulating the requirements of multiple mechanisms into a complete matrix can aid the designer in finding common factors among mechanisms. Reviewing the latitude of these requirements is vitally important in determining trade-offs. It is also helpful to realize that new views on mechanisms and motors, even if they require development, need not be costly or schedule impacting. Simplicity and commonality can greatly improve system reliability while achieving mission objectives.

A system approach to mechanism design has been successfully applied here to maximize reliability, minimize weight, achieve low power consumption and maximize commonality among the designs. Through example, it has been demonstrated that a system approach to mechanism designs can meet the unique requirements of the International Solar Polar Mission and the normally encountered requirements of precision spaceborne imaging instrumentation.

ACKNOWLEDGEMENTS

The work under this Subcontract (Subcontract No. NCAR S9003) was funded by UCAR's Prime Contract ATM 77-23757 with the National Science Foundation through a transfer of funds from the National Aeronautics and Space Administration.

TABLE 1: ISPM CXX MECHANISM REQUIREMENTS MATRIX

	Redundant (R) Failsafe (F)	Inertia ($gm-cm^2$)	Speed	Position Requirements	Position Repeatability	Life Cycles Incl. Test	Weight (gms)
WLC Door	F	33	45°/sec.	±180° Failsafe Open	N/A	2241	125
XXT Door	R	23	N/A	One time open 270°	N/A	51	169
A1-A3 Apertures	F	Low	40°/sec.	5 positions	±0.004 mm	55	314
D4 Occulter	-	Low	N/A	±0.13 mm 0.0025 mm steps 2 directions	±0.0025 mm	200	246
WLC Filter	RF	105	N/A	10 positions	±0.75 mm	4965	212
XXT Filter	RF	1530	N/A	15 postions	±0.75 mm	8617	263
WLC Shutter	RF	173	40°/sec.	Open/Close same side	±0.5 mm	4965	183
XXT Shutter	RF	173	40°/sec.	Open/Close same side	±0.5 mm	836,200	183
Cooler Cover	R	50	N/A	One time open 270°	N/A	51	213

TABLE 2: COMPARISON OF XXT FILTER WHEEL DESIGNS

Requirements	Traditional Design	Redundant Motor Design
Low Weight (263 gms max)	372 gms	213 gms
Low Power (2.68 watts max)	2.25 watts	2.3 watts
Volume (excluding filter wheel)	5cm x 9cm x 14cm	5cm x 5cm x 5cm
Minimize Moving Parts	33 parts	7 parts
Gears	Yes	No
Single Point Failure Potential	Yes	No
Hydrocarbon Outgassing	None	None
Particulate Generation	External Gears	None
Radiation Resistance	Yes	Yes
Meeting Torque, Speed and Inertia Requirements	Yes	Yes
Motor Torque	7.2 gm-cm	360 gm-cm
Gearmotor Torque	972 gm-cm	N/A
Vibration Test at 60 g's	Not Tested	Passed

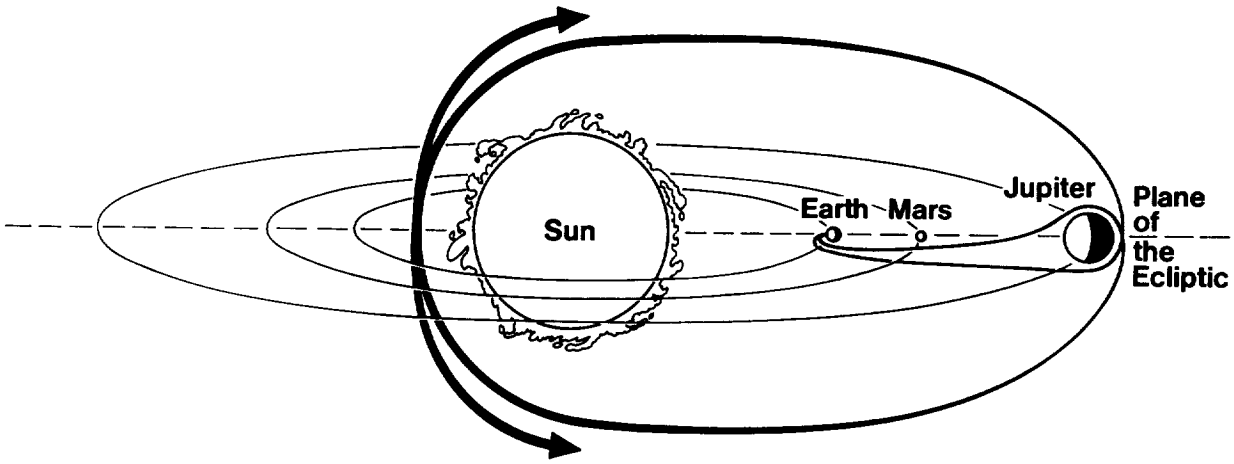

Figure 1. ISPM Mission Profile.

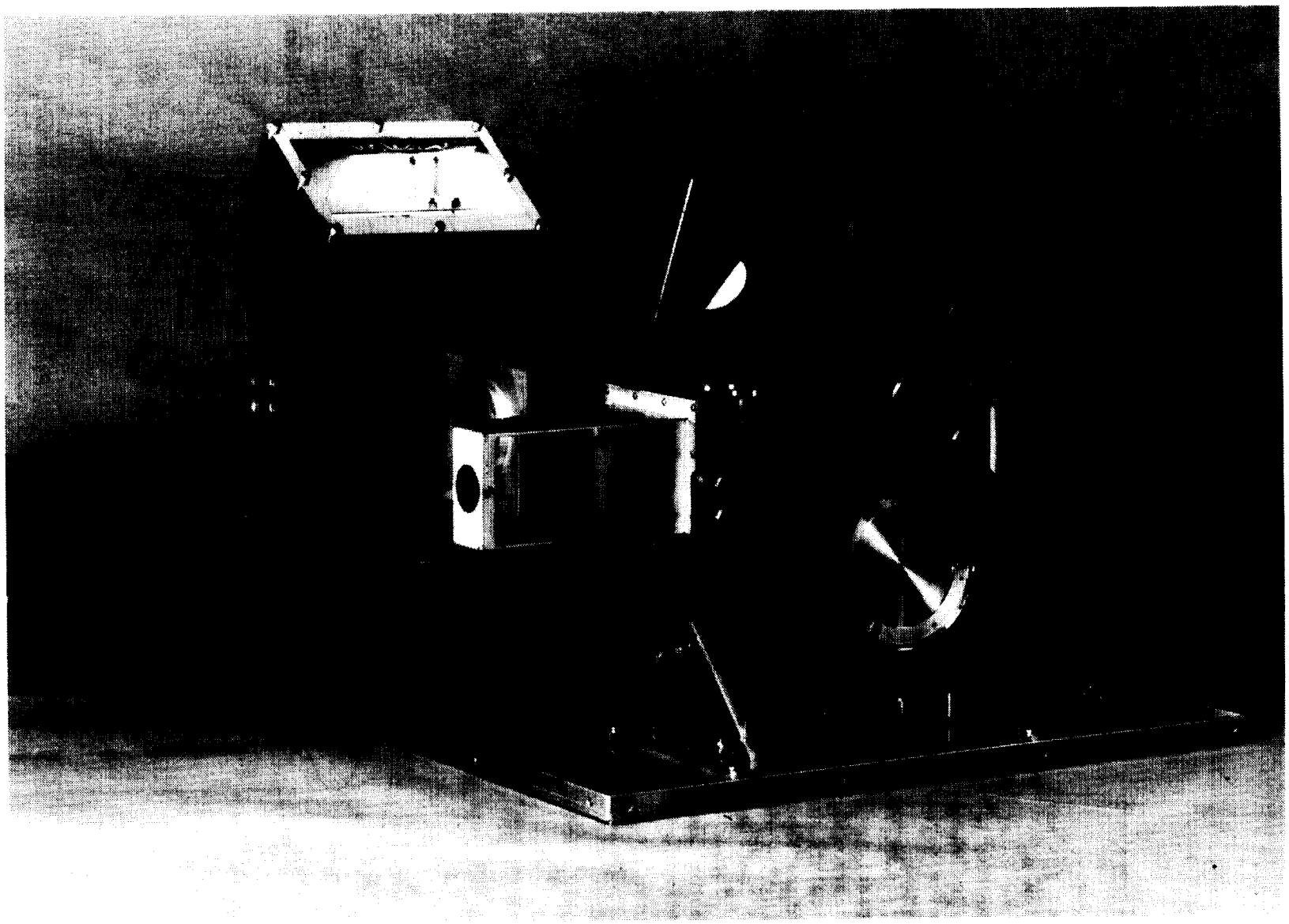

Figure 2. CXX Instrument Mock-Up.

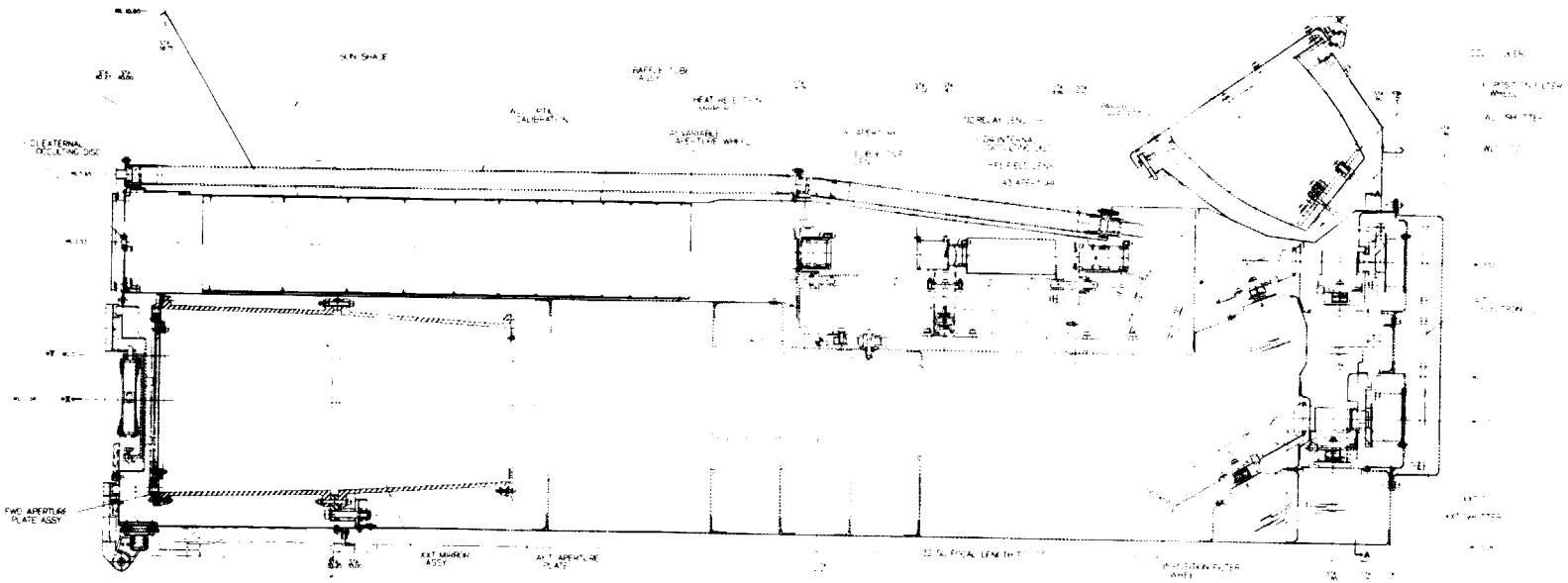

Figure 3. White Light Coronagraph/X-ray XUV Telescope.

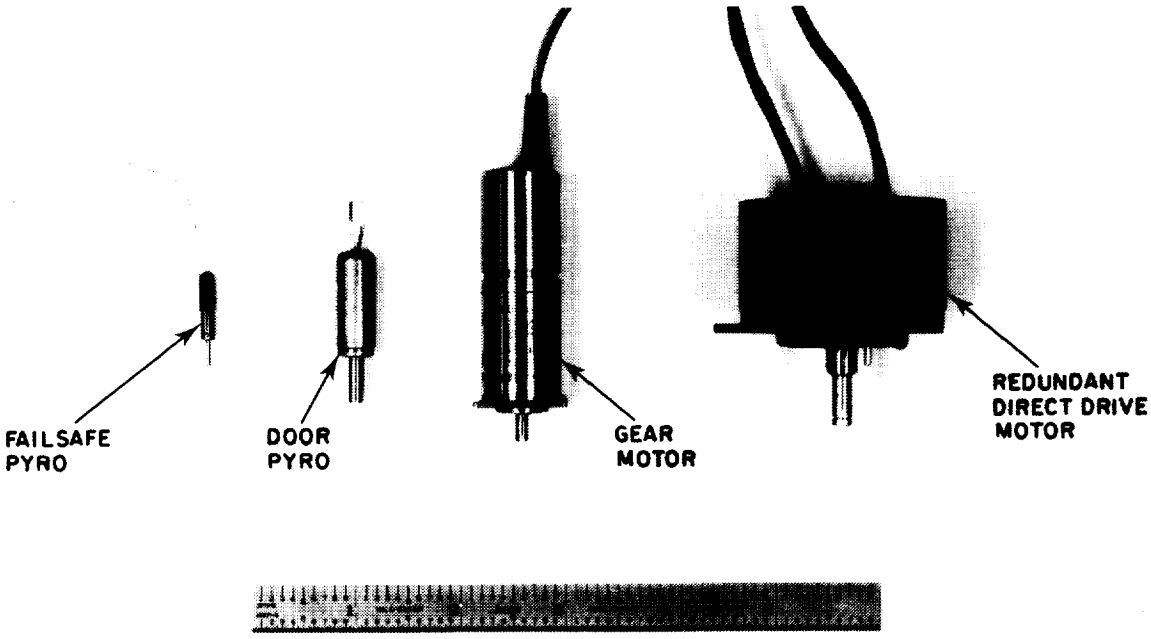

Figure 4. CXX Pyrotechnics and Motors.

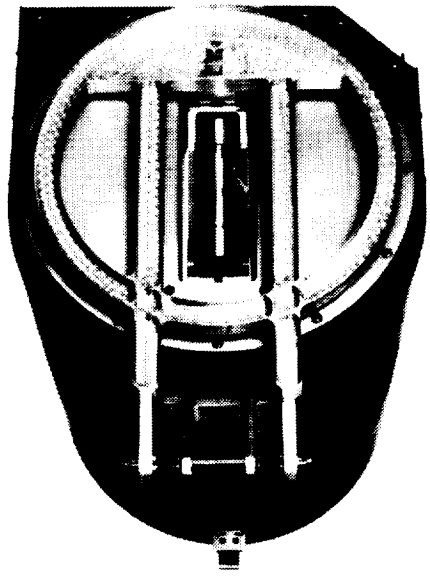

Figure 5. XXT Door.

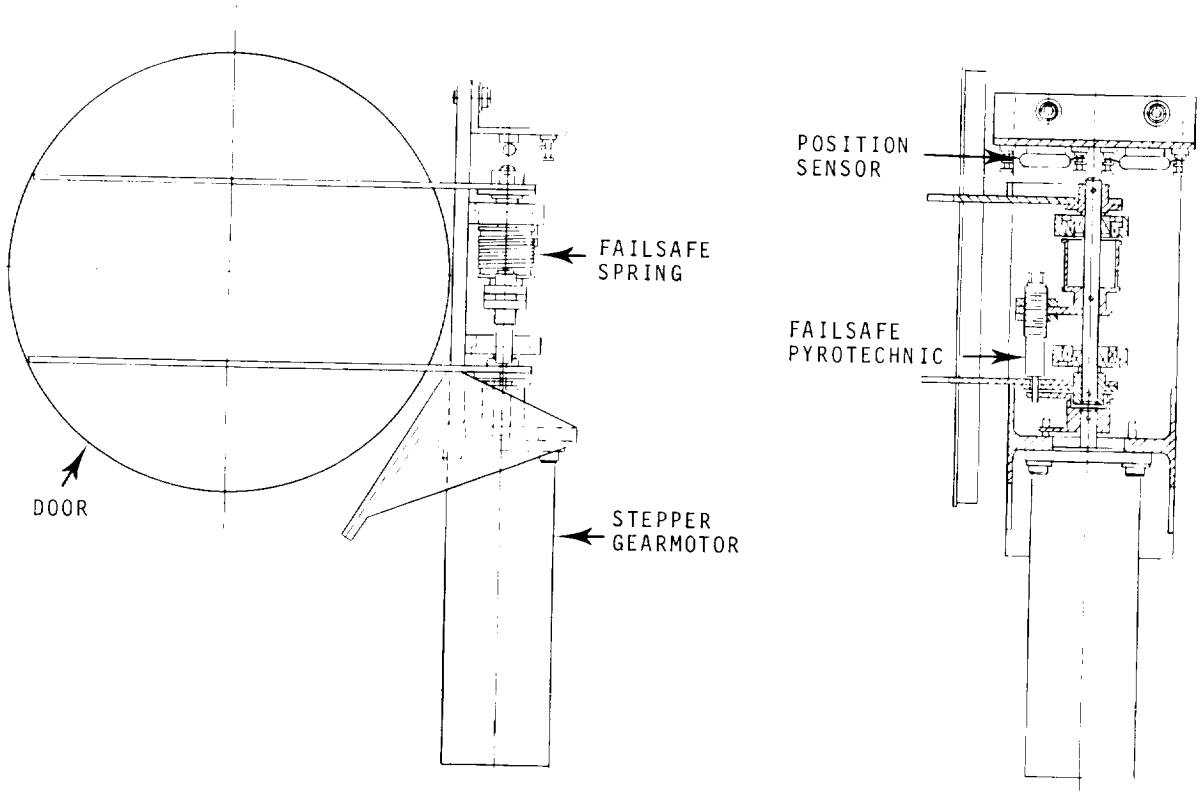

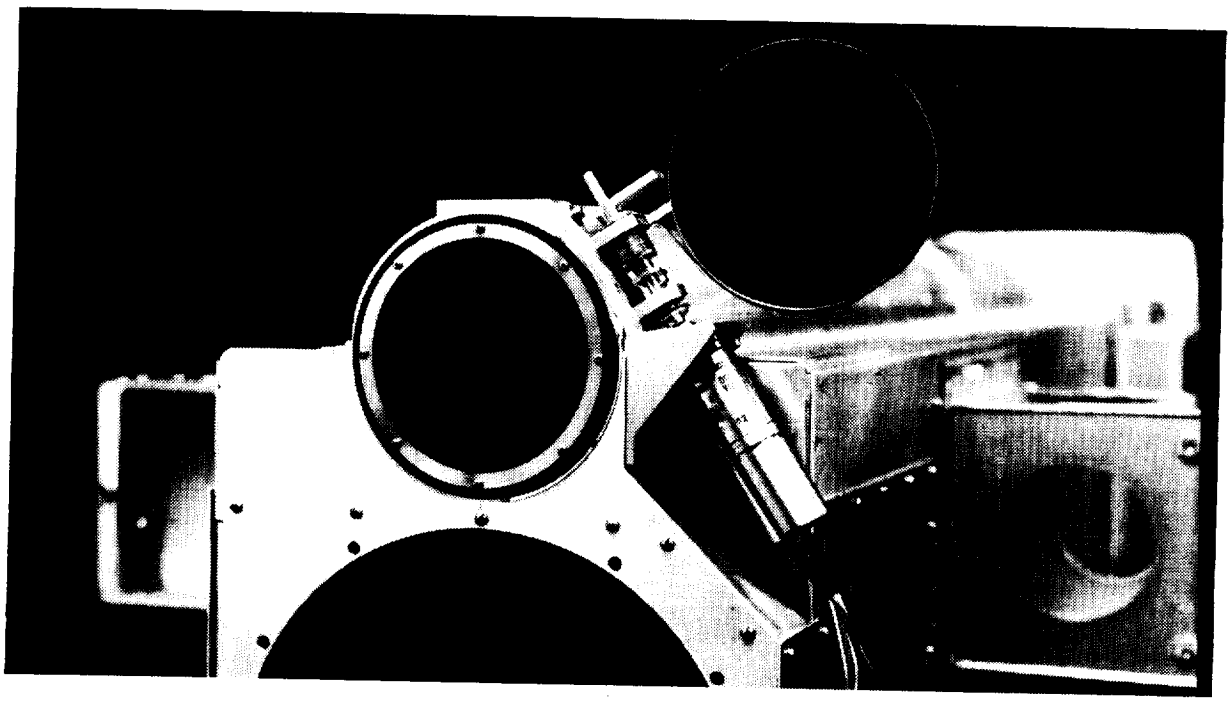

Figure 6. WLC Door.

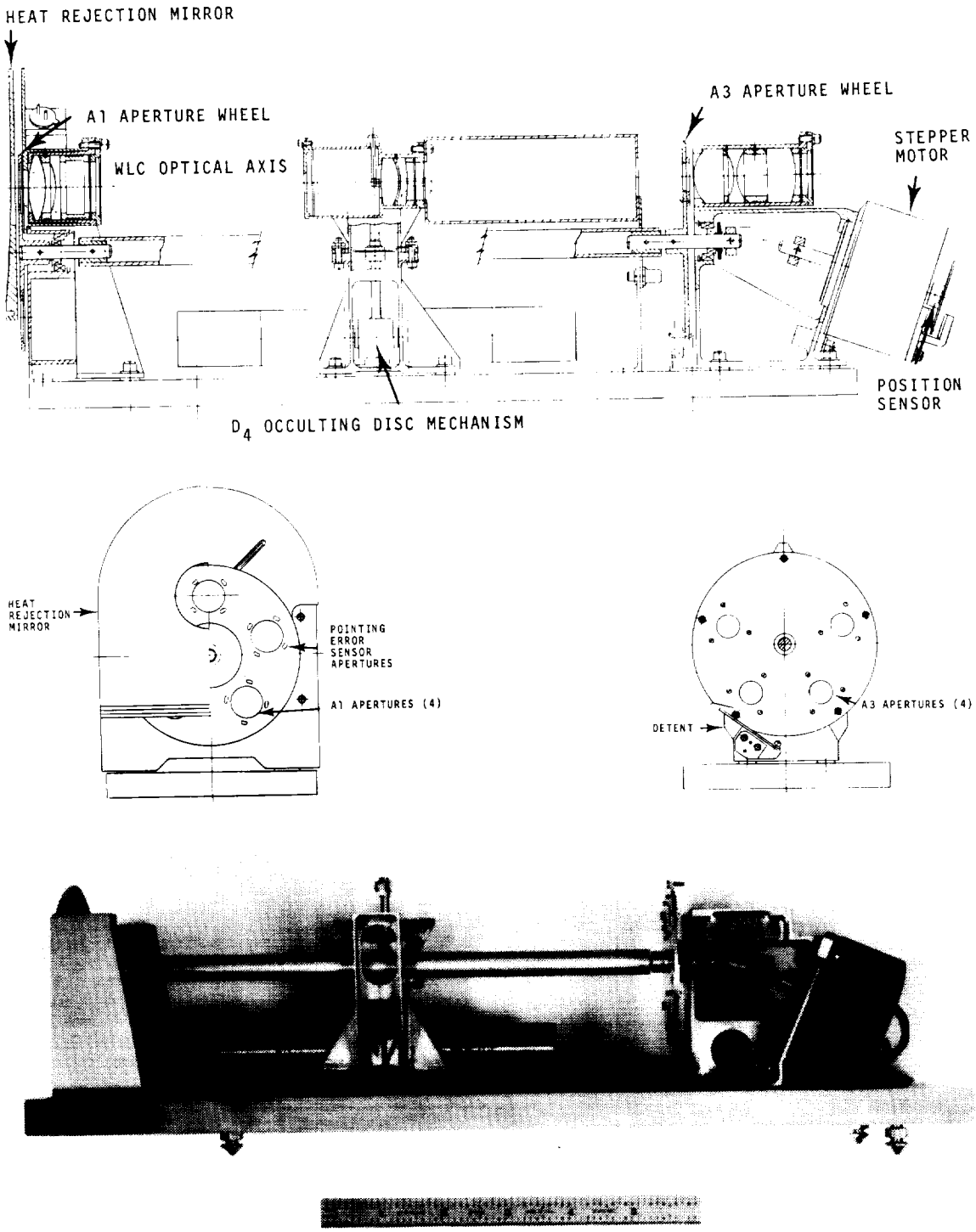

Figure 7. $A_1 - A_3$ Aperture Mechanism.

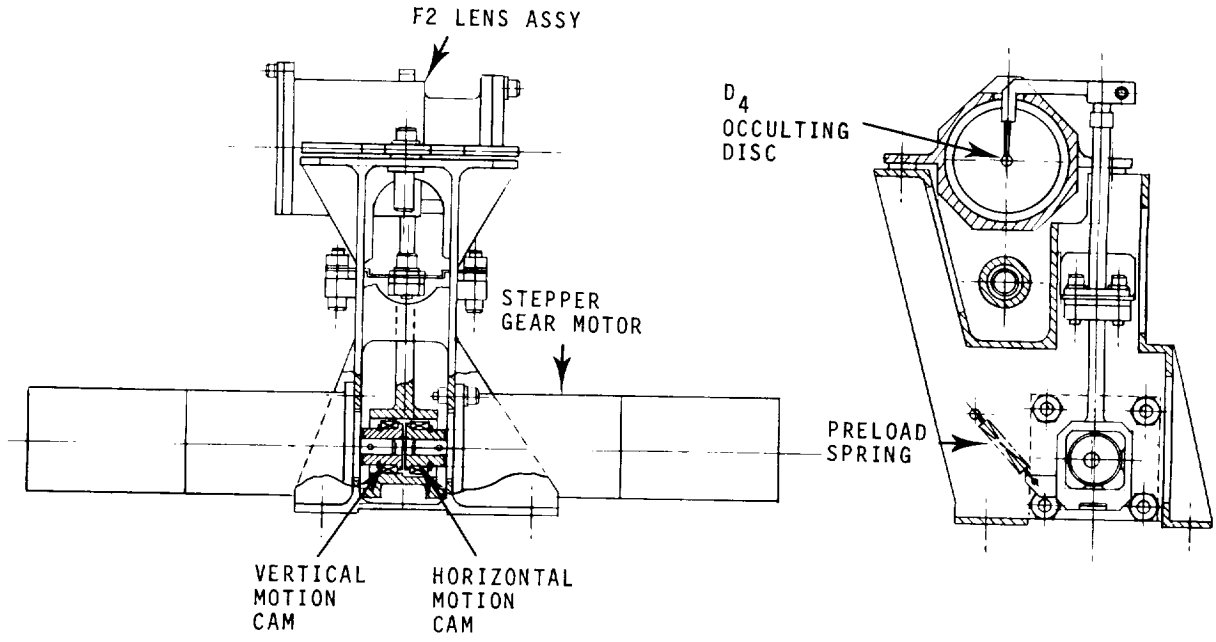

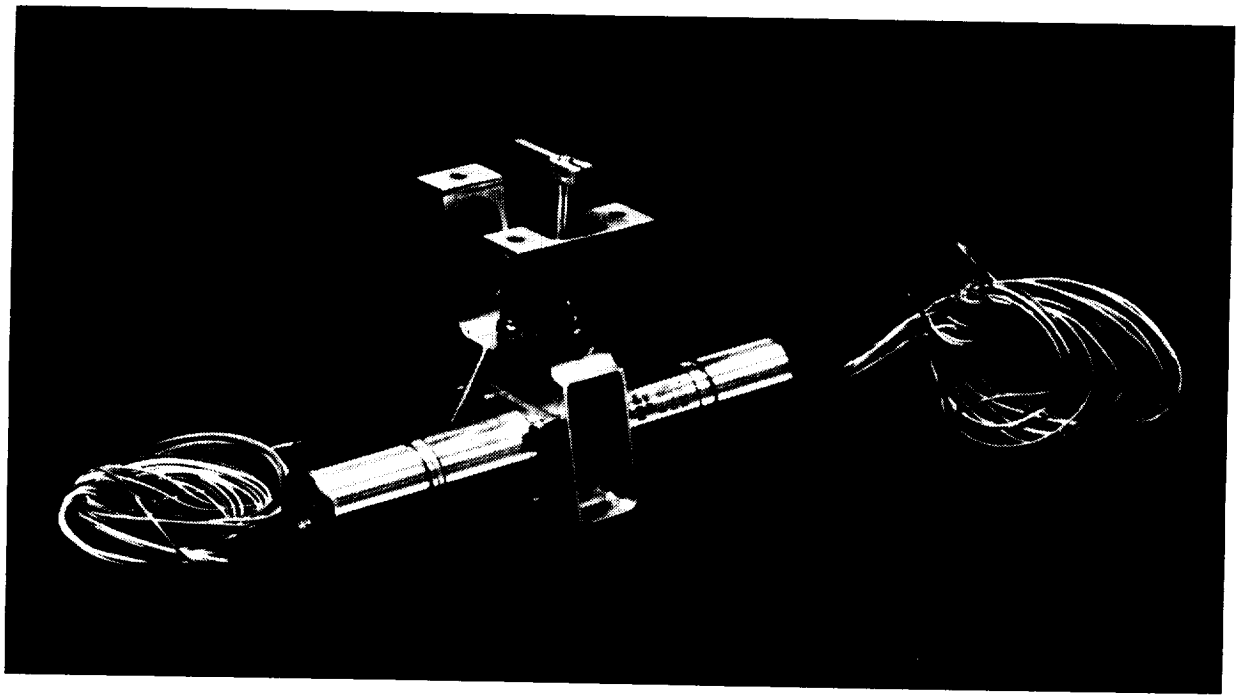

Figure 8. D_4 Internal Occulting Disc.

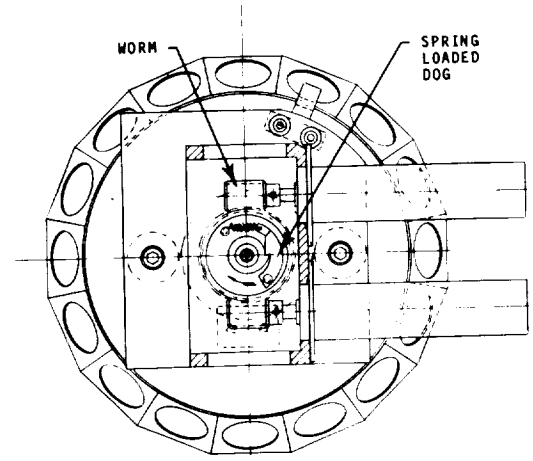

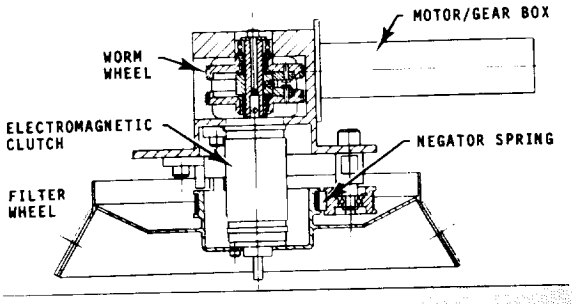

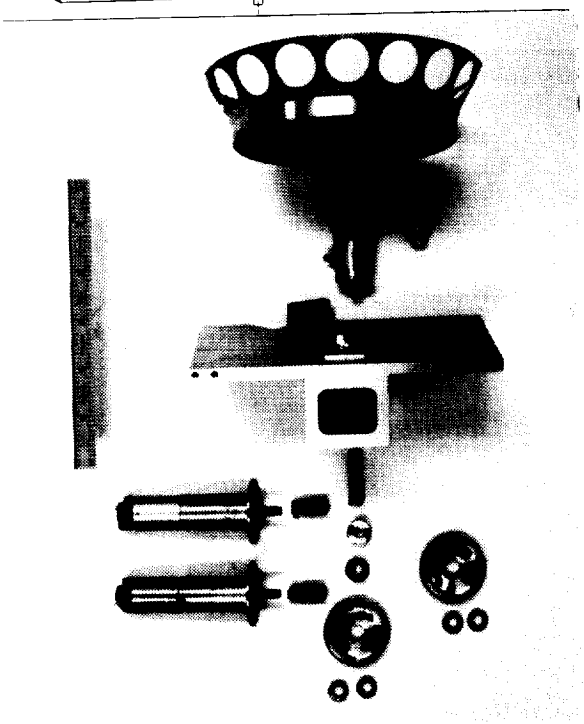

Figure 9. XXT Filter Wheel. (Traditional Design).

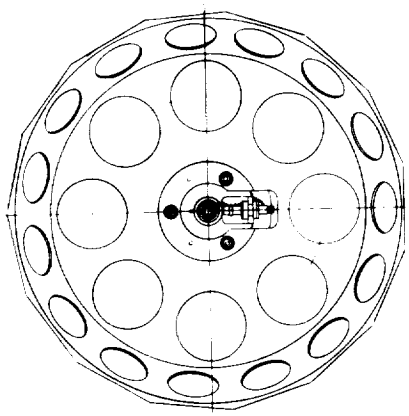

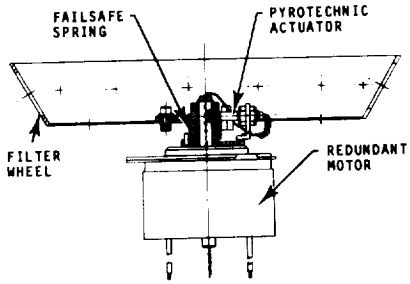

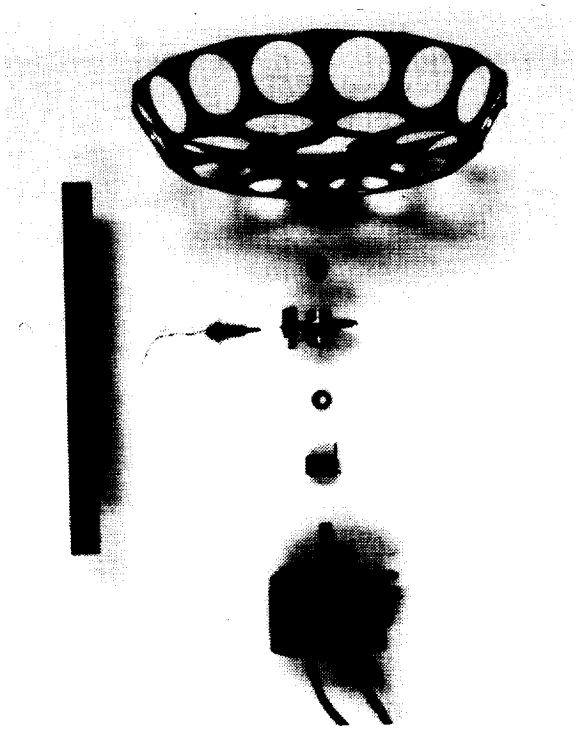

Figure 10. XXT Filter Wheel. (Redundant Motor Design).

COALIGNMENT OF SPACECRAFT EXPERIMENTS

Robert E. Federline

National Aeronautics and Space Administration
Goddard Space Flight Center
Greenbelt, Maryland

ABSTRACT

On February 14, 1980, the Solar Maximum Mission, SMM, satellite was launched into orbit with experiments to monitor solar activity. To obtain common-object observations experiments must be coaligned within 90 arc-seconds of the spacecraft pointing vector. Hardware was designed to minimize structural and thermal distortions of the experiment support plate. Coalignment was provided through control of a unique interface which combined flexible blades to limit load transfer and spherical seats for alignment reference.

This document describes the hardware used to achieve coalignment and more importantly identifies the techniques utilized to achieve the coalignment of experiments on SMM.

I. INTRODUCTION

On February 14, 1980, NASA launched the Solar Maximum Mission satellite into a near-earth orbit. The Solar Maximum Mission (SMM) Solar Observatory is illustrated in Figure 1.

On board were eight highly sophisticated research experiments monitoring solar activity in different portions of the spectrum. During this period of maximum activity in the sun's eleven-year cycle, particular attention is directed to solar flares and flare-related phenomena. To achieve this

scientific goal, simultaneous common object viewing is required. This in turn requires a precise coalignment of the experiments and a stable platform from which observations can be made.

There are, of course, many techniques which can provide precise coalignment on the ground, but these prove impractical when applied to space flight use. Spacecraft hardware in general must be lightweight and highly reliable. Attachments must be accessible at all times and be repeatable. Experiments must not affect one another or the spacecraft to any degree which would affect control or performance. Most importantly, all experiments must survive the launch into orbit and perform as predicted. Further, schedule must be maintained throughout.

II. COALIGNMENT REQUIREMENT

The requirement for common object viewing established the specification for coalignment. Because experiments had not yet been selected, their fields of view were undefined. That, coupled with an inability to agree on the exact size of a solar flare, caused the alignment specification to be defined in terms of experiment boresight. The experiment boresight is the centerline of the experiment field of view. The specific requirement was to provide a stable platform for in-orbit solar observation where the experiment boresights would be coaligned to the solar pointing vector within 90 arc-seconds. The solar pointing vector is defined as the boresight of the fine pointing sun sensor. Because its location could be adjusted in orbit by software modifications, the specification translated to coalignment of experiment boresights within 180 arc-seconds of each other.

The approach selected to fulfill this coalignment requirement is based on providing a single plate where experiments are mounted to both sides. The major components of the SMM are depicted in Figure 2. The Multimission Modular Spacecraft (MMS) keeps the experiments pointed at the sun. The plate is isolated from thermal and mechanical distortions originating in its support structure and in the experiments. This provides the stable platform. To align the instruments, an alignment template is used which accurately defines the experiment interface. With optical reference surfaces for three-axis determination, the alignment template provides the common link between the experiment boresight through the interface to the spacecraft hardware. With a unique template for each experiment, individual experiment boresights are aligned to a common optical vector.

III. DESIGN

Early in the program, concept studies were conducted to determine the best method of providing a stable platform capable of maintaining experiment alignment. The results indicated that, to be stable, the support must be isolated both structurally and thermally from its environment.

The first step is to isolate the support plate from its support structure. This is effected mechanically through true kinematic support. The plate is supported at only three points; one at each side and one in the center. A 3.8 cm (1 1/2") diameter spherical bearing with a break-away torque of less than 0.9 newton-meters (eight inch-pounds) is installed at each support point. Additional bearings are installed at the base of the center strut and in a trapeze joint at one side of the plate. Thermal isolation of the support

plate is achieved by wrapping the plate and the support structure in 20 layers of aluminized mylar super-insulation. The support structure at both sides is constructed of welded titanium plates. The center strut is a tube 10.2 cm (4") in diameter with 0.6 cm (one-quarter inch) walls. It was fabricated from graphite-reinforced epoxy by Hercules, Inc., of Magna, Utah. The use of titanium and graphite epoxy provides thermal resistance and conductively insulates the plate from the support structure.

The second step is to isolate the support plate from the experiments. Thermal isolation is achieved with thermal blankets and titanium in the experiment mounts. Mechanical isolation is very difficult because load isolation and coalignment are conflicting requirements. The solution lies in the design of the experiment mounts. A well-defined experiment interface can be aligned with precision, while a flex-blade type of mount minimizes load transfer, permitting the plate to remain stable. Forces resulting from hardware shifts during launch and thermally induced dimensional changes are first localized by the flex mounts and then converted to bending within the mount itself. No measurable effects are experienced by the support plate, permitting it to remain stable. The minor changes in the orientation of the interface plane causes negligible misalignment. Therefore, status changes or malfunctions in any single experiment do not affect the stability of the support plate or the alignment of experiments.

The experiment support plate is designed as a single dip-brazed assembly. The technique used to construct the Experiment Support Plate is illustrated in Figure 3. Aluminum core strips 1.6 mm (1/16") thick are machined with slots and tabs. The slots interlock as core strips are assembled at right angles to each other, forming a 10.2 cm (4") grid cell structure. Aluminum facesheets 3.2 mm (1/8") thick are machined with slots and 3.81 cm (1 1/2") holes. As the facesheets are fitted over the core structure, the tabs on the core strips protrude through the facesheet. The tabs are twisted over, locking the core and facesheet together. Welding flux is applied to the joints, and the complete assembly is dip-brazed as a unit at McDonnell Douglas in Long Beach, California. The support plate, 1.5 m (5 feet) by 1.8 m (6 feet) by 10.8 cm (4 1/4 inches) is one of the largest single dip-brazed structures of its type to exist. After brazing, the support plate is heat treated, fog-quenched and aged to produce material properties only slightly below the T-6 values.

The 3.8 cm (1 1/2") diameter holes through the facesheets were centered in each of the 10.2 cm (4") core cells. Each cell is identical on both sides which allows attachments to be made at any point. Magnesium corner reinforcement brackets are installed internal to each cell where experiment mounts are to be installed and where loads require stiffening doublers.

Experiment mounts fit through the holes in the facesheet and into the cell. Figure 4 shows details of the experiment mount design. With the aid of a backing plate, the experiment mounts are rigidly bolted to both the front and the back facesheets of the support plate. Internal to the mount is a titanium stud machined in the form of a flex blade. Experiments are constrained to use

three mounts. The weak axis of two blades is radially oriented to the stiff blade. Accessibility to the experiment attachments normally results in a right triangle configuration with the stiff blade at the apex. Spherical bearings and seats on the top of each experiment mount define a unique interface for each experiment. It is the function of the alignment template to identify and correlate these unique interfaces.

IV. COALIGNMENT TECHNIQUE

The alignment templates are accurately machined from tooling plate and contain an integral interface to accommodate a master alignment gage. Experiment mounting holes are not installed at this time. Optical measurements are made between an optical cube installed on the template and the master gage. If the template cube should require replacement, the old cube and the new cube can be related through the master gage.

Meanwhile, fabrication of the experiment base structure, without mounting holes, has been completed. The alignment template is attached to the experiment base structure. The mounting holes are simultaneously machined into both pieces in an "in-line" machine operation. Once separated from the template, assembly of the experiment onto its base structure continues with the following restrictions: (1) The completed instrument must be aligned to the hole pattern in the base structure. The hardware on the spacecraft side of the interface has limited capability to compensate for gross misalignment. For this design, the hardware limitation is 30 arc-minutes. (2) An alignment reference must be installed on a stable portion of the experiment structure. The reference must be aligned with the boresight within the tolerance of our

measurement facility to see it. For the facility used on SMM, this value is five degrees. (3) Finally, the three-axis bias values between the experiment boresight and the experiment reference cube, and between the experiment reference cube and the alignment template cube must be measured. These are the minimum system requirements. If arc-second coalignment is important, the experimenter will, of course, do much more. It is the accuracy with which he identifies the bias values and the care with which he designs and constructs the experiment while monitoring shifts and compensating for effects that ultimately determine the precision of the final alignment.

Once the interface holes have been installed in the alignment template, the holes are inspected and the cube is verified against the master gage. The template is next fitted with weights for mass simulation. Bearing halves are installed in the interface holes. The bearing halves in the template now define a single unique interface. Next, the template is used to locate test experiment mounts on an alignment fixture. While mounted to the alignment fixture, the gravitational effects on both the unweighted and weighted template are measured by the 180 degree re-orientation technique.

The template is used to locate test mounts in a vibration fixture prior to the experiment acceptance test. For critically aligned experiments, optical measurements should be made, both before and after testing, which relate a fixed reference on the test fixture to the references on the template and on the experiment. This will establish the stability and repeatability of the

experiment and also determine the template-to-experiment reference cube bias values. It is usually after vibration and during experiment calibration that the final bias between the experiment boresight and the experiment reference cube is measured.

The alignment template and the bias values are used to locate the experiment mounts in the support plate. Shims are installed between the experiment mount housing and the support plate to co-planarize mount sets and to insure a good fit to the support plate. Using a template to control the interface, the experiment mounts are adjusted to optically align the template reference to the main pointing vector. On SMM this was the boresight of the fine pointing sun sensor as defined by its template reference and associated bias values. Once adjusted to the correct position, the experiment mounts are dowel-pinned to the support plate. The interface is now aligned and securely locked in place. From now on, only fine alignment adjustments can be made. In two of the axes, this is accomplished by placing ground shims between the bearing seat and the top of the flex blade in the experiment mount. Adjustment of the third axis is accomplished by exchanging the nominal concentric bearing seats with bearing seats of a known offset. One feature of this mount design is that, while close tolerance parts are contained in the alignment path, the actual attachment of the experiment has ample clearance. This permits easy installation and removal of experiments from the support plate at all times.

V. ALIGNMENT VERIFICATION MEASUREMENT

Once all experiment mounts are aligned and pinned to the support plate, the plate is installed in its support structure. Gravity influence measurements are made on the empty support plate as the plate is oriented first up and then down. Unweighted templates are installed on the plate, and measurements are repeated and expanded to include template reference cubes in both gravity orientations. Similar measurements are repeated for weighted templates as shown in Figure 5 and again for flight instruments when they become available. In Figure 9, the support plate with flight experiments installed is shown in an intermediate position between optical measurements. Before a critically aligned experiment is installed on the support plate, gravity influence measurements are performed on it in the same optical test fixture previously used for its template. With all experiments installed on the support plate, the final optical measurement becomes the baseline from which alignment shifts are monitored throughout the observatory integration and test program. The most critical test of the coalignment is launch simulated vibration. In Figure 7, the SMM Observatory is shown in the vibration test facility.

A detailed analysis using NASTRAN is used in parallel with the collection of measured data to predict optical vector alignments. This provides a check on the measured data by identifying questionable values for detailed investigation. Conversely, the measured data is used to validate and revise the math models. This cross-check of alignment data accounted for the

discovery and correction of several inconsistencies in both the measurement technique and the analysis. It also produced a high level of confidence in the accuracy of the math models used for structural analysis.

VI. SYSTEM CONSIDERATIONS

On the surface, this coalignment process appears to contain tremendous expenditures in material, scheduling, and manpower. Relative to material cost, the hardware is completely passive with no complicated mechanisms. Close tolerance machining is required as in any alignment system. The most complicated device is the optical facility equipment required for gravity re-orientation measurements.

In terms of schedule, the majority of the time-consuming optical measurement activities are in parallel with experiment construction,and even then they are phased relative to one another. The time schedule becomes critical when experiments are mated to the support plate and the observatory is proceeding through the integration and environmental testing. By then, coalignment is complete and locked in place, and only shift measurements are performed. Should alignment corrections become necessary, shim sizes are calculated and only verification measurements are required to insure that proper results are achieved. Finally, on SMM not all components require the full coalignment process. Once the experiments were defined, it was found that only two require critical coalignment. Two others require a de-scoped version, while the remaining four have sufficiently large fields of view that the mechanical tolerances are adequate to insure their coalignment. To successfully achieve the coalignment of spacecraft instruments, the design

must accommodate all experiments equally with the most complex and sensitive instrument in the complement. However, with a firm understanding of the capability of the system, its error sources, and their effects, a rational decision can be made in de-scoping procedures to achieve economy in cost, personnel, and schedule.

To understand hardware response and to assess an error budget, a series of developmental tests was required. Some of these tests were: flex blade stiffness measurements, bearing break-away torque measurements, zero-torque attachment effects, interface repeatability measurements, installation sequence effects, and adjustment sensitivity measurements. A demonstration of the template procedure, complete with vibration shift and realignment measurements, was made. A full-scale structural test model of the instrument module was constructed which included mock-up experiments. The structural test model was subjected to vibration, acceleration, thermal balance and a comprehensive set of optical alignment tests.

VII. RESULTS

The real proof of any system or design is in the results. Using the optical cubes mounted on the experiment baseplates, the alignment shift of each experiment after vibration was measured. The results are shown in Table 1. The maximum shift for any single experiment is 18 arc-seconds. Note that the combined measurement uncertainty of the facility for these types of measurements is $\pm$ 10 arc-seconds. The allocation for vibration shifts was 45 arc-seconds.

Using the measured position of the experiment reference surfaces and the bias information, the in-orbit location of the experiment boresights was predicted. The results are shown in Figure 8. This is boresight location data and does not show the extent of the field-of-view overlap for common object viewing. All except three are within the 90 arc-second error circle. No attempt was made to correct these three pointing vectors because one, the ACRIM, has an extremely large field of view; the other two, the FCS and the WLCP, both possess raster capability of several arc-minutes.

Results in orbit indicate that the coalignment goal was achieved. One month after launch, quick-look data was extracted for the critical instruments. The data is shown in Figure 9. The critical instruments lie within a 90 arc-second error circle. Note that both the primary and secondary fine-pointing sun sensors show significant shifts. This was traced to an imprecise identification of the boresight of the sensors and does not represent a hardware shift. Software compensated for this alignment.

In September, 1980, the SMM Project Office at the Goddard Space Flight Center issued this statement: "In-orbit experience has demonstrated that the mutual alignment requirement has been met. Analysis is underway to identify the boresights of the instruments to the 10 to 15 arc-second level of accuracy. This must be done by analyzing scientific data, which is a time-consuming process."

VIII. CONCLUSION

The in-orbit coalignment of experiments has been demonstrated. The success of the alignment system is the total of the success of the hardware design, the alignment techniques, the tests, the measurements, and analysis. No

single element can stand alone. But the simplicity of the system and its ability to adjust to diverse hardware and programmatic demands remove it from the one-time use category. With minor modifications, the coalignment system and its hardware can be adapted to a variety of alignment and coalignment applications.

Table 1

Experiment Baseplate Alignment Shifts Pre to Post Vibration

Experiment	Acronym	Arc-Seconds Y	Arc-Seconds Z
Fine Pointing Sun Sensor	FPSS	-4	+3
Ultravoilet Spectrometer/Polarimeter	UVSP	+16	+6
Hard X-ray Imaging Spectrometer	HXIS	-	-
Flat Crystal Spectrometer	FCS	+2	-8
Bent Crystal Spectrometer	BCS	-7	+5
White Light Coronagraph/Polarimeter	WLCP	+0	-18
Active Cavity Radiometer Irradiance Monitor	ACRIM	-10	+9
Hard X-ray Burst Spectrometer	HXRBS	-	-
Gamma-Ray Experiment	GRE	-	-

Facility Measurement Accuracy $\pm$ 10 arc-seconds

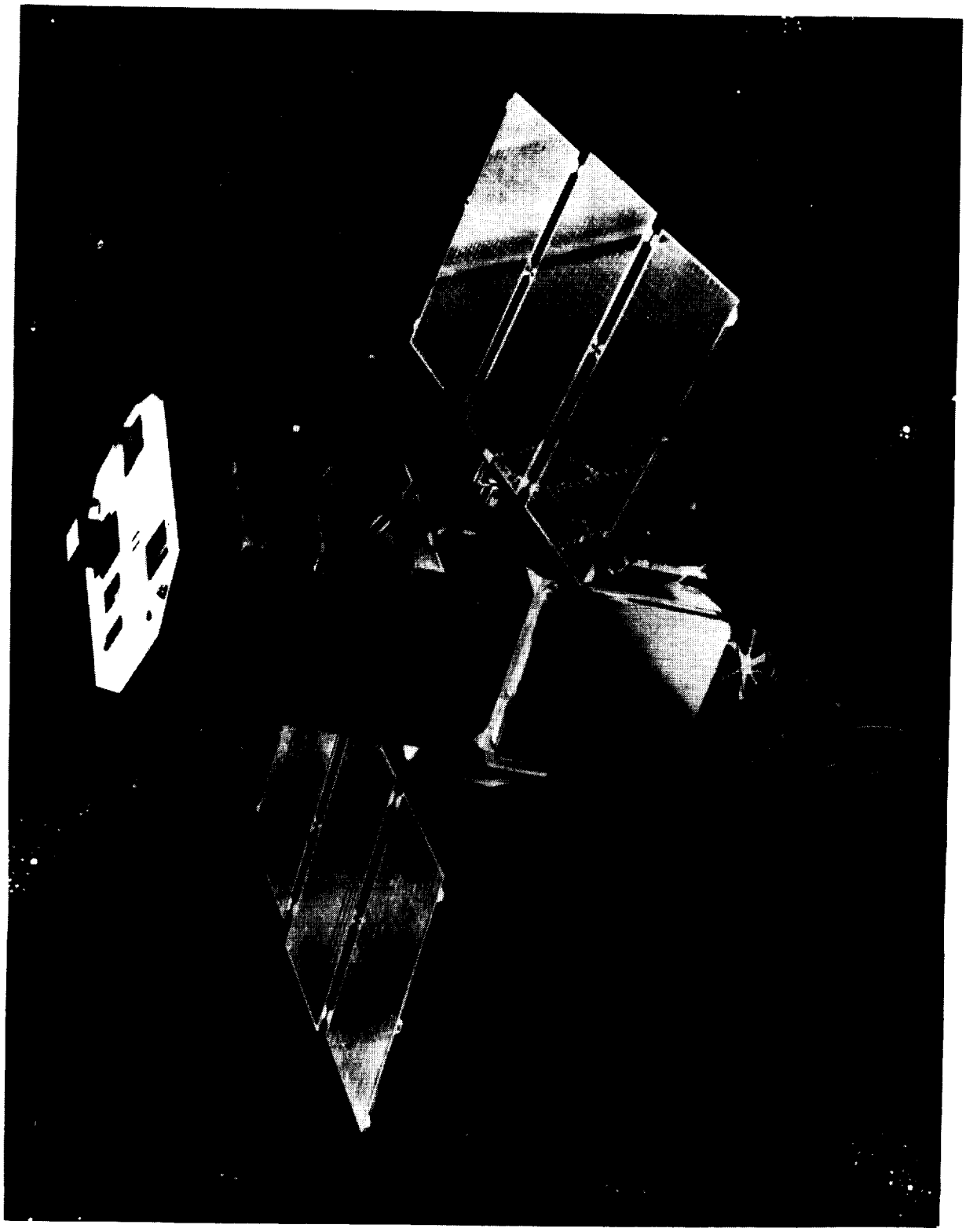

Figure 1.- Solar Maximum Mission Observatory

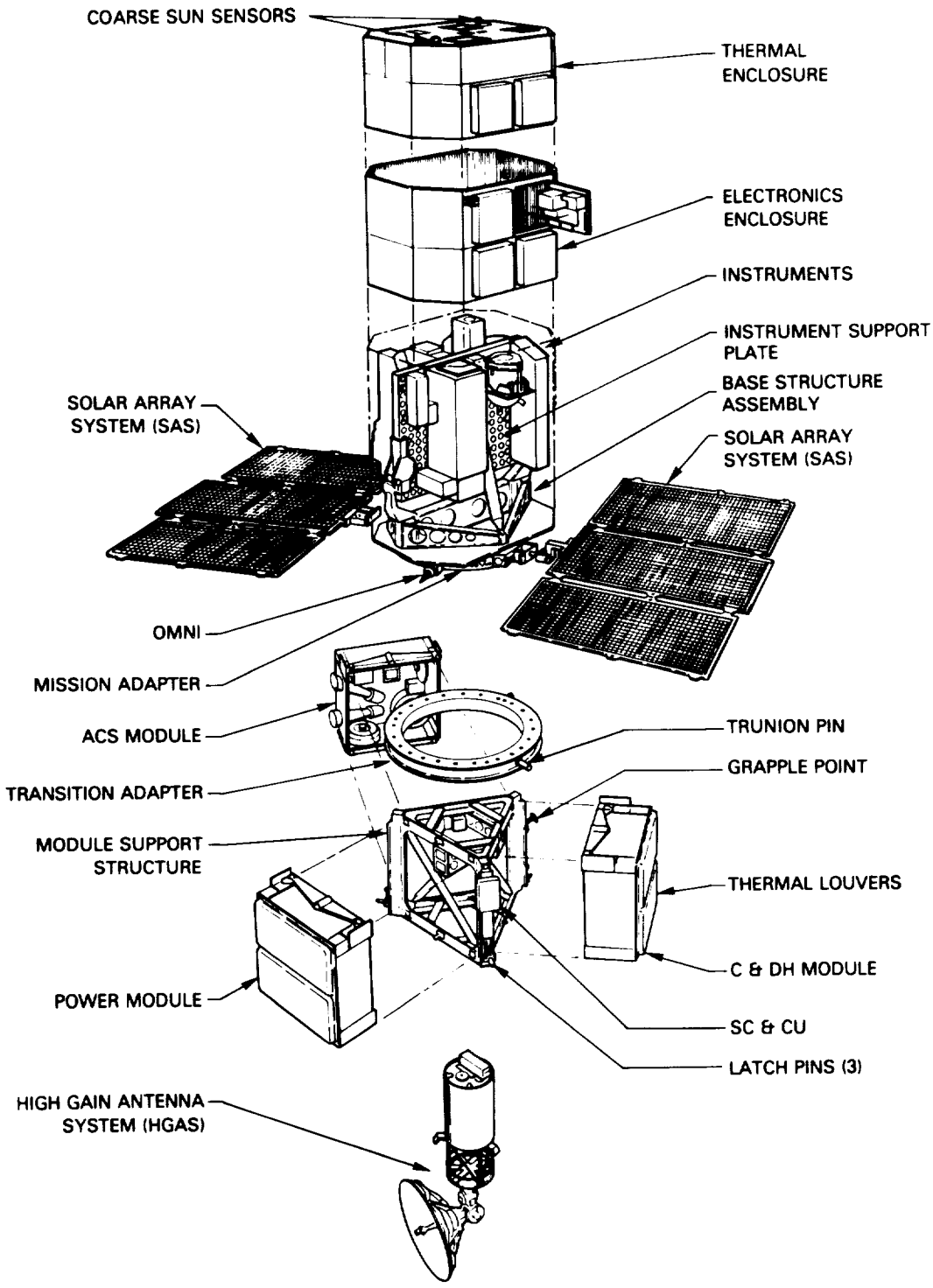

Figure 2.- SMM Observatory Exploded View

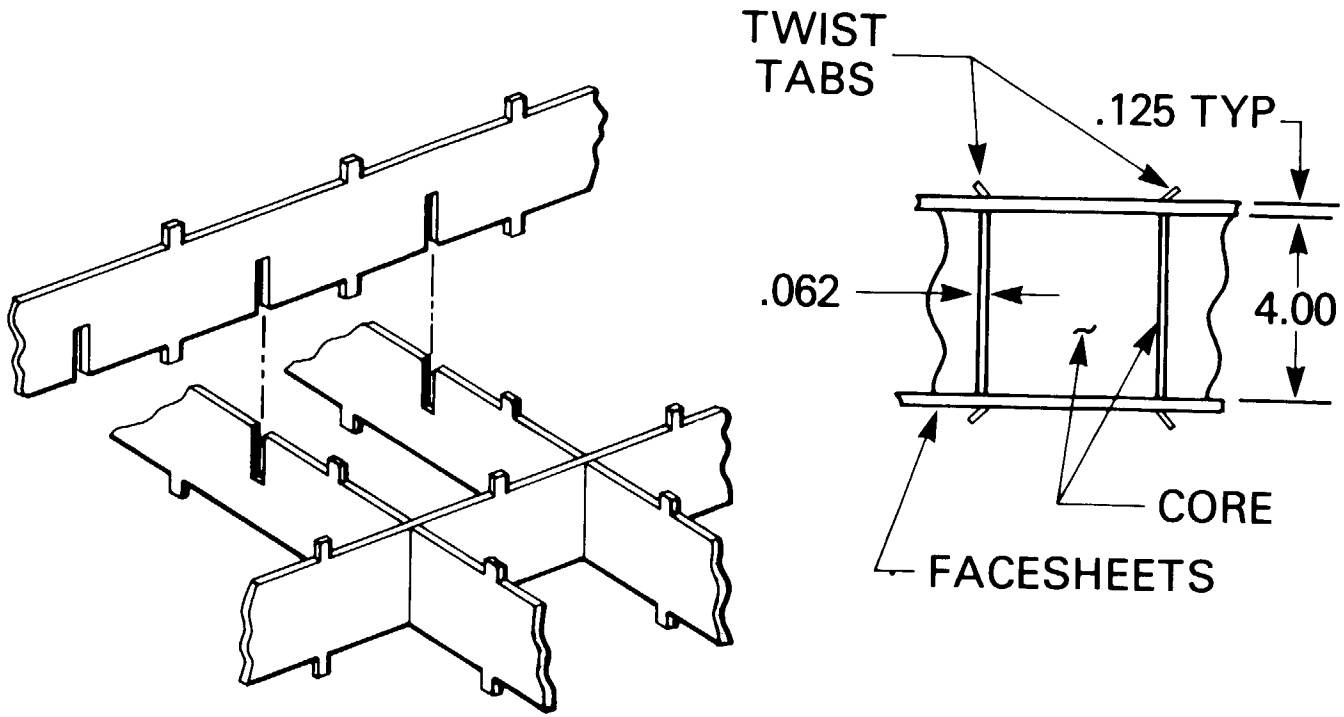

Figure 3.- Experiment Plate Construction

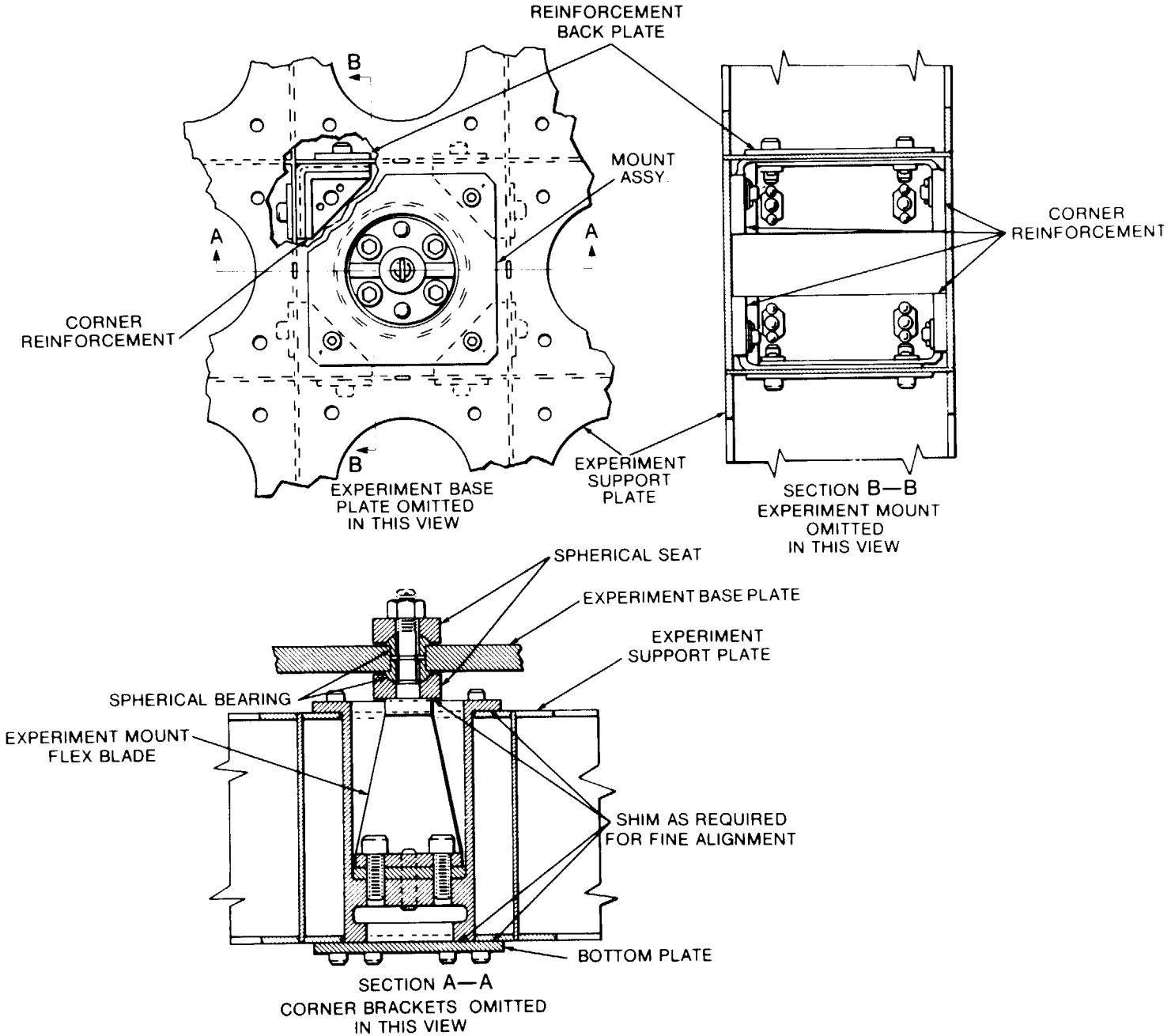

Figure 4.- Experiment Mount Details

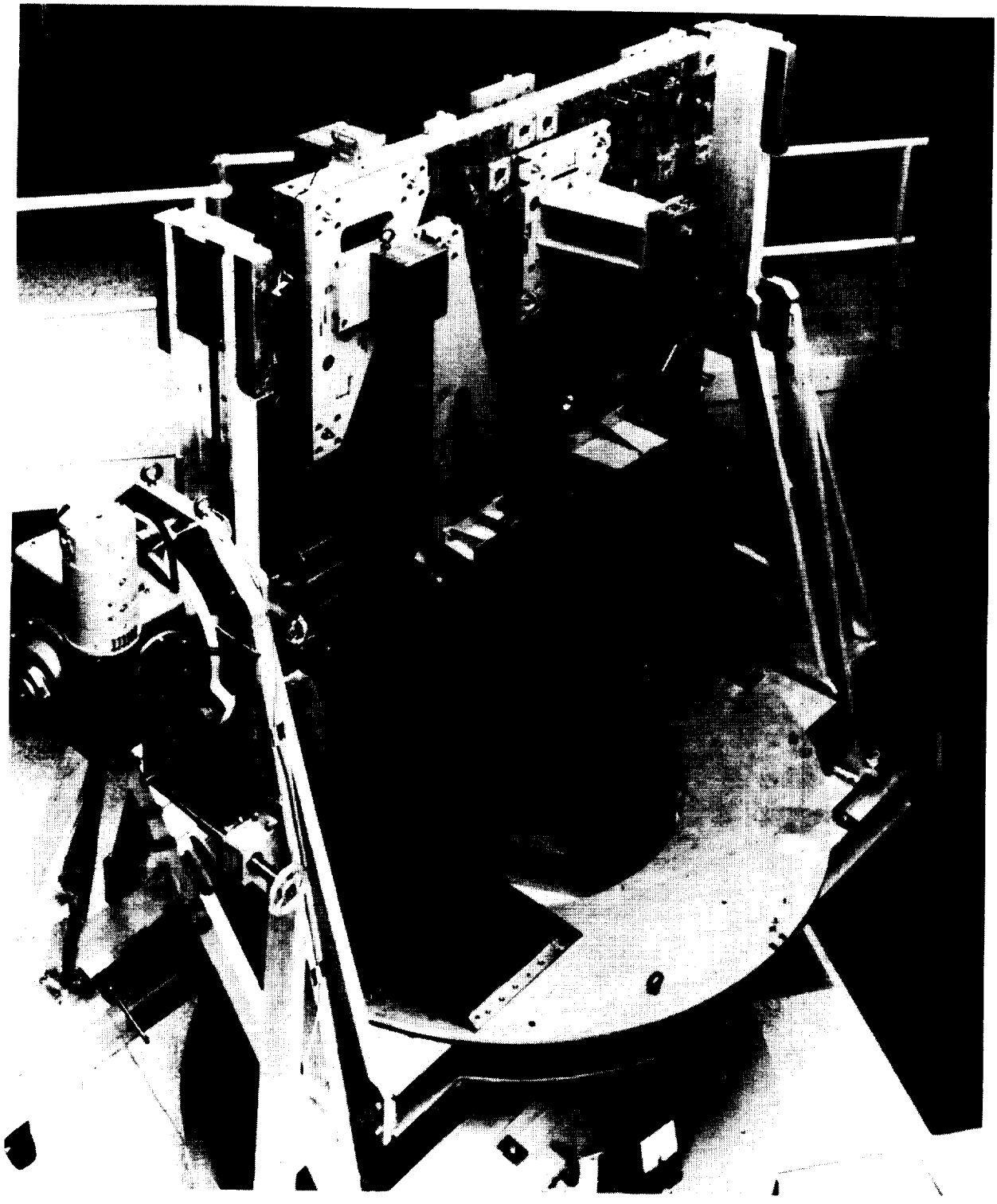

Figure 5.- Experiment Plate with Weighted Templates Optical Measurement, Positive Orientation

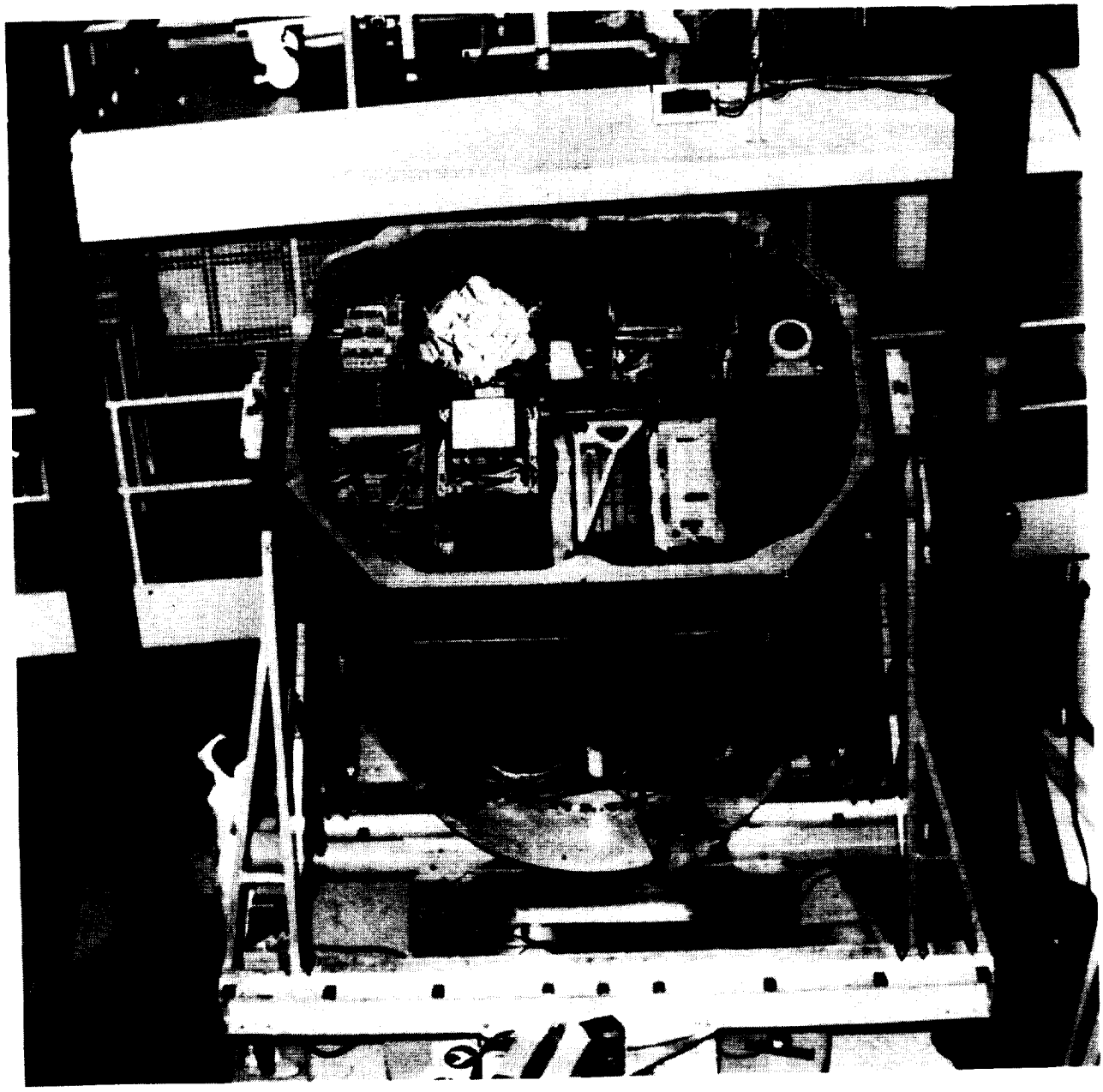

Figure 6.- Experiment Plate with Flight Instruments, an Intermediate Orientation between Optical Measurements

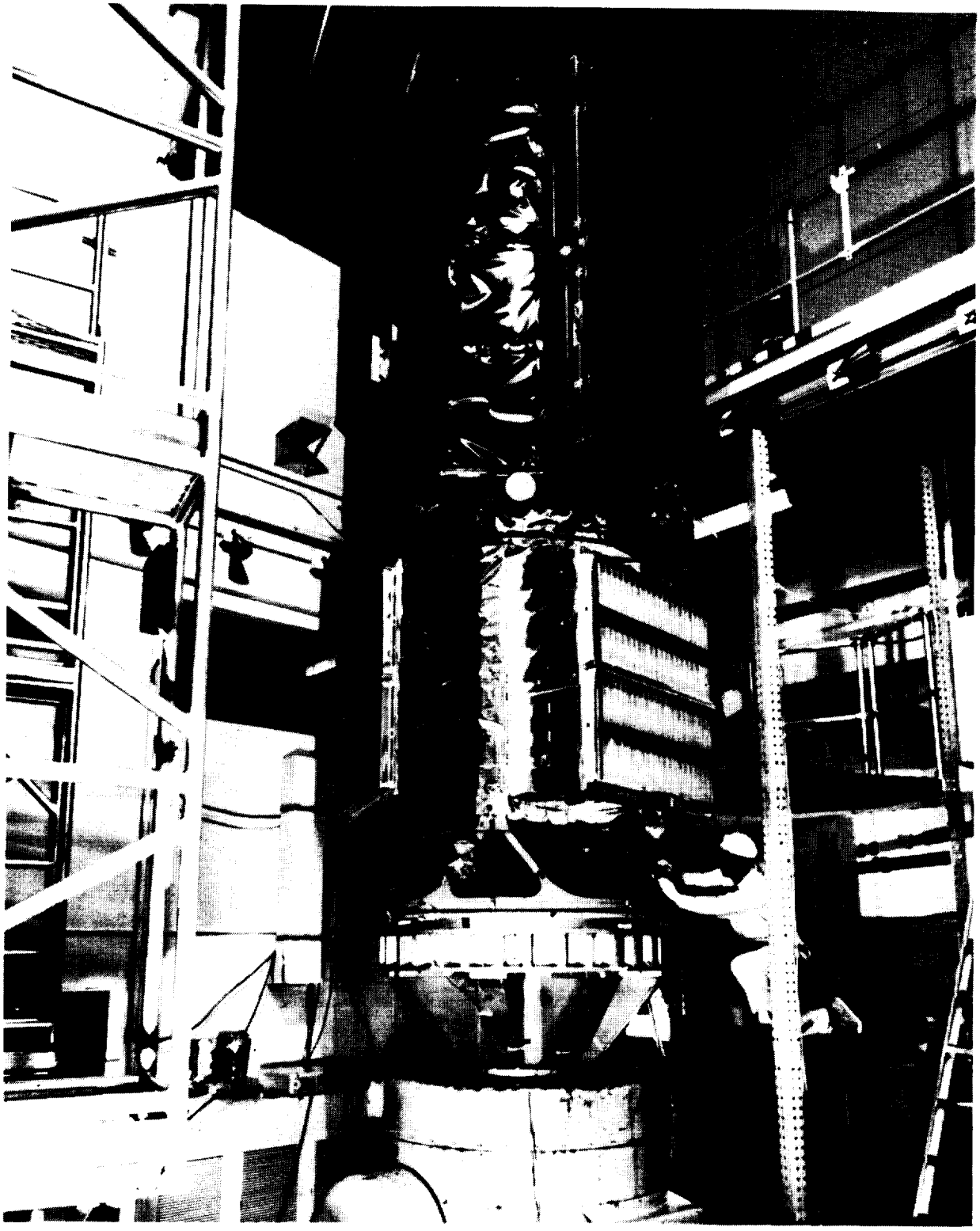

Figure 7.- Solar Maximum Mission Observatory Vibration Test

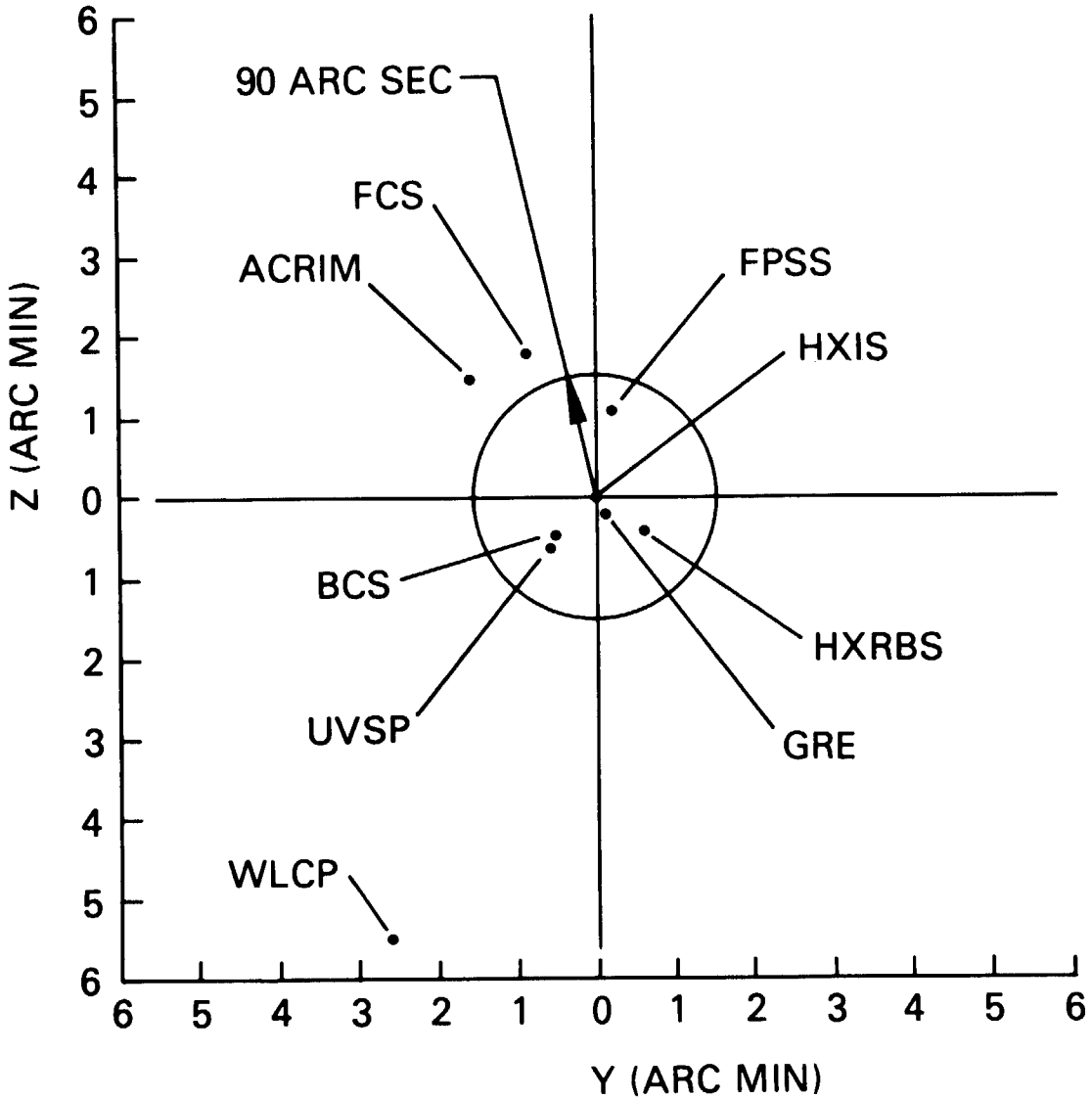

Figure 8.- In-Orbit Experiment Boresight Prediction

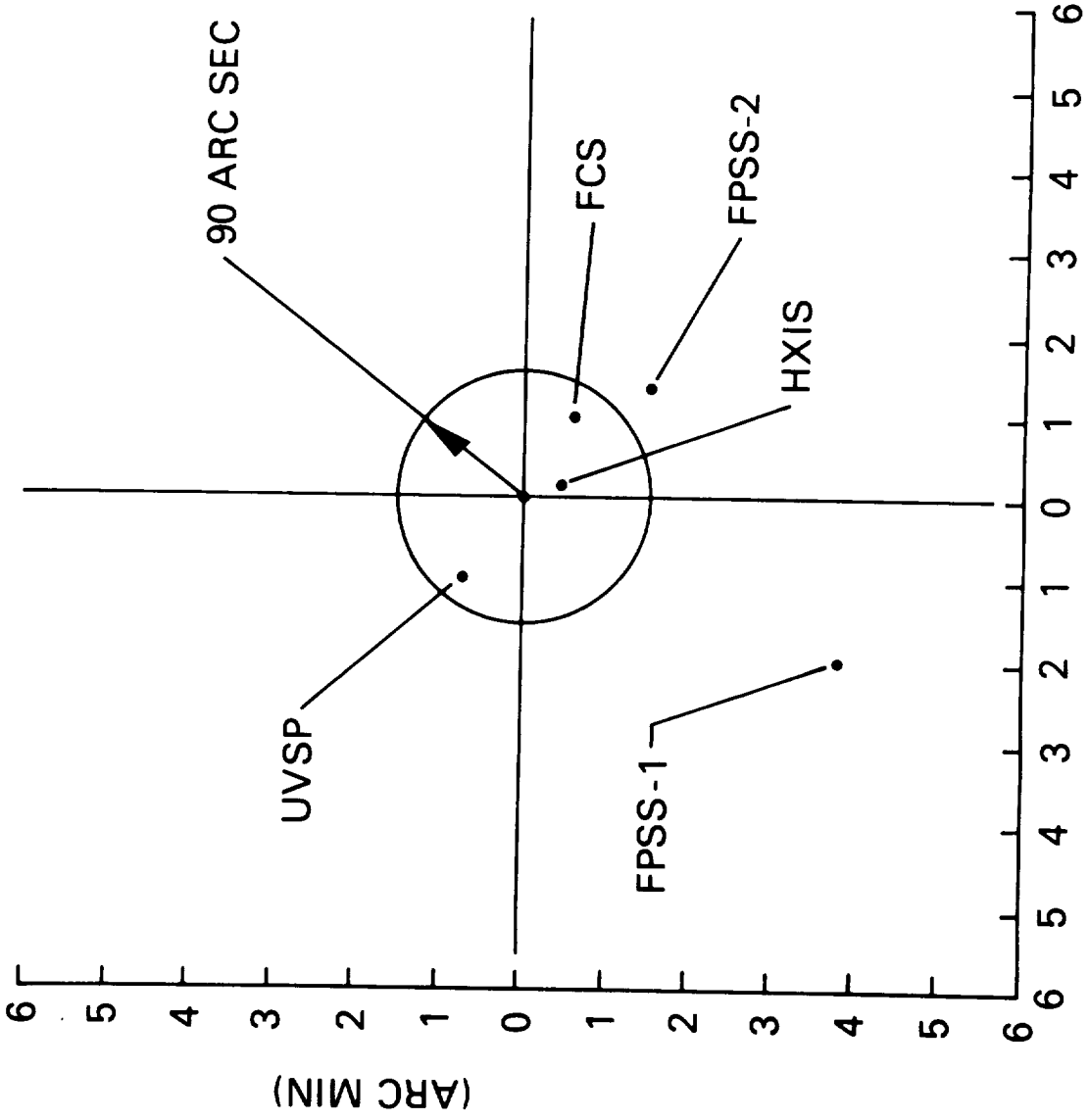

Figure 9.- In-Orbit Experiment Boresight Results (3/80 Data)

ZERO GRAVITY TESTING OF FLEXIBLE SOLAR ARRAYS

D. T. Chung - Lockheed Missiles & Space Co., Inc.
L. E. Young - Marshall Space Flight Center

ABSTRACT

In 1973, the George C. Marshall Space Flight Center (MSFC) began a technology program to demonstrate or develop solar array technology capable of meeting solar electric propulsion (SEP) mission requirements. Two of the most demanding requirements were the need for solar array electrical performance of at least 66 watts per kilogram, and the capability to extend and retract in the zero gravity of space. A contract was initiated with the Lockheed Missiles and Space Company (LMSC) to develop the solar array design and demonstrate or develop the required technology. This program resulted in fabrication, and ground testing, leading to flight of a full-scale wing (124.5 m^2) as an experiment on Shuttle. As a result of the above requirements, the array structural weight had to be reduced to such an extent that Kapton, instead of the conventional aluminum honeycomb materials, was used in the design as the substrate for mounting solar cells.

In order to develop the solar array design and prove the feasibility for extension and retraction in space, a series of "zero-g" flights in a KC-135 aircraft was a part of the technology test program. Six full-size panels (36.83 cm. x 398.78 cm. each) and 12 half-size panels were extended and retracted in the "zero-g" provided by the KC-135.

A test structure was specifically designed and built by LMSC for "zero-g" flight testing and is easily modified, depending upon the test specimen configuration. It mounts directly to the aircraft floor, with the specimen contained to survive ground handling and flight loads. The test structure is fully automatic for extension and retraction; however, there is a manual override to continue testing in the event of a power loss to the drive motors.

The flexible solar array test specimen (6 panels or 12 panels) was successfully extended and retracted numerous times in the KC-135 aircraft within the "zero-g" period of flight. Five flights have been successfully conducted with blanket specimens containing various panel stiffening patterns, standard cell simulation, thin cell modules, low cost cell modules and reflectors.

The flights have significantly contributed to the flexible solar array design development and ultimately to the potential success of the SEP Solar Array Shuttle flight experiment.

INTRODUCTION

Lockheed Missiles & Space Co., Inc., (LMSC) in Sunnyvale, California, in conjunction with the National Aeronautics and Space Administration (NASA)/Marshall Space Flight Center (MSFC) in Huntsville, Alabama, has had the responsibility for the design, development, manufacturing, and zero gravity flight testing of the flexible solar array specimens of various configurations. The specimens were required to automatically extend or retract successfully during a zero gravity maneuver of the KC-135 aircraft. When successful extension or retraction occurs, the flexible solar array panels demonstrate hands-off proper unfolding or folding, respectively.

HISTORY

The Zero Gravity Program was started in 1957 at Wright-Patterson Air Base in Dayton, Ohio. The first 3 years were a difficult period because authorized funds were not available. The original aircraft was a C-131 and its pilots were Air Force Captains Gene Kerr, deceased, and John Simons, retired. During those first 3 years, numerous problems occurred. Two of the more significant ones were periodic loss of oil pressure resulting in propeller control problems, and zero gravity time which was too short — 15 seconds (maximum). Consequently, no sponsors were available to fund the program. However, the two pilots continued to make unauthorized maneuvers and recorded data and eventually alleviated the lost oil pressure problem. Finally, a sponsor was obtained and proper funds were made available. The original aircraft was then refurbished and used until 1960.

The original C-131 was then replaced with the first KC-135 aircraft, and the most significant gain was achieved: increased zero gravity time of 25 to 30 seconds instead of 15 seconds. Also, it was a standard KC-135 with a modified hydraulic system to prevent cavitation.

Since 1957 and up to the present time, a total of ten aircraft were used; three C-131s, presently all retired and seven KC-135s, of which three are retired, one crashed into the side of a mountain and another one crashed upon approach. The remaining two are still very active. One is dedicated to wing lift testing at NASA/Edwards in California. The other is dedicated to various NASA centers and military funded programs and is located at NASA/Ellington AFB in Houston, Texas.

Figure 1 shows the KC-135 aircraft trajectory and significant information for a zero gravity maneuver.

FLEXIBLE SOLAR ARRAYS

All zero gravity testing of flexible solar arrays was sponsored by NASA/ Marshall Space Flight Center (MSFC) under Contract Number NAS8-31352.

The first three tests utilized the full-size six-panel configuration. The primary objectives were the following:

1. Demonstrate proper solar array foldup in a zero gravity environment
2. Determine a minimum efficient level of stiffening that assures proper array foldup during array retraction in zero gravity
3. Determine array extension/retraction rates for satisfactory operation
4. Obtain film and acceleration history data during zero gravity operation to acquire design improvement information.

The last two tests utilized the half-size six- and twelve-panel configurations. Their primary objectives were the following:

1. Demonstrate that the flat fold solar array foldup design, using a significant number of panels in a half-scale model, will properly fold in a zero gravity environment

2. Observe retractions using several guide wire configurations in order to obtain best possible flat fold operations

3. Utilize the KC-135 aircraft test facility and test fixture hardware regardless of solar array panel sizes

4. Obtain film and acceleration history data during zero gravity operation of the model to evaluate the design

5. Obtain temperature history data during zero gravity operation of the model to evaluate its effect on the design.

The test structure (Figures 2 and 3), which is bolted to the aircraft floor, is designed to do the following:

1. Automatic extension/retraction and array tension capabilities

2. Manual override in case of loss of aircraft power

3. Variable rate control within predetermined time limit

4. Preload capabilities to prevent damage during shipment, aircraft takeoff, landing, and high g level during flight maneuvers

5. One g support for the extended array to preclude damage to cell simulators and panel stiffeners

6. Working surface for changes of panel stiffening configuration

7. Walk-through surface for flight crew members.

SOLAR ARRAY MODULE (SAM) — SEPTEMBER 1976

This test specimen consisted of six full-size panels with glass cell mass simulators bonded to 0.0051-cm (2 mil) thick mylar substrate. A two-guide wire negator system, located approximately 25 percent in from each specimen edge and integrated to the hinge line with guide wire retainers, was used to provide panel direction guidance and support during extension and retraction operations. The panel stiffening material was fiberglass epoxy with a cross section of 0.058 cm x 0.254 cm (0.023 in. x 0.100 in.) and consisted of maximum, medium, and minimum stiffening. (See Figure 4.)

Pictorial documentation was provided by two movie cameras, one stationary and another hand-held, and one still camera. Colored tape was strategically located on the panels to aid in determining the shape of the panel. An optical grid located opposite to the movie cameras was used to establish panel curvature during extension and retraction operations.

Zero gravity testing lasted three days with the following results, conclusions, and recommendations:

1. The stiffening material (fiberglass epoxy) was taped to the kapton substrate, and thermal expansion differences were not considered. This problem has to be resolved prior to any space flights, and one suggestion is to have sleeved stiffeners.

2. Inconsistent g loads created deflections in the fold and hinge lines during retraction causing reverse bending of the panels. This is an undesirable condition. However, the panels did right themselves prior to closeup. Three 180-degree bend memory springs of beryllium-copper material, 0.030 cm x 0.635 cm x 3.81 cm (0.012 in. x 0.25 in. x 1.50 in.) were used at the center and guide wire positions of the fold and hinge lines, and folding improved. In addition, guide wires are to be located under a stiffener.

3. The flat fold array foldup design was sufficiently demonstrated to operate successfully in a near zero gravity environment of a space flight operation.

4. Prior to an actual space flight, aircraft testing of the final panel design with the exception of the solar cells (replaced with glass mass and size simulators) will be done.

5. Test method selected is the best method available for the demonstration desired. It provided a sufficient amount of information on array panel motion in a low gravity environment, which can be used to advantage in future development testing.

6. Selected slow and fast rates did not appear to affect foldup operations of the panels.

7. The colored tape and optical grid is not needed to determine shape and curvature of the panels.

CONCENTRATOR SOLAR ARRAY — APRIL 1978

The test specimen (Figures 5 and 6) consisted of two pup tent reflector pane assemblies made from aluminized kapton and two full-scale panels (0.571 m x 3.988 m) using glass mass and size simulators bonded to 0.0051-cm thick mylar substrate. It also contained a thin cell (0.0051 cm) electrical module mounted on the inboard (stationary base side) panel. Stiffener configuration on half panels is around the perimeter and inboard at the quarter points. Stiffener configuration on the reflectors is around the perimeter and seven intermediate

points across the pup tent. A two-guide wire system, located under the panel stiffener quarter points, was used to support the test specimen during extension and retraction operations.

Documentation was pictorial only, and was the same as the previous test. In addition, a television video cassette was used which provided immediate evaluation of the operation. It was extremely valuable because daily evaluation was necessary to determine results.

Testing was done over three days and following are results, conclusions, and recommendations:

1. Interference of the moving cover support fittings and one of the side support tables caused much difficulty while in flight. Under these conditions, only minor adjustments were made and only manual testing was continued. Since then, the test support hardware has been redesigned and the problem eliminated.

2. Static electrical charges on the reflectors prevented them from taking a planar shape. (Two sides of the same tent curved toward each other.) Manual assist did not eliminate the problem. A slip sheet was placed between reflector surfaces to alleviate interface sticking. In addition, the aluminized surfaces were grounded to the structure. Some improvement was noted. Another idea was added, which was spraying static guard in the pup tent (back side of the reflective surface). Subsequent reflector and panel profiles were very good.

3. Some reverse bending of the panels did occur under higher g loading, but in all cases they righted themselves prior to closeup (Figure 7). Design improvements and further testing will overcome the problem.

4. It is feasible to incorporate in-plane concentrator reflectors into a flat fold solar array system.

5. Zero gravity testing provided invaluable assessment of array panel design. It is also a logical in-process test to check out design worthiness.

6. Instant replay television camera system provides excellent coverage for immediate postflight review and analysis. This is an excellent tool in providing guidelines for the course of action.

LOW COST TERRESTIAL CELL SOLAR ARRAY — MAY 1979

The test specimen was made up of three full-scale panel (0.762 m x 3.988 m per panel) solar arrays. Two panels consist of solar cells and glass slide mass and size simulators. One panel has only mass and size simulators. Stiffener configuration on half panels are around the perimeter and inboard at the quarter point (Figure 4, minimum stiffening). A two-guide wire system was used to support the test specimen during extension and retraction separations.

Documentation was pictorial, namely, movie and still cameras, as well as the instant replay television cassette recorder. In addition, a digital g counter was included, and it was located in view of the movie camera to relate the g levels to the test specimen shape and motion.

Zero gravity testing took two days and following are results, conclusions, and recommendations:

1. Design changes to the test structure were demonstrated in flight and the results were positive.

2. The flat fold array foldup design again demonstrated its adequacy, and there were no significant problems during any extension or retraction operations.

3. The g counter and test specimen shape and motion relationship idea is a good one. Unfortunately, because of its size and camera distance, the g-level counter was impossible to read. This relationship is very important to a final panel configuration. A recommendation was made to include both a visible g counter setup and a temperature sensor as part of the instrumentation.

ONE-HALF SCALE SIX PANEL SOLAR ARRAY — SEPTEMBER 1979

The test specimen consisted of six half-scale panels (0.381 m x 1.994 m per panel) solar array and each contained glass slide mass and size simulators. In order to achieve half-scale to full-scale panel stiffness equivalency, the half-panel stiffener configuration consisted of a longitudinal one at the fold line and three transverse ones, one at the center and one each located approximately 12.5 percent in from the end. The longitudinal and transverse stiffeners were not joined. There were three different sets of guide wire systems:

1. Under center, 5.08 cm from outer stiffeners and free end. See Figure 8 (Five-guide wire system).

2. One each located 5.08 cm from outer stiffeners. See Figure 9 (Two-guide wire system).

3. Same as No. 1 except move the two intermediate guide wire systems between the center and outer stiffeners. See Figure 10 (Five-guide wire system).

INSTRUMENTATION

Studies of film of the panel test specimen extension/retraction motions revealed the need for measurement of accelerations perpendicular to the extended panel test specimen plane. A knowledge of these accelerations would facilitate correlation with panel folding characteristics.

In this test, an accelerometer (Klister servoaccelerometer Model 303) was mounted in the base of an equipment rack with its axis perpendicular to the floor of the aircraft. Four 6-volt batteries in series provided power. The rack also contained an x-y recorder (Moseley Model 135) which measured acceleration. Recorder power was provided by the aircraft 115 vac, 60 Hz source. The output of the accelerometer was connected to the x-input of the recorder. Sensitivity of the accelerometer was 1.0 volt/g. The rack was located in the field-of-view of the recording cameras on the opposite side of the panel test specimen such that the arm of the recorder was easily observable by the cameras. Recorder controls were adjusted such that right and left limits of arm deflection represented +0.05 g and -0.05 g, respectively. An operator was required to remove the accelerometer input when accelerations with magnitudes greater than ±0.05 g were experienced. Test periods with accelerations outside these limits were classified as no test conditions.

The test time span was three days and following are the results, conclusions, and recommendations:

1. The first day, 25 maneuvers were dedicated to extension and retraction operations using the five-guide wire system. Although some puckering occurred, in all cases the panels righted themselves prior to closeup.

2. Significant temperature decrease which did not occur on previous flights.

3. Two-guide wire system was a total disaster in that random reversed bending of the hinge and fold lines occurred during retraction. Assistance was provided to closeup the test specimen.

4, A five-guide wire system was used and after nine maneuvers and a significant decrease in temperature, all following retraction operations were failures.

5. Wherever a transverse stiffener is located, a guide wire shall be within 5.08 cm from it to eliminate a reverse fold direction.

6. Continuity between transverse and longitudinal stiffeners is necessary to provide a picture frame effect to achieve proper fold and hinge line movement.

7. Hinge and fold line loop clearances shall be minimized to decrease undesirable amounts of relative panel motion at the start of folding.

8. The foldup design should be demonstrated in the KC-135 environment, but a g-level limit should be established. If that limit is exceeded, a no test condition is declared.

9. The KC-135 aircraft flight test zero gravity simulation remains the best available tool for proper zero gravity operation of the array.

10. The instrumentation worked well except for high frequency noise observance in the recorder arm deflections. This noise was an annoyance when studying film of the test operations, but was not sufficiently large to void recorder data.

HALF-SCALE TWELVE PANEL SOLAR ARRAY — JUNE 1980

A change was made in the definition of panel size. The original size (half-scale) was 0.381 m x 1.994 m. The present size (half-scale) is 0.1905 m x 1.994 m, and a full-scale panel size is now 0.381 m x 3.998 m.

A series of recommendations were made based on the evaluations and analysis of the previous flight. These recommendations were incorporated into the design, and additional objectives (Reference, page 4) were added to the zero gravity test program. They were the following:

1. Demonstrate that the flat-fold solar array foldup design, using a significant number of panels in a half-scale model and including recommendations of the previous KC-135 aircraft flight, will properly fold in a zero gravity environment.

2. Demonstrate the validity of the picture frame concept with hairpin-type springs located at the transverse panel stiffeners of the frame.

3. Demonstrate that the amount of hinge and fold line loop is adequate to eliminate undesirable relative panel motion when folding begins.

4. Scaling down the twelve half-panel mass to 0.075 g for one g testing indicated that the guide wire does not have to be under a stiffener for this panel configuration.

The test specimen consists of a twelve half-scale panel (0.1905 m x 1.994 m per panel) solar array (Figure 11). Four panels contain glass slide mass and size simulators, and the remaining eight are made up of aluminum platelet mass and size simulators. Each stiffener configuration is a picture frame, two longitudinal ones, 0.216 cm from the hinge and fold line and five transverse ones approximately equally spaced across the panel. All twelve panels have this frame. Across each hinge and fold line is a spring-loaded delta (double) hinge design featuring hairpin-type springs made of 0.0356-cm diameter spring steel. The springs are taped to the frame at the intersection of the transverse and longitudinal stiffeners, thus achieving frame continuity. In addition, they also provide panel-to-panel continuity (Figure 12). The two-guide wire system is the baseline. However, the design has provisions to add one, two, or three more guide wires.

INSTRUMENTATION

The instrumentation for this test was the same as that discussed in the previous test with the following exceptions:

1. An electronic circuit was incorporated between the output of the accelerometer and the x-input of the recorder. The was done to attenuate frequencies above 10 Hz and to limit input levels to the recorder to the range of ±0.05 volts even during periods when g levels exceeded ±0.05 g.

2. A cabin temperature display circuit was added such that cabin temperatures were observed by the recording cameras. This temperature circuit consisted of an analog device AD 590 solid state temperature sensor with its output connected to the y-input of the same x-y recorder. The y-pointer on the recorder arm was increased in size so so that it was easily observable by the cameras. The scale on the recorder was ajusted to display the range of $40^{o}F$ to $90^{o}F$.

Zero gravity testing took three days,and following are the results, conclusions, and recommendations:

1. As documented on film, all extensions and retractions were successful.

2. Spring-loaded delta hinge design provided a pup tent shape as soon as retraction started, and it demonstrated proper and controlled folding throughout its total travel distance.

3. Rates did not appear to affect the operation.

4. Guide wire tensions were changed from 0.226 kgm (0.50 lb to 0.113 kgm (0.25 lb) and all subsequent extensions and retractions were successful. Guide wire tension loads are based on natural frequency and g-level requirements and will vary based on those requirements.

5. On the second day of testing, one of two guide wires broke during the first retraction. Folding shape and motion look good, so a decision was made to continue testing. Subsequent tests continued to show good folds, resulting in an increased level of confidence of the hinge design.

6. After guide wire repair and subsequent tests, guide wire drag was noted. But like the broken wire, operations were not affected.

7. Pulled out delta hinge pin on the three final retractions with one of the acceleration levels at 0.12 g. Folding was still successful.

8. During extensions, sticking occurred near the edges where the flat conductor cables are taped to the panels. This was due to inadequate taping procedures. This is an area of concern, so special attention must be provided for any flight hardware.

9. The instrumentation arrangement worked very well and proved to be a substantial asset to the analysis of camera data. In this test, the effects of cabin temperature on the panel test specimen folding characteristics were not observable.

CONCLUDING REMARKS

Zero gravity testing in the KC-135 aircraft of flat fold flexible solar array test specimens has sufficiently demonstrated the adequacy of the panel design. The aircraft flight crew has provided invaluable assistance and has significantly contributed to the design and development of the flexible solar array, and ultimately to the potential success of the Solar Electric Propulsion (SEP) Solar Array Shuttle Flight Experiment Program.

REFERENCES AND ACKNOWLEDGEMENTS

1. R. V. Elms, Lockheed Missiles & Space Co., Inc., SEPSAFE Program Project Leader, Zero Gravity Testing Final Reports, 1976 to 1980.

2. L. E. Young, Marshall Flight Space Center (MFSC), SEPSAFE Program NASA Coordinator.

3. R. Shurney, Marshall Flight Space Center (MFSC), NASA Zero Gravity Testing Coordinator.

4. D. Griggs, Retired, Johnson Space Center (JSC), NASA Zero Gravity Test Director.

5. L. Magers, Johnson Space Center (JSC), NASA Zero Gravity Test Director.

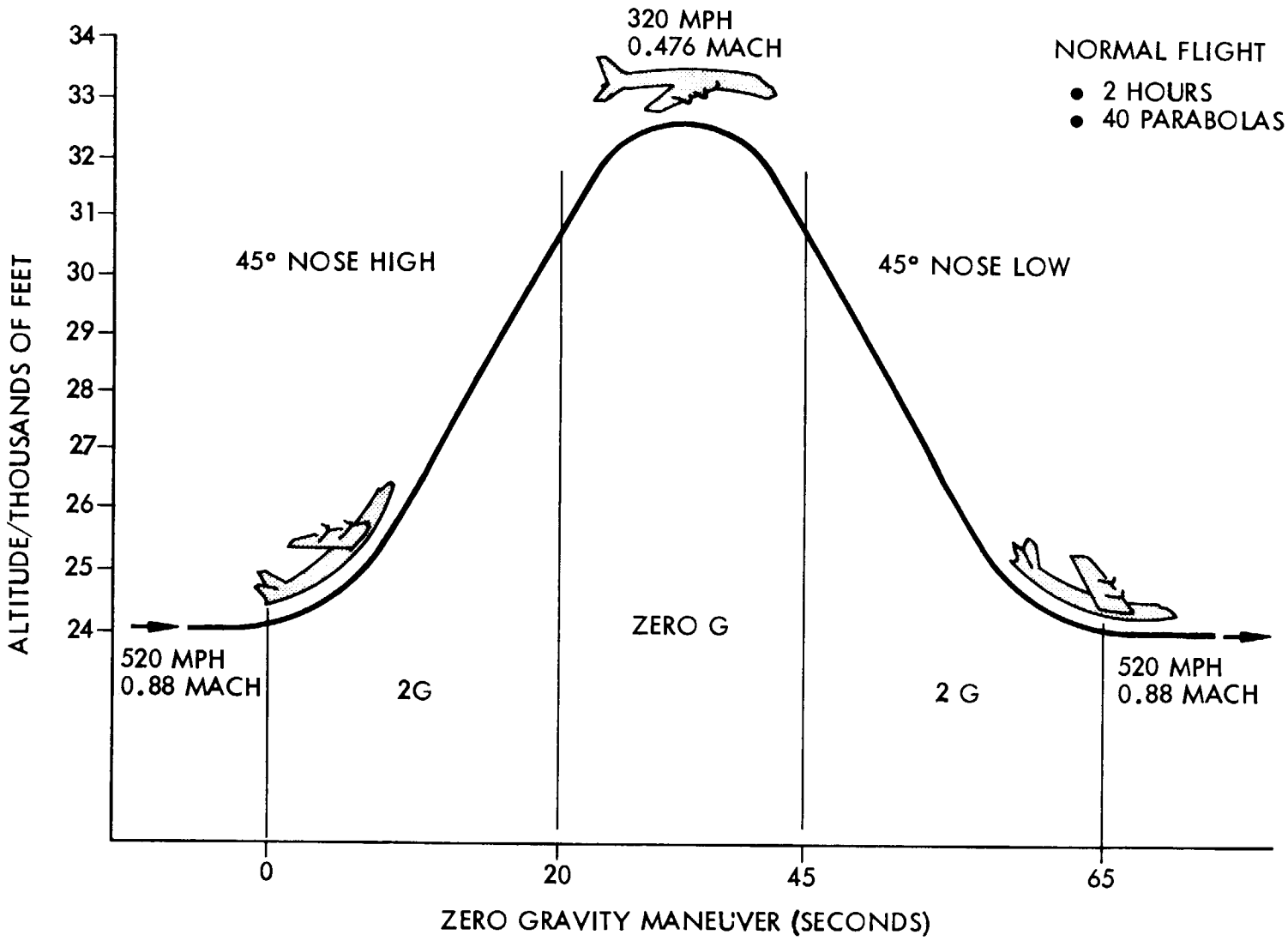

Figure 1. KC-135 Aircraft Trajectory

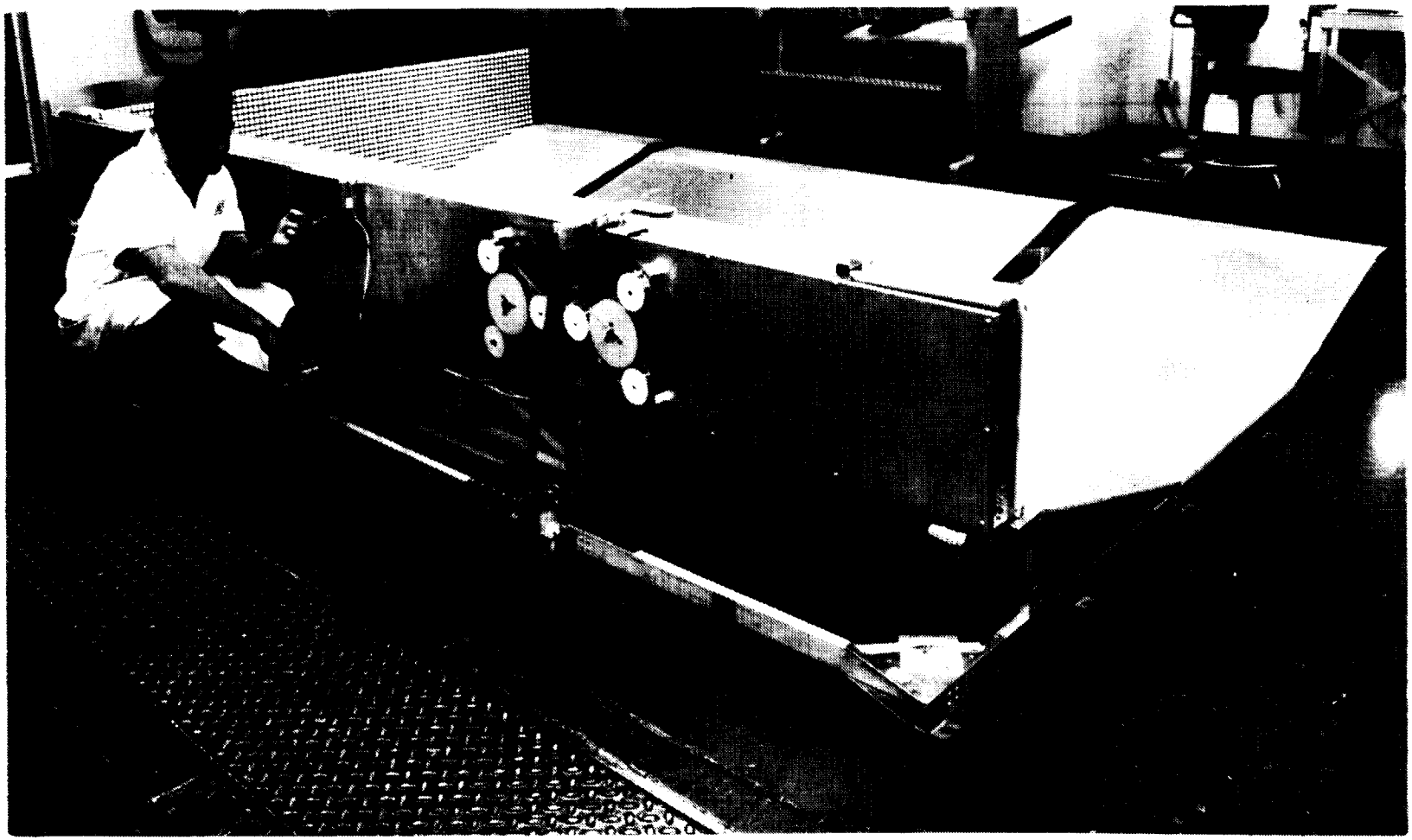

Figure 2. Zero-Gravity Test Solar Array Module and Support Table (Technology Evaluation)

Figure 3. KC-135 Zero Gravity Flight Test Structure

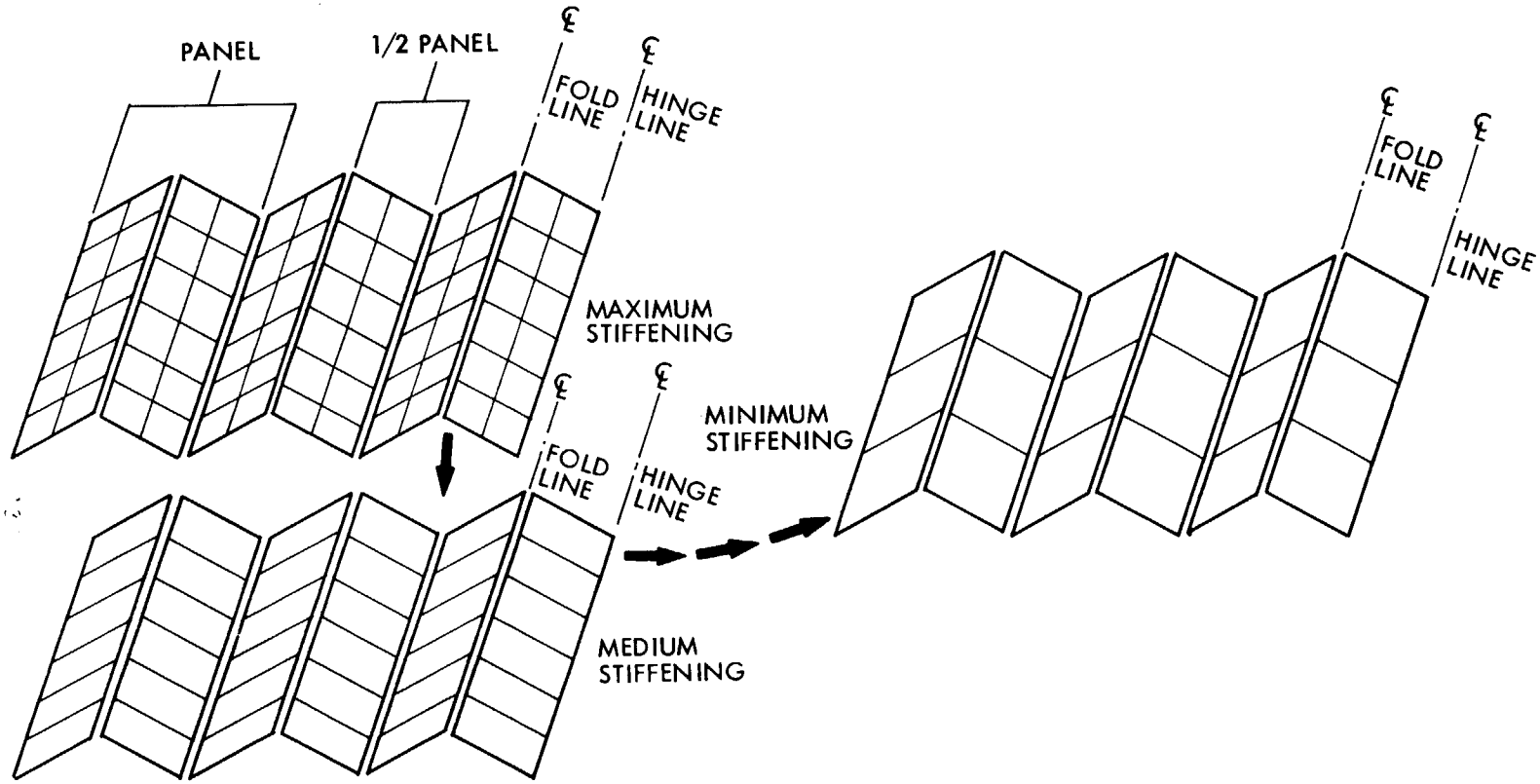

Figure 4. Test Panel Stiffening Configuration

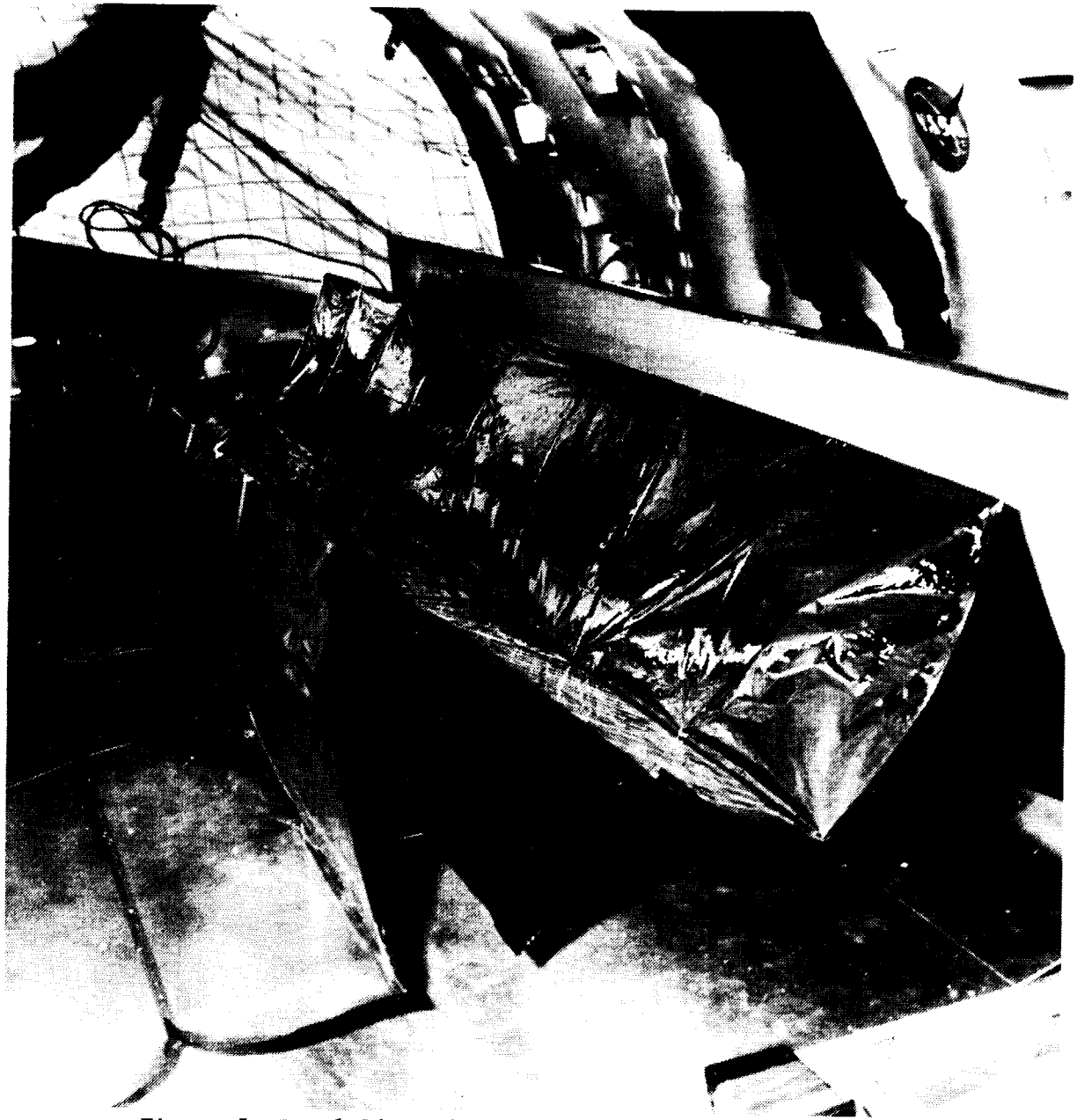

Figure 5. Panel Planarity at Full Deployment and Zero g

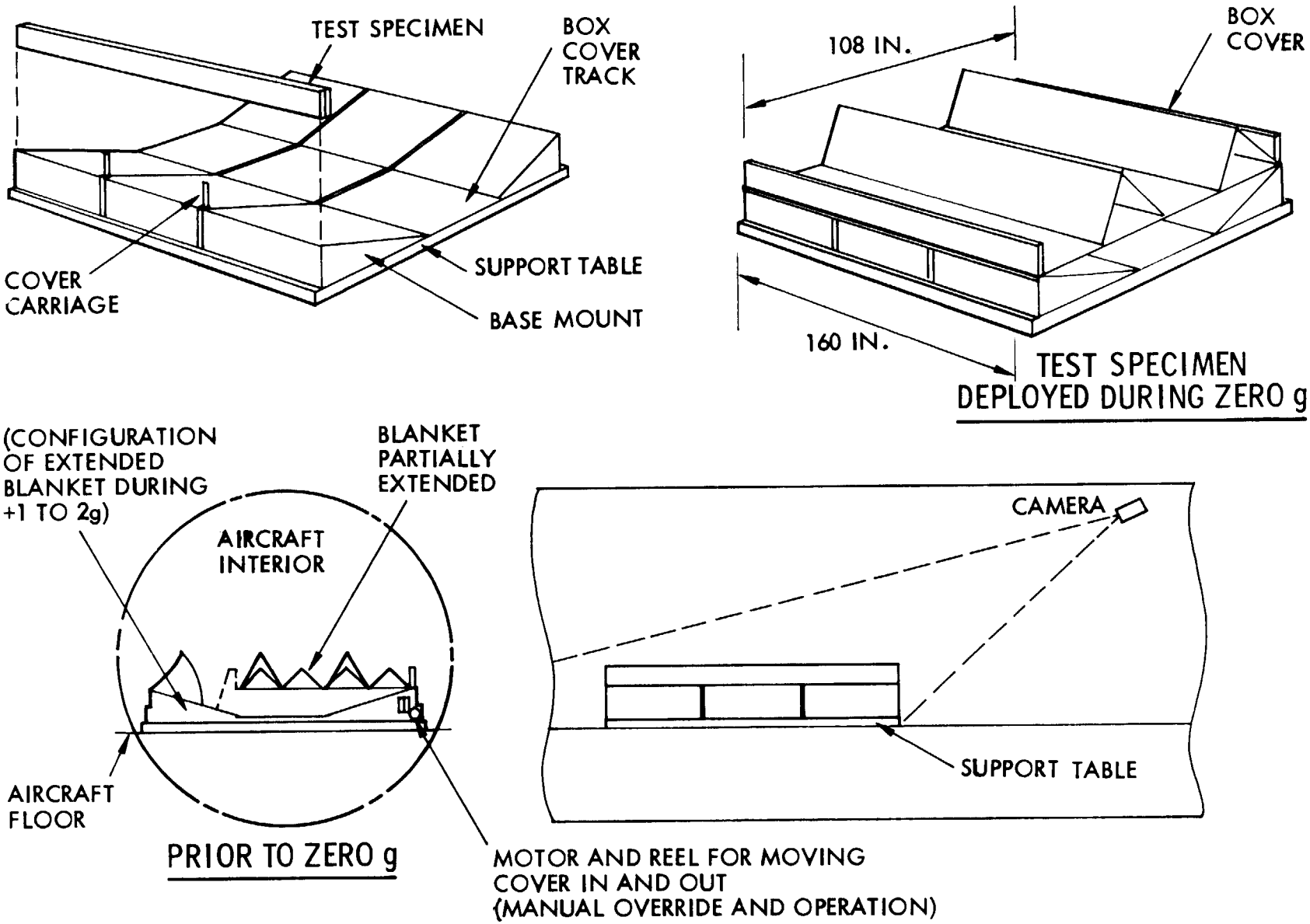

Figure 6. Concentrator Array KC-135 Test Setup

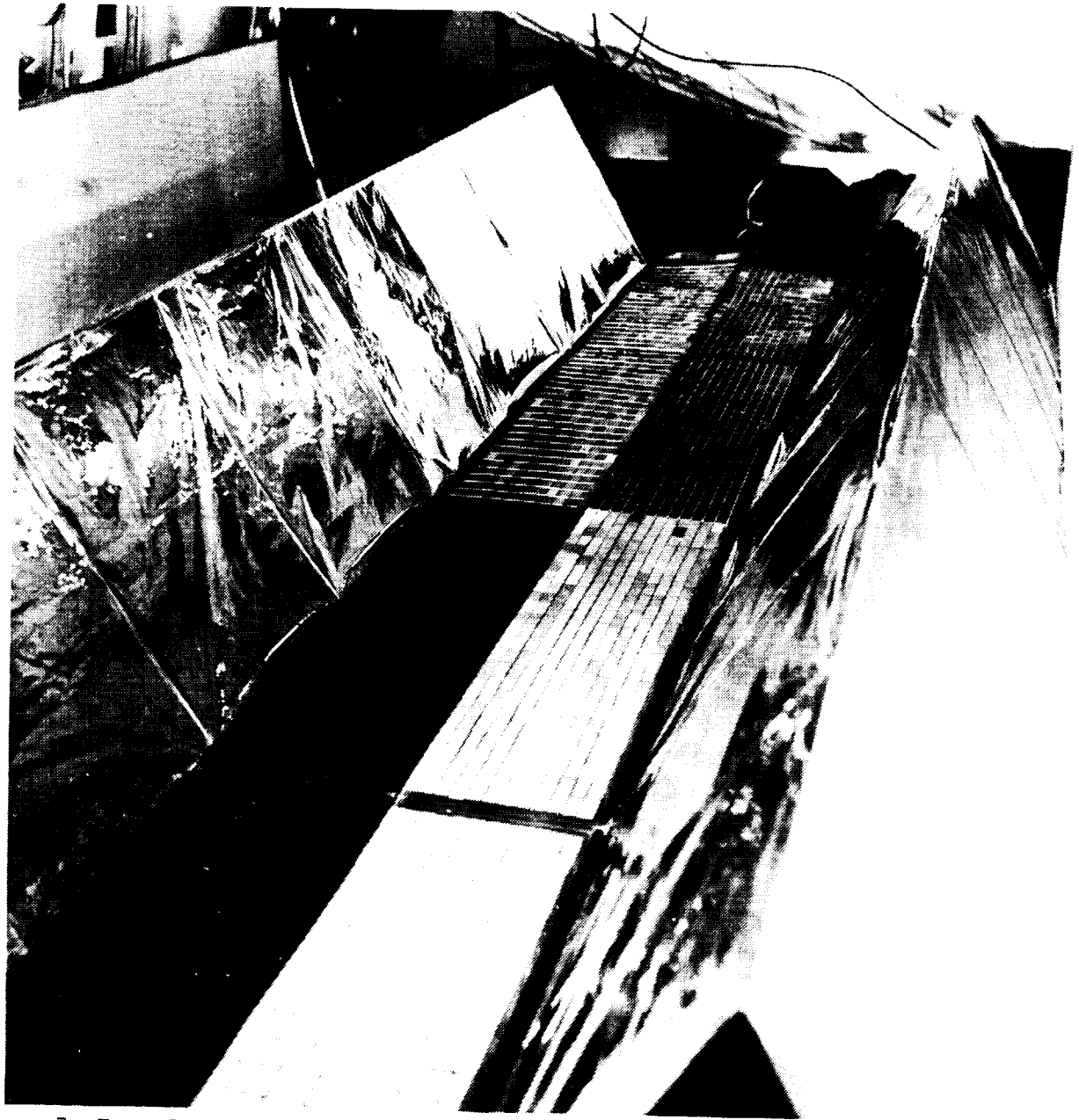

Figure 7. Test Speciment Nearing Full Deployment Under Slight Negative g Loading

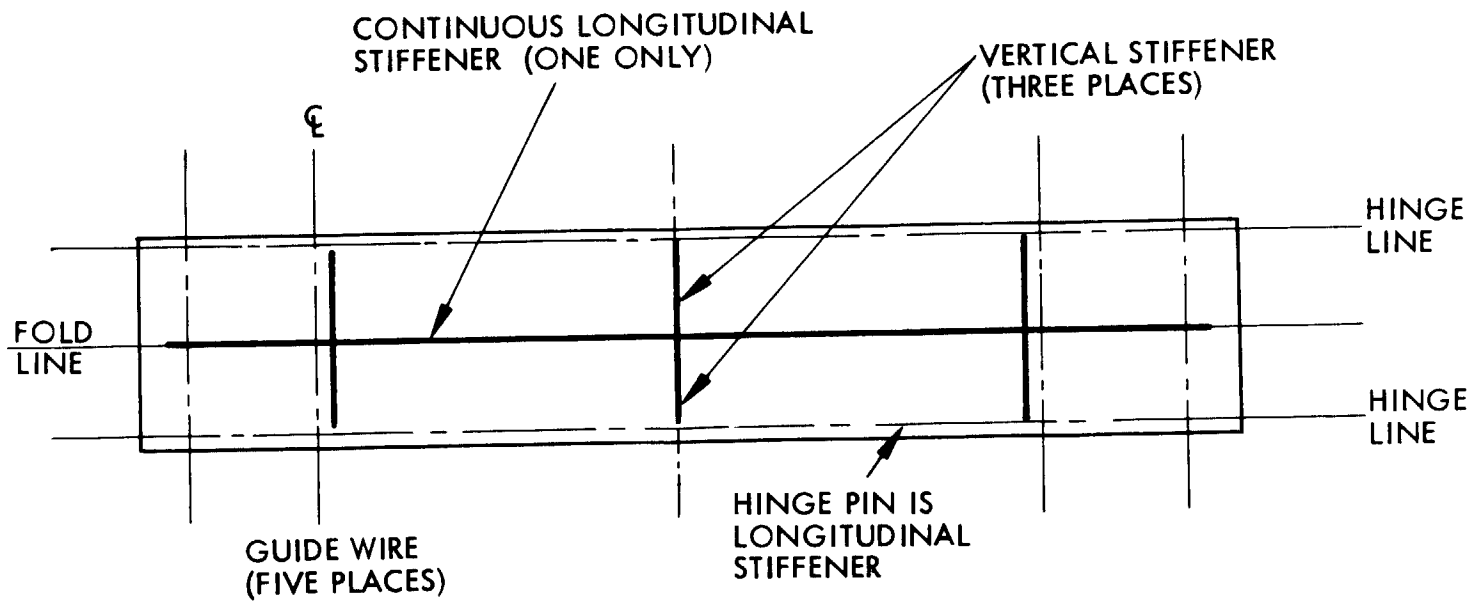

Figure 8. First Five-Guide Wire Blanket Test Configuration

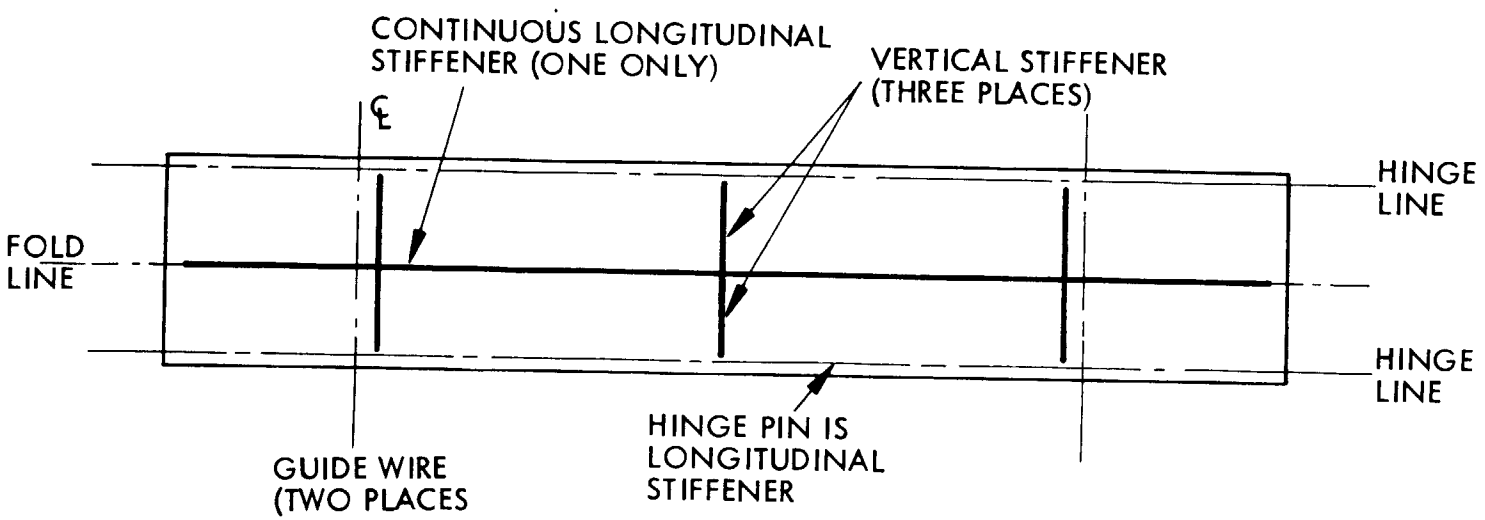

Figure 9. Two-Guide Wire Blanket Test Configuration

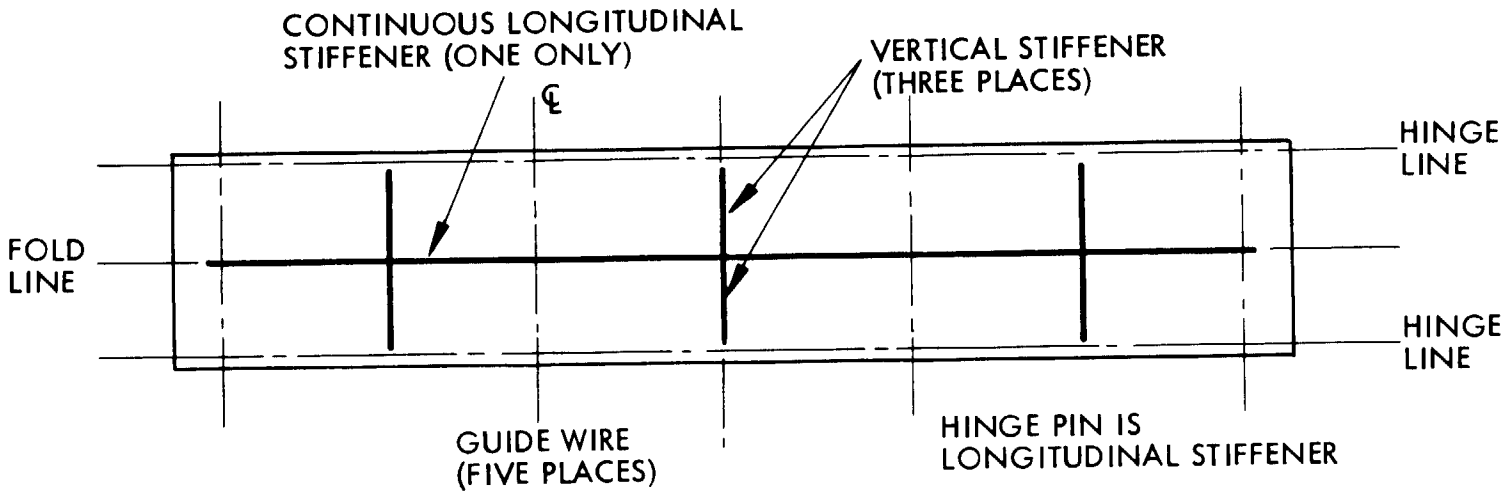

Figure 10. Second Five-Guide Wire Blanket Test Configuration

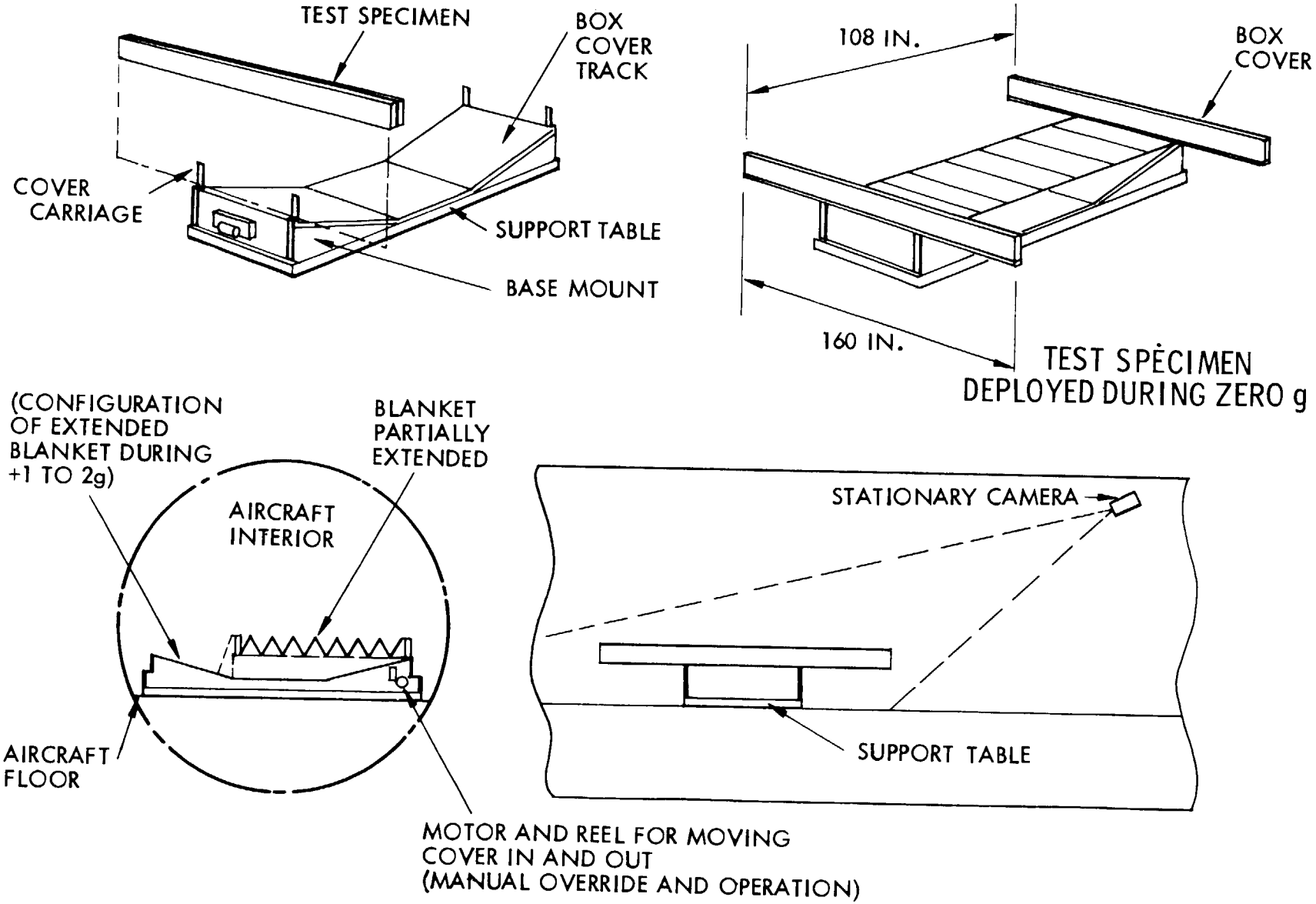

Figure 11. One-Half Scale Solar Array KC-135 Flight Experiment

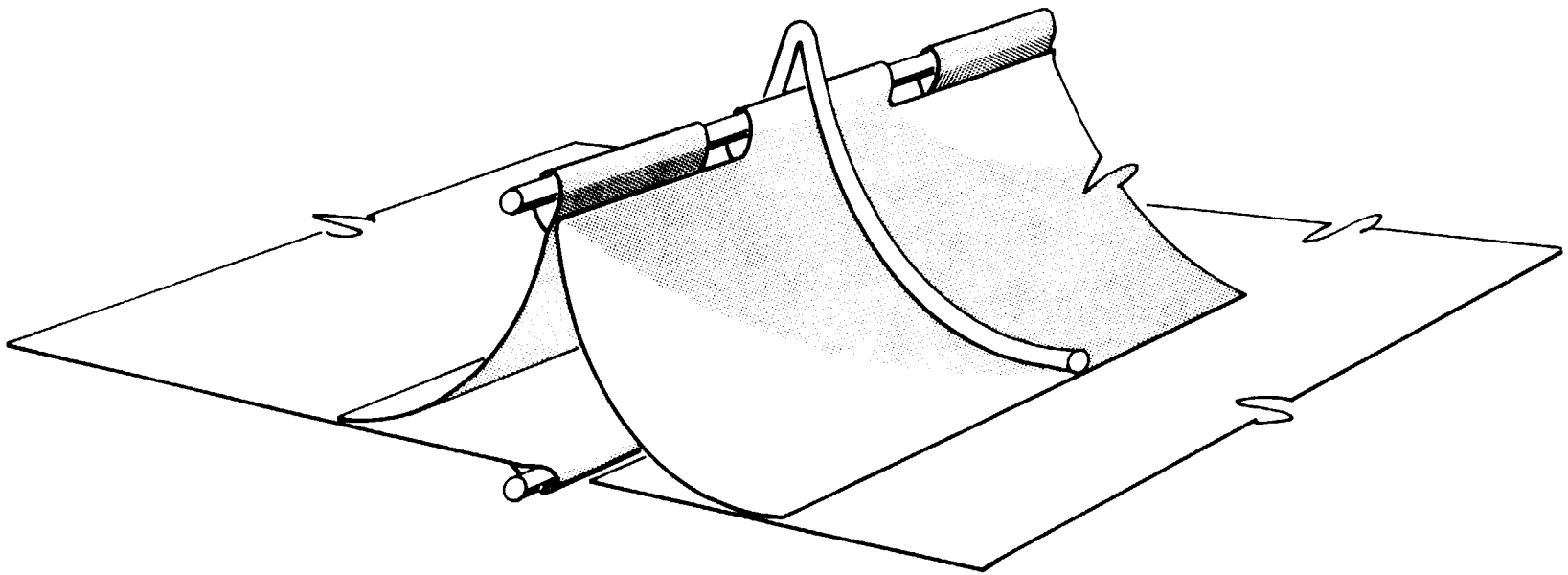

Figure 12. Spring-Loaded Delta Hinge

SPACE-DEPLOYABLE BOX TRUSS STRUCTURE DESIGN

John V. Coyner, Jr.* and William H. Tobey*

ABSTRACT

This paper summarizes the development status of Denver Aerospace's deployable box-truss structure. Potential applications for this structural system are described briefly. Structural and component design requirements derived from these applications are discussed. Components of prototype 4.6-m cubes which incorporate graphite/epoxy structural members, fittings, and mechanisms are described. The benefits of the component designs and their respective manufacturing processes are presented.

INTRODUCTION

Large Space Systems (LSS) launched aboard the STS Orbiters during the 1980s will use deployable antennas and platforms rather than structures manufactured or assembled on-orbit. The deployable structures present significant design challenges, and several different approaches are being pursued to meet them. These approaches can be grouped generically as radial rib, hoop-column, or truss structures. In this area, Denver Aerospace is developing a deployable box-truss structural system applicable to flat and curved antennas, platforms, and beams. The system features compact stowage, step-by-step deployment, high deployed precision, convenient payload attachment points, and adaptability to a wide variety of structural configurations.

Regardless of configuration, a box-truss structure such as the one shown in Figure 1 is composed of repetitive deployable frames. The frames are shaped by telescoping diagonal braces that span both frame diagonals. Two of the frame sides are hinged in the middle and fold toward each other for stowage. The hinge mechanism contains springs and an overcenter latch mechanism that drives the deploying structure and provides an impulse at deployment completion to apply tension to the truss diagonals and an antenna surface, if present.

The truss deploys in a sequence of steps that can be monitored and controlled by astronauts on the Shuttle Orbiter's aft flight deck. This sequence dissipates the deployment energy in an incremental manner, thereby reducing the possibility of producing structural failure in the deploying truss.

The following sections discuss the designs for all structural elements and mechanisms in the deployable box-truss. Specifically covered are the hinges, telescoping braces, structural members and fittings, and deployment drive/latch mechanisms that are designed for low-cost production and high

*Martin Marietta Denver Aerospace, Denver, Colorado

reliability and, at the same time, are capable of supporting launch, deployment, orbit transfer and operational loads. Potential operational systems range from small diameter (15 meter), offset-fed parabolic reflectors to 300-meter diameter systems that use either continuous trusses or box-truss hoops capable of supporting stretched membranes, meshes or arrays, both flat and curved.

Aspects of the design evolution that has taken place to bring the system to its present level of maturity are presented. The full-scale hardware elements are prototypes of composite-membered frames, cubes, and trusses. This evolutionary process has focused on reducing cost and weight and on increasing structural and thermal performance and reliability. While this process has been taking place, significant progress has also been made in applying the box-truss component technology to other structural configurations such as tetrahedral trusses and deployable masts.

APPLICATIONS

NASA, DOD, and industry studies have identified requirements for satellites that are much larger than present satellites. The space applications potentially requiring LSS technology include: phased-array radars, communication systems, radiometers, laser system support, space power systems, radio astronomy telescopes, etc. Consideration of the capabilities of the STS Orbiter clearly shows that very lightweight deployable structures will be required. Figures 2, 3, and 4 illustrate a variety of systems that can be implemented using Denver Aerospace's deployable box-truss.

DESIGN REQUIREMENTS

Practical, deployable large space systems must: (1) meet operational antenna and payload requirements for deployed shape accuracy and dynamic and thermal performance; (2) be compatible with launch in, and deployment from, the STS Orbiter; (3) use the Orbiter efficiently; and (4) be capable of withstanding loads imposed by orbit transfer propulsion systems. Analyses have shown that the Orbiter launch and orbit transfer loads are the dominant drivers of structural member and fitting sizes. Maximum loads in localized box-truss axial members and fittings range from 400 to 4000 newtons and minimum gage components are sized to accommodate 400-n loads. Deployment actuators, typically springs, are sized to overcome frictional resistance and provide tension to the antenna surface and truss diagonal braces while keeping the deployment energy below the amount necessary to fail the deploying structure due to excess kinetic energy.

COMPONENT DESIGNS

As shown in Figure 1, the deployable box truss is composed of three types of structural members: vertical members, surface tubes, and diagonal tapes. The vertical members are typically flanged square tubes as shown in Figure 5. This design facilitates compact stowage and restrains the telescoping diagonal tapes during launch. Each vertical member's load carrying capability can be varied easily by changing its flange dimensions. In a minimum gage truss, the flanges are omitted.

Figure 6 shows a 4.6-m laminated graphite/epoxy vertical member before installation in a truss frame. The member is assembled, from the five components shown, using room-temperature-cure adhesive. The central square tube is autoclave-cured on a silicone rubber mandrel within a two-part aluminum mold. The flange sections are autoclave-cured in a female aluminum mold. The finished vertical member is substantially stronger and stiffer than required for a 4.6-m deep truss because the member's cross section was designed to be applicable for truss frames up to 10-m by 10-m. The key features of this design are its: low-cost, low coefficient of thermal expansion (CTE); easily variable structural characteristics; compact stowage; and compatibility with launch restraint and load requirements.

The surface tubes, Figure 7, are autoclave-cured on an aluminum mandrel that has a reduced end diameter to provide an integrally-molded end fitting. This eliminates the need for separate fabrication and installation steps for reinforcements at the hinge pin locations. The benefits of this design are low cost, low CTE, and easily tailorable structural parameters.

Figure 8 illustrates the diagonal braces that telescope for stowage and deployment inside each frame. Their flat tape and tube configuration uses integrally molded end stops as shown. The stowed flat tube extends from the corner fitting to the surface tube's midlink hinge when stowed (Figure 5) to protect the flat tape during launch. The four tapes are linked by a crossover fitting that performs functions in addition to bridging the gap between the stowed, deploying, and deployed diagonals. Each crossover fitting, restrained by cup-and-cone shear ties on the vertical members when stowed, holds the midlink hinges in place and provides a compression load path between adjoining vertical members during launch. As in all the box truss components, the diagonal braces and their fittings are designed for low cost, weight, and CTE. Further, the tape cross section can be increased by a factor of three, if required, without impacting any other components in order to accommodate higher loads in the vicinity of an orbit transfer stage interface.

The box-truss structural members are joined together at the cube corner fittings. As shown in raw form in Figure 9, these compression-molded, graphite fiber reinforced components provide the flanges and cavities to accept the surface tube and diagonal brace hinge pins and the vertical member square tube and fins. The fitting's top plate, which supports stowed compression loads, is the location for the deployment-release solenoid latches. The fitting material, Fiberite E21718, is a mixture of 13-mm graphite fibers in an epoxy resin matrix. Compression molding these components with this material reduces production costs by 70 percent and CTE by 80 percent compared to machined metallic fittings.

Perhaps the most interesting mechanism in the deployable box truss is the midlink hinge and overcenter latch mechanism shown in Figure 10. Except for steel hinge pins and springs, these devices are fabricated entirely with laminated graphite/epoxy materials to substantially reduce the coefficient of thermal expansion compared to metallic hinge/latch assemblies. All of the graphite/epoxy components are simple layups and are produced in bulk quantities. After the individual parts are shaped, they are assembled in a fixture that provides

the precise alignment and drilling guides required for surface tube alignment and proper overcenter latch operation. The mechanical advantage of the overcenter latch multiplies the torque of the latch drive spring dramatically as its surface tube approaches and achieves full deployment. Figure 11 shows this mechanical advantage as a function of the angle between the surface tube halves. This torque multiplication is necessary to reach full deployment because both diagonal braces in a truss frame are placed in tension, typically 40-n or more, when the frame deploys. This tension level is set high enough to prevent the diagonal braces from slackening under operational load conditions. This eliminates nonlinear truss dynamics. Thus the midlink hinge/latch is a low-cost low-CTE device that meets several structural and mechanical requirements.

CONCLUSIONS

The Martin Marietta Denver Aerospace deployable box truss is a state-of-the-art space structure system. With little modification, its components can be used to form platforms, dishes, rings, and beams. Its development to prototype status is coinciding with the firming of requirements for such structures in the 1980s and early 1990s. Each component in the truss has been carefully designed to be low in cost, reliable and versatile and to meet the demanding requirements imposed by manufacturing, assembly, test, launch, deployment, and deployed operations. This attention to detail is reflected in the finned square tube vertical members; tubular surface tubes with integral end fittings; compression molded, graphite-reinforced corner fittings; telescoping diagonal braces; and the midlink hinge/latch. The only metallic parts are the hinge pins and deployment/latch drive springs, all other components are graphite epoxy. The result is a truss system that stows compactly and has high stiffness and thermoelastic stability after deployment.

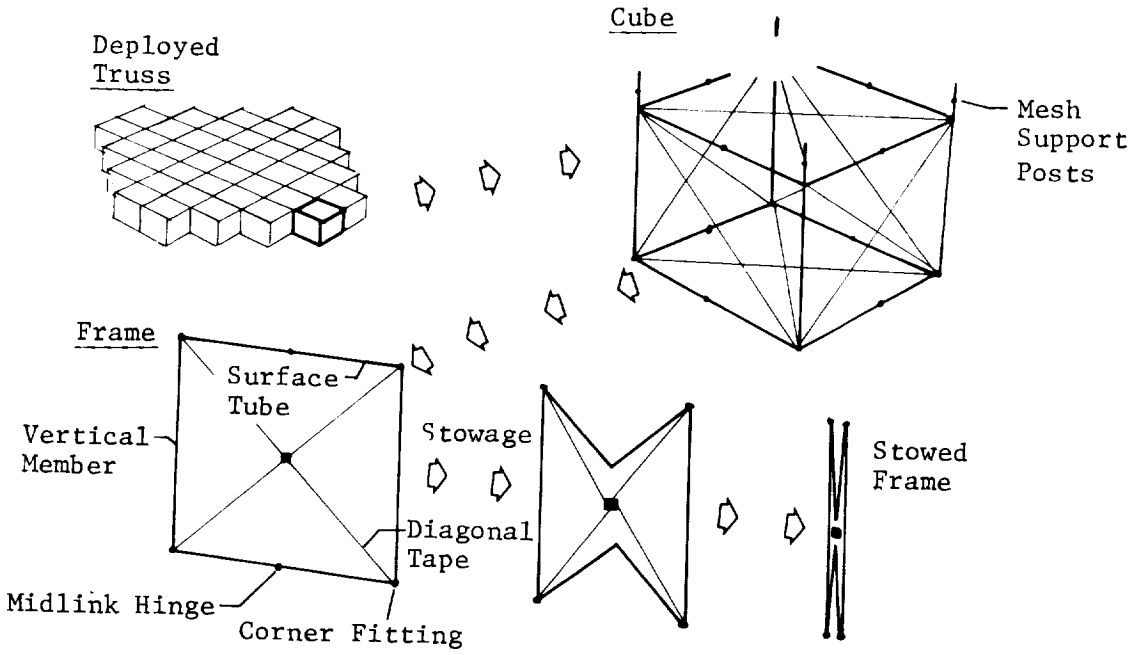

Figure 1. All Box-Truss Structures Use Deployable Frames to Form Platforms, Dishes, Rings and Beams.

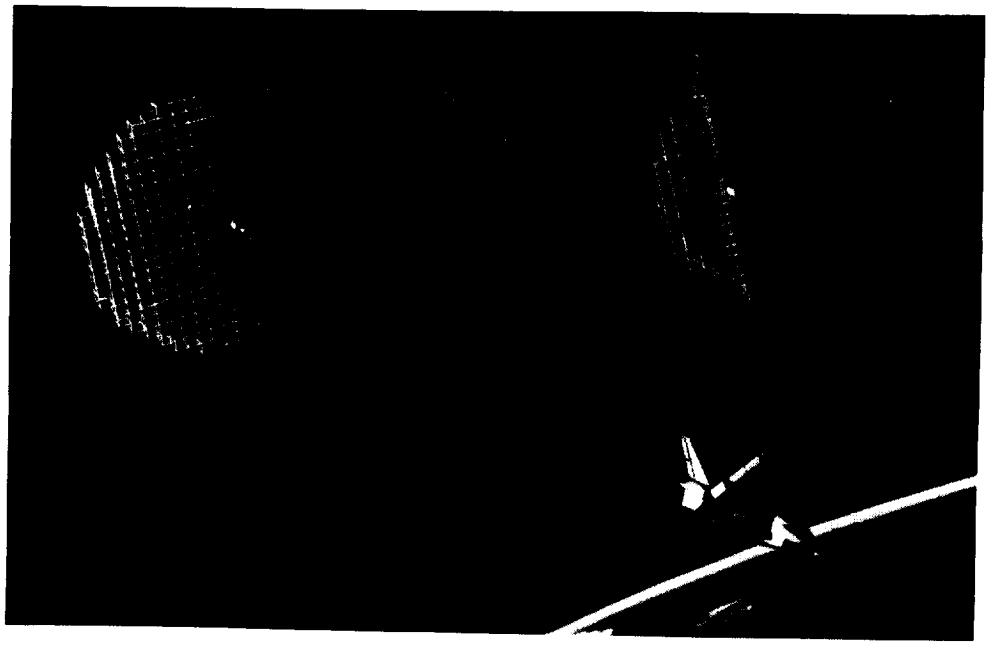

Figure 2. Planar Antenna Arrays and Platforms Can Take Advantage of the Box-Truss' Stiffness, Strength and Thermoelastic Stability.

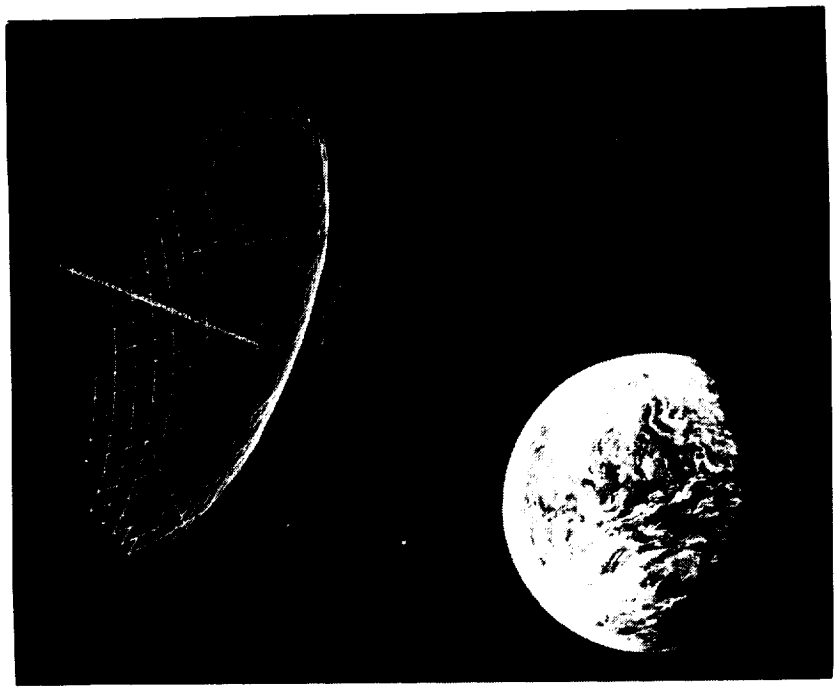

Figure 3. Parabolic Deep Space Network and Radio Astronomy Satellites Can Operate at Frequencies Up to 30 Ghz When Equipped with Appropriate Mesh Reflectors.

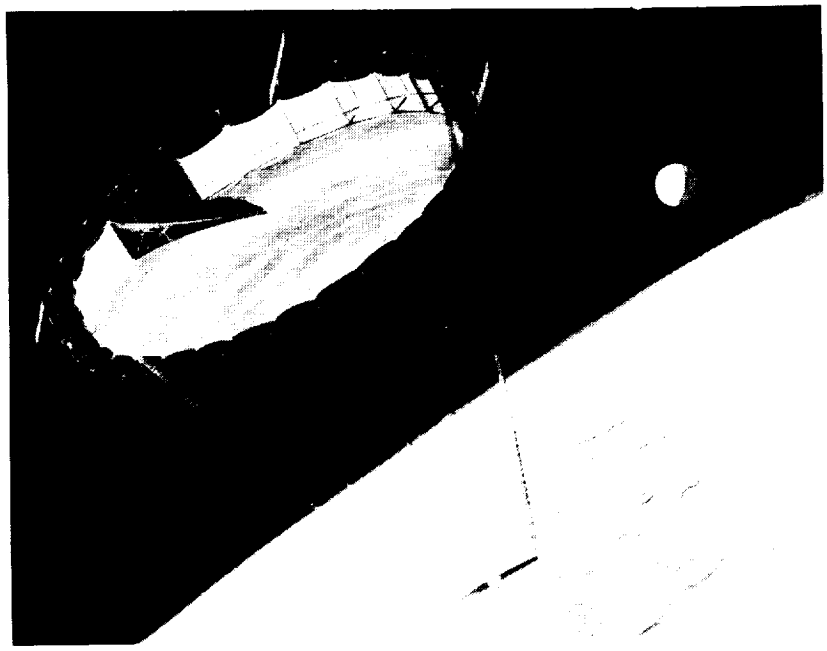

Figure 4. Combining an Electrostatically Controlled Membrane Mirror with a Box-Truss Ring Can Yield Radiometer Spacecraft Capable of Operating at Higher Frequencies Than Systems Using Mesh Reflectors.

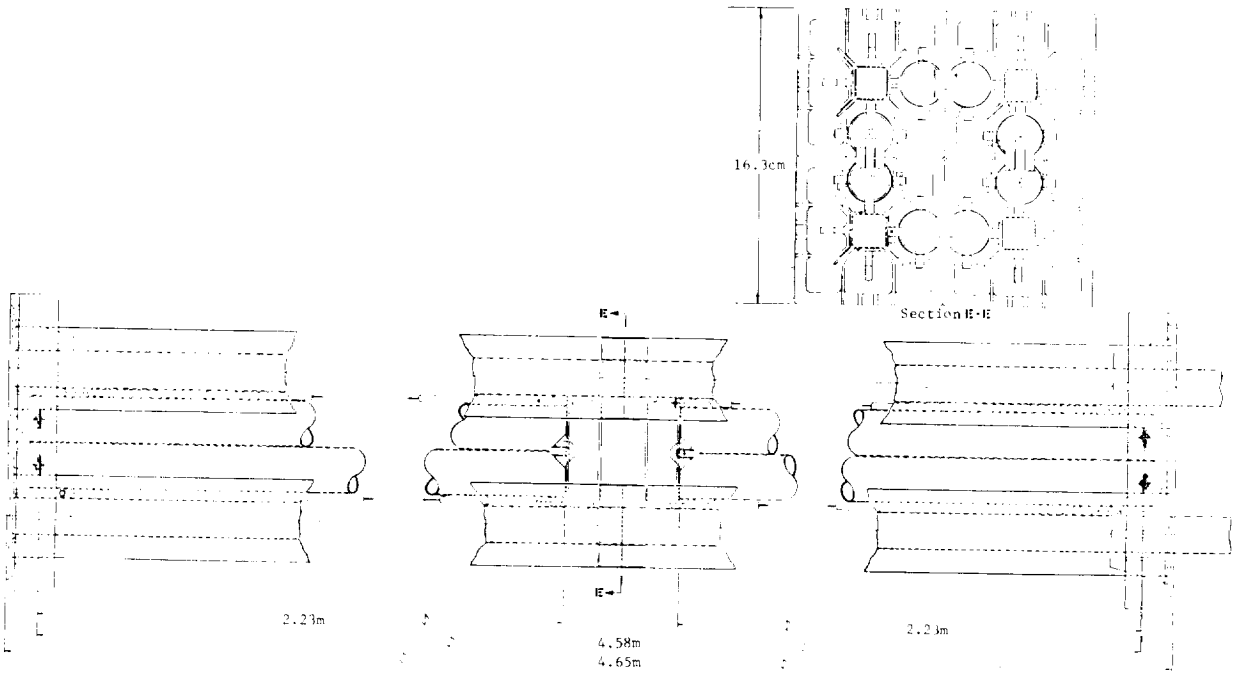

Figure 5. A Box-Truss Cube Stows Efficiently and Provides Positive Launch Restraints for All Components.

Figure 6. The Vertical Member's Column Allowables Can Be Varied Easily by Varying the Fin Construction.

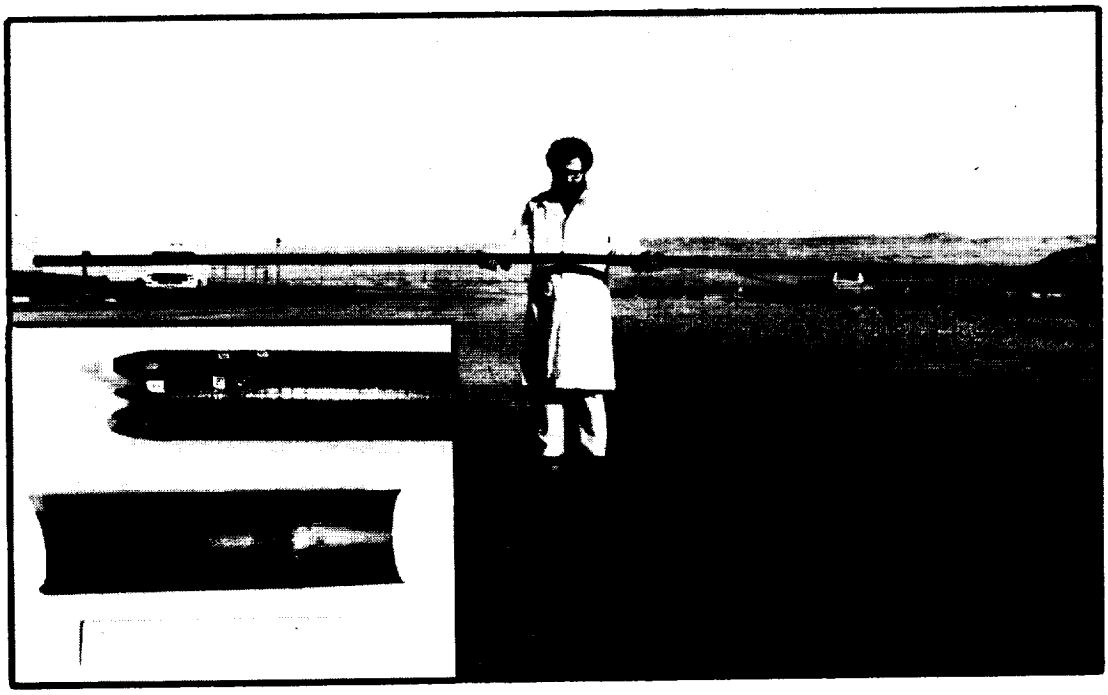

Figure 7. The Surface Tube Halves Feature Low-Cost Integrally Molded End Fittings.

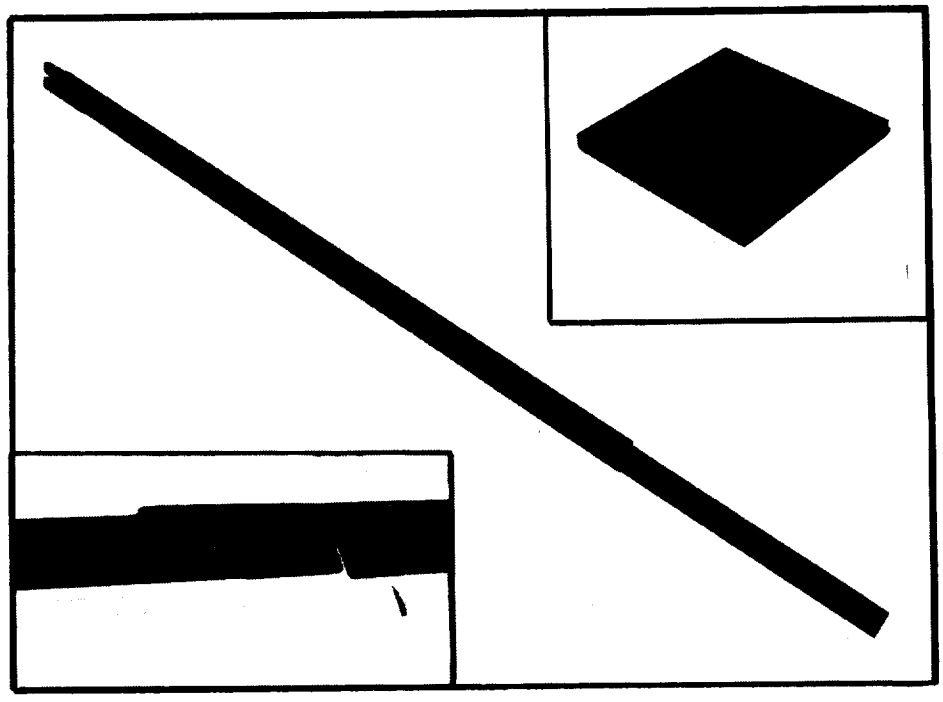

Figure 8. The Diagonal Braces Inside Each Frame Stow Securely and Compactly.

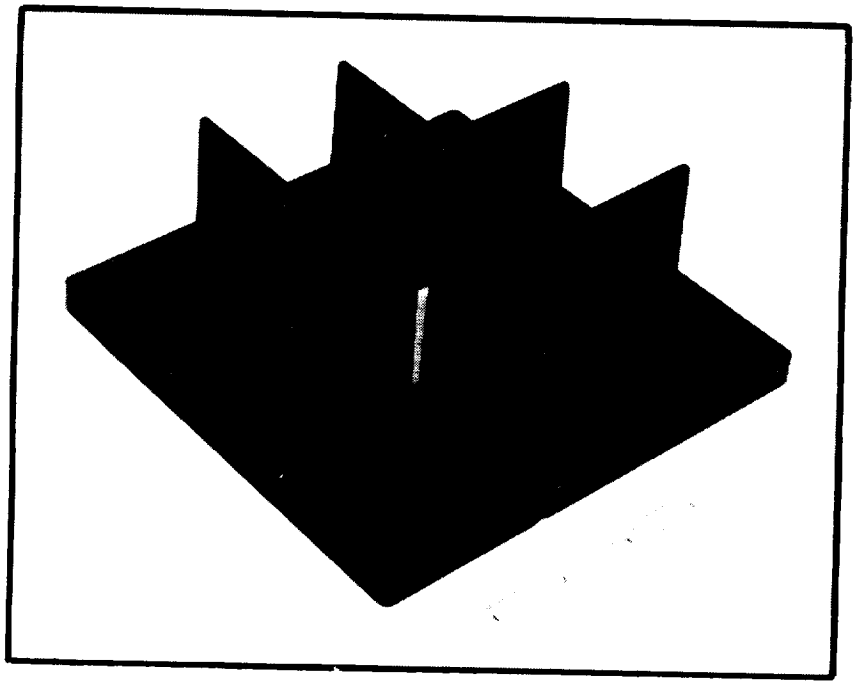

Figure 9. The Compression-Molded Graphite Fiber-Reinforced Corner Fitting Joins the Box-Truss Structural Members.

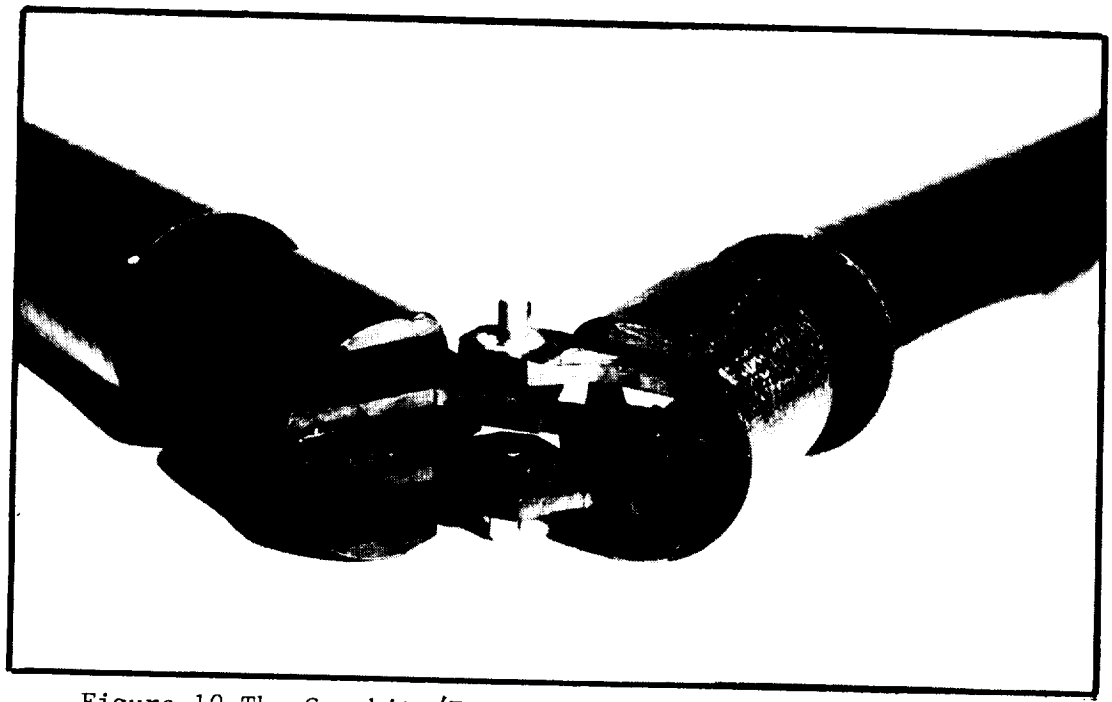

Figure 10. The Graphite/Epoxy Midlink Hinge Assembly in Each Surface Tube Contains an Over-Center Latch That Drives Deployment and Locks the Tube Straight.

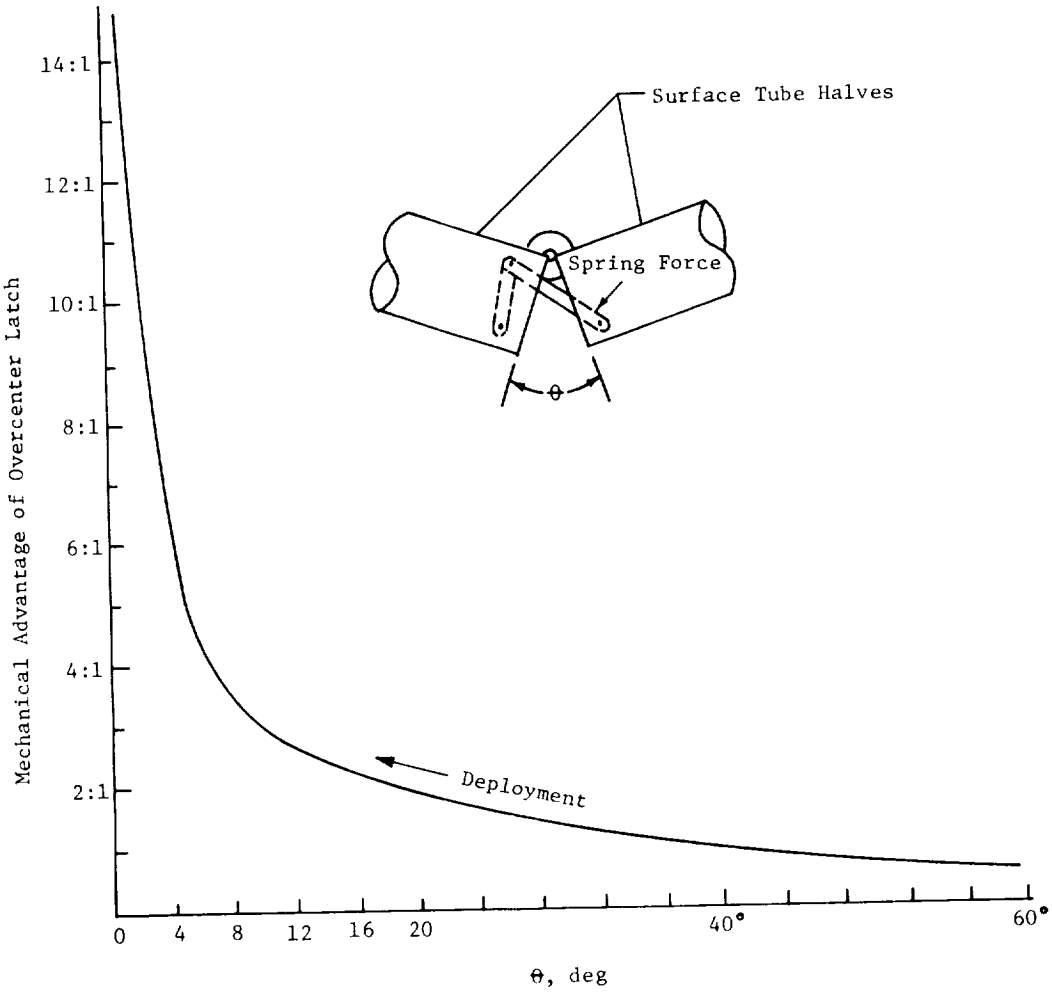

Figure 11. The Overcenter Latch Multiplies the Torque of the Drive Spring to Complete Deployment.

ON THE DESIGN OF LARGE SPACE DEPLOYABLE MODULAR ANTENNA REFLECTORS

By J. W. Ribble and A. A. Woods, Jr.
Lockheed Missiles & Space Company

ABSTRACT

Within the aerospace community, many ways are currently being investigated to assemble, erect, or deploy large reflector surfaces in space. One concept, potentially applicable to the construction of reflectors up to several hundred meters in diameter consists of individual deployable modules which are assembled in orbit into the final structural configuration. When designed for transport to orbit by the STS Orbiter, each module can be stowed in a package 25 cm in diameter by 17 m long, resulting in a deployed hexagonal measuring 28 m across the corners. The initial study summarized in this paper has indicated that this deployable modular approach will support erection of 400 m reflector apertures for operation up to 2 GHz with a single Space Shuttle Flight. Multiple launches can allow increased aperture sizes up to the limit of efficiency dictated by the use and maturity of full space erection or space fabrication techniques.

INTRODUCTION

Development of the Space Transportation System will permit truly large scale space structures to be placed in low earth orbit. Accordingly, NASA has begun studying various possible techniques for transporting and constructing such structures.* One such technique involves tightly packaging many individual deployable modules into the Space Shuttle Orbiter cargo bay, transporting them to orbit, and then deploying and assembling the modules into a completed structure. The primary features of such a concept are: 1) each module is an autonomous structural element which can be attached to adjacent modules by connecting at three points in each surface plane, 2) the upper surface is a folding hexagonal truss plate mechanism which serves as the supporting substructure for a reflective surface and 3) the entire truss and surface can be folded into a cylindrical envelope in which all truss elements are essentially parallel.

The initial effort described in this study demonstrated concept feasibility through development of a subscale engineering model possessing all the mechanical features (characteristic of a full size module) such as folding joints, module attachment points, deployment mechanisms, and surface attachment methods. In addition, studies have estimated potential performance characteristics for radio frequency antenna reflectors constructed from these modules, and preliminary packaging methodologies and erection scenarios have been prepared.

*Supported by Contract NAS1-14887, Sub-Task 14, under the direction of NASA-Langley Research Center, Langley, Virginia, Harold Bush, Project Director.

MODULE DESCRIPTION

The heart of the modular antenna concept is the individual deployable module. The general arrangement of one module is shown in Figure 1. Each module is made up of small diameter (1.27 cm), thin wall (.4 mm) tubes which are hinged so as to stow as a cylindrical package approximately 25 cm in diameter by a length of about 5/8 the diameter of the deployed modular segment. The module deploys into a space frame structure with a truss supported hexagonal reflective mesh front surface and a triangular rear support frame connected to the front surface by cross braces. Each module is of a depth equal to .86 times the diameter across the corners of the hexagon.

Deployment is achieved by operating a jackscrew mechanism located at the center of the module which separates the center pivots of the two sets of radial arms in the upper surface truss. During this motion the arms rotate outward and downward to deploy the surface. The perimeter arms, which are hinged at the center and folded parallel to the upper radial arms in the stowed position, are allowed to deploy by the deploying radial arms. The deployment energy for the perimeter arms is obtained from springs within the center fold joint, shown in Figure 2. When the arm reaches its fully deployed position (straight), this spring activates a latch, locking the arm into the open position. Thus the six perimeter arms form, when deployed, a rigid hexagonal outer hoop. The rotation of the jackscrew shaft also pays out three cables from drums located beneath the jackscrew mechanism (see Figure 3). These cables route along the sides of the jackscrew mechanism, then inside three of the upper radial arms, emerge at the tips of each of these arms, and terminate at the corner fittings of the lower arm members. Therefore, as the cables are payed out, they allow the lower arms and cross brace members to deploy away from the upper arms. The deployment forces for deployment of these members are supplied by spring loaded joints located at the mid-span fold joints of each set of cross braces and the center fold joint of each bottom frame member. Each of these springs also operates a latch to lock the joint in its fully deployed position. The cable spool pays out slightly more cable than required for the deployment motion to insure that there is no residual cable tension in the deployed module.

The completed demonstration model of the individual module is shown in Figure 4 and stowed in Figure 5.

PERFORMANCE STUDIES

The kinematics, joint concepts and deployment mechanism of the modular antenna demonstration model can be scaled directly to Orbiter cargo bay proportions. The only significant change required to produce a full scale antenna model is to increase the length of the individual struts. The useful size of the Oribter cargo bay, after allowing room for Astronaut ingress/egress to the bay, is a cylinder 4.5 m (15 ft) in diameter by 17.1 m (56 ft) long. This limits the module size by constraining strut lengths to the 17 m cargo bay length. This constraint leads to 28 meters across the corners of the hexagonal face as a maximum practicable module size compatible with STS launch.

The mass of an individual module vs module diameter is given in Figure 6, and corresponding mass fractions are shown in Figure 7. It can be seen that for larger module sizes the predominant mass in the module is the reflective surface itself with the parasitic mass fraction of the supporting structure and deployment mechanisms reducing to less than 25%. In comparison, current technology antenna reflectors have structural mass fractions in excess of 70%.

The radio frequency performance of the modular antenna concept is shown in Figure 8, and Figure 9 depicts current projected large scale antenna application missions which can be supported by the concept. The major limitations in operation frequency of an antenna is deviation in the reflective surface from the true desired parabolic surface. The two major contributing factors to deviations in the case of the modular antenna concept are 1) deviations from a parabolic contour due to the flat mesh panels, and 2) thermal distortions of the structure. The results of each of these deviations can be seen in the figure. The "flats approximation" deviation can be seen in the form of the curve families. If the antenna size is increased by increasing the size of the individual modules, the RMS deviation of the flat mesh from the desired parabolic surface increases and the possible frequency of operation suffers. This is a normal consequence of increasing antenna size. But, if the modular antenna size is increased by using more and more modules of a given size, the additional grid points on the desired parabolic surface actually decreases the overall surface RMS deviations, thus increasing the possible operation frequency. Thus, the performance of the reflector can be tailored to specific needs by adjusting the module size and the number of modules. Thermal distortions are always detrimental, however, and can be seen in the figure to cause a flattening of the performance curves as reflector size is increased. At extremely large diameters, the thermal surface errors would dominate the analysis, limiting the performance of the reflector in spite of increased numbers of modules.

REFLECTOR ASSEMBLY

Erecting large antennas in space requires construction of large numbers of modules, packaging them for launch into earth orbit, and deploying and assembling the completed modules in the space environment. Practical means of modifying and/or repairing these structures are also required to make such systems truly economical.

Attaching elements one to another to form larger assemblies will probably provide the largest single challenge to the construction of large space structures. Certainly the assembly task of connecting modules together to form large, extremely accurate antenna reflectors poses a major challenge and module design requirement. Figure 10 shows a design solution for the module to module attachment joints located at the corners of the reflective surface. The exclusive use of axial motions for activation and deactivation of the latch allows the module deployment cable to perform double service as a latch release cord. Mechanical advantages in the cam motions allow the module to be pushed into place and latched for installation. For removal, the cable is pulled, retracting the spring loaded plunger and retracking the the latch cam. The wedging action of the cams against the conical seat and

the edge of the module corner fitting against the center pin eliminate freeplay and provide a load path wheelbase through the joint. Other fastening devices, turn fasteners, screw threads, could be used to attach each module to the cap plate, but they would close approach by an astronaut to release the module. Using the cable release, an astronaut can perform the attachment release for both joints at each module corner from the base end of the structure, thus saving valuable EVA time and eliminating the danger associated with operating a man in close proximity to the reflective mesh.

A transport and antenna module erection scenario is depicted in Figure 11. Modules for a reflector assembly are loaded into a transport cannister which is in turn loaded into the STS Orbiter cargo bay. When the Orbiter achieves the desired orbit, the cargo bay doors are opened and the module cannister relocated above the cargo bay as shown in Figure 9A and B. The Payload Installation and Deployment Aide (PIDA) being developed by Johnson Space Center or an equivalent handling system can be used to affect this position change. The Orbiter RMS is then used to grasp the first module by its deployment jackscrew drive. The module cannister is designed to open sequentially and release one module at a time from its support frames. The RMS is then used to position the module away from the Orbiter and to deploy the module as shown in C. Once the module has been deployed it can be released by the RMS to be installed into a reflector assembly, D. As additional modules are deployed, the cannister structure is peeled back upon itself layer by layer to provide access to the lower items. After the last module is deployed, E, the cannister framework is closed and returned to the cargo bay by the PIDA, F, for return to earth.

CONCLUSIONS

The kinematic studies and Engineering Demonstration Model developed during this study have fully verified the deployment kinematics, stowing philosophy, and deployment sequencing for large deployable antenna modules. Mesh attachment methods compatible with full scale modules have been devised. Parametric studies of large modular reflectors have established size, mass and aperture frequency capabilities for these assemblies. Preliminary studies have been made devising means of delivery modules to orbit, and once there, of assembling the modules into complete modular antenna reflectors. The basic feasibility of creating mass efficient modules, erectable into large structures in space has been established.

Figure 12 shows an artist's concept of the eventual outcome of modular antenna research. Using a modular approach, spaceborne antenna reflectors of up to 400 m in diameter designed for operation at frequencies of 2 GHz are possible using one STS launch and reflectors of up to 1 km in diameter are feasible using multiple flights.

REFERENCES

1. Russell, Campbell and Freeland; A Technology Development Program for Large Space Antennas; Paper No. IAF-80-A33, Thirty-First International Aeronautical Congress of the International Astronautical Federation, September 1980.

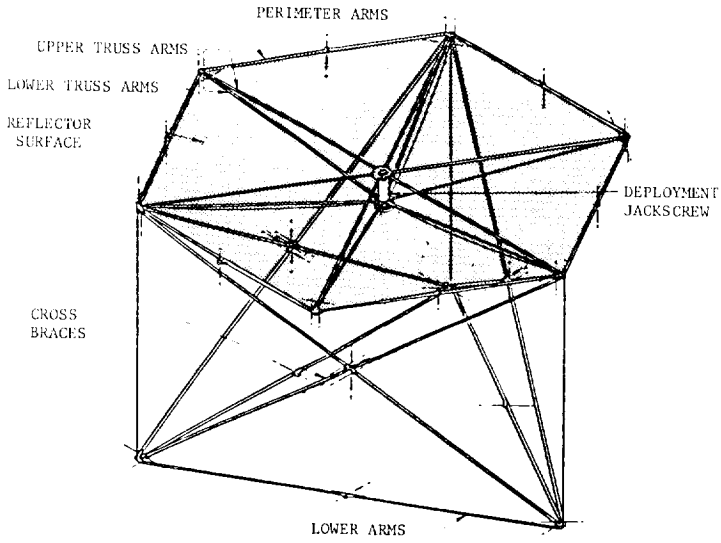

Figure 1. General Arrangement, Deployable Module

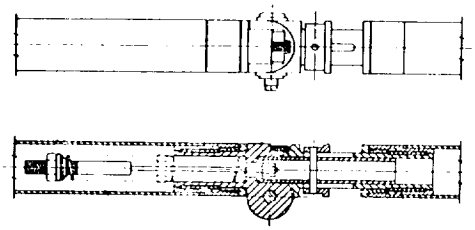

Figure 2. Center Fold Joint-Perimeter Arm

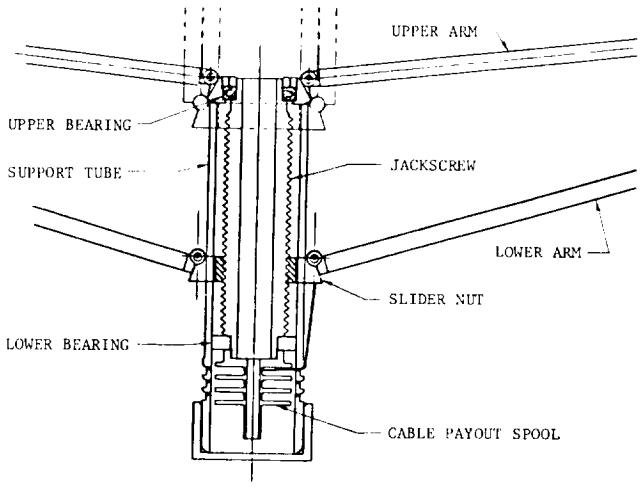

Figure 3. Jackscrew Deployment Mechanism

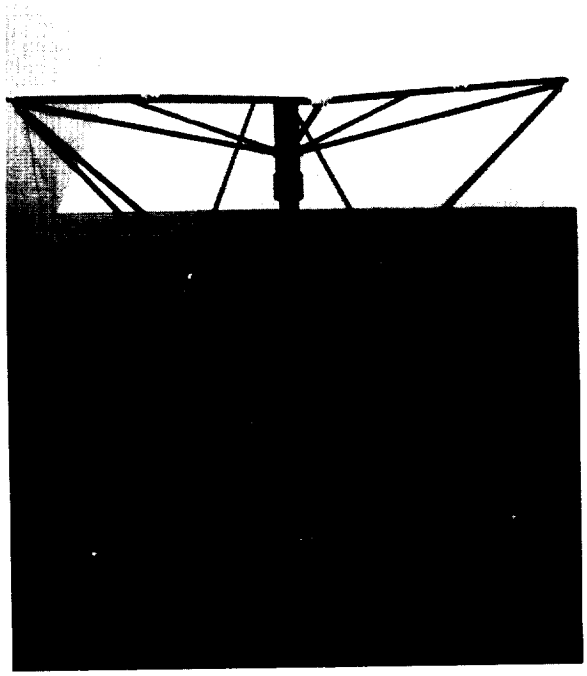

Figure 4. Modular Antenna Demonstration Model - Deployed

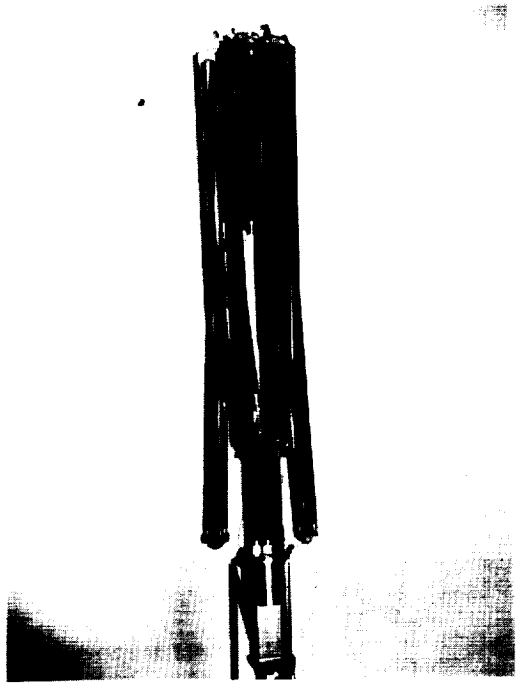

Figure 5. Modular Antenna Demonstration Model - Stowed

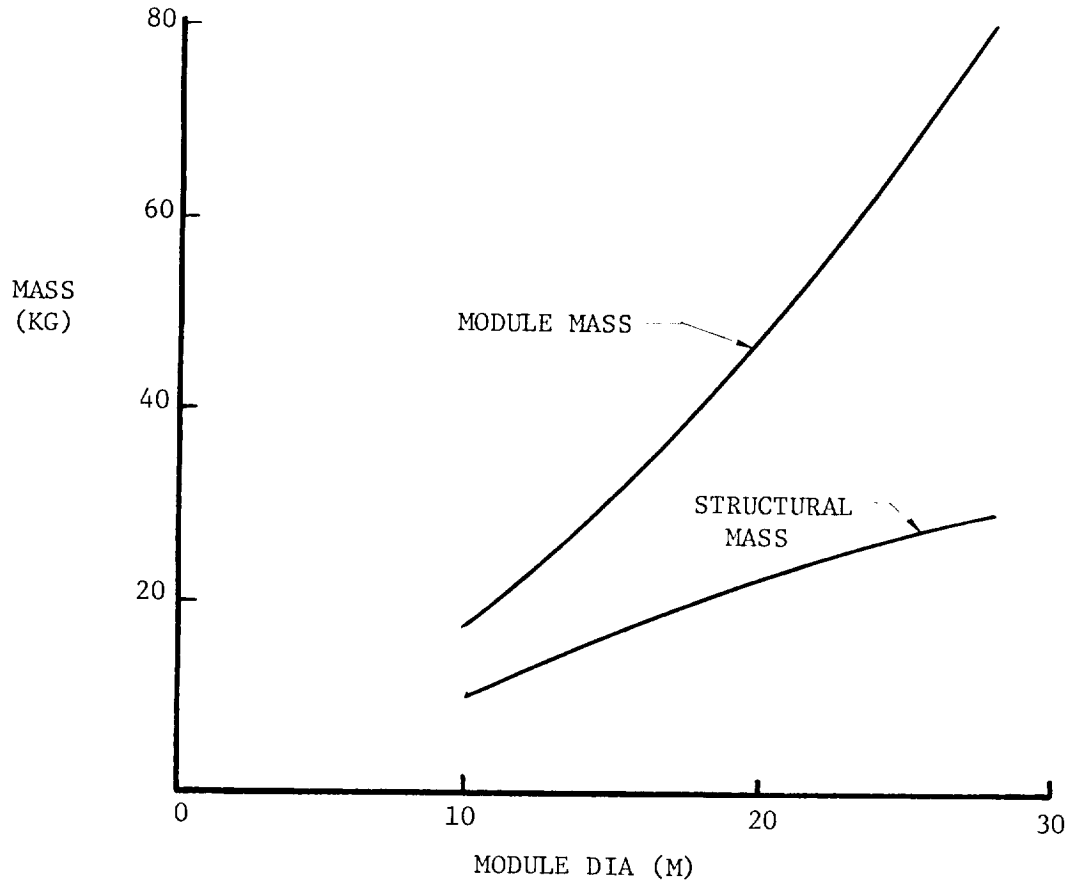

Figure 6. Module Mass vs Size

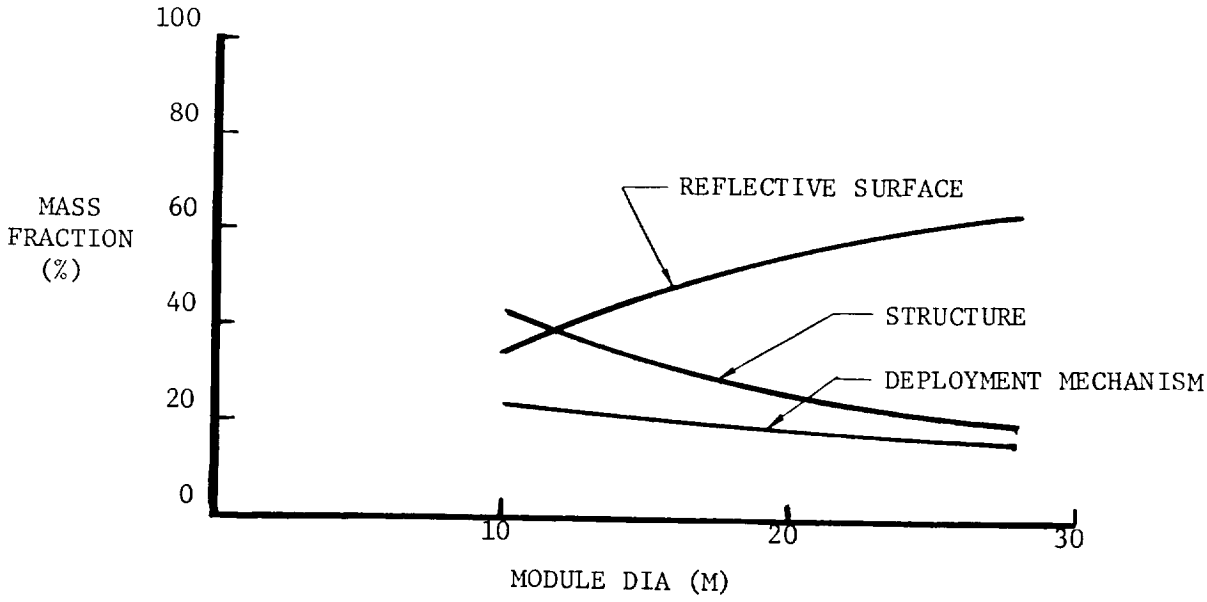

Figure 7. Module Mass Fractions vs Module Size

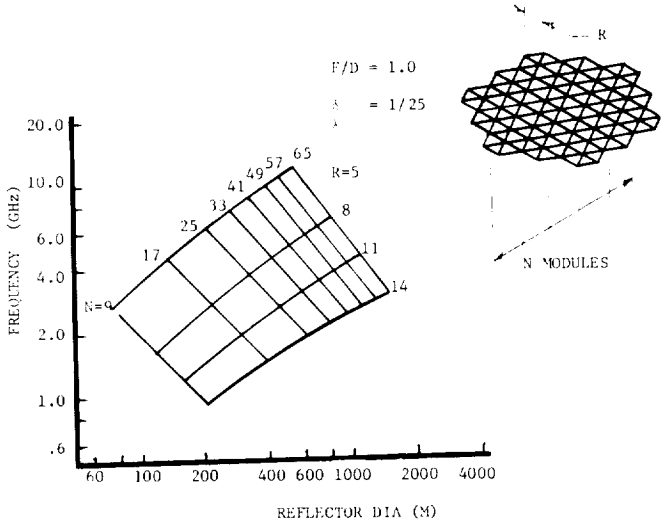

Figure 8. Reflector Frequency vs Size (Inc. Thermal Effects)

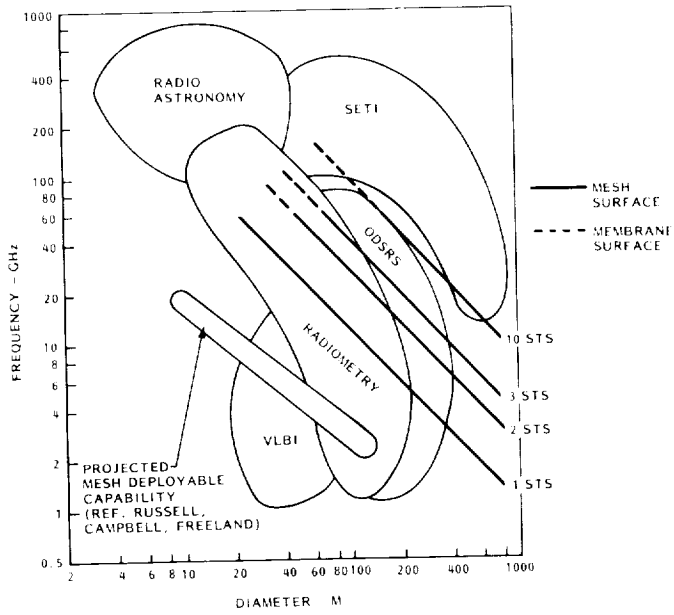

Figure 9. Modular Antenna Projected Applications

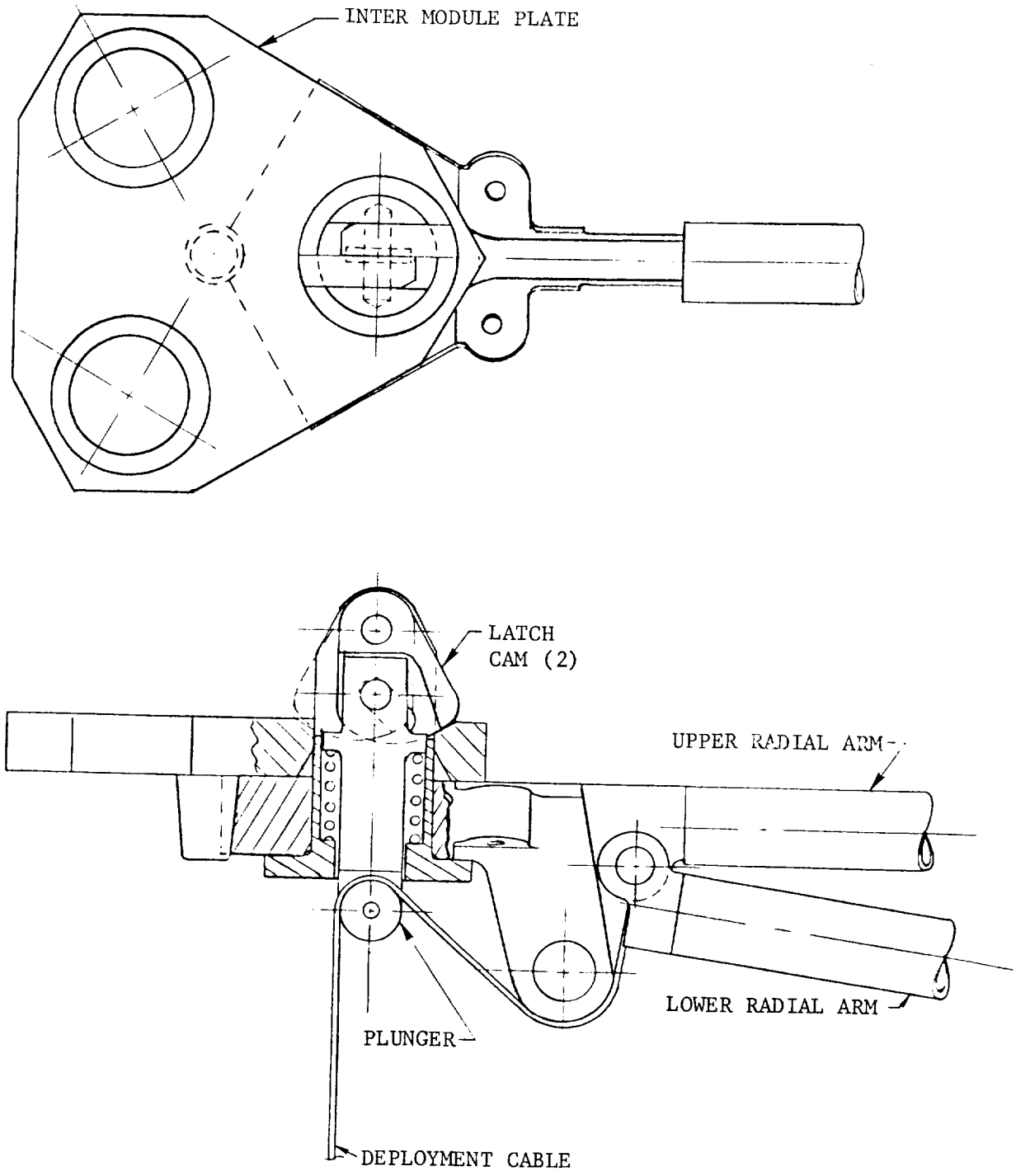

Figure 10. Module to Module Joint

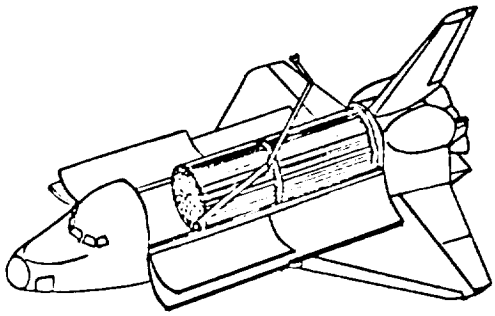

A. SHUTTLE ORBITER IN DEPLOYMENT ORBIT

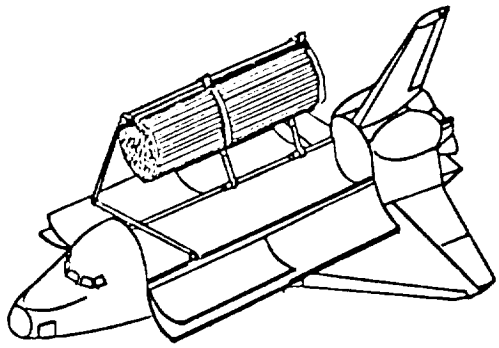

B. MODULE CANNISTER DEPLOYED BY PIDA OR EQUIVALENT PAYLOAD HANDLING MECHANISM

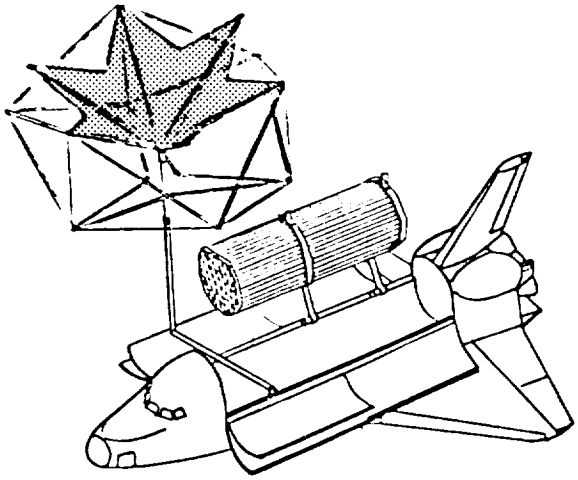

C. FIRST MODULE REMOVED FROM CANNISTER AND BEING DEPLOYED

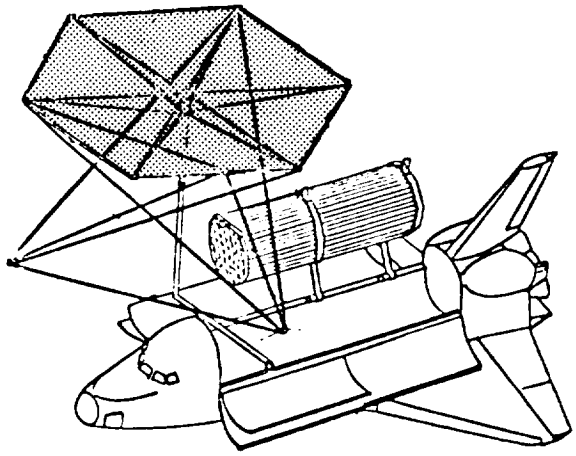

D. FIRST MODULE DEPLOYED AND READY FOR HANDOFF TO REFLECTOR ASSEMBLY

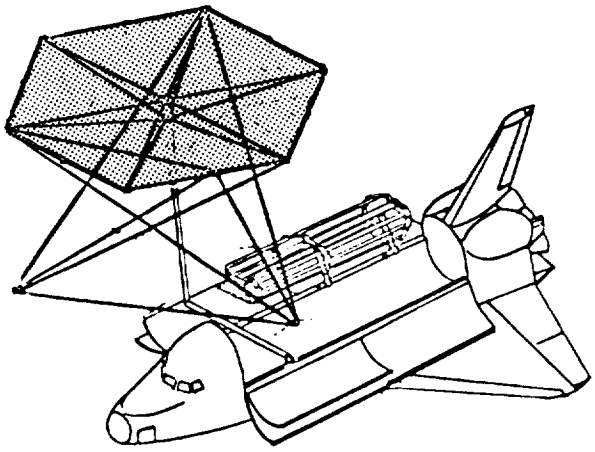

E. LAST MODULE DEPLOYED AND READY FOR HANDOFF TO REFLECTOR ASSEMBLY

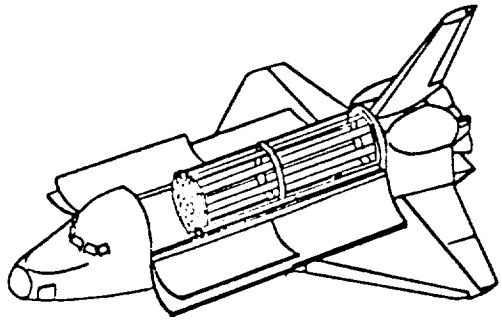

F. MODULE CANNISTER RECLOSED AND REPACKED INTO ORBITER CARGO BAY FOR RETURN TO EARTH

Figure 11. Module Deployment Scenario

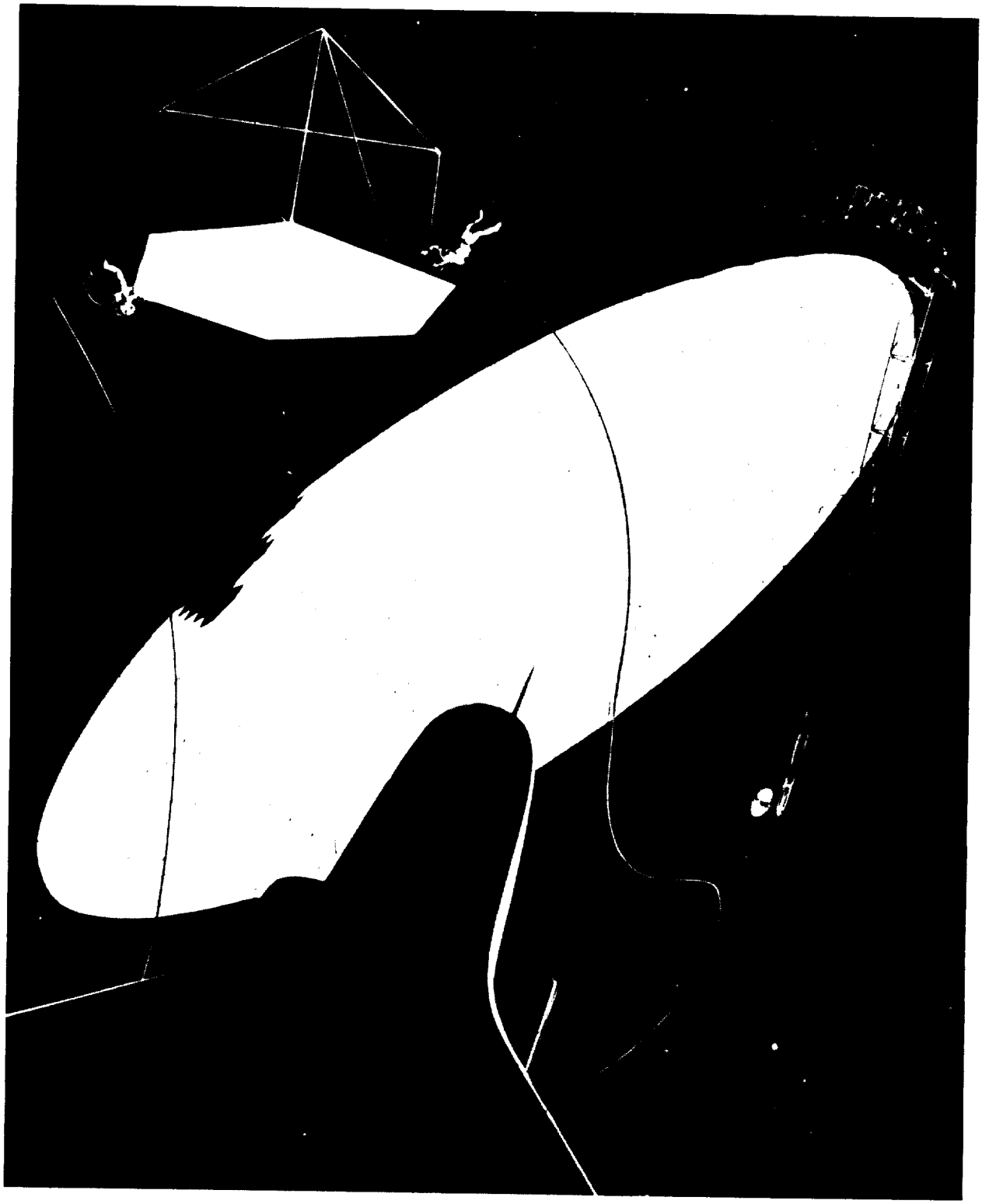

Figure 12. Artist's Concept of Large Aperture Modular Antenna

THE TECHNOLOGY DEVELOPMENT METHODOLOGY FOR A CLASS OF LARGE DIAMETER SPACEBORNE DEPLOYABLE ANTENNAS

William D. Wade & Verdinal C. McKean

Lockheed Missiles and Space Company

ABSTRACT

The NASA community has identified applications for large diameter deployable antennas to provide radiometer measurements of soil moisture content for better water shed control, an electronic mail system, two-way voice radio telephone service, emergency land mobile satellite communications, vehicle fleet dispatch, utility power monitoring and satellite to earth microwave power transmission. The designs and hardware development for the predecessor to such antennas which are being developed at Lockheed Missiles and Space Company under contract to the Jet Propulsion Laboratory and in support of the NASA Large Space Structure Technology Project Office, Langley Research Center are the subject of this paper. The development of a 55-meter diameter (.64-acre) offset wrap-rib reflector antenna, for demonstration and evaluation of a full scale 100-meter diameter (2.1-acre), intended for operational usage of S-Band frequencies, is being fabricated to demonstrate technology readiness.

The application of thermally stable graphite epoxy materials in flexure is discussed and deployment mechanism designs that are adaptable to both the proof of concept and the full scale 100 meter system with no modification to the basic concept are presented. The ground deployment test techniques and mechanisms developed for ground demonstration and evaluation of large size antenna structures are presented to illustrate the complexities involved in supporting antenna structural elements in excess of 25 meters in length.

INTRODUCTION

The advent of the Shuttle Transportation System has provided the opportunity for the consideration of reuseable or recoverable satellite systems. This coupled with the increased payload capability has created a new philosophy, within the NASA community, regarding the viability of advanced system concepts that may not have been fully demonstrated in the 1-g environment. These advanced systems will provide missions with heretofore unheard of capabilities. NASA has developed a new approach to technology development that will catalyze the various subsystems into useable mission profiles. The catalyst being used is the "focus mission" concept (Ref. 1). A "focus mission" is one which is used to identify the critical technologies that are sure to be needed for a broad class of particular mission applications. Under this concept, the requirements for the various missions are compared and synthesized into one mission that will support the required technology development. One of the identified critical paths on the technology road map involves the development of large aperture, high radio frequency antenna systems.

One of the concepts selected for development by JPL as part of the NASA Large Space Systems Technology (LSST) Program is the Wrap-Rib Reflector Antenna. During 1978 under a JPL funded program at Lockheed Missiles and Space Company (LMSC), parametric analyses were conducted to determine the compatibility of the wrap-rib reflector to the "focus mission" requirements. The results of this study indicated that all of the near term (1985 - 2000) needs could be met using the current design concepts and available materials technology. These results, shown in Figure 1, indicate the offset wrap-rib mission compatibility. The textured blocks represent potential near term mission requirements as identified in Ref. 2. The long term requirements derived from Ref. 3 are shown in dashed lines. Antenna capabilities are within the envelope represented by the solid line. These realizations provided the impetus for a 1979 initiation of the hardware development phase of the JPL/LSST program. The methodologies being applied to that program developed are described herein.

Identified Large Deployable Antenna Applications

A summary of the potential large space systems missions is presented in Figure 2 (Ref. 2). This NASA mission model clearly identifies the need for precision shaped reflector antennas with apertures from 10 m to 300 m. Once the shuttle becomes operational and the antenna technology has been demonstrated, it is anticipated that the mission model will grow significantly in scope.

WRAP-RIB ANTENNA TECHNOLOGY

The wrap-rib parabolic reflector is based on an approximation to a paraboloid of revolution. The wrap-rib antenna is comprised of radially emanating gores between ribs which take the form of parabolic cylinders. The parabolic cylinders more closely approximate a true paraboloid of revolution as the number of gores is increased. Figure 3 illustrates the physical appearance of the resulting reflector (Ref. 4).

The gores are fabricated from a flexible membrane material which is usually a knitted or woven fabric of electrically conductive material. The gores are sewn to parabolically curved cantilevered ribs terminated at the central hub structure in a hinge fitting. For launch the antenna is folded into a package size which will fit into the shuttle cargo bay. During stowage the ribs are rotated on the hinge pin, then elastically buckled and wrapped around the hub. Once in space, the reflector is deployed by release of the stored rib energy through a deployment restraint mechanism which simply controls the rate of energy release and therefore the deployment rate. Figure 4 shows deployment of a wrap-rib antenna, including some details of the hub assembly.

Structural Configuration

There have been two rib design configurations applied to the wrap-rib reflector concept, i.e., the open or C-shaped rib cross section and the closed or lenticular cross section, both of which are illustrated in Figure 5.

Figures 6 and 7 are photographs of actual hardware fabricated into the two shapes. The choice between the two is dictated generally by the desired stiffness and diameter of the reflector. The C-section can be employed up to about 20 m in diameter while the lenticular section is theoretically useful from about 15 m to above the 300 m class (Ref. 4).

Regardless of the cross-sectional shape used, the design requires that the ribs provide a dimensionally stable support structure in the space environment for the reflective mesh surface, and the ribs must be capable of being wrapped into the allowable storage envelope for an indefinite length of time without appreciable dimensional changes occurring.

Reflective Surface Technology

The reflective mesh surface is composed of an electrically conductive knitted or woven fabric. The strands or yarns in the fabric can be of several basic materials either organic or metallic in nature. For most materials, adequate reflective properties are obtained through the use of either electroless plating or electroplating with a good conductive material, e.g., gold, silver, aluminum, etc. The diameter of the wires and the distance between them are dictated by the highest antenna radio frequency.

CURRENT JPL/LSST ANTENNA TECHNOLOGY PROGRAM

The present JPL/LSST program at LMSC is chartered with the responsibility for the technology development of a 55-meter diameter offset wrap-rib antenna. The driving requirement for the efforts on this project is that all aspects of the design and manufacturing must be scalable to a unit with a 100 m diameter with no change to the basic concepts. As configured, the JPL/LSST technology design requirements focus on an antenna operational frequency of 3 GHz, a hardware focal-length-to-offset-diameter ratio of 1.5, antenna surface figure of 1/30 of a wavelength and space shuttle compatibility.

To provide a frame of reference, the 100 m reflector when fully deployed in the Houston Astrodome, would occupy all of the playing area between the football goal posts and have a surface error of less than 3 mm (0.12 in) RMS referenced to the design paraboloid. The feed support tower for this unit would be as tall as a 68-story building and have a known, stable positional accuracy between the ends to within 6 mm (0.25 in). It is not reasonable to expect that this full scale antenna could ever be completely deployed in the 1-g environment.

Rib Fabrication Technology Development

The main structural elements of the wrap-rib reflector are of course the ribs themselves. These ribs are required to have a high specific stiffness, and have a low thermal coefficient of expansion. The only present state of the art materials that provide adequate margins against the technology requirements are graphite epoxies. The emerging metal matrix composites (MMC) which utilize a metal such as aluminum or magnesium as the matrix binder

instead of a resin system, show great promise in future antenna application. This MMC technology requires additional development prior to its use in design application.

Graphite epoxy ribs are produced by placing sheets of epoxy impregnated graphite fabric and/or tape onto a tool of the desired cross-sectional shape. The layup is trimmed, vacuum bagged and placed in an autoclave to cure by temperature and pressure. Since LMSC's autoclave can accommodate layups up to a length of only 7.5 meter, the ribs for the 55-meter (180-foot) reflector must be fabricated in segments. Lenticular rib segments, made in two halves (Figure 5), are bonded together in the flattened state to form 6-meter segments. These segments are then spliced together and trimmed to obtain the finished rib.

Previous tooling methods have been based on machined graphite, machined aluminum, cast ceramic and fiberglass design approaches. These types of tools required long manufacturing time, weighed 1 - 1.5 tons, and cost a great deal of money to produce. These concerns initiated activity on the design of a new rib segment layup and cure tooling approach.

Previous tooling at LMSC utilized high temperature fiberglass. While adequate for development efforts, repeated usage caused serious degradation in the tool surface quality and created porous cracks through the tool making it difficult to achieve an adequate vacuum level. Two other disadvantages were the tooling weight (approximately 900 Kg) and the thermal mismatch (approximately 13 x 10 Exp - 6/°F) between the cured part and the tool itself. Trade studies performed to evaluate the alternate materials for the tooling included machined aluminum, machined bulk graphite, machined invar, and ceramics. While each of these materials offered some improvement over the fiberglass, they were all very heavy and, more importantly, prohibitively expensive. It was obvious, therefore, that a "new" approach to the tooling had to be developed.

LMSC since the early 1960's had been producing wrap-rib reflectors using aluminum ribs. These ribs were fabricated in both the C-shape and lenticular cross section using a technique known as bump forming. This process involves the use of a power brake fitted with a bumping die working against a rubber platen. The sheet aluminum was yielded into the desired cross section by proper setting of the power brake. It occurred to the designers of the current reflector that this aged technique might be applied to the tooling fabrication. Instead of using aluminum, invar was chosen as a more appropriate material due to the inherent low coefficient of thermal expansion. The tool that resulted eliminated all of the previous design limitations. It reduced the thermal mismatch by an order to magnitude, decreased the tool weight from 900 Kg to 45 Kg, produced a reliable reuseable non-porous surface, and reduced the projected tooling cost by a factor of 5.

Reflector Deployment Control

This deployment control mechanism, called the "re-wrap" concept is essentially a reel-to-reel tape drive. With the reflector in the stowed configur-

ation, a restraint tape is attached at the central hub and wrapped circumferentially along every third rib. This tape then travels over a set of 45° bevel idlers, through a slack take-up mechanism and terminates at a spool that is a part of the central hub (see Figure 8). The bevel idlers are mounted to a gear-driven carriage ring mounted on bearings. In operation, the drive motor is energized, driving the carriage ring. This causes the tape to travel over the bevel idlers, and re-wrap around the central spool. This gradually releases the radial pressure on the stowed ribs, allowing the stored energy to deploy the ribs at a controlled rate. For stowage, the operation is simply reversed causing the ribs to again wrap around the central hub.

A kinematic model of the mechanism shown in Figure 9 was fabricated to demonstrate the operation. This model identified the need for an additional degree of freedom in the bevel idler design. The action of the tape moving over the idlers produces a significant level of frictional force in a direction parallel to the idler axis as depicted in Figure 10. This friction develops because the tape must contact and leave the idler at a different longitudinal position. The only mechanism for this to occur is through slippage between the tape and idler. As a result a design investigation into methods of providing for the longitudinal motion without slippage was undertaken.

Figure 11 illustrates schematically the results of that study. This dual-axis bearing idler consists of a helically grooved, ball bearing mounted, roller mount. The 45° helix groove machined into the shaft provides the captive feature for the roller axle which is formed as a 45° pitch spring. Local pockets are machined into the shaft to allow clearance for the rollers. This configuration should provide low friction for the required two degrees of freedom.

Rib Root Design

Activities prior to the JPL/LSST program identified design concerns in the interface of the lenticular rib to a hinge at the hub. The design requirements for this hinge are to:

- provide for flattening of the rib for stowage,
- provide for 90° rotation of rib for stowage and deployment, and
- provide for maximum, deployed stiffness transfer from the rib to the hub.

The previous approach attached the hinges to the flanges of the lenticular structure. This required that the lateral fixity and resulting stiffness be provided by the graphite shell as shown in Figure 12. The evolved design developed to improve the stiffness of the previous configuration is shown in Figures 13 and 14. By providing a transition from the hexagonal shape to the lenticular shape in a titanium root section, it was possible to increase the local thickness of the shell to an extent that the hinging, latching and stopping loads are no longer of concern and the full stiffness potential of the rib cross section can be realized.

Ground Test Development

The ground test deployment of the 55 meter (180 feet) diameter reflector as part of the JPL/LSST program presents some challenging engineering problems. The ribs designed for space do not have sufficient stiffness to support themselves during the deployment event. They must therefore be supported at several positions along their length in a zero gravity simulation. This requires that the support system provide six degrees of freedom at the point of rib attachment without aiding the normal zero G deployment motion or rib stability. Another consideration has to do with the deployment motion. The unwrapping ribs will follow a spiral path similar to that shown in Figure 15. The deployment test equipment must be capable of compensating for this motion.

The scheme developed to allow the deployment motion of the four rib three gore test structure is illustrated in Figure 16. The 1-g support is provided by a balance beam. This beam, attached to an overhead track by a lanyard, is free to pivot both in the horizontal and vertical direction (see Figure 17). The reflector interface mount is rotated counter to the hub deployment direction and rate to maintain the rib motion in an appropriate radial direction and therefore within reach of the balance beam.

CONCLUSIONS

At the mid-point of this Offset Wrap-Rib Technology Development Program, LMSC has, as is indicated in the text, succeeded in adapting and evolving the flight demonstrated wrap-rib deployable antenna technology into a technology which supports the requirements for 50-to 150-meter diameter spaceborne offset antenna systems. The Jet Propulsion Laboratory funded program has advanced this technology to the point of demonstration through full scale hardware development. When completed in 1983 this program activity will have proven through the full scale antenna segment testing the readiness of technology to support 50-to 150-meter offset antenna missions and in the process will have significantly advanced space technology.

REFERENCES

(1) Freeland, R. E. and Campbell, T. G.; Deployable Antenna Technology Developement for the Large Space Systems Technology Program; AIAA/NASA Conference on Advanced Technology for Future Space Systems, Hampton, VA, May 8 - 10, 1979, NASA CP-2118.

(2) Russell, R. A., Campbell, T. G., and Freeland, R. E.; A Technology Development Program for Large Space Antennas; Thirty-First International Astronautical Congress of the International Astronautical Federation, Tokyo, Japan, September 21 - 28, 1980, Paper No. IAF-80A33.

(3) Powell, R. V.; A Future for Large Space Antenna; 7th AIAA Communications Satellite System Conference, San Diego, CA, April 23 - 27, 1978.

(4) Woods, A. A. and Wade, W. D.; An Approach Toward the Design of Large Diameter Offset Fed Antennas; AIAA/NASA Conference on Advanced Technology for Future Space Systems, Hampton, VA, May 8 - 10, 1979.

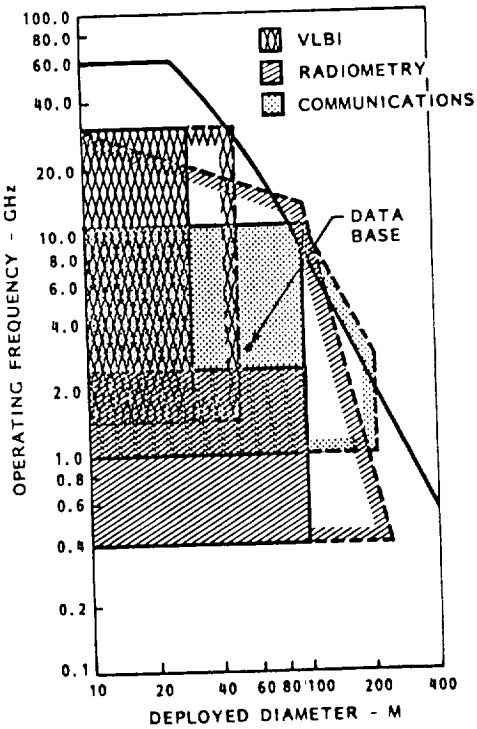

FIGURE 1. OFFSET WRAP-RIB ANTENNA MISSION CAPABILITY

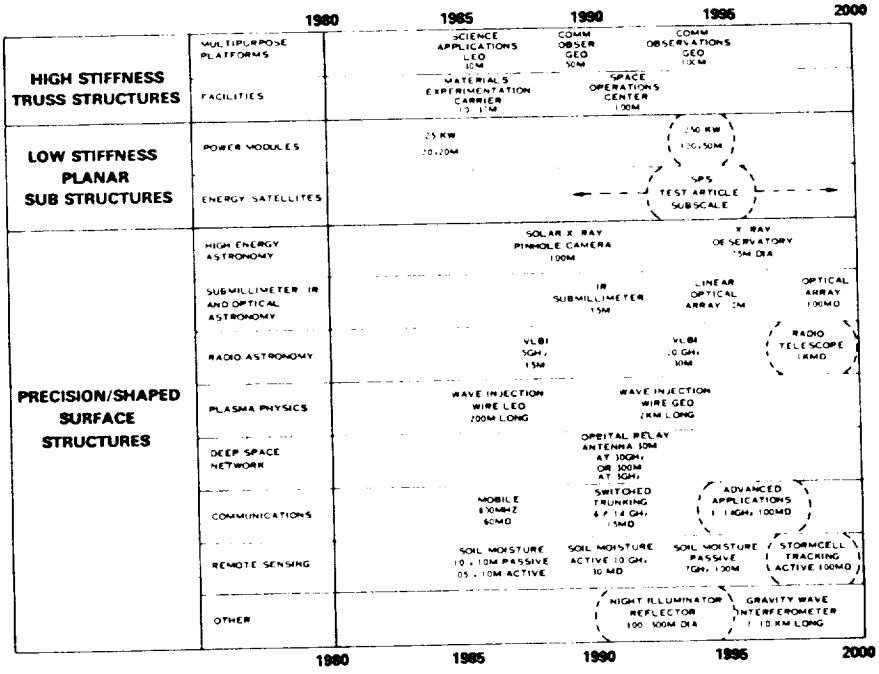

FIGURE 2. POTENTIAL LARGE SPACE SYSTEMS MISSIONS

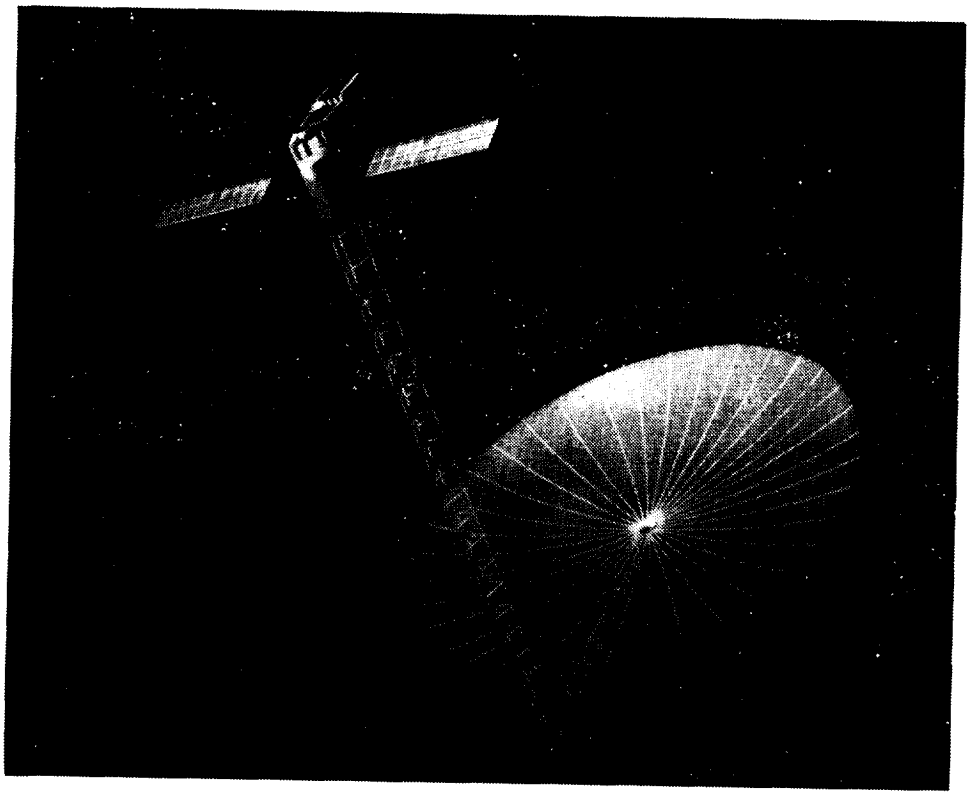

FIGURE 3. OFFSET PARABOLIC WRAP-RIB REFLECTOR

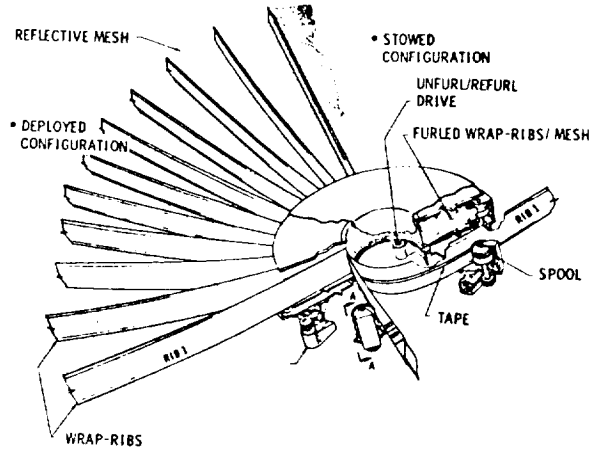

FIGURE 4. REFLECTOR DEPLOYMENT MECHANISM

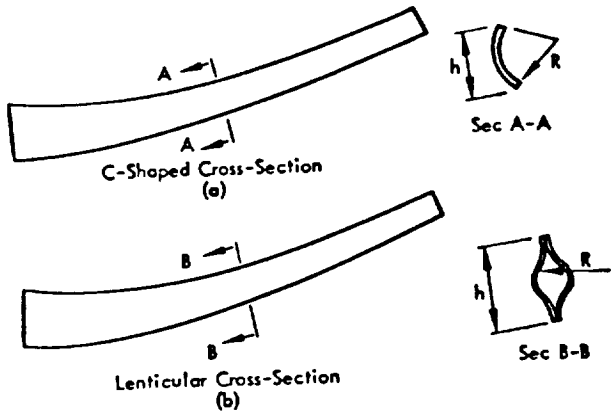

FIGURE 5. DEVELOPED RIB DESIGNS

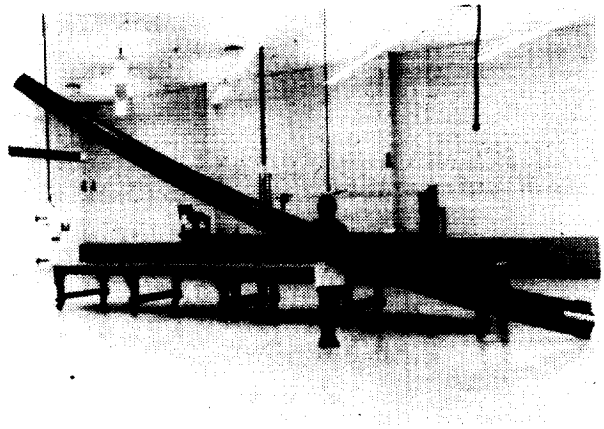

FIGURE 6. 6.9 M GRAPHITE EPOXY LENTICULAR RIB

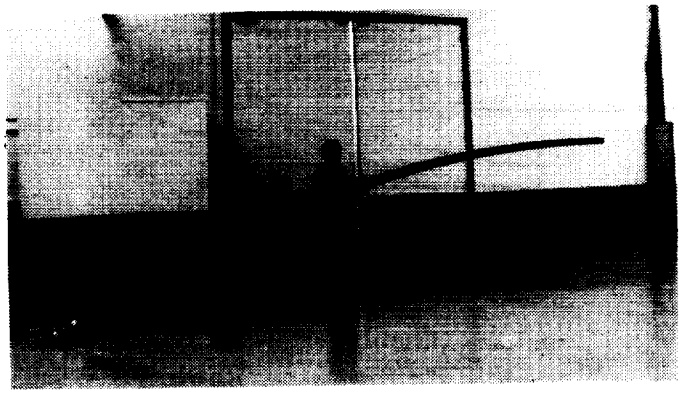

FIGURE 7. 7.0 M GRAPHITE EPOXY C-RIB

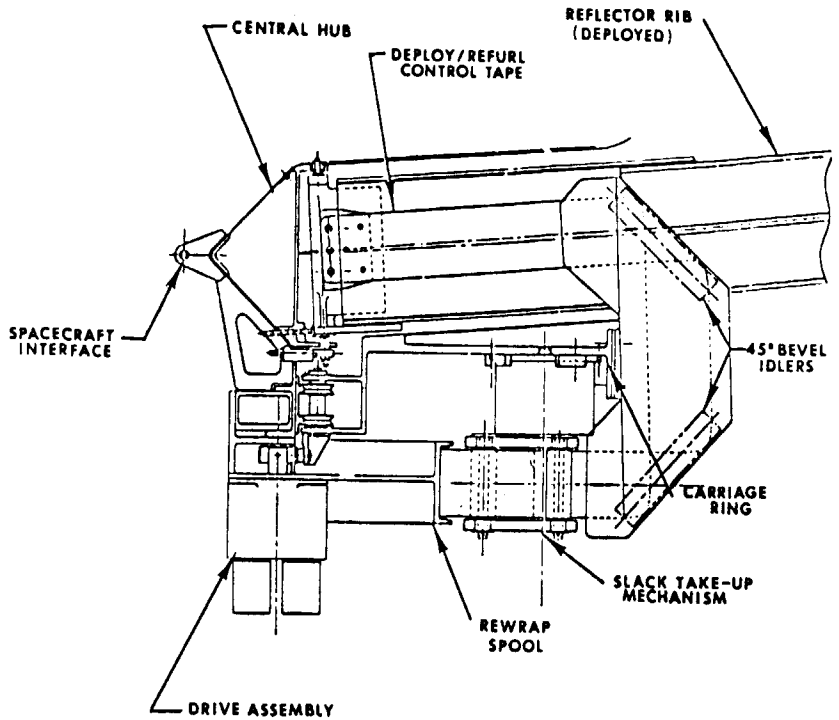

FIGURE 8. DEPLOYMENT CONTROL MECHANISM

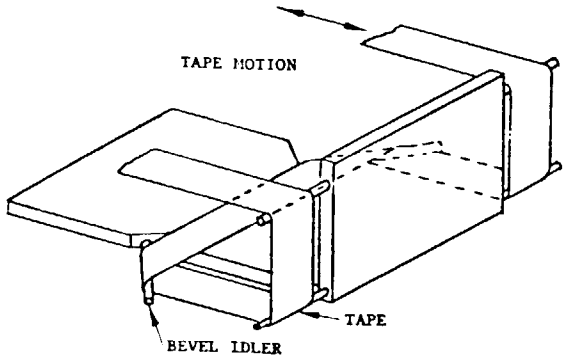

FIGURE 9. KINEMATIC MODEL OF THE DEPLOYMENT CONTROL MECHANISM

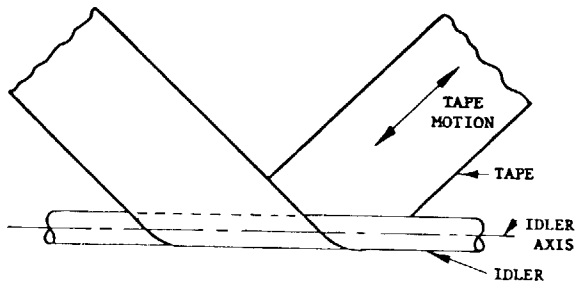

FIGURE 10. THE TAPE MUST SLIP ALONG THE IDLER AXIS

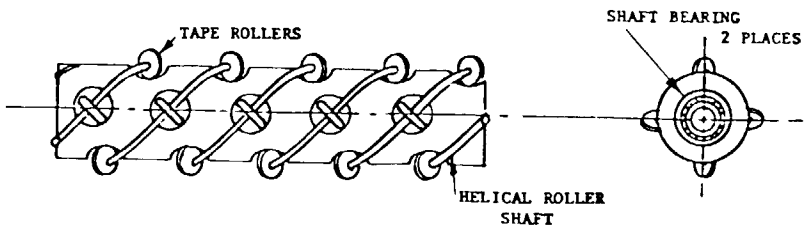

FIGURE 11. DUAL AXIS BEARING

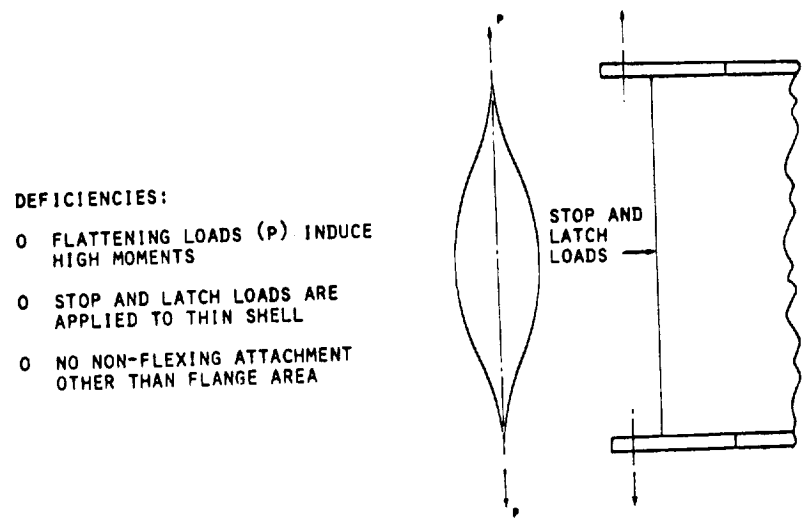

FIGURE 12. PREVIOUS RIB FLATTENING CONFIGURATION

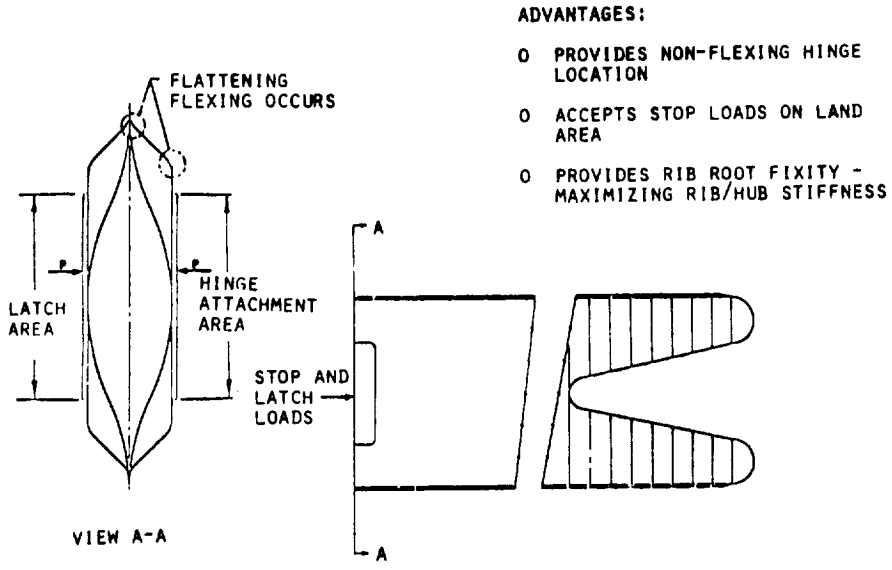

FIGURE 13. NEW TITANIUM RIB ROOT SECTION

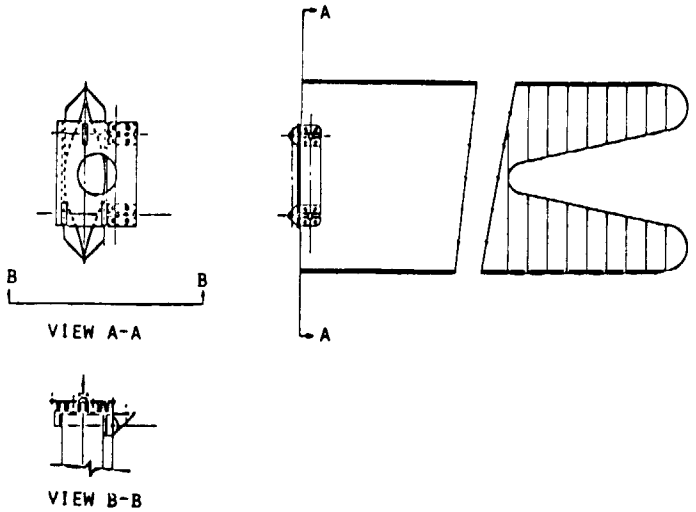

FIGURE 14. NEW RIB HINGE CONFIGURATION

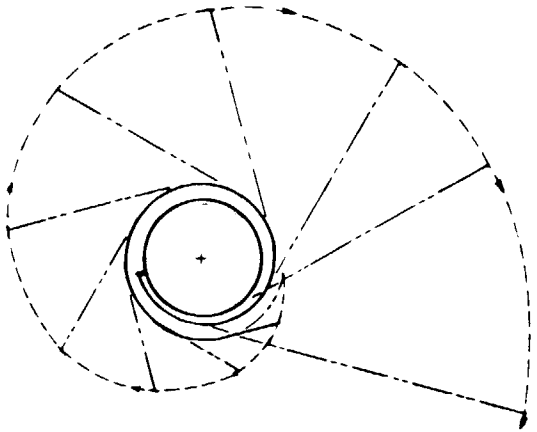

FIGURE 15. SPIRAL PATH OF A DEPLOYING RIB

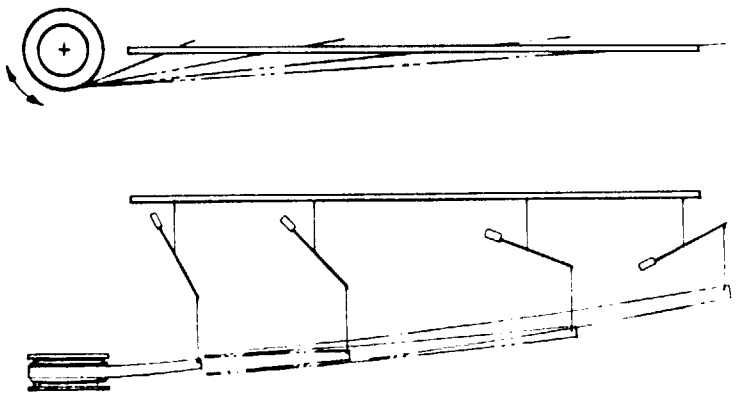

FIGURE 16. SHOWN ARE VARIOUS STAGES OF THE DEPLOYING RIB AND THE TEST SET UP

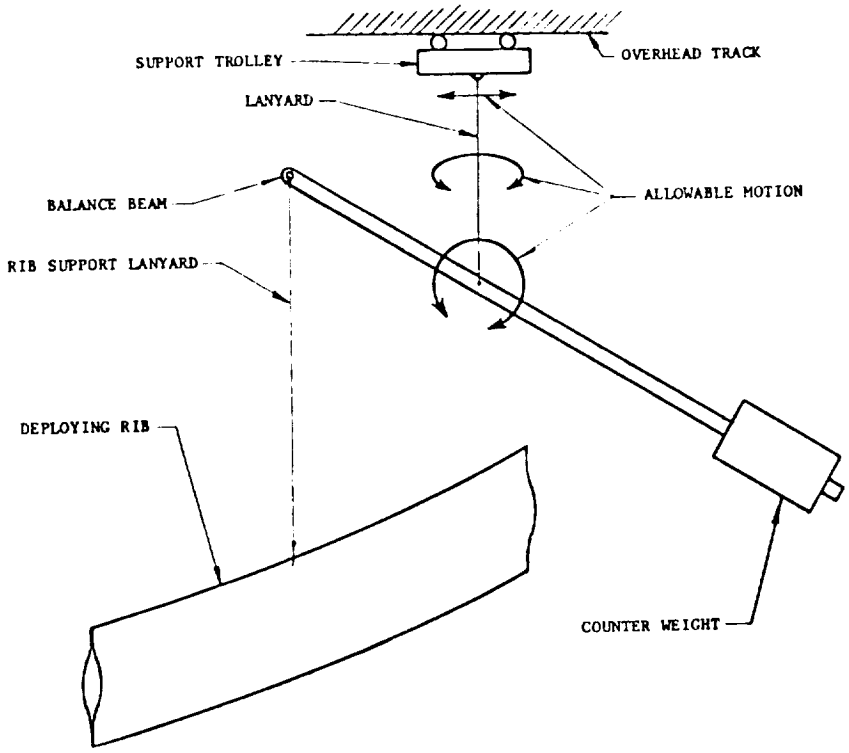

FIGURE 17. DYNAMIC RIB SUPPORT SCHEME

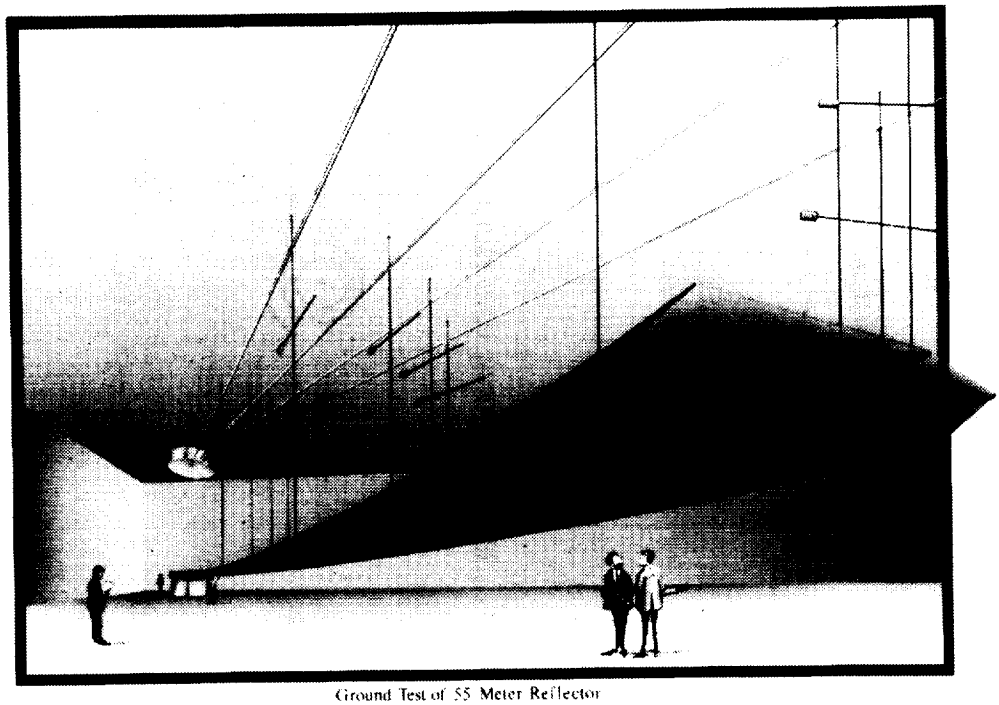

Ground Test of 55 Meter Reflector

FIGURE 18.

HIGH FREQUENCY DRIVE MECHANISM FOR AN ACTIVE CONTROLS SYSTEMS AIRCRAFT CONTROL SURFACE

Hugh E. Smith

Lockheed-Georgia Company

SUMMARY

The mechanism discussed herein was developed under a Lockheed-Georgia Company "Unconventional Controls Concept Program" for aircraft. It was successfully utilized on a wind tunnel model tested during January 1980 in the company's Transonic Blow-Down Tunnel. The mechanism is also applicable to a flying aircraft.

INTRODUCTION

Unsteady transonic aerodynamic data on supercritical wings with active controls are needed to support the growing effort in energy efficient transport aircraft design. Flutter tests on supercritical wings have indicated a pronounced transonic dip in the dynamic pressure flutter boundary, and there is a need for further tests and studies to fully explain the unsteady aerodynamic processes which are occurring at and near the wing flutter condition. In addition, since an active flutter suppression system may contribute to the efficient use of the supercritical wing on future transport aircraft, a need exists for unsteady transonic aerodynamic data on a number of fast acting control surface configurations.

To acquire some of these data an unsteady test facility was developed for use in the Lockheed-Georgia high Reynolds number blowdown transonic wind tunnel. A two-dimensional supercritical airfoil with a trailing edge control surface was driven sinusoidally at high frequency. (Fig. 1 & 2) The unsteady pressure response of the airfoil to the surface motion was measured utilizing high response Kulite pressure transducers. From this, the effect of Mach number and Reynolds number on the unsteady control effectiveness of the driven surface was determined for later comparison to predictions from current unsteady transonic airfoil codes. These comparisons provide a basis for the validation or correction of the predictive methods, which are in turn, essential to the design of active flutter suppression systems.

One of the most significant design problems in the development of the wind tunnel model needed to acquire this new type of data was that of actuating the control surface at the required frequencies under the extremely high loadings incurred on the model. This paper describes the innovative mechanism which proved necessary to accomplish the control actuations in the presence of the many severe constraints imposed by the tunnel installations environment.

CONTROL SURFACE DRIVE MECHANISM
(BY CONVERSION OF LINEAR MOTION TO ROTARY MOTION)

As with most complex mechanical systems, not one but several interrelated mechanical subsystems have been utilized

to accomplish our purpose. Two of the key innovative subsystems have been the subject of two separate patent disclosures. Their descriptions are as follows:

(a) Low Inertia-Anti-Backlash Drive Mechanism for High Frequency (150 Hz) Oscillation. (Fig. 3 and 4)

(b) Compact-Anti-Backlash Drive Mechanism for Conversion of Rotary Motion to Linear Motion. (Fig. 5 and 6)

The first converts linear motion to rotary motion while the second accomplishes the opposite.

It would have been advantageous to have driven the control surface from both ends simultaneously to minimize torsional wrap-up over span. However, the cost of solving the synchronization problem appeared prohibitive. During the development phase, a number of hydraulic actuator manufacturers were encountered who were certain their actuators and controllers could accomplish our purpose. Unfortunately, all of the hydraulic systems considered had a maximum operating frequency of approximately 90 Hz.

For this system the primary driving force is provided by a large (65g) electrical solenoid actuator originally purchased as a "shaker" for dynamic cycling of "flutter" test specimens. (Fig. 7) This "shaker" is powered by a typical control unit which permits rapid reversing (cycling) of the applied force.

The low inertia control surface drive mechanism is utilized in this application to impart an oscillating motion to an airfoil model control surface. The closely coupled drive mechanism is designed to achieve minimum torsional wrap-up and backlash of the connecting mechanism for optimum mechanical efficiency and low inertia. Conventional approaches usually involve the use of eccentric linkages similar to those found on early locomotive drive wheels. However, preliminary analysis revealed that this easier method utilizing a rapidly reciprocating actuator mounted 90^{o} to the driven drive shaft and coupled via an eccentric arm would not work. The restricted access to the model control surface area caused by the test facility wall structure (Fig. 8) further aggravated the problem by demanding a longer driven shaft than would otherwise have been necessary. Had a shaft of sufficiently low inertia to satisfy the frequency requirement been actuated in said manner most of the actuator motion would have been lost in shaft torsional wrap-up with little or no resulting motion of the control surface itself. These and other criteria dictated an unusual solution to a common problem.

Present applications of the principle utilized normally employ balls traveling in spiral grooves around the periphery of a cylinder such as those found in the so-called "yankee" or "ratchet" screwdrivers. However, this mechanism utilizes eccentrically mounted fixed rollers at

ninety degree increments along the actuator interior. All rollers track in the same helical square cross-sectioned groove cut in the driven shaft. (Fig. 9) The roller eccentric mounting permits pre-loading the mechanism to eliminate backlash. The close coupling of the mechanical parts minimizes weight and inertial loading, thereby reducing power requirements and permitting higher (150 Hz) frequency operation.

The control surface is fabricated from graphite composite laminate with a hollow core for minimum inertia and maximum stiffness. A hollow titanium torque tube extends the length of the control surface leading edge and is then flanged and keyed to the main driven oscillating shaft.

The control surface angular position is monitored by a variable impedance transducer. It operates on the principle of impedance variation caused by eddy currents induced in a conductive target. Electromagnetic coupling between the transducer and the target is dependent upon the separation distance. The output voltage of the system is proportional to the distance between the face of the sensor and any metallic (conductive) target. In this instance the target is a cam mounted on the oscillating control surface shaft. Obviously, a varying gap occurs as the shaft oscillates. Control surface angular position is determined by comparison of digital voltmeter readings with a calibration curve.

CONTROL SURFACE SHAFT LEAF SPRING LOADING MECHANISM
(BY CONVERSION OF ROTARY MOTION TO LINEAR MOTION)

Prior to operation the desired moment arm of an applied leaf spring load is selected. It is set by properly meshing an external gear on the oscillating shaft with an internal gear on a cam. During operation this variable tension leaf spring counterbalances the air load on the oscillating flap to control amplitude and/or frequency. Tensioning is varied by an electrically reversible motor with a worm gear reduction unit coupled to a ball bearing screw nut and sliding shaft assembly. (Fig. 5) Rotary motion of the sliding shaft is prevented by a unique keying method. First a slotted ball bushing (Fig. 10) is modified by insertion of a "spreader key". (Fig. 11) This spreader key aligns the ball bushing liner (floating recirculating) ball chambers with the outer ball bushing shell and prevents them from rotating. Thus a path is provided for a "guide key" (Fig. 11) which is then inserted in the sliding shaft assembly. Position of the sliding shaft and attached leaf spring is monitored by a linear potentiometer.

During testing, unsteady aerodynamic pressures on the airfoil and oscillating control surface are measured utilizing thirty-eight specially encapsulated high response differential pressure transducers. Four subminiature accelerometers also in the oscillating flap transmit inertia data. A strain gauge bridge on the oscillating drive shaft provides torsion information.

This mechanism was bench tested to 150 Hz in 1979. It was successfully utilized on a wind tunnel model tested in January and February 1980. (Fig. 12 and 13)

The purpose of the test was to measure the unsteady aerodynamic pressures on the two-dimensional LG6-616 airfoil with a 25% chord full span trailing edge control surface. Surface angle, hinge moment, surface and wing accelerations, steady pressures and incremental unsteady surface pressures were measured with the wing at a fixed angle of attack and with the flap oscillating at frequencies up to 150 Hz.

The model was mounted in the two-dimensional solid sidewalls of the test facility using standard tunnel fixtures in the south wall and special fixtures in the north wall. These special fixtures included a new tunnel window fitting, a new support pedestal and support brackets for the flap actuation system previously described.

The installation of the model and actuation system was such that model angle of attack could be adjusted using the normal tunnel remote control.

The unsteady tests were preceded by a short series of steady tests to determine the steady pressures for a range of surface settings at fixed angles of attack. During this steady testing the balance spring was calibrated to determine the relationship between the balance spring settings and the steady flap angle over a range of Mach numbers and Reynolds numbers.

Following the steady testing, the electrodynamic shaker was actuated and unsteady model data was recorded over a range of control surface frequencies, Mach numbers and Reynolds numbers.

The effects of varying these test parameters are shown in Figures 14 thru 16. Oscillograph traces of oscillating surface motion versus induced dynamic pressure disturbance are shown for comparison. The mechanism has proved very successful in meeting all its operational requirements. Its components functioned well and showed minimum wear resulting from the extensive testing. It appears that more precise adjustment of the cam actuator eccentric rollers can even further reduce system backlash during the tests planned for the latter half of 1981.

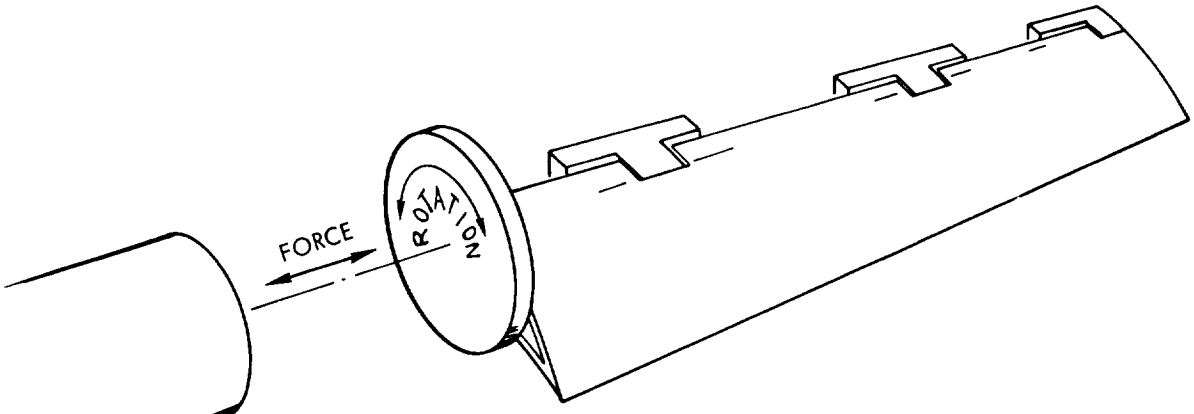

MAXIMUM APPLIED RECIPROCATING FORCE 75#

FORCE ACTUATOR TRAVEL = 0.12 IN. (±0.06 IN.)	MAXIMUM TRAVEL CONDITIONS
REQUIRED ROTATIONAL MOVEMENT = 20°(±10°)	
FREQUENCY 60 Hz	
FORCE ACTUATOR TRAVEL = 0.024 IN. (±0.012 IN.)	MAXIMUM FREQUENCY CONDITIONS
REQUIRED ROTATIONAL MOVEMENTS = 4° (±2°)	
FREQUENCY 160 Hz	

FIG. 1 SURFACE ACTUATION REQUIREMENTS

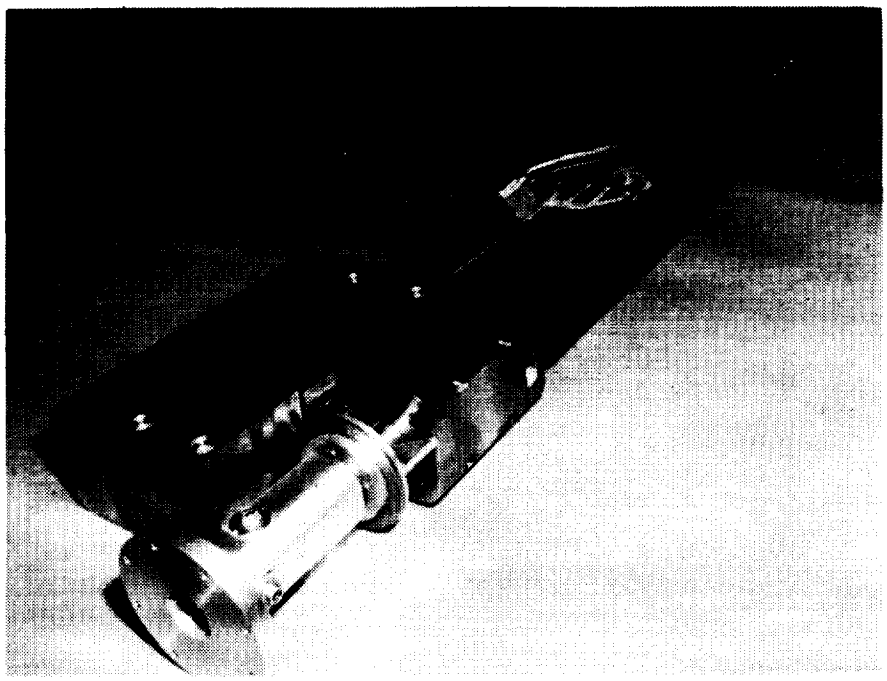

FIG. 2. WING, SURFACE AND ACTUATOR ASSY.

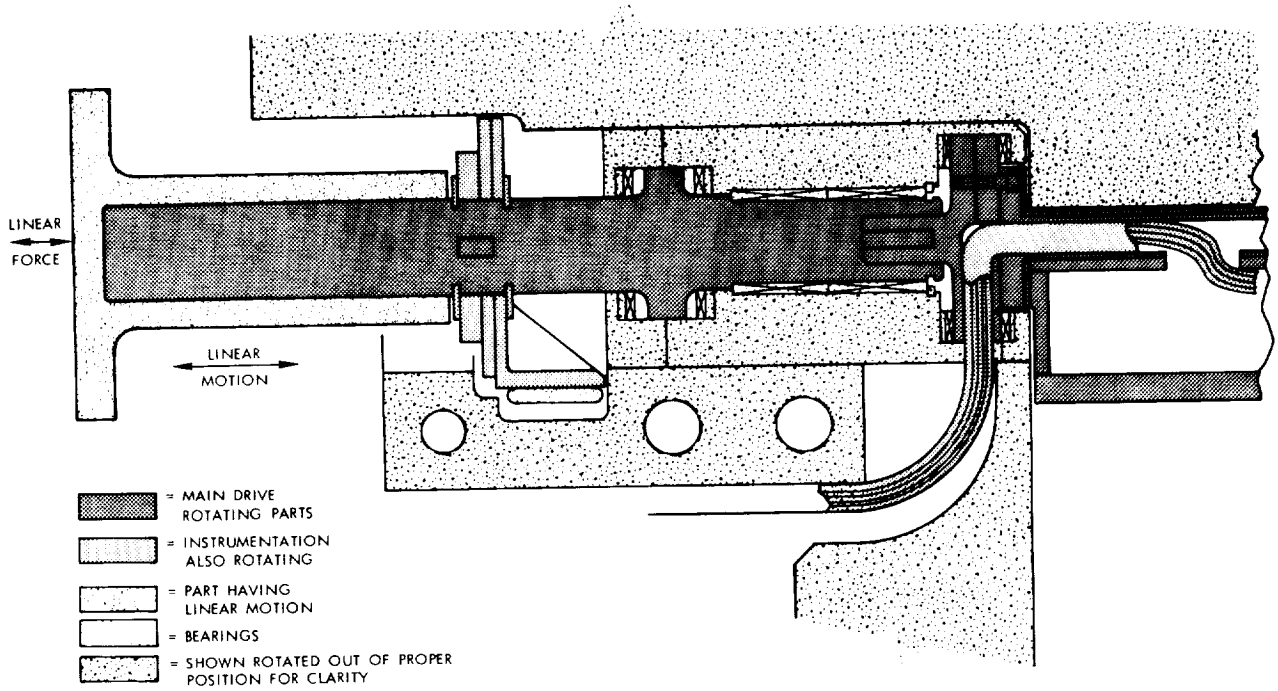

FIG. 3. SURFACE & ACTUATOR ARRANGEMENT (LINEAR TO ROTARY MOTION)

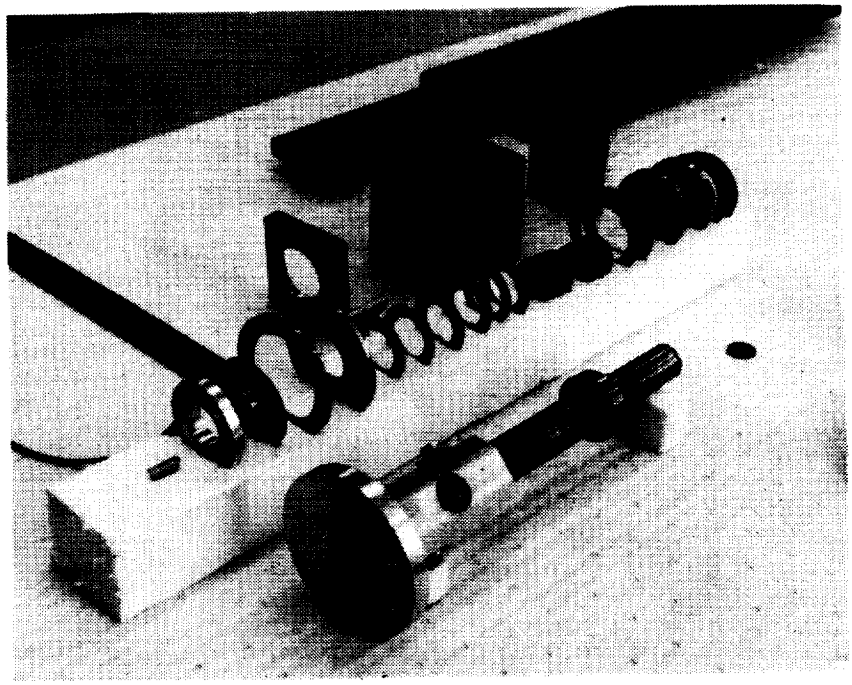

FIG. 4. SURFACE ACTUATOR COMPONENTS

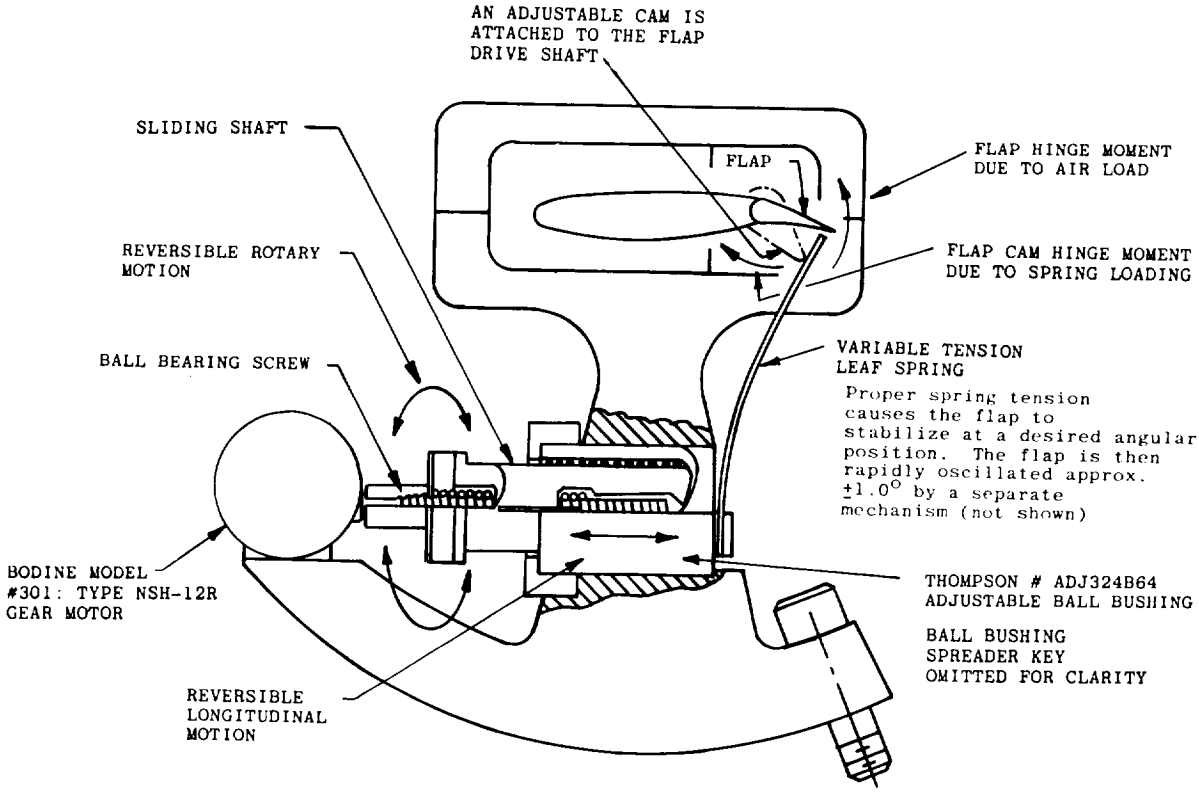

FIG. 5. CONTROL SURFACE LOADING MECHANISM (ROTARY TO LINEAR MOTION)

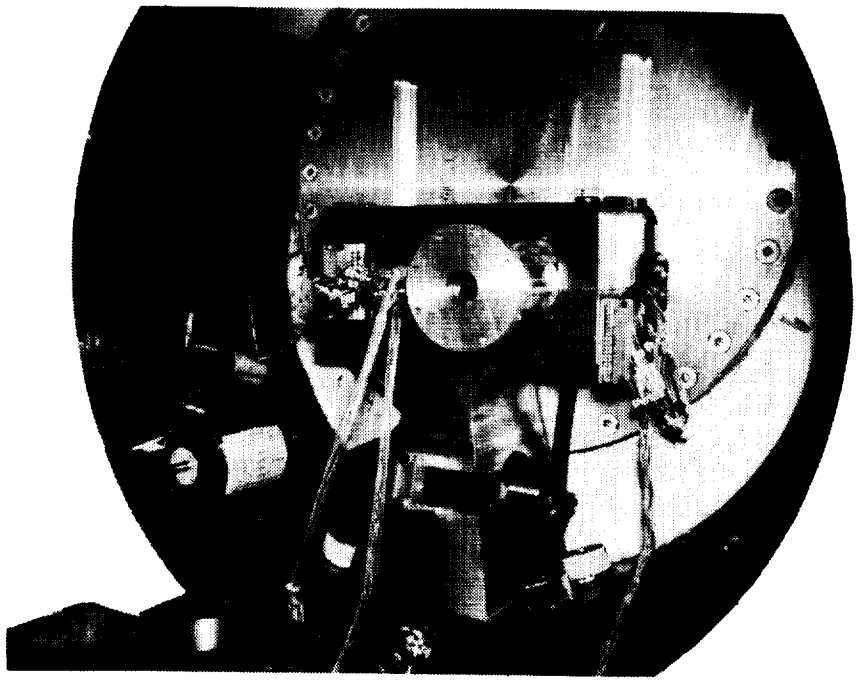

FIG. 6. SURFACE MECHANISM INSTALLATION

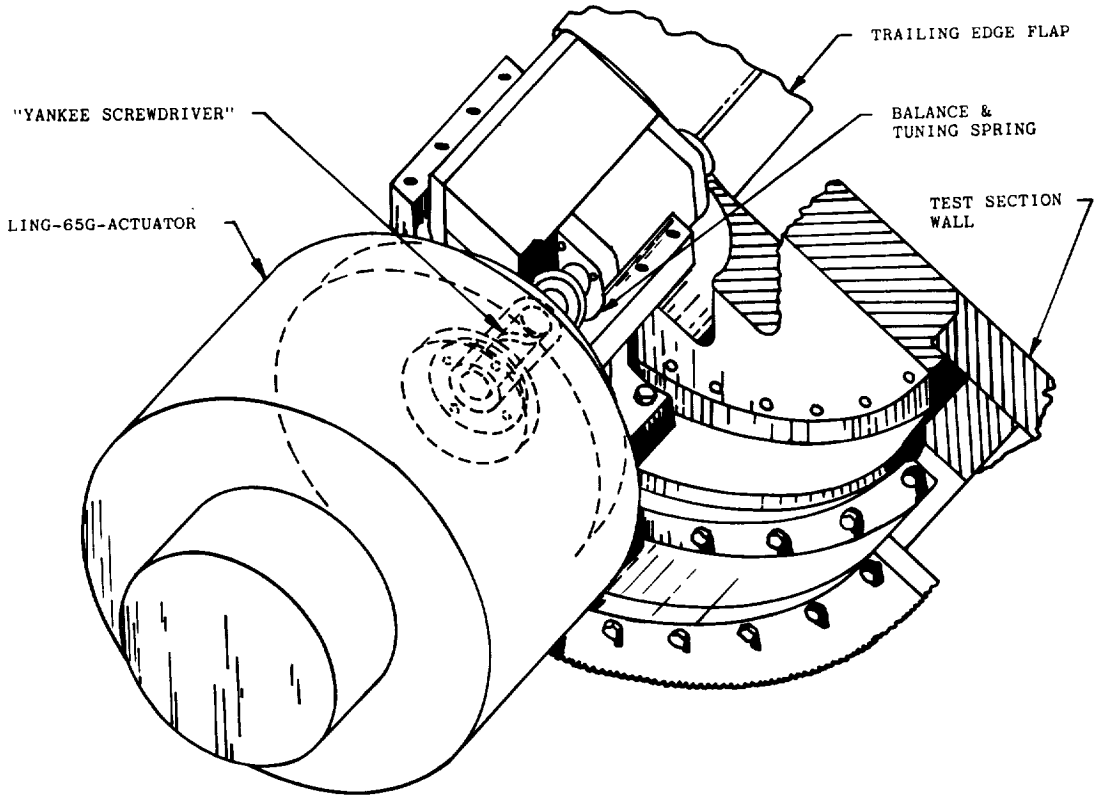

FIG. 7. SURFACE ACTUATOR AND MECHANISM ARRANGEMENT

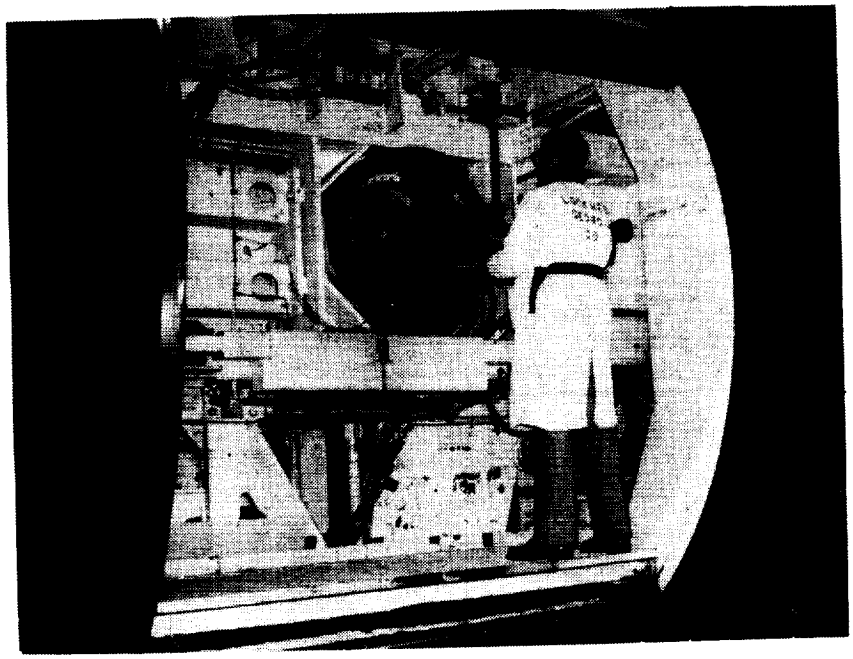

FIG. 8. SURFACE ACTUATOR AND MECHANISM INSTALLATION

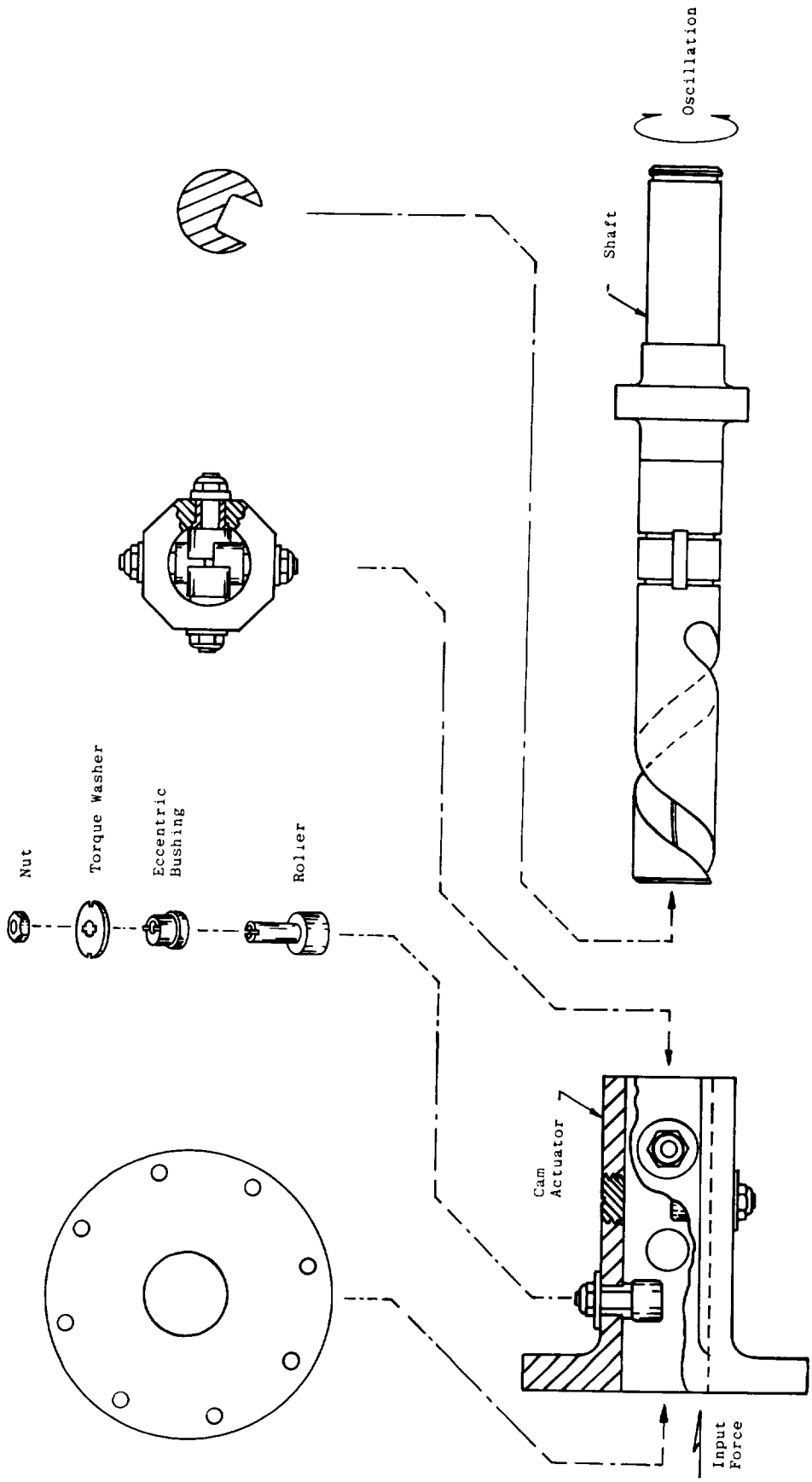

FIG. 9. CAM ACTUATOR DETAILS

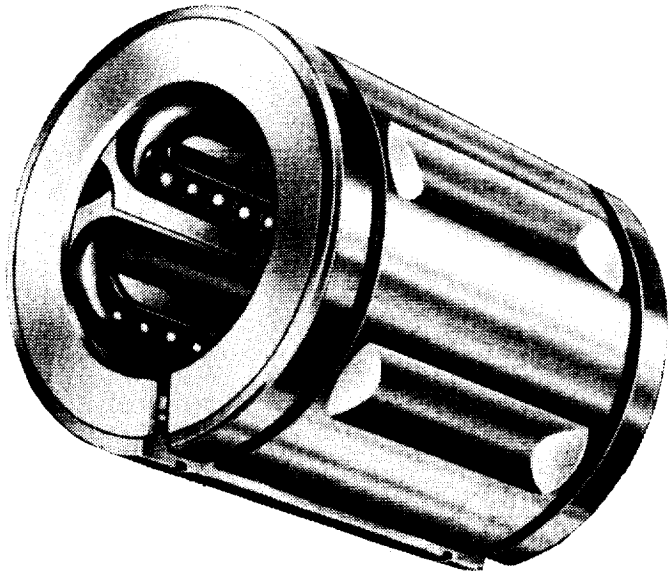

FIG. 10. LINEAR MOTION BALL BUSHING

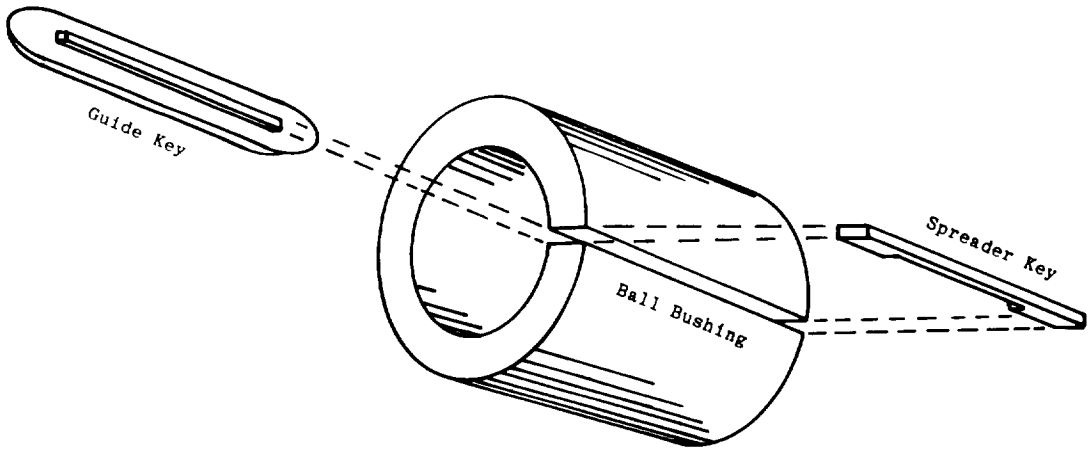

FIG. 11. BALL BUSHING MODIFICATION

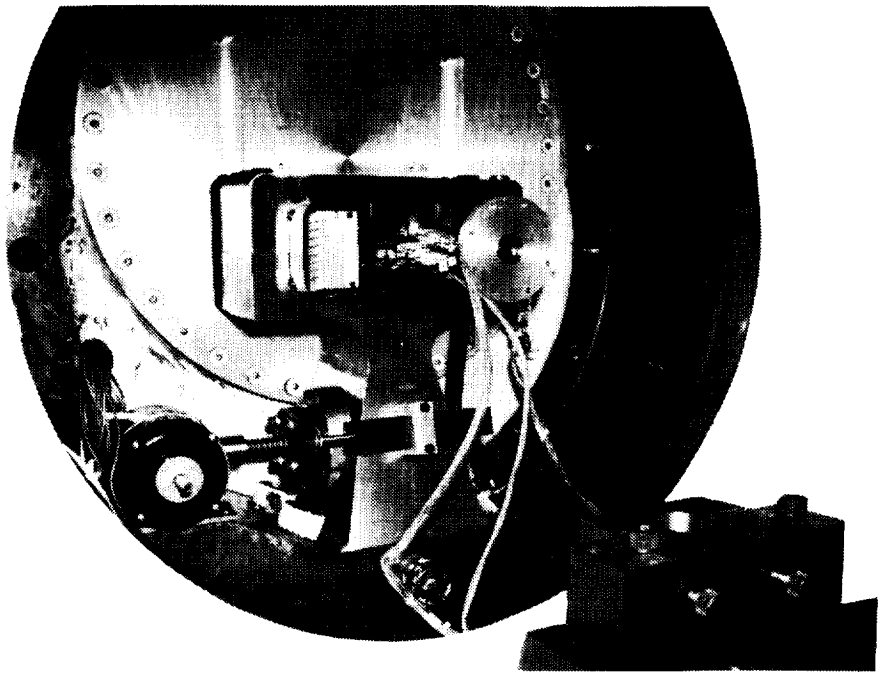

FIG. 12. CONTROL SURFACE MECHANISM INSTALLATION

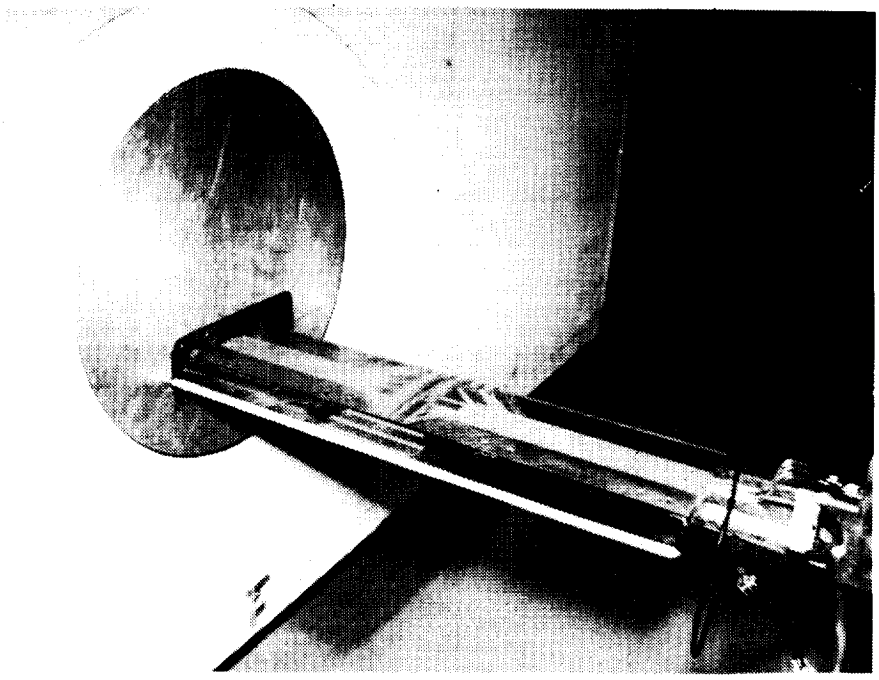

FIG. 13. WING AND CONTROL SURFACE INSTALLATION

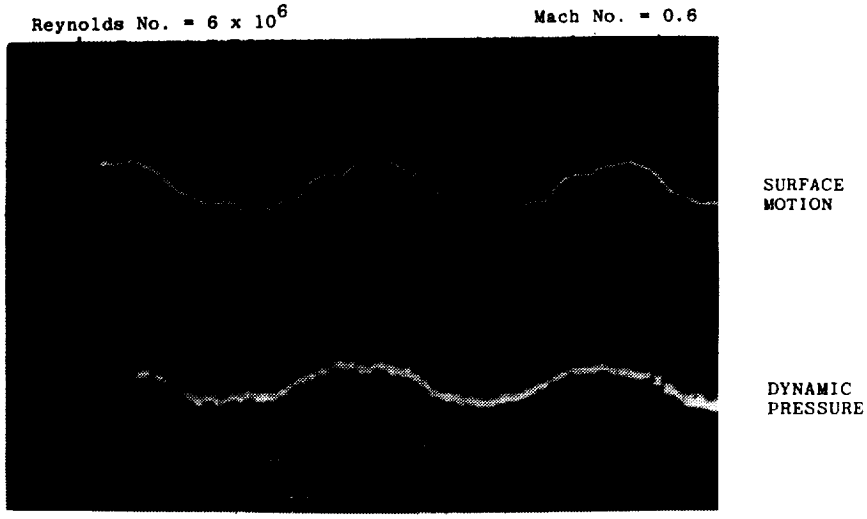

FIG. 14. FREQUENCY = 50 Hz

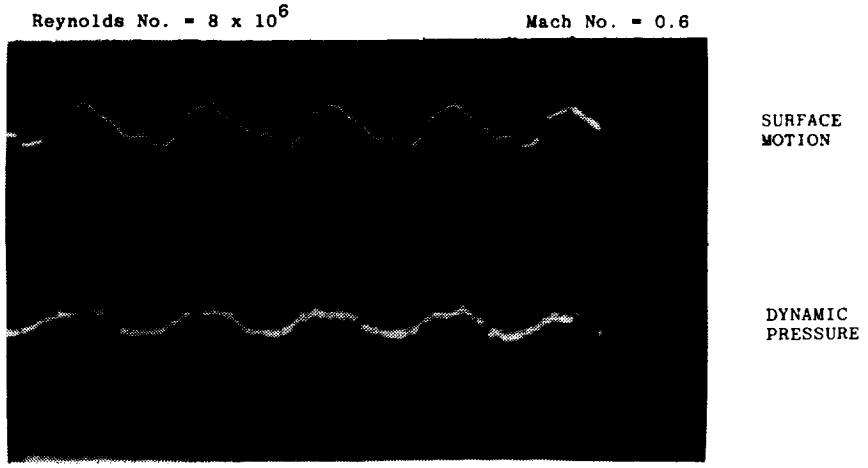

FIG. 15. FREQUENCY = 100 Hz

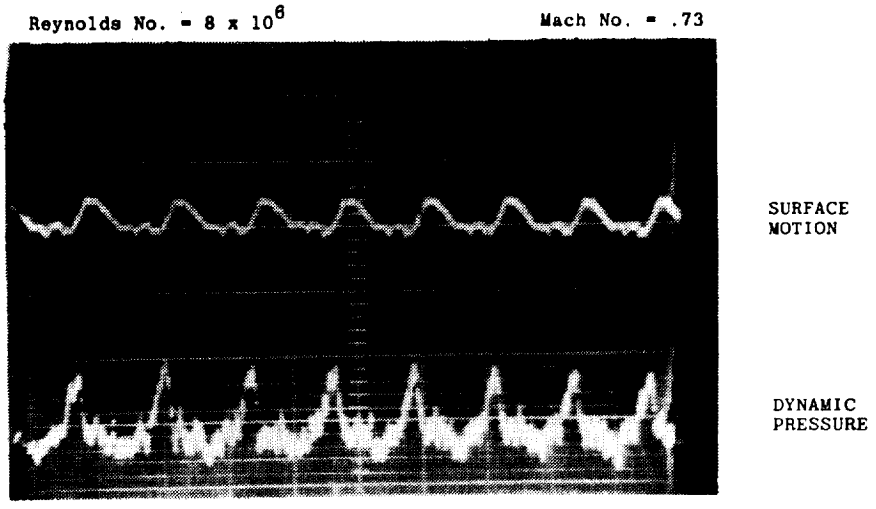

FIG. 16. FREQUENCY = 150 Hz

A BAPTA EMPLOYING ROTARY TRANSFORMERS, STEPPER MOTORS AND CERAMIC BALL BEARINGS

W. Auer
TELDIX
Heidelberg
Germany

ABSTRACT

The utilisation of rotary transformers as an alternative to slip rings for the power transfer from solar panels to a satellite's main body could be advantageous, especially if an AC bus system is taken into consideration. Different approaches with main emphasis on the electro-magnetic design were investigated and showed efficiencies of up to 99 % with a 3 kW power capability. A solidly preloaded pair of ball bearings with ceramic balls assures proper transformer air gaps and acceptable torque changes over temperature and temperature gradients. The BAPTA is driven by a direct drive stepper motor with inherent redundancy properties and needs no caging mechanism.

INTRODUCTION

For future high power satellites with a primary power of several kW's, the utilisation of a Bearing and Power Transfer Assembly (BAPTA) with rotary transformers as an alternative to slip rings for the power transfer from the solar panels to the satellite's main body, could be advantageous. In combination with an AC bus system, benefits concerning, for instance, reliability and weight can be achieved.

In Fig. 1 as an example a block diagram for the power supply of a TV broadcasting satellite, employing an AC bus is shown, indicating the rotary transformers. The DC voltages, generated by solar cells, are converted to AC voltages of a medium frequency by power converters, situated at the yokes of the solar panels. Because the solar panels follow the sun, the radiators of the converters can be mounted such as to be averted from the sun; therefore, the heat, generated by the converter losses, can be

directly radiated in the direction away from sun. No heating up to the satellite's main body occurs.

The AC power is transferred via the rotary transformers to a regulator which adds the two power channels by appropriate voltage and phase conditioning of the two power converters. The necessary signal feedback with the control loops is not shown for clarity reasons.

The AC bus power is available to several subsystems which may condition the AC power according to specifications: For instance, transform the bus voltage to defined AC voltages by small transformers, isolating the subsystems in a galvanic sense. The DC voltages may be obtained by simple rectifying or phase sensitive rectifying, allowing for voltage control.

A part of the AC power is fed via a rectifier to a battery and to the DC bus from which the subsystems, which have to operate also during eclipse (e.g. attitude control), are supplied. The positions of TV broadcasting satellites are chosen so that eclipses occur only after midnight local time in the receiving area.

In anticipation of this application TELDIX developed under contracts of DFVLR a BAPTA with two rotary transformers - for reliability/redundancy reasons - with a direct drive stepper motor and solidly preloaded ball bearings, employing ceramic balls.

DESIGN CONSIDERATIONS

The main requirements were the following:

- Power per BAPTA ..... 3 kW
- Transformers per BAPTA ..... 2 × 1.5 kW each
- Frequency ..... 10 kHz
- Efficiency ..... 99 %
- Outer Diameter ..... < 250 mm
- Length ..... < 300 mm
- Speed nominal ..... 1 Revolution/day
  maximal ..... 1 Revolution/30 min
- Step angle ..... about 18 arc sec
- Design life ..... 7 to 10 years
- Environmental conditions ..... according to TV-SAT specs.

These requirements were reflected in several design approaches.

The main points of discussion concerned the following:

1. General design
2. Transformer investigations
3. Bearing and housing problems
4. Drive and angular read-out components
5. Signal transfer

To 1: The rotary transformer may be built with a cylindrical (radial) or an axial air gap. If - as it is the case - two transformers per BAPTA are specified, only a design with radial air gaps can overcome the tolerance build-up without requiring costly adjusting procedures. The assembly can be as well straightforward in that stators and rotors can be mounted in their respective housing parts with good accessibility for measuring and documentation purposes; after that they can be easily assembled by pushing the rotor housing into the stator housing.

In addition, the mechanical interfaces between housing parts and transformer parts are concentric with the air gap surfaces, resulting in excellent accuracy properties.

To make full use of this accuracy potential, an adequate ball bearing arrangement for the suspension was developed, comprising two angular contact ball bearings, mounted on both sides of the transformer assembly (Fig. 2).

To 2: Two interrelated problem areas must be considered, that is, the core (magnetic active material) and the windings.

Two core materials were investigated: laminated and ferrite. Laminated materials allow for high induction values. Properly processed materials may also be used for the intended frequency range (about 10 kHz). But it turned out that laminated materials are difficult to apply for a rotary transformer. Especially the different flux directions - radial and axial - make it nearly impossible to derive an attractive design.

Good results were achieved with ferrite materials. The cores are built from rings, forming in a cross section a U-shaped core for both primary and secondary sections (Fig. 3).

This approach has also the advantage that different lengths of transformers with different power ratings may be designed with the same core elements.

It should be also noted that ferrite cores have the potential for utilization with low losses at higher frequencies

than the specified 10 kHz. Also rectangular shaped voltages can be used. Last but not least, investigations have shown a high radiation resistance of ferrites (Ref. 3).

Three winding types were studied, both theoretically and experimentally: Stranded wire, helix and foil windings.

Stranded wire technology is well known from high frequency applications. For a power transformer, it is essential, for low copper losses, to achieve a high fill factor. Since a fill factor of about 40 % only is possible, the results were not too promising (Ref. 4).

With laminated helix and foil windings, a fill factor in the order of 80 % could be realized. Skin effect losses should be small enough in both cases.

A study showed that the stray flux, penetrating the windings, could cause losses which are higher for the helix than for the foil winding technology. Early tests confirmed these theoretical results (Fig. 4).

To 3: The housing should provide a rugged but lightweight compartment for the transformers. The housing material should have also a good electrical conductivity for electromagnetic and electrostatic purposes. It should be a good thermal conductor and, concerning thermal expansion coefficient, match closely enough the ferrite of the transformers and the steel of the ball bearing rings. Considered were aluminum alloys, steel and titanium alloys. The latter material was rejected because of poor thermal conductivity. Models were built with steel and an aluminum/silicon alloy with comparatively low thermal expansion.

The ball bearings are arranged in a back-to-back configuration. At given diameter/distance/contact angle relations, an adjusted preload tends to be constant not only over temperature but also temperature gradients. Even a solid preload is possible (Ref. 5).

The chosen arrangement assures proper transformer air gaps in the whole temperature range and, therefore, reliable operation under thermal environmental conditions.

Ball bearings of this size are able to carry the launch loads without any caging mechanism.

To avoid lubrication problems, ball bearings employing ceramic balls are used. This approach was space qualified in the course of the development of a double gimballed momentum wheel.

These bearings meet by a wide margin the design life and can be utilized in a wide temperature range, which is essential due to the heat generated by the transformer losses.

TELDIX has also manufactured ball bearing made totally from ceramic material. In a life test, a bearing unit accumulated to the present time more than 10 million revolutions. This makes these ball bearings an attractive alternative to those described above.

To 4: Different drive principles were investigated, such as DC motors with gears, both brush and brushless types, direct drive DC motors, stepper motors with reduction gears and stepper motors with inherent reduction mechanisms (direct drive), needing no additional bearings.

The last mentioned type was selected as a result of a trade-off process which included the assessment of weight, electrical and mechanical expense, interface with electrical and mechanical subsystems of the satellite, and reliability. This friction type stepper motor (Ref. 6) has, without a further reduction gear, a single step capability in the order of 10 arc sec. Despite the fact that the steps have a tolerance in the order of 20 %, depending on the torque, the positive angular movement per commanded step allows by counting an estimation of the accumulated angular movement. Therefore, perhaps even a "synchronisation" per revolution, accomplished by a simple "zero pick-off", may be sufficient for appropriate operation.

At ESTL, three such friction type stepper motors were successfully thermal vacuum tested for many millions of steps, against varying torques. This motor was also fully space qualified in an application as a gimbal drive in a double gimballed momentum wheel. It is also utilized for other mechanisms, as antenna pointing mechanisms.

In an investigation (Ref. 7), the effect of off-set angles of the solar panels for attitude control purposes was studied.

In this application, attitude control signals "override" - within certain limits - the synchronous speed signals. The pointing accuracy of the solar panels to the sun is in this approach of a second order importance; therefore, the above mentioned tolerance build-up would have no significant impact. It should be also mentioned that this motor has inherent redundancy properties.

To 5: Signal transfer is necessary, for instance, to command and control power converter operation.

It is obvious that one thinks first about a telephone type carrier system, where the signals are modulated, for instance, as a pulse pattern and transferred via the rotary transformers. But an investigation showed that a signal slip ring arrangement (low power) is by far the best solution with respect to cost and reliability.

FURTHER IMPROVEMENT OF EFFICIENCY

As shown in Fig. 4, with a foil winding an efficiency of 98.1 % at full power (1.5 kW per transformer) was achieved; this is valid for a primary to secondary voltage ratio of 1:1. At a ratio of 1:3.3, primary 30 V to secondary 100 V, the efficiency dropped to only 96 % with an unacceptable heating up of the mechanism. **This loss of 4 percent of 3 kW means a heat generation of** 120 W in this comparatively small mechanism.

The loss budget for the transformer with 96 % efficiency was the following: Iron losses amounting to 3.3 W and total losses of about 60 W. The calculated copper losses, that is, resistive and skin effect losses should be in the order of 6 W. The difference of about 50 W was the subject of an intense theoretical study.

In the course of this effort, a numerical analysis of the stray flux has revealed that this flux is essentially in the axial direction with **the defined field strength a function of the** radius (Fig. 5).

The flux strength B_σ penetrates the laminated windings. In Fig. 6 left, an axial view of a laminated foil winding, consisting only of two laminations, separated by an insulation foil, is shown in principle together with B_σ. The alternating field strength induces a voltage in this winding, which causes a short circuit current, indicated by arrows, circling only inside the transformer. Additional copper losses are the result.

These losses can be reduced considerably, if the laminations are crossed, as indicated in the Fig. 6 right. The induced voltage is smaller than in the above case and can approach zero, if the crossing is made at the proper location of the winding, which depends on the flux **profile over the radius.**

The winding technology to achieve this crossing of laminations was developed and implemented in the rotary transformer.

The results confirmed the theoretical predictions: The total losses were as low as about 15 W in the most favorable

voltage/current combination, at a power of 1.5 kW. In Fig. 7, the efficiency η, the losses P_V, the copper losses P_{Co} and the iron losses P_{Fe} are shown at a constant transferred power of 1.5 kW with different currents and voltages corresponding to the 1.5 kW value.

It should be noted that a further efficiency potential of 99.3 % is given, assuring that an efficiency of 99 % should be achievable during production.

Thermal vacuum tests at about 10^{-5} mbar with full power transfer were conducted at different temperatures. The heating up was measured at the "hot spot" in the middle of the primary winding. At + 50 °C test temperature, a winding temperature of 76 °C was measured at - 20 °C, + 21 °C.

This transformer has a main inductance of 245 µH and a stray inductance of 3.74 µH.

RESULT OF BAPTA DEVELOPMENT

The following results were achieved in the course of the development efforts of a BAPTA with rotary transformers:

- Power per BAPTA ..... 2 × 1.5 kW
- Efficiency ..... 99 %
- Outer diameter ..... 123 mm
- Inner diameter ..... 50 mm
- Length ..... 220 mm
- Mass ..... 8.2 kg
- Step angle ..... ≈ 10 arc sec
- Motor torque ..... > 0.5 Nm
- Friction ..... ≈ 10^{-2} Nm

These results compare favorably with the requirements, stated above.

CONCLUSION

It has been demonstrated that it is possible to **build** a BAPTA with rotary transformers, showing favorable properties for the employment in high power satellites. It is believed that the penalties of weight and efficiency, compared with a slip ring BAPTA, are compensated, if an AC bus system is employed, which has the additional advantage of having low electrical noise properties.

It should be also mentioned that other applications for rotary transformers in spacecraft exist. For instance, for remote sensing satellites with high pointing requirements, the torque noise of a BAPTA with slip rings limits the pointing accuracy of the instruments. This can be overcome by using rotary transformers.

The availability of high efficiency rotary transformer BAPTA's should be a stimulation to take these devices into account for future projects.

REFERENCES

1. Lucius, G.: Studie über die Entwicklung eines Drehtransformators ...
   Abschlußbericht für DFVLR-BPT, Vertrags-Nr. RV 21-V9/74-QH-91-205-23, Juli 1976.

2. Lucius, G.: Studie über die Entwicklung eines Drehtransformators ...
   Abschlußbericht für DFVLR-BPT, Vertrags-Nr. 01 TO 105A-V 12 WRT 2075, März 1978.

3. Resch, W.: State of Ferrites after Exposure to High-Energy Radiation, Siemens Review XL1 (1974) No. 6.

4. Marx, S.H. and R.W. Bounds: A Kilowatt Rotary Power Transformer, IEEE Transactions on Aerospace and Electronic Systems. Vol. AES, No. 6, November 1971.

5. Auer, W.: Untersuchungen über die Änderung der Vorspannung durch Temperaturdifferenzen in der Lagereinheit.
   SYMPHONIE-Report 15 020 - 287, Mai 1973.

6. Moll, H.: Schrittmotoren mit hoher Winkelauflösung, Feinwerktechnik und Meßtechnik, 86. Jahrgang 1978, Heft 4.

7. Renner, U.: Attitude Control by Solar Sailing - A Promising Experiment with OTS-2, ESA Journal 79/1.

8. Auer, W.: BAPTA with Rotary Transformer, ESA-Symposium 'Photovoltaic Generator in Space', Heidelberg 15-17.04.1980.

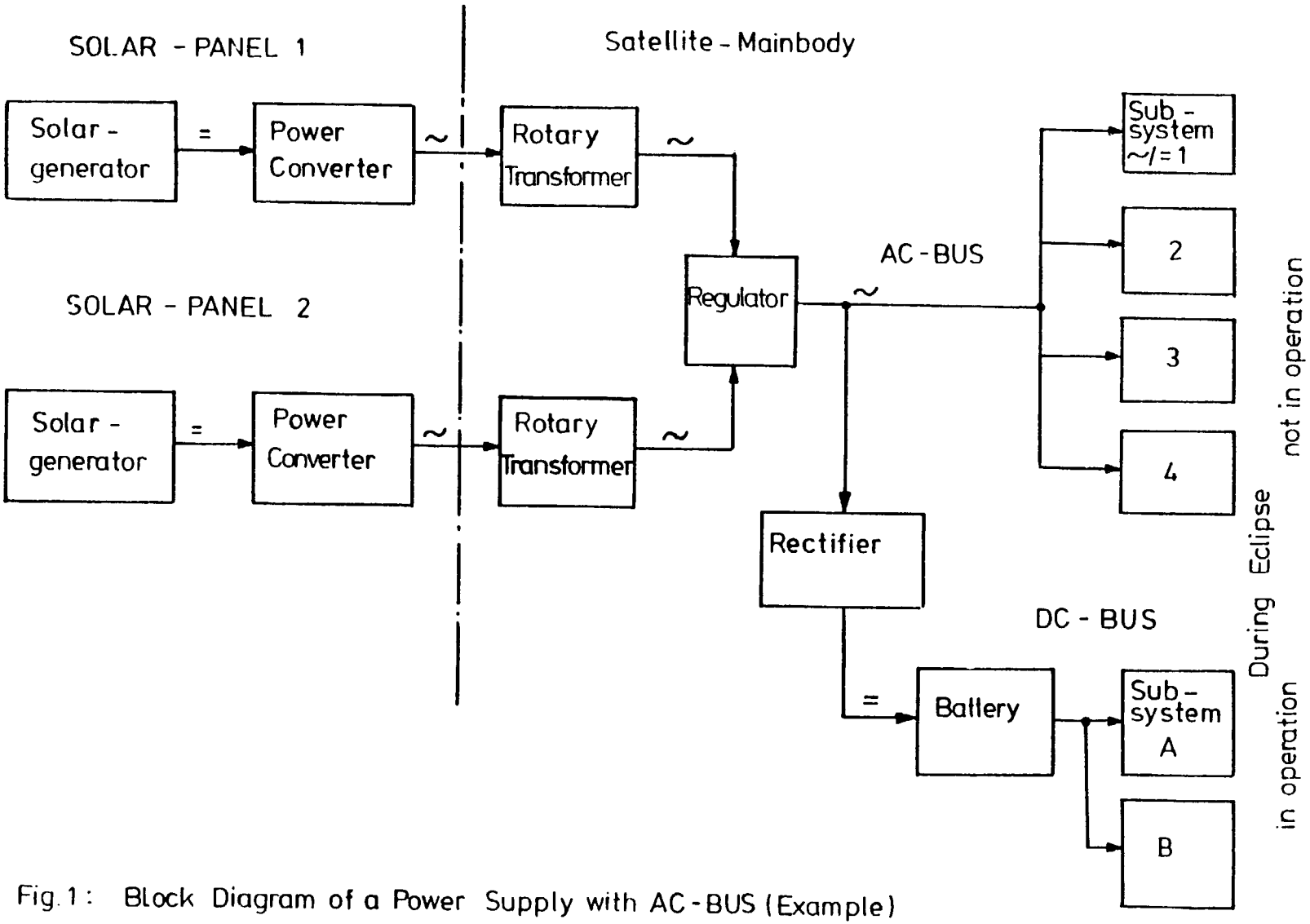

Fig. 1: Block Diagram of a Power Supply with AC-BUS (Example)

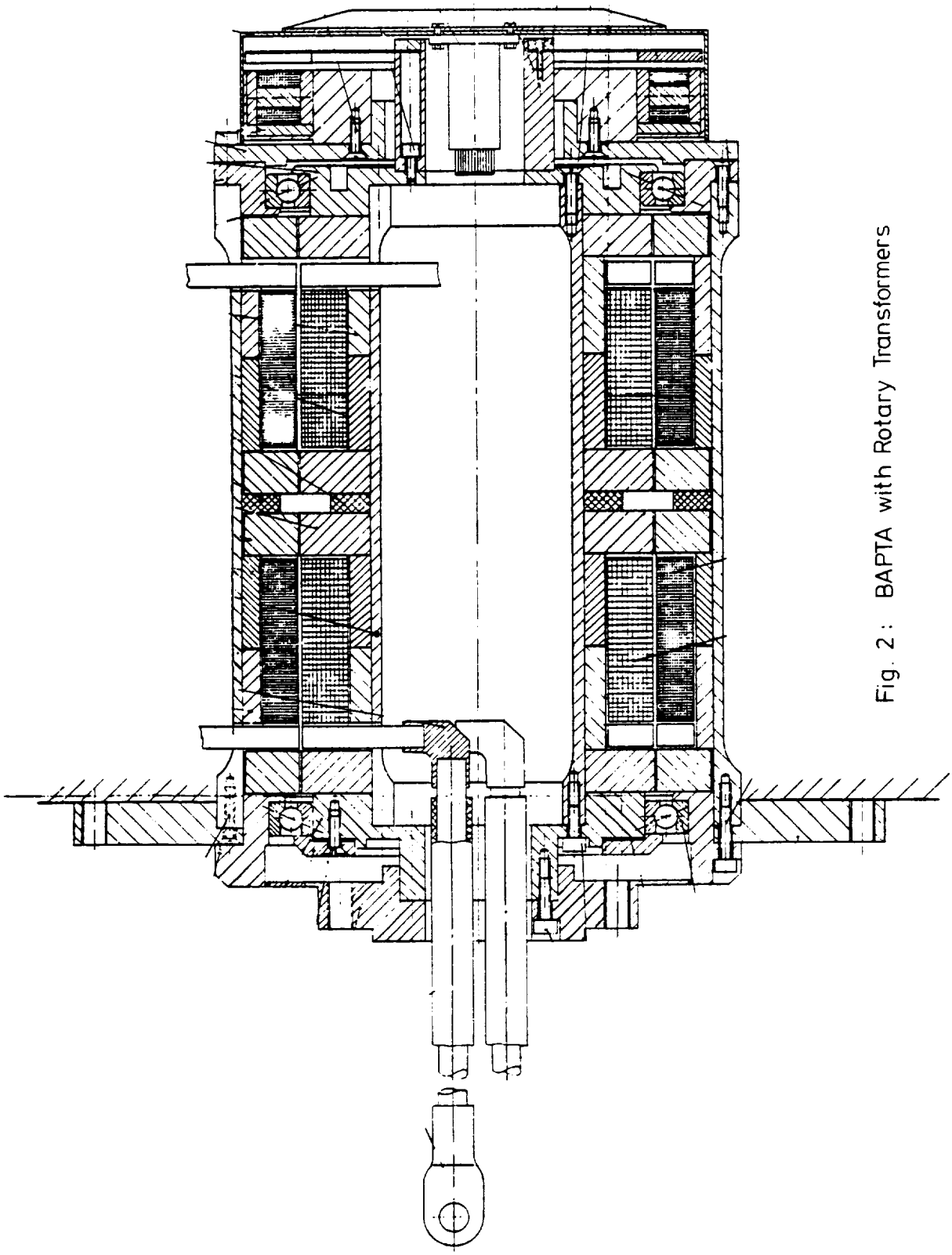

Fig. 2 : BAPTA with Rotary Transformers

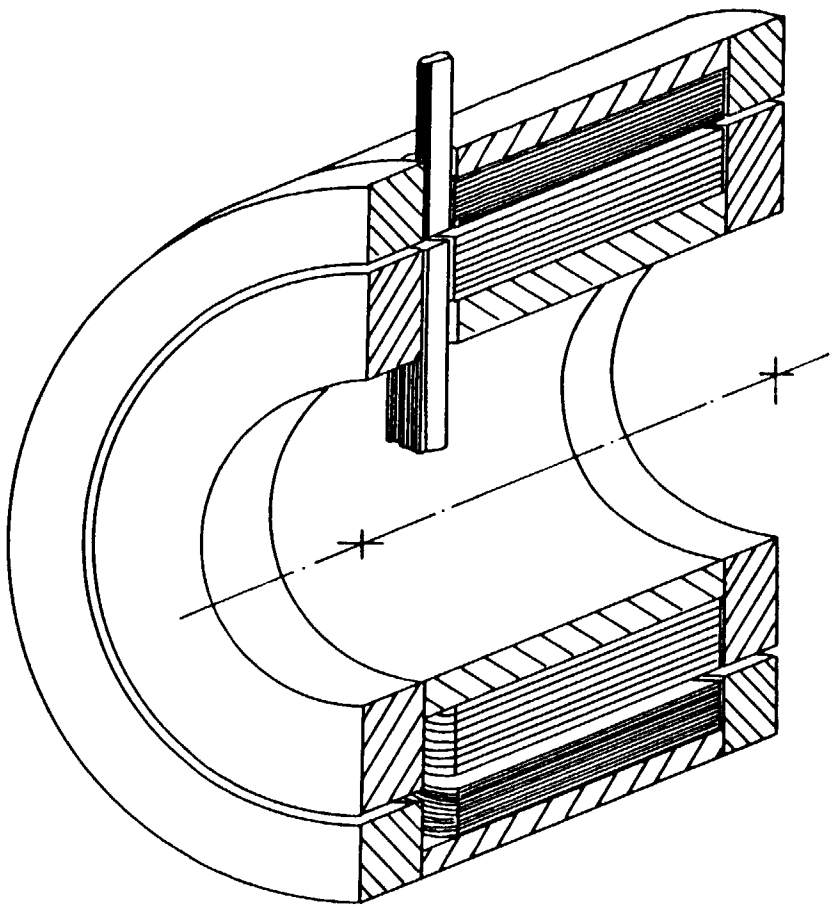

Fig. 3 : Arrangement of Ferrite Core and Foil Windings

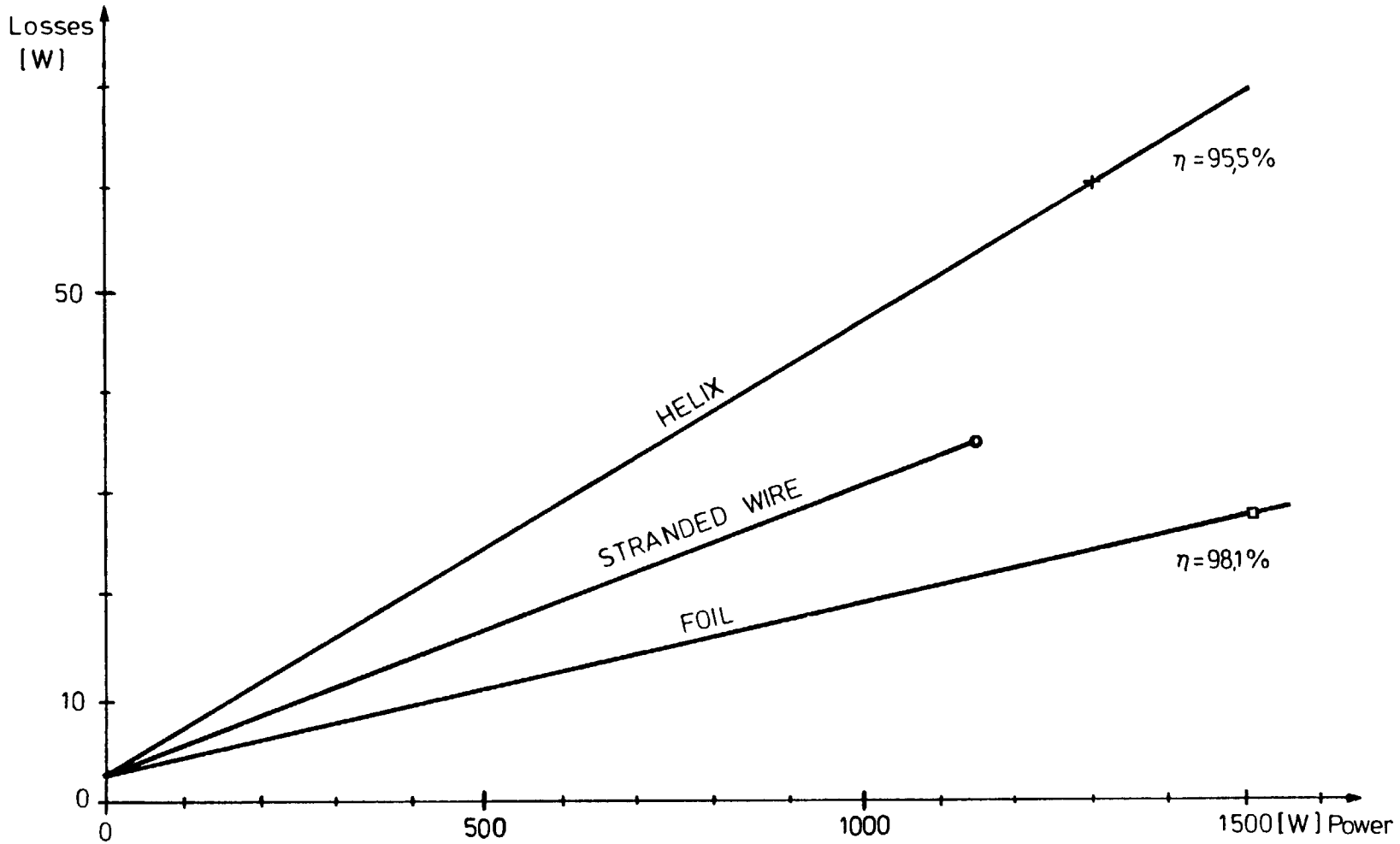

Fig. 4: Losses over Power for different Windings

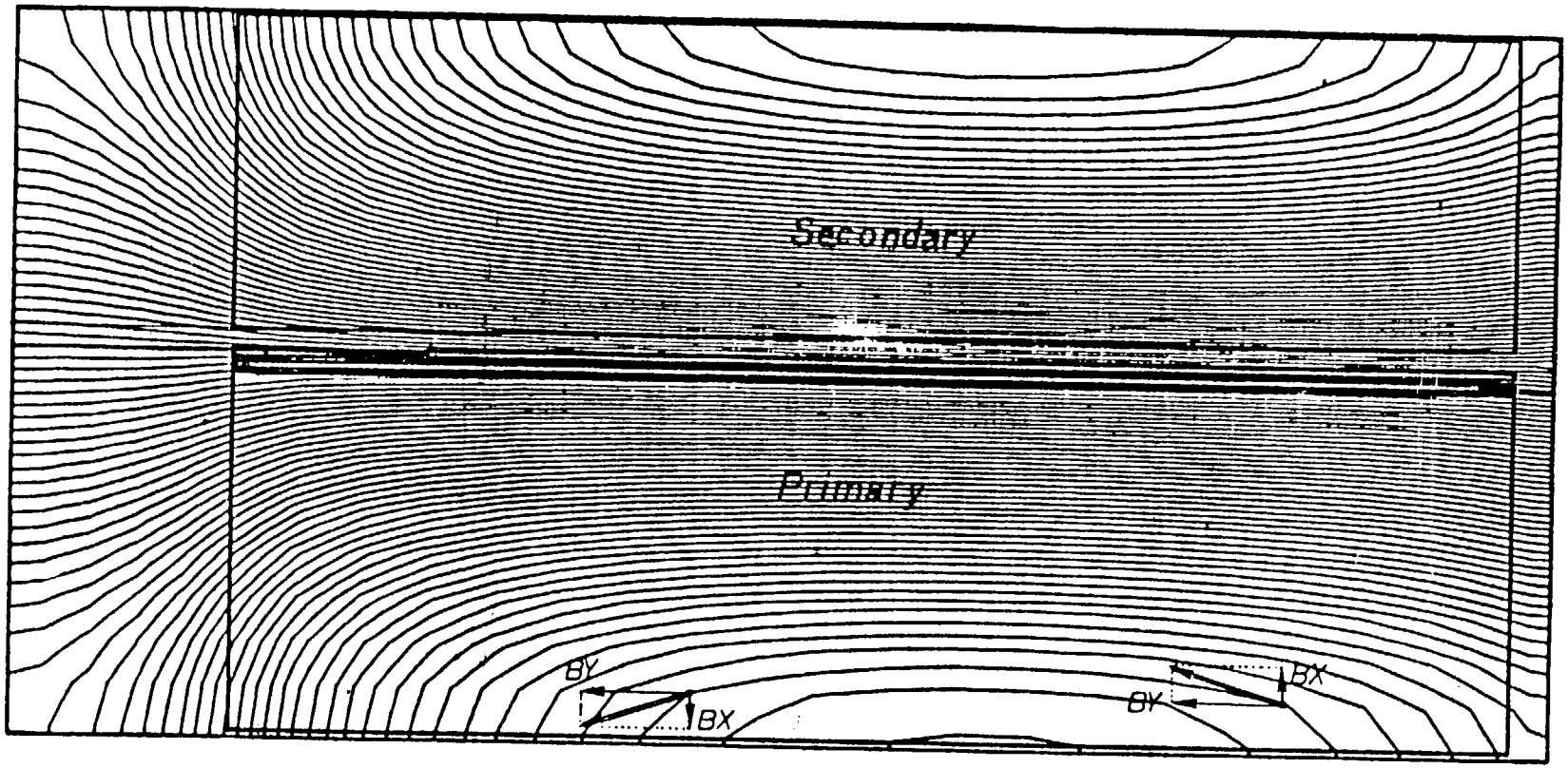

Fig. 5: Stray Flux through the primary and secondary Windings

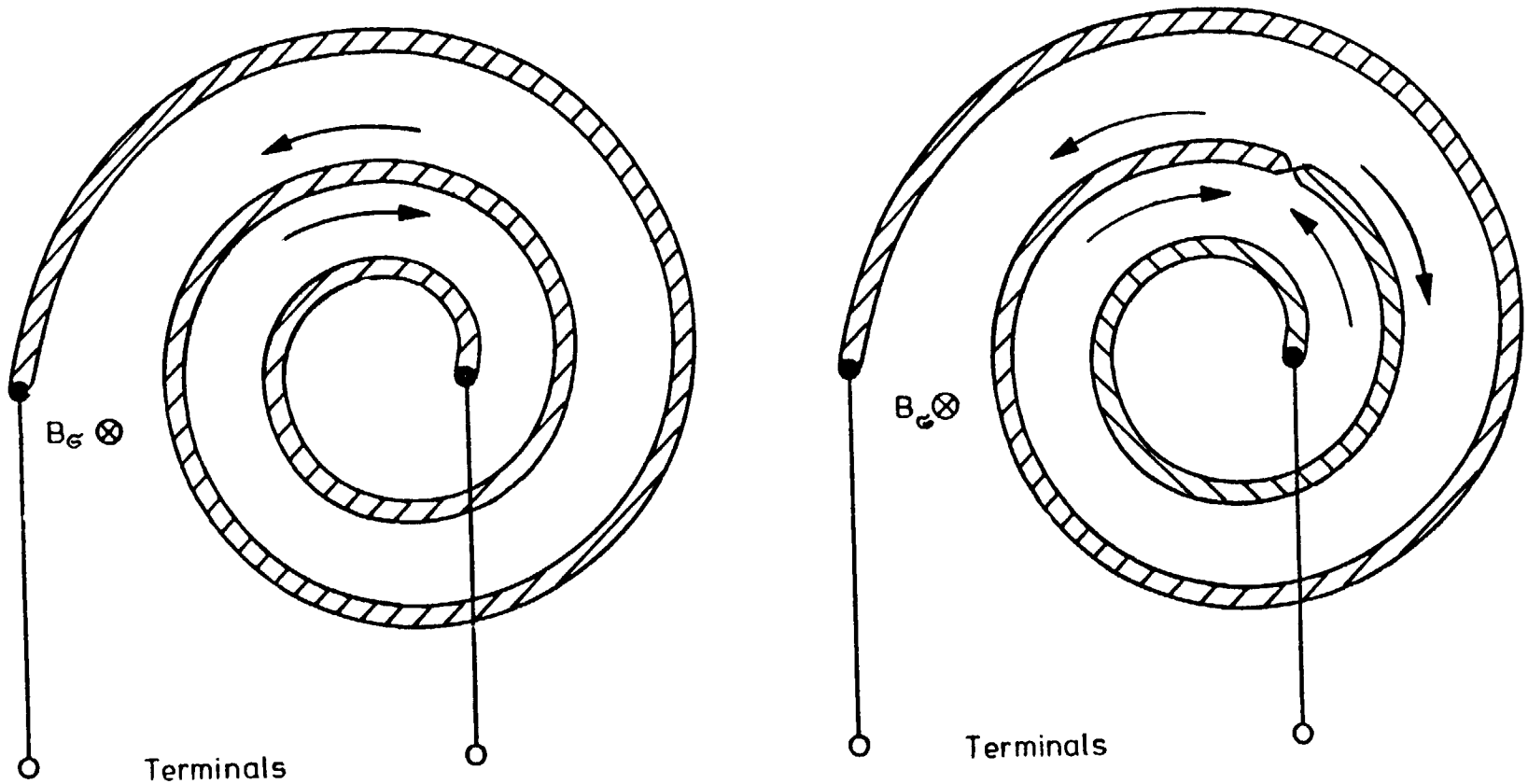

Fig.6 : Stray Flux induced Losses

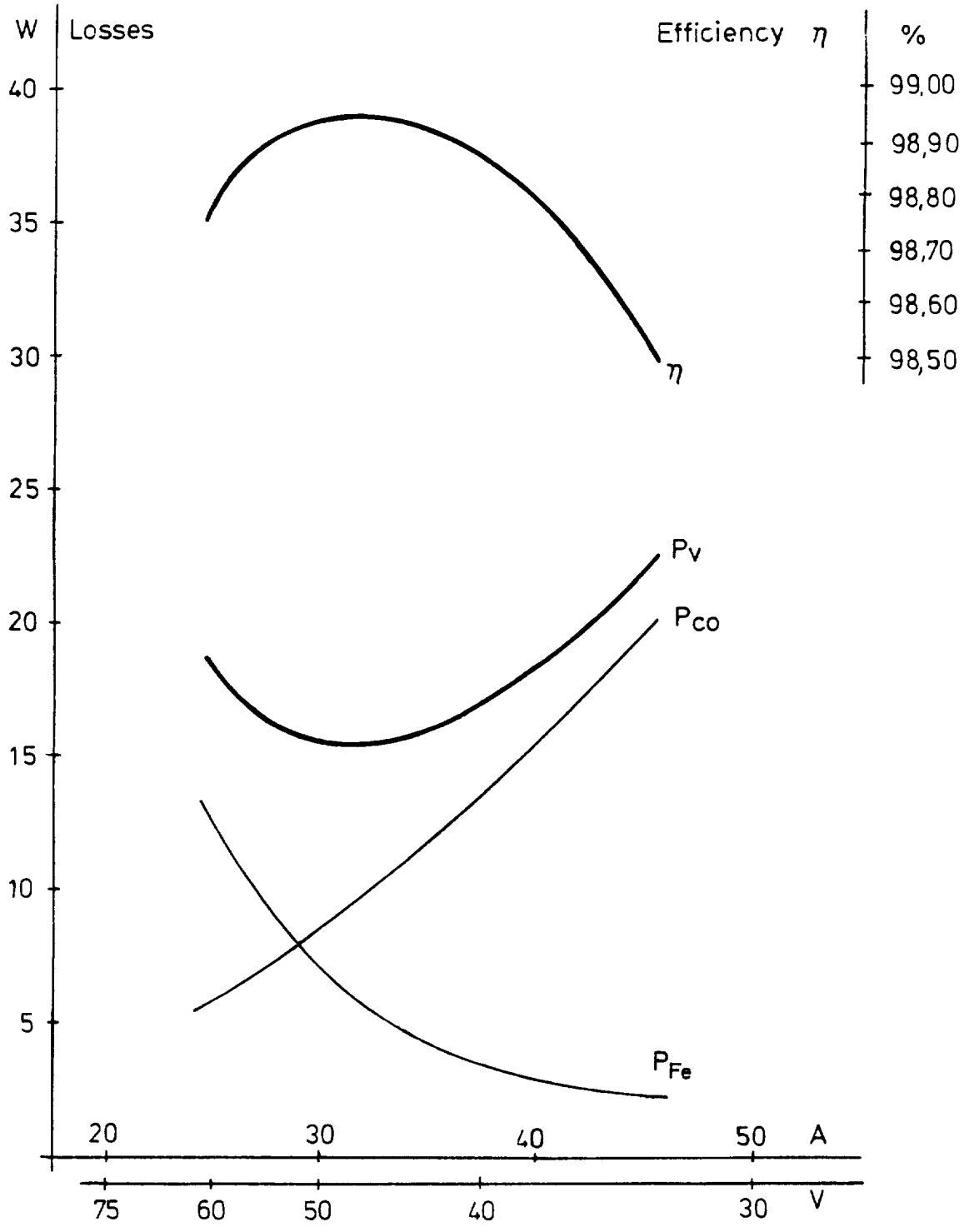

Fig. 7: Losses and Efficiency

A MECHANICAL DRIVE FOR RETRACTABLE TELESCOPIC MASTS

By M. E. Humphries*

ABSTRACT

There is a continuing requirement for lightweight extendable structures to deploy and support flexible solar arrays. One such structure is a telescopic mast deployed by compressed gas. This provides a simple and lightweight solution for mission applications requiring a single operational deployment, but is not inherently well adapted to missions requiring mast retraction. To meet the need for multiple operation cycles an alternative mechanical drive system has been developed by BAe which has the capability for mast retraction. The manner in which the mechanism design has evolved to the present development model status is described in this paper.

INTRODUCTION

During 1979/80 a contract funded under the Advanced Supporting Techology Programme (ASTP) and coordinated by ESA was undertaken. The aim of the contract was to develop a mechanical drive system capable of deploying the BAe telescopic mast, and thereby providing a back-up to an existing pressurised gas deployment system. The mechanism design had to be compatible with existing mast interfaces, and offer an improvement in performance where possible. In addition it had to extend the growth potential of the telescopic mast by meeting new requirements such as multiple operational cycles for Shuttle-borne missions.

THE GAS SYSTEM

The existing gas-driven telescopic mast (figure 1) consists of commercial aluminium alloy tubing with a wall thickness of 0.5mm and tube diameters varying from 40 mm to 150 mm in 5 mm steps. Each tube is nominally 2 metres long, depending on mast length and number of tubes. Front end collar fittings clamped around flares on the outboard end of each tube contain adjustable bearing pads (which run on the outer surface of the next smaller tube) and sprung latches (which lock that tube out when fully deployed. The inboard end of each tube has bearing pads (which run on the inside of the surrounding tube), sliding gas seals, bonded collar fittings (which provide an end stop for tube travel), rebates for latch engagement at the end of travel and ramping fingers to release the next tube section and therefore ensure sequential deployment of the tubes.

* British Aerospace, Dynamics Group, Bristol Division, Filton, England.

Mast deployment is controlled by the rate of admission of nitrogen gas through an orifice and by an escapement mechanism mounted at the base of the mast and connected to its tip by a cable. Mechanical backlash of the assembly is eliminated by incorporating interference fits between tubes and bearing pads which utilise the inherent flexibility of thin walled tubing. Each moving tube has a guidstrip bonded to it which acts as a key to prevent relative rotation of the tubes during and after deployment.

MECHANICAL DRIVE

Design Requirements

The mechanical drive concept had to embody the two major advantages of the gas system, i.e. simplicity and low mass. It also had to be compatible with the existing mast design and the range of available tube sizes, the most critical being tubes of 40 mm dia. and 3.0 m long. The mechanism had to provide controlled deployment at a rate between 20 mm/sec and 200 mm/sec against the highly variable load resulting from latching forces, inertia forces and tube bearing pad friction; the latter varies due to the effects of tube tolerances on the interference fits at the tube joints. The maximum accumulated force was estimated to be 240 N. In addition to typical spacecraft launch vibration and thermal/vacuum environmental constraints, there was a requirement that the mechanism must be capable of operating under typical lateral accelerations due to spacecraft manoeuvres.

Concept Trade-Off

In the process of establishing a preferred concept many candidate concepts were derived, several of which, by early inspection, failed to meet the basic requirements and were thus eliminated. The remaining eleven concepts were subjected to further investigation and a trade-off. One of the major factors influencing the assessment of each concept was performance characteristics such as low mass, complexity/reliability, controlability and low sensitivity to the launch environment. Another factor was the configuration of critical interfaces which included compatibility with existing mast hardware and solar array configuration, and this tended to bias the trade-off towards an electrically powered, internally mounted device. Other aspects considered were ease of assembly, test qualification status and growth potential.

The winning concept (figure 2) was a device that used existing technology capable of deploying a large number of relatively long tubes. It had the advantages of being relatively easy to test and could be fitted to the existing mast as a complete unit. The device has a mode of operation similar to that of a conveyor belt. In simple terms, an endless flexible element

supported by a column mounted within the tube stack makes contact with a projecting lug on one side of the innermost tube. The tube is driven through its stroke and the next tube is pulled into contact with the drive element. The process is then repeated for each tube and results in a continuous and sequential deployment of any number of tubes, so enabling a wide range of mast lengths to be deployed.

The element is driven by an electric motor which can also provide retraction of the mast when its direction of motion is reversed. A lead screw device was placed as a close second choice in the trade-off, but was penalised mainly by its greater mass and limitations for applications using long tubes.

Mechanism Design

Various aspects of the winning concept were subsequently examined in order to evolve the optimum configuration which satisfied all the design requirements. Further trade-off studies were undertaken to select the type and number of flexible elements to be used in the conveyor belt. The type of flexible element to be used was selected from a number of options which fell into the broad categories of metal tapes, posidrive belts and miniature pitch chain drives from which the chain drive concept was selected.

The deciding factors in favour of a chain drive were its ability to cope with the small radius of curvature at the outboard sprocket, high loads, an adverse environment and its fundamental suitability for positive drive conveyor type applications. A stainless steel chain having a pitch of 3.75 mm was selected and modified to provide the required interface. It had a tension load capability of 800 N and was sufficiently small to minimise any impact on the availability of space for the support structure.

The inherent requirement of driving each tube at an interface point remote from the central axis of the tubes was thought to generate forces which could lead to jamming of the mast at the end of deployment of each tube. However, subsequent analysis of the effects of offset forces showed them to be relatively minor, their effect being limited to an increase in deployment forces of less than 3% This result had a major impact on the selection trade-off for the drive chain configuration, making the simple and more compact single chain system the most favourable option.

It was soon evident that mounting the mechanical drive system within the tube stack would severely limit its configuration and size due to the restricted volume available within the base of the stowed mast. This would have had an adverse effect on accessibility of the mechanism, and hence its maintainability, and could preclude the provision of a manual override for future missions. The baseline concept was therefore reconfigured to permit the use of an external drive unit by incorporating diverter sprockets at the base of the mechanism to isolate the tube stack from the drive chain. The final configuration is shown in figure 3.

Detailed analysis of the elastic extension of the relatively long chain indicated that it became excessive when subjected to operating loads. This would have led to slack in the drive chain in addition to the slack generated by differential thermal expansion between the chain and its support structure which could cause it to become entangled with or disengaged from the drive and guide sprockets. It was therefore essential to provide residual tension in every section of the chain, and this led to the inclusion of a tensioning device at the base of the mechanism. This device has a scissor-like configuration which is capable of compensating for wear, creep, thermal effects and chain elasticity regardless of the direction of motion, i.e. for both mast deployment and retraction. This is only possible because the scissor device has the ability to rotate as a whole unit and thereby always applies a load to the slack side of the drive chain wherever it occurs.

An essential element of the mechanism is the support tube on which the outboard idler sprocket is mounted. During actuation of the mechanism this support tube acts as a long strut under axial compression, with a small end moment applied due to the friction torque at the sprockets bearings. Therefore it must be rigid enough to resist Euler buckling. In addition, the support tube must possess a high stiffness to mass ratio to avoid excessive tip deflections arising from lateral accelerations imposed during spacecraft manoeuvres and the launch phase. The solution chosen comprised a round carbon fibre tube with diametrically opposed recesses to accommodate the drive chain. Even using this configuration it was necessary to support the tip of the structure during launch. This was achieved by providing a support/sliding interface between the tip of the support tube and the innermost tube. This means of support can also be used at other positions along the length of the support tube according to the specific stowed frequency or deflection requirements applicable during the launch phase.

A result of lateral accelerations applied during deployment of the mast can be large movements of the support tube and the drive chain due to the unpredictable nature of the applied forces; this could adversely affect the drive interface between the chain and the telescopic tubes and restrict the capability of the mechanism to deploy long slender tubes. In addition, the drive chain could possible impact on adjacent components causing damage and debris. An intermediate step to solving this problem was the introduction of guide channels integral with the support tube which provided location between the chain and the tube at discrete intervals. This solution, plus a residual chain tension, limited deflection of the chain during launch. The spacing of the supporting points permits a limited degree of adjustment of the fundamental frequency of the chain and the elimination of self-excited oscillatory effects such as those generated by bearing friction and chordal action.

Since the chain is positively located in the support tube by guide channels, the problem of structural deflection during deployment was solved by providing a self aligning drive interface. This interface limits the relative lateral movement of the chain and drive lugs by deflecting the support tube in unison with any tube irregularities. This solution also makes the

mechanism completely insensitive to lateral accelerations during deployment of the mast but retraction relies on the ability of the support tube to relocate with each interface guide as it travels inwards. To assist this action the tip of the support tube was profiled and the mast mechanism outboard support housing provided with a bell mouth to ensure final relocation when retraction was complete.

The tubes are driven from the inboard end by drive lugs which comprise an annular member with two teeth which project radially inwards. The annular ring is locally relieved where tube bearing pads occur to permit local flexing of the tube walls beneath the pads (figure 4).

Also projecting radially inwards from the annular ring are four pads of MoS_2 impregnated nylon which are circumferentially disposed to align with continuous smooth surfaces along the outside of the support tube. This provides the self-aligning interface. The two projecting teeth are spaced apart to allow the drive chain to run between them, contact between the two components being achieved by the insertion of extra wide chain side plates at selected intervals along the length of the chain. When contact is made the tube is driven through its stroke without any possibility of slippage. The shape of the purpose built side plates ensures that the drive load acts along the axis of the chain and is transmitted to it as a shear force (figure 4).

The space between the drive plates of the chain can in theory be made an exact factor of the spacing of the tube drive lugs when the mast is in the deployed state. This would provide ideal synchronisation and perfectly continuous deployment of the mast. However, this is neither practical nor desirable as it would be extremely difficult to cater to manufacturing and assembly tolerances and would require the use of profiled side plates which would generate separation forces that must be reacted across the sliding guide surfaces of the mechanism. Instead, a lag was introduced into the deployment sequence by increasing the pitch of the drive plates by the same amount. This was sufficient to cater to mechanism synchronisation but, more importantly, could cater to any adverse effects of differential thermal expansion and thermal gradients between the chain and the telescopic tubes. This is a major advantage of using a non-captive drive interface but as a consequence the mast motion is not completely continuous.

The drive chain is driven by a sprocket at the base of the mechanism, and has a diameter which determines the torque/velocity requirement for the drive shaft. This provides a degree of tuneability which obviates the need for further gearing and permits the use of a direct drive motor. To meet the torque requirements, a brushed samarium cobalt D.C. torque motor is used, controlled by a velocity feedback control system which also limits the acceleration of the system as the drive is transferred to subsequent mast tubes. The feedback element is an optical encoder mounted directly to the drive shaft. The motion of the mast is not enclosed within the control loop but is effectively driven by a constant velocity source through a highly compliant coupling, i.e. the drive chain. The oscillatory tendencies of this configuration are swamped by the friction forces between the tubes and the

chain compliance tends to control the rate at which the drive forces are applied, hence minimising mechanism jerk.

The estimated mass of the flight standard mechanical drive system is approximately 3 kg. A breakdown is given in table 1. This figure is based on the use of 2 m long tubes and shows a significant mass benefit when compared with an equivalent gas deployment system which would have a mass of almost 5.5 kg.

THE DEVELOPMENT MODEL

To verify the functional capability of the mechanical drive and its critical mechanical interfaces a development model was made which interfaced with an existing three element telescopic mast 5.5 m long (figures 5, 6). The build standard reflected the limited scope of the tests and deviations from the flight design were made to minimise manufacturing costs and schedule. The major deviations were the use of an aluminium support tube, which was stiffness representative, a non representative method of chain lubrication and the use of an existing motor drive unit. This drive unit has been designed for slewing experimental payloads and incorporates a 100:1 gear reduction unit and D.C. torque motor which provides an almost constant output. This is necessary to simulate the velocity controlled system of the flight configuration which was not available. A micro-switch actuated by tube latch engagement was used to cut the supply power to the motor at the end of deployment. An additional switch was incorporated in the tensioning mechanism to prevent the possibility of overload.

TEST RESULTS

During the test programme the mast was supported in a vertical position by a tripod assembly and deployed vertically (figure 7) under ambient conditions. A dummy mass of 8 kg was attached to the tip of the mast to simulate a representative payload mass and also demonstrate the ability of the mechanism to deploy against the design level axial loads. The self aligning interface between the tubes and the mechanism was verified by deploying the mast at an inclination of 6^{o} from the vertical, thereby imposing a lateral acceleration component to represent a typical flight condition.

The nominal mast deployment velocity was 50 mm/sec as shown in figure 8. This plot, which has been derived from cine film, shows two distinct pauses in the mast motion. The first pause of 0.1 seconds duration, was unexpected and was caused by a rapid increase in friction forces at the position where the first tube is latched out. The second pause represented the intended lag in synchronisation and lasted for 0.2 seconds. A trace of motor current showed that the pauses in motion did not produce significant impulse loads.

The tests also revealed that the self-aligning interface between the tubes and the mechanism was necessary in order to compensate for misalignment between the tube stack and the support structure.

The capability of the mechanism to retract under power has not yet been proved as the present mast hardware does not allow automatic delatching of the adjacent tube elements. However, retraction by manual override has been demonstrated.

FUTURE DEVELOPMENTS

The following activities are planned for the continued development of the mechanical drive:-

- The design and manufacture of an automatic unlatching system to provide a retraction capability for the existing mast.
- Thermal/vacuum testing and final selection of a preferred lubrication technique for the drive chain.
- Manufacture and vibration testing of a mass/stiffness representative model.
- Incorporate an expanding roller system that will constrain the tip of the support tube on the longitudinal axis of the mast and thereby facilitate the retraction of long slender tubes whilst subjected to adverse lateral accelerations.

These developments are considered to be vital stages of a programme which would lead to a viable mechanism for space applications.

CONCLUSIONS

Test results on the mechanical drive have indicated that the system is capable of deploying a typical telescopic mast under ambient conditions. The design can be considered for a wide range of space applications since, in theory, there is no limit to the number of tubes that can be deployed.

The mechanical system offers a number of advantages over a gas driven system, such as the ability to retract and also provide a significant mass saving. Further testing is planned in order to prove such aspects as automatic retraction of the tubes and successful operation in a space environment.

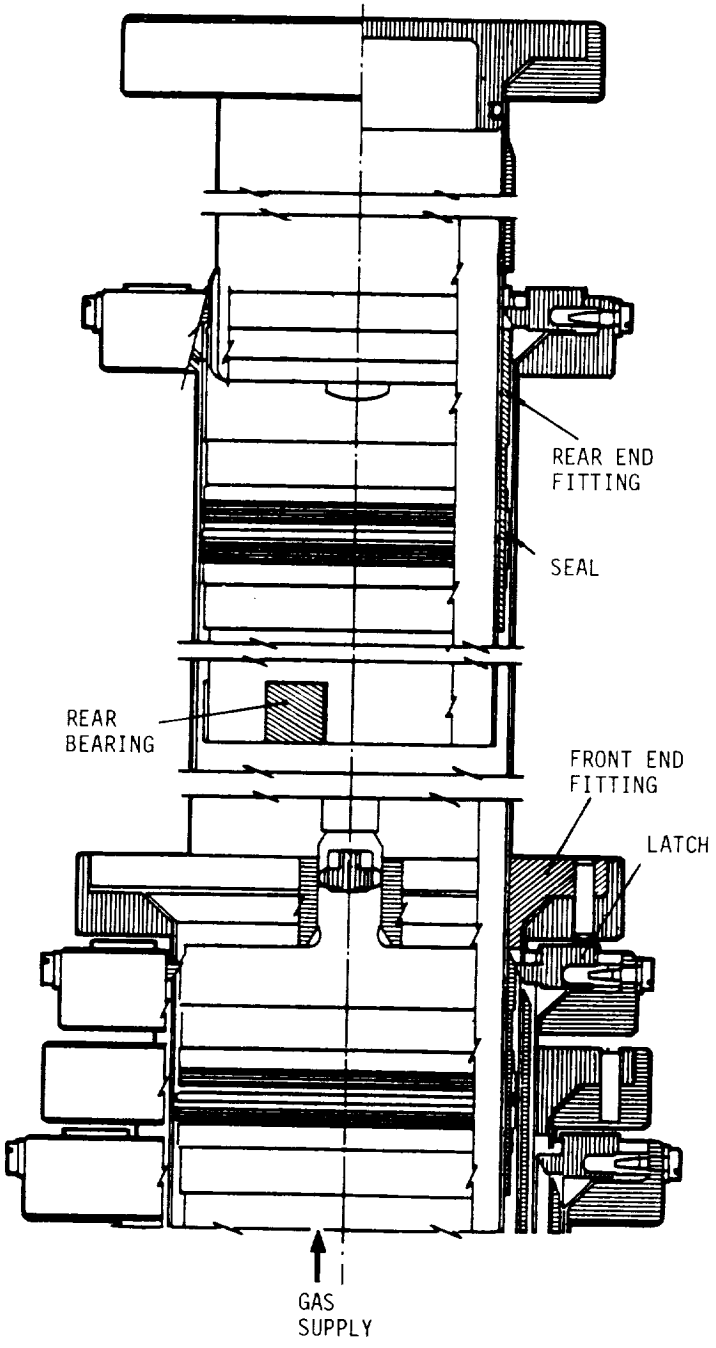

Figure 1: Telescopic Tubes and Fittings

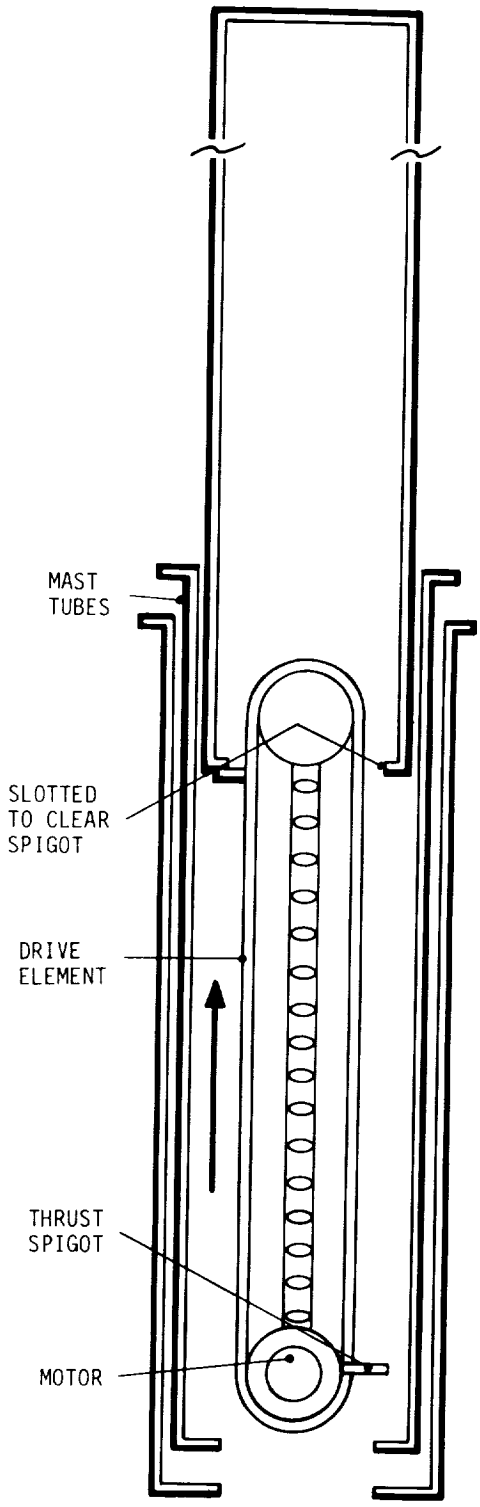

Figure 2: Mechanism Concept

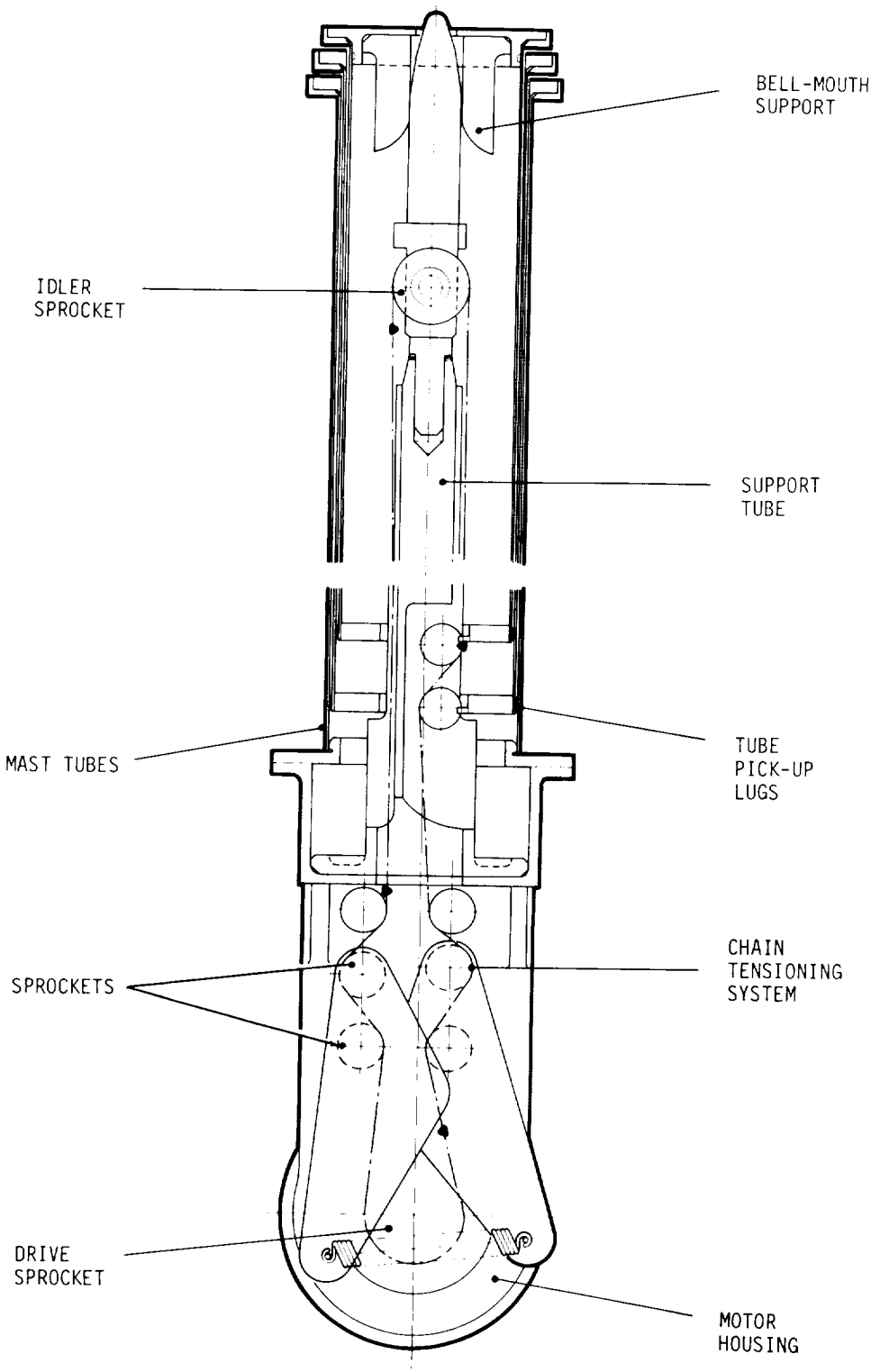

Figure 3: Final Configuration

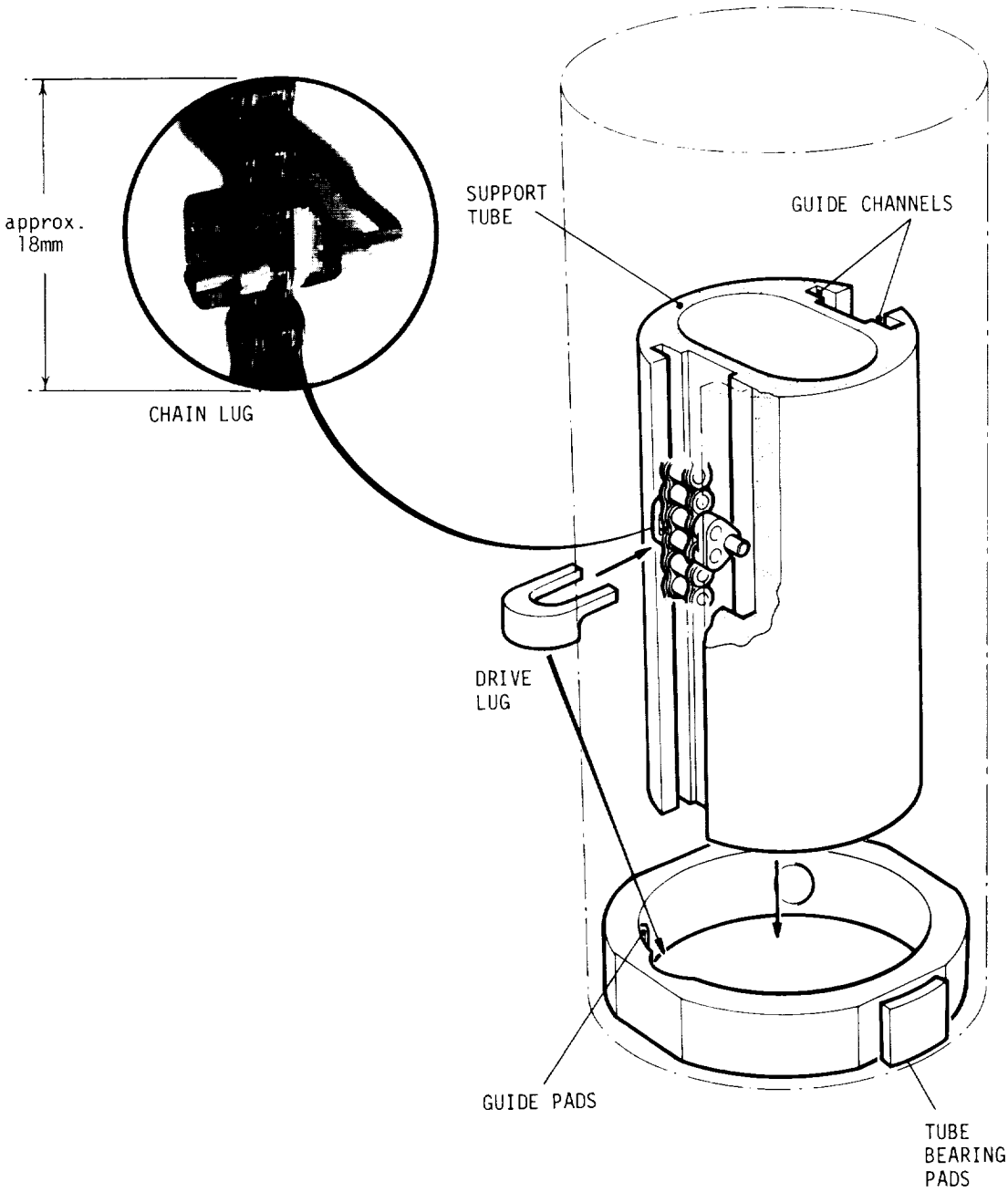

Figure 4: Schematic of the Self-aligning Interface

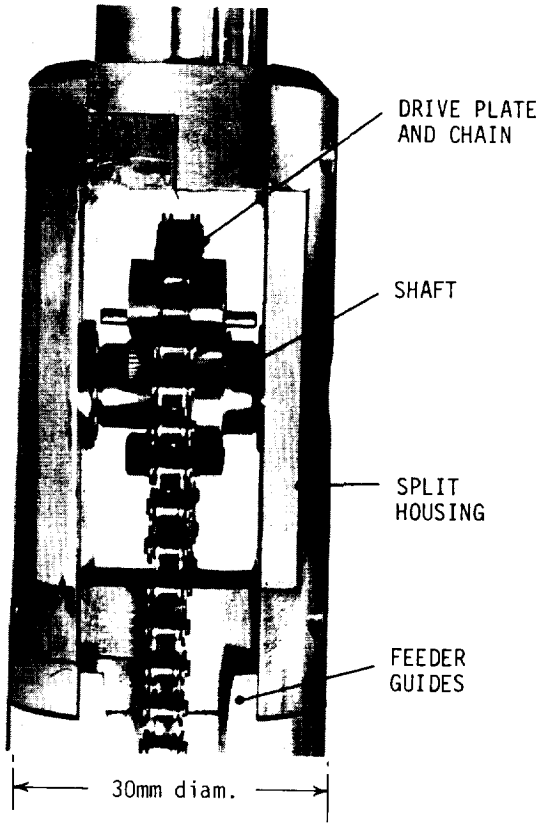

Figure 5: Top Idler Sprocket Assy. Development Model

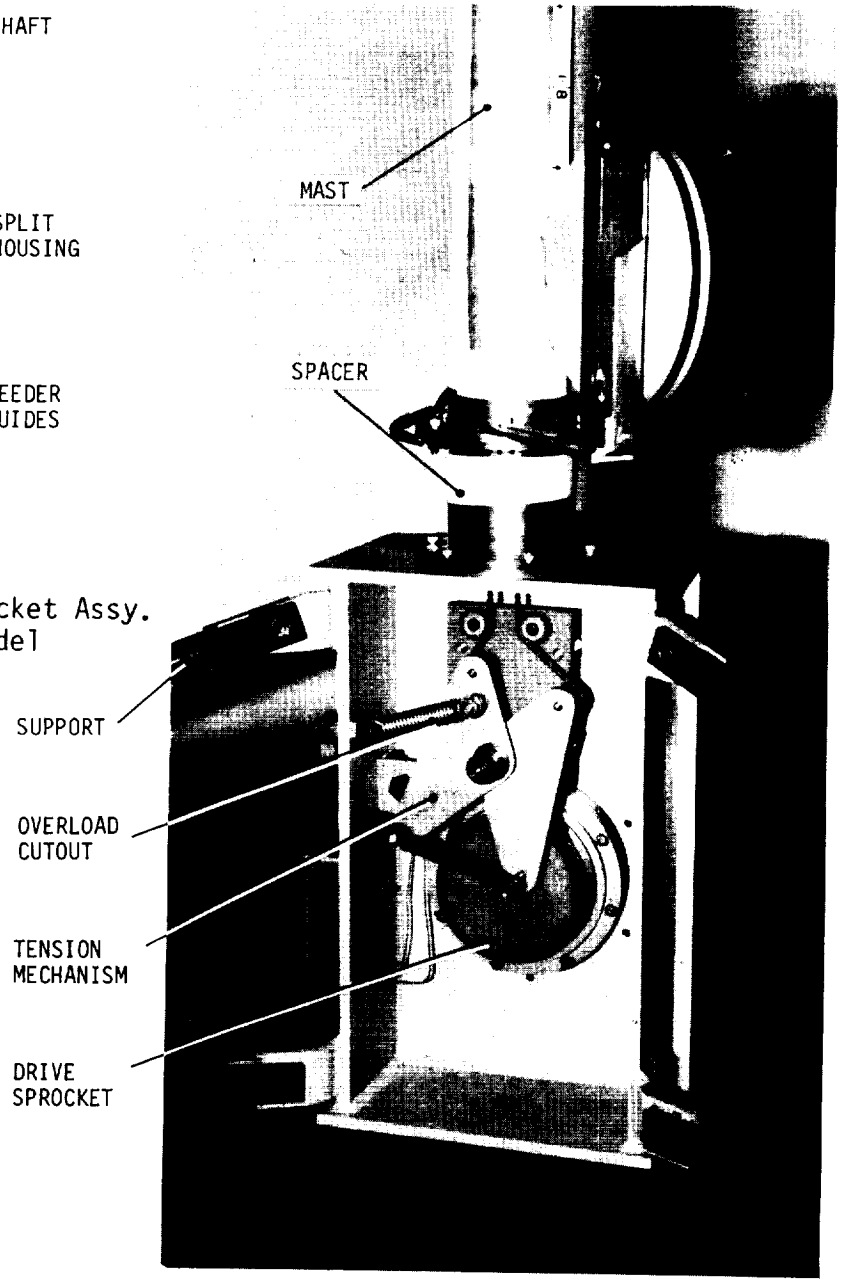

Figure 6: Development Model Base View

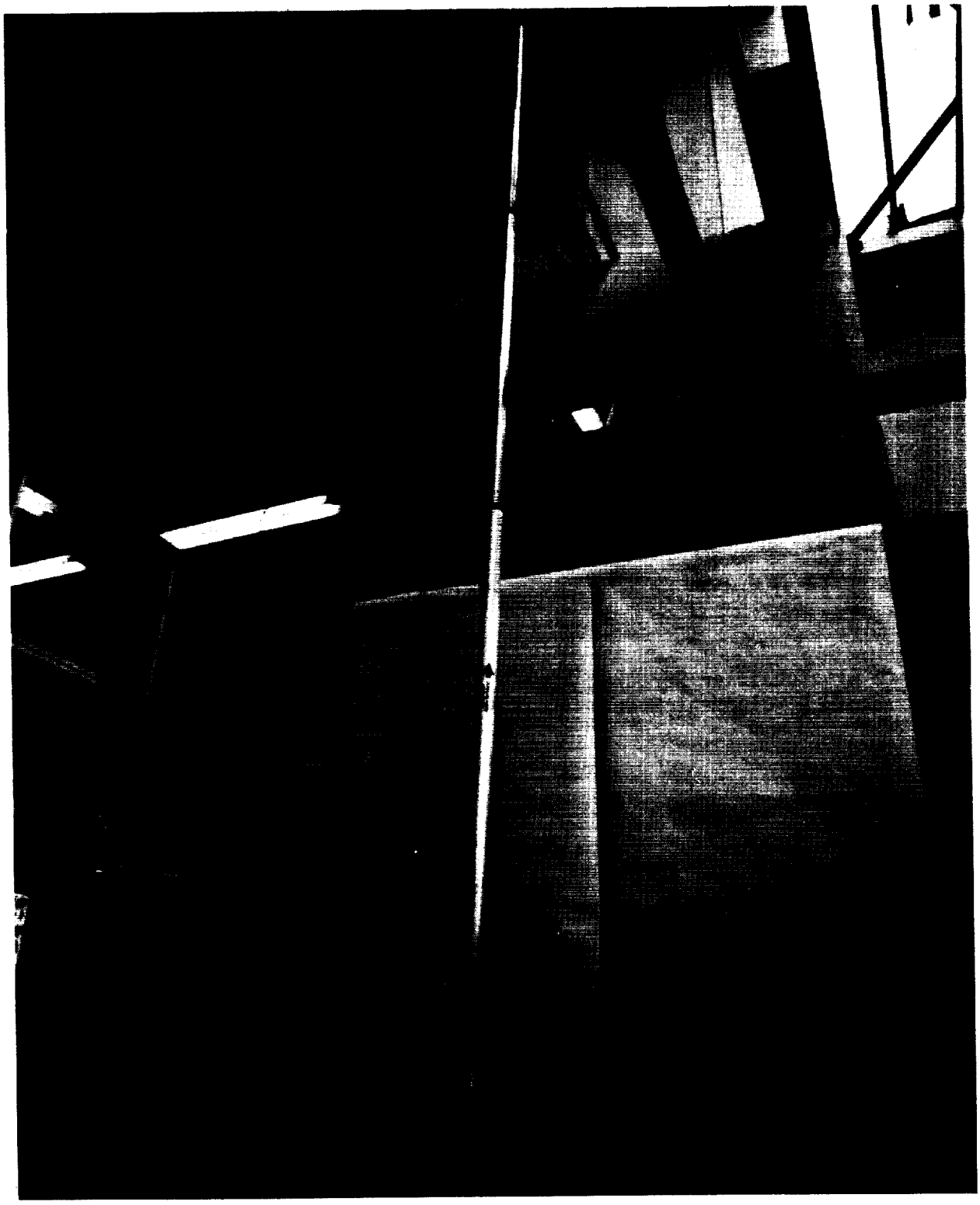

Figure 7: The Three Element Mast under Test

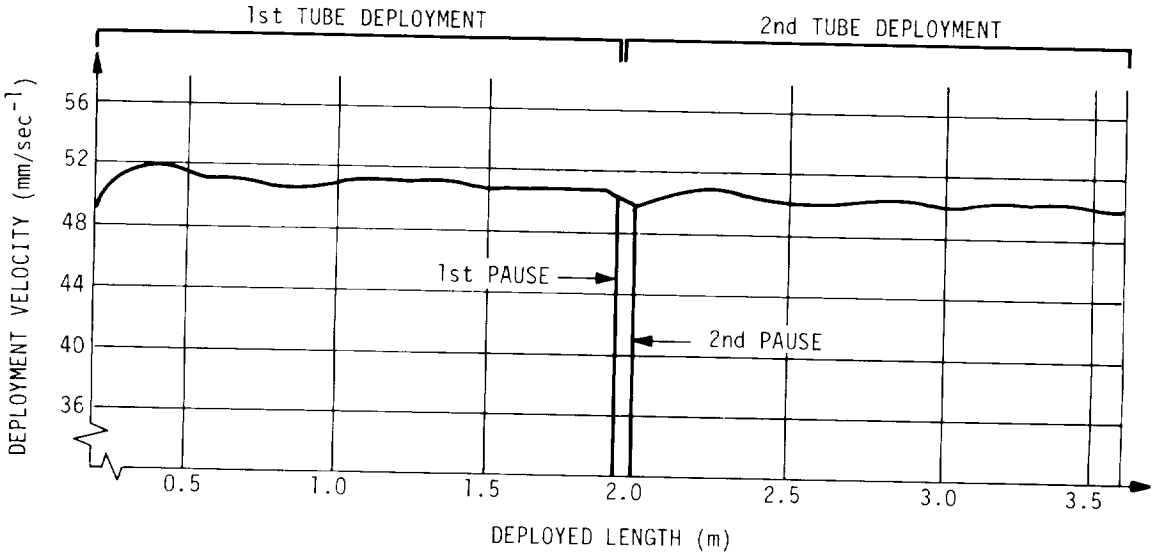

Figure 8: Velocity Profile for The Three Element Mast

ASSEMBLY	MASS (kg)	MASS (lb)
STRUCTURE	0.38	0.84
DRIVE ASSEMBLY	0.31	0.68
TRANSMISSION ASSEMBLY	1.42	3.12
MAST I/F ELEMENT	0.12	0.26
ELECTRONIC PACKAGE	0.80	1.76
Total System	3.03	6.66

Table 1: Estimated Mass Breakdown of Mechanical Mast Drive (for 2m tubes)

DESIGN AND DEVELOPMENT OF AN OPTICAL SCANNING MECHANISM (OSMA) WITH MINIMUM MOMENTUM TRANSFER

Leandro B. Fernández Sáinz, Erardo Herrera,
José M. Bajo, Harry J. Mallard.
SENER, S.A., Dept. Aerospacial. Madrid. Spain

ABSTRACT

The Development Model for an Optical Scanning Mechanism Assembly (OSMA) is described as being two equal inertial masses which collide with each other to minimize the momentum transfer to the satellite and other mounted instruments.

The design criteria for the Mirror, the Compensating Inertia and other components are given. The details of the design are discussed and related test results are presented, which show the validity of the design concept for momentum compensation.

INTRODUCTION

In oscillating scanners it is desirable to minimize the transfer of momentum to the spacecraft. Thus the moving elements need to be properly designed so as not to cause intolerable disturbances to other satellite-mounted instruments.

The Optical Scanning Mechanism Assembly (OSMA) here presented has equal inertias for both the Mirror and Compensating Inertia which collide with each other to produce the oscillatory motion and give a minimum momentum transfer, as specified in Table 1.

With this idea in mind, a conceptual design was derived and later a development model was built and tested.

The data generated during the tests have been used to verify the principle and the design, to confirm and support the analytical methods and to establish the techniques of measurement themselves.

DESCRIPTION

The OSMA consists of the mechanical and electronical units.

The mechanical unit, given in Figure 1, is made of the following elements: Mirror, Compensating Inertia and Support Structures, Pivots, Off-Loading Mechanism, Bumper Devices, Motor and Sensors. The components are listed in Table 2.

The Mirror Structure is the central piece made in the shape of a cross which supports the small square mirror in the center and the anvils at either end of its longer arms. This structure simulates the inertia and mass of the actual elliptical mirror. It has also adjustments to modify the inertia and the position of the center of gravity. The structure was made of Aluminium, except for the two anvils, which are made of stainless steel.

The external frame of the Mirror is called the Compensating Inertia Structure and is made of four rectangular tubes and two discs on the rotational (scanning) axis. There are welds in between the tubes and the discs, and each pair of tubes is also welded at the upper and lower corners, where they give support to the Bumper Devices.

Support to the above two structures is given by the U-shaped structure that can be seen in Figure 1.

The mechanical elements connecting the moving structures to the support are Flexural Pivots. The pivots are cantilever 5016-800, especially processed and of welded construction. Their positioning and fixing method are given in Figure 2, 3 and 4. This last figure shows the design details for permitting relative motion between the discs.

Since the type of pivot was selected to comply with the linearity spec, two pairs of Off-Loading Mechanisms have been incorporated in the design in order to withstand the launching loads. Each of these mechanisms is made of Cu-Be and consists of a clamp which holds one of the moving discs to the support structure. After the pyrotechnic cuts the holding rod, the clamp relaxes into its groove on the support and allows the free motion of the moving disc. The free motion of the whole structure is produced by releasing the two pairs of discs.

On the other hand, the oscillatory motion within the active range of ± 5 degrees is produced by the simultaneous collisions that take

place between the anvils on the mirror and the pads at the tip of the cantilever springs of the Bumper Devices.

Under each of the springs there is a layer of silicone rubber that dampens reverberation between collisions. The materials for the springs and pads have been stainless steel and 16% carbon filled delrin, respectively.

At the time of the collisions frictional energy loss is compensated by the pancake torque motor which is mounted on the Compensating Frame, thus leaving the movement of the mirror undisturbed in between collisions.

Finally, the electronical unit controls the motion and feeds the motor. In the OSMA two 18000 line optical encoders have been used. One of them is connected to the Mirror and the other to the Compensating Inertia as is detailed in Figure 2. The torsional rigidity of the mounting shaft was determined to have relative displacement below 2 micro radians between the structure and the encoder disc, during motion.

DESIGN CRITERIA

Compensating Inertia

The design of the compensating frame presented an optimization problem for the following reasons:

On the one hand, the frame cannot interact with the scanning field during its motion. Also the collision points on the Bumper spring have to be located as far as possible from the rotating axis in order to make them more effective and decrease the power consumption.

On the other hand, the inertia of the frame has to equal that of the mirror in order to have a stable, oscillatory motion.

These conflicting criteria have posed a lower limit to the inertia reached by Aluminium. The deviation actually reached is 25% over the goal of 0.25 Nm^2.

This figure could, alternatively, be improved by manufacturing the frame with carbon fiber.

Flexural Pivots

The criteria for selecting the pivots are as follows:

- Linearity during active scan	0.125%
- Maximum range	$\pm$ 8.91 degrees
- Life	2.9×10^9 cycles
- Static load	13.5 N
- Dynamic coefficient	2

During testing it was noticed that the pivot characteristic is very sensitive to the fitting pressure. Because of this, the pivots are held in position by means of clamps and screws (See Fig. 5). A small key which fits into the internal shots of the pivot is used for adjustment (See Fig. 6).

Bumper Devices

The positioning of the spring at rest was studied in order to give minimum frictional losses at the contact points during motion.

The turnaround time is as high as possible, to be compatible with the efficiency requirement of 25%.

A number of cycles should be above 2.9×10^9 (10 years).

Off-Loading Mechanism

This mechanism is a very convenient feature of the OSMA design since it is possible to fix the moving parts when needed during assembly and tests, as well as meeting the intended original goal of withstanding the launching loads.

The friction coefficient determined by tests has been bigger than 0.25, which gives capability to withstand loads of above 700 N.

TEST RESULTS

Tests to determine the repeatability, linearity, efficiency, pointing stability and power requirement have been done during the development of the model.

However, only the results obtained when measuring the wear of the collision pads and the momentum compensation are presented below due to

limit of space.

One of the questions in mind when starting the development program was to determine the rate of wear in the collision pads. Their position, initial and final dimensions, as well as the mark left on the anvil are sketched in Figure 7.

An approximate estimate of the contact wear can be obtained by the fact that the thickness of the spherical pad, which was initially 1 mm, is reduced by half after 200 hours of continuous operation. It was also noted that the wear is initially very rapid and decreases as the area of the contact increases, and when that area becomes approximately 3 mm in diameter the wear reduces to almost a negligible rate.

The parameters to compute the wear rate can be taken as follows,

- Operation frequency : 7.2 Hz
- Duty cycle : 200 Hrs
- Mean Load : 5.3 daN.

The fundamental question is that of the aptitude of the OSMA design for momentum compensation.

By design, the momentum transfer is mainly found around the scanning axis, since the existing forces and torques can only come from the motor and pivot reactions, and from the lack of instantaneous collisions at the bumpers.

The set up for measuring the transfer is the one sketched in Figure 8. It consists of four equal cantilever beams for displacement of the whole OSMA at the interface points. These displacements have been measured by means of strain gauges placed as close as possible to the clamping points.

The measured natural frequency of each beam was 35.7 Hz., which has given a dimensionless response factor of 1.053 at an operating frequency of 8 Hz., that factor being 1.04 at 7 Hz.

On the other hand, the strain sensitivity was 394.74 micro-deformations per volt.

When functioning, the output from the strain gauge was a sinusoidal signal with an amplitude of 20 mvolts peak to peak. Thus the

interface forces has been determined to be 3.6 gr with an average of 2.5 gr. This gives a torque of 1.011×10^{-3} Nm, and a torque transfer per second of 16.98 Nm/sec. at 8.4 Hz.

CONCLUSIONS

It was easy for the mirror structure to reach the specified value for the moment of inertia. However, it was not so in the case of the compensating structure because of the need to maintain sufficient rigidity. Thus the manufacture of the Compensating Inertia unit should be undertaken first and then that of the mirror, since to coincide both moments of inertia is of importance so as to decrease vibrations originated at the collision points.

The structure, mechanism and instrumentation in the mechanical OSMA complies easily with the specified weight of 25 kg. The OSMA unit itself weights 13 kg.

The idea of using optical encoders has shown to be a valid one. However, care should be taken not to over-specify its number of lines. A maximum number of lines would seem to be better, but the higher the number of lines used the higher its sensing capability is. This would complicate its adjustment and make the output signals prone to errors from vibrations and center shift displacement.

Even though the flexural pivot has the advantage of being free from friction, it is too unpredictable for such a precise mechanism as the OSMA is intended to be. Besides its center shift displacement, which makes the alignment difficult, its torsional rigidity is uneven with angular displacement. The pivots have to work under traction in order to improve the resulting linearity of motion and they seem to change their constitutive relation with the fitting pressure and with vibrations.

The material used to smooth the collisions was carbon filled delrin (16%). This material has proved to be very good in this application.

It has been shown from all the tests carried out that the present concept for moment of momentum compensation in oscillating mechanisms is valid, although the obtained value is double the specified value, this latter being extremely low indeed.

ACKNOWLEDGEMENTS

The OSMA system was built with the assistance of our colleagues in the Manufacturing Group to whom full credit must be given.

We also wish to acknowledge the constructive comments and help from Mr. H.M. Briscoe and Dr. R.H. Bentall of ESTEC during the project.

TABLE 1. REQUESTED PARAMETER

PARAMETER	SPECIFIC GOAL
Scan Active Range (^{o})	± 5
Null Pointing Direction (^{o})	± 1
Nominal Scan Frequency (Hz)	8.4
Nominal Scan Period (sec)	.119
Scan Efficiency	.25 (T)
Scan Linearity	.125%
Along Scan Repeatability (rad)	2.6×10^{-5}
Pointing Stability (rad)	2.0×10^{-6}
Start/End Scan Precision (rad)	4.0×10^{-6}
Start Jitter (rad)	30
Start Time(minutes)	pitch,yaw 7.8×10^{-3}
Momentum Transfer (Nms)	roll 9.2×10^{-3}
Power (W)	
Start-up, Operation	30, 15

TABLE 2. COMPONENT SUMMARY

ITEM	MANUFACTURER	DESCRIPTION
Flex Pivot	Bendix, Utica, N.Y.	12.7 mm dia. Electron Beam welded
Motor	Aeroflex, Long Island, N.Y.	Pancake Torque Motor
Encoder	Dr. Heidenhain, Tranreut, Germany	Optical 18000 lines
Guillotine	Holex, Holister, Cal.	To cut 3 mm dia. bar

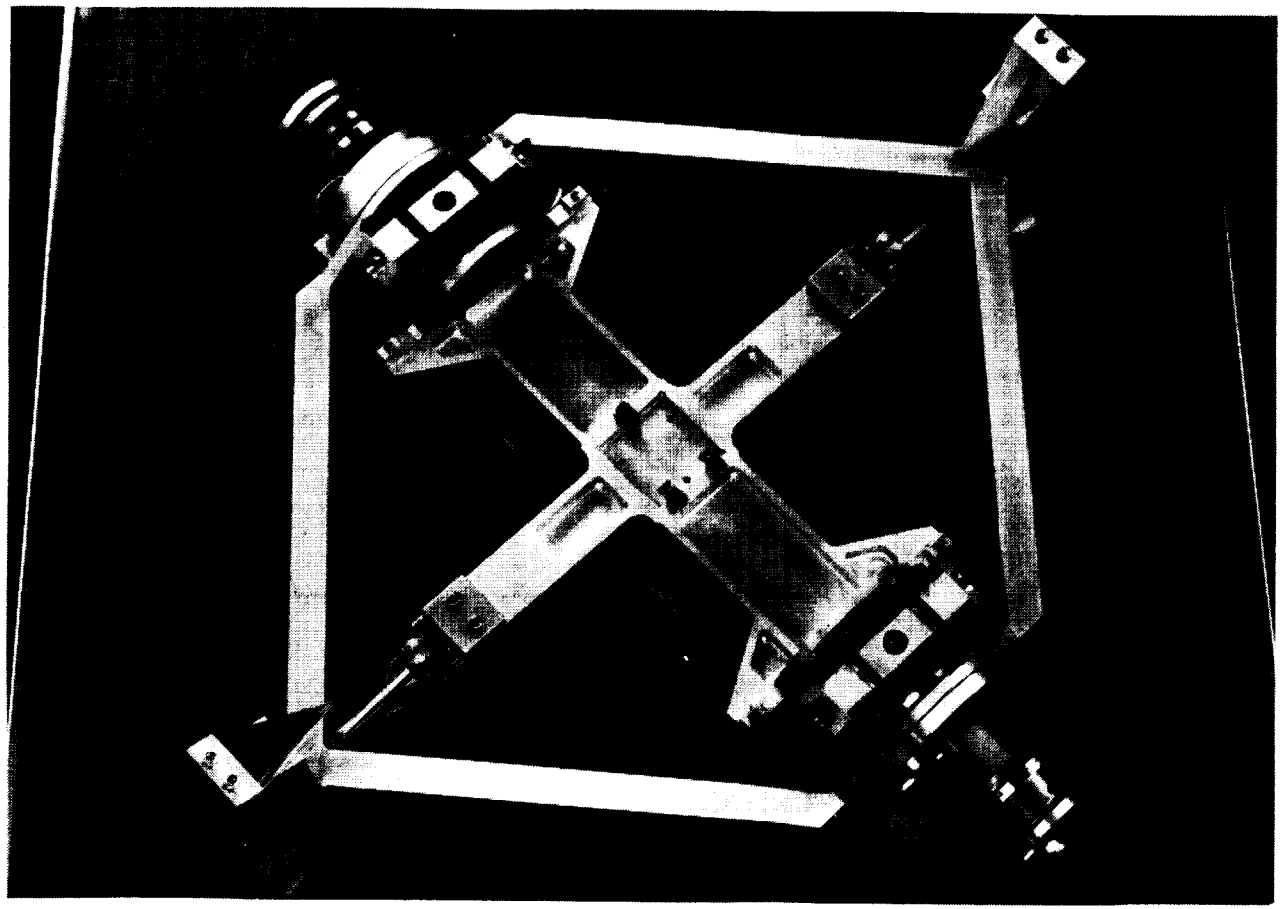

Figure 1. Development Model of the Optical Scanning Mechanism Assembly (OSMA)

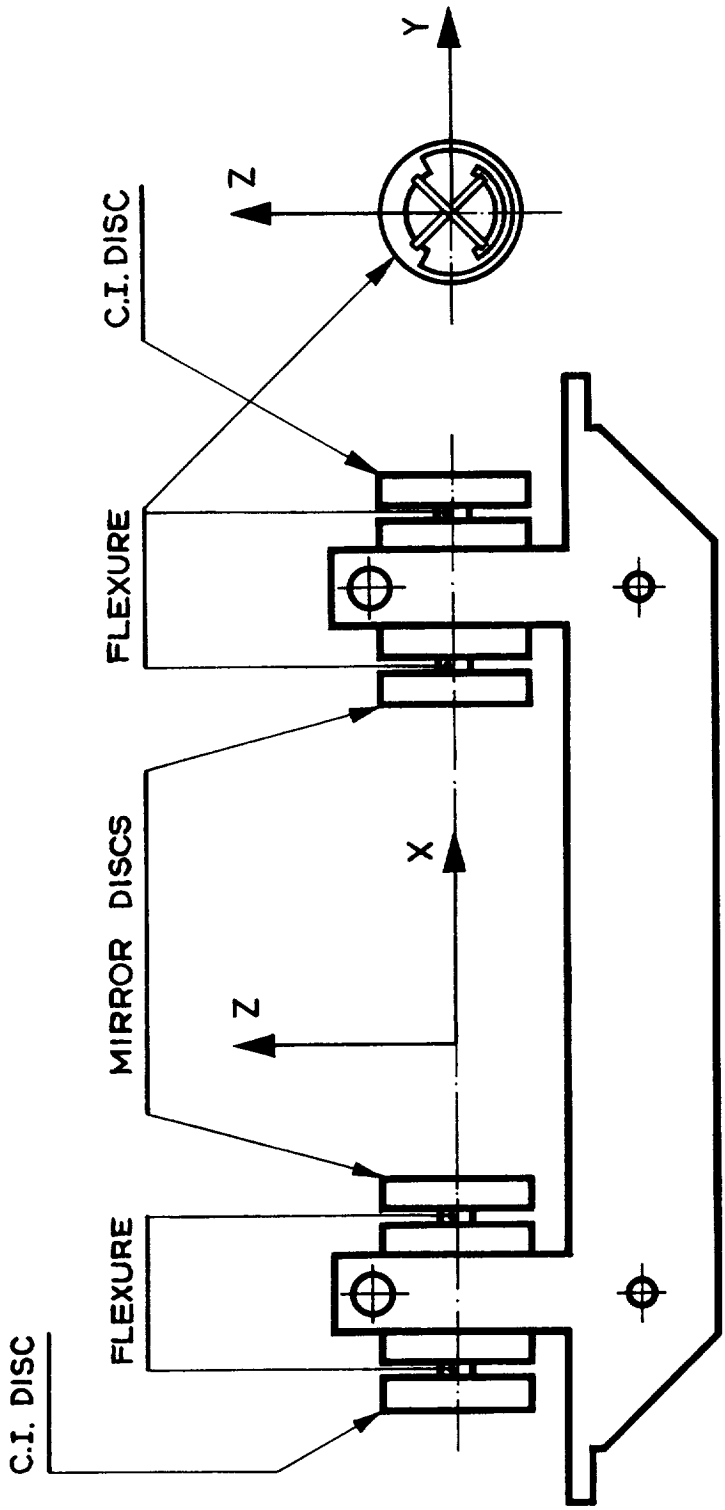

Figure 2. Location of the Flexural Pivots

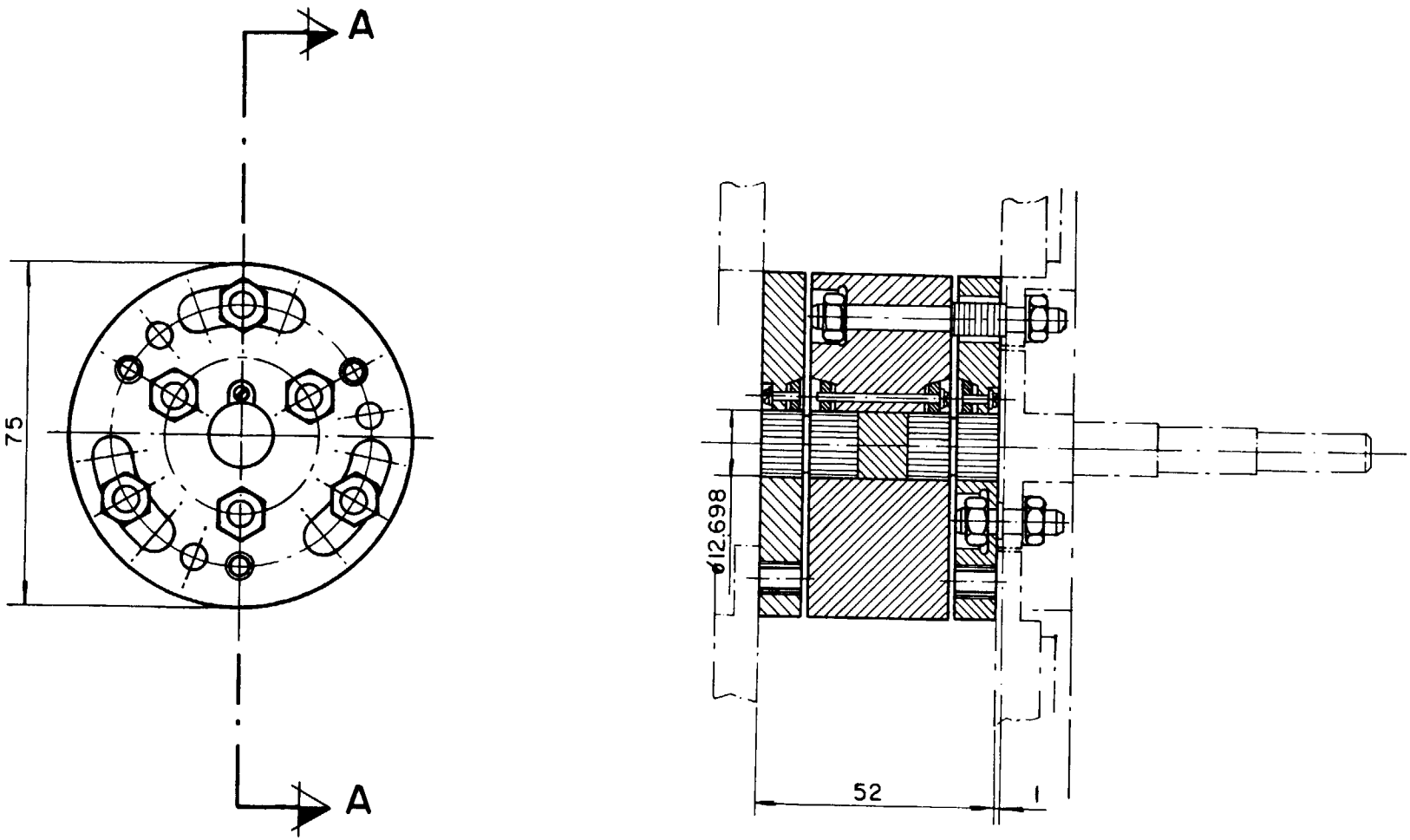

SECTION A-A

Figure 3. Left hinge mechanism and support for the Mirror encoder

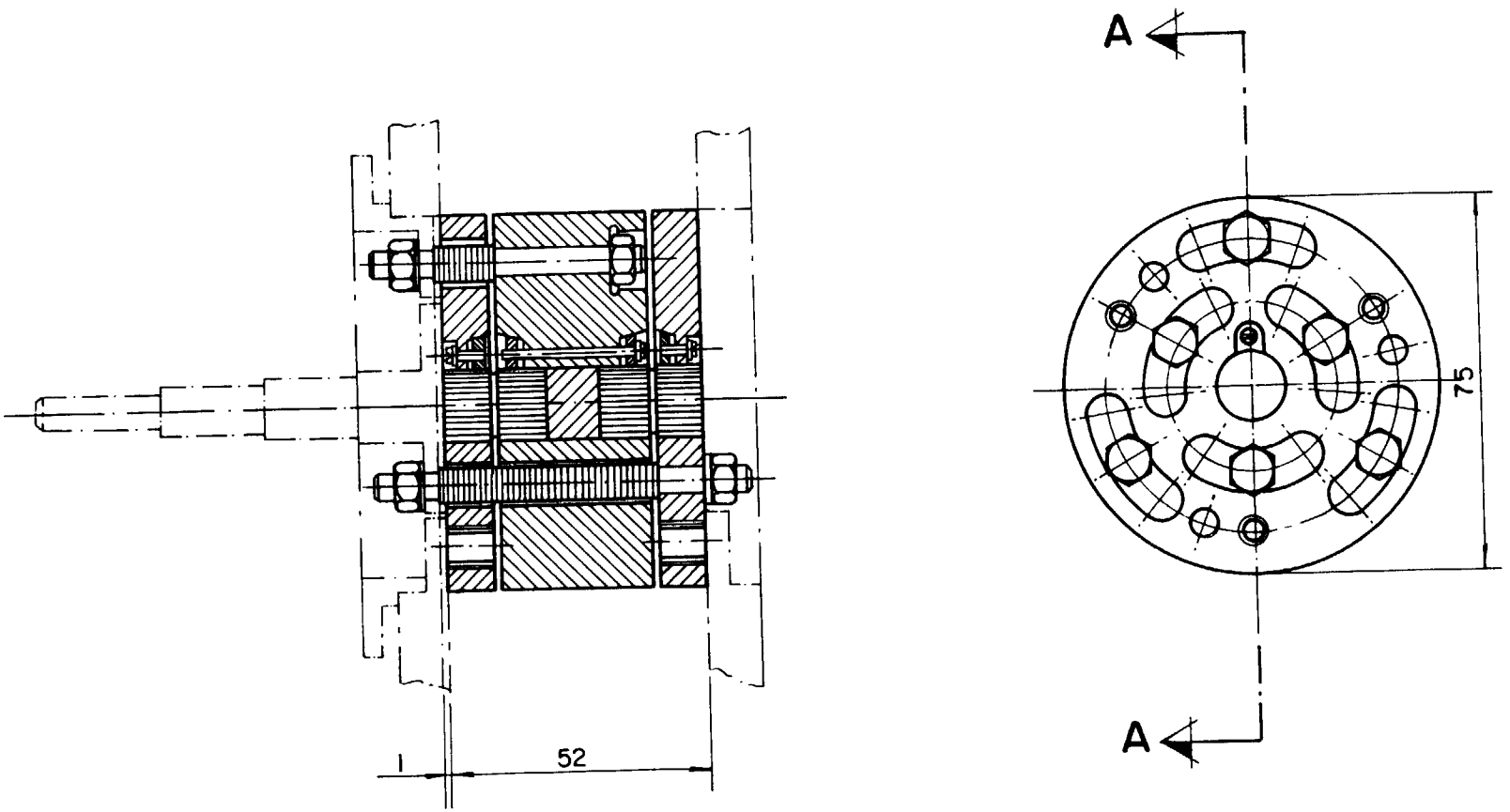

SECTION A-A

Figure 4. Right hinge mechanism and support for the Compensating-Inertia encoder

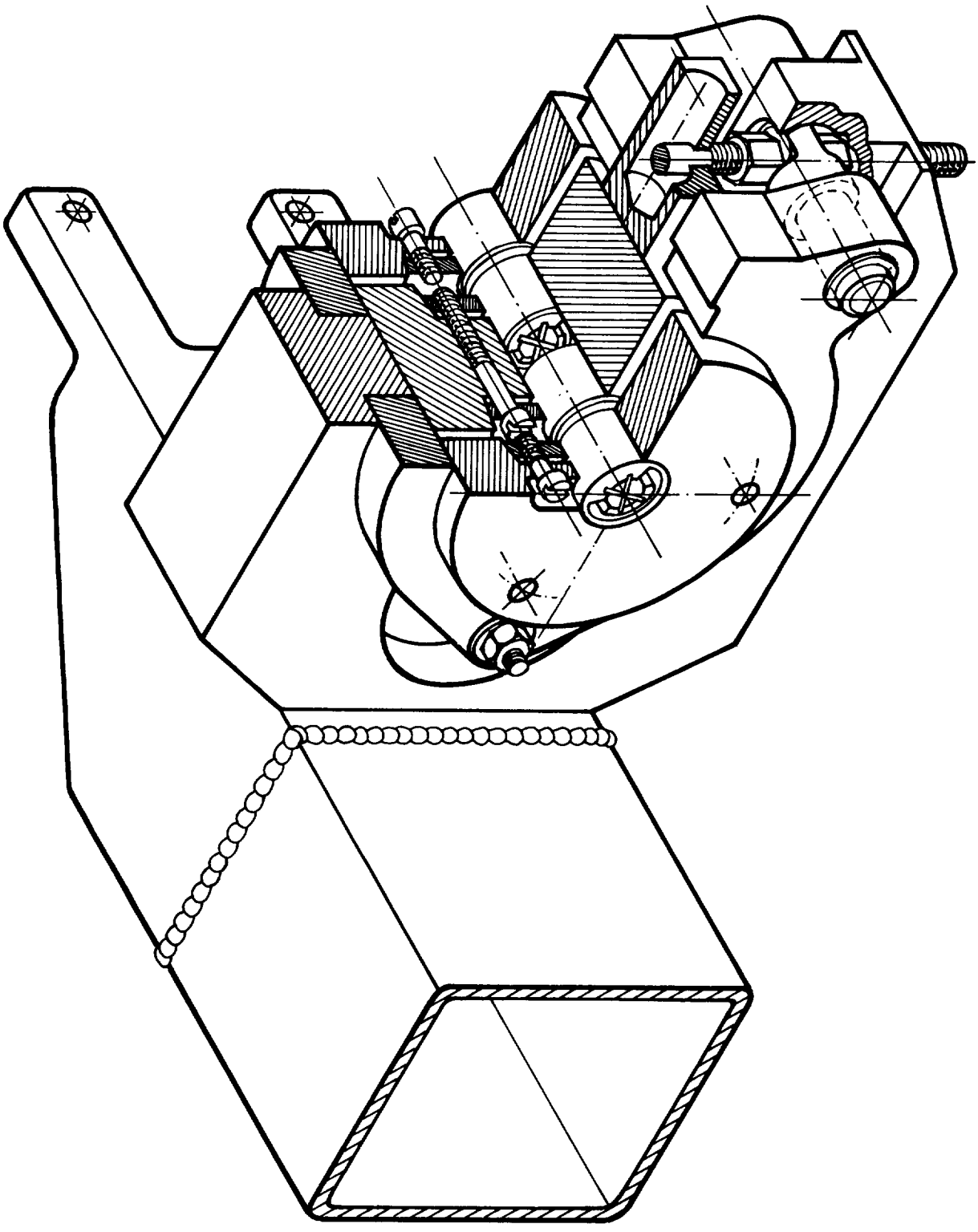

Figure 5. Off-Loading Mechanism. Device to hold the pivots

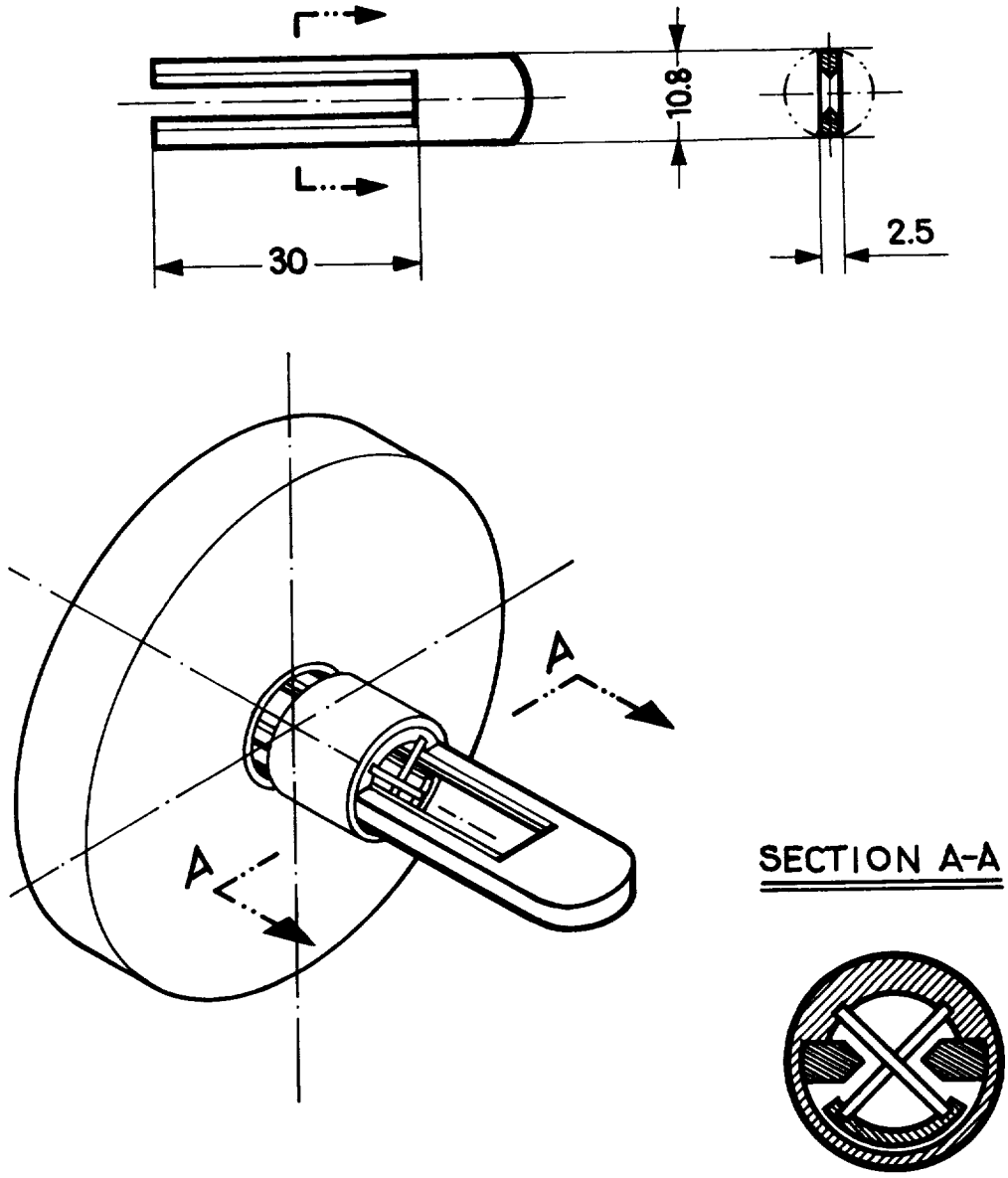

Figure 6. Key for positioning the flexural pivot

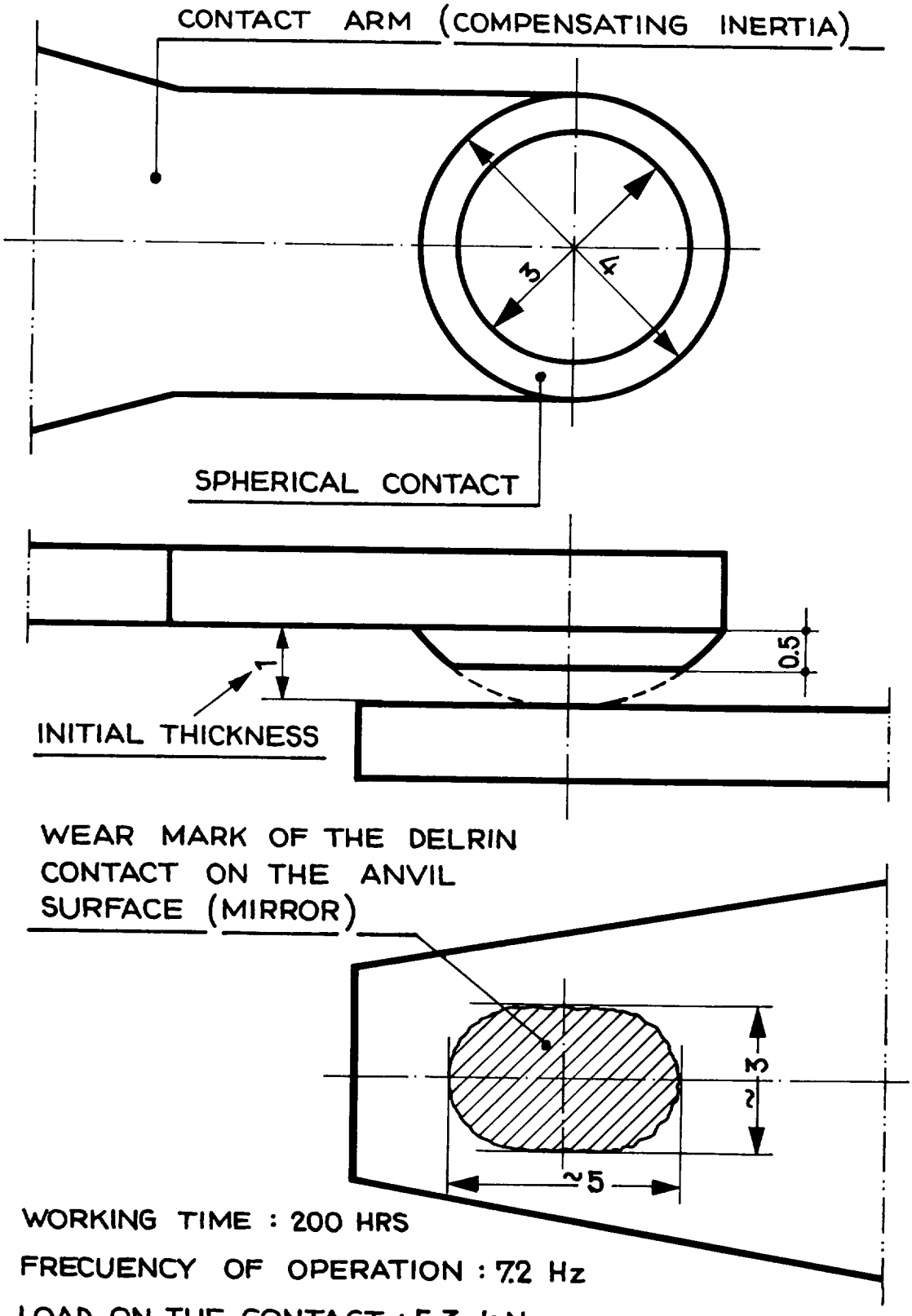

Figure 7. Geometry of wear in the contact points

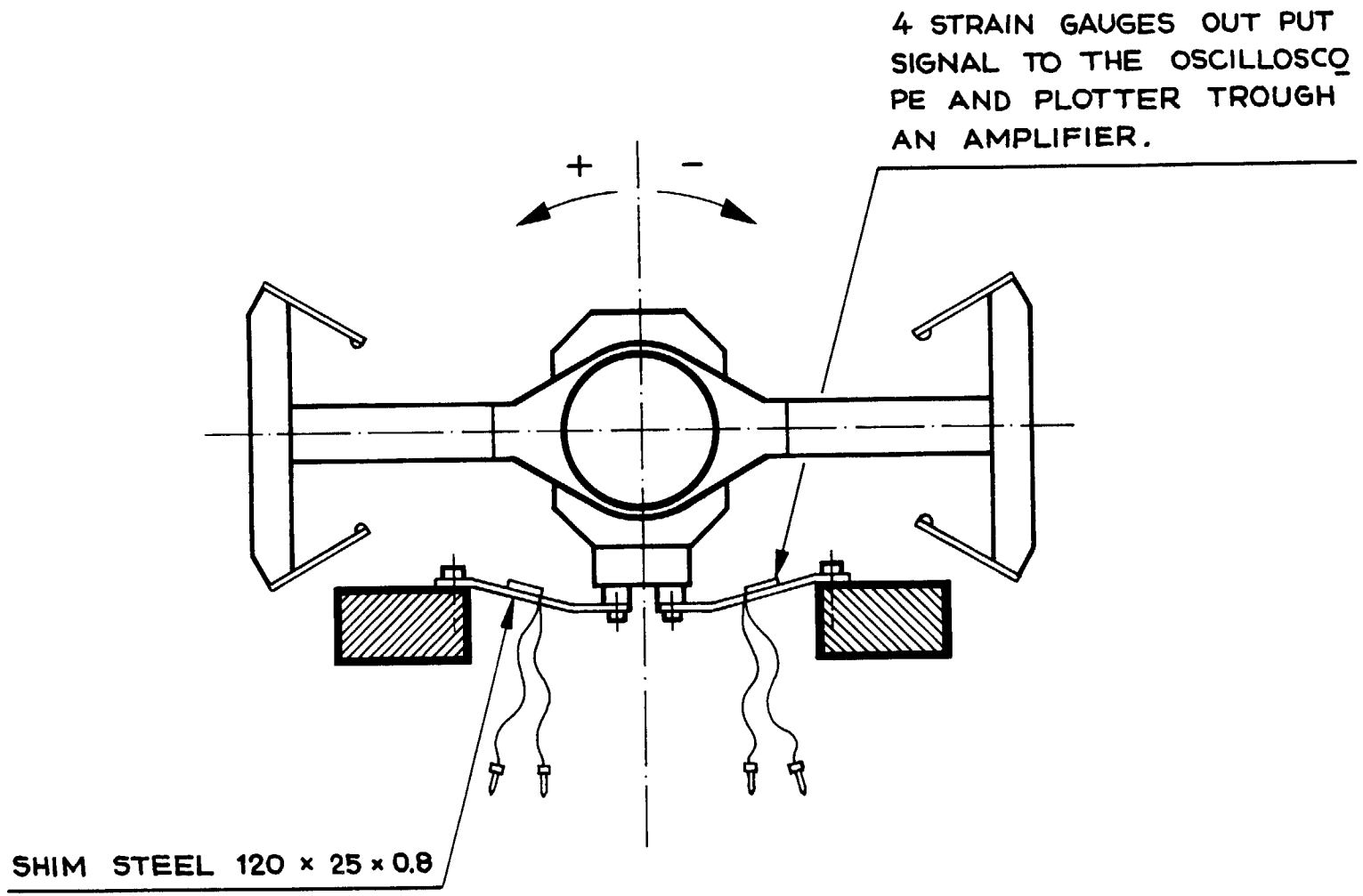

Figure 8. Set up for measuring the Momentum Transfer

SOFA : SYSTEME D'ORIENTATION FINE D'ANTENNE
(an antenna fine pointing mechanism)

Bernard HUBERT and Pierre BRUNET

Société Nationale Industrielle Aérospatiale
CANNES, FRANCE

ABSTRACT :

AEROSPATIALE's SOFA is a device designed for the highly accurate, 2-axis pointing of antenna or any feature installed on a spacecraft.

The SOFA system, now pending an AEROSPATIALE patent, is particularly suited to the transmit-and-receive antennae of Television Satellites. It is one of the requisites for a Radio-Frequency type deviation detector.

The major characteristics of this system is complete freedom from friction and wear-out, resulting in numerous advantages, such as outstanding precision, virtually endless service life, high simplicity and reliability.

The sizing method is described and performances are analysed. The results from analogue simulations are presented.

A functional model of the electrical and mechanical parts has been built and subjected to on-ground tests using a 2-axis platform simulating the spacecraft's motions. The results obtained are thoroughly in keeping with the predictions and simulations. A qualification model is under test. Various possible applications of the SOFA system are mentioned.

1 INTRODUCTION

Telecommunication satellites as a rule and television satellites in particular require increasingly fine antenna pointing accuracies. Despite increased sophistication, the conventional means do not meet the present demands. As a matter of fact the earth sensor-kinetic wheel assembly, even with one or 2 degrees of freedom does not guarantee accuracy values of 0.1° let alone of 0.05°.

Furthermore, the overall pointing budget has to take into account the misalignments and thermal deflections.

Certain improvements have been made to the latest projects: Increase in the number of Earth sensors, location of the sensors on the tower supporting the antenna feed, reflector reorientation device for misalignment compensation.

However, these improvements are not sufficient. On the contrary the adoption of a radio frequency sensor, whose major asset is the use of a radio electrical path very close to that of the useful beam, is a decisive break through for pointing accuracy.

This sensor may be used to control the overall satellite's attitude. That configuration ensures the best possible accuracy for the antenna used in receiving the beacon's signal.

Alternatively, this sensor may be used to pilot only the beam delivered by the antenna receiving the RF beacon signal. The latter concept ensures high accuracy in pointing the transmit antenna and fair accuracy in pointing a receive antenna other than the transmit antenna.

In this case, the orientation mechanism is interlaid between the antenna's reflector and the spacecraft's structure, with the source remaining in a fixed position on the spacecraft, e.g., on a tower. The reflector's position is then continuously adjusted to nullify the error signal delivered by the RF Sensor.

The beam is permanently orientated towards the on-ground Beacon through an independent control loop whilst the satellite itself is stabilised by conventional means with regard to earth centre.

The antenna fine pointing system, the so-called SOFA developed by AEROSPATIALE CANNES, is the subject of the descriptions hereinafter, which also cover the efforts conducted to demonstrate the performances of the system.

An application has been filed for a patent to cover such system.

2 SPECIFICATION AND CONSTRAINTS

The specifications adopted are suited to utilisation for the transmit antenna of the French TV Satellite.

The main data to be considered in the conceptual design and sizing of the pointing system may be summarised as below :

- satellite's in orbit weight : 1,000 Kg
- thruster's torque : 10 Nm
- inertiae : Ix = Iz = 25,000 m2 Kg
  Iy = 900 m2 Kg
- solar panel's rotation by 0.15° steps
- solar panel's torsion inertia = 50 m2 Kg
- solar panel's minimal oscillation period = 3 sec
- satellite stabilisation accuracy = 0.3°

- maximal perturbation torque in orbit corrections : 0.8 Nm (misalignment of thrusters and dissymetry of thrust).

The most stringent typical perturbation effects to be considered in beam pointing are under the following conditions :

- a spacecraft oscillation, period 24 hours, amplitude 0.3°
- 0.05 Nm torque steps on the reflector during station keeping
- spacecraft body oscillations at a period of 3 sec and an amplitude of 0.02°
- the signal from the radio frequency is assumed to be affected by a random noise, density 2.8 10^{-4}°/Hz $^{1/2}$ within the 0 - 15 Hz band, say a variance of 1.1 10^{-3} degrees (1 σ)
- the 10 Kg elliptic reflector whose inertias are 5 and 9 m2 Kg.

The beam pointing error added to the sensor error is required to stay below 0.01 degree (1 σ).

Taking into account the amplifications the adopted vibration level specifications are :

- 40 g on the longitudinal axis
- 30 g on the transverse axis

with the reflector's C. of G. 15 cm above the mechanism's axis.

The temperature limits selected are - 120° + 80°.

3 DESCRIPTION OF THE MECHANISM

3.1 General presentation

The system developed by AEROSPATIALE Cannes, the SOFA (système d'orientation fine d'Antenne), is an antenna fine-pointing device absolutely free from friction or any source of wearout and having infinite resolution.

- The principle is illustrated in figure 1. Two plates, the lower one mounted on the spacecraft and the upper one clamped to the reflector, are linked by a deformable element, the central spring, acting as a ball joint.

The forces required to orientate the reflector are provided by 4 circumferentially located linear motors.

The mechanical system furthermore includes :

- travel stops
- a locking device for launch phase
- an electromagnetic temporary locking device

A control loop electronics drives the current into the coils depending on the sensor's error signal. Each of the above element is detailed hereinafter.

3.2 The spring

The spring utilised is a beryllium copper cylinder having a superimposed and alternated series of 120° spaced slits (figure 2).

The properties of such a deformable system are well-fitted to the problem :

- the bending stiffness (0.1 Nm/degree) selected is a fairly small one to reduce the permanent electrical consumption,

- the other motions are not damped but they remain very small even when in resonance excited by the thrusters,

- the spring's stresses and fatigue during on-orbit operations are quite negligible.

3.3 The motors

Each motor consists of a magnetic circuit with permanent magnets which is attached to the reflector clamped platform of a flat coil attached to the spacecraft mounted platform (fig. 3).

Interaction between current running through the coil and magnetic field generates a force according to Laplace's law :

$$\vec{F} = 2.l.n.\ \vec{I} \wedge \vec{B}$$

which is proportional to the current value.

Only one motor is used on each axis while the opposite motors are used for redundancy.

Each coil counts 800 turns for 45 Ohms, stop piece limit deflection to $\pm$ 1.5° in the present configuration, which permits to compensate a beam deflection of approximatively $\pm$ 3°.

For example a 35 mA current is necessary to rotate the reflector by 0.5° (approx. 1° for the beam) which amounts to 55 m W.

3.4 Locking device for launch

Of course this hinged device has to be secured to carry the reflector throughout launch. The device chosen is an adaptation of the system previously qualified for the retraction of solar arrays. Three 120° spaced shoes are tilted to bottom on the 3 stops which motion compresses the spring by 4 mm (figure 1).

The assembly is locked by a kevlar cable, the tension of which provides overall assembly prestess.

Tension is applied through a deformable lever that has tension-regulating action wherever deflections are felt.

At the time of on-orbit deployment, a pyro-cutter releases the system. Each contact shoe is returned by a spring that frees the stops as well as the reflector-supporting plate, which takes up its nominal operation position after expansion of the central spring.

3.5 Temporary locking

A temporary locking device can be incorporated to restrain the two platforms into zero position.

This system consists of an electromagnetically driven flip-flop locking device. Two similar 90° spaced devices are used.
Their distance to centre is 10 cm. With the spring as the third attach point, restraint is thoroughly ensured.

This system would be used only in the event of failure of the on-ground RF beacon, which would only be temporary, or in the event of dual failure of the RF sensor and the on-board SOFA system.

4 PERFORMANCE ANALYSIS

4.1 Pointing accuracy

After analytical study and with the selected adjustment, the expected errors are as follows :

- noise leads to 2 10^{-3} degree depointing (3σ)
- the spacecraft's daily oscillations are quite negligible
- the effect of solar panel's rotation steps gives 4 10^{-3} degrees in the East-West direction
- the 0.05 Nm torque which may occur during stationkeeping shows 1 sec peaks at the beginning and end of each manoeuvre which peaks have an amplitude of 1.5 10^{-2} degree
- such other sources of error as the roll or pitch desaturations give errors less than 1 10^{-3} degree.

4.2 Analogue simulations

The mathematical model was simulated on an analogue computer, and many simulations were performed, which provided checking of the selected setting and verification that the variation of parameters, particularly of the filter's setting, was not critical.

The findings are that the performances obtained are absolutely compliant with predictions.

The spacecraft body's oscillations are indeed reduced to the extent nominally predicted (see figure 4).

Figure 6 shows the effects of a torque on the reflector and of sensor noise, as well as the effect of integral control.

A 0.05 Nm torque gives peaks of 1.10^{-2} degree (duration 1 sec), and the $2.5\ 10^{-3}$ degrees ($3\ \sigma$) noise gives a pointing error of $1.5\ 10^{-3}$ degrees ($3\ \sigma$).

Even with substantial noise, the driving current for the motors can be filtered and is a fair measurement of SOFA rotation apart from the transient phenomena. Finally, as the system's equivalent band-pass is 1 Hz, the antenna's structural modes should necessarily be greater than 5 Hz to ensure good frequency decoupling.

5 FUNCTIONAL TESTS

A functional development model was built from the motors spring and driving electronic, see figure 5.

The test set up utilised suggeststhe operational conditions :

- the mechanism is installed on a table with 2 degrees of freedom providing simulation of the spacecraft roll and pitch motions (see figure 7)
- the reflector is simulated by the inertia of a rectangular metal frame
- the radio frequency sensor is simulated by an optical system : the picture of a flood light is shaped after reflection on a mirror (which is fixed to the moving part) at the centre of 4 photo electric cells.

The noise of stability of the error signals are better than 0.5×10^{-3} degrees.

Figure 8 shows the principle of sensor simulation.
With this set-up the different sorts of perturbations were tested in quite realistic conditions, namely :

- torque on reflector (figure 6)
- spacecraft's oscillations at various frequencies
- satellite depointing
- noise on the sensor signal (figure 6)
- acquisition with great initial depointing.

The results obtained provide adequate verification of the shape of responses and the values obtained by both the analytical study and the analogue simulations (figure 6).

The consistency of all above results is a verification of the mathematical model and demonstrates that the parameters of the control loop law have indeed been mastered.

6 RELIABILITY

The electronic is designed for pointing the beam to a particular angular distance from the beacon.

To improve reliability, such presetting is performed on board prior to launch, but there is a register that enables refinement of such setting and corrections of the misalignments or zero errors.

The electronic and motors are fully redundanced and no cross-coupling is needed between those elements owing to the high reliability.

The reliability of the electronic part calculated with quality (E2) components over 7 years is 0.995.

The reliability figure for the largely over-dimensioned mechanical part is 0.9996 and undergoes no degradation over time, as the spring is the only element that is stressed after pointing mechanism release, with the very high reliability of 0.99999.

7 STATUS OF DEVELOPMENT

The model was utilised in very numerous tests for 1 year.

A qualification model was built with no change made to the functional elements, i.e., spring and motors. The locking system is an adaptation of some already qualified systems.

The qualification tests are under way to completion.
Adaptation to a given mission can be done smoothly with minor changes to essential elements.

Adaptations are in progress for different applications, particularly a model including position sensors that enable a reflector to be locked to a given position or to the position of a first reflector itself locked by control loop to an RF sensor as described herein.

8 CONCLUSION

The SOFA described here is a system that permits to solve, under optimal conditions the problem of fine antenna pointing.

The SOFA offers numerous advantages, namely :

- very high pointing accuracy = 1.10^{-2} degrees (3σ) to be added to RF sensor's accuracy on beam pointing, even during orbit controls
- small weight (4 Kg including electronic) and power consumption (less than 1 W)
- very high reliability and virtually endless service life of the frictionless, free-from-wear mechanical part
- small outline dimensions and easy accommodations by all configurations
- small height minimising the effects of defocusing

Using the SOFA leads to very significant relaxation of the system constraints, as the SOFA

- puts up with simplified stabilization of spacecraft body
- allows great relaxation of the alignment and thermal deflection requirements on the various constituents of the antenna and on the sensors.

Thus, the SOFA system largely simplifies satellite attitude control, as well as all alignment and stability constraints of structures .

Several applications are possible :

a) antenna fitted with a SOFA and an RF sensor ensures both transmit and receive functions or transmission alone, as the receive antenna requires no accurate pointing

b) an antenna fitted with a SOFA and an RF sensor plus another antenna also equipped with a SOFA reproducing the evolutions of the first one. This set-up corrects all attitude control errors.

c) the SOFA's electronic is designed to permit orientation of an antenna beam's axis on a different direction from that defined by the RF sensor's on-ground beacon. This variable offset is telecommanded.

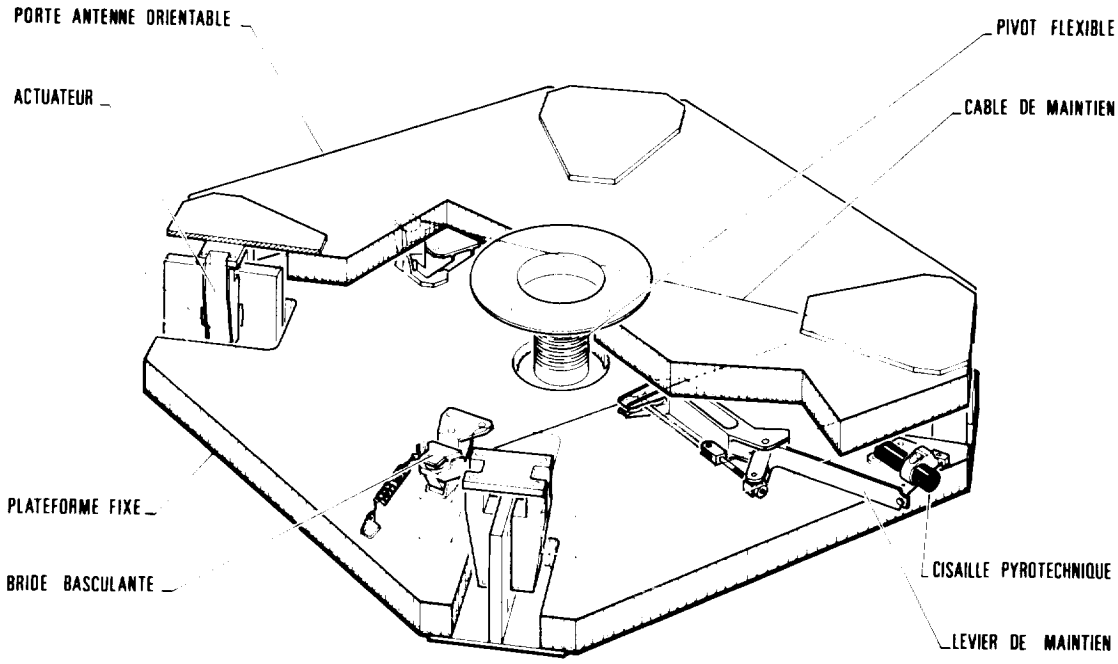

Fig. 1 SOFA Device

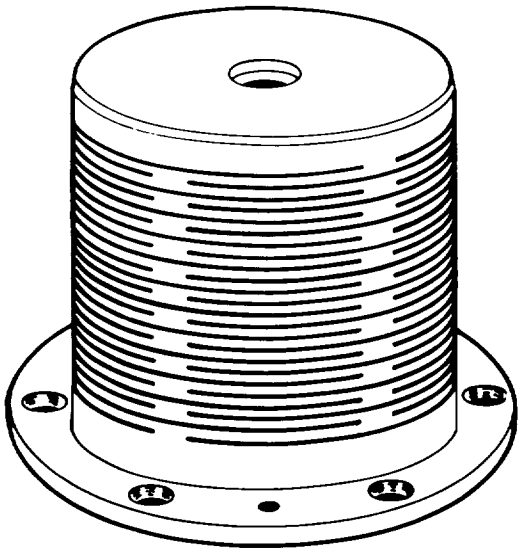

Fig. 2 Flexible pivot

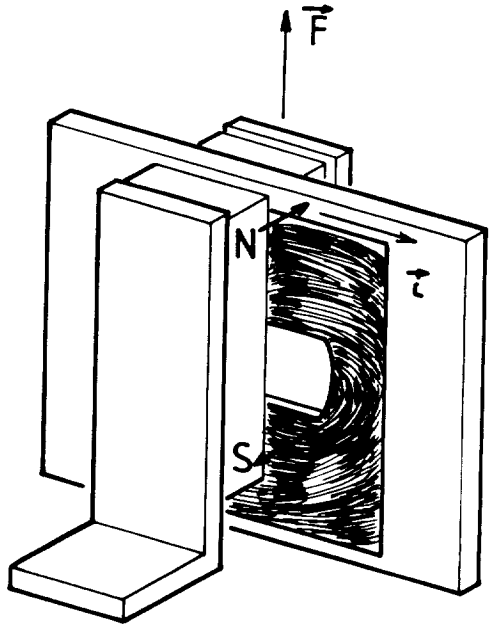

Fig. 3 Actuator principle

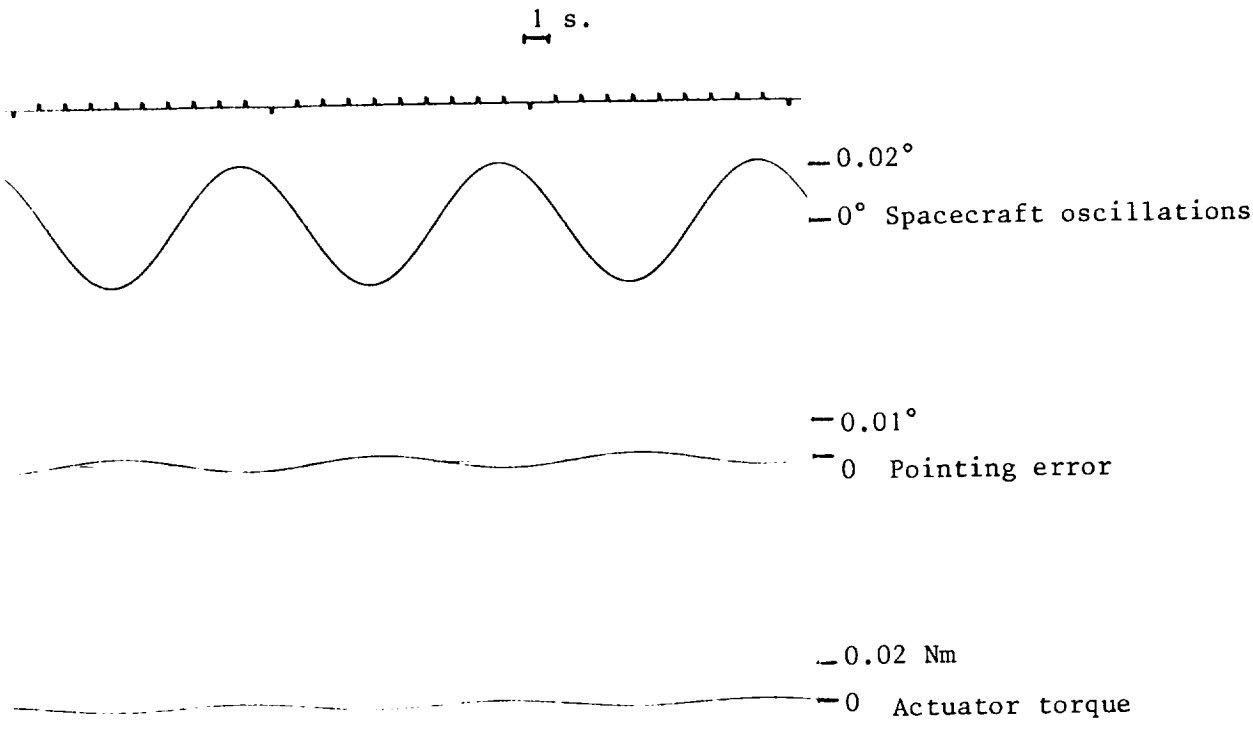

Fig. 4 Spacecraft oscillations effect

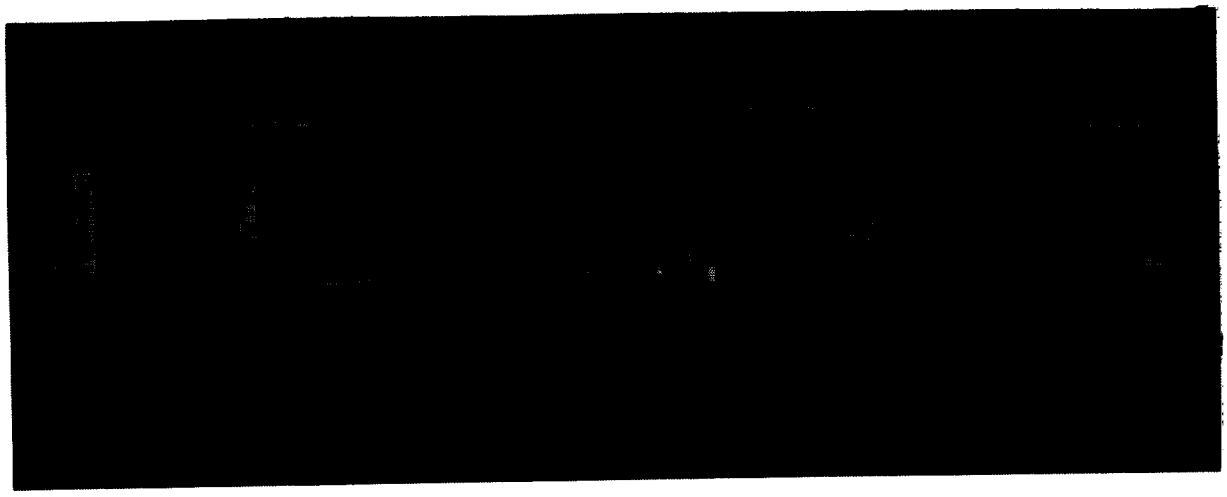

Fig. 5 SOFA Bread-Board Model

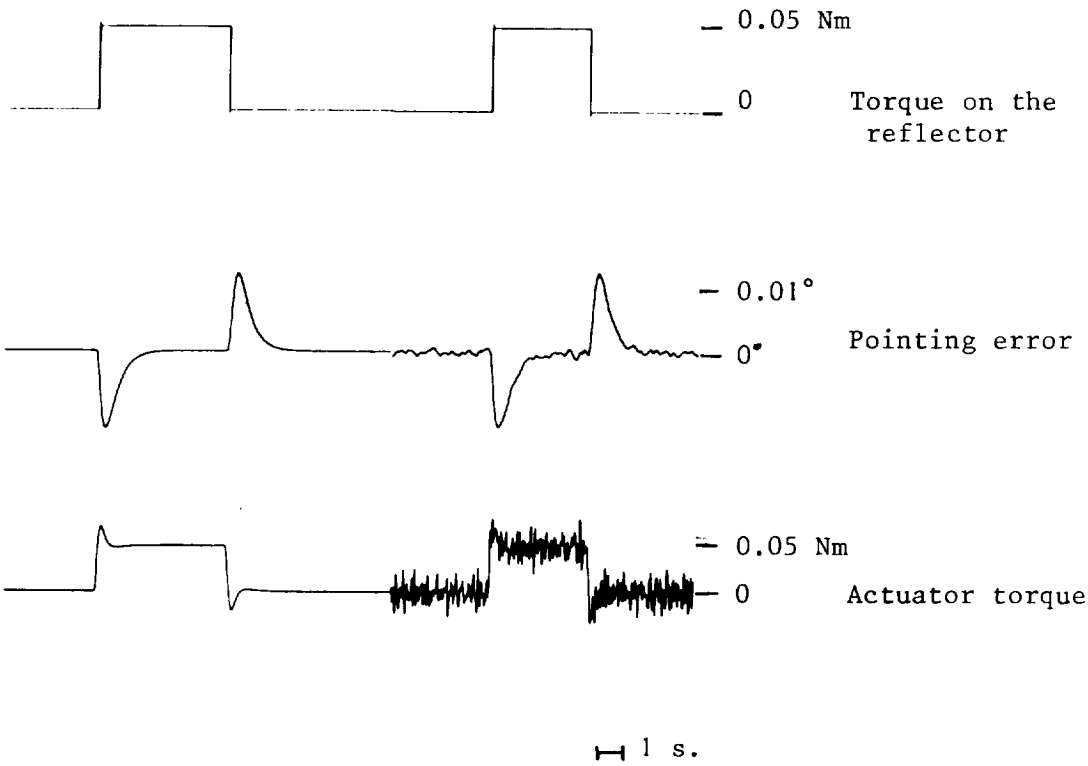

Fig. 6 Simulation and test results

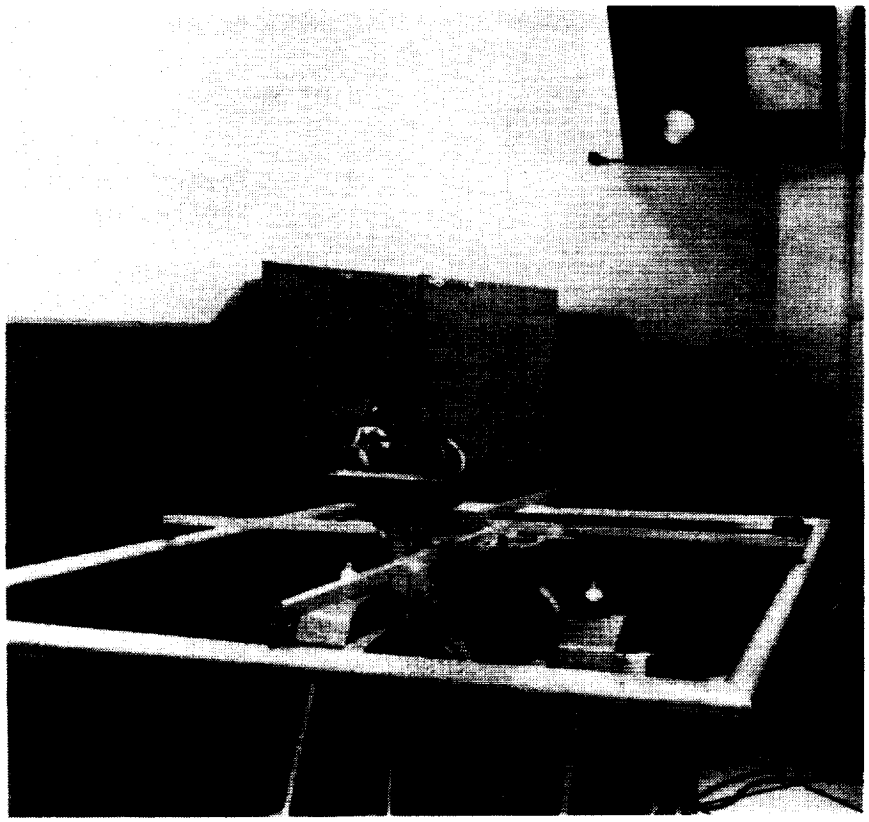

Fig. 7 Dynamical test facilities

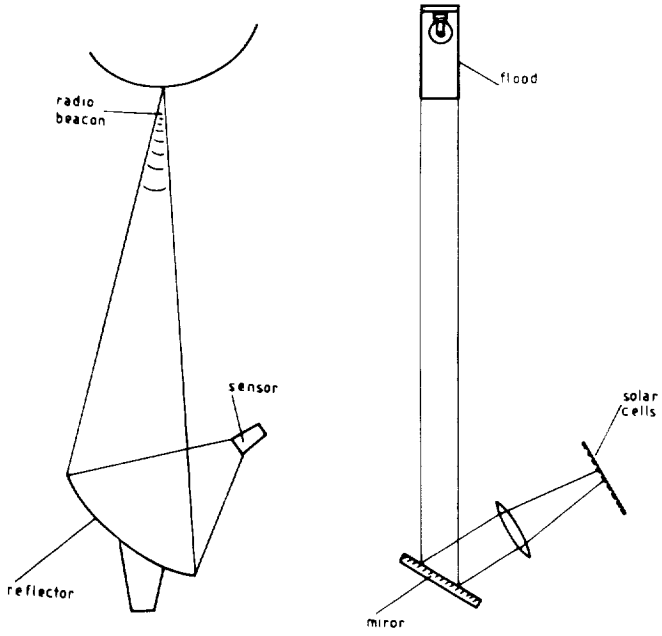

Fig. 8 R.F. Sensor optical simulator

AN ANTENNA POINTING MECHANISM FOR LARGE REFLECTOR ANTENNAS

Hans Heimerdinger
Dornier System GmbH
Friedrichshafen/Germany

ABSTRACT

An Antenna Pointing Mechanism (APM) for large reflector antennas on direct broadcasting communication satellites was built and tested. After listing the requirements and constraints for this equipment the model is described, and performance figures are given. Furthermore, results of the qualification level tests, including functional, vibrational, thermovacuum and accelerated life tests are reported. These tests were completed successfully.

INTRODUCTION

Direct broadcasting from orbit to homes is an objective of television broadcasting authorities. The aim is to attain acceptable screen quality when using paraboloid reflectors with a diameter of approximately one meter, located on a roof top. This and the regulations of the World Administrative Radio Conference (WARC) for noninterference with neighboring countries require the use of large reflector antennas on the direct broadcasting communication satellites in geostationary orbit and direction of the spot beam very precisely to the small coverage areas in Europe.

The Antenna Pointing Mechanism described here is the intermediate coupling and decoupling member between the heavy satellite and spot beam reflector antenna. The APM is a two-axis cardan-type suspension with direct drive motors and precise angle pick-offs. It is driven by its own control electronics, which in turn are controlled by tracking electronics on the spacecraft. A closed-loop control is assumed, with an RF signal from the ground indicating the beam deviation. During launch the antenna is locked rigidly to the spacecraft structure via the APM.

REQUIREMENTS

The large antennas were assumed to have moments of inertia up to 6 m^2 kg. In order to reduce the attitude control requirements of the spacecraft stabilized in three axes by momentum wheels, the error in each of the two orthogonal pointing axes of the mechanism should be below 0.01 degrees.

Due mainly to the large flexible solar arrays, the satellite will never come to a complete rest. As the mechanism compensates these residual spacecraft movements in a dynamic mode, a maximum speed of 0.1 degree per second is assumed. Design life was planned to be 10 years with at least 7 years of continuous run. For reorientation or repointing of the antenna beam, angular freedoms to ±4 degrees were required.

Beyond these driving requirements, some environmental requires were (1) interface temperatures from -70 to +65°C, (2) sine vibration input up to 18 g, and (3) a natural frequency above 100 Hz in lateral directions with the launch phase condition.

DESCRIPTION OF SOLUTION

Overall Description

Many of the design characteristics are based on the experience gained with previously built models: a vibration model and an engineering model (Figure 1). While the engineering model was of aluminum in circular configuration, the manufacture of the carbon fiber plastic (CFP) frames of the Q-Model required a square or rectangular configuration. Presently, the Q-Model of the Dornier antenna pointing mechanism is compsoed of the following items and characteristics:

- o Frames of carbon fiber plastic (CFP)
- o Inside/out arrangement of the gimbals
- o Wobbling disc direct drives
- o A very stiff- and direct-path off-load device
- o Compact unit, testable and adjustable before integration
- o Modular design of frames, drives, bearings, angle pick-offs, and off-load.

This Q-Model is shown as a photograph on Figure 2, as a block diagram in Figure 3, and as a cardan suspension in Figures 4 and 5. A detailed description follows:

Mechanism Bearings

Angular contact ball bearings were preferred to flexural metallic pivots because of their higher load capacity and the absence of center shift. The

size is rather large, to prevent damage by residual loads during vibration, since 100% off-loading is not attainable. The cage is of bronze and the balls of tungsten carbide with a thin layer of titanium carbide. An additional layer of MoS_2 on races and cages serves for lubrication.

The bearings are installed with a preload. Thermal distortion between the base plate (aluminum) and the inner frame (CFP) is compensated by the spring rate of the inner frame bracket, which carries the resolver. To ensure symmetric loading of the ball bearing, a spherical bearing is incorporated in this bracket. A special means for compensating thermal distortion between the two gimbal frames of CFP is not required.

Structure

To get a compact, readily clamped, and mountable unit, the stiff base plate was made by filigree milling of aluminum instead of using the satellite structure as a base plate. Two brackets of aluminum connect the base plate to the inner gimbal frame. Inner and outer gimbal frames are of a compound material design, with CFP walls and inserted titanium fittings. The inner frame is rectangular, with tubular sections of rectangular cross section, which are bonded together at the edges. The outer square frame has walls of open U-profile. During launch, its edge fittings directly transfer antenna loads to the off-load device. The fittings housing the bearings in both frames are of titanium also.

Off-Load Device

The off-load device consists of mainly of four lever pairs engaging the edge fittings of the outer frame, as well as the base plate. Thereby, a very short load path is achieved which bypasses launch loads from the bearings. Pre-tension of the levers is provided by a steel cable that can be cut pyrotechnically. After this cutting, the levers are opened by springs.

Relocking Device

This device, in the center of the mechanism, is designed to relock it in a central position upon telecommand in case of problems within the drive system. The relocking cone is driven – forward and reverse – by a DC gearmotor and a ball screw. It maintains its final position without being powered, by the self-jamming effect of the high ratio (1:1670) gear.

Resolvers

Consideration of reliability and accuracy led to resolvers as angular position pick-off. The type used here is a three-speed high-precision housed version that has already been qualified for space applications. It is driven by a special coupling, being stiff to torsional loads but soft to axial loads.

Motors

The stepper motor on each axis is a unique design which has been developed especially for this application. The motor consists of rotor and stator, where only the stator with its 24 coils is supplied with DC power. The rotor is a membrane, the rim of which is pulled down to the stator by a number of coils. As there is a slight cone angle on the stator opposite to the rotor membrane, a down-gearing effect between rotor and stator – without gear teeth but by friction only – provides a very small angular relative displacement when eight of the coils in the stator are switched stepwise. Step sizes down to 0.003° or below are achievable. As there is friction only between rotor and stator transferring the torque, the step size depends on the rotor load. This effect, in turn, provides a very smooth starting characteristic of this wobbling disc type of motor.

Mechanism Functions

The mechanism, during a mission, will first release the off-load device by cable cutting with one of the two pyrotechnic cutters. The next function will be the fine pointing of the antenna in both axes according to steering signals from external electronics. In this main operational mode, the mechanism compensates satellite motion up to 0.2 Hz dynamically. In the repointing mode, as the third function, the mechanism rotates the antenna up to ±4 degrees thereby shifting the beam coverage from one country to another. Thereafter fine pointing can start again.

As already mentioned, the mechanism is able to recenter the antenna mechanically upon telecommand. This fourth function is reversible without limitation, although this is a failure recovery device only.

PERFORMANCE AND TEST DATA

Overall dimensions and mass figures are as follows:

Height 130 mm and squarebase width 450 mm, 6.3 kg mass. The dynamic tests were performed with a fixed step frequency of 40 steps per second, but there is a potential frequency increase to above 125 steps per second.

Testing was performed in four phases:

a. function tests
b. vibration tests
c. thermo-vacuum tests
d. life tests.

a. Function tests were conducted in the atmosphere as single-axes tests with a gravity-compensating suspension representing an antenna. Function tests in the thermo-vacuum chamber were performed with constant weight loads of 0.2 Nm.

With the separated resolvers, angular errors below 15 arcsec were measured. The angular range of the mechanisms was above ±4 deg. Step sizes without load were up to 0.0025 deg, and with load up to 0.0016 deg.

Angular speeds:

Without loads	0.1 deg/sec
With weight load of 0.3 Nm	0.065 deg/sec
With weight load of 6.24 M^2 kg	0.1 deg/sec

Cross-coupling, that is, a disturbance from the active axis to the other passive axis, was not observed. An oscillation of the inertia package after stopping the motor could not be detected.

b. Vibration tests were conducted with the mechanism clamped and loaded by a stiff antenna package. The design criterion of 50 g response at the package center of gravity at excitation in lateral directions was verified without any damage to the model.

Vibration inputs were:

- lateral sine vibration up to 18 g
- axial sine vibration up to 20 g
- random vibration with 15.4 g rms (max. 0.6 g^2/Hz at 50 Hz).

Measured natural frequencies of the mechanism were:

- 110 Hz in the x-direction
- 100 Hz in the y-direction
- 420 Hz in the z- or axial direction.

The bearings were free of backlash and their friction torques were not changed after the vibration test.

c. The thermo-vacuum tests were conducted in an oil-free chamber with superinsulation and radiators to simulate the satellite thermal conditions at qualification levels. The motors were supplied with constant current. The chamber pressure was always below 10^{-5} mbar.

In addition to soak tests at -30°C and at +60°C, the critical temperature tests were:

- cold test with -5°C at the satellite interface and -70°C antenna interface
- hot test with +50°C satellite interface and +65°C antenna interface
- negative gradient test with +50°C satellite interface and -40°C antenna interface
- positive gradient tests with +10°C satellite interface and +65°C antenna interface.

During each temperature test case, the behavior was observed and function tests were performed. The behavior was not changed by the temperature

or the temperature gradients. A performance decrease was measured in operating speed only. Although the increase of copper resistance in the motor coils was compensated by the electronics, a 20% reduced speed was measured when one motor had to perform at its upper thermal limit. This is a motor characteristic. No damage or wear was observed after these tests.

d. Life tests were were at first conducted with the motors separately, with doubled step frequency (80 Hz).

The accelerated life tests and qualification tests which were conducted at the European Space Tribology Laboratory in England used the same temperature levels as mentioned before. Again there was no damage or wear to be detected after 7 months of testing. The optical test method used there detected no cross coupling between the two axes. A zero shift of 0.01 deg in x-axis and of 0.02 deg in y-axis was measured during eclipse conditions. Such a shift is acceptable because during eclipse no operation is required.

Using the optical test method, again no temperature-dependent behavior was observed except for the speed decrease. The optical test method was known to have angular errors below 0.0026 degrees.

CONCLUDING REMARKS

The mechanism proved to be a valuable construction with further development potential for adaptation to certain satellite programs. The significant technology features of the APM are:

- long-term dry lubrication with small angle oscillating ball bearings
- the use of CFP frames for achieving thermal stability in highly loaded three-dimensional structures
- the direct drive wobbling disc stepper motor with tiny steps and minimum power consumption
- the very stiff, reliable and light-weight off-load device.

ACKNOWLEDGMENT

My company and I want to acknowledge the assistance of personnel at ESTEC in Holland and at ESTL in England for their valuable discussions and support during the testing at ESTL. This development work was funded by the DFVLR-BPT in Cologne, Germany.

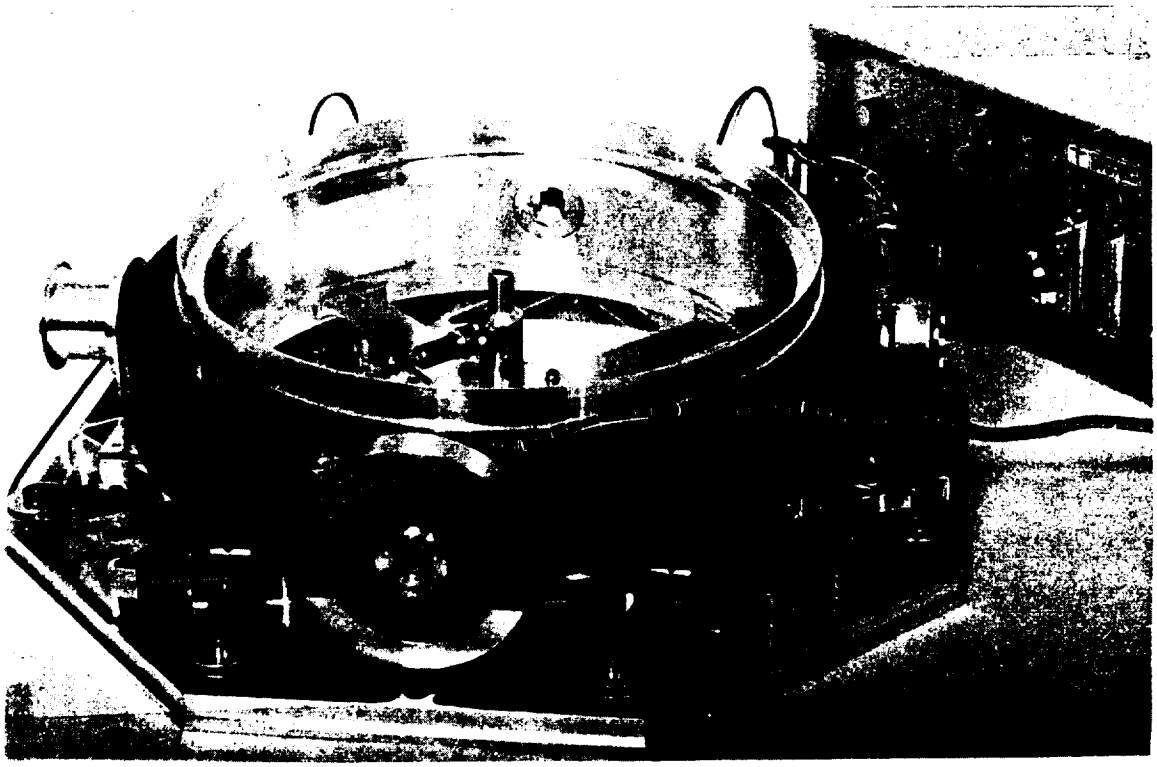

Figure 1: APM Engineering Model

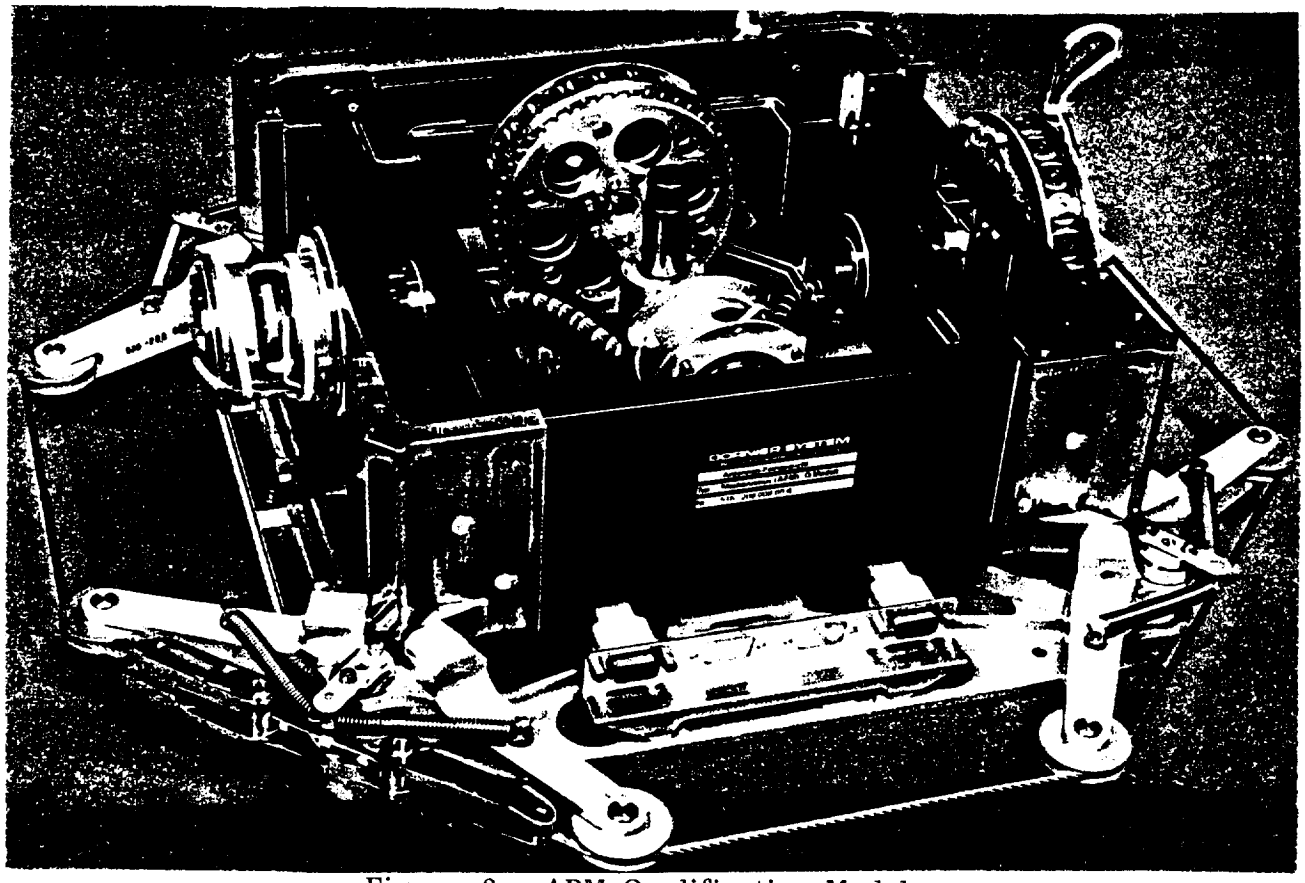

Figure 2: APM Qualification Model

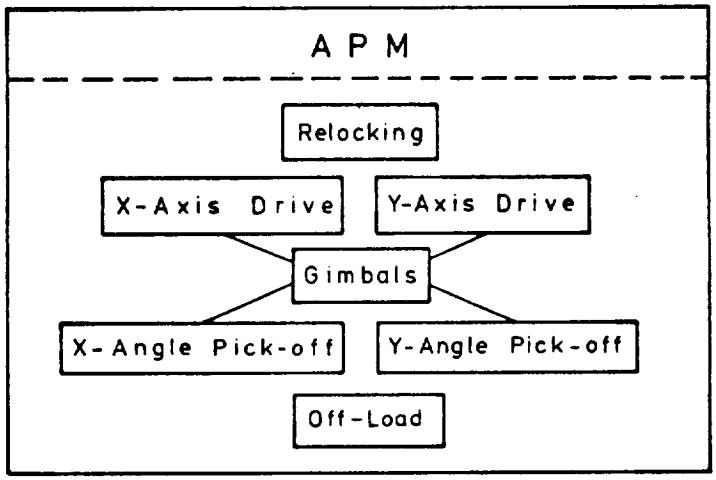

Figure 3: APM Block Diagram

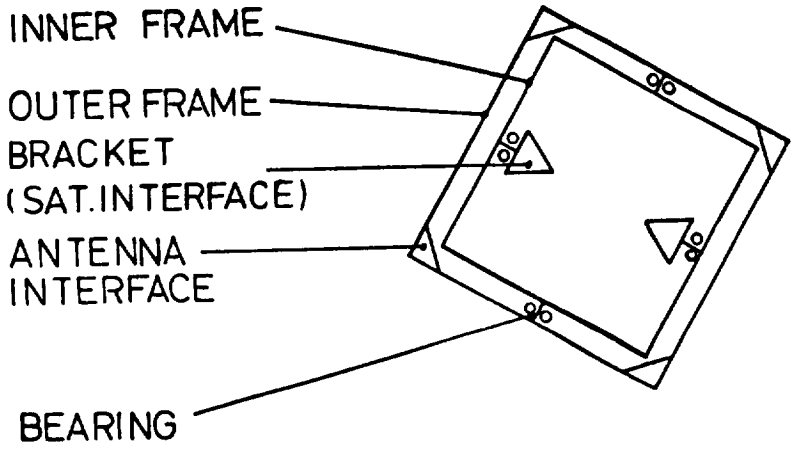

Figure 4: APM Cardan Suspension, Schematic

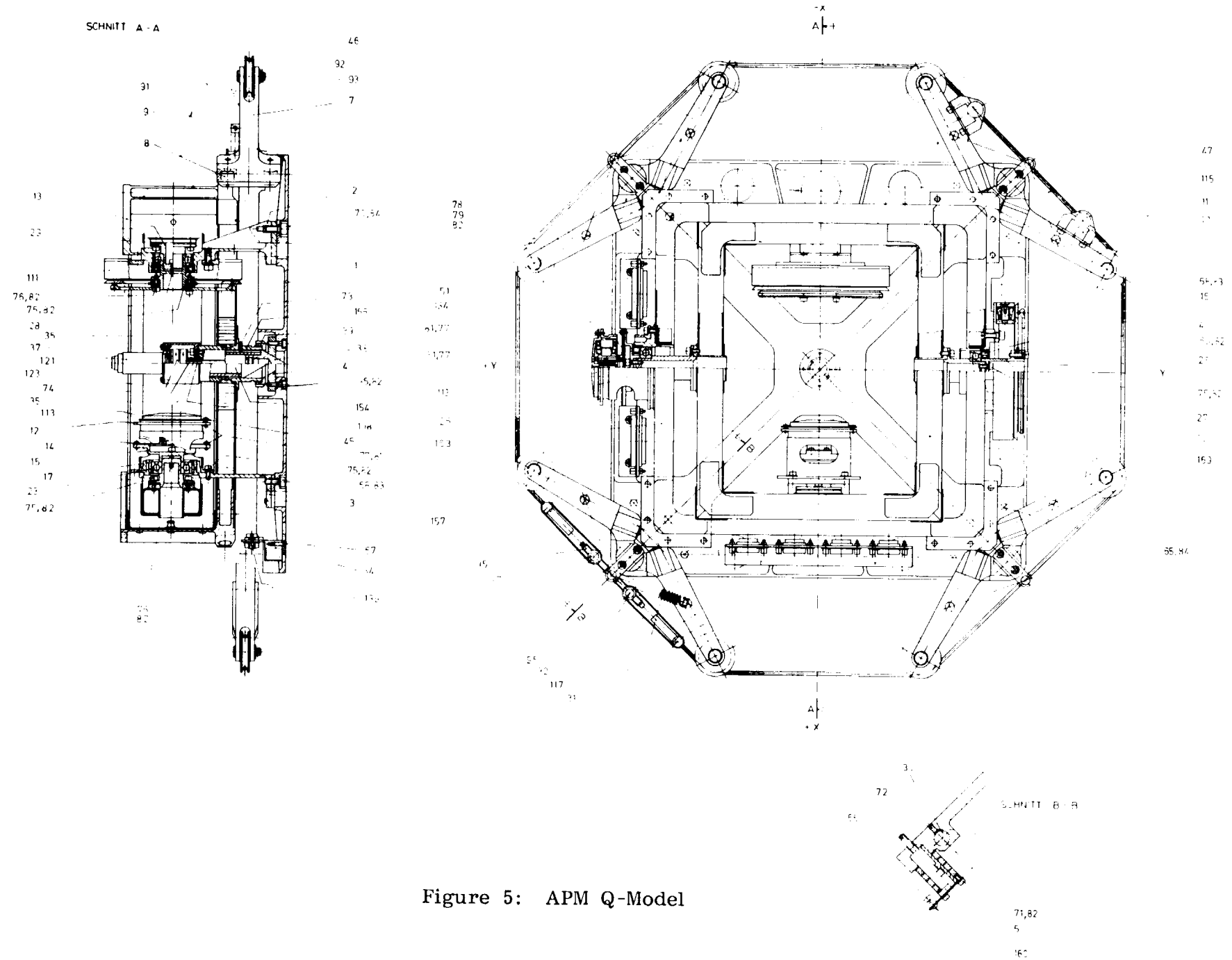

Figure 5: APM Q-Model

A DRIVE UNIT FOR THE INSTRUMENT POINTING SYSTEM

R. Birner* and M. Roth*

ABSTRACT

The requirements, capabilities and unique design features of the IPS Drive Units (DU) are presented. The DU's are identical for all three gimbal axes (elevation, cross elevation and azimuth) and provide alternating rotation of shaft versus the housing of ± 180 degrees. The design features include:

- two ball bearing cartridges using cemented carbide balls coated with TiC layer
- redundant brushless torque motors and resolvers
- a load by-pass mechanism driven by a DC torque motor to off-load the bearings during ascent/descent, ground transportation and to provide an emergency braking capability
- cabling over each gimbal axis by means of cable follow-up consisting of 13 signal and 15 power flat band cable loops

The qualification of the DU is in progress. Test results of disturbance torque characteristics are presented.

INTRODUCTION

The DU's described in this paper were designed for the ESA Instrument Pointing System (IPS). Figure 1 shows IPS subsystem configuration and the arrangement of the 3 DU's within the gimbals in launch mode.

The DU function is to

- generate the necessary torques to control the pointing accuracy and to erect and stow the payload
- provide the angular freedom of gimbals with low disturbance torques
- measure gimbal positions
- carry the ascent, descent and ground loads of the integrated gimbal system without detrimental effects on the ball bearings
- provide flexleads for power and signal interfaces
- brake gimbal motion in case of control failure which could lead to damage of orbiter and consequential crew safety hazards

*Messerschmitt-Bolkow-Blohm GmbH, Germany

- self align the zero position to facilitate P/L stowage within the capture range of the latches

- provide a manually actuated shaft lock to provide a back-up in case of a failure of the load by-pass or torque motors

The DU performance requirements are summarized in Table 1. The small angle disturbance torque requirements and their definitions are given in Figure 2.

DESIGN DESCRIPTION

The DU design is shown in Figure 3 and is illustrated in schematic form in Figure 4. The DU is composed of the following constituents:

- Bearing Subassembly which houses the torquers and resolvers

- Load By-Pass

- Cable Folow-Up

Bearing Subassembly

The bearing subassembly consists of a main shaft, an intermediate shaft, two bearing cartridges, the motors and the resolvers.

The main shaft carries the loads of the launch and landing phase and is disengaged from the intermediate shaft during these phases in order to protect the high precision bearings. The intermediate shaft is linked to main shaft for rotational deflections by means of a spring preloaded stop.

Bearings and Lubrication System

The bearing disturbance torque is a major system parameter influencing pointing control performance for small payloads.

The selected bearing configuration consists of one radial thrust bearing cartridge containing duplex angular contact bearings, face-to-face mounted,and a radial bearing preloaded by a diaphragm. The bearing races are made from steel 440 C, the balls are 2 µm TiC coated tungsten carbide (WC 6 Co) and the retainers are 5 percent aluminium bronze. The bearing precision is ABEC 9. The balls are ground to AFMBA grade 5. The lubrication applied is the visco static oil FORMBLIN Z 25 as recommended by ESA. A labyrinth seal assures protection and continuous lubrication of bearings.

Motors and Resolvers

The system requirement on man motion disturbance error leads to a peak torque demand of approximately 10 Nm. Since the operation of the drives is essential for the stowage of payload redundant motors were selected. The selected motors are pancake type 12 pole brushless torque motors with cobalt samarium permanent magnets, commutated by redundant single/multispeed resolvers. The single speed windings of the resolvers are necessary to provide a position signal for coarse acquisition and for erection/ stowage manoeuvres.

Load By-Pass

The Load By-Pass (LBP) is used to unload the ball bearings during ascent/descent and to act as an emergency brake in case of a failure of the IPS range/rate control. Figure 5 shows a section view of the LBP which is made up of the following major components:

Two adjacent conical slotted clamprings (1), housing (2) with bonded on friction lining (3), wedge segments (4) which provide the radial force to enable the braking via the clampring and the actuation mechanism.

The clamprings are screwed on the shaft and their segments act like flat springs radially but provide enough stiffness in tangential direction to transmit the braking torque. The actuation of the LBP is performed by means of a DC torque motor (8) integrated in the main shaft. Its rotor (9) turns the spindle (12) which has one right and one left hand thread. The nuts (11) engage/disengage the wedge via the disks (6). The wedges are dry lubricated and provide a low coefficient of friction which allows a high brake torque of a relatively small axial force. As the wedges have the freedom to move radially with respect to the disks (6), thermal deflections and manufacturing tolerances do not alter the radial force on the clamprings.

The LBP needs only short term power for operation due to the self locking feature of the threads on the spindle.

Development vibration testing revealed the need of an additional device to prevent inadvertent loosening of the brake. This device shown in Figure 6 consists of turnable hub (13), a fixed toothed ring (14), two springs (15) attached to an intermediate ring (17) and a ball ratchet. The actuator motor (9), when energized, turns the hub and unlocks the ball ratchet. The hub rotates until it reaches its stop on the intermediate ring where it is locked again by the ball ratchet. During this movement the spring

ratchet is released preventing back rotation of the spindle after stand still of motor. For reverse motor rotation, the ratchet functions vice versa.

For payload stowage and to accommodate torques at ascent/descent, the LBP is equipped with two form clutches one of which provides self alignment of zero position at a capture range of 0.5 degrees. This function is achieved by a wedge shape of the clutch. The second clutch is rectangular and is to carry the major torques. The clutches are suspended in preloaded springs to avoid potential damage during engaging while the shaft is rotating at emergency braking operation.

A pin actuated by an EVA lever provides a back-up in case of LBP failure thus avoiding need for jettisoning for this event.

Cable Follow Up

The purpose of the cable follow up (CFU) is solely for the transmission of signals and power to and from the gimbals. Any torques exerted by the flex leads are undesirable.

Initially a roll-around flex lead configuration as per Figure 7 was selected based on advantages over a spiral configuration with respect to space, weight and ideal rolling leading to very small theoretical disturbance torques. Tests on a development model including the full number of signal and power lines showed an unexpected irregularity of rolling motion. The flat conductor cables lifted from the shaft at larger angular excursion forming parasitic loops. These loops became suddenly unstable at certain positions and generated intolerable disturbance torque peaks while transition to the desired loop shape occurred. Thus, a spiral configuration had to be adopted as shown in Figure 7. For EMC reasons signal and power lines are housed in separate chambers. The cables integrated in the cable follow up are as follows:

Signal Chamber:

10 flat conductor cables 18 x AWG 24
Kapton insulated

3 flat bands, each consisting of
10 twisted shield pairs
125 Ohm and 75 Ohm

Power Chamber:

18 flat bands, each 18 x AWG 20
PTFE insulated

TESTING

Although the qualification program is not yet fully concluded, the following major tests have been completed in compliance with the requirements:

- Performance tests on
  disturbance and angular freedom
  torquers and resolvers
  brake and form clutch (torque load 2500 Nm)
  electrical interfaces and power

- EMC test: radiated and conducted emissions

- TV test at operating and nonoperating temperatures including performance tests on disturbance torque and braking

- Shock test; 20 g/10 ms per MIL-STD-810 B/5/6, 3 axes

- Life test on
  bearings and load by-pass torque motor

Qualification with respect to sine/random vibration is currently on hold due to newly redefined much more severe environmental loads which are now being studied regarding its impact on structural design. A redesign may result from this study.

Disturbance torque tests were performed on the bearing subassembly, bearing subassembly with integrated torque motors, cable follow up and on the complete drive unit with simulated on orbit loads of approximately 300 N radial and 150 N axial. This was achieved by tilting of the drive unit and use of extra mass attached to the drive unit housing in a set-up shown in Figure 8.

The Figures 9 and 10 present records of disturbance torque tests on the CFU and the bearing subassembly at small angle displacements. The shape is roughly in the form of parallelograms. At increasing angles the parallelograms extend mainly in the axis of displacement as figure 9 indicates. The CFU exhibits no friction. The bearings show, besides friction, an important part of a spring characteristic. Figure 11 shows the disturbance torque of the complete DU including the disturbance torques of the torque motors which contribute considerably to the spring and hysteresis torque.

CONCLUSION

A drive unit compatible with the IPS system requirements has been developed. Reusability, gimbal structure/payload separation, safe stowage of payload in case of main bus failure with associated power restriction and safety aspects led to drive unit design with features not available in conventional drive units, i.e., electromechanical load by-pass with low short term power demand, mechanical self alignment of zero position, emergency braking capability and manual locking device.

A roll around cable follow-up configuration showed torque anomalies in application where ± 180 degrees rotation and a high number of flex loads are required. The spiral configuration performed as desired and deflection tests in the range of arc seconds revealed that no friction is generated at this range. Disturbance torque tests at assembly levels revealed the contributors to friction, hysteresis and spring torques.

TABLE 1

DRIVE UNIT PERFORMANCE REQUIREMENT

- Position Accuracy	10 arcmin
- Drive Motor	
Stall torque	15 Nm
Ripple torque	2.25 %
Cogging torque	0.1 Nm
Hysteresis torque	0.3 Nm
Power	65 Nm at 10 Nm
- Load By-Pass	
Braking torque	600 Nm
Power	18.5 V/7.8 A
- Cable Follow Up	
Angular Freedom	± 185 deg
No. of leads	538
- Mass	74 kg
- Operating temperature range	+ 20 to + 70°C
- Life	10 years or 50 missions

TABLE 2

DRIVE UNIT DISTURBANCE TORQUE TEST RESULTS

Small Angle Disturbance Torque at ± 0.1 deg Deflection at Zero Position

Friction Torque T_f Ncm	1.5 ÷ 2.7
Hysteresis Torque T_H Ncm	4.8 ÷ 7.0
Spring Constant C_D Nmm/rad	79 ÷ 112

Brushless Torque Motor Disturbance Torques

Cogging Torque p-p	0.03 Nm
Hysteresis Torque 0-p	0.09 Nm
Ripple Torque p-p	1.3 %

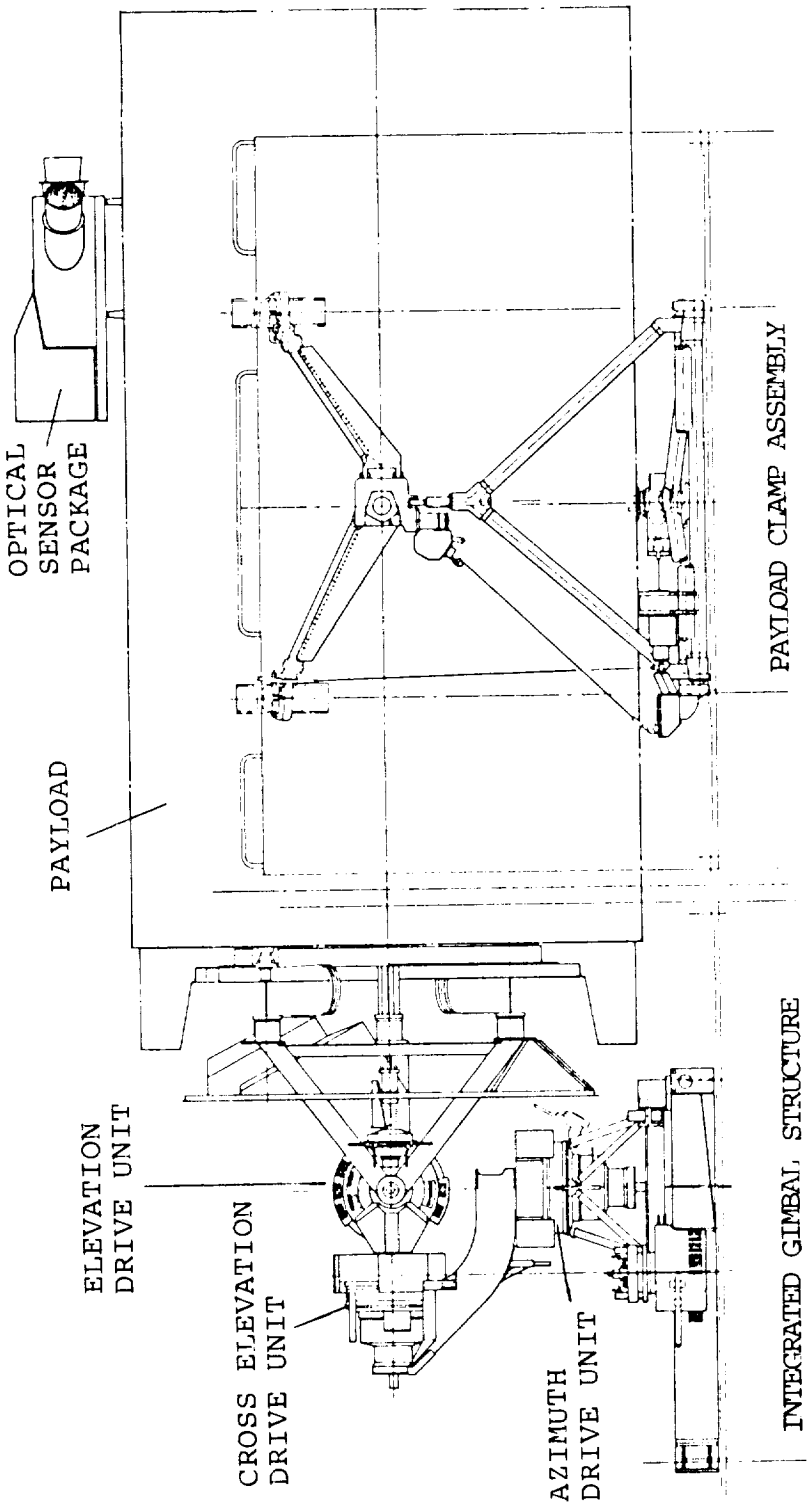

Figure 1. Instrument Pointing System

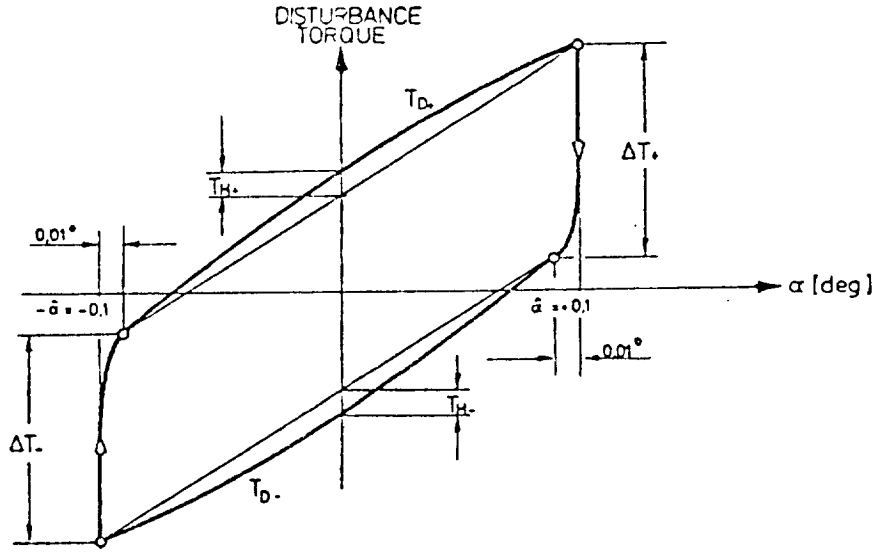

Friction Torque T_f	$\leq$ 4 Nm
Hysteresis Torque T_H	$\leq$ 14 Ncm
Spring Constant C_D	$\leq$ 170 Nm/rad

Figure 2: Small Angle Disturbance Torque Definition and Requirements

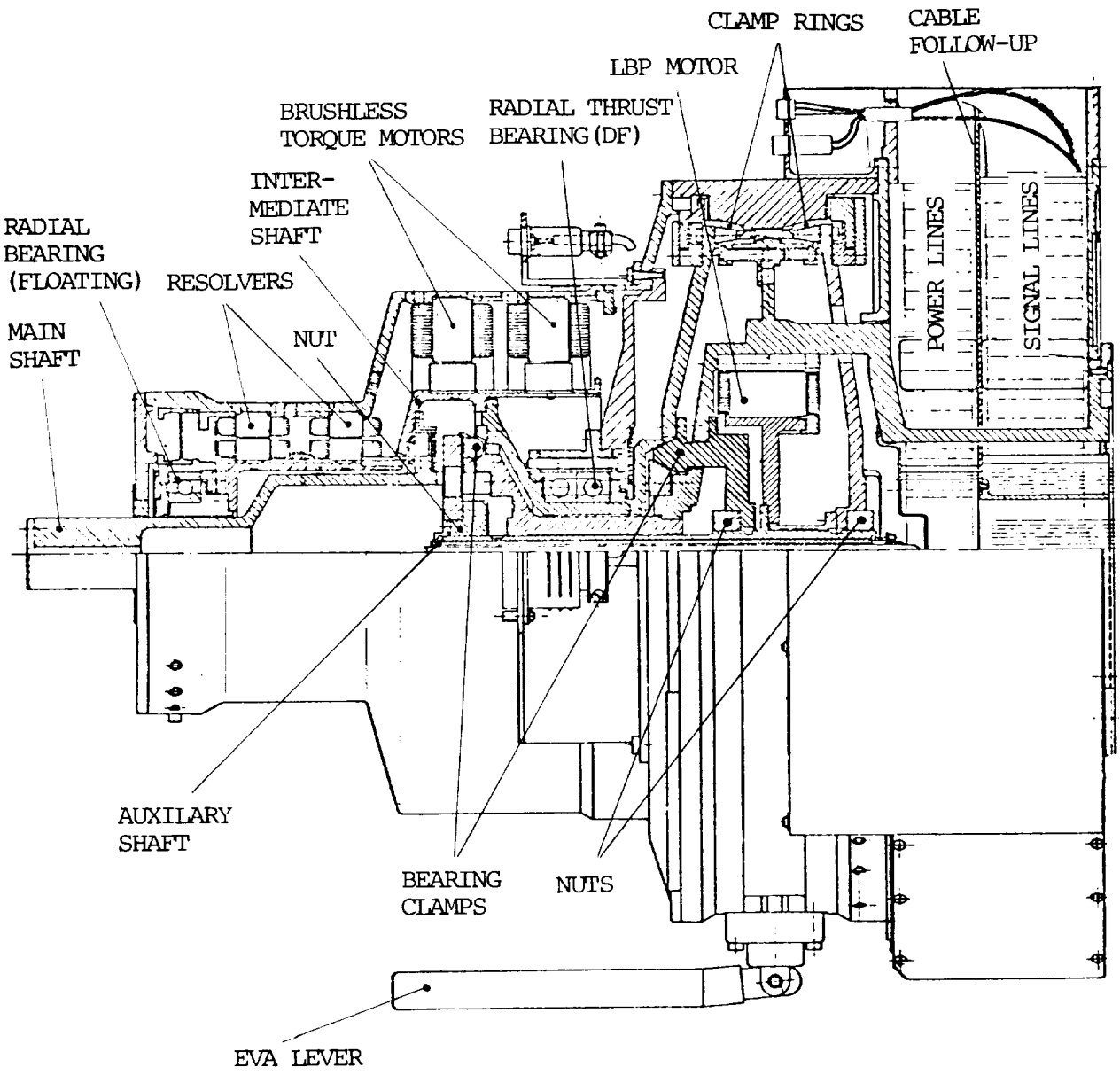

Figure 3: IPS Drive Unit

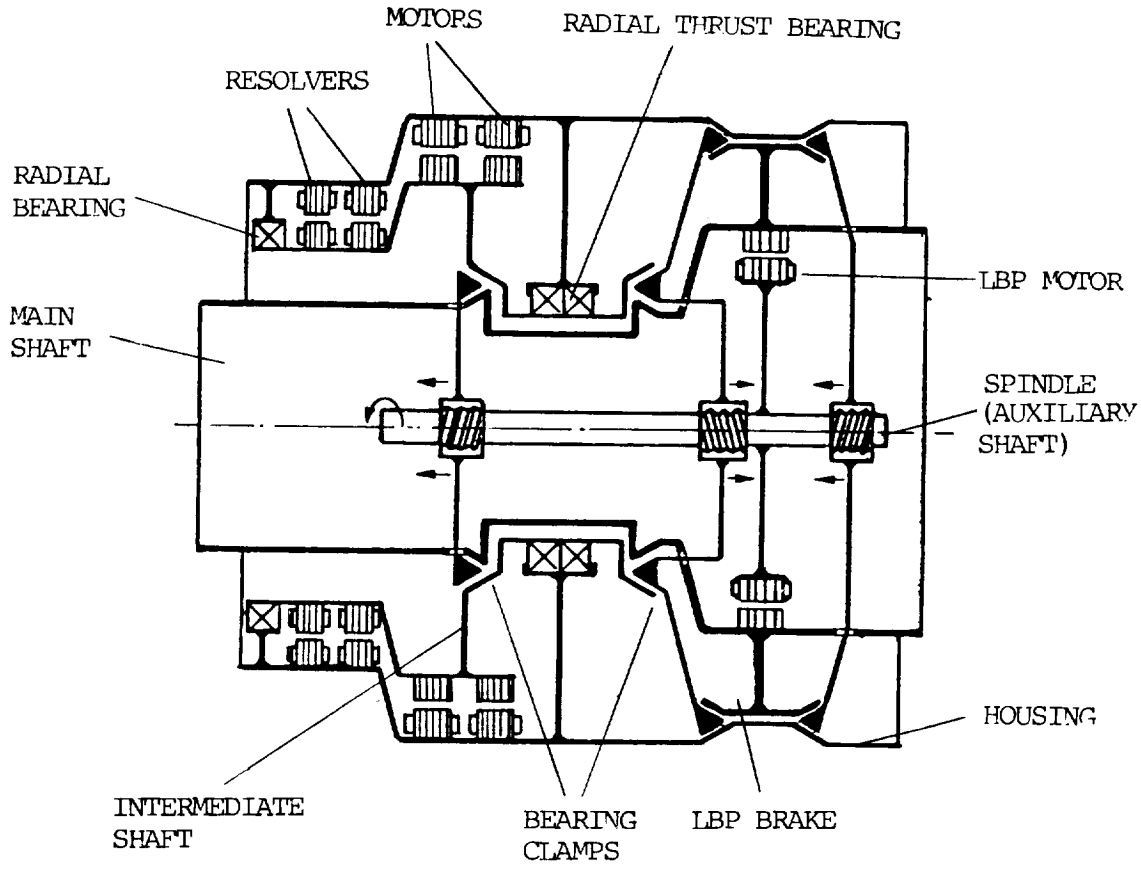

Figure 4: Drive Unit Mechanical Schematic

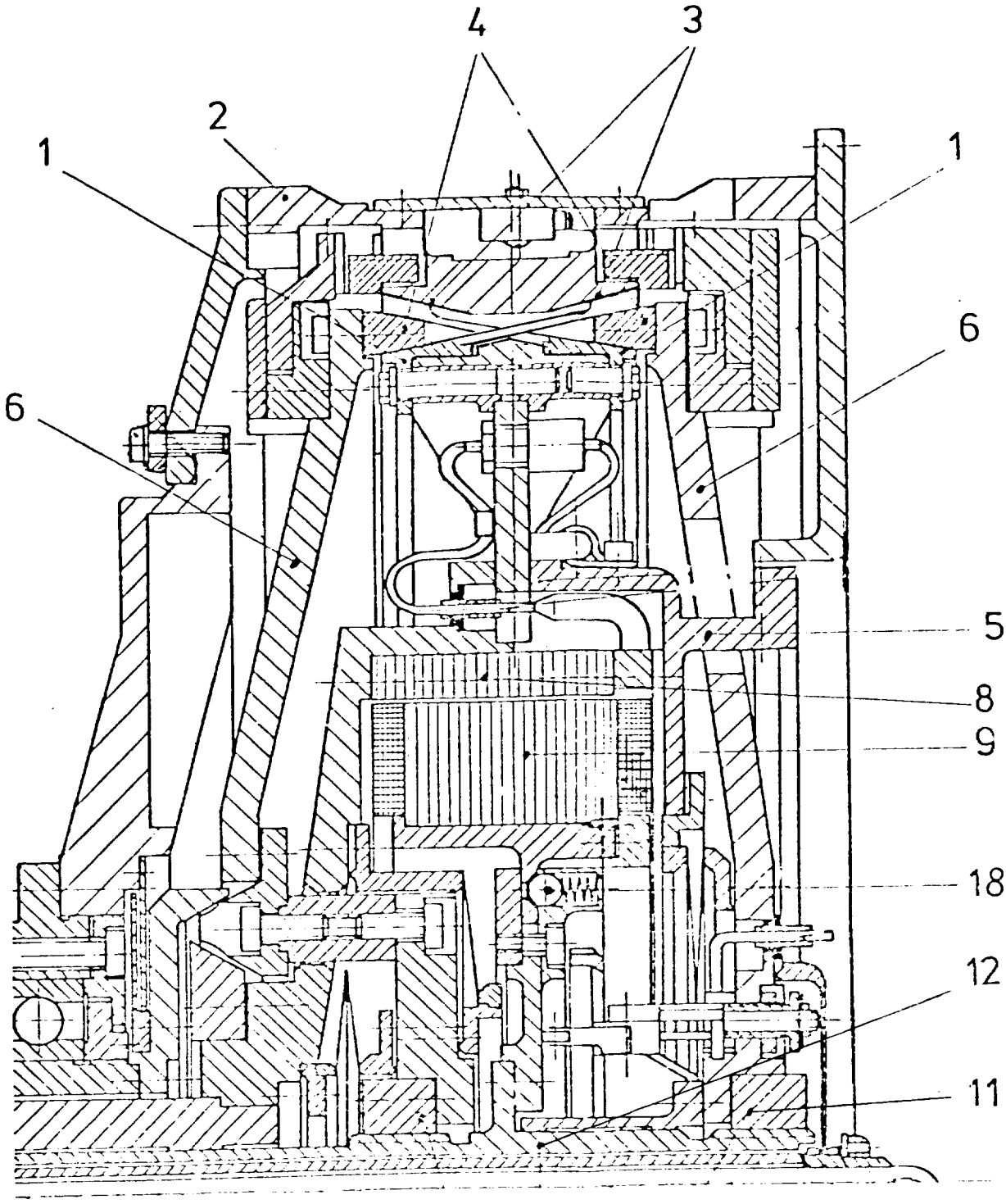

Figure 5: Load By-Pass

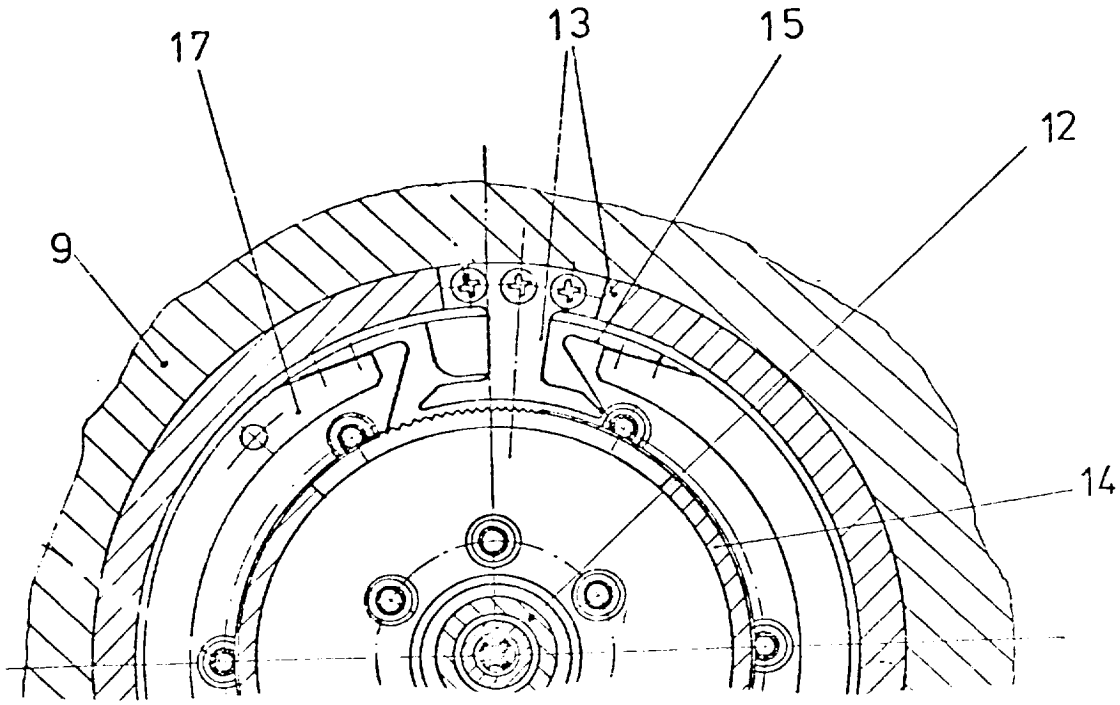

Figure 6: Load By-Pass Ratchet

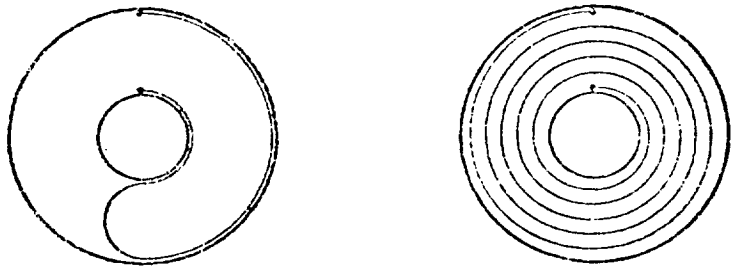

ROLL AROUND LOOP SPIRAL

Figure 7: Flex Lead Configurations

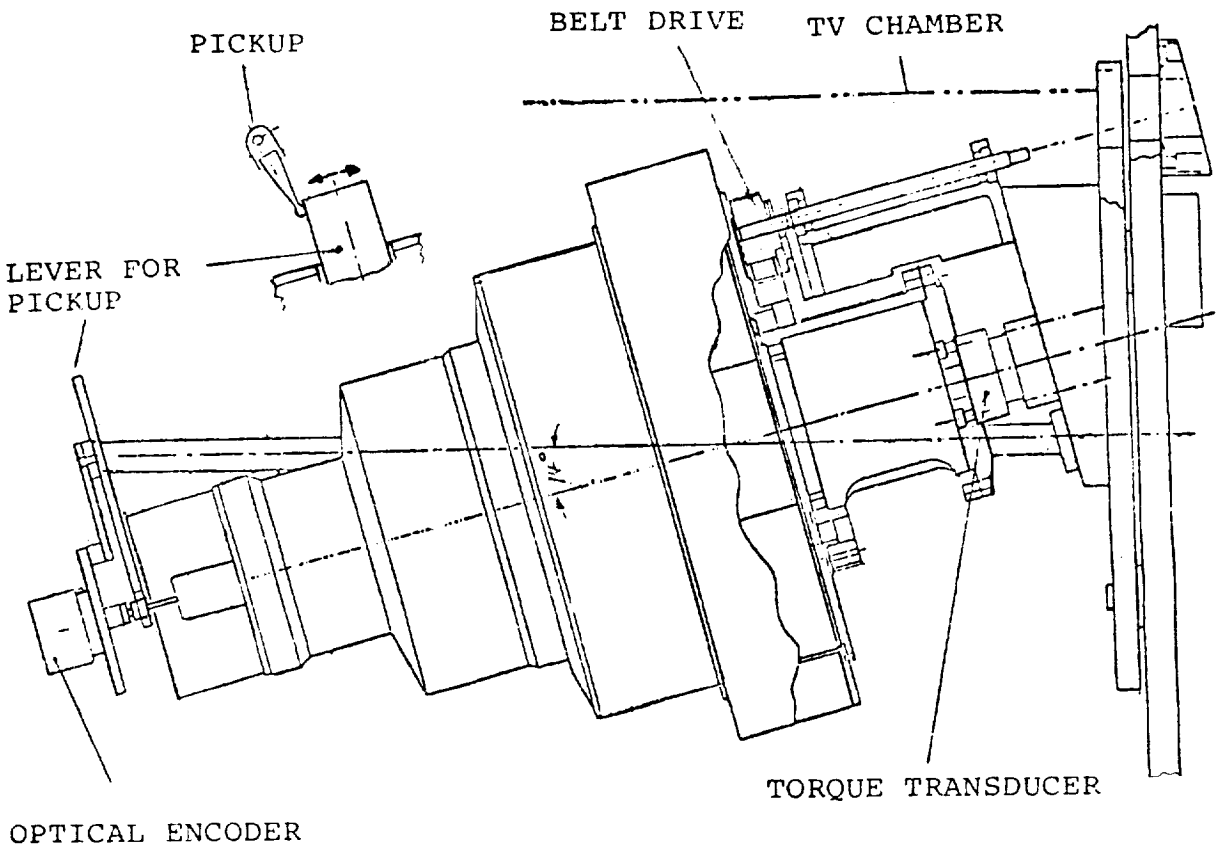

Figure 8: Mechanical Test Set-Up for Disturbance Torque Measurement

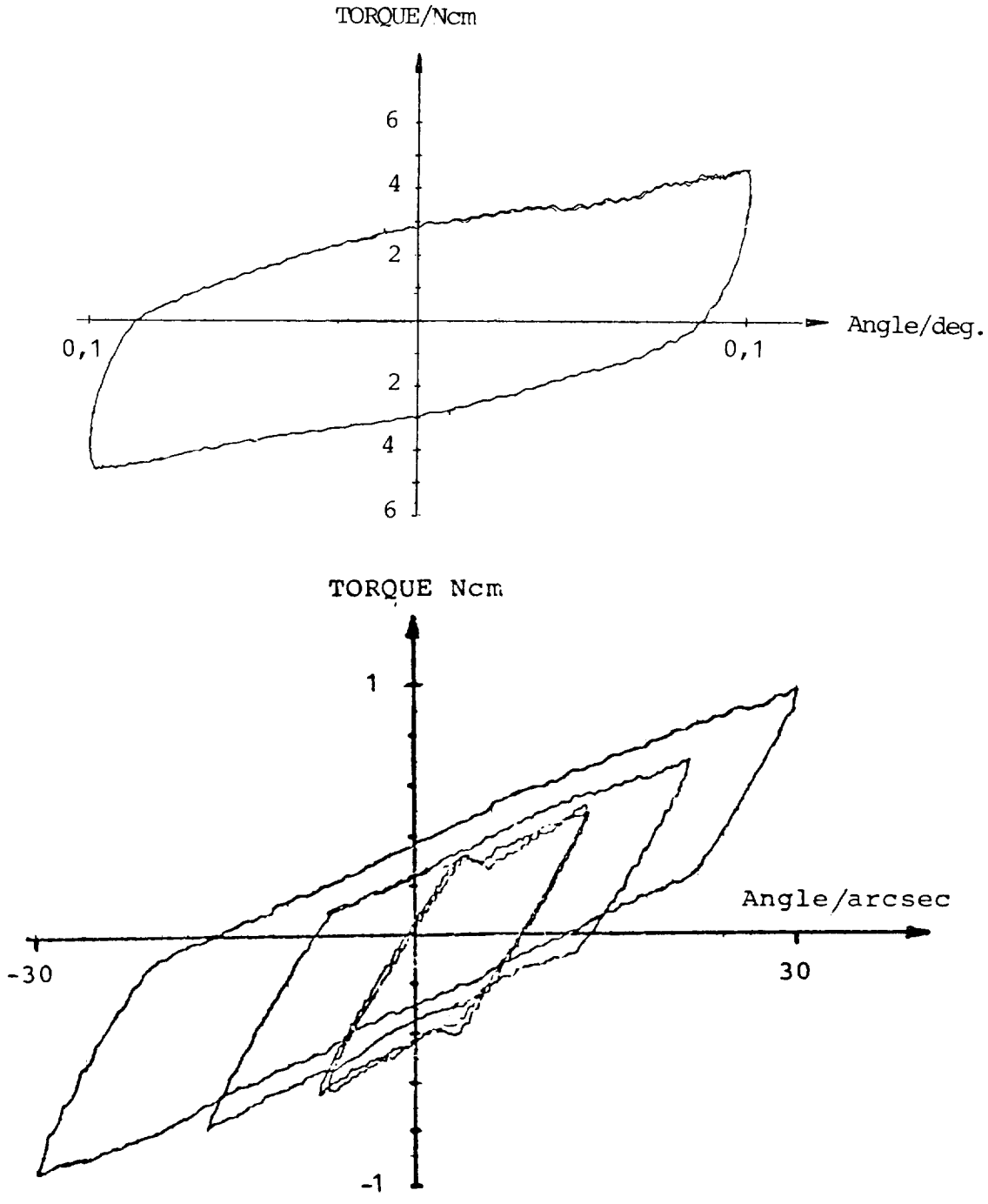

Figure 9: Measured Small Angle Disturbance Torque of the Cable Follow-Up

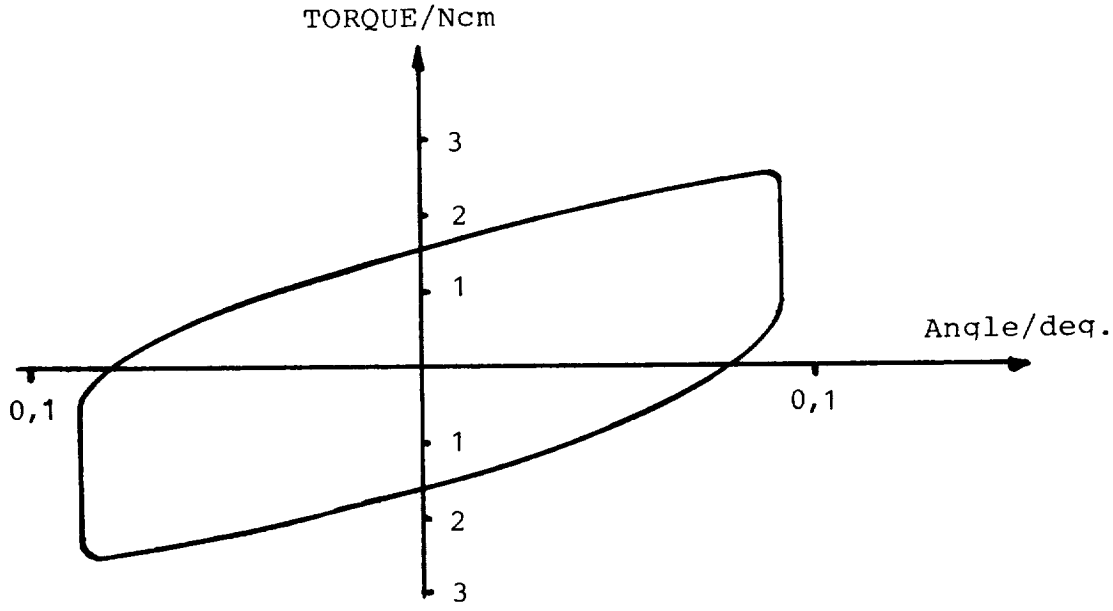

Figure 10: Measured Small Angle Disturbance Torque of Bearing Subassembly

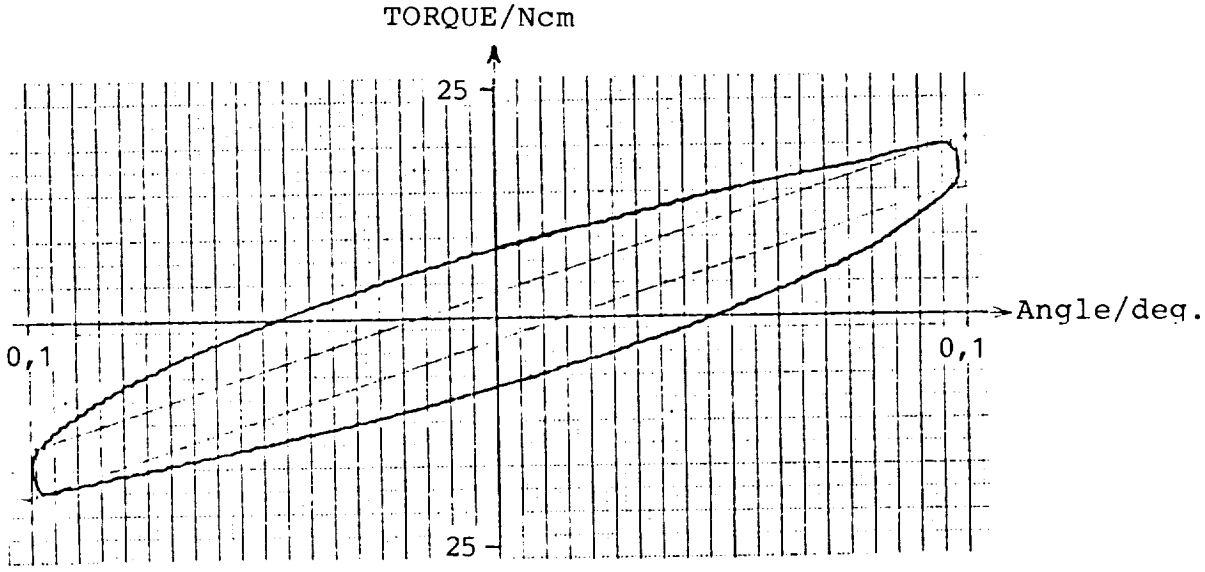

Figure 11: Measured Small Angle Disturbance Torque of the Drive Unit

SRB DEWATERING SET

By Robert E. Wickham

John F. Kennedy Space Center

SUMMARY

The Solid Rocket Booster (SRB) Dewatering Set is a system that is designed to prepare the Space Shuttle SRB's (two per Shuttle flight) for being towed back to port, the first step in recovering and refurbishing the SRB's for reuse on subsequent Shuttle missions.

INTRODUCTION

After about two minutes into the flight, the SRB's separate from the Orbiter/External Tank and parachute into the ocean. The parachutes are automatically detached from the SRB after impact. A sealed chamber on the SRB forward end (called the forward skirt) provides 27,216 Kilograms (Kg) (60,000 lbs) of buoyancy. Added buoyancy is needed to float the approximately 75,751 Kg (167,000 lb) SRB (splashdown weight). This buoyancy is provided by air trapped in the upper portion of the rocket motor. The predicted SRB attitude after stabilization is vertical (spar buoy mode) with the rocket nozzle in a Keel position.

SYSTEM DESCRIPTION AND OPERATION

The SRB Dewatering Set consists of a Nozzle Plug, Control Console, Remote Control Unit, Power Distribution Unit, Umbilical Cable, Interconnect Cables and various handling and storage items. The Nozzle Plug (NP) is a remotely-controlled, tethered (by an umbilical cable) underwater vehicle that is launched from the Retrievel Vessel (RV) by a crane, maneuvers on the surface of the ocean over to the SRB, descends down the side of the SRB and is positioned below the SRB nozzle. A TV camera mounted at the top of the NP central core is used by the Control Console operator to visually guide the NP during descent and docking. The NP is then driven up and locked into the nozzle. Compressed air is passed through the umbilical from the RV, through the NP and into the SRB motor. As the air pressure builds up, the water inside the SRB is expelled causing the SRB to rotate to a near horizontal (log mode) attitude on the surface of the water. A sealing bag on the NP is inflated that blocks the SRB nozzle throat and prevents further entry of sea water into the SRB. A flexible hose is deployed from the forward end of the NP that drops to the bottom of the SRB. Compressed air

is again introduced into the SRB causing the remaining water to be expelled through the hose, down a tube (past a check valve) inside the NP and out numerous discharge holes downstream of the inflated bag. Upon completion of this final dewatering, the umbilical is disconnected and the umbilical lines are capped. A towing line from the RV is attached to a 18.3 meter (60 foot) long tow line attached to the front of the SRB. The SRB is then towed behind the RV back to the SRB Disassembly Facility at the Kennedy Space Center. A sketch of the system is shown in Figure 1.

NOZZLE PLUG

The NP is 4.2 meters (13 feet 11 inches) tall, 2.1 meters (7 feet - 0 inches) across at its widest point, and has a central core 76 centimeters (cm) (30 inches) in diameter. A simplified sketch of the NP is shown in Figure 2 . Fully ballasted and with all fluids at recommended levels, the NP weighs approximately 1542 Kg (3400 pounds) in air. Sealed chambers augmented by flotation foam, which is included in the total in-air weight, create a small positive buoyancy in water. The NP is powered by six thruster motors, two of which provide vertical thrust and four horizontal thrusters mounted near the center of gravity at 90-degree intervals. All thrusters are Kort Nozzle type and are fully reversible in direction of thrust. Except for some forward pitch angle during horizontal movement, the NP remains vertical during all maneuvering. The NP is able to be propelled vertically up or down, or horizontally (laterally or turning), or combinations of vertical and horizontal if so desired. The umbilical hangs beneath the NP in a catenary that allows free motion of the NP in any direction. The NP is stable with its longitudinal axis vertical. The center of gravity (CG) is approximately 165 cm. (65 inches) up from its base, and the center of buoyancy (CB) is approximately 23 cm. (9 inches) above the CG. On the surface of the water, approximately 38 cm. (15 inches) of the NP is above the water surface.

The electrical and air umbilicals are married together to a point about 3.7 meters (12 feet) below the NP where they are then separated. The electrical cable enters a junction box on NP leg no. 1 and is routed through the leg into the NP central core while the air hose does likewise through the opposite leg no. 3. This utilizes the legs as protective enclosures and eliminates the drag that would be caused by running these umbilical components externally.

CONTROL CONSOLE

The Control Console is the command center for SRB dewatering operations. From this console located on the RV bridge, the operator sends commands to the Nozzle Plug via the electrical cable portion of the umbilical cable

The electrical also carries information from the NP that is displayed on the Control Console by meters, lights, and video monitor.

REMOTE CONTROL UNIT

During launch of the Nozzle Plug, control is exercised using the Remote Control Unit. Attached to the Control Console by a 15.2 meter (50 foot) electrical cable, the Remote Control Unit controls the thrusters as the Nozzle Plug is maneuvered across the ocean surface to the SRB. Once the Nozzle Plug is adjacent to the SRB, control is transferred to the Control Console for the remainder of the mission.

UMBILICAL CABLE

The umbilical cable consists of an electrical cable and an air hose that are joined together. Floats are added at selected intervals to a portion of the umbilical assembly, beginning about 53.4 meters (175 feet) from the Nozzle Plug and continuing to the Retrieval Vessel end.

POWER DISTRIBUTION UNIT

Electrical power enters through a signal conditioner called the Power Distribution Unit (PDU) and is then distributed to using functions. The PDU contains fuses, transformers, relays, circuit breakers, and motor starters for the electrohydraulic motor/pump units.

INTERCONNECT CABLES

The interconnect cables are used to transfer electrical power and/or signals between the PDU and Control Console, the PDU and the power sources; between the Control Console and the Remote Control Unit; between the Control Console and auxiliary TV monitor and TV taping equipment; and between the Control Console and the air manifold located near the air compressor.

TRADE STUDIES

During the early phases of design, it was decided to perform certain trade studies to ensure that the best design paths would be chosen for

our particular application. I will state here without attempting justification for either method that a program decision had already been made to use a remotely-operated vehicle instead of a diver-operated vehicle. The trade studies selected were:

1. Propulsion System: Electrical vs Hydraulic[1]
2. Structural Materials Selection[2]
3. Umbilical Disconnect Location[3]
4. Water Discharge Systems[4]

A discussion of each trade study follows.

PROPULSION SYSTEM

In order to decide whether to propel the NP with an electrical or hydraulic system, several pertinent variables were modeled using a graphics computer (ADAGE) tied to analog computers and a UNIVAC 1110 for real time simulation. Three problem areas were addressed in this simulation; namely, (1) operator response time to vehicle motions due to wind and wave actions, (2) propulsion delay time, or the time it takes to translate the operator's commands into thrust, and (3) vehicle response time, or the time it takes the vehicle to respond to thrust forces. On the NP, studies were conducted to determine the required amount of thrust per motor; motor locations; motor thrust direction; total NP mass and moment of inertia; and drag:rotational, horizontal and vertical.

It was decided to have four horizontal thrusters at or near the vertical CG, acting in X-Y coordinate pairs, and two vertical thrusters at the base of the NP. The thrusters would be Kort Nozzle Type, fully reversible. The computer simulation showed that rapid reversals of thrust direction would be required during docking. Hydraulic thrusters provide rapid thrust reversing capability, while electric thrusters are considerably slower to reverse, so hydraulic thrusters were selected.

Once this decision was made, other functions not requiring large hydraulic demand (TV tilt) or not functioning during thruster demand times (locking arms actuation) were designed to operate hydraulically. Hydraulic system pressure is provided by two lightweight, aircraft type electrohydraulic motor/pump units, designed to be submerged in a reservoir at the base of the NP Central Core. These motor/pumps are powered by a 440 volt, 400 Hertz electrical supply via a 60 KW generator. The reservoir is pressure compensated to be slightly higher than ambient.

STRUCTURAL MATERIALS SELECTION

Materials were required that were lightweight, strong, and corrosion resistant. Other considerations were cost, availability, ease of fabrication and reliability (no unreasonable dependence on manufacturing techniques). The materials studied were stainless steels (300, 400 series), carbon steel, aluminum (5000, 6000 series), titanium and plastic. Titanium and plastic were eliminated due to cost, availability, and ease of fabrication considerations. The carbon and stainless steels were eliminated due to weight considerations. Of the remaining materials, several tempers of 5083, 5086, and 6061 alloys were analyzed. 6061-T6 was chosen, mainly due to its ready availability. Fasteners would be 304 stainless steel, coated with a mastic to prevent crevice corrosion. Any dissimilar metals to be mounted would be separated from the aluminum by a non-conducting material to prevent galvanic corrosion.

UMBILICAL DISCONNECT LOCATIONS

Prior to this study, the concept was to disconnect the umbilical at some predetermined point or points prior to towing the SRB/NP back to port. In addition, this study recommended cable types, connector types, umbilical strength member, and recommended against multiplexing any functions.

The study recommended to have two umbilical disconnect points, one at the RV and one located 6.1 meters (20 feet) from the NP. After further evaluation, it was decided to change the disconnect point at the RV to a point 61 meters (200 feet) from the NP. This would trail enough umbilical during towing to enable access to the umbilical end without getting the RV too close to the SRB. The disconnect point near the NP would shorten the trailing umbilical during in-port towing to preclude damage from curious boaters who might venture too close to the SRB.

The rest of the items recommended by the study were adopted. These included not multiplexing anything, but going with point-to-point interconnection; the connectors recommended were in-air disconnect, pressure balanced oil filled type. The integral strength (Kevlar) was specified as 26,670 newtons (6000 lbs.) strength (later upgraded to 44,450 newtons (10,000 lbs.)). A cut-away view of the electrical cable is shown in Figure 3.

WATER DISCHARGE SYSTEMS

Two alternatives were studied: blowing air into the SRB to force the water out, and pumping the water out. A baseline dewatering time of 3 hours

was established prior to the study. A worst case condition of 305,639 liters (80,750 gallons) of entrapped water would require a discharge rate of 1701 liters per minute (450 gallons per minute) to meet the 3 hour dewatering baseline.

For the pump method, it is important that the pump inlet pressure exceed the rated net positive suction head of the pump. In order to assure that this occurs during the entire pumping operation, it is necessary to transfer air into the casing as the water is removed; thus two hoses are required, one for water discharge and one for air replacement. Since the pump must operate during the entire dewatering cycle, the umbilical cannot be disconnected and towing commenced until the SRB dewatering is completed.

The air pressure system is simpler in that only an air hose and pressurized air supply are required. Also, the final log mode dewatering (about half of the dewatering time is consumed in this portion) doesn't require the air hose (umbilical) to be connected once the SRB casing has been pressurized. Using the air pressure method, the umbilical can be disconnected and towing begun much sooner than with the pumping method.

Based on the above considerations, the air pressure method was selected. The air supply options consisted of pressurized bottles, or bottles with a make-up compressor, or a compressor alone. We chose to use the compressor alone due to the large area required to store the bottles.

LOCKING ARMS

One mechanism of interest is called a Locking Arm. There are three Locking Arms on the NP located 120 degrees apart just above the Inflatable Bag. These Locking Arms are in a stowed configuration until the NP is in the SRB nozzle. When the bumpers on the NP lower legs are depressed by contact with the SRB nozzle, switches are actuated that power indicator lights on the Control Console. When this occurs, the console operator turns on a switch that extends the Locking Arms into an extended (deployed) position. The lower legs prevent further entry into the Nozzle, and the Locking Arms prevent the NP from being discharged from the Nozzle.

The Locking Arms are actuated by a 2070 Newtons/sq.cm(3000 psi) hydraulic system. Hydraulic flow is controlled from the Control Console by actuating a four-way solenoid valve. A double acting hydraulic cylinder moves a rod that pushes out to deploy the Locking Arms from the stowed to the extended position, and pulls in to retract the arms back to the stowed position. All of the hydraulic cylinders are manifolded together from the four-way valve. In the extended position, the Locking Arms upper braces have an over-center mechanical lock that tends to keep the arms in the extended position. With the nozzle plug locked into the SRB nozzle, the bag fully inflated, and a 6.9

Newton/sq. cm (10 psi) pressure inside the SRB casing, the loading on each locking arm upper link (the heaviest loaded portion of the locking arms) will be as shown in Figure 4.[5]

CONCLUDING REMARKS

A full-size SRB Simulator called the Ocean Test Fixture was used to verify that the SRB Dewatering Set can successfully accomplish its intended function. The SRB Dewatering Set has been extensively tested in the ocean with the sea conditions at or near the upper end of the operational limit established as a design goal, which is with waves as high as 2.4 meters (8 feet). All aspects of the SRB Dewatering Set have been successfully demonstrated.

REFERENCES

1. Bennett, G. J., "Electrical and Hydraulic Propulsion Trade-Off Studies for the NASA Dewatering System", Naval Undersea Center*, San Diego, CA, September, 1975.

2. Estabrook, A. R., "Structural Material Selection of Nozzle Plug for NASA Dewatering System", Naval Undersea Center, San Diego, CA, September 1975.

3. Cashdollar, H., "Umbilical Disconnect Locations for a Dewatering System for NASA", Naval Undersea Center, San Diego, CA, September 1975.

4. Estabrook, A. R., "Water Discharge Systems Trade-Off Study for the NASA Dewatering System", Naval Undersea Center, San Diego, CA, September 1975.

5. "Design Data Manual for the Solid Rocket Booster Prototype Dewatering System", Naval Ocean Systems Center, San Diego, CA, July, 1977.

ACKNOWLEDGEMENTS

1. A prototype SRB Dewatering Set was developed by the Naval Undersea Center*, San Diego, CA, under Contract NDPR CC-51247A from the John F. Kennedy Space Center, NASA.

2. Subsequent development engineering was provided by both the Naval Undersea Center* and the Planning Research Corporation/Systems Services Company, Kennedy Space Center, Florida.

*Now called the Naval Ocean Systems Center.

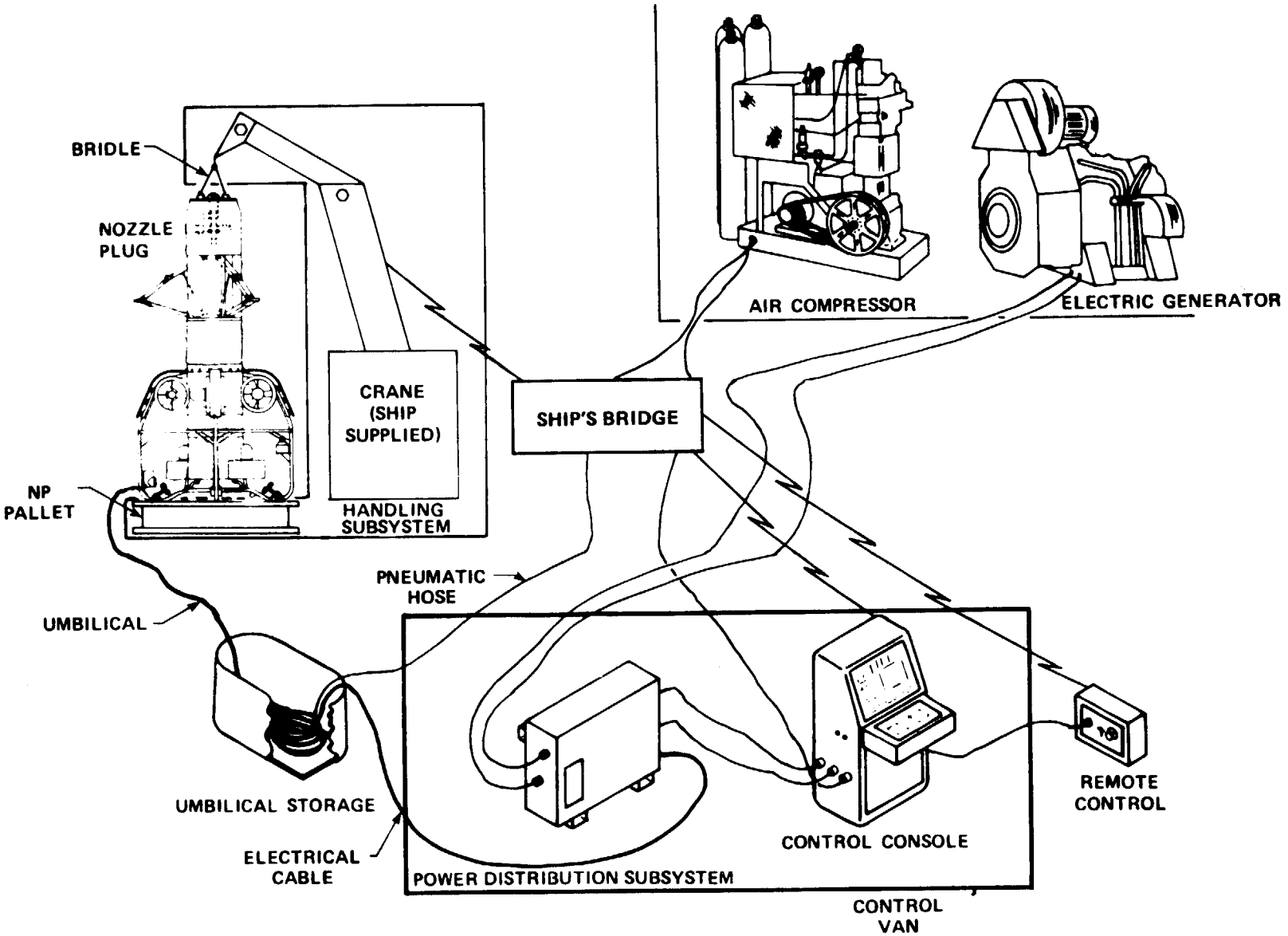

Figure 1. SRB Dewatering Set System.

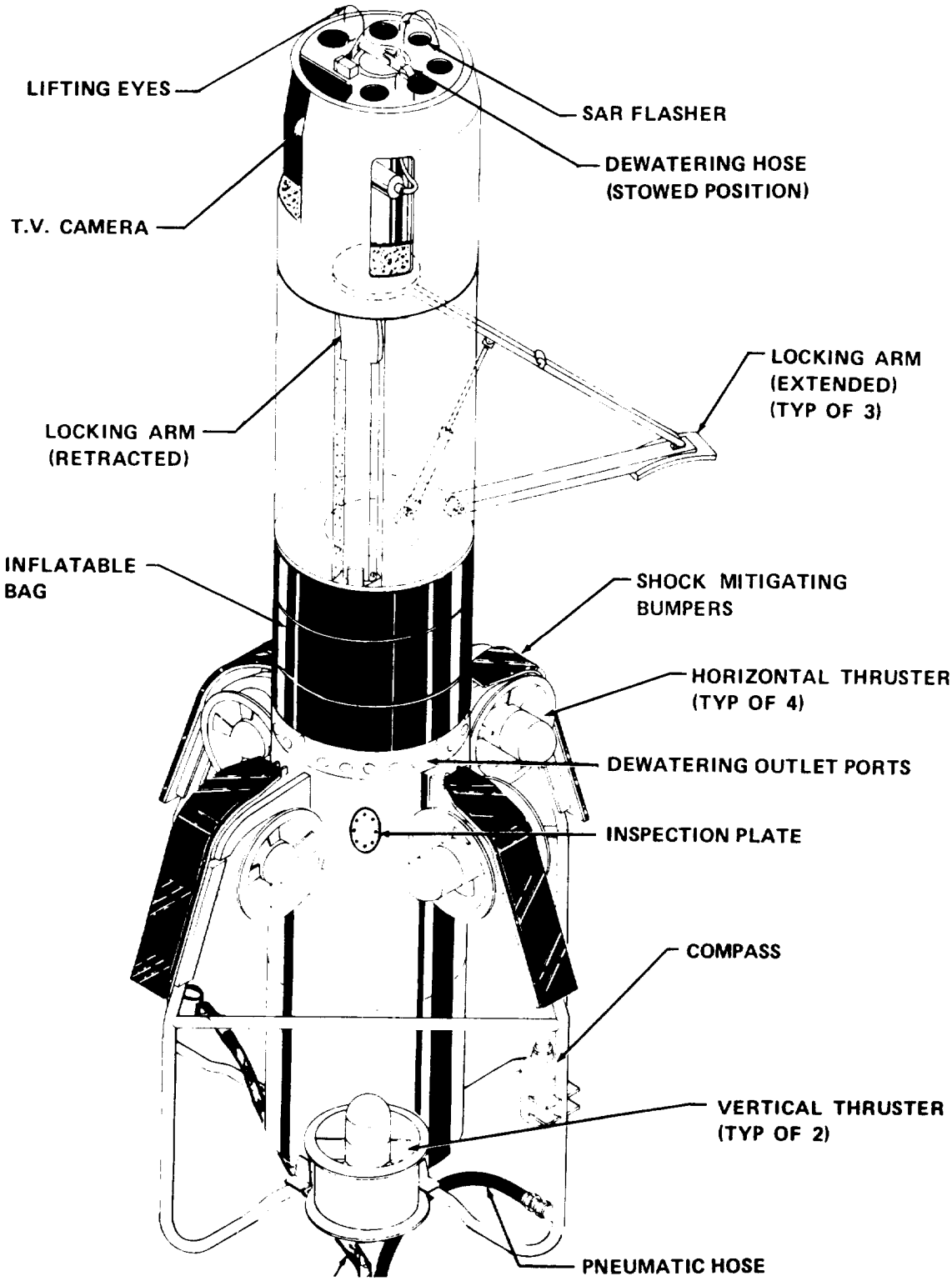

Figure 2. Nozzle Plug

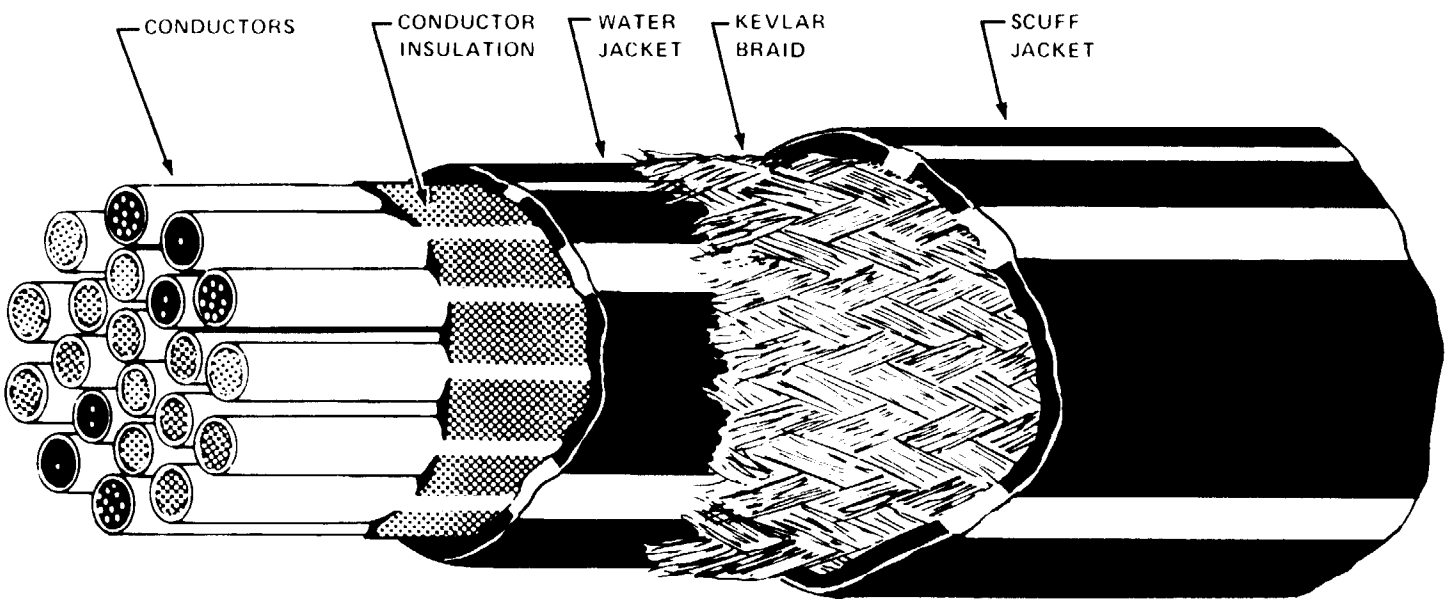

Figure 3. Electrical Umbilical Cable Cross Section

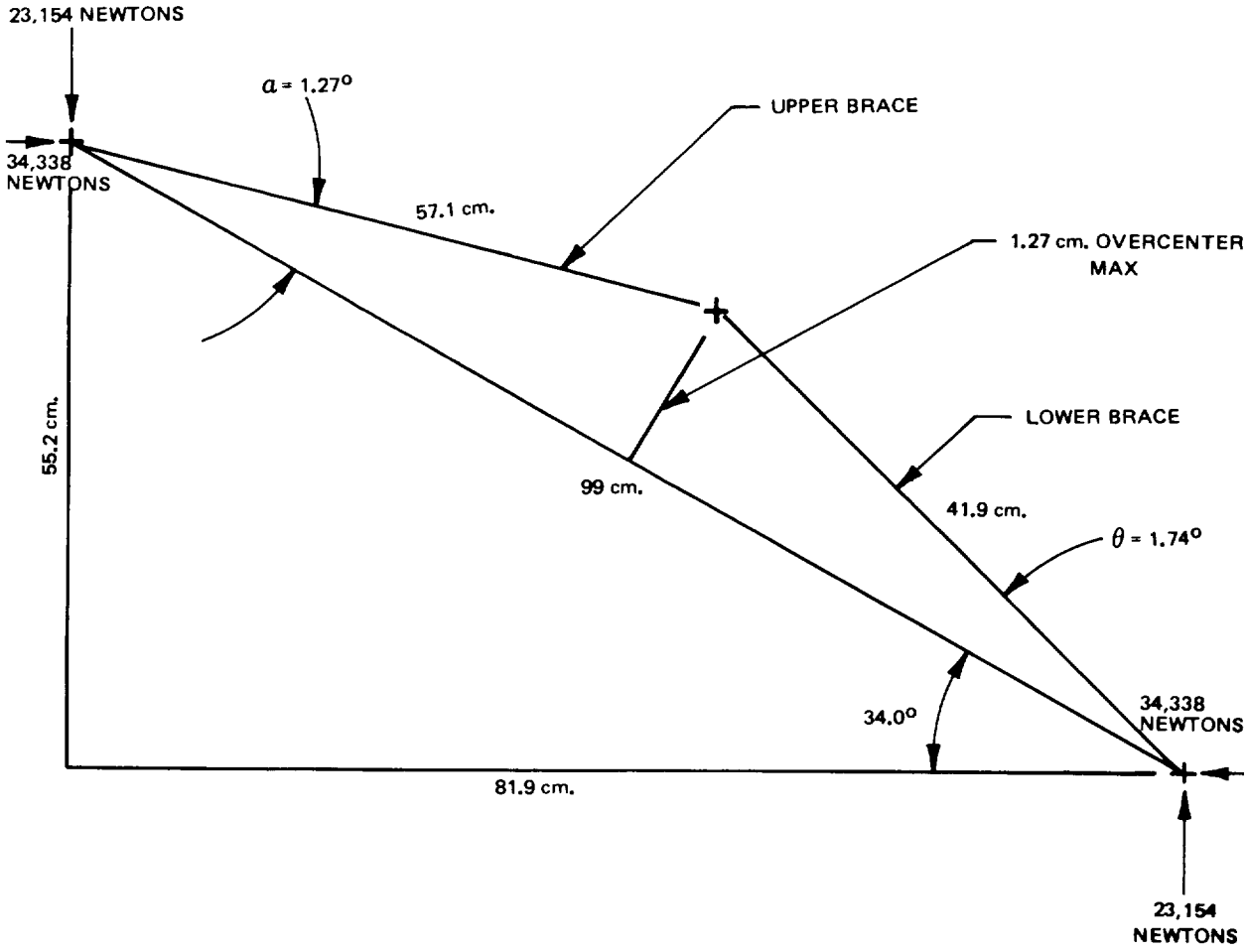

Figure 4. Locking Arm Loading, Extended Configuration

SPACE SHUTTLE MAIN ENGINE - HYDRAULIC ACTUATION SYSTEM

Gerhard Geller and Carl D. Lamb
NASA-Marshall Space Flight Center

ABSTRACT

The Hydraulic Actuation System of the Space Shuttle Main Engine consists of five electrohydraulic actuators and a single engine filter used to control the five different propellant valves, which in turn control thrust and mixture ratio of the Space Shuttle Main Engine. The Hydraulic Actuation System has several unusual design features, is built to severe requirements, and has overcome many design and test problems during the development phase of its maturation.

After over 500 tests on a hot firing Space Shuttle Main Engine, the Hydraulic Actuation System has demonstrated the capability, accuracy, and reliability necessary to control the combusion process of the engine.

INTRODUCTION

The Space Shuttle uses for its propulsion system a pair of Solid Rocket Boosters and a trio of liquid fueled rocket engines, which are known as the Space Shuttle Main Engines. These engines, using liquid oxygen and liquid hydrogen for fuel, have variable thrust capability, and must, therefore, be controlled by five valves having very precise control over their instantaneous position and rate of rotational speed in reaching that position. The Hydraulic Actuation System provides this control with a precision of 98.7 percent or an error in position no greater than 1.3 percent of full scale rotational travel for critical positions. There are two basic configurations of hydraulic actuators, although, because of small additional variations, four different part numbers are used. Figure 1 shows a completed preburner valve actuator.

NOMENCLATURE

SSME - Space Shuttle Main Engine
MOVA - Main Oxidizer Valve Actuator
MFVA - Main Fuel Valve Actuator
RVDT - Rotary Variable Differential Transformer
OPOVA - Oxidizer Preburner Oxidizer Valve Actuator
SSW - Servoswitch
SSV - Servovalve
HAS - Hydraulic Actuation System
FPOVA - Fuel Preburner Oxidizer Valve Actuator
CCVA - Chamber Coolant Valve Actuator

BODY

Description

The actuators weigh approximately 25 pounds apiece and are about 12 x 10 x 10 inches in size. Each actuator is composed of the following components:

a. Two electrohydraulic servovalves.

b. Two electrohydraulic servoswitches for control of redundancy features. One for fail-operate and one for fail-safe modes of operation.

c. Two hydraulic pistons with rods and a crank (see figure 2).

d. An output shaft with bearings and seals.

e. A rotary transducer (RVDT) (redundant channels).

f. A pneumatic piston.

g. A cam-controlled pneumatic sequence valve.

h. A body (aluminum 7175-T736) with connecting passages and covers (see figure 4).

i. Two spool-type valves (Shuttle valve and bypass valve).

Operation (Figure 3)

In normal operation, an electrical signal from the SSME electronic controller is sent to servovalve number 1, which meters flow through the Shuttle valve and the bypass valve to the hydraulic pistons. The pistons rotate the output shaft, which is connected to the propellant valve on one end and to an RVDT on the other end. The RVDT provides a shaft position signal which is sent to the electronic controller. The pilot stage return flow of both servovalves is vented to the hydraulic return line via a passage to a seal warming helix around the valve end shaft seal. If the shaft position signal from channel 1 RVDT does not agree with the command signal from the channel 1 electronic controller, the fail-operate servoswitch is energized, which connects hydraulic pressure to the left end of the Shuttle valve and moves it to the right. The passages from number 1 servovalve are then blocked, and the passages from the number 2 servovalve are connected through the Shuttle valve and the bypass valve and on to the hydraulic pistons. The performance of the actuator will be the same as it was while using servovalve number 1 prior to the failure.

If the RVDT shaft position signal from channel 2 does not agree with the command signal from the channel 2 controller, or if there is other evidence that the actuator or electronic controller is

malfunctioning, the fail-safe servoswitch will be deenergized, which removes pressure from the left end of the bypass valve and allows the right end spring to move the valve to the left until it contacts the spring loaded stop on the left end. The bypass valve in this position blocks the passages from the servovalves, and also blocks the hydraulic piston passages, locking the output shaft in a fixed position. The HAS is capable of maintaining hydraulic lockup of all five actuators for up to 10 minutes with a maximum drift of 4 percent of full scale shaft rotational travel. When the pneumatic control applies pneumatic pressure to the actuator, the pressure on the right end of the bypass valve moves it further to the left by compressing the stop spring. This valve position connects the hydraulic pistons together through a timing orifice, and allows the pneumatic shutdown piston to rotate the shaft and close the valve within a specified time limit. In the preburner actuators, when the shaft has turned to a position where the valve is partially closed, a cam (mounted to the shaft) opens the pneumatic sequence valve allowing pressure to continue on to the next actuator in the engine shutdown sequence.

Design Requirements

Some of the design requirements the HAS is required to meet are as follows:

Hydraulic Supply Pressure - 2,700 to 3,500 psig

Hydraulic Supply Temperature - 35^{o}F to 250^{o}F

Pneumatic Supply Pressure - 700 to 800 psia

Warmant Flowrate - 2.5 gpm maximum/per engine

Rotational Travel - 86^{o} (MOVA, MFVA) 79^{o} (OPOVA, FPOVA, CCVA)

Slew Rate - 150 to 370 percent per second - MOVA
180 to 370 percent per second - MFVA
150 to 305 percent per second - OPOVA, FPOVA, CCVA

Vibration Environment - 7.5 hours at maximum random vibration of 33.7 grms with transient shock levels to 200 g peak

Required Output Torque - 4,400 in/lb - MOVA
1,800 in/lb - MFVA
650 in/lb - FPOVA, CPOVA
1,428 in/lb - CCVA

Hydraulic Flowrate - (Total) - 1.5 to 12 gpm (all five actuators)

Unusual Design Features

a. Push-push type piston arrangement.

b. Lack of positive connection - piston to rod.

c. Redundancy of design in all electrical aspects.

d. Use of servovalve for switching.

e. Housing out of forged solid block.

f. Warmant helix flow.

g. Lucite housing during development (see figure 5).

h. Tuff-tride process for connecting rod ball ends.

i. Hard anodize for pneumatic cylinder.

j. MFV heater to maintain hydraulic fluid temperature prelaunch.

Problems During Development

During its development phase, the HAS evolved from development to operational status with a series of surprising failures and some very novel solutions. Once, while undergoing a vibration qualification test, an actuator was shaken to destruction because a control accelerometer had been inadvertently placed in a node, thus allowing an overtest to occur. The unusual solution to this was to set up a pair of controlling accelerometers, which effectively limited response by sharing control functions during the subsequent vibration test.

Another development during vibration test was the failure of a flapper on a servovalve caused by the beating of the flapper against its housing. The novel solution was to keep the servovalve electrically energized during vibration, which is its normal mode of operation during powered engine flight, anyway.

A lesson learned during development concerned a servovalve which was found to malfunction because of contamination introduced when an actuator was removed by uncoupling the hydraulic supply line first instead of the return line first. It seems that the slight static head in the return side caused a backflow which clogged one of the orifices. A simple procedural change now prevents this by requiring the return line to be the first to be disconnected, and the last to be connected.

During the first endurance test on an actuator, there were several galled or abraded surfaces associated with the piston, connecting rod, and crank mechanism (see figure 4) experienced during the test. The

ball-head of each connecting rod was particularly badly eroded. To correct this problem, a series of holes were drilled into the bottom half of the ball-head communicating with a single hole coming out the top of the ball. This helped the flow of lubricating hydraulic oil to the top of the ball and then the ball was "tuff-trided", which improved the bearing surface capabilities demonstrably.

The piston was given a radius cut at the bottom of the skirt to round off the sharp edge and the cylinder walls were hard anodized. These measures cleared up the problem of early wearing of the cylinder walls.

The crank pin and monoball materials were changed several times and a new reduced friction monoball bearing with different clearances was selected. All these measures improved the actuator's endurance capability to its present level of being able to perform 55 Space Shuttle missions before requiring refurbishment.

During early manufacturing operations on the actuator housings using a Milwaukeematic numerically controlled machine, a group of housings had to be scrapped because of two internal passageways that intersected when they should not have. A lucite see-through housing was then utilized as a preproduction proof sample housing for all machining operations. This enabled a very valuable check on the accuracy and correctness of all automatic machine operations.

When actuator design was about 90 percent complete, a new requirement to be capable of hydraulic lockup for 10 full minutes was instituted. Since the original design requirement called for only a 5-second lockup capability (with drift limited to 4 percent of full scale travel), it was decided to test the existing design, which has a diametral clearance of .000110 to .000140 inches on the spools for a 10-minute lockup capability. The actuator met the new 10-minute requirement without any redesign. That was pure luck (or maybe overdesign originally). Another surprise during the development phase was that actuator internal friction was greater than originally anticipated, resulting in a condition where the pneumatic piston was too small to shut down the actuator under all operating conditions. This was corrected by using a step pneumatic piston with two different bores. The biggest surprise during development perhaps was that the crank (see figure 5) would fail in fatigue, very close to its full life cycle. A beefed-up redesign adequately laid this problem to rest.

CONCLUSION

The HAS has performed satisfactorily in over 500 hot fire Space Shuttle Main Engine tests and has demonstrated that it can accurately, reliably, and safely perform its function of controlling propellant valve position on the SSME.

ACKNOWLEDGMENT

The SSME HAS has been developed for Marshall Space Flight Center - NASA under contract with Rocketdyne Division of Rockwell International Corporation and via a subcontract with the Hydraulic Research-Textron Corporation. The bulk of the design, development, and testing effort has been performed by Hydraulic Research under close supervision of Rocketdyne and MSFC. The project has had some unique development problems, but it has been successful, and for that reason both Rocketdyne and Hydraulic Research deserve commendation from MSFC/NASA.

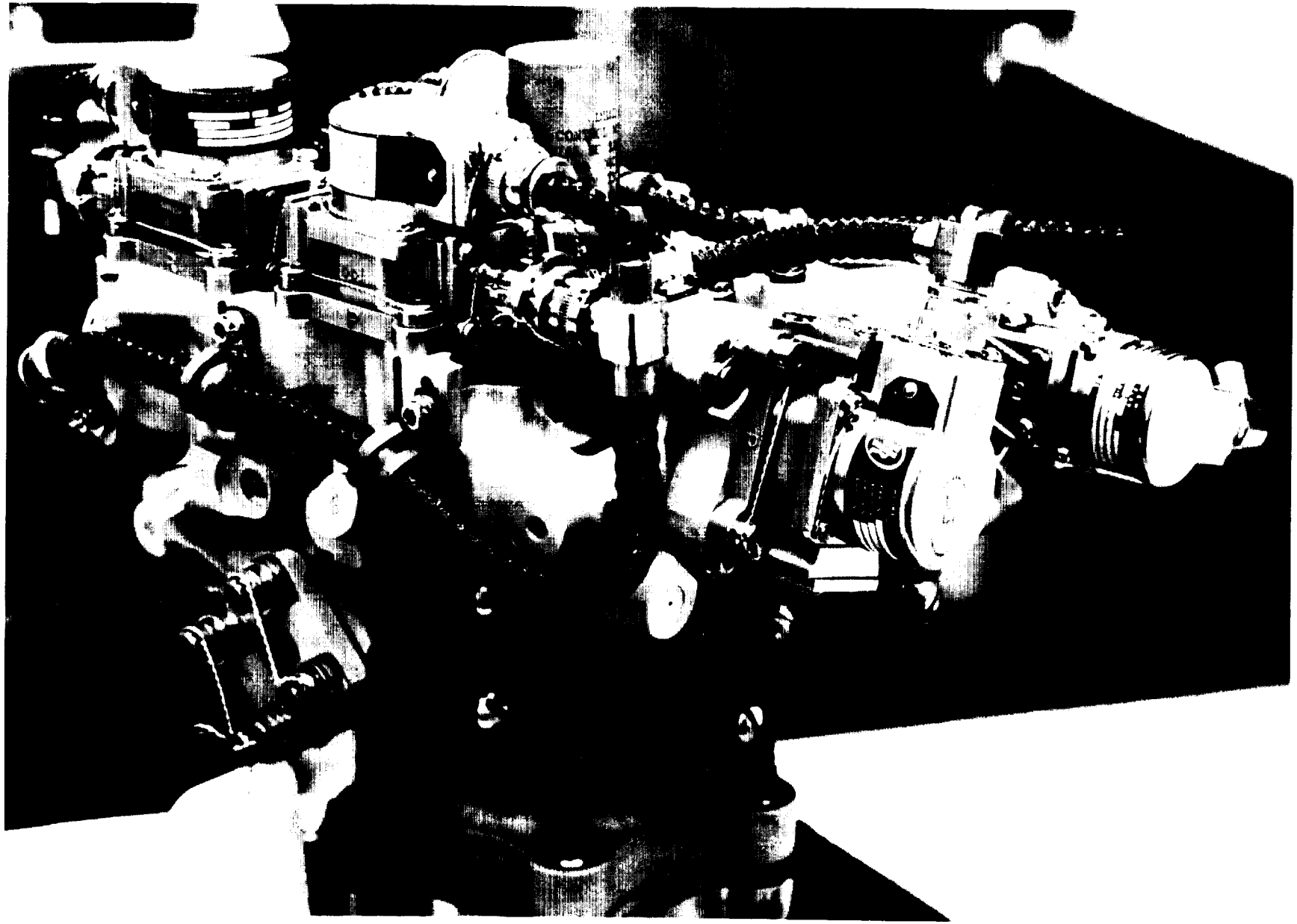

Figure 1. Pre-Burner Valve Actuator

PREBURNER VALVE ACTUATOR

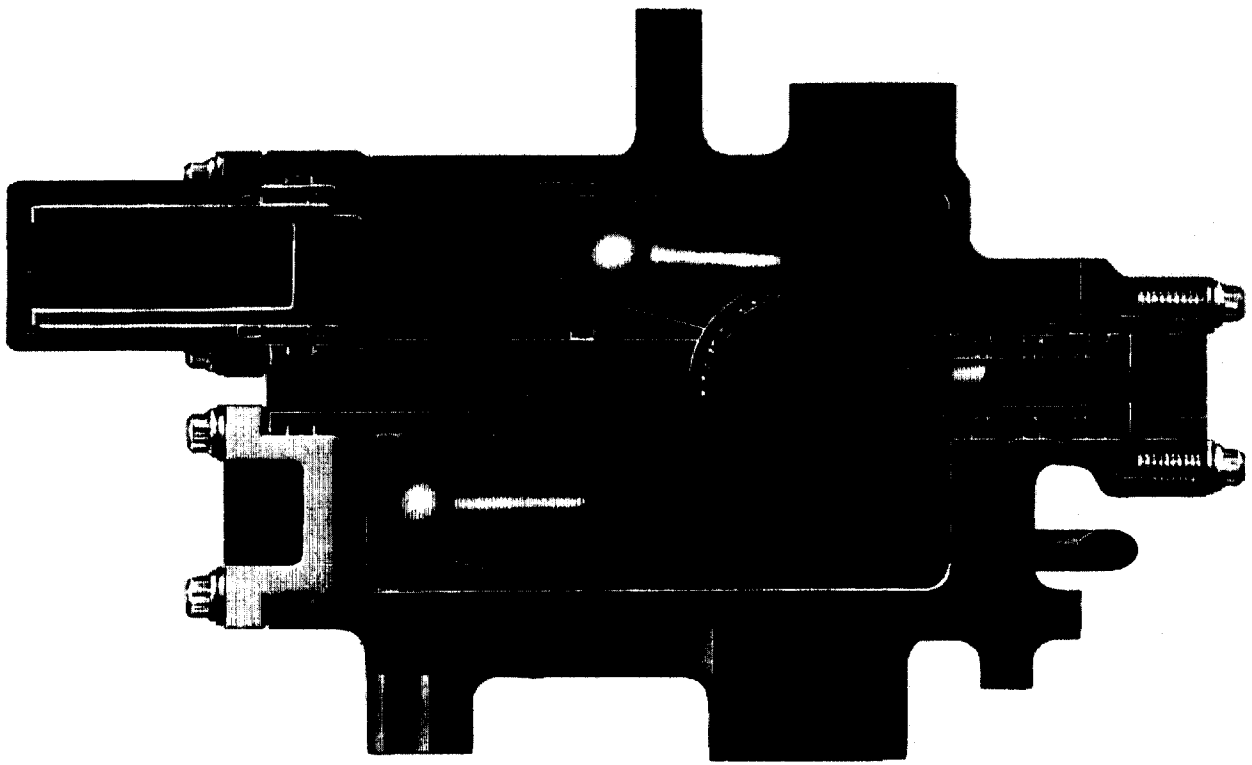

Figure 2. Pre-Burner Valve Actuator Components

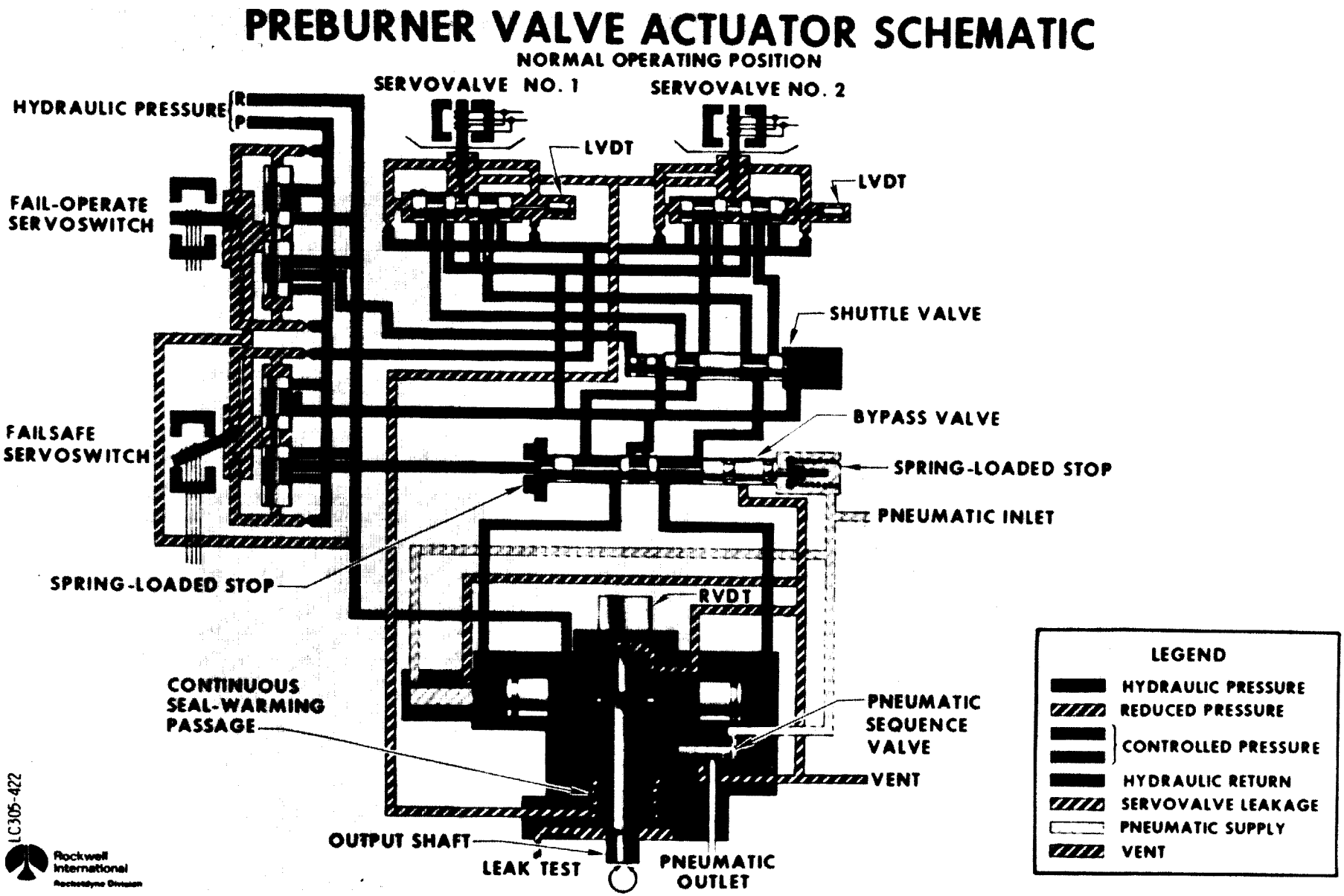

Figure 3. Pre-Burner Valve Actuator Schematic

Figure 4. Piston, Connecting Rod, Crank Subassembly

Figure 5. Lucite Housing

DEVELOPMENT OF A WINDOW PROTECTION ASSEMBLY FOR A SHUTTLE EXPERIMENT

Obie H. Bradley, Jr.*

ABSTRACT

A window environmental protection assembly has been developed for the Shuttle Infrared Leeside Temperature Sensing (SILTS) experiment. The assembly consists of a carbon phenolic composite window mount which contains two silicon windows, a fibrous environmental protection plug to protect the windows during launch operations and ascent heating, a release mechanism used to jettison the plug just prior to atmospheric entry, and two pin puller mechanisms which retain the plug. The plug will be released from the window mount assemblies using pneumatic pin pullers and separation springs in the release mechanism. The assembly was designed and tested to withstand the severe mechanical and thermal environments which could be experienced at the top of the Shuttle Orbiter vertical stabilizer during the ascent, on-orbit, and entry periods of the Shuttle trajectory.

INTRODUCTION

The Shuttle Infrared Leeside Temperature Sensing (SILTS) experiment is a data acquisition system which is scheduled to fly on the Space Shuttle in the 1981-82 time frame. The purpose of the experiment is to place a scanning infrared detector at the top of the Shuttle vertical stabilizer to obtain temperature data over the top surfaces of the fuselage and left wing during the atmospheric entry period of the Shuttle trajectory. Through analysis of the data, heating rates will be determined which will be used to develop analytical procedures and techniques for designing future generation reentry vehicles.

An artist's conception of the Shuttle orbiter with SILTS installed is given in figure 1(a). Located within the modified vertical stabilizer structure are three major subsystems, as shown in figure 2. These include a dome assembly, a data and control module, and a high pressure nitrogen gas module. The scanning infrared detector is located within the dome assembly. Shuttle high temperature silica tile insulation is used on the outside of the SILTS pod for thermal protection. Two separate conical infrared window cavities extend through the insulation on the hemispherical nose to allow the infrared detector to view the Shuttle fuselage and wing. Two environmental protection plugs are installed in the window cavities to protect the infrared windows during launch operations and ascent heating. These plugs will be ejected prior to atmospheric entry using a pressure activated release device and separation springs.

The SILTS experiment will be activated approximately 300 seconds prior to atmospheric entry (see figure 1(b)). At this time valves will be opened on the nitrogen gas module to allow flow for window cooling. Static pressure

*NASA Langley Research Center, Hampton, Virginia

from the window coolant line will be used to actuate four pin pullers (two per window) which retain window protection plugs. The plugs will then be ejected from the window cavities by spring plungers on the plug release mechanisms. The plugs will be ejected in the direction of the upper surfaces of the left wing and fuselage, and they will impact on these surfaces at low relative velocities. During atmospheric entry, the infrared detector mounted in the dome assembly will scan between the two window ports through which the infrared energy emitted from the top surfaces of the Shuttle is focused on the detector. Nitrogen gas, ejected through holes around the exterior of each window mount, will reduce the convective heating on the surfaces of the infrared transmitting windows by film cooling. The design goal is to maintain window temperatures below 93° C (200° F) through the data period. The data period begins at the time of atmospheric entry of the Shuttle and ends when the relative velocity drops below 1219 m/sec (4000 ft/sec).

This paper describes the details of the window protection assembly which includes the infrared transmitting windows, the window mounts, the window protection plugs and release mechanisms, and the pin puller assemblies which retain the plugs.

DESIGN REQUIREMENTS

The SILTS experiment, including the electronics, infrared windows, and window protection system, had to be designed to survive a relatively severe set of environments resulting from the Shuttle ascent and descent trajectories and on-orbit conditions. During on-orbit periods, temperature extremes ranging from -101° C (-150° F) to 38° C (100° F) can be experienced by the structure at the vertical stabilizer tip. The assembly was also required to withstand a 177° C (350° F) hot soak on entry during each of six missions. A random vibration spectrum requirement was imposed as described in table 1 resulting in a composite acceleration of 30.8 G (root mean square) for each of the three principal orthogonal axes. All parts of the assembly were required to be extremely clean and low outgassing to prevent contamination of the infrared windows. In addition, the assembly performance could not degrade as a result of being exposed to natural environments such as salt spray, humidity, ozone, and lightning. Unique requirements were imposed on individual parts of the assembly. These are discussed below.

The two infrared transmitting window assemblies were required to isolate the dome assembly from the extreme thermal environment which will be present around the tip of the vertical stabilizer during atmospheric entry. The window assemblies were to be designed "fail-safe" so that if an anomaly occurred such that nitrogen gas was restricted from providing window coolant, the infrared windows and the window mounts would survive one entry and prevent the dome structure temperatures from exceeding 260° C (500° F). Above this temperature there was danger of losing bond line adhesion for the thermal protection tile system. This was a particularly difficult requirement because thermal analyses indicated that peak window temperatures could reach 1188° C (2170° F) and peak window mount temperatures could reach 1464° C (2668° F) during a design trajectory entry with window plugs ejected and no window

coolant gas available. The analyses considered convective heating rates on the windows equal to 29 percent of free stream reference heating rates. The window assemblies also were required to survive a differential pressure equal to one atmosphere.

The window protection plugs were required to withstand all the launch pad environments and the ascent heating which would be experienced during their one mission lifetime. Temperatures approaching 593° C (1100° F) are expected on the surface of the plugs during ascent. The plugs must separate cleanly at experiment activation at very low relative velocities since the plugs will impact on the top surfaces of the Shuttle. Also, it was desirable that the material selected for the window protection plugs be soft and compliant.

The plug release mechanism, which remains with the window protection plug after separation, and the pin pullers, which are fixed in the window mount, were required to allow redundant release. In the event of loss of coolant gas before experiment activation, the pin pullers were required to retain the plugs through the entry trajectory. The very limited space available in the dome assembly constrained the size of the pin puller assemblies. The infrared scanning detector required most of the internal volume of the dome assembly to scan from one window to the other. During a scan by the detector, the clearance between the front surface of the insulation blanket on the detector housing and the interior surface of the aluminum dome is approximately 28.45 mm (1.12 in.).

As a baseline constraint, pyrotechnic devices were not allowed. This removed a number of options from design consideration.

DESCRIPTION OF ASSEMBLY

The window protection assembly consists of two silicon windows held in a charring ablator composite (carbon phenolic) window mount assembly, a fibrous thermal protection plug made of fibrous insulation, a pivoting release mechanism, and two pneumatic pin pullers which retain the plug. The complete assembly is shown in figure 3. The window mounts are clamped to the interior of the dome assembly using C-shaped aluminum clamps which are attached to the aluminum dome with A-286 alloy screws. Two pin puller assemblies are located on each window mount as shown in the figure. The pins from the assemblies extend through the window mount to engage the release mechanism for the window protection plugs.

A machined window mount assembly is mounted at each of the two viewing ports located in the dome assembly (see figure 4 and figure 5). The window mounts have a maximum diameter of 110.5 mm (4.35 in.) and a minimum internal diameter of 50.8 mm (2.00 in.). Each window mount contains two silicon windows for redundancy. Each of these windows is 6.15 mm (0.242 in.) thick and 59.44 mm (2.34 in.) in diameter. Metallic "E" seals of Inconel 718 alloy are provided on the inboard side of the exterior window and on the outboard

side of the interior window. These seals press against a spacer ring machined out of Haynes 188 alloy plate. A retainer ring also of Haynes 188 mounts against the interior face of the window mount and makes contact with the interior silicon window over a very narrow line opposite the "E" seal to minimize edge moments in the window during thermal excursions. The retainer ring is held in place with screws which thread into barrel nuts inserted in machined slots in the window mount as shown in figure 3. The screws and barrel nuts are also of Haynes 188 alloy. The window mounts were machined out of billets of a chopped fiber carbon-phenolic material designated by trade name FM5055. These billets were formed by processing carbon fabric impregnated with a phenolic resin in molds at 163° C (325° F) under pressure of 20.7 MPa (3000 psi). This material was selected based on its performance in solid fuel rocket nozzles and its low thermal conductivity. Some of the problems associated with using this material are discussed later in this paper.

Nitrogen coolant gas fittings are located in tapped holes which penetrate the window mount as illustrated in figure 3. Six window coolant fittings are installed in each mount. These fittings are of 347 stainless steel construction. Extruded tubes of 1.02 mm (0.040 in.) O.D. with 0.25 mm (0.010 in.) wall thickness extend through the mount and are brazed into the threaded fittings using 20 percent silver brazing alloy. The tubing extends from the window mount assembly back to a brazed bulkhead pressure manifold fitting.

Two pneumatic pin puller assemblies fit into each window mount assembly as shown also in figure 3. Two A-286 alloy screws are used to secure the pin pullers to wire-thread inserts installed in the carbon-phenolic window mount. A pin puller assembly consists of a cylinder, piston, seals, spring and cap. The cylinder is 36.58 mm (1.440 in.) long with an internal diameter of 5.84 mm (0.230 in.) and an external diameter of 10.03 mm (0.395 in.). The piston is 56.90 mm (2.240 in.) in length. The pin end of the piston is 2.41 mm (0.095 in.) in diameter. A spring sized to provide enough force to keep the piston extended during random vibration fits over the piston. An end cap screws on the external threads on the cylinder to close the assembly. The spring end of the piston extends through the end cap so that the piston can be manually retracted from inside the dome assembly. The maximum stroke of the piston is 5.08 mm (0.20 in.). Figure 6 shows a complete pin puller assembly. A photograph of the assembly is given in figure 7. All metal parts of this assembly except the spring are of 347 stainless steel construction. The spring is 302 stainless steel. Journal type seals of Vespel SP-21 polyimide were machined to fit the precision reamed internal cylinder walls. Both seals used a press fit on the piston to assure very low leakage around their internal diameters. The external seal surfaces were hand polished to the proper fit with the cylinder internal diameter. The larger seal was pinned to the piston after final fitting. A preformed 1.52 mm (0.060 in.) O.D. tube to supply the actuation pressure was vacuum brazed into the cylinder wall using 82 percent gold/18 percent nickel brazing alloy. Prior to assembly, the external surfaces of the seals and the internal cylinder walls were burnished with molybdenum disulfide to reduce friction.

Window protection plugs were designed to fit the conical cavities which penetrate the silica tile insulation installed on the dome assembly. An assembly view of a plug is shown in figure 8. The plug is approximately 78.7 mm (3.1 in.) thick and the smaller diameter is 50.8 mm (2.05 in.). The sides of the plug have an included angle of 55°. A photograph of the complete window plug is given in figure 9. The plug is constructed of Flexible Reusable Surface Insulation (FRSI). This insulation is used over many areas on the top surfaces of the Shuttle. It is an aramid fiber felt coated on one side with a white silicone coating and its use is normally restricted to areas where the peak temperature does not exceed 371° C (700° F). But, previous testing on the Shuttle program had shown that it could be used in a one-mission application at temperatures in excess of 538° C (1000° F). The plug is made up of a number of layers of the FRSI bonded together using RTV 566 silicone adhesive.

The pivoting plug release mechanism which was designed to secure the plug into the window cavity, and to provide a means to release the plug and eject it from the cavity is shown in figure 8 as part of the window protection plug assembly. The release mechanism consists of a plug retainer which is bonded into the plug, a release housing with a pivoting release bar, and two plungers with separation springs. All of the parts were fabricated using 6061 aluminum alloy. The mechanism is installed by first slipping the pivoting release bar under the pins extending through the window mount assembly. Then the plug is attached by using a single screw through the plug retainer and into a locking thread insert located in the top of the release housing. The two spring plunger mechanisms press against the external window with a maximum force of 0.363 Kg (0.8 lb) each. TFE teflon pads cover the ends of the plungers to prevent damage to the surfaces of the I. R. windows. Scotch Y966 transfer adhesive is used to secure the pads to the plungers. The assembly is designed such that release by either of the pins will allow the whole plug assembly to separate. If only one pin is actuated, the pivoting release bar will rotate to clear the remaining pin. The total weight of the window plug and separation mechanism is 124 grams (0.27 lb). Using this weight and the energy stored by both springs, the theoretical maximum separation velocity is 0.42 m/sec (1.38 ft/sec).

DESIGN PROBLEMS

The severe mechanical and thermal requirements imposed a number of design problems for the window protection assembly. Most of these problems centered around materials selection and fabrication.

The selection of the material for the window mounts was an interesting example. Many different designs were conceived to meet the mechanical design requirements. Most of these, however, could not meet the requirement of withstanding entry temperatures on the exposed surfaces of 1464° C (2668° F) and still provide the thermal isolation necessary. The design which was selected called for the selection of a composite material which could take all of the thermal and mechanical loads, and the design placed additional demands on the machinability of the material. Many close tolerance

penetrations, tapped holes, and mating surfaces were required. It was found that the carbon-phenolic composite which was selected could meet the requirements which were imposed. Diamond tipped grinding tools and ultrasonic drills were used for all cutting operations. Coarse grit tools and high surface speeds were required to give the finish which was desired. Since carbon-phenolic is rather porous, only pure water was used during the cutting and drilling for cooling and particle removal to help assure that the final machined parts were free of contamination.

Following the machining operations on the window mounts, radiographic inspection revealed no positive flaws. A solvent wipe procedure using ethanol, however, revealed tiny cracks in the material extending from the tapped holes in which the threaded inserts for the pin puller attachment were located to the milled holes for the forward section of the pin puller cylinder. This area is shown in figure 10. The decision was made to qualify the window mounts with the cracks in these thin sections to show that this was not a serious design problem.

A problem which had to be resolved in the pin puller design was to control gas leakage from the pin puller assembly over the operational temperature range -101° C to 38° C (-150° F to +100° F) and following 177° C (350° F) hot soaks which are expected during each atmospheric entry. Pressure to actuate the pin pullers was supplied from the window gas coolant system. Leakage from this system was undesirable because it could compromise experiment data time. The amount of gas which could be carried with the experiment was limited by physical dimensions and weight considerations. And, since the gas provided coolant for the windows and pin puller actuation, as well as cooling the infrared detector by use of a Joule-Thomson cryostat, it was imperative to make conservative use of the gas available. It was undesirable to operate the pin pullers at the maximum system pressure of 20.7 MPa (3000 psi) because this would compound the leakage problem. And, to operate the pin pullers at 186 kPa (27 psi) which was to be supplied to the window coolant ports would have resulted in a much larger piston design to achieve the required actuation force. Therefore, a modification was provided to the pressure system to provide pressure at the pin pullers of 2.07 MPa (300 psi) maximum. The system is shown in schematic form in figure 11. A coil of 0.25 mm (0.010 in.) I.D. tubing was used to control the flow rate through the system. This coil was sized to allow flow equivalent to a 0.18 mm (0.007 in.) orifice. A bulkhead tee fitting downstream of this coil was modified by adding a 0.56 mm (0.022 in.) orifice in the line to the window coolant ports. This provided a 2.07 MPa (300 psi) static pressure at the tee if no leakage occurred at the pin pullers. Any leakage, however, reduced the pressure to the pin pullers and reduced flow rate to the window coolant ports. This can be seen in figure 12. The leakage was controlled by special attention to the seal design in the pin puller assemblies. Journal type seals were necessary to carry the moment caused by the window protection plug separation spring forces applied at the tips of the pins. These seals had to be hand polished to properly fit with the cylinders. A force gauge was used during the polishing operation to measure the sliding friction of the seals against

the cylinder walls as an indication that proper fit had been obtained. Teflon (TFE) was first evaluated as the seal material, but this material proved unsatisfactory. After properly sizing the seals, a 177° C (350° F) hot soak was applied to the assembly. The teflon permanently deformed at this condition causing excessive leakage around the seals following cooldown. Vespel SP-21 was then evaluated and was found to provide the desired characteristics. Seals machined from this material were unaffected following the hot soak and cooldown. Also, these seals provided better performance at the coldest operating temperature of the seals, -101° C (-150° F). Leak rates at room temperature for each pin puller assembly were generally less than 1000 standard cubic centimeters per minute (SCCM). The maximum pressure which was required to actuate the pin pullers under load was 1.03 MPa (150 psig).

The soft, fibrous material used for the window protection plug caused a problem in the fabrication of the plug. The material could not be bonded together and cut to give the desired contour. Instead, it was found that each layer of the material had to be cut separately and bonded together in a female mold.

TESTING

A test hardware assembly was fabricated to be used during the certification testing of the window protection assembly. This hardware is shown in figure 13. This hardware was necessary to duplicate the Space Shuttle interfaces during the environmental testing.

Functional tests of the pin pullers and plug ejection system were performed before and after each of the environmental tests. To simulate a zero G condition for the functional tests, the plug was attached by cable to a pivoting bar which was counterweighted such that the force applied by the cable on the plug was equal to the weight of the plug.

Although analysis indicated that stresses in the window mount assembly would be small when the assembly was subjected to a differential pressure loading, the assembly was tested for this loading condition in the test hardware assembly. A maximum pressure difference of 155 kPa (22.5 psi) was applied using dry nitrogen gas and no anomalous behavior was observed.

A rain test was performed to show that rain water would not soak into the waterproofed plug or migrate past the plug in the launch configuration. Post-test inspection of the plug and assembly indicated that all requirements were met.

The test hardware assembly was subjected to the random vibration spectrum described in table 1. Shortly after starting the test, the window protection plug separated from the assembly. Upon inspection, it was found that two different anomalies had probably contributed to the failure. First, it was found that the screw which attaches the plug to the release mechanism

was not long enough to engage the locking threads in the mechanism. The screw was supposed to be a standard 12.7 mm (0.5 in.) long, but measurements showed it was only 11.43 mm (0.45 in.) in length. This problem was cured by using a 14.22 mm (0.56 in.) long screw to assure that the locking threads were well engaged. The second problem which was found to contribute to the failure was that the caps on the pin puller assemblies had not been safety wired as per procedure. The vibration environment had caused the caps to back off several threads. This had reduced the preload on the pistons from the springs, possibly allowing the pistons to retract slightly. The vibration test was rerun with the problems corrected with complete success. The assembly completed 156 seconds of run time in each of three axes. A functional separation test following the vibration demonstrated that the mechanism would perform as required.

Possibly the most severe test was the thermal certification. The first part of the test was an ascent heating simulation. For this test, the window protection assembly was installed in the certification test hardware. The temperature of the top surface of the window plug was controlled to follow an analytically predicted temperature curve through an ascent environment. This curve is given in figure 14. A quartz lamp heater was used to supply the heat input. The assembly was placed in a vacuum chamber to run this test, and the chamber pressure was controlled during the test to approximate an ascent trajectory. The maximum temperature reached on the top surface of the plug during this test was 566° C (1050° F). Following cooldown in vacuum, the assembly was removed from the chamber and another functional test was performed. The window plug separated cleanly as desired. Following this test, the assembly was placed back in the vacuum chamber without a window protection plug installed to undergo an entry simulation test. For this test, the temperature of the exterior window was controlled to match an analytically predicted temperature curve which was calculated based on the Shuttle design entry trajectory (see figure 15). The maximum temperature expected on this curve was 1188° C (2170° F). A vacuum pump was attached to the side of the hardware assembly to maintain a vacuum on the interior side of the window mount assembly throughout the test. The pressure on the exterior side of the assembly was controlled to approximate the entry trajectory pressure expected. Following the test, the window mounts and pin puller assemblies were inspected and found to be in very good condition. The seals in the pin pullers were damaged, but this was expected.

Two window mount assemblies were installed in a dome assembly which was used in the thermal vacuum testing of the whole SILTS experiment. For this test, the window protection plugs were not installed because no insulation was applied to the dome to provide side support for the plugs. Rather, the plug release mechanisms were installed without the fibrous plugs. The temperature of the dome assembly was lowered to approximately -101° C (-150° F) in vacuum (10^{-6} mmHg) and allowed to stabilize. When the valves on the pressure system were opened, both plug release mechanisms separated as required.

CONCLUSIONS

Testing has shown that the window protection assembly to be flown on the vertical stabilizer of Space Shuttle as part of the SILTS experiment will perform as required. The assembly was subjected to a random vibration environment equivalent to 30.8 G (root mean square) overall and a severe thermal environment simulating ascent and entry heating. The fibrous window protection plug has met all the requirements of providing protection for the I. R. windows and being ejected prior to atmospheric entry. The window mount assemblies have demonstrated that they can withstand one entry with no coolant gas flow for "fail-safe" design.

ACKNOWLEDGEMENTS

The author acknowledges all the design contributions of R. K. Dail and H. C. Halliday at Langley Research Center, and the contributions of many engineers and technicians at Rockwell International - Space Division, and Johnson Space Center.

TABLE 1

RANDOM VIBRATION DESIGN ENVIRONMENT

FREQUENCY	SPECTRAL DENSITY
30 TO 100 Hz	PLUS 12 dB/ OCTAVE
100 TO 600 Hz	1.2 g^2/Hz
600 TO 2000 Hz	MINUS 9 dB/ OCTAVE

COMPOSITE - 30.8 GRMS

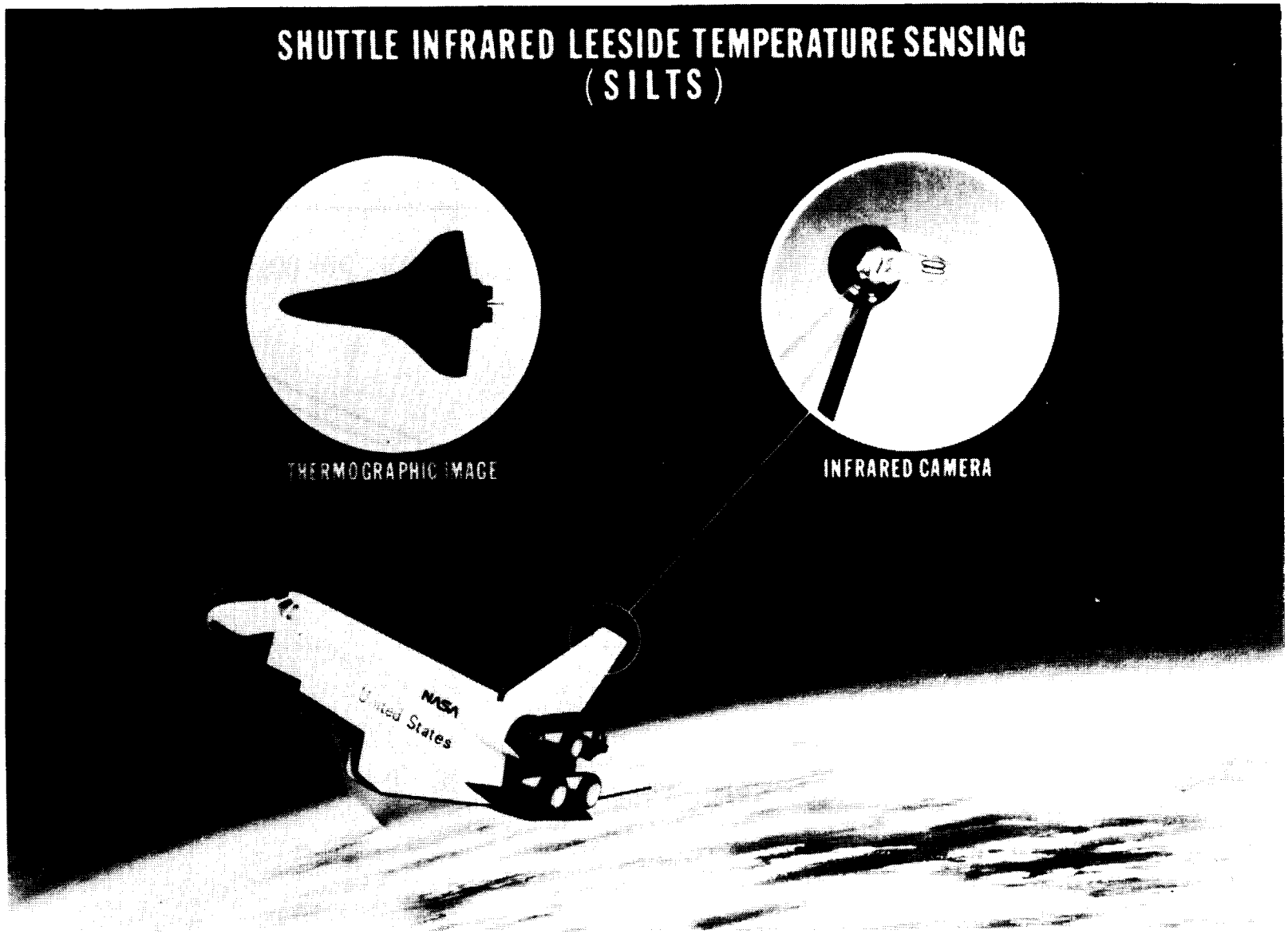

Figure 1-a. Shuttle Orbiter with SILTS experiment

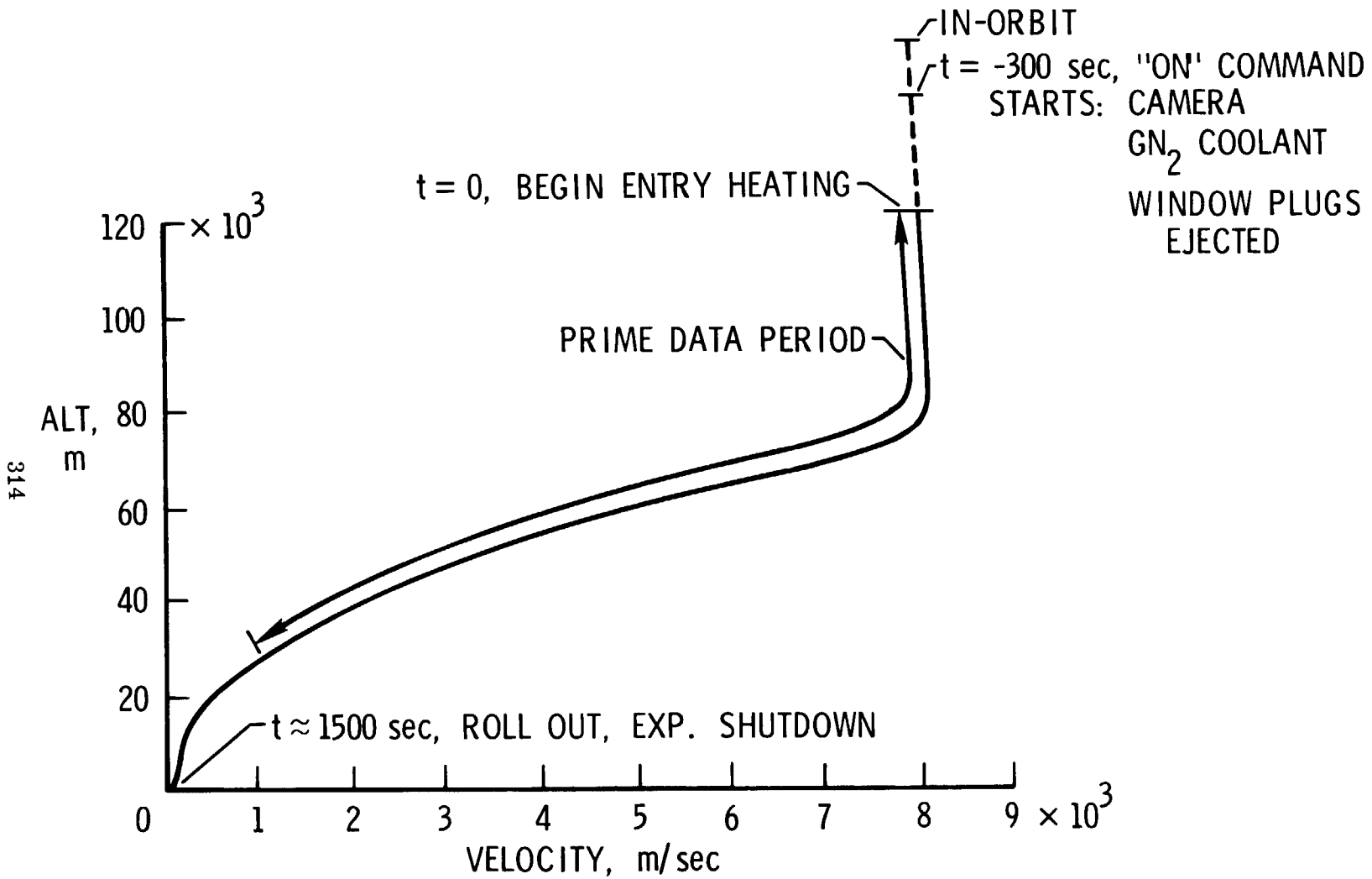

Figure 1-b. SILTS experiment overview--Orbiter entry

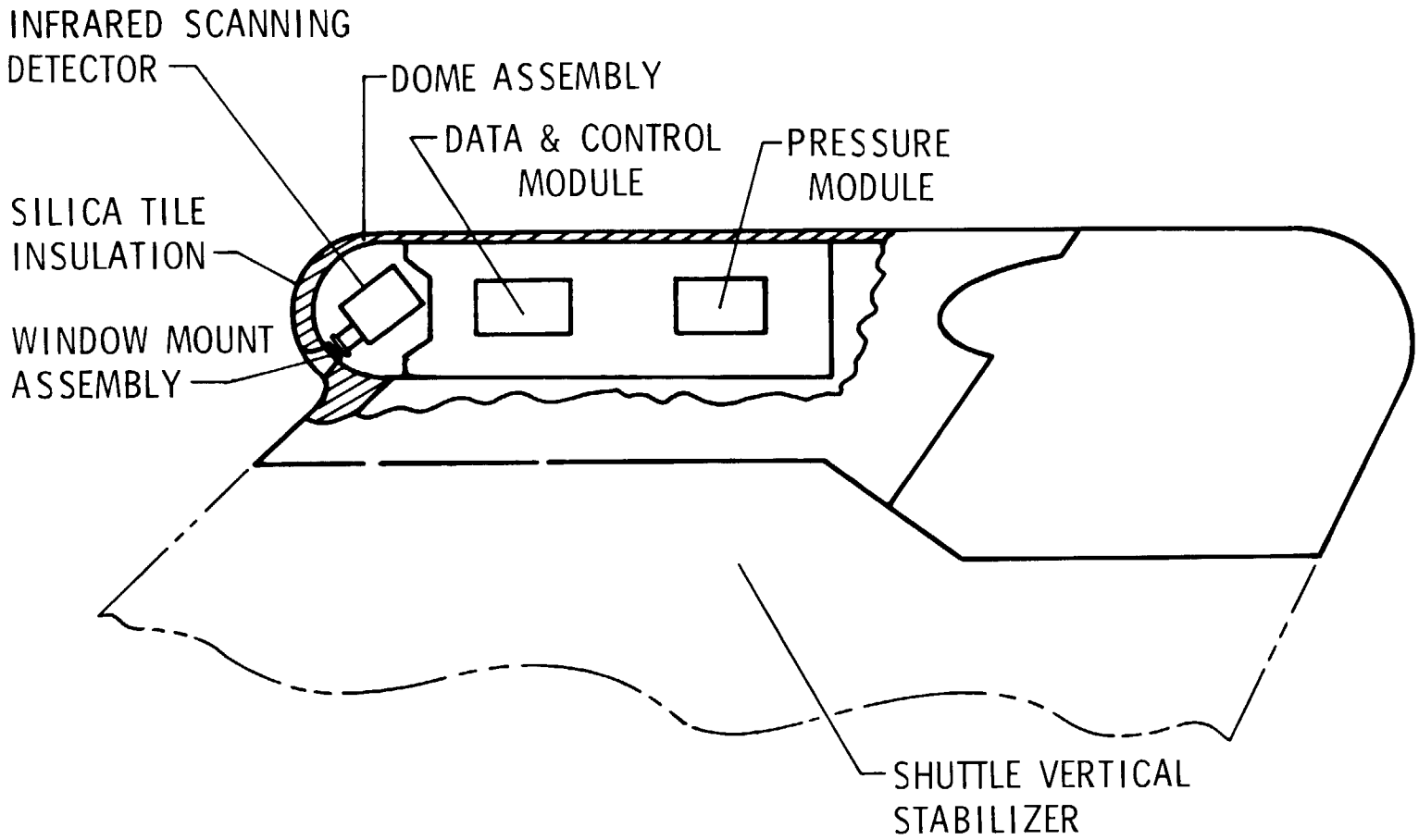

Figure 2. SILTS subsystems in Shuttle vertical stabilizer

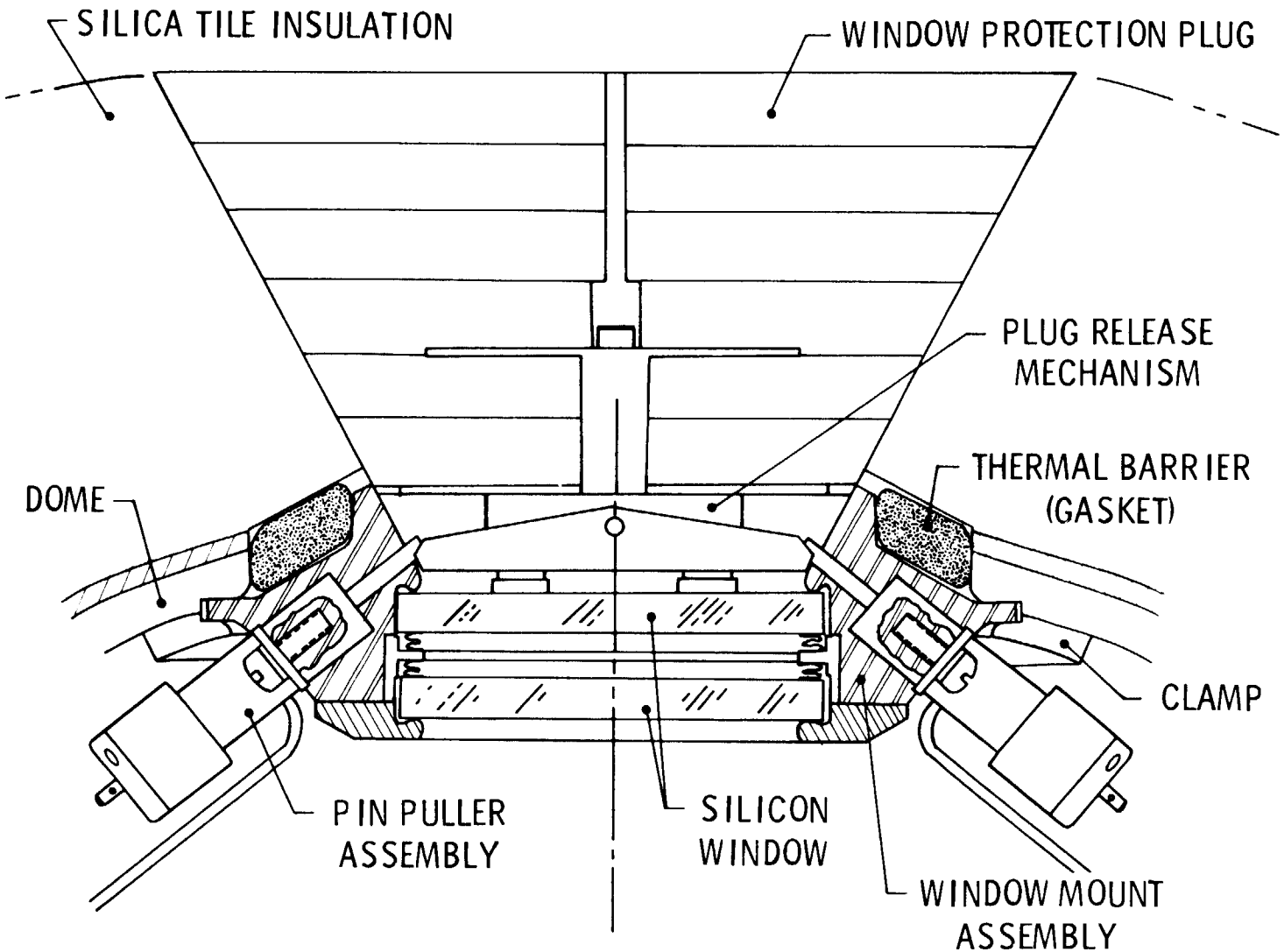

Figure 3-a. Window protection assembly

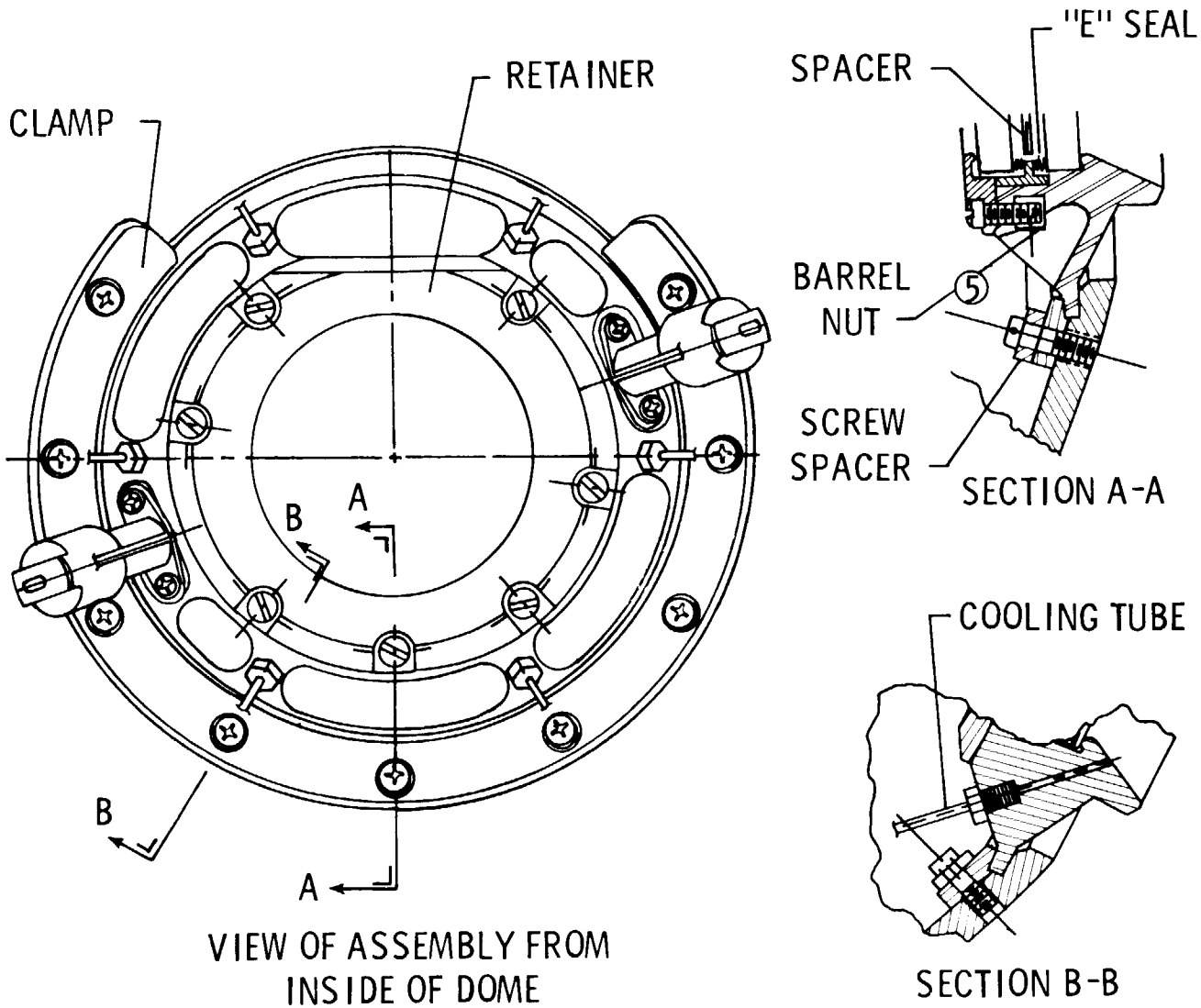

Figure 3-b. Window protection assembly

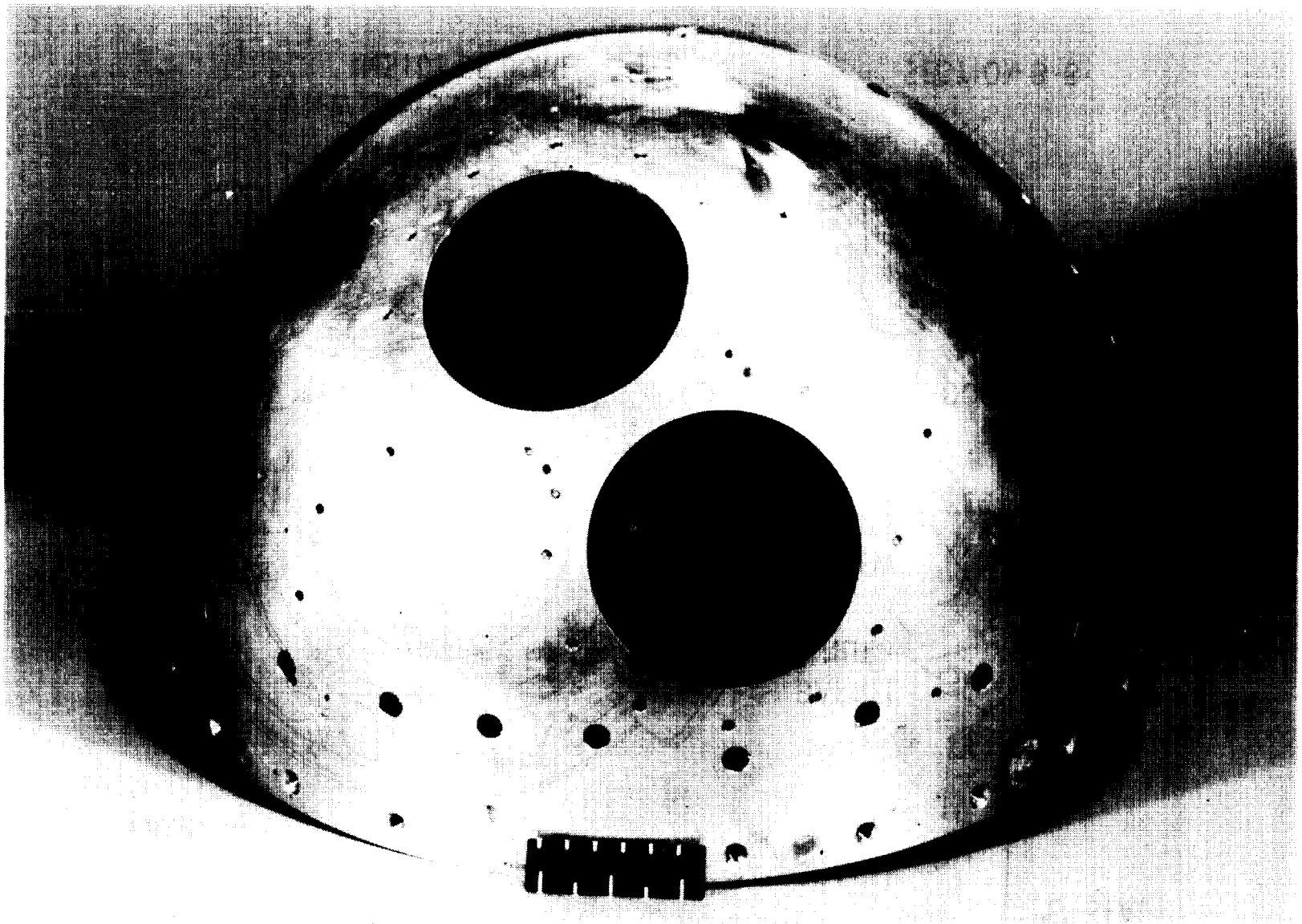

Figure 4. SILTS dome with window mount assemblies installed

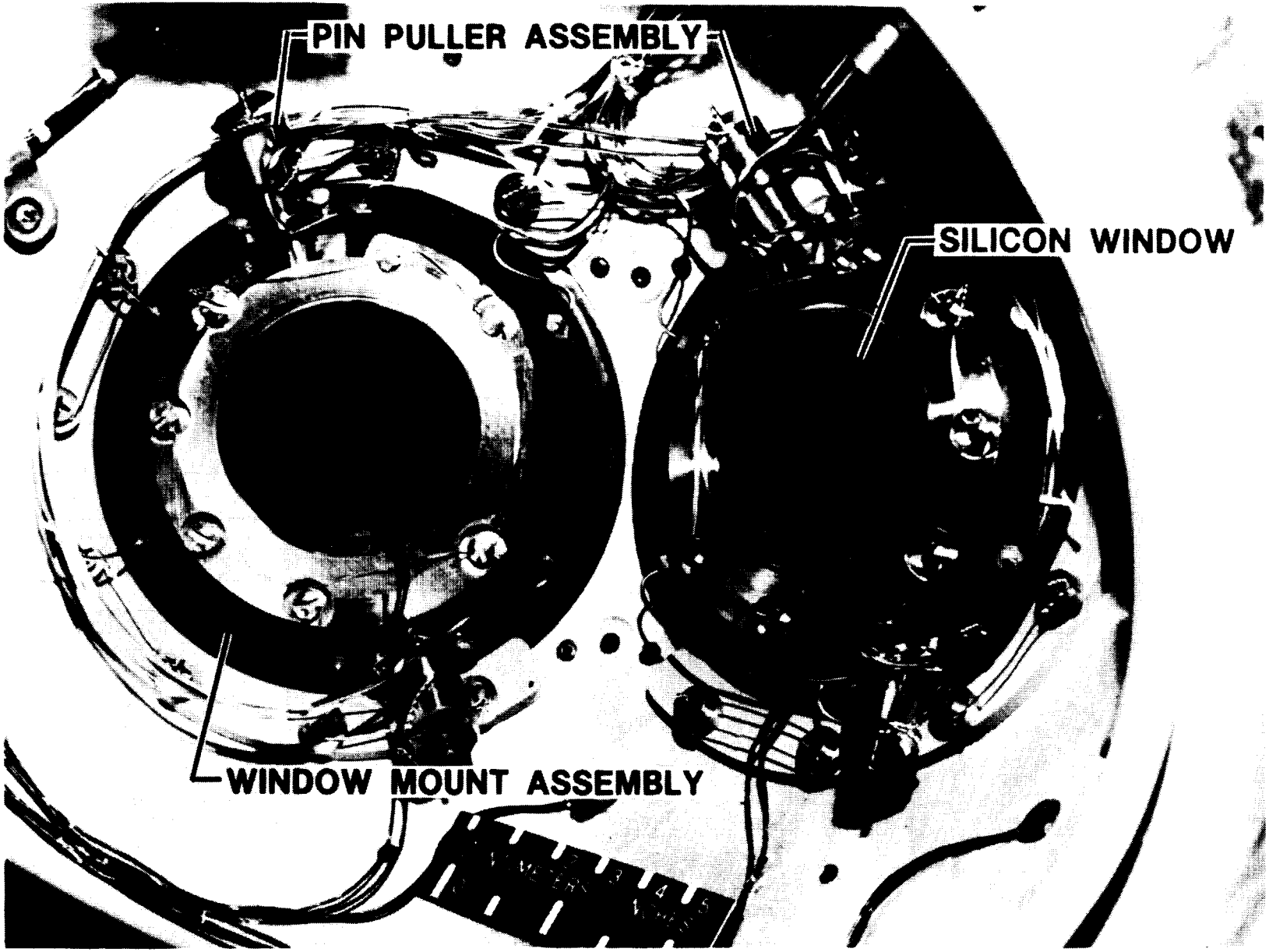

Figure 5. View of window mount assemblies from interior of dome

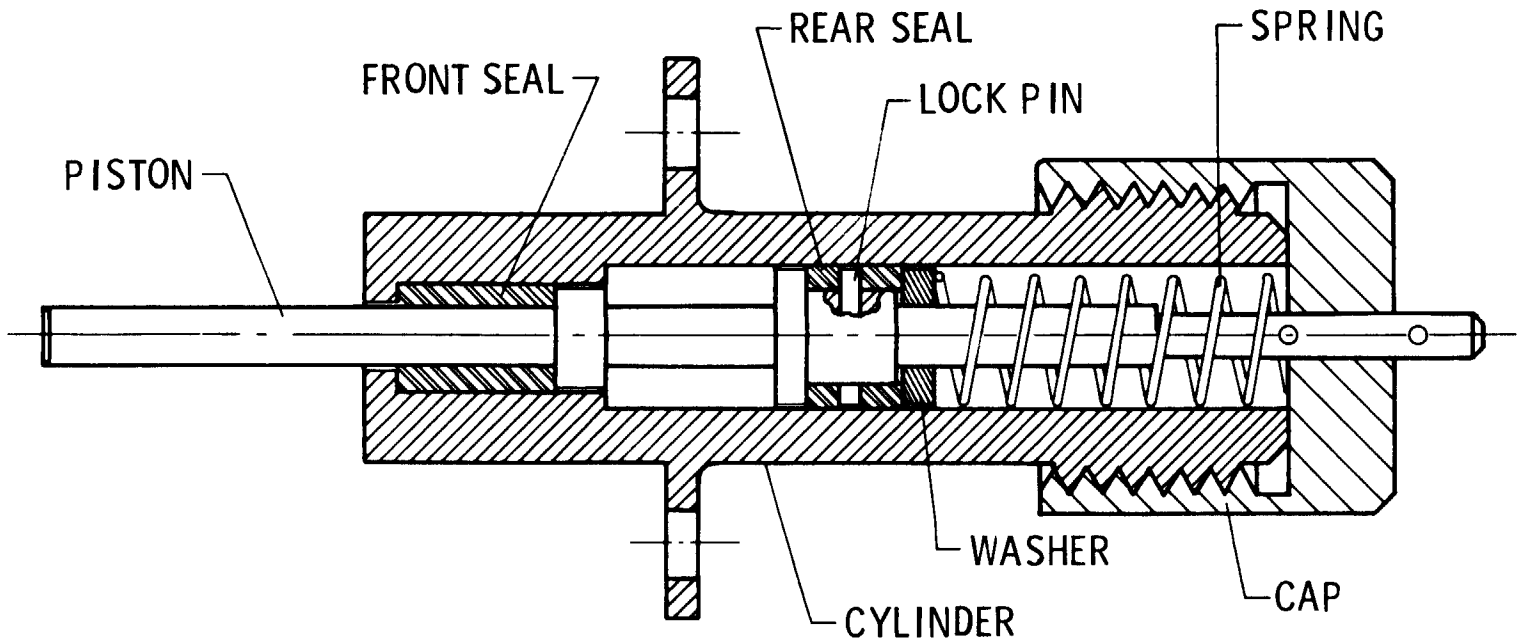

Figure 6. Section view of pin puller assembly

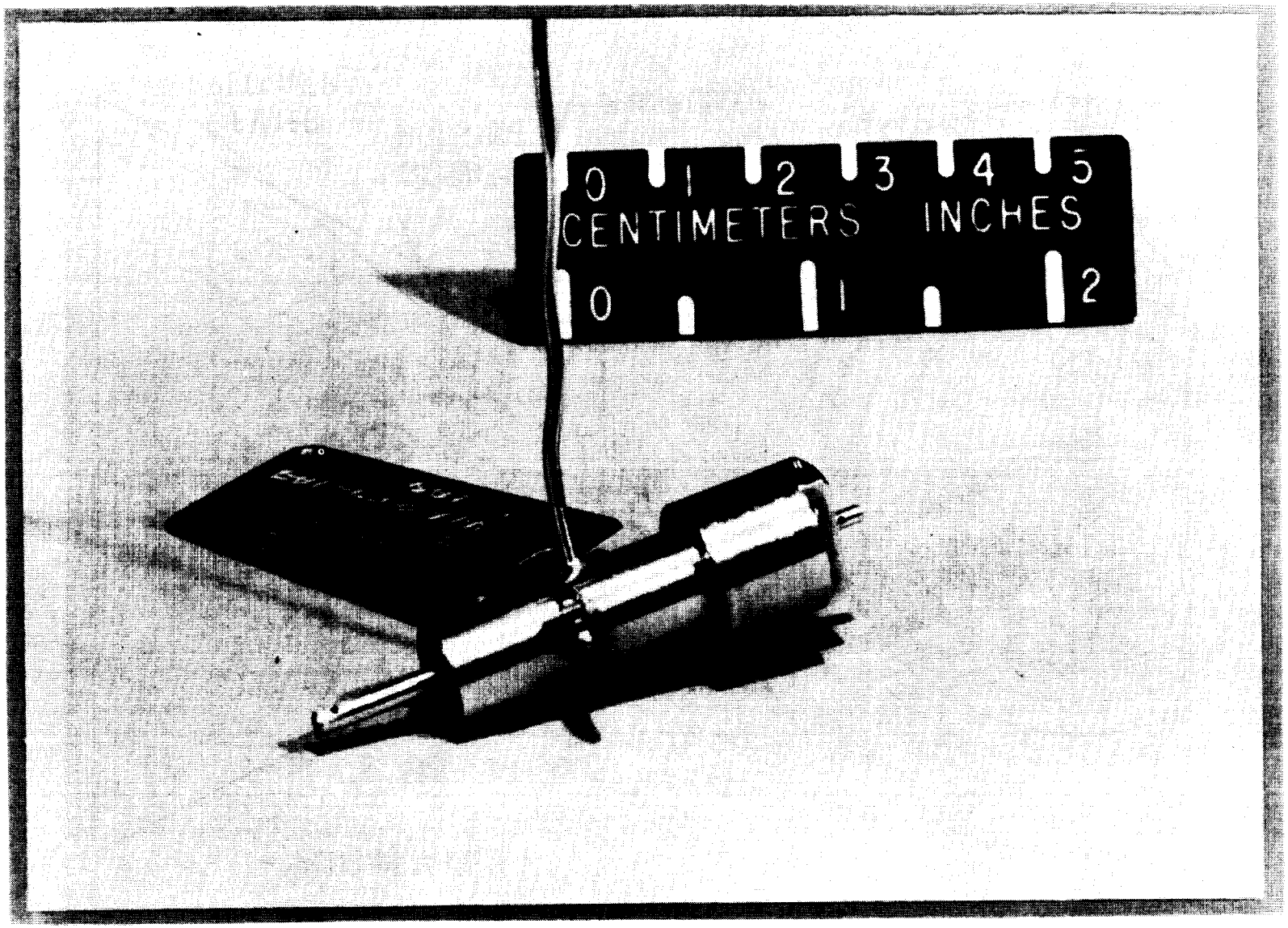

Figure 7. Photograph of complete pin puller assembly

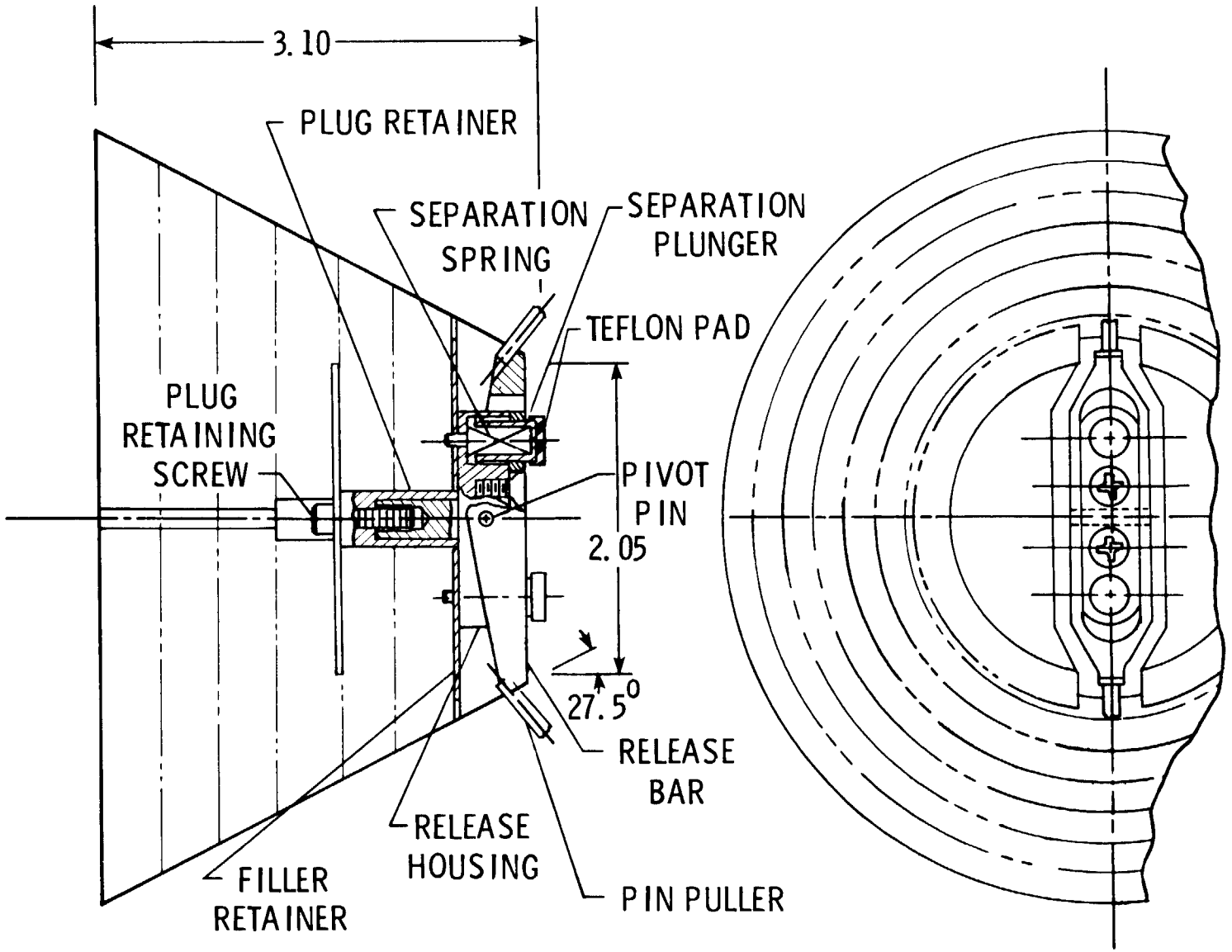

Figure 8. Window plug assembly

Figure 9. Photograph of window plug assembly

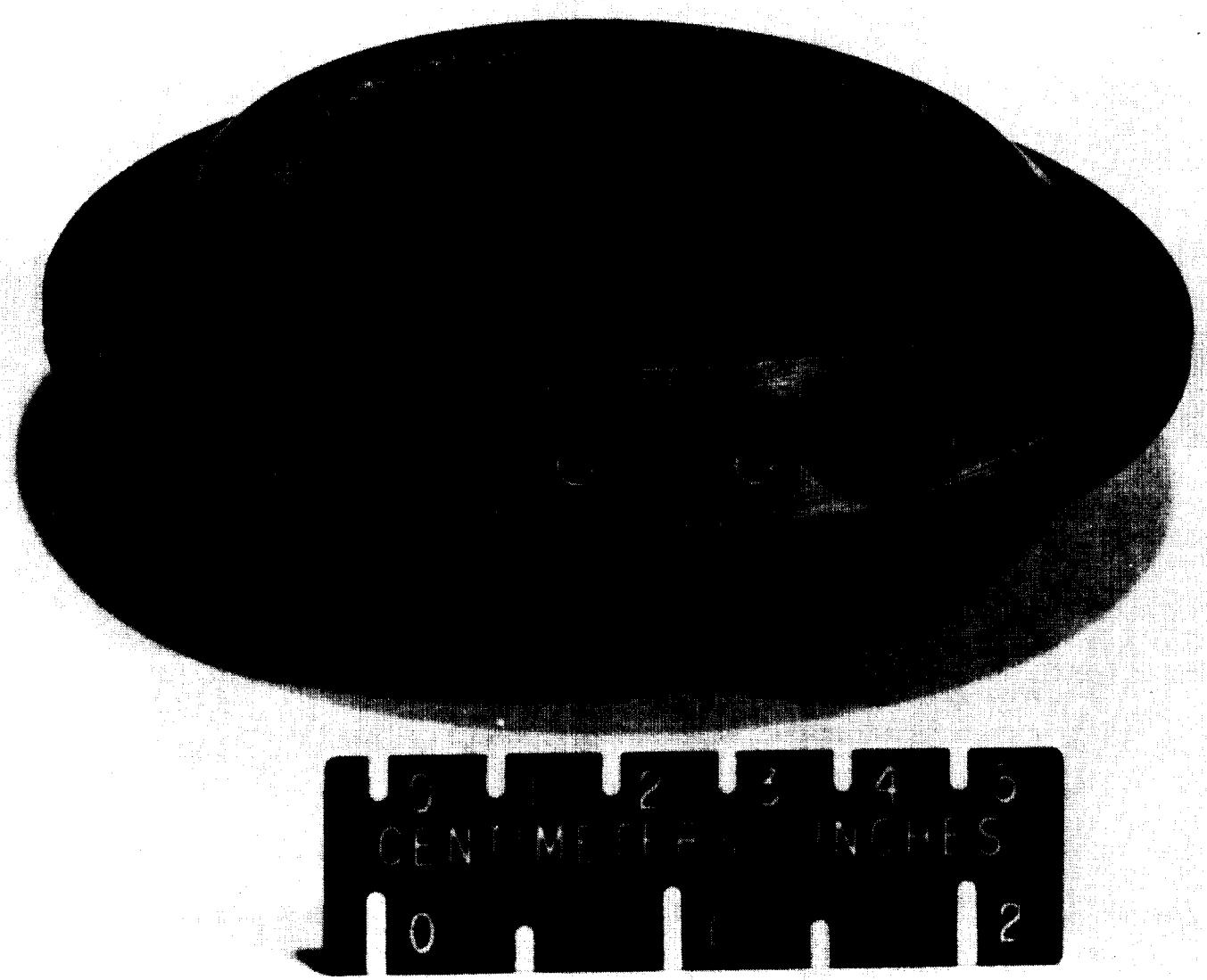

Figure 10. Photograph of machined carbon phenolic window mount

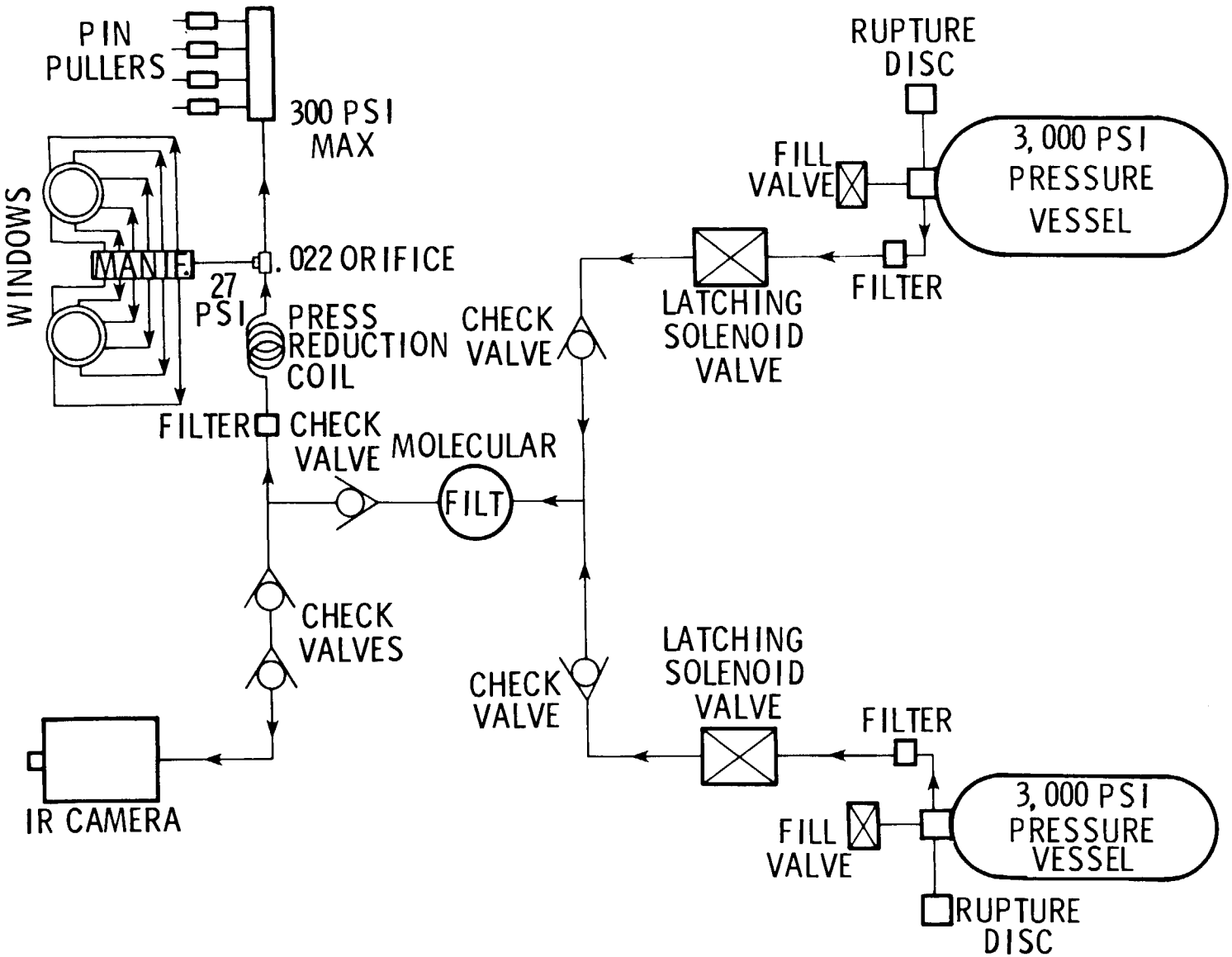

Figure 11. Pressure system schematic

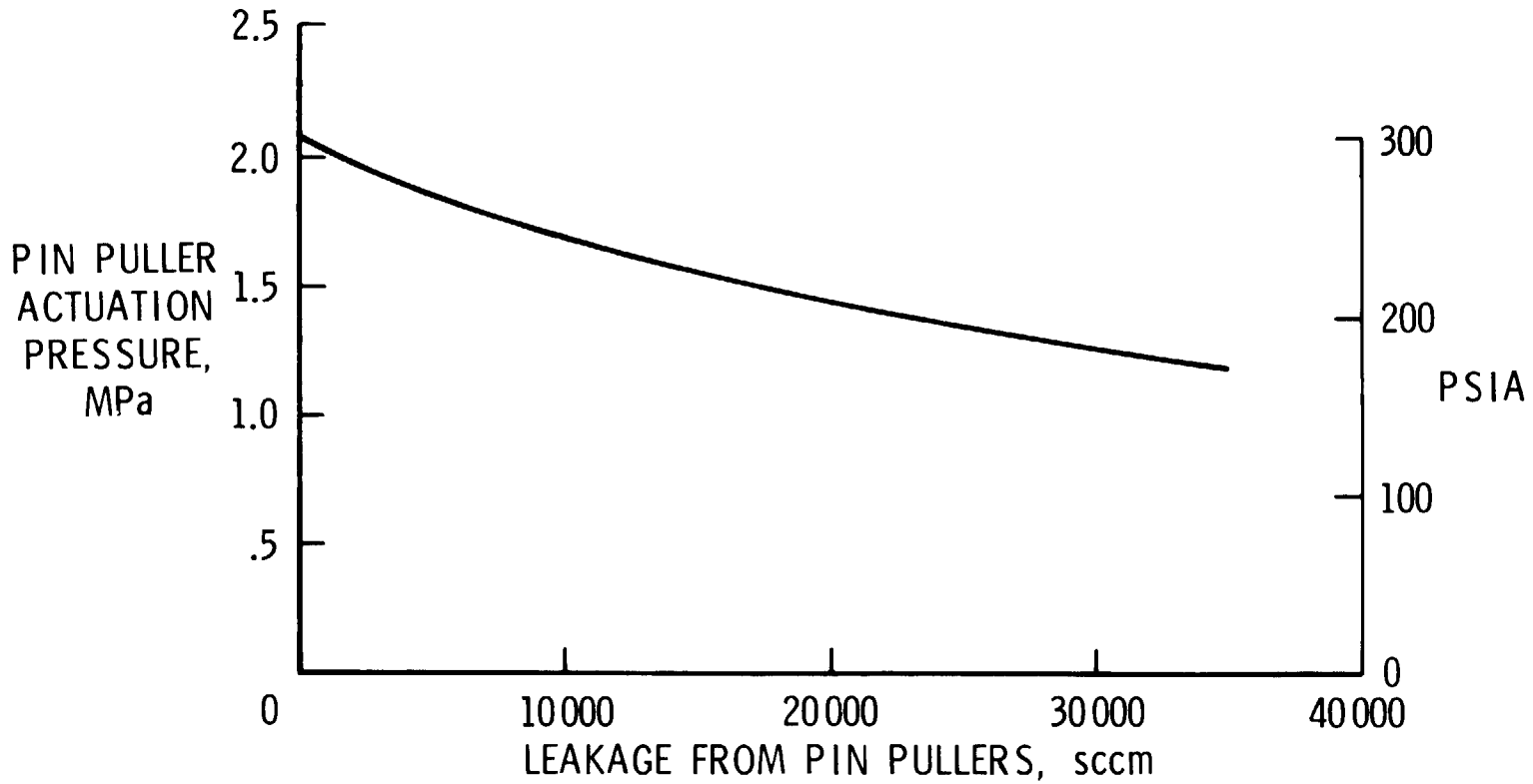

Figure 12. Pin puller pressure vs. leakage

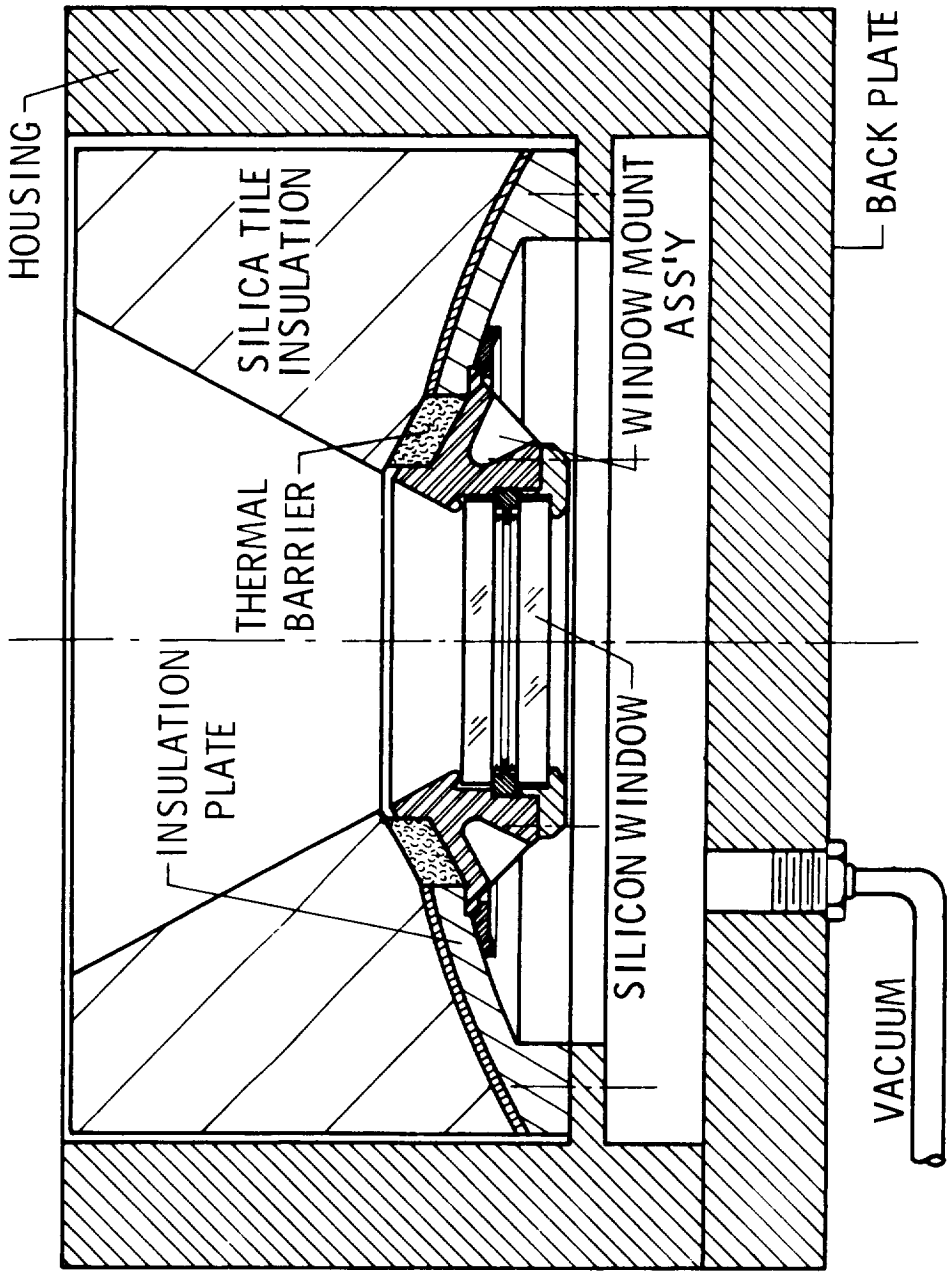

Figure 13. Certification test hardware

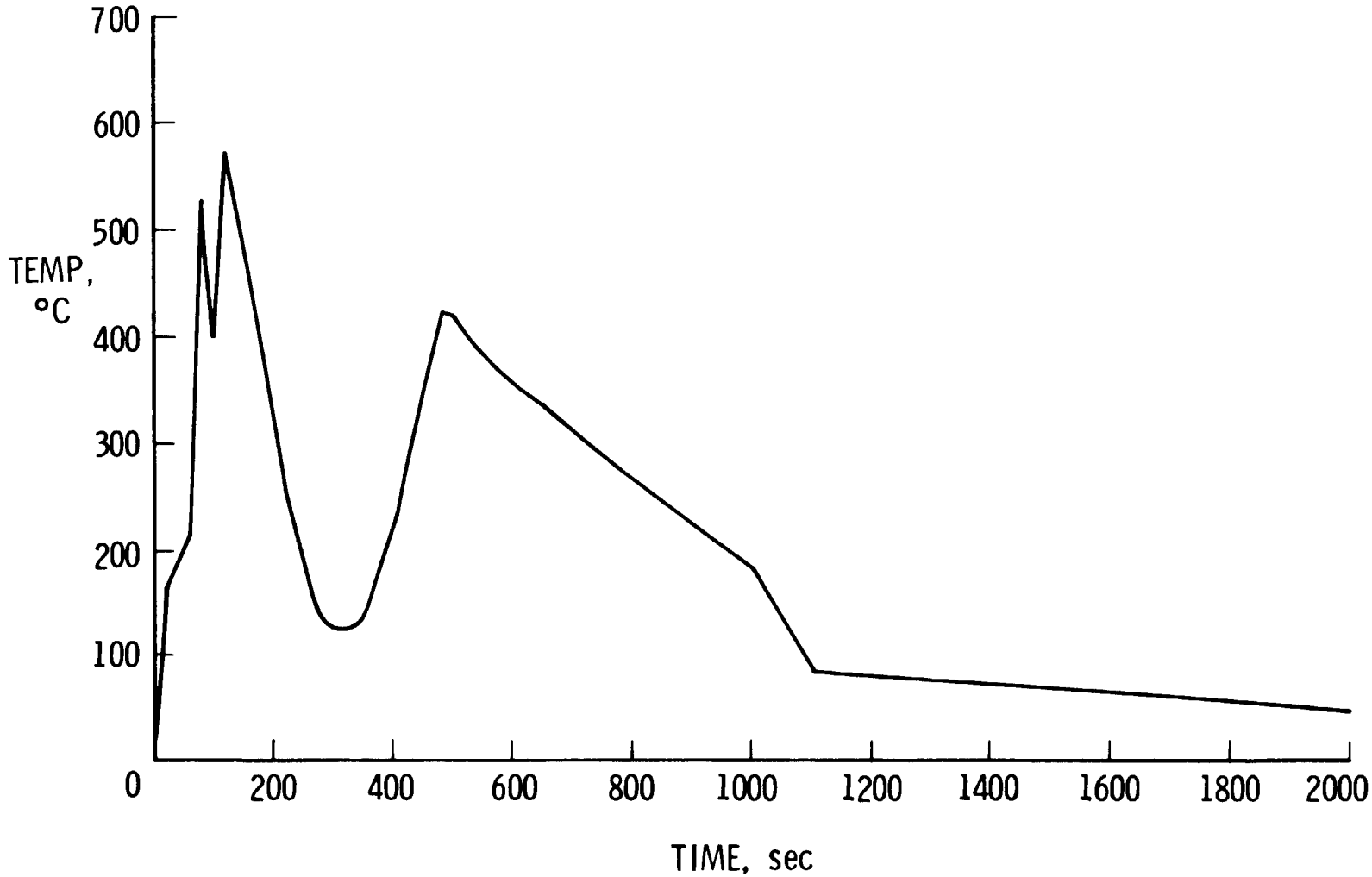

Figure 14. Temperatures predicted for the exterior surface of the window protection plug during ascent

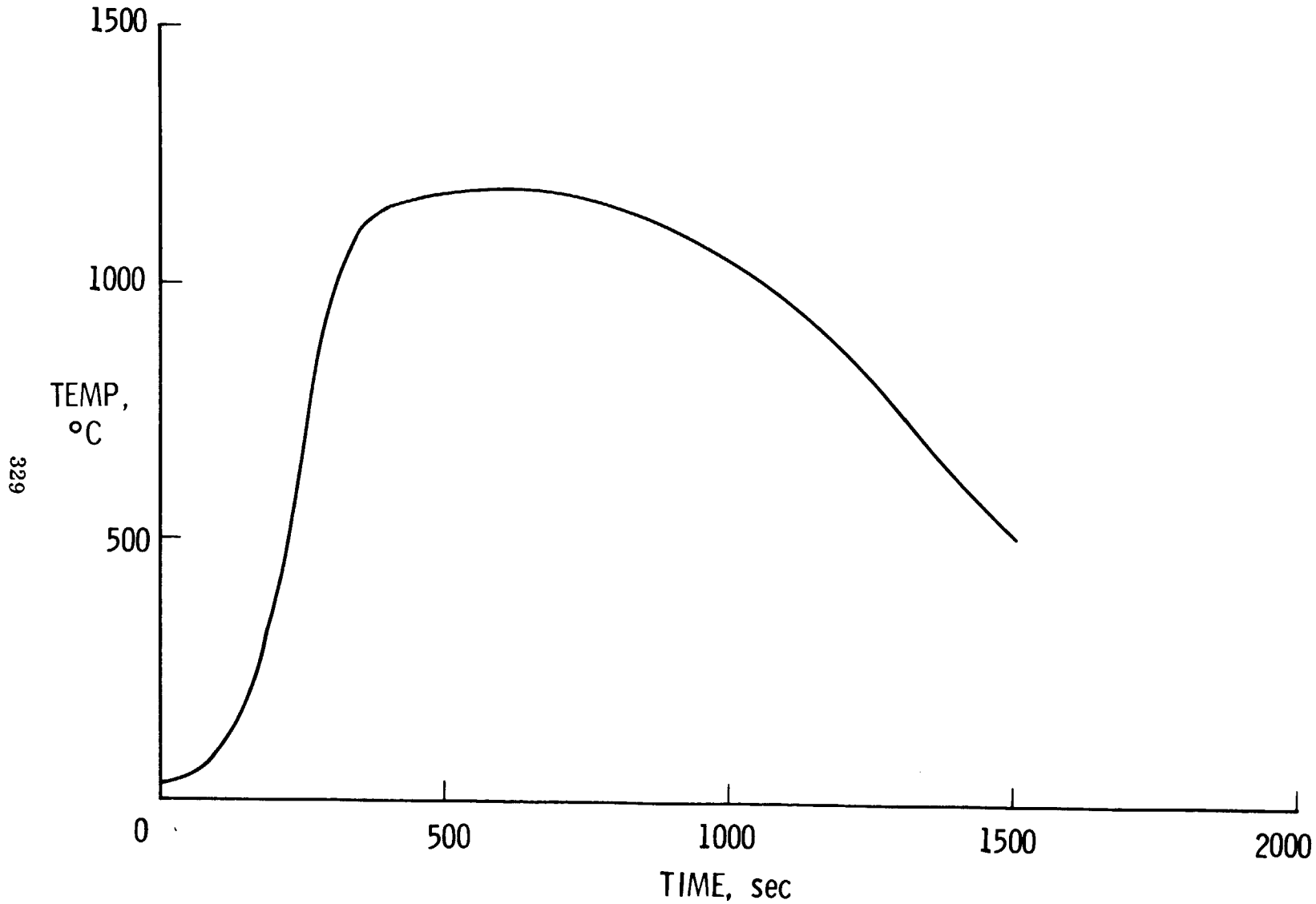

Figure 15. Analytical temperature prediction for exterior window with no coolant gas

LATCH MECHANISM FOR THE SPACE TELESCOPE*

Hubert F. Schmidt

Lockheed Missiles & Space Company, Inc.

ABSTRACT

Latch mechanisms to secure, release and relatch deployables on the Space Telescope are being developed by Lockheed Missiles and Space Company, Inc. under contract to Marshall Space Flight Center. The Space Telescope is designed for launch in the Space Shuttle with consideration for on-orbit maintenance and earth return capability. This on-orbit maintenance and earth return requirement created unique design problems. Not only is a manual override of any space telescope mechanism a requirement, but the forces required to override must not exceed the astronauts' capability. Physical and visual access must be designed for, including simple and standard tool usage. Earth return requirement in effect dictates the need for relatching or securing the Space Telescope deployables. Thermal gradients, if not properly designed for, could cause unacceptable conditions, especially when trying to secure lengthy components. The latch mechanisms are mechanical pre-loading devices composed of a four-bar linkage driven by an electro-mechanical rotary actuator. This paper describes the latch mechanism requirements, unique design features, analytical highlights and the development testing.

INTRODUCTION

Placed in orbit by the Space Shuttle, (see Figure 1) the Space Telescope will perform its many functions in an environment impossible to duplicate on Earth. Atmospheric filtering, haze, twinkling, and light pollution will be eliminated.

The Space Telescope will have 10 times better resolution than ground-based telescopes; it will be able to see objects that are 50 times fainter and 7 times farther away than those we now observe.

The Space Telescope overall is a cylinder 14.3 meters (43 feet) long and 4.7 meters (14 feet) in diameter (see Figure 2). The Optical Telescope Assembly will comprise a 2 meter class reflecting telescope.

*Work was sponsored by the NASA, Marshall Space Flight Center, Alabama. under contract NAS8-32697.

The Scientific Instruments Package will provide the means of converting the telescope images to useful scientific data. The Support System Module will contain a very precise stabilization system, the communications system, and the power system. Electrical power will be supplied by solar panels. The Space Telescope can be serviced and repaired while it is in orbit, and scientific instruments, as well as worn out or failed spacecraft components, will be replaced on-orbit. When major overhauls are considered necessary, the Space Telescope will be returned to Earth for major repairs and improvements and then be replaced in orbit.

Three different types of deployables are mounted on the Space Telescope. Two high gain gimballed antennas, an aperture door and the European Space Agency (ESA) supplied solar arrays (2), are to be deployed once the Space Telescope is on-orbit. For ascent and return, these deployables must be secured. To keep extra vehicular activity (EVA) time to a minimum, all deployables must be able to be remotely unlatched, deployed and be able to be remotely latched again. Only in case of a failure shall an EVA be used for problem correction.

The solar arrays are unfurled after spacecraft deployment by the shuttle orbiter and are retracted prior to retrieval. Both arrays rotate about the pitch axis during slew maneuvers to maintain solar cell surface normal to the sun during observations. The Space Telescope utilizes an average of 2.3 KW for operation of all subsystems and instruments.

This paper describes the design of the latches used to secure, release and relatch the two stowed solar arrays (see Figure 3). To limit the scope of the subject, the description will confine itself to the latch and will not include the mating fittings of the solar arrays.

REQUIREMENTS

The latch design was constrained by envelope restriction, redundancy, astronaut override features, remote operation, temperature extremes, and 5-year life verification requirements. The envelope restrictions and temperature extremes were the main design drivers.

DESIGN CRITERIA

The two latch mechanisms to secure each SA are mounted to the Space Telescope. Figures 4 and 5 show an overview of the stowed SA and the location of two latch assemblies. Figure 3 shows the hinge

point of the SA creating a three-point support for the SA. Lockheed as the integrating contractor had the requirement to provide mounting support for the SA during ascent, orbit and return. In order to take axial loads at only one latch point, the aft latch assembly, and not the SA hinge, created a special problem for the SA contractor. Any thermal gradient would result in an axial load at the SA point. Once the solar array is unlatched, however, the thermal gradients will cause a mismatch at the interface to be overcome by the latch upon relatching. Here is where the design divides into two main areas: (1) the interface between the SA and the latch seat has to be able to center itself to carry all loads once secured, and (2) the interface between the latch pawl and latch fitting. The latter interface requirement then drove the design features. The latch needed only to provide a clamping force, similar to a compressing joint with a tension bolt.

DESIGN DESCRIPTION

The latch assembly is shown in Figure 6. A four-bar linkage is driven by an electro-mechanical rotary actuator incorporating redundant permanent magnet stepper motors with one harmonic drive gearhead. The output shaft of the rotary drive unit is connected through a universal type linkage to the crankshaft of the latch assembly. The engagement pawl and pawl arm are connected to a lever via two compliant torque rods. These torque rods are the unique feature of the latch design. A force by the linkage against the lever, with the pawl engaged to a solar array fitting, will twist the rods, resulting in a relative rotational motion between the pawl arm and the lever. Figure 8 shows a cross-section through the lever, pawl arm and torque rods. The splined torque rods engage the splined pawl arm, with strain gages fastened to the torque rods. The strain gages are used to calibrate the final latch forces and define the setting for the preload limit switch.

A 3.2/1 single stage pinion gear is attached to the crankshaft to aid the astronaut to manually operate a latch. The rotary drive unit with its magnetic detent in the stepper motors creates a resistance to unpowered rotation. Torque applied to the output shaft of the rotary drive unit will cause it to backdrive through its harmonic drive. A hex for a wrench on the pinion shaft of the external gears provides the access for the astronaut to manually operate the latch in case of power failure. The detent in the stepper motor also provides the natural locking feature for the latch in either the open or closed position. Mechanical stops have been provided with redundant limit switches for either the open or closed (fully preloaded) position.

Redundancy is designed into every rotating joint of the latch. No one single point bearing failure will render the latch inoperable. Figure 7, shows a cross-section through the linkage and crankshaft. The spherical rod ends have Teflon lined ball joints; the pivot shaft through the rod end has roller bearings for redundancy. All other rotating joints have a combination of Teflon lined journal bearings acting as inner race for the rolling elements of the needle bearings. The inner race outer surface contacting the needles is hardened to 58 RC. As a back-up feature, the adjustment bolt located in the pawl arm, can be used to flip the pawl away.

Aluminum 7075 is used for the side plates and linkages. The lever, torque rods and pawl arm are made from 15-5 PH stainless steel. All needle bearings are lubricated with a low outgassing grease, Bray Oil Company, 3L-38RP (use of dry lubricant was ruled out for usage on the Space Telescope). The lubrication is applied by an immersion process developed by the Lockheed Missiles and Space Company. The grease used has been tested by NASA and is documented in a NASA Technical Memorandum (Ref. 1).

ANALYTICAL HIGHLIGHTS AND DEVELOPMENT TESTING

The latch operation is shown more graphically in the series of Figure Numbers 13, 14 and 15. To fully understand the function of the torsion rod, it is important to note that in Figure 14, the pawl, Item 6 has engaged the interfacing solar array fitting and therefore any further counter clockwise rotational motion by Lever, Item 1 will reduce the gap (1.3 MM) between pawl, Item 6 and Lever, Item 1. Proper sizing of the torsion rod and gap adjustment provides a proper margin of power for the drive unit acting at the crankshaft. Mechanical testing of the proto-type latches revealed an unexpected large compliance (low spring rate). The increased compliance in the linkage and latch structure precluded reading full preload and significantly reduced the drive unit torque margin.

Instrumentation and kinematic analysis showed that the latch stiffness must be increased by a factor of eight to meet an increased preloading requirement with a torque margin of 1.0 for the drive unit. To meet this requirement, several latch components were modified, basically by increasing the cross-sections of the support structure, and changing of bolt patterns.

Results of a finite element model indicate an eight-fold stiffness increase over the original tested latch. The stiffness of the tested latch was about 6 100 NM/Rad (54,000 in-lb/Rad), while the improved version indicates a system stiffness increase to 52 000 NM/Rad (460,000 in-lb/Rad).

Figures 9 through 12 are the highlights of further analyses of

the stiffened latch. The mechanical advantage (Figure 9) is considerable once the crankshaft comes to the end of its travel.

The pawl preload curve (Figure 10) shows the pawl contact at about 89 degs of crankshaft rotation and then a rapid preload increase. The drive unit capability is approximately 55 Joules (490 in-lb) to preload the latch, a good margin to work with. The impact of low temperature operation of -73°C (-100F) will be investigated to determine if usage of active thermal control can be avoided.

The manual override torque required for the astronaut to operate the latch, using a 12-inch extension wrench, should not exceed 34 Joules (300 in-lb). Figure 12 shows that 27 Joules (240 in-lb) torque will operate the latch. The 27 Joules includes the backdriving force of approximately 19 Joules (171 in-lb) for the drive unit.

CONCLUSION

A preload latching device with redundant features has been developed for use in 9 different applications on the Space Telescope. The latch provides forces equivalent to a tension/compression bolt. The latch is powered by a one-stage harmonic drive stepper motor drive unit. Astronaut override capability is provided to operate the latch in case of power failure.

ACKNOWLEDGEMENT

The development of the latch past its concept has been greatly enhanced by the efforts of Messr. Herb Greenfield and Joe Wilson of Lockheed Missiles and Space Company, Inc.

REFERENCES

1) NASA TECHNICAL MEMORANDUM No. NASA TM 78162; by E. L. McMurtrey; dated March 1978; George C. Marshall Space Flight Center, Marshall Space Flight Center, Alabama.

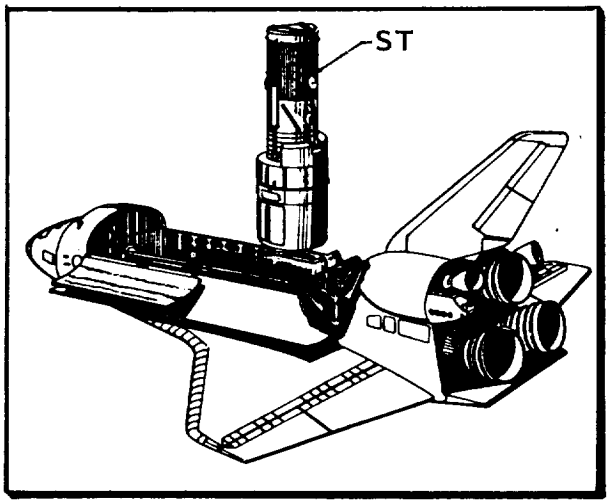

Figure 1. ST and Shuttle

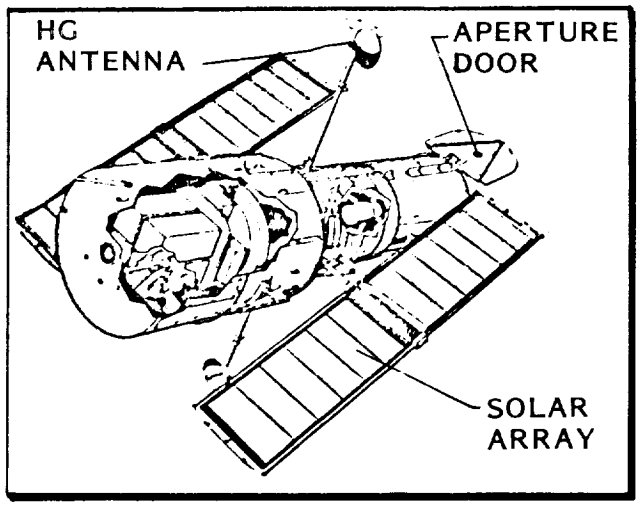

Figure 2. Space Telescope

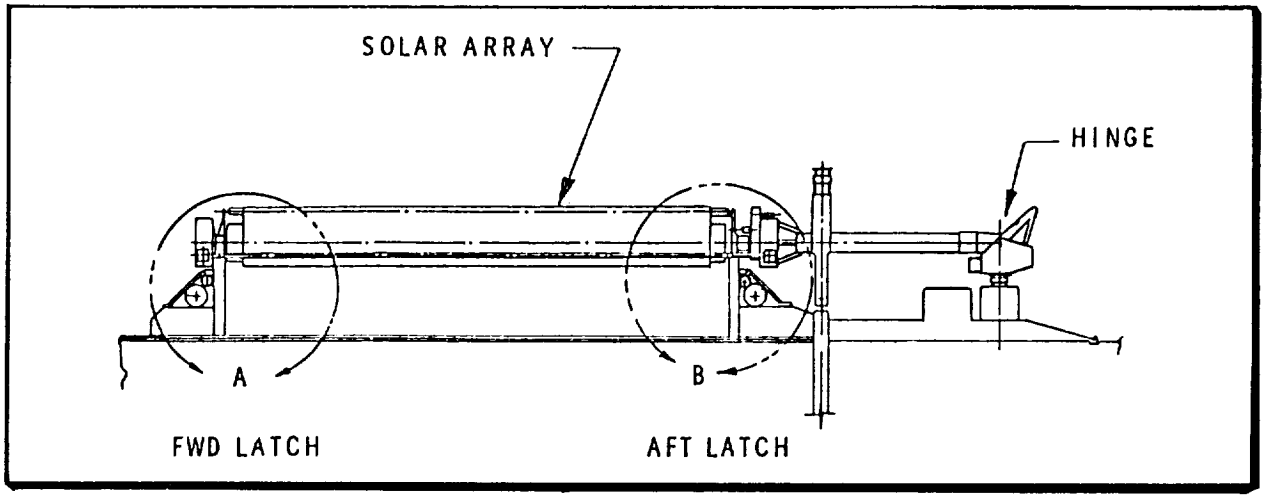

Figure 3. Solar Array Support System

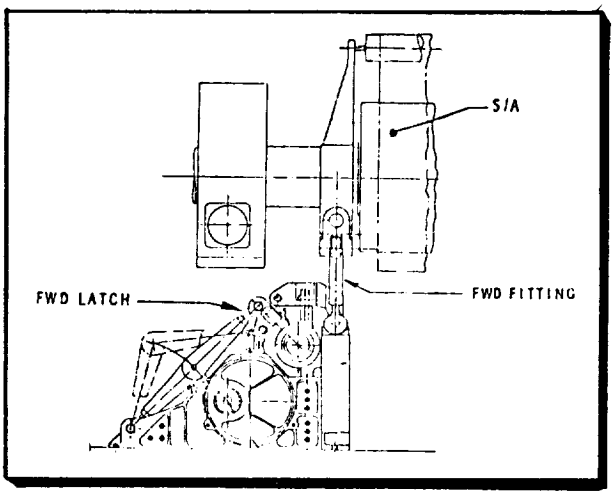

Figure 4. Detail A

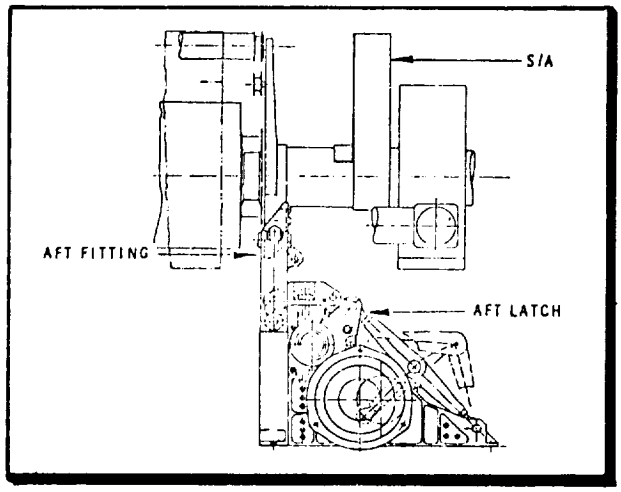

Figure 5. Detail B

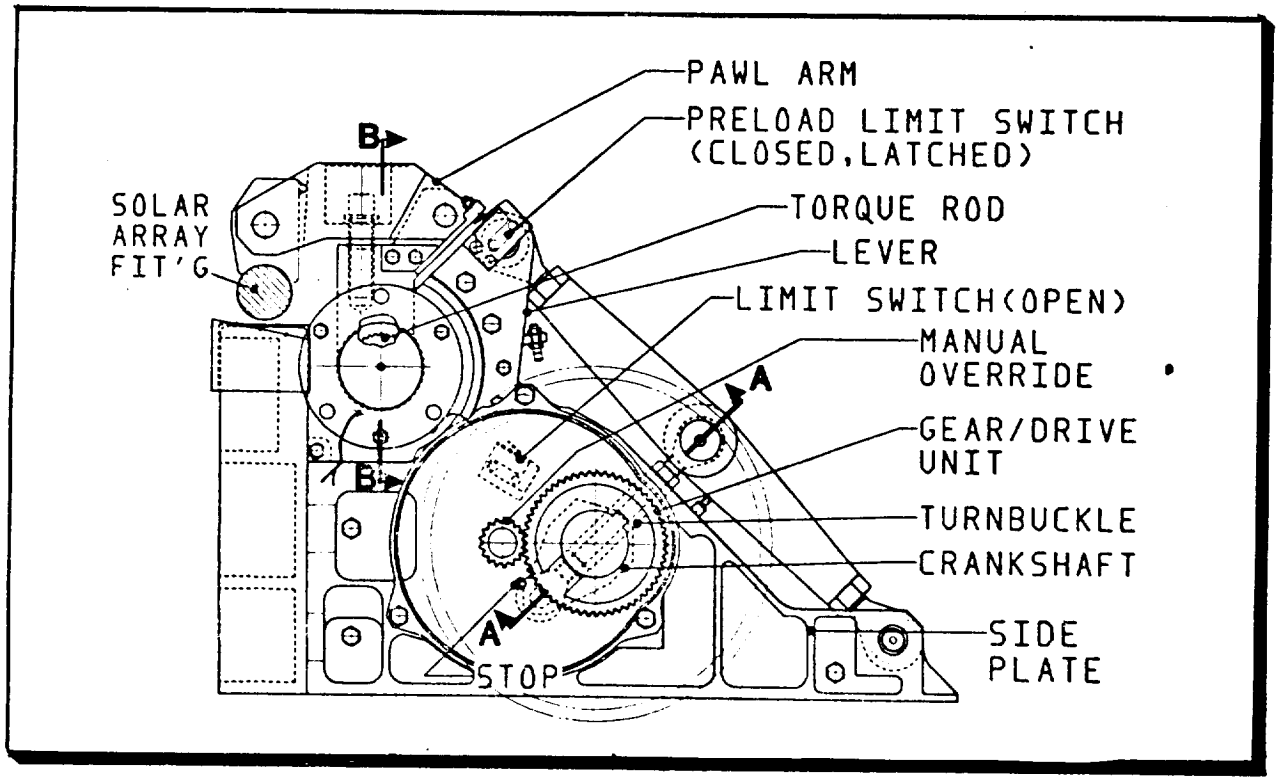

Figure 6. Latch Assembly

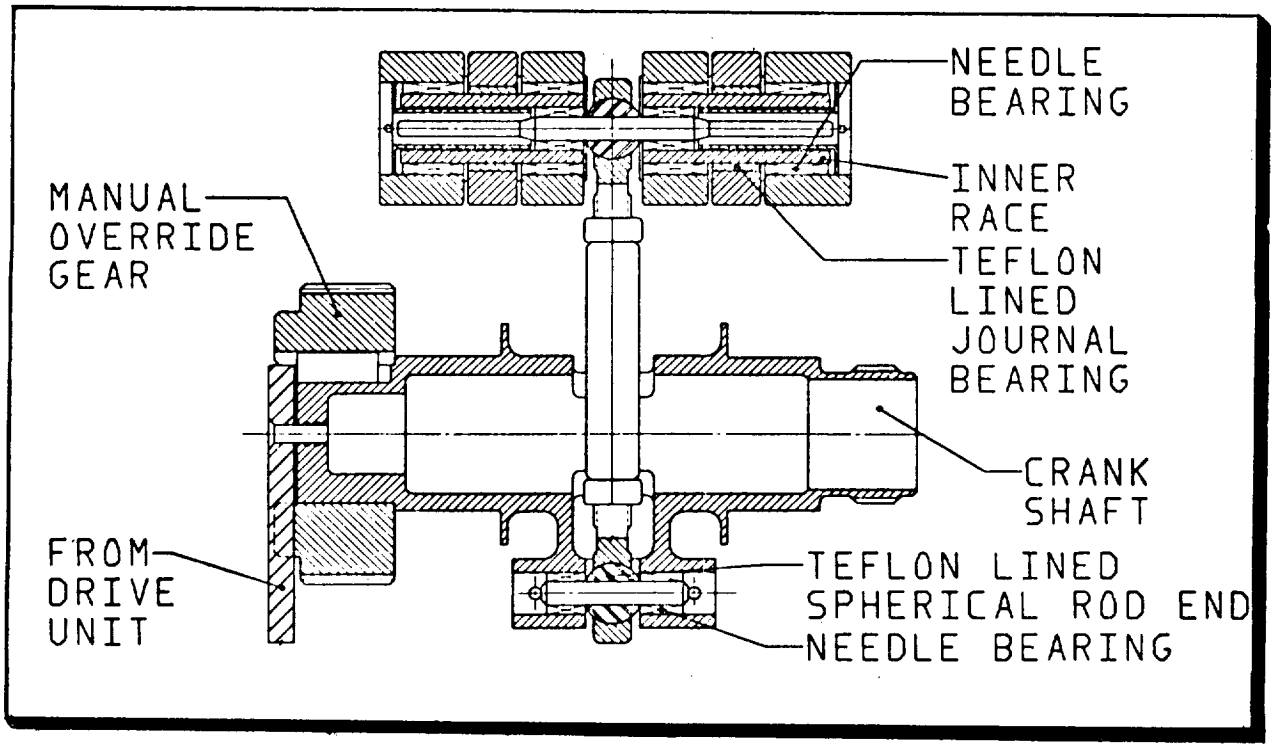

Figure 7. Latch Assembly - Section A-A
(rotated 45 deg ccw)

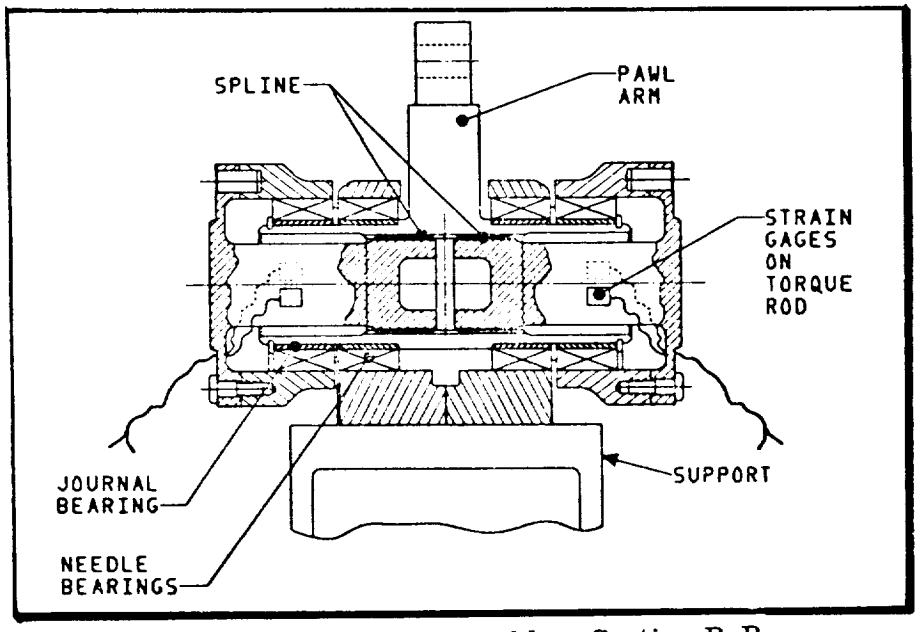

Figure 8. Latch Assembly - Section B-B

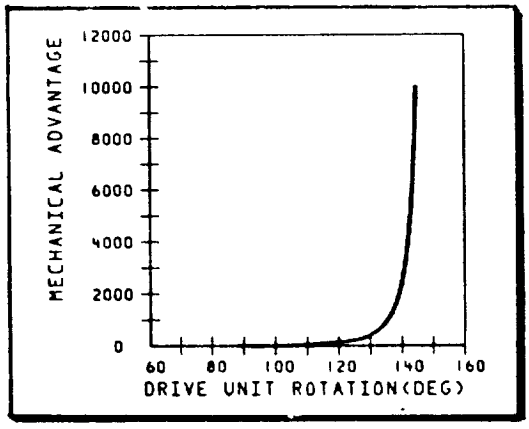

Figure 9. Mechanical Advantage

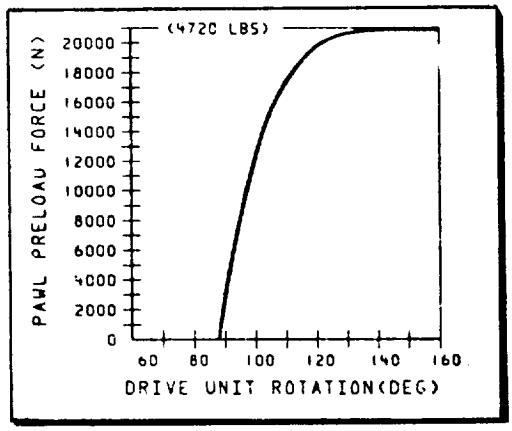

Figure 10. Pawl Preload Force

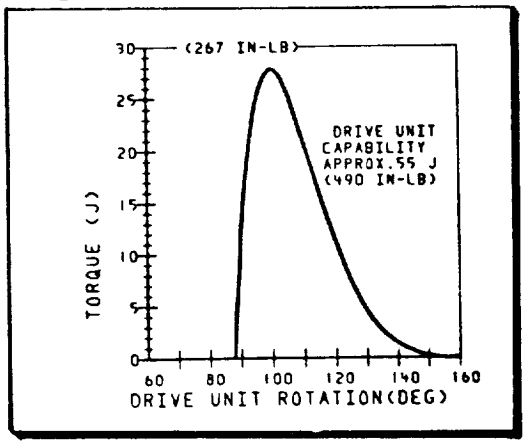

Figure 11. Drive Unit Utilization

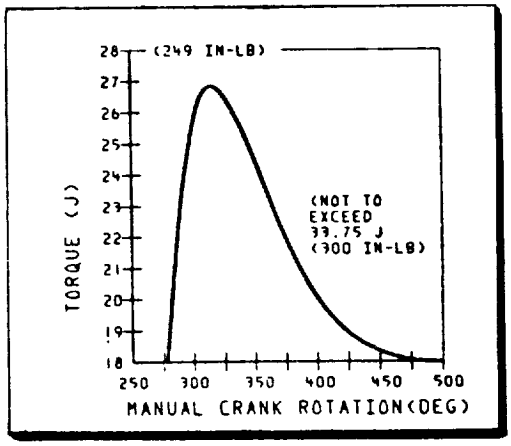

Figure 12. Manual Override

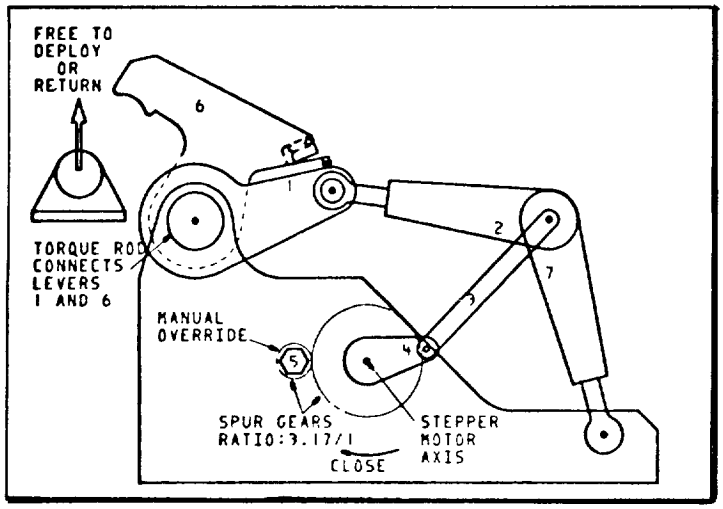

- Latch fully open. Lever, item 1 against mechanical stop.
- Crank shaft, item 4 ~160 Deg from closing position.
- Limit switch open
- Payload free to deploy or return.

Figure 13. Latch Open

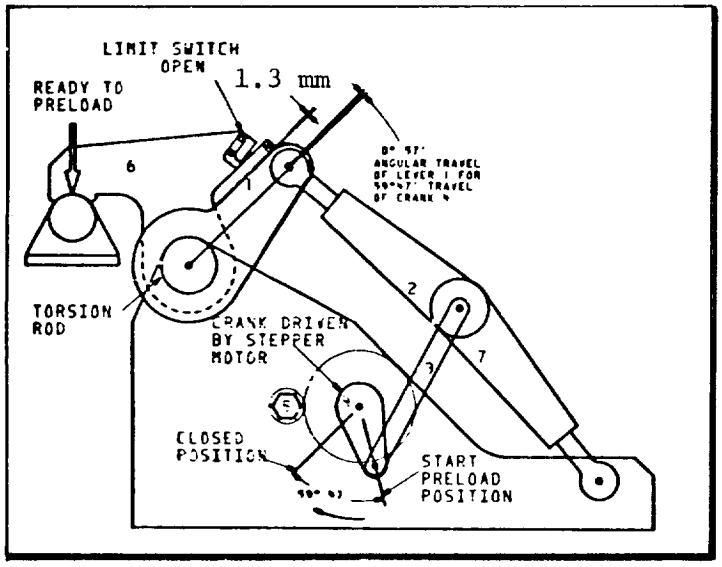

- Levers items 2 and 7 not straight
- Crankshaft, item 4 ~60 Deg from closing position.
- Limit switch still open
- Lever, item 6 stopped
- Lever, item 1, 1.3 mm from closed position

Figure 14. Latch Ready to Preload

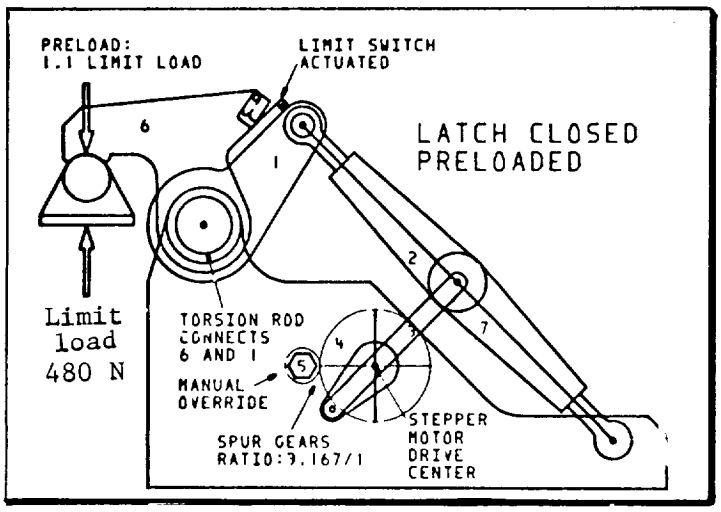

- Levers items 2 and 7 straight
- Crank shaft, item 4 and connecting rod item 3 are aligned straight
- Torque Rod twisted 57 arc min.
- Limit switch actuated
- Stepper motor detent holds latch closed.

Figure 15. Latch Closed - Preloaded

A FULLY REDUNDANT POWER HINGE FOR LANDSAT-D APPENDAGES

By

Frank E. Mamrol

And

Donald N. Matteo

General Electric Company
Space Division

ABSTRACT

As spacecraft appendages become larger and more complex, and as the potential need emerges to retract these appendages for retrieval by Space Shuttle, the requirement for a reliable power driven hinge for deployment/retraction of such appendages becomes increasingly apparent. Such a hinge has been developed at General Electric to deploy both the Solar Array and the Antenna Boom for NASA-GSFC's Landsat-D spacecraft.

This paper describes the configuration and testing of this hinge which is fully mechanically and electrically redundant and, thereby, can sustain a single point failure of any one motor (or its power supply), speed reducer, or bearing set without loss of its ability for function. Because of the universality of the basic hinge design, the same hinge (with suitable structural modifications) is used at three different locations on the Landsat spacecraft; both the inboard and outboard hinges for the TDRSS Communications Antenna Boom and as the root hinge for the Solar Array.

Another requirement which is becoming increasingly more important is that of high bending stiffness of the deployed hinge. This requirement is especially difficult to satisfy about the functional axis of the hinge. This design uniquely utilizes the capability of the stepper motor drive to remove the flexibility of the drive train from the joint stiffness equation when the hinge is loaded against its stop. This feature precludes gapping of the joint under spacecraft maneuver loads even in the absence of a latching feature. Thus retraction is easily accomplished by motor reversal without the need for a solenoid function to remove the latch. This capability is utilized in the Landsat-D Outboard Antenna Boom Hinge where on-orbit reconfiguration allows minimizing vehicle inertias for maneuvering. For extreme load conditions, a non-reversible, spring-loaded latch

is easily incorporated, as is the case for the Landsat-D Boom Root Hinge.

INTRODUCTION

The Landsat-D spacecraft, NASA's latest orbital earth resources instrument platform, requires two large deployable appendages. These are a 2.31 m wide by 5.92 m long Solar Array and a 3.83 m long Antenna Boom. To deploy these appendages, General Electric has designed a set of fully redundant power driven hinges which provide the required redundancy for all single point mechanical and electrical failures, as well as sufficient stiffness to satisfy appendage deployed natural frequency requirements imposed by attitude control considerations.

While redundancy in a mechanical drive system is readily achieved by the incorporation of a back-up motor and speed reducer, most systems fall short of complete redundancy at some point where both drive trains couple into a single output shaft. Moreover, reliability is usually further compromised by the necessary utilization of overrunning clutches to free the system of the failed drive train. Finally, bearing redundancy is usually achieved at the expense of joint bending stiffness. This paper describes the unique solution to all of the above challenges in the Landsat-D Power Hinge developed by General Electric Space Division.

REQUIREMENTS

The Landsat-D spacecraft requires power driven hinges at three locations, both root hinge and outboard hinge of the TDRSS Antenna Boom, and the root hinge of the Solar Array. Figure 1 depicts these locations on the instrument module of the spacecraft. Note that the Solar Array is of the single wing design and is not planar. This configuration resulted in a very long array of high inertia and a deployment sequence involving synchronized rotation about four hinge lines simultaneously. The Antenna Boom requires two hinge lines and carries an active payload, the Gimballed Antenna and associated RF electronics. Moreover, in order to reduce spacecraft inertia for on-orbit maneuvering, the outboard hinge is required to be retractable.

The above system level considerations resulted in the following hinge requirements: (normal spacecraft environmental requirements have been deleted from this list for brevity.)

- Both Boom Hinges shall be power driven.
- The Root Solar Array Hinge shall be power driven and shall act as the rate controller for the three outboard spring driven hinges through a system of synchronization cables.

- All power hinges shall be fully redundant and tolerant of any single point mechanical or electrical failure.
- The minimum output torque of the power hinge shall be 40.7 Nm (360 lb.in) including the effects of torque transmission limitations of the unpowered motor.
- The minimum deployed stiffness of the hinge shall be 8×10^4 Nm/rad (7.1×10^5 lb. in/rad) about any axis.
- Both inboard hinges shall include a mechanical latch.
- All hinges shall provide a telemetry indication of full deployment.
- All hinges shall be capable of powered retraction. (Only the Outboard Boom Hinge is required to be retracted in flight.)

DESIGN SOLUTION

Description

The power hinge consists of two modules mechanically in series. Figure 2 shows the Landsat-D Antenna Boom Upper Hinge. The module consists of a Rapid Syn 23H-503 series stepper motor coupled to a TRW Globe 1A2119-4 speed reducer. The speed reducer output shaft is spline coupled into the shaft on which two duplex pairs of angular contact bearings are mounted. The characteristics of the module are listed in Table I. The two modules are the parts of the power hinge that provide the torque, and may be adapted to various structural hinge configurations. The output of the two modules are joined by a shaft, while the housings are attached to the separate hinge fittings.

Redundancy Features

Note that the hinge employs two complete drive trains, each including a stepper motor, a speed reducer, and an independent set of bearings. The drive trains are in series with each other. Thereby, the torque from either drive train is transmitted through the other to be delivered to the load and reacted by the spacecraft structure. By this means, the hinge is tolerant of a completed jam-up of any element (motor, speed reducer or bearing) and is still capable of delivering the output torque of the unfailed drive train to the load. The inherent lack of bending stiffness of two sets of bearings acting in series is overcome by the straddled yoke arrangement which provides a long wheel base for each bearing set such that shaft bending loads are reacted principally by bearing radial loading.

TABLE I

POWER MODULE COMPONENT CHARACTERISTICS
MANUFACTURERS RATINGS

Stepper Motor		
	Step Angle	1.8°
	Rated Voltage	28 VDC
	Resistance per Phase	80 OHMS
	Inductance per Phase	70 mH
	Weight	.72 kg (1.58 lb)
Speed Reducer		
	Gear Reduction	647:1
	Torque Multiplier	524
	Max Continuous Torque	11.3 Nm (100 lb. in.)
	Max Intermittent Torque	22.6 Nm (200 lb. in.)
	Momentary Stall Torque	56.5 Nm (500 lb. in.)
	Min. Life	1000 hours
	Weight	.44 kg (97 lb.)

Operation

Applying power to one stepper motor rotates one hinge fitting relative to the other, transmitting torque through the unpowered module. The potential torque transmitted through the hinge is:

$$T = T_m R \eta \tag{1}$$

where T_m is the torque of the motor, R is the ratio of the speed reducer, and η is the torque efficiency of the speed reducer. However, the maximum torque that can be transmitted is that limited by the slip of the unpowered motor:

$$T = \frac{T'_m R}{\eta} \tag{2}$$

where T'_m is the magnetic detent torque of the motor.

Rotation takes place in the bearings that are in the hinge fitting to which the operating module is attached; the second set of bearings is inoperative. Thus, the hinge is mechanically redundant. With separate power supplies for each motor, the hinge is electrically redundant. Failure of any functional element is overcome by switching to the other module.

Lubrication

Molybdenum disulfide is used for lubrication in all required locations. The races of the ball bearings in the motor and in the hinge brackets are coated with the lubricant bonded with sodium silicate. The gears of the speed reducer, the integral ball bearings of the planetary stages and the ball bearings supporting the output shaft were cleaned of the original grease and tumbled in molybdenum disulfide powder. This lubricant provides adequate lubrication for the limited life with relatively little change in drag over the temperature range while meeting the outgassing requirements for spacecraft.

Latching

The requirements for the stiffness and strength of a hinge with the appendage in the deployed position are usually greater than for when the appendage is deploying. The Landsat-D antenna boom upper hinge has no latch, but the required deployed stiffness is achieved as follows: the moving hinge bracket contacts the fixed hinge on mechanical stops at the end of the deployment. A switch closure a very short distance before the stops contact starts a counter that, after 2048 pulses to the motor, cuts off power to the motor. During those 2048 pulses to the motor, the torque of the module winds deflection into the gear train and hinge brackets, preloading one against the other. No more torque can be wound into the hinge than the backdrive capability of the unpowered motor when it slips. The stiffness of the hinge is now that of the hinge brackets, not the module drive train. This is analogous to the preloading of a structural joint. The stiffness of the joint is that of the joined parts, not the bolt, until the load exceeds the preload of the bolt. The stiffness of the hinge is that of the hinge brackets until the applied load exceeds the torque wind-up of the module. The boom upper hinge external applied torque requirement is less than this wound-in torque; therefore, no other latching mechanism is required. The boom lower hinge and the solar array require a positive latch. These hinges similarly wind into a stop. A tapered latch is spring driven into a notch which contacts on the side to prevent backing up of the hinge. The spring driving the latch into engagement wedges the hinge into the stops in the deployed direction and the latch in the retracted direction. The switch that initiates the pulse counting for shut-off is actuated by the latch dropping into the notch.

TESTING

Speed Reducer

A series of tests was made to characterize a motor/speed reducer combination. The motor and speed reducers were the manufactured stock items differing from the final spacecraft adaptations in that the motor bearings were grease lubricated and the speed reducers were lubricated with Beacon 325 diester oil per MIL-G-3278A. The motor and speed reducer are coupled with an adapter as shown in Figure 3 driving an inertia. Figure 4 shows the pulley and weights driven through the gear box.

A simplified set of hinge brackets was fabricated for development testing and characterizing the performance of the power module. The torsion load was applied by a pulley and weight system where the weight was reacted by a separate bearing not in the hinge. Thus, the hinge felt only torsion. The hinge and loading pulley are shown in Figure 5. The power supply for supplying motor pulsed current is shown in the foreground. Tests were made by placing weights on the pan and operating the motor to lift the weights at a particular pulse rate, 100 percent pulse width. The power supply was reduced until the motor no longer raised the weights with continuous motion. At this point, pulses would be skipped, and motion then continued. The electrical parameter measured was the current in the common return of the four field coils. The current was measured with a coil type ammeter where the inertia of the armature integrated the current pulses for a steady indication. At voltages relatively low compared to the spacecraft's bus, output torques reach the maximum as listed by the speed reducer manufacturer.

The bus voltage of the Landsat-D Instrument Module can vary between 22 and 33 volts at the times when deployment is to occur. At this high voltage, the motor would draw as much as 0.29 amperes producing 160 Nm (1416 lb. in.) at the output shaft of the speed reducer. The speed reducer manufacturer's ratings are understandably conservative for a failure-free long life. For Landsat-D application, the speed reducer operates less than one revolution during the mission. Allowing for several revolutions occurring during testing, the life requirement is very short. Little of that time is probably at maximum torque. It is appropriate to allow a torque rating higher than the manufacturer's for a short time. Extensive analysis or testing to determine the limits of this speed reducer was not done. It was, however, operated at 90.4 Nm (800 lb. in.) for a short time, after which the gears and bearings were inspected. There was no visible effect of this loading so a rating of 56.5 Nm (500 lb.in.) was tentatively established. The measurements were made for several weights up to this limit, and pulse rates of 31.25 to 125 Hz., in both directions. The results are shown in Figure 6.

As previously stated, the maximum torque that can be transmitted through the redundant pair is the torque to slip the unpowered module. Measurements were made with the same pulley and weight pan. Weights were added until the shaft turned. This is defined as break-away torque. In

addition, lesser weights were put on the pan, and the pulley assisted to start rotation of the shaft. If the shaft did not continue to rotate after the assist was removed, more weights were added. When the shaft continued to rotate, this was defined as running torque. The averages of three such measurements in both directions, at ambient and -40°C, are listed in Table II.

TABLE II

Unpowered Back Drive Torque-Power Module

	Breakaway	Running
Ambient	50.0 (442)/49.7 (440)	30.4 (269)/31.6 (280)
-40°C	51.4 (455)/54.0 (478)	42.1 (373)/43.5 (385)

Clockwise/Counterclockwise torque in N m (lb.in.)

The data indicate a substantial effect of temperature on the running torque, but little on breakaway torque. From this it might be expected to specify 30 Nm (265 lb.in.) as the minimum torque limit for the redundant hinge. The magnetic detent torque of the test motor (T'_m of Eq.2) was lower than what can be expected of other motors. Therefore, the minimum back driving torque was specified to be 40.7 Nm (360 lb. in.) Torque limiting was achieved by current limiting the power supply so that the motor stall torque is between 56.5 (500) and 40.7 Nm (360 lb. in.) when the supply voltage is between 33 and 22 volts. The power supply regulates motor current by having a fixed voltage on the base and an emitter resistor for each motor phase switching transistor. The performance of the power module when driven by the regulated power supply is shown in Figure 7.

A flight configuration hinge assembly was loaded with dead weights about the boom bending axes in turn, while measuring deflections. Angular deflection about each of the axes due to a unit torsional moment about an axis was derived for each of the boom bending axes. These values are listed in Table III.

TABLE III

UPPER HINGE TORSIONAL DEFLECTION RATES

Radians/Nm (Radians/lb. in.)

Moment perpendicular to axis of rotation

$\frac{d\theta_x}{dM_x}$	$\frac{d\theta_y}{dM_x}$	$\frac{d\theta_z}{dM_x}$
1.10 E-6 (1.24 E-7)	1.07 E-6 (1.21 E-7)	2.18 E-6 (2.46 E-7)

Moment about axis of rotation

$\frac{d\theta_x}{dM_y}$	$\frac{d\theta_y}{dM_y}$	$\frac{d\theta_z}{dM_y}$
5.30 E-6 (5.99 E-7)	11.6 E-6 (13.1 E-7)	small

CONCLUDING REMARKS

The development of these hinges is now complete through successful spacecraft level full scale deployments on the Landsat-D mechanical test model. It is believed that the development of these hinges represents a significant contribution in the area of spacecraft appendage deployment mechanisms and should form the basis for development for deployment/retraction devices made necessary by future shuttle recoverable missions.

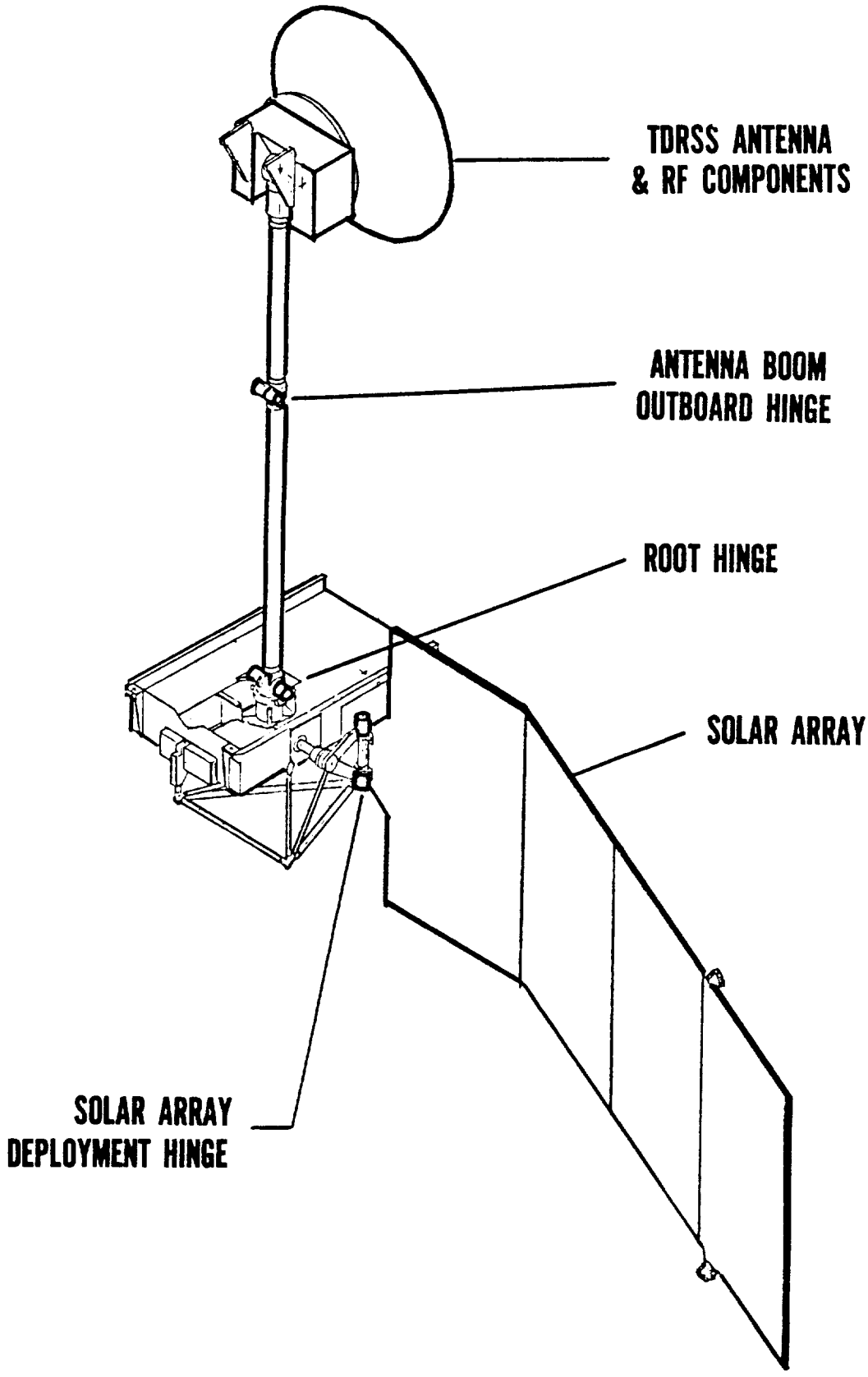

Figure 1. LANDSAT D Instrument Module

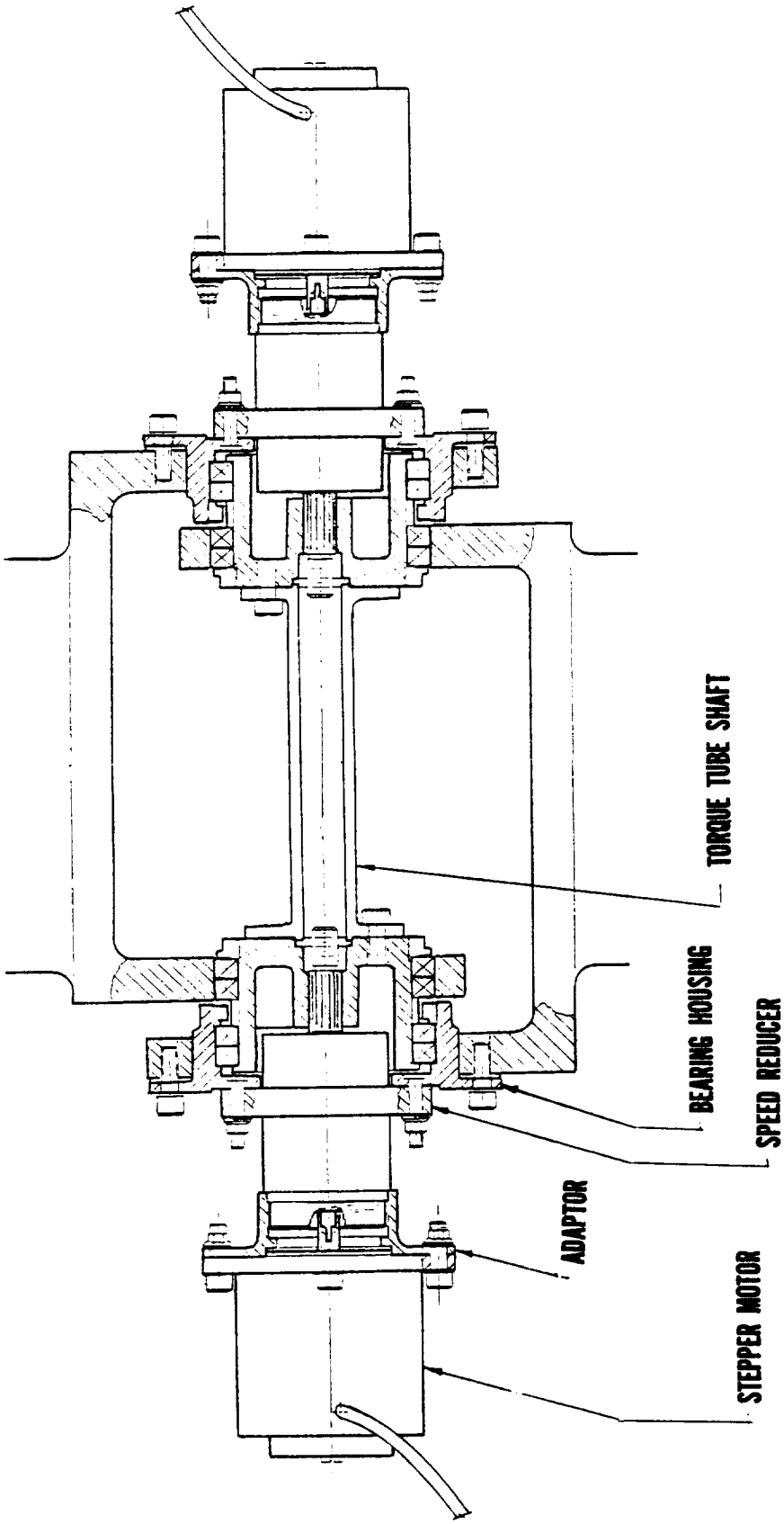

Figure 2. Redundant Power Hinge

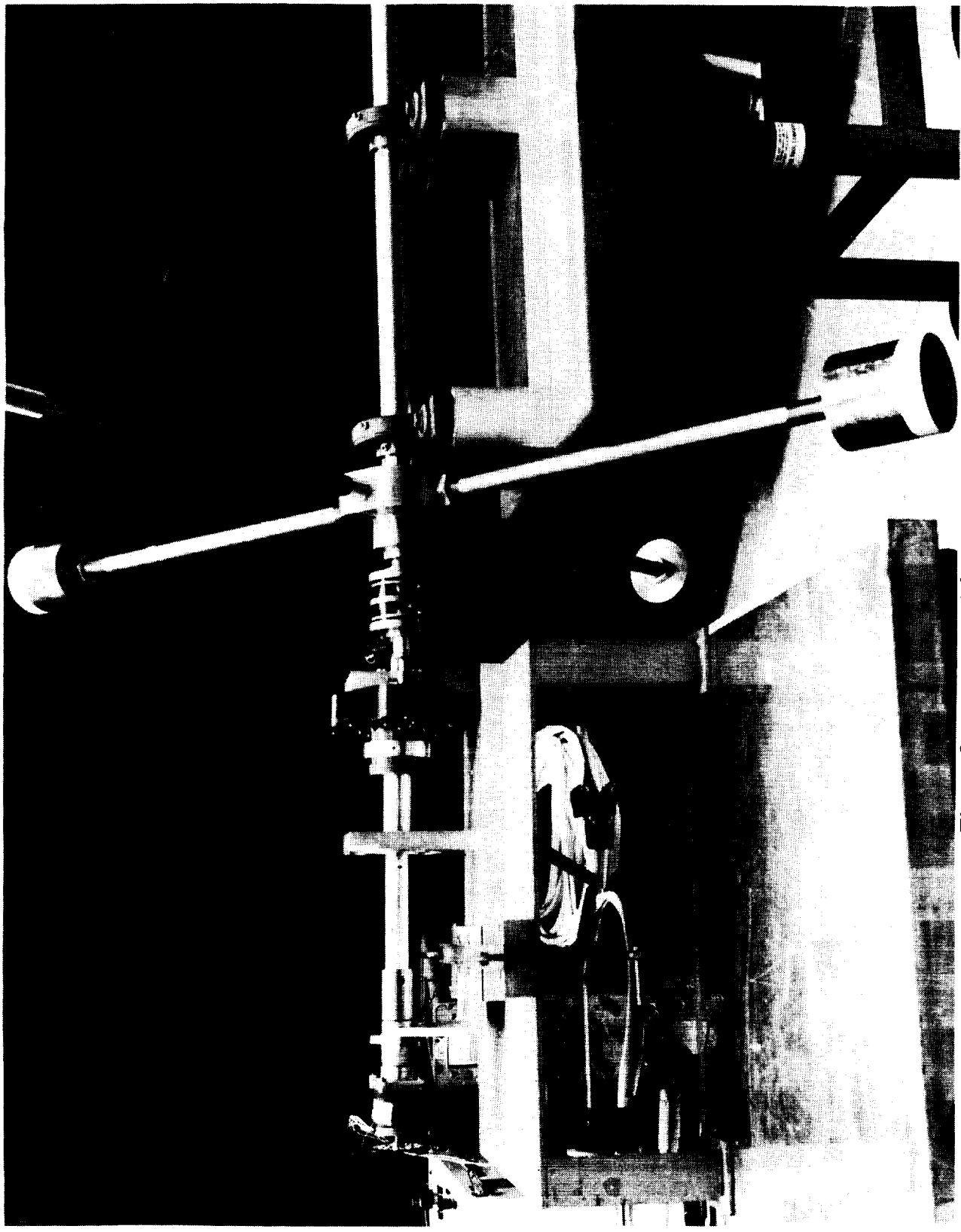

Figure 3. Power Module Driving Inertia

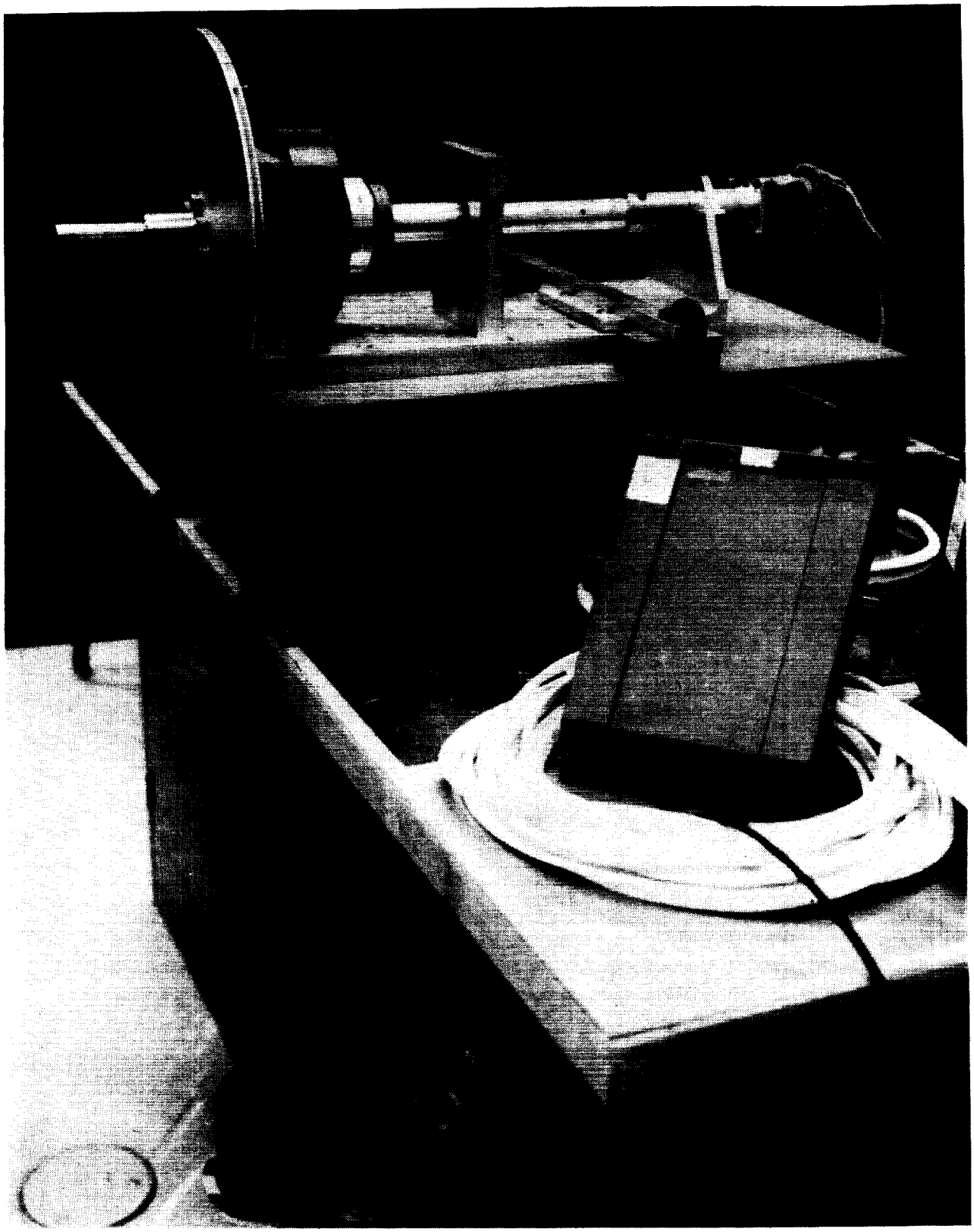

Figure 4. Torque Measurement

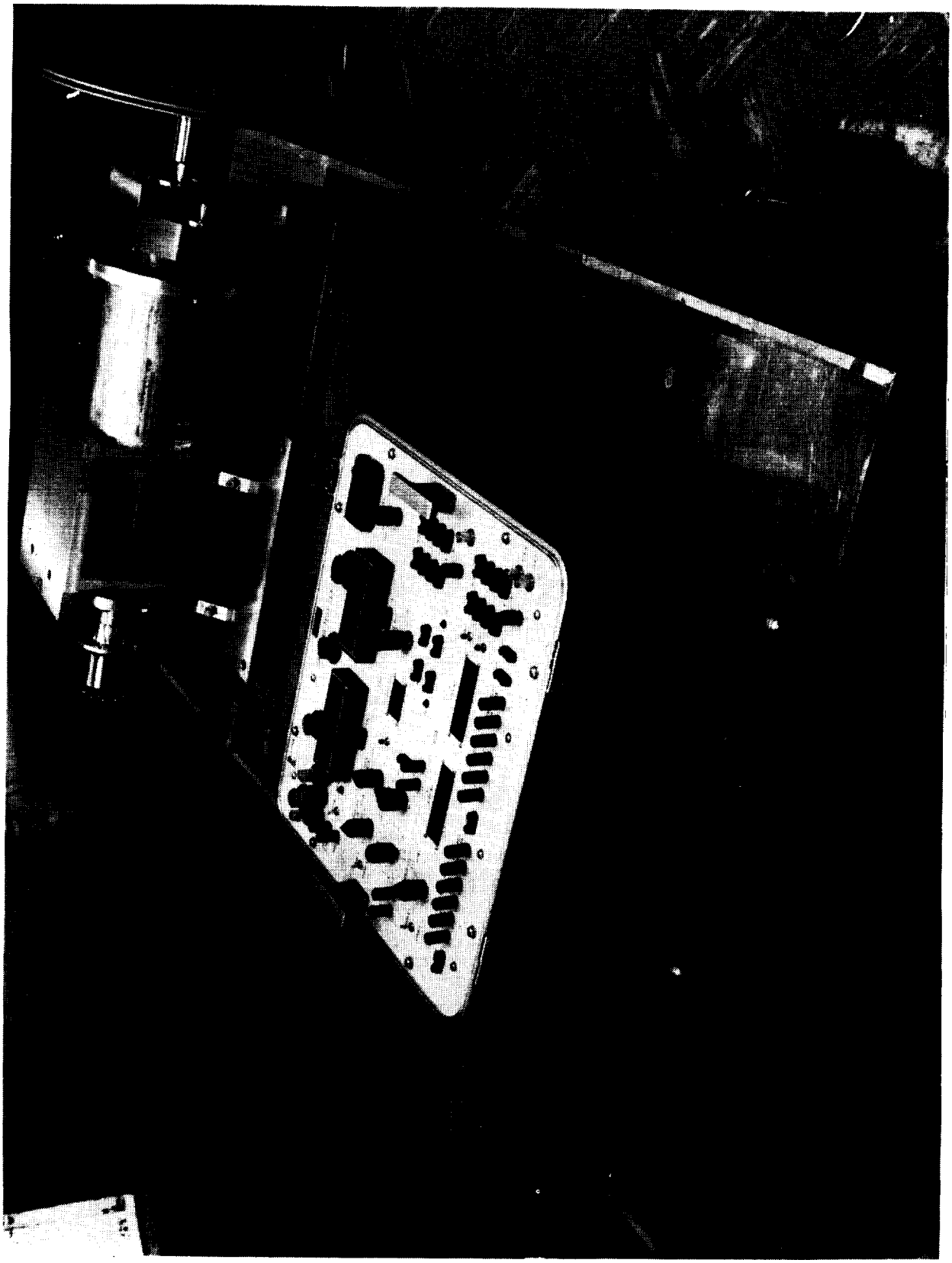

Figure 5. Power Hinge Development

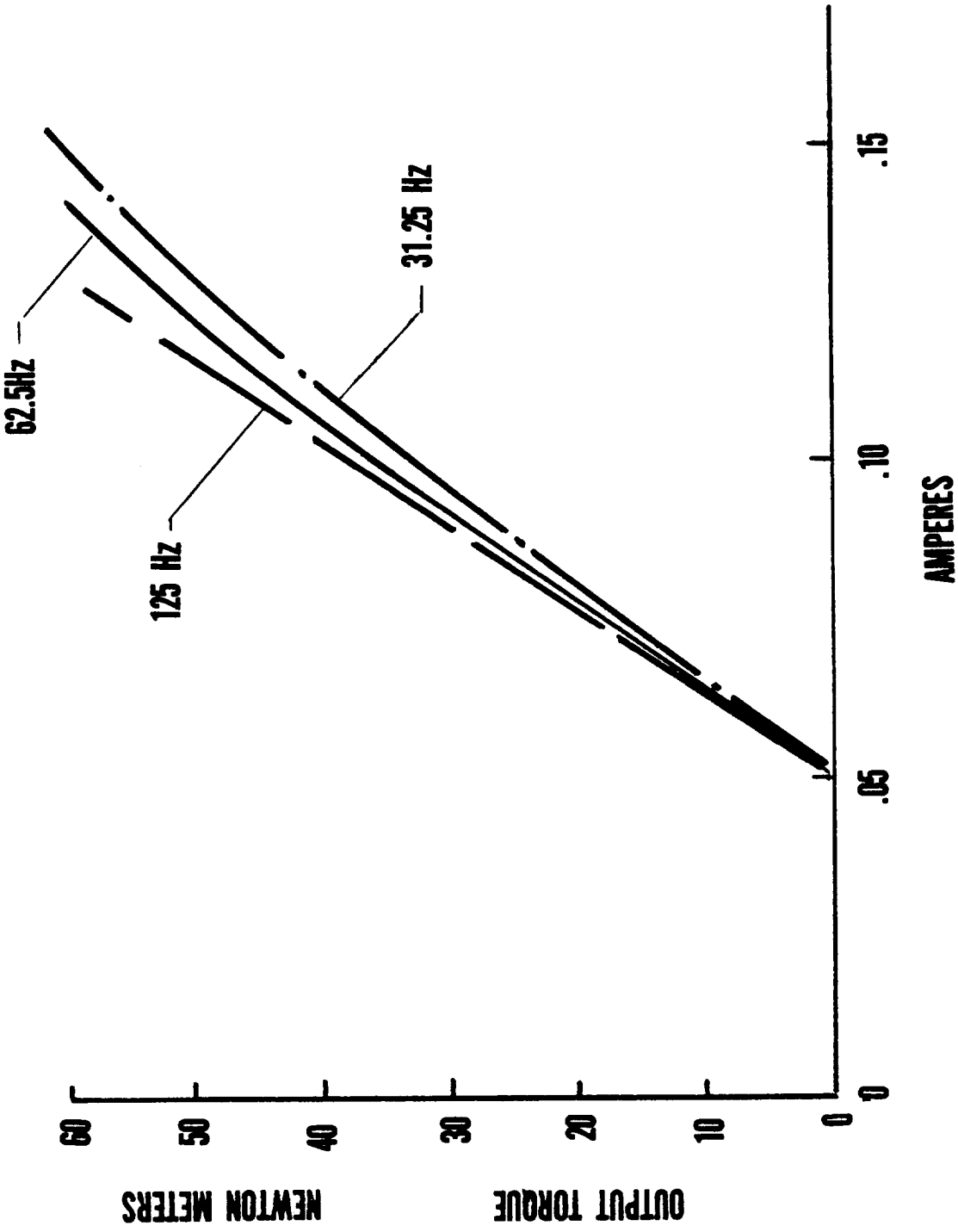

Figure 6. Performance of Power Hinge

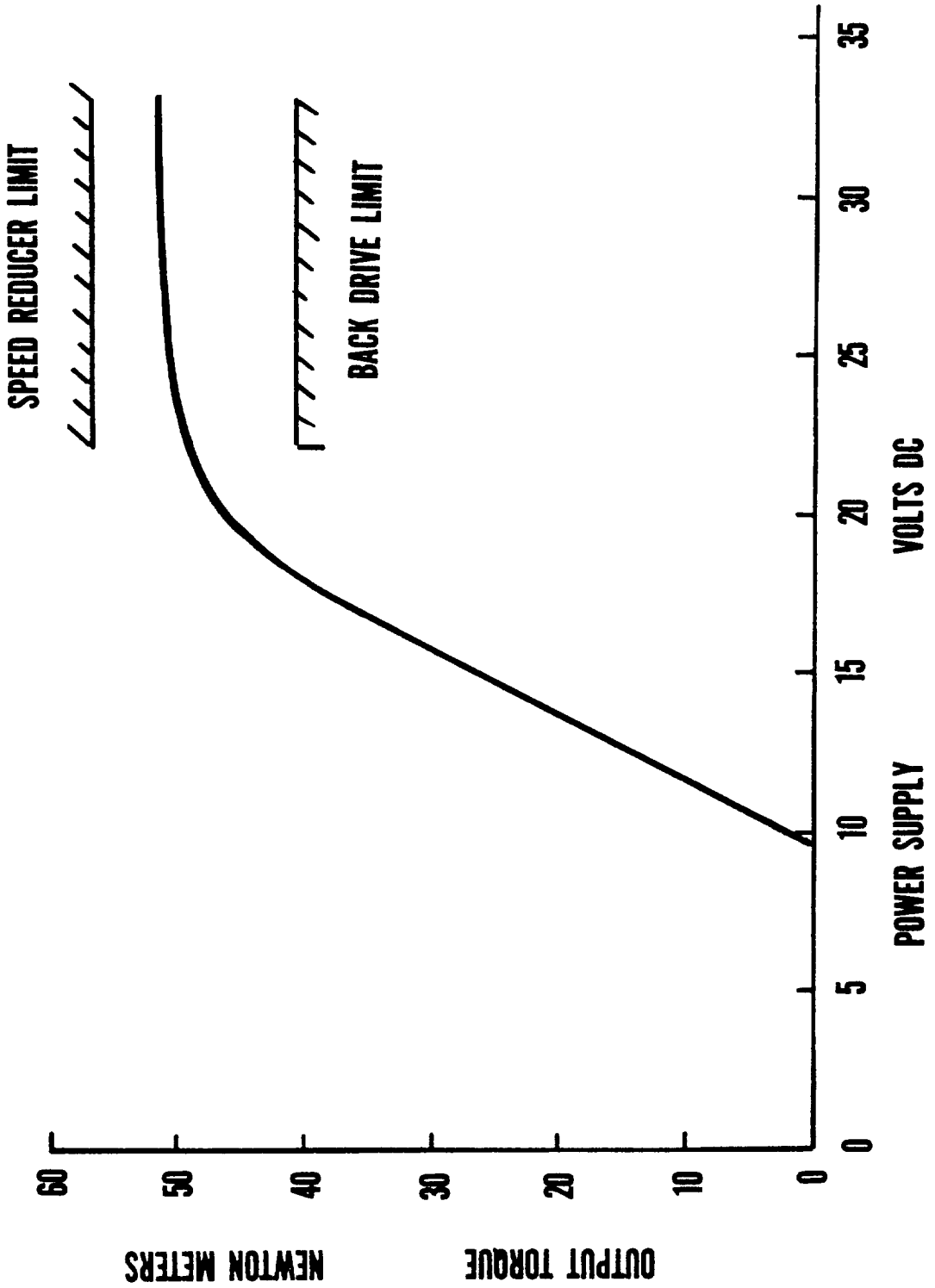

Figure 7. Performance with Regulated Power Supply

COMPARATIVE EVALUATION OF OPERABILITY OF LARGE SPACE STRUCTURE CONNECTORS

By Jack Stokes*

ABSTRACT

Several connector concepts have been undergoing evaluation in the Neutral Buoyancy Simulator at the Marshall Space Flight Center as part of the ongoing evaluation of the assembly of large space structures. Evaluation of the connectors was limited to operability during structure assembly. Parameters for evaluating the fasteners included subject comments and hardware damage. Evaluation results include a rank ordering of the candidates with descriptions of the acceptable and unacceptable points of each. General design recommendations established as a result of neutral buoyancy testing are defined. Recommendations include detailed hardware and operational design requirements.

INTRODUCTION

The Marshall Space Flight Center (MSFC) Neutral Buoyancy Simulator (NBS) has served as a test bed for various large space structure concepts over the last four years. Test requesters desiring to evaluate their various erectable, deployable, and fabricated structures relative to assembly operations have used this underwater test medium. The NASA Large Space Systems Technology (LSST) Project Office has collected assembly operations data from each of these simulations via "over-the-shoulder" monitoring for its Man/Machine Assembly Analysis. The purpose of this analysis is to determine the most cost-efficient assembly technique for any large structure or system. It addresses techniques ranging from totally manual to totally automated assembly methods.

In support of the test series, the NBS is equipped with a Shuttle cargo bay mockup, complete with an operational remote manipulator arm (Fig. 1). The manipulator is equipped with a standard end effector mockup or a special end effector, as required, e.g., opposed jaw end effector. An operational underwater mockup of the Manned Maneuvering Unit is also available.

Realistic structural assembly techniques, procedures, and timelines have been developed in the simulated space environment. The various structures have been evaluated relative to crew and RMS interfaces. Of specific interest are the various techniques for attaching structural members and utilities to form a completed space platform.

*NASA - Marshall Space Flight Center

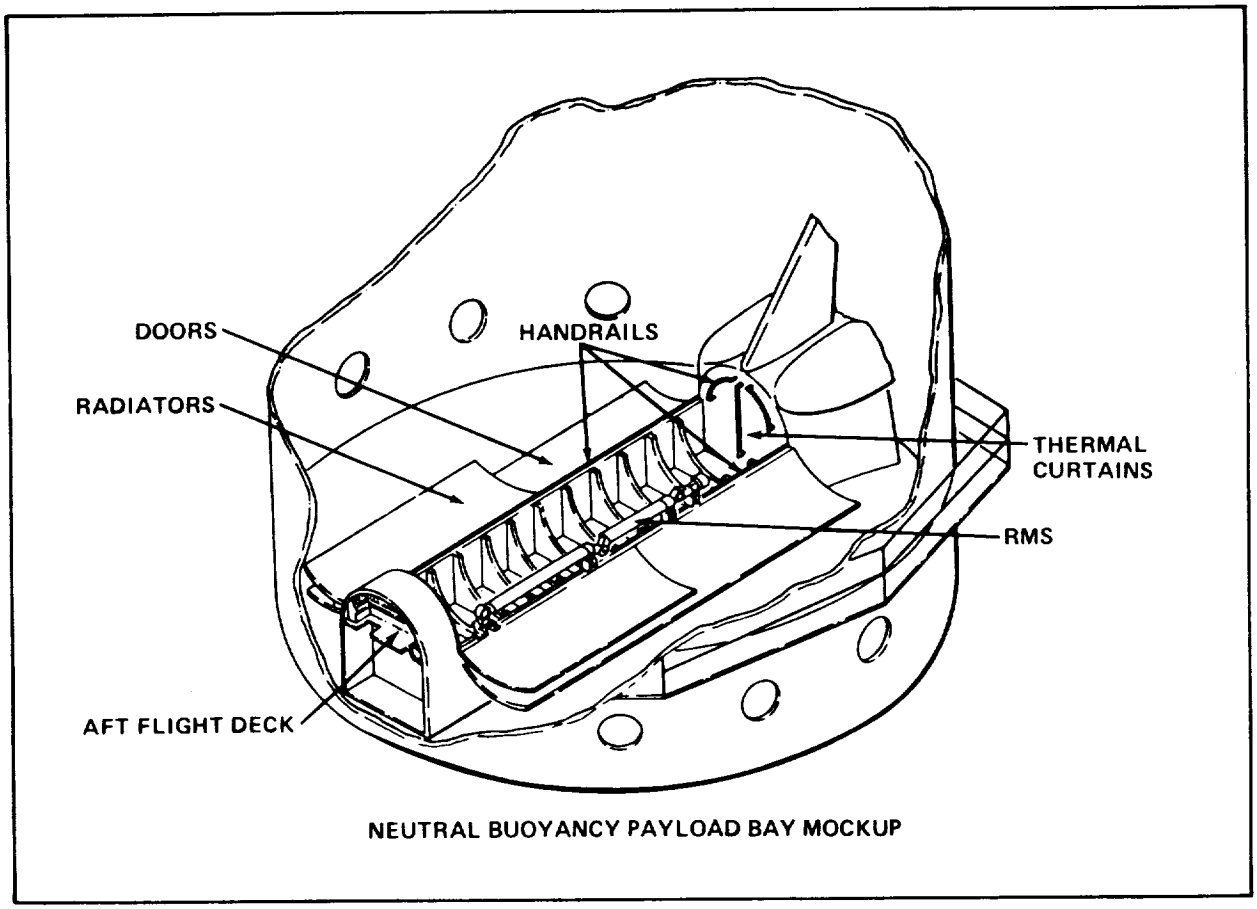

Figure 1. MSFC Shuttle Cargo Bay Neutral Buoyancy Mockup.

NOMENCLATURE

LaRC	Langley Research Center
LSST	Large Space Systems Technology
MSFC	Marshall Space Flight Center
MIT	Massachusetts Institute of Technology
NBS	Neutral Buoyancy Simulator
PVC	polyvinyl chloride
RI	Rockwell International

HARDWARE DESCRIPTION

The connectors addressed herein in order of testing include:

1) The MSFC spike connector

2) The RI electrical connector

3) The LaRC snap-joint union

4) The RI ball/socket connector

5) The MIT cluster slip-joint

6) The Essex lap joint

7) The Vought module-to-module coupler

8) The Vought automatic coupler.

The terminology of the seven connectors is that used by each test requester.

The MSFC aluminum spike connector (Fig. 2) was designed to position "fabricated" tribeams in the form of a prismatic truss. For assembly, the spike was inserted into a female receiver located in the end of a capped tribeam. Once inserted, the spike was retained by a T-handle retaining pin. Two of the three spikes per cluster were rigid, while the third had a compressible spring-loaded shaft which permitted the attachment of a rigid beam within a fixed space.

The RI electrical connector (Fig. 3), somewhat different from the other connector examples, is planned to suffice as a mechanical and electrical connector concept for a yet-to-be-defined space structure. This type of connector will permit the integration of power and data cables across structural members containing cable bundles. Once the beams are mechanically mated, they will permit power and data to be transmitted about the structure through an internal cabling system.

Four LaRC aluminum snap-joint unions, attached to aluminum cluster joints (Fig. 4), restrained 5.48 m (18 ft) epoxy-graphite beams in the form of a tetrahedron. The three base and upper apex snap-joint unions were firmly attached to a simulated assembly fixture. The test subjects were required to align and snap together the two connector components. Once the components were mated a rigid connection existed between the beam and the cluster.

The RI ball/socket connector was used in a similar assembly technique. It also restrained beams [9.14 m (30 ft) long cylindrical aluminum members] in a tetrahedral form. The assembly fixture for the RI structure required only two base connectors (along the cargo bay sill) in contrast to the four required for the LaRC tetrahedon. As depicted in Figure 5, the node or ball attached to the beam end was placed into and restrained by the socket. The sockets were arranged on the connector cluster in a geometry which permitted a tetrahedral assembly of the beams. The ball was initially loosely captured in the socket, with approximately 30° alignment error available. Rigidization of the connector was accomplished by hand screwing a large jam nut which butted against a flat socket plate.

The MIT structure was assembled by attaching 3.0 m (9.84 ft) PVC columns together using sliding sleeve lock joints. Even though a flexible joint was initially evaluated, all subsequent evaluations used a rigid connector, as depicted in Figure 6. All references and discussion concern this latter design, which has continued to receive minor modifications through the various tests. The connector consisted of two tubular members, one with an alignment node at the end and the other with a matching receiver for the node. Once the node of one connector component was positioned in the receiver of the other, the

sliding sleeve lock was moved by the crewman over the two shafts to rigidize the members together. In the initial concept the sliding lock was to the cluster component. In later variations, the sleeve was attached to the beam component. A central cluster and 12 perimeter clusters consisting of various members of tubular connector components were required for structure assembly.

A fastening device, an end cap, developed by the Essex Corporation, was designed for capping tribeams fabricated by the MSFC/Grumman beam machine. The end caps and the beams were restrained by the RI ball/socket connector. Therefore, it shall not be further addressed in this paper, as that connector has been previously addressed. However, the Essex-designed lap joint is of interest, in that it permitted the attachment of two fabricated tribeams at perpendicular angles to each other. As depicted in Figure 7, the test subject had to position the square lap joint to one face of a tribeam. The lap joint was temporarily restrained by alignment tabs. Once the lap joint was restrained to the beam face, the subject attached four overcenter fasteners (two per longron) which rigidized the beam to the lap joint. The second beam was then positioned 90° to the longitudinal axis of the first beam, and the same attachment procedure was performed.

Two connectors of interest were designed and manufactured for testing by the Vought Corporation. The first was an interconnect device which, when used in unison with three others on the structure end face, attached deployable modules together. As depicted in Figure 8, the module-to-module coupler was a quick-connect probe-drogue device, which had a self-locking capability and could accommodate a ten-degree misalignment error. The other fastener, a quick-connect coupler (Fig. 9),was also a probe-drogue device which permitted the attachment of a fixed-length strut in a fixed space without the need for a compressible end fitting, such as the MSFC spike connector. Spring-loaded pins in the probe slid into a grooved guide in the female receptacle until the pins locked into centering holes, thus restraining the probe in the drogue.

CONNECTOR ASSESSMENT

The eight connector concepts were evaluated relative to operability. No consideration was given to the structural or materials qualifications of each. Such information may be obtained from the various test requesters or from the author.

The numerical ranking of each connector, as indicated in Table 1, is a subjective rating by the author, based upon neutral buoyancy test observations and test subject comments occurring during the tests and during the debriefings. Also, connector or structure damage resulting from difficulties in mating the connector components is a consideration in making the assessments. Any rating is open to discussion and is intended as an estimate based on qualitative results.

The various comparison parameters or considerations of the evaluation are described, along with assessment of each connector relative to each parameter. The assessment is summarized in Table 1. Each connector is ranked per evaluation parameter, with the highest number (10) considered the best connector for that parameter and the lowest number (1) representing the worst for the

TABLE 1. RANK ORDER OF CONNECTORS RELATIVE TO OPERABILITY

CONNECTOR	STRUCTURE	CONNECTOR SIMPLICITY		EASE OF ASSEMBLY				EASE OF DEMATE	FRAGILITY	CREW SAFETY	TOTAL
		ASSY CLARITY	TRNG REQ'D	EASE OF ALIGN.	EASE OF MATE	CONN. MATE VERIFIC.	CREW RESTR. REQ'D				
MSFC SPIKE CONNECTOR	PRISMATIC TRUSS	6	5	5	3	3	5	3	4	2	36
RI ELECTRICAL CONNECTOR	FLEX CABLE TO TASK BOARD	3	3	8	3	3	5	8	3	8	44
LaRC SNAP-JOINT UNION	TETRA-HEDRON	7	4	5	4	2	4	4	2	7	39
RI BALL/SOCKET CONNECTOR	TETRA-HEDRON	9	9	9	9	9	9	5	9	9	77
MIT CLUSTER SLIP-JOINT	AREA STRUCTURE	6	5	8	6	8	9	9	5	7	63
ESSEX LAP JOINT	PRISMATIC TRUSS	5	5	8	5	9	8	7	2	9	58
VOUGHT MODULE-TO-MODULE COUPLER	DEPLOYABLE TRUSS	9	9	9	8	9	9	6	8	9	76
VOUGHT QUICK-CONNECT COUPLER	DEPLOYABLE TRUSS INTER-CONNECT MODULE	8	6	9	7	7	9	9	6	9	70

parameter. A summary total of the ranking points for each concept appears in the far right hand column. This number represents the overall evaluation ranking for each connector, with the highest number representing the most operable connector and the lowest number indicating the least operable. Operable in this case is defined as the combination of five comparison parameters: connector simplicity, ease of assembly, ease of demate, fragility, and crew safety.

All of the connectors basically performed the required assembly tasks, some more effectively than others.

Connector Simplicity

The first comparison parameter was devised to indicate how obvious the mating technique for a connector was to the test subject or operator. It is assumed that the more simple the connector, the more obvious its attachment and/or separation. This parameter is subdivided into two parameters: "Assembly Clarity" and "Training Required." The former considers the intuitiveness of the operator to make the connection, while the latter considers the degree of training required to verify that the operator would not damage the connector or harm himself while successfully completing the operation. The most simple connectors being most obvious to mate, and the ones requiring the least training to mate were the ball/socket connector and the module-to-module coupler. It was apparent for each connector that the node was to be inserted into the receiver, to be accomplished without significant skill. In descending order of rank relative to assembly clarity were the quick-connect coupler, the snap-joint union, the cluster slip-joint connector tied in rank with the spike connector, the lap joint, and finally the electrical connector. Relative to training the ranking in descending order was the quick-connect coupler, followed by a tie among the spike connector, the cluster slip-joint connector, and the lap joint, followed by the snap-joint union, and finally the electrical connector. It was not intuitively obvious that the hand grip of the electrical connector shaft had to be pulled to make the electrical mate. The lap joint required several phases of assembly, as well as having somewhat confusing over-center latches. The snap joint union required some training so that the operator could verify that the connector was fully mated.

In general, there were no real difficulties in understanding or learning how to operate the candidate connectors.

Ease of Assembly

This consideration addressed the ease with which the test subject could align and mate a connector. It is somewhat related to the previous parameter. However, it was demonstrated on several occasions that subjects had difficulties in assembling some connector components even with thorough training.

Four subparameters fall under Assembly Ease. They are, "Ease of Alignment," "Ease of Mate," "Connector Mate Verification," and "Crew Restraints Required."

Ease of Alignment is concerned with alignment of the connector components prior to connection. A connector which required little or no alignment was considered better than one which required close alignment. It was possible to mate fairly simply all evaluated connectors. Three connectors (ball/socket connector, module-to-module coupler, and quick-connect coupler) were rated highest, followed immediately by the electrical connector, the cluster slip-joint and the lap joint. The least easy to align were the spike connector and the snap joint union.

Once alignment was accomplished, ease of mating was addressed. Considered here was how easily the components mated. Variables affecting ease of mating were skill and/or strength required to mate the components. Highest ranking was given to those connectors which went together with the least effort. The most easily mated connector was the ball/socket connector, followed closely by the module-to-module coupler, then the quick-connect coupler. Next in order were the cluster slip-joint, lap joint, and snap-joint union. There was a tie for last between the spike connector and the electrical connector.

As connector mating occurred, the operator required feedback as to whether the connector was properly assembled. All connectors required a visual inspection to verify mating; however, some could be verified by feel.

A three-way tie for the highest ranking was among the ball/socket connector, the lap joint, and the module-to-module coupler. Immediately below came the cluster slip-joint followed by the quick connect coupler. Then much lower in the rating fell the spike connector and the electrical connector, with the snap-joint union ranked lowest.

The final subparameter for ease of assembly was whether crew restraints were required for the test subject to mate the connector. The highest rating was for that connector which could be assembled by the subject without the aid of foot restraints or handholds other than the structure itself. Four candidates were tied for top position. They were the ball/socket connector, the cluster slip-joint, the module-to-module coupler, and the quick-connect coupler. Immediately below in the ranking was the lap joint, rated slightly lower because of its size and bulkiness. The spike connector and electrical connector were rated significantly lower because the operator required much more body stability to complete assembly, though foot restraints were not absolutely required. However, foot restraints were required for the lowest ranked fastener, the snap-joint union.

Ease of Demate

Though most connectors were not designed for planned separation, or demating, this function must be considered for contingency purposes. The quick-connect coupler and cluster slip-joint were considered the easiest to separate, and therefore received the highest ranking. The electrical connector was ranked just below because it required some stabilization of components and of the operator to break the connection. The lap joint was next, as release of several latches was required to separate the beams. The module-to-module coupler ranked next lowest. This would have been ranked higher if more room had been available between the connector and structure to perform the release function. The ball/socket connector ranked next lowest, as a tool was required

to release a restraining latch in order to release the ball. Following the ball/socket connector was the snap-joint union, which also required a tool to release the segments. However, a definite alignment skill was required. Lowest ranked was the spike connector, as it was extremely difficult for the operator to compress the spring in the spring-loaded spike to release the connector from its beam.

Fragility

The parameter of connector fragility is an assessment as to the ruggedness of the connector during the mating or demating operation.

"Sensitivity to structural alignment" is deemed an important consideration under fragility, because it has been determined in neutral buoyancy testing that connector segments require some free play when initially mated in order to prevent overloading of the partially made connector by the operator or by the structure members. The less the flexibility between components during mating and demating, the greater is the risk of damaging or failing the connector.

Ranking of the connectors relative to fragility is as follows. The connector providing the most flexibility following initial component mating was the ball/socket connector, which provided misalignment flexibility of approximately 30° in all directions about its centerline. The module-to-module coupler was ranked next highest, with misalignment adjustment of 10° in any direction. There was very little flexibility in the rest of the connector concepts. The next lower ranked cluster slip-joint provided some minor adjustment prior to closing of the sleeve. The spike connector was ranked next lowest, as it had some alignment flexibility as the probe tip was initially inserted into the receiver in the end of the beam. The electrical connector was ranked next down, as alignment was critical in order to make the electrical connection. The electrical connector was not integrated into a structural member; hence, it was not possible to assess any potential hardware damage occurrences.

The lap joint and the snap-joint union were rated lowest, as hardware damage occurred with each during mating. The lightweight beam braces were susceptible to damage if any misalignment occurred between beams during lap joint connection. The tabs on the snap joint were susceptible to bending or fracture if the beams were at all misaligned during connector assembly.

Crew Safety

The final parameter of comparison is one of the most important, that being crew safety. The large majority of the candidates were considered safe to operate by a pressure-suited crewman. The ones judged best were the ball/socket connector, the lap joint, the module-to-module coupler, and the quick-connect coupler. The electrical connector was rated slightly lower only because it has electrical power close to the crewman. However, it nominally appeared safe. The snap-joint union and the cluster slip-joint were rated slightly below the electrical connector, because conceivably one might inadvertently pinch a glove between the sliding components, though this situation has yet to be demonstrated. By far, the worst design relative to safety is the spring-loaded spike

connector. The spike throw was approximately eight inches with sufficient force to penetrate a pressure suit. This concept, as presently designed, is the only one unequivocally recommended to be dropped from consideration for larger structures assembly.

CONCLUSIONS

Of the eight large space structure connector concepts evaluated, the Rockwell ball/socket connector was ranked highest overall for operability, followed very closely by the Vought module-to-module coupler. In descending order below these two concepts were the Vought quick-connect coupler, the MIT cluster slip-joint, the Essex lap joint, the Rockwell electrical connector, LaRC snap-joint union, and finally the MSFC spike connector.

It should be understood that two connectors, specifically the electrical connector and the ball/socket connector, were early prototypes and as such were incomplete in design. Likewise, the spike connector and the cluster slip-joints were concepts only and not actually considered for flight. Development effort on the snap-joint union has continued and a slightly modified version will be tested in the near future at MSFC. The module-to-module coupler is seriously being considered for a flight design. The quick-connect coupler, though not presently planned for flight, has great potential and should be considered for use where appropriate.

In summary the following general connector design recommendations are made.

o First and foremost, the connector should be completely safe for crew operation. A design goal should be that no stored energy shall exist in any of the components prior to, during, or following mating of components. If stored energy components do exist, the energy level should be kept to a minimum.

o Connectors requiring mating by a crewman should be hand-operated without the necessity of tools. Likewise, release of the device should be by hand, or, at the most, a simple tool. Assembly should require one hand only. Connector mating should occur without the need for additional crew restraints or assembly aids.

o The components should be attachable without critical alignment being a requirement. As a design goal the connector should be capable of being made without visual access.

o Since pressure-suit gloves are very bulky and difficult to operate, the connector should require very low effort by the crewman to attach the components.

o The connector should be assembled in a two-step process. The components should be initially restrained together, but with alignment flexibility among the components. Once structure final alignment is complete, the connector components should be lockable.

o The crewman should have a positive indication that the connector has been made, either through feel or visual access.

o If a connector has a cluster of similar components, it should be immediately obvious to the crewman which components properly mate.

o Design consideration should be given to transporting groups of connectors so that they can be easily controlled without harming the crewman or damaging either the connector or the surrounding hardware, and be removable from the stowage apparatus in order of need.

o Connector operation should be intuitively obvious, and require minimal crew training.

o Forethought should be given to connector design if the connector will be exposed to multiple cycles or harsh environments, such as underwater. Data gathered from the test environment or as a result of test conditions may not be directly applicable to one-time assembly in space.

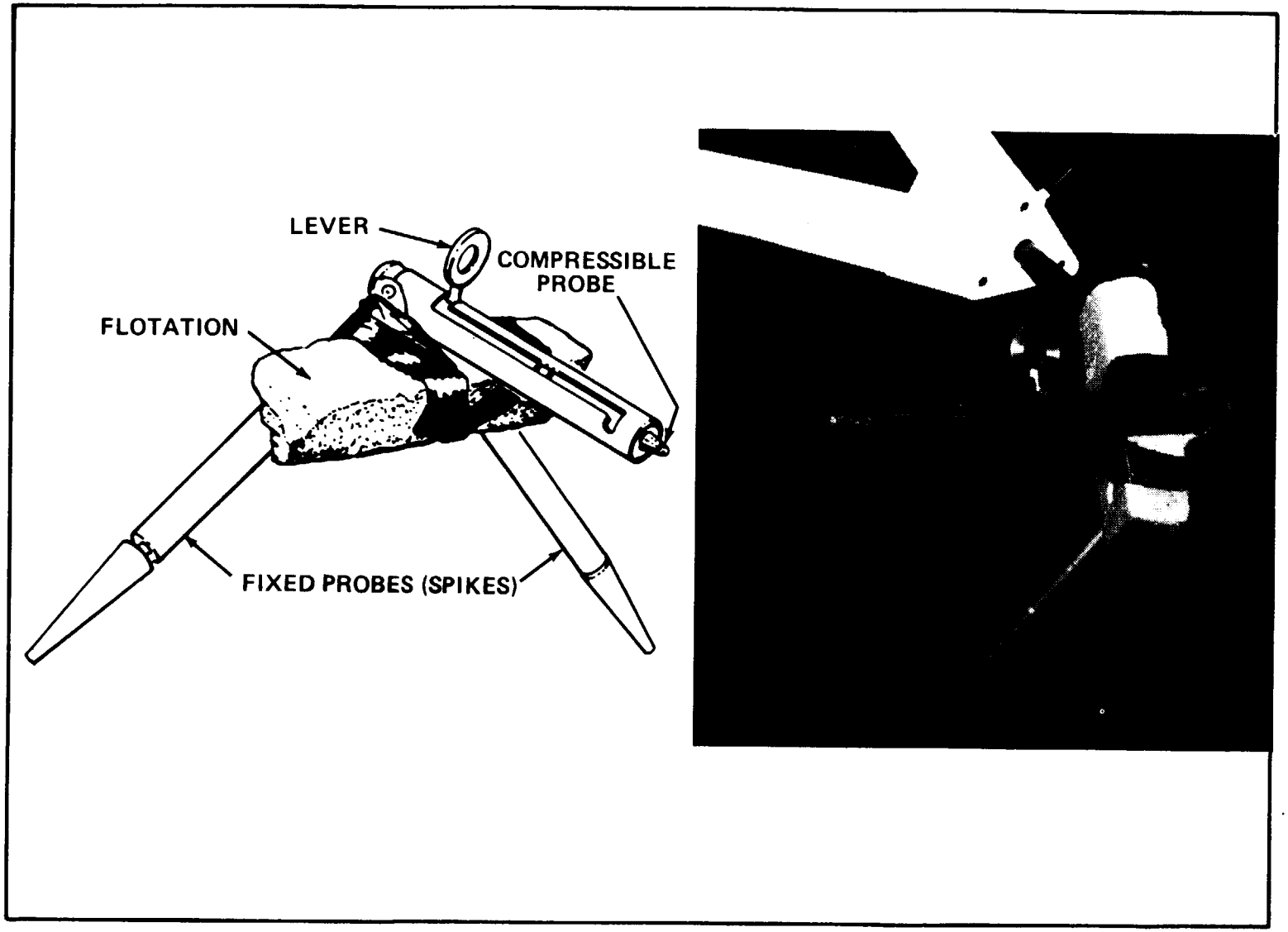

Figure 2. MSFC spike connector.

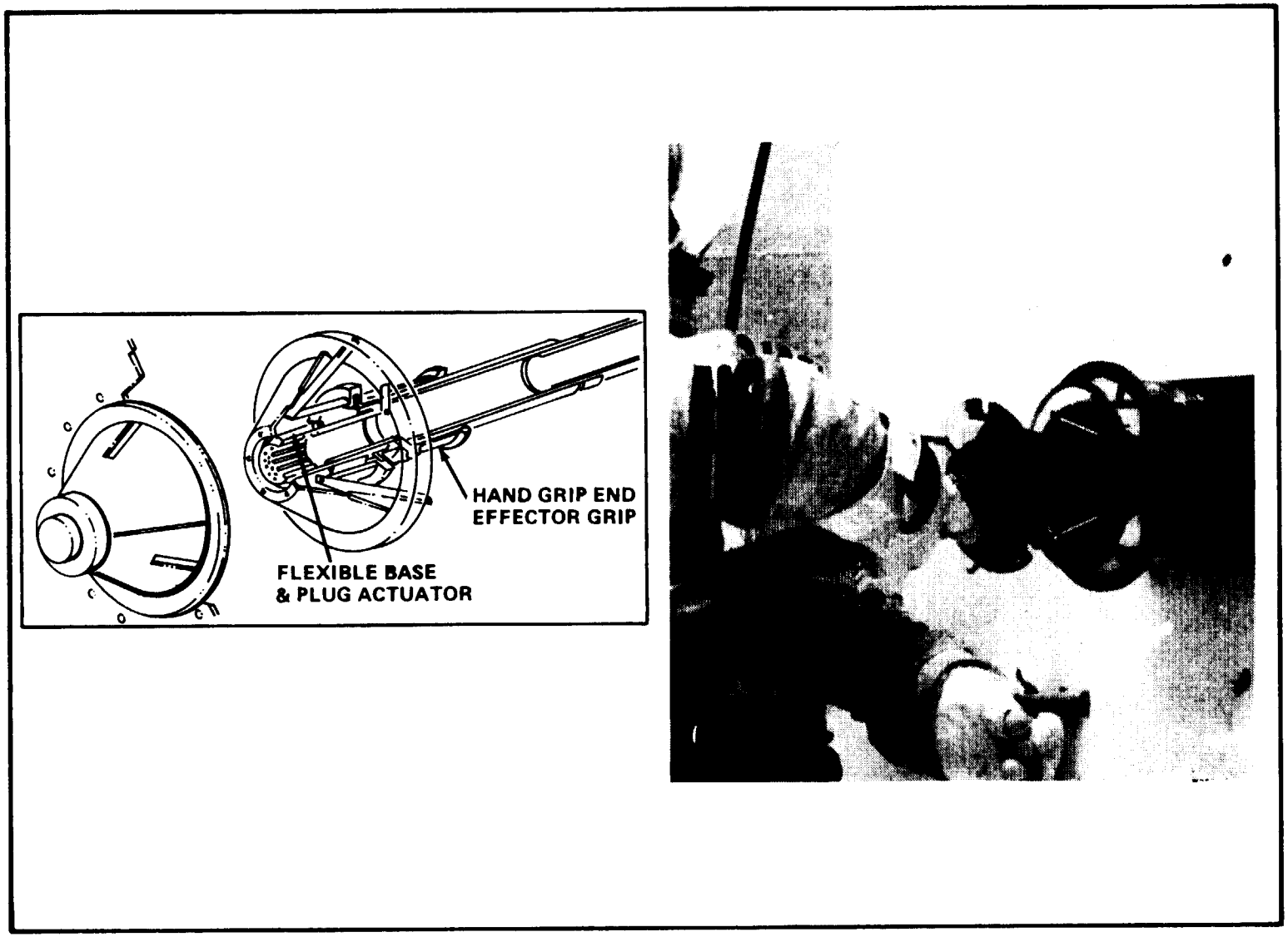

Figure 3. RI electrical connector.

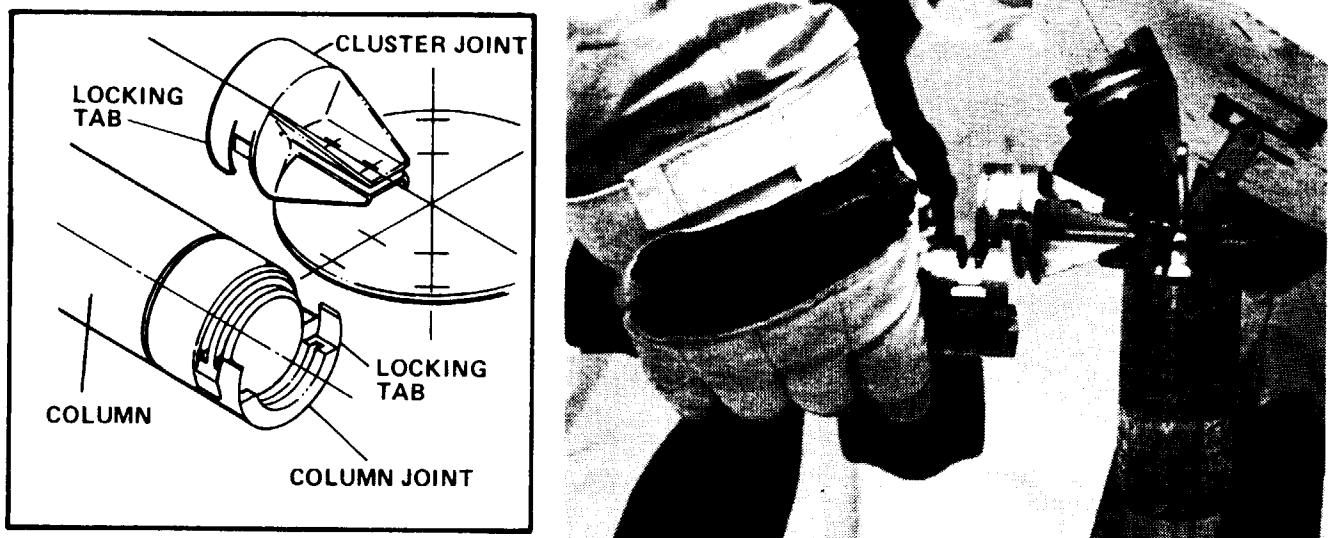

Figure 4. LaRC snap-joint union.

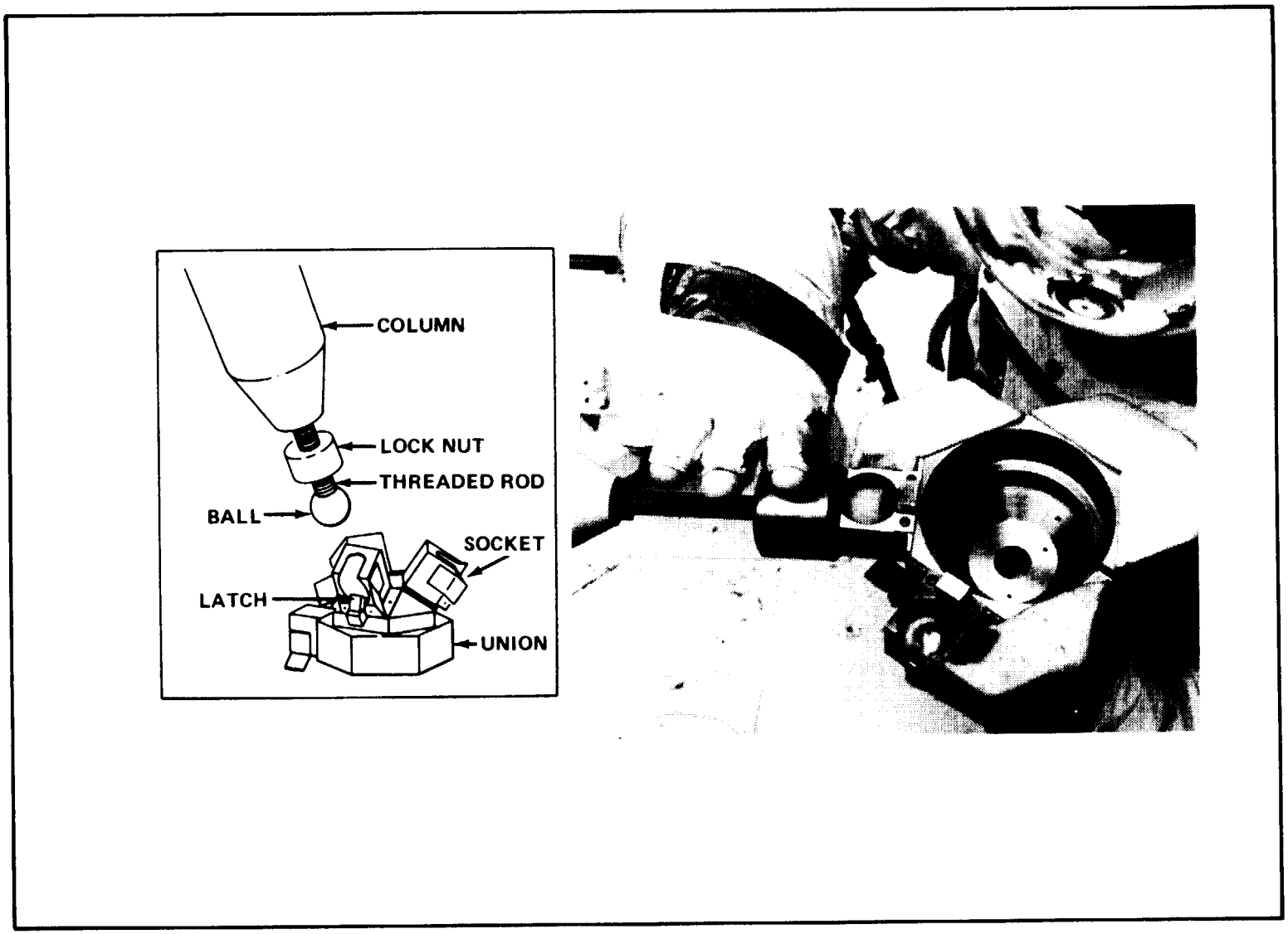

Figure 5. RI ball/socket connector.

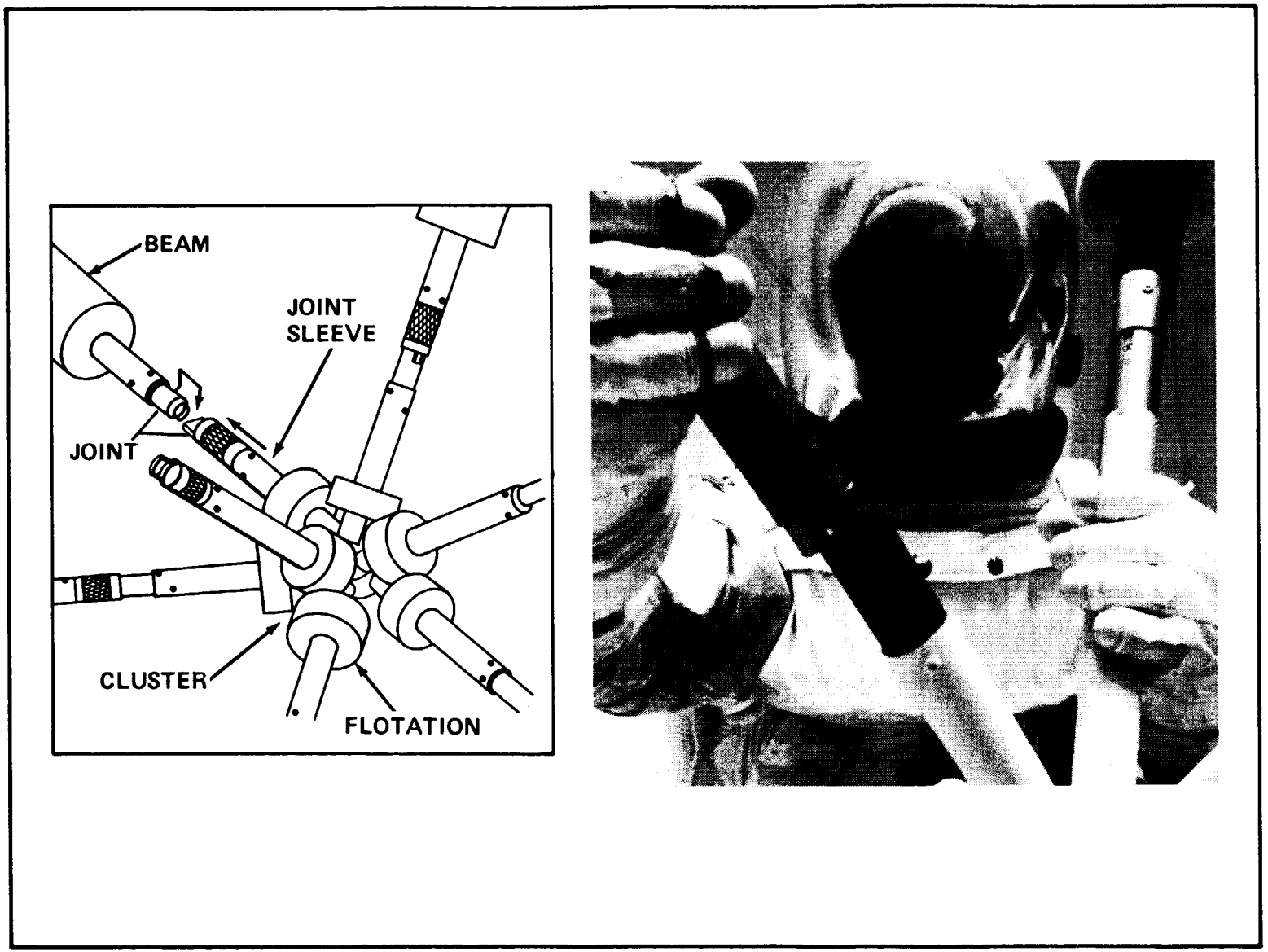

Figure 6. MIT cluster slip-joint.

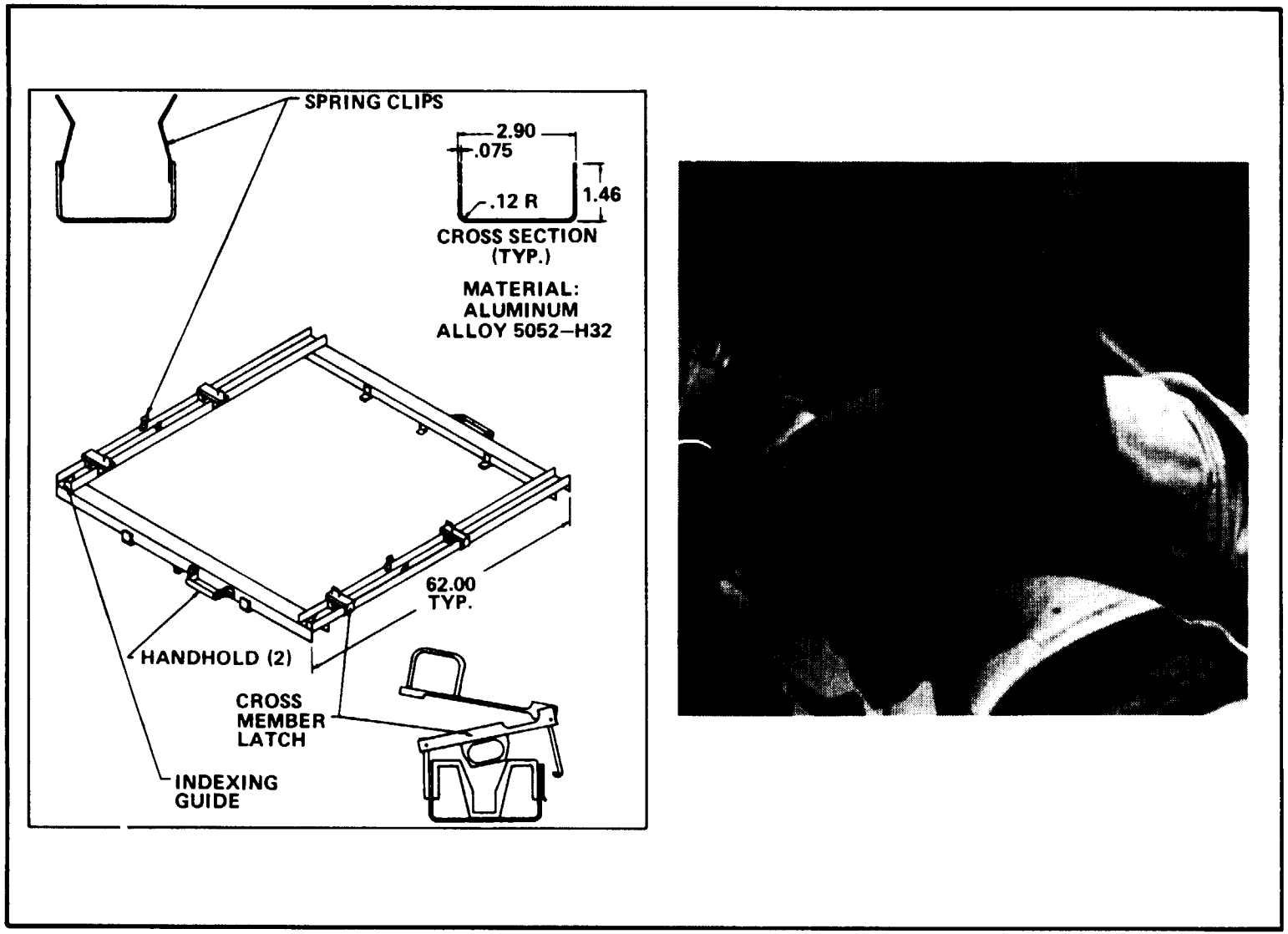

Figure 7. Essex lap joint.

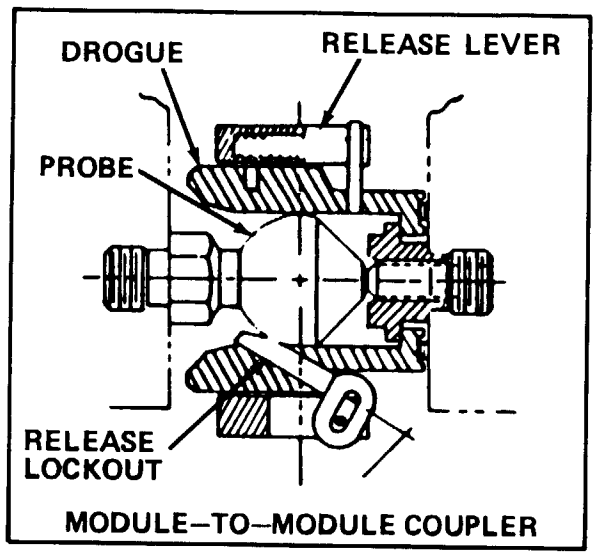

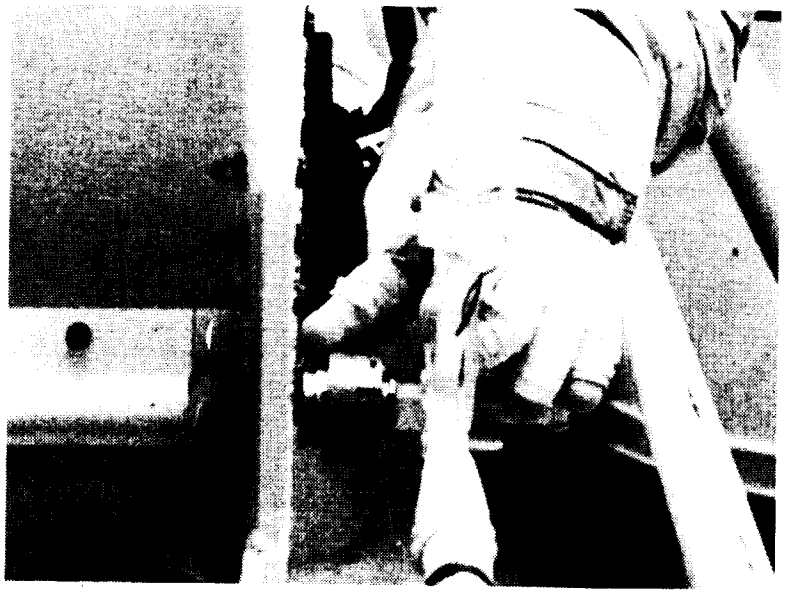

Figure 8. Vought module-to-module coupler.

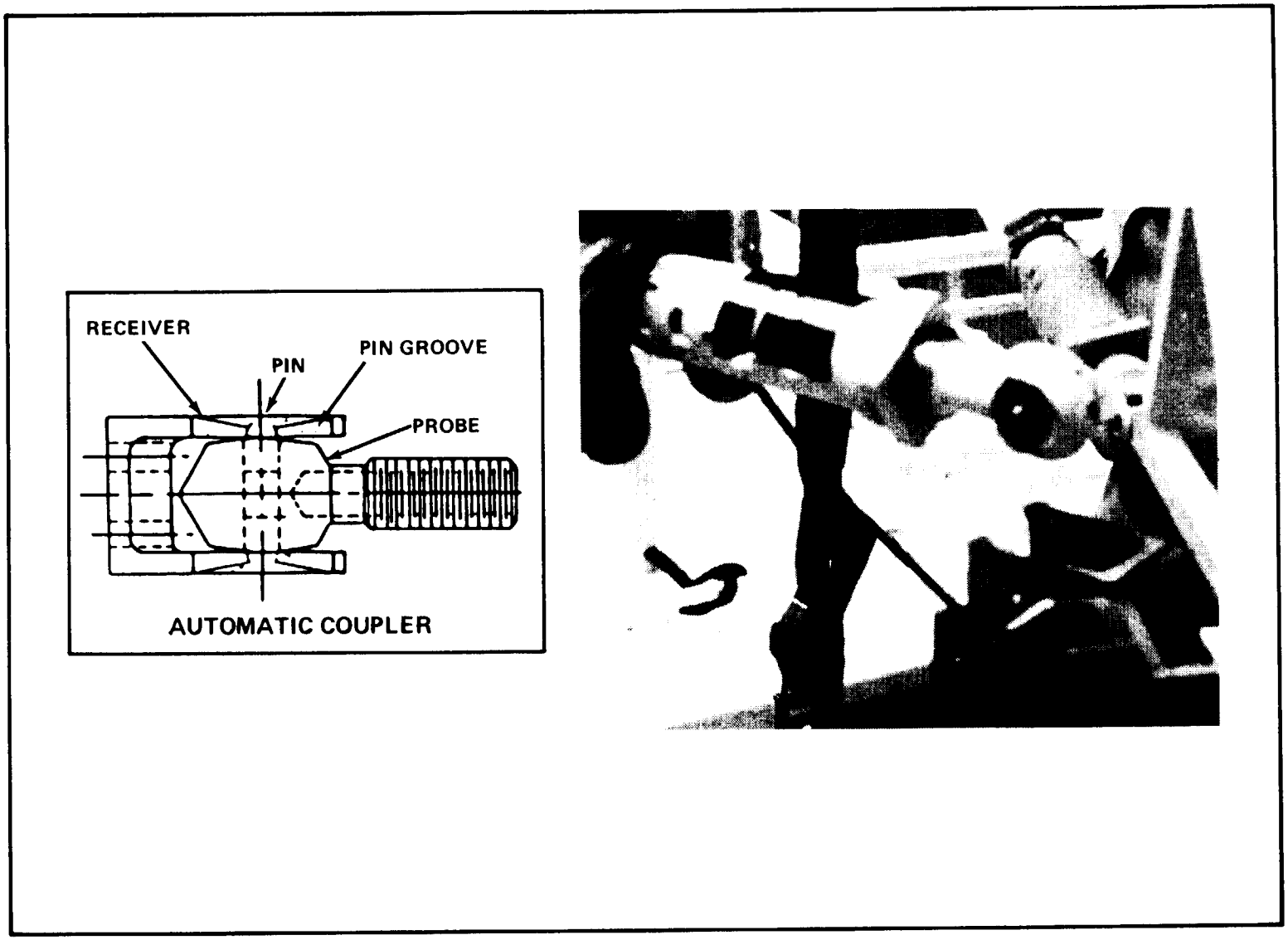

Figure 9. Vought quick-connect coupler.

A CLAMP MECHANISM FOR DEPLOYABLE THREE-TON PAYLOADS

R. Birner* and H. Ral*

ABSTRACT

The requirements, capabilities and unique design features of the IPS Payload Clamp Assembly (PCA) are presented. The PCA is designed to have the flexibility to accommodate a wide payload range varying from 0.5 m to 3 m in diameter and from 500 kg to 3000 kg mass. This is being achieved by modular clamp design in connection with replaceable struts. The design features include clamping of payload in a statically determined way and actuation of clamp latches by means of single linear actuator via ropes. The vibration and TV environmental conditions for the mechanism are extremely severe. A structural and prototype model has been built. The qualification testing is in progress. Test results of the operating characteristic are presented. In addition, problems of tribology are highlighted.

INTRODUCTION AND DESIGN REQUIREMENTS

In the frame of the development of IPS (Instrument Pointing Subsystem), which is designed to facilitate extremely precise pointing of payloads in orbit and flown on the shuttle, the design had also to provide for clamping and deployment of these payloads (P/L). The mechanisms described in this paper were developed by MBB which subcontracted the clamp units to Contraves. According to the task of IPS, a payload of up to 3000 kg had to be held in statically determined way within a standard pallet of the shuttle during ascent and descent and to be deployed and stowed for on orbit operation.

Furthermore, it was required to decouple the payload from the gimbal subsystem during ascent and descent in order to avoid dynamic impact and to minimize forces introduced to the P/L.

Deflections of the pallet had to be considered such that mainly tangential forces are introduced into the P/L.

The mechanisms which should release the P/L attachment elements had to be activated electromechanically, as hydraulic and pneumatic devices were considered to be not suitable with respect to the wide specified temperature range from -150°C up to +120°C, because of outgassing requirements and some other reasons such as power supply-, control-, weight- and maintenance-problems. In case of failure in the activation system automatic clamping of the P/L by spring force should be possible by EVA.

An overall View of IPS is shown in Fig. 1.

*Messerschmitt-Bolkow-Blohm GmbH, Germany

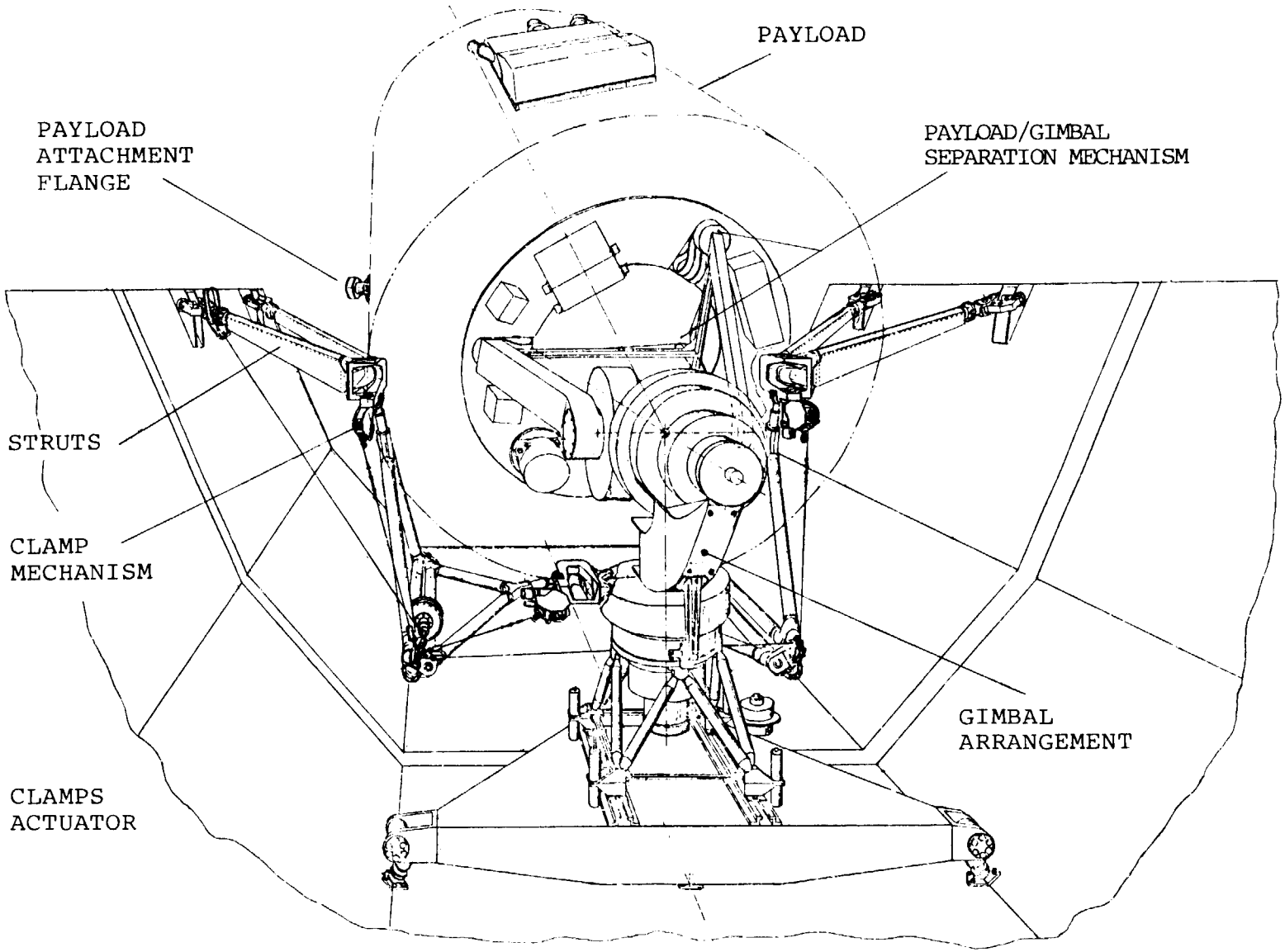

Figure 1: IPS - Overall View

CONCEPT DEVELOPMENT

During the design definition phase of the IPS-Project, an optimum had to be found for the four main mechanical requirements.

- statically determined load transfer from P/L to a deflecting pallet
- deployment and clamping of the payload
- stowage and gimbal decoupling
- flexibility for size and mass of payload

The design approach for the first requirement was a P/L suspension shown in Fig. 3 which allows translational and rotational deflection of each clamping point consisting of the Clamp Unit and the Payload Attachment Flange (PAF). In parallel to this, the following two concepts for P/L stowage operation were considered (see Fig. 2)

A) positioning of P/L vertically into clamps, clamp P/L, separate gimbal system from P/L

B) positioning of P/L in front of clamps, push P/L horizontally into clamps by P/L-gimbal separation mechanism, clamp P/L

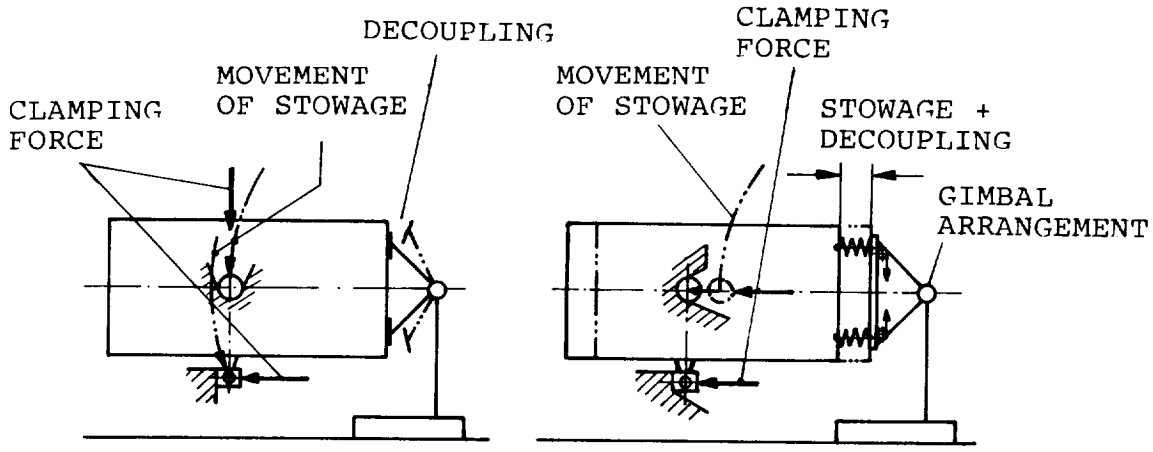

Figure 2: Payload Stowing Concepts

Solution A requires a high torque of the gimbal motors depending on P/L length for guiding it into the clamps. The reason for this is a certain force for guiding of spring-loaded elements on the P/L which must be implemented to cover pallet deflections, when the P/L is stowed.

A second disadvantage is the necessity to introduce a very complicated mechanism for decoupling the P/L from the gimbal system.

Solution B requires positioning of P/L in front of clamps.

Pushing of P/L into clamps is performed in connection with separating the P/L from gimbal system. So two actions are accomplished simultaneously.

Another advantage is the independence of guiding force from P/L dimensions to be provided by the separation mechanism.

For guiding of the P/L into the clamps during stowage, all three gimbal axes have to be controlled with full motor power. That means that also in emergency case the nominal power must be available.

However, if this is not the case, the P/L can be positioned suitable for latching by subsequent turning around each of the gimbal axes into resolver zero position and clamping with emergency power.

For these reasons the solution B was chosen.

As a consequence of this and the stowage direction identical with P/L-centre line (i.e., shuttle roll-axis) clamping points had to be arranged within a plane vertical to that axis.

Having in mind the requirement for P/L flexibility and statically determined fixation of the P/L within the shuttle pallet, a compromise between centric load transfer by the struts from clamp units to pallet and functional requirements for PAF's and clamping mechanism had to be found.

Elastic pallet deflection due to loads at ascent and descent and thermal gradients must allow for ± 35 mm maximum movement radial to the P/L between PAF and clamp unit. This necessitates the use of a spherical bearing on the PAF (Fig. 3).

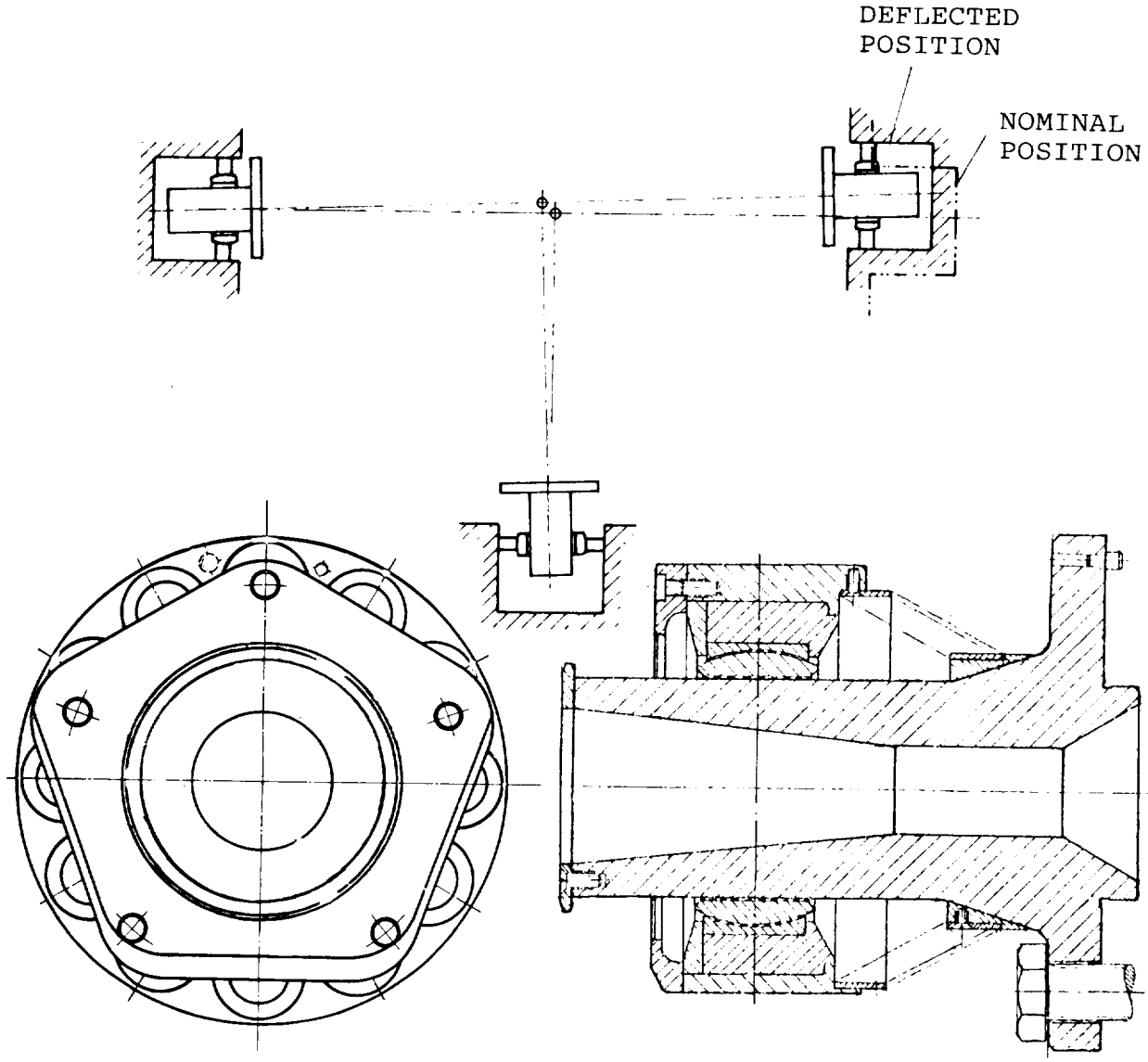

Figure 3: Payload Suspension to account for Pallet Deflections

This bearing had to be designed such that it is able to slide under high flight loads on a trunnion fixed on the P/L. Furthermore, an element enclosing that spherical bearing is required to guide the P/L into the clamp housings which could be situated out of their nominal position.

These guiding criteria in connection with the need for a good flight load distribution led to a polygon-element with five flats.

To hold and release the polygon element, a movable key bolt was chosen which acts vertically to the trunnion axis on which the spherical bearing slides (Fig. 4).

The head of the key bolt mates with one of the polygon flats. From this configuration, a force of about 100000 N in axial direction of the key bolt results. This load has to be carried by the clamping mechanism elements.

To activate the key bolt two fundamental possibilities were considered

- Driving of each key bolt by an individual actuator.

- Releasing of all three key bolts by a common actuator via steel ropes and locking by spring force.

The latter solution was chosen based on the following rationale:

- In case of a failure it makes no difference whether one or all 3 mechanisms cannot be activated as safe landing is only possible with 3 clamps closed.

- All 3 clamps can be closed to guarantee safe landing by spring force when the ropes are separated from the common actuator by single EVA (Extra-vehicular Activity).

- Due to design restraints for areas around the clamp housings, complications had to be expected for thermal control for the first solution.

- Low complexity (one actuator instead of 3 required)

The arrangement of the actuating mechanisms can be seen on Fig. 4.

The dimensions had to be kept as compact as possible because of design restraints for the clamp mechanisms almost from all sides of the clamp housings by strut and PAF-interface.

Safety aspects demand that the key bolt shall be locked automatically by spring force.

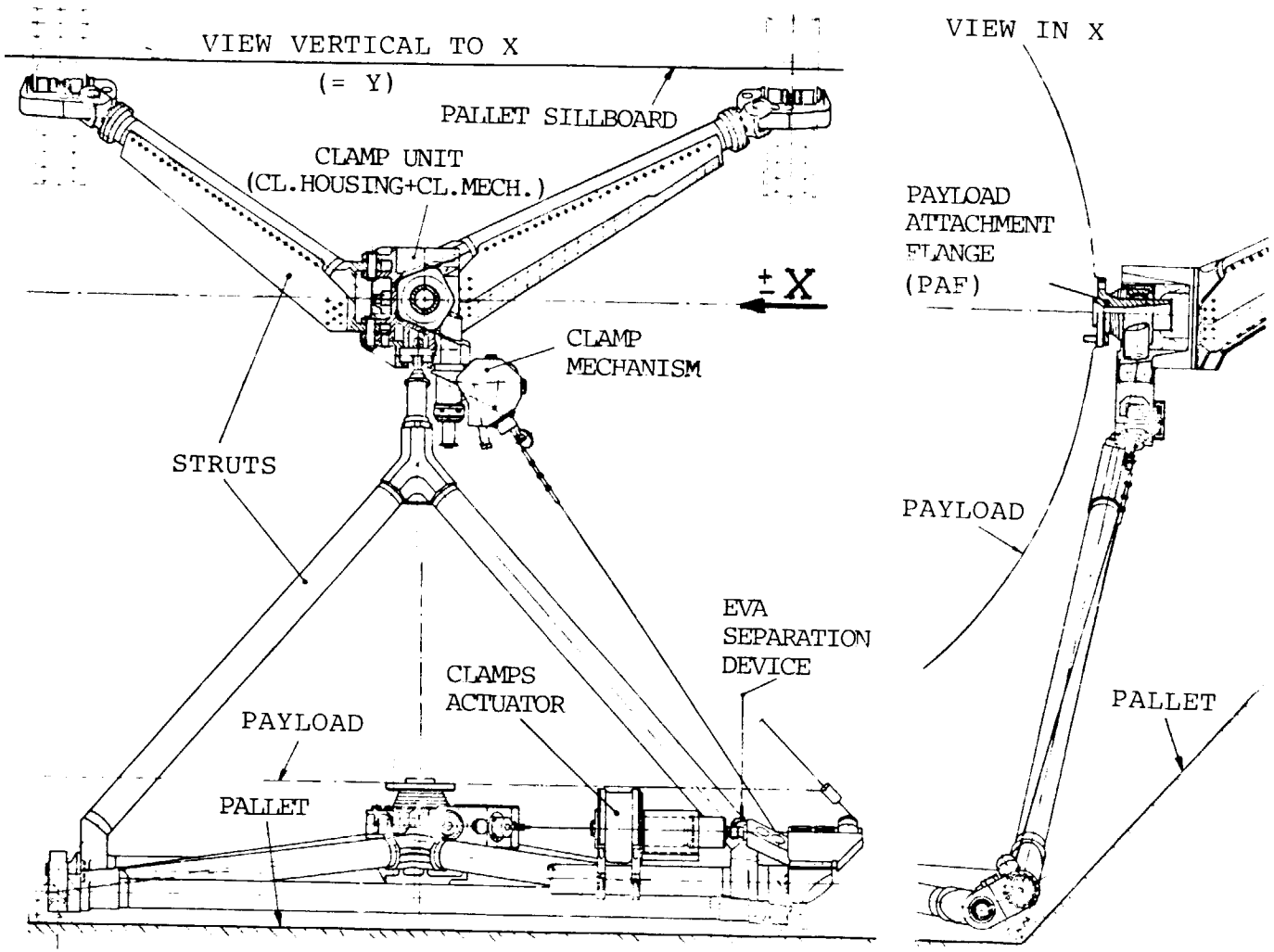

Figure 4: Arrangement of Clamp Mechanisms and Actuator within IPS-PCA

DESIGN DESCRIPTION

Clamp Mechanisms

The clamp mechanism (CM) was designed as a plug-in unit mounted into a clamp housing. The key bolt is actuated by double toggle joint levers as shown in Fig. 5 schematically.

To release the P/L the key bolt is pulled back into the clamp housing by about 57 mm. Safe locking such that the above mentioned 100000 N can be sustained shall be possible with minimum play between polygon and clamp housing when the polygon has the upper specified temperature of +120°C and the housing the lower one of -100°C.

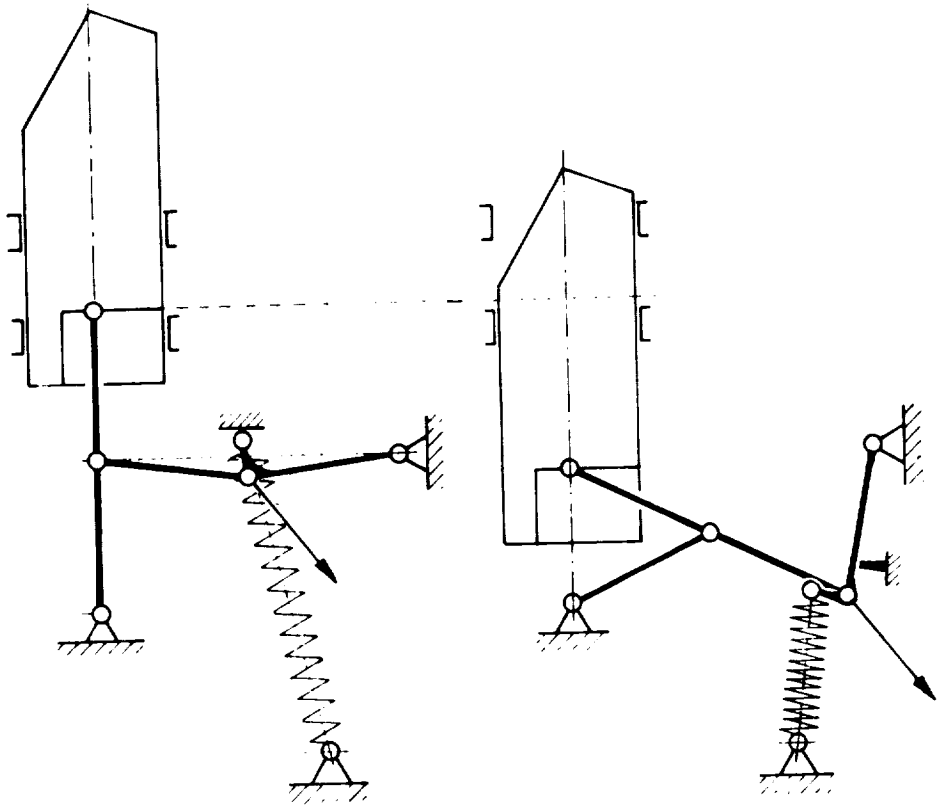

Figure 5. Principle of Clamping Mechanism

Due to design restraints imposed by strut interface, the primary toggle joint levers had to be integrated into the key bolt instead of location at the rear end of the key bolt. At one end, the toggle joints are adjustable to account for tolerances of polygon, key bolt and clamp housing.

The key bolt "locked position" as shown in Fig. 6.1 can be adjusted by nuts in steps of 60°, corresponding to 0.25 mm in key bolt axis. The primary toggle joint levers must be exactly in straight position when the key bolt is locked to give maximum load carrying capability.

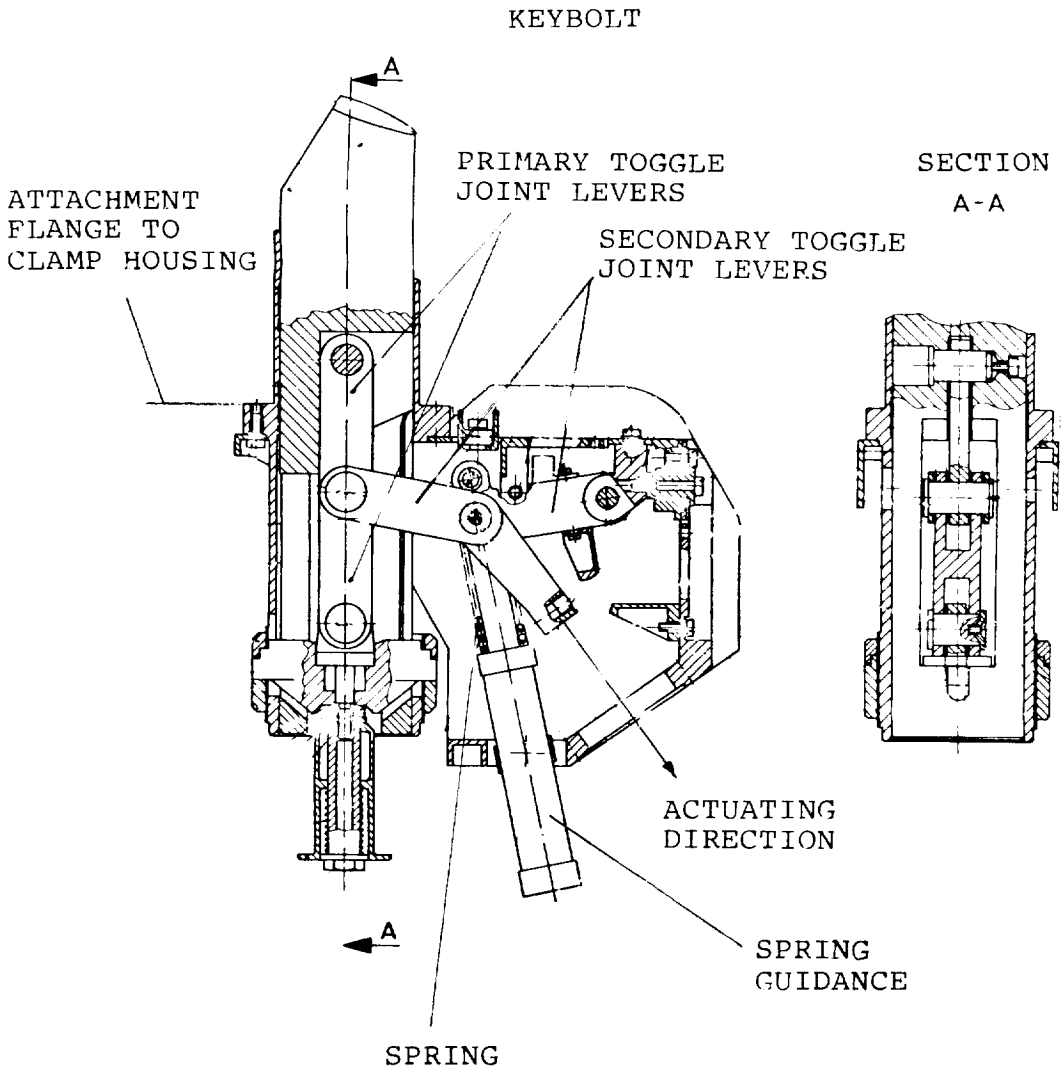

Figure 6.1: Clamp Mechanism locked

The "secondary" toggle joint is adjusted such that the stroke of the steel rope is minimized and limited by a stop.

All joints are lubricated with dry MoS_2-Film (Tiolube 460). The key bolt runs in two slotted bushes of Vespel SP1.

A fully guided compression spring activates the mechanisms for locking when the steel rope is released by the actuator. The point of attack of that spring is located on a specially shaped angle lever which is part of the secondary toggle joint to provide a starting force when the mechanism is unlocked (Fig. 6.2).

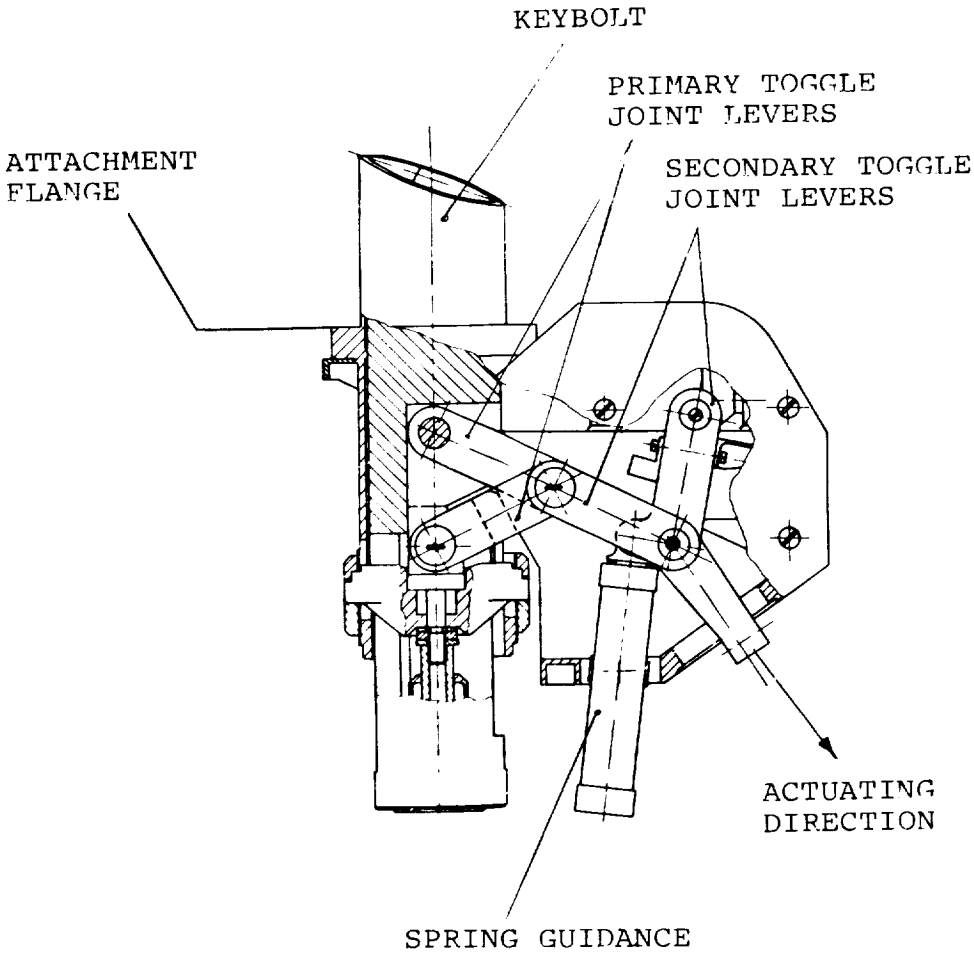

Figure 6.2: Clamp Mechanism unlocked

The locked and unlocked position is indicated by redundant and individually adjustable limit switches.

The force versus stroke of the rope of three mechanisms measured in vacuum (3 ÷ 6) · 10^{-5} Torr at +120°C and -76°C is shown in Fig. 7 and 8.

The single wires of the steel rope are coated with MoS_2-sliding lac (Molycote 321 R) before twisting.

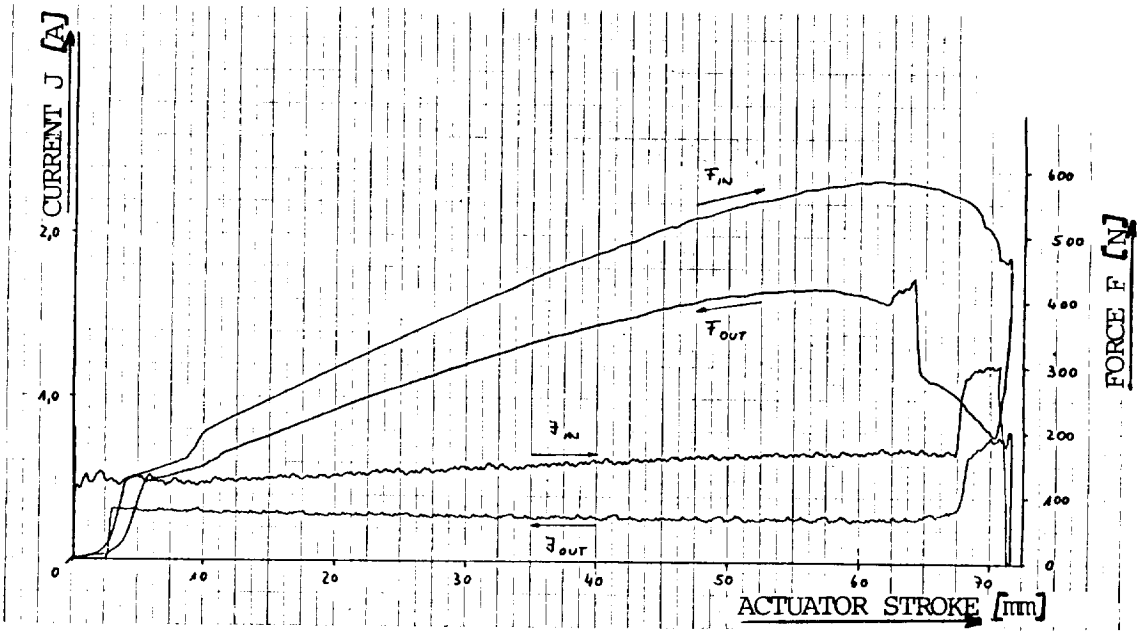

Figure 7: Force versus Stroke of 3 Clamp Mechanisms at +120°C in Vacuum

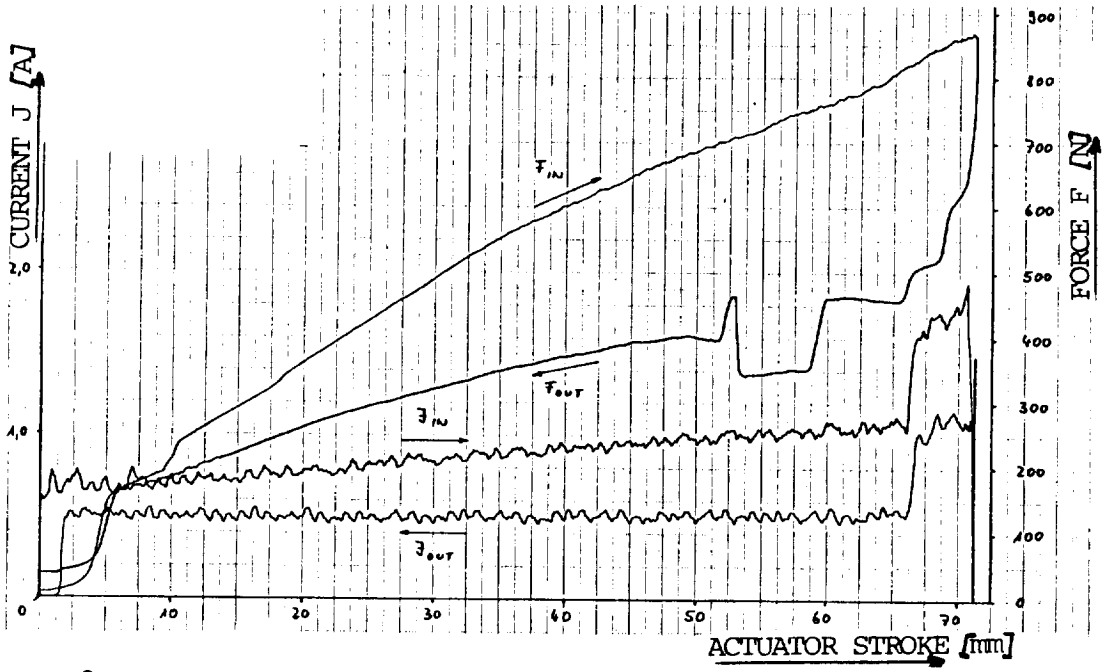

Figure 8: Force versus Stroke of 3 Clamp Mechanisms at -76°C in Vacuum

Clamps Actuator

The clamps actuator was designed on the basis of the following electrical and mechanical restraints and criteria:

max. power consumption 87 W over 0.1 sec
mean power consumption 50 W over 70 sec
DC-voltage source of 19 + 0.5 V with current limited 4.3 A
max. force 2000 N
max. stroke 80 mm
max. operating temperature +120°C/-20°C
active heating by heater mats
O-ring seal of static joints
two brush pancake torque motors acting on one common axis for redundancy

The transformation of torque into linear force is performed by a "Transrol"-spindle which has a wide range of aircraft application (i.e., actuation of flaps). The main features of this spindle are:

- mainly rolling instead of sliding elements
- very low friction and thus high efficiency
- high life-time

The nut of the spindle is situated in the rotating axis of the motor; the spindle is fixed on a welded membrane bellow consisting of 2 x 15 pairs of membranes. The bellow is supported in the middle on the spindle to give stability at 1 bar differential pressure. The membrane bellow was chosen as it represents an element with minimum dimensions at maximum linear elasticity and vacuum tightness. The bellow is protected by one fixed and one moving bushing.

A scheme of the actuator is shown in Fig. 9.

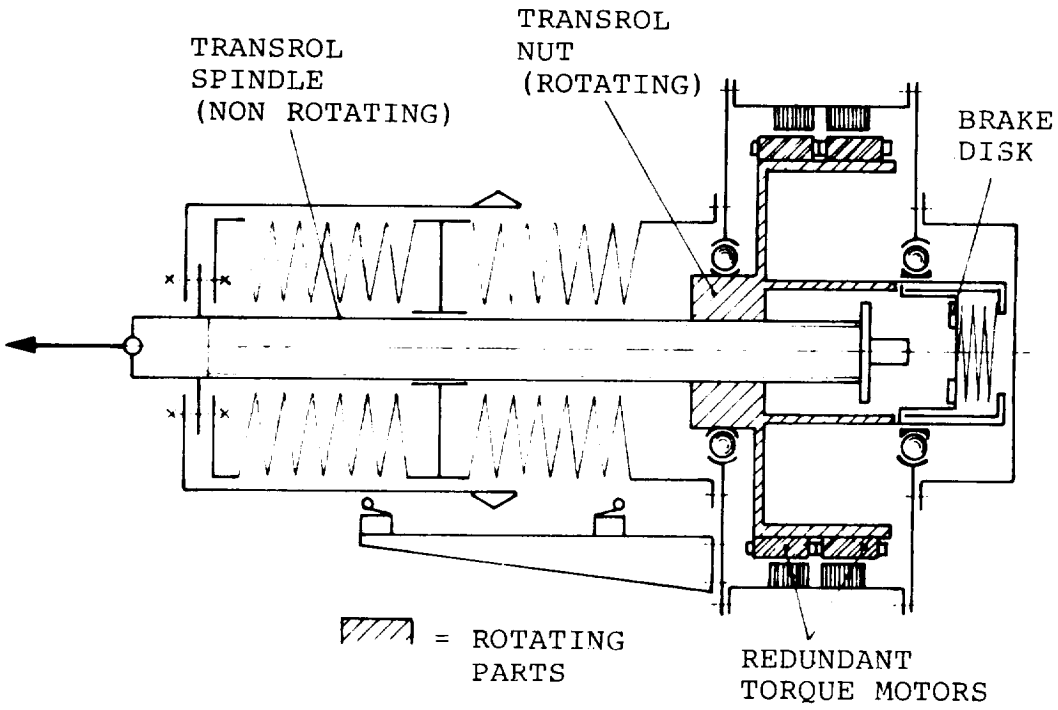

Figure 9: Scheme of Clamps Actuator

The front end of the actuator is supported and guided in extended position to give a definite position for the limit switches and to reduce vibration on the spindle/nut assy.

The spindle is fitted with stop in both directions.

As the spindle is not self-locking, a spring-loaded brake disk is applied on the axis of the motor to support the braking torque of the brush ring in retracted position (maximum load on the spindle induces max. torque on the nut).

Fig. 10 shows a photo and an explosion scheme of the Transrol spindle type SV. The high pull force capability of about 8000 N of this actuator, generated by a motor torque of 1.8 Nm, results from the high contact surface, the specially shaped thread and the high number of rolling grooved elements Ⓒ of that spindle. After one revolution, each roll jumps out of the race and is pushed back within a tunnel Ⓔ in the nut for one pitch by the lift ring Ⓓ.

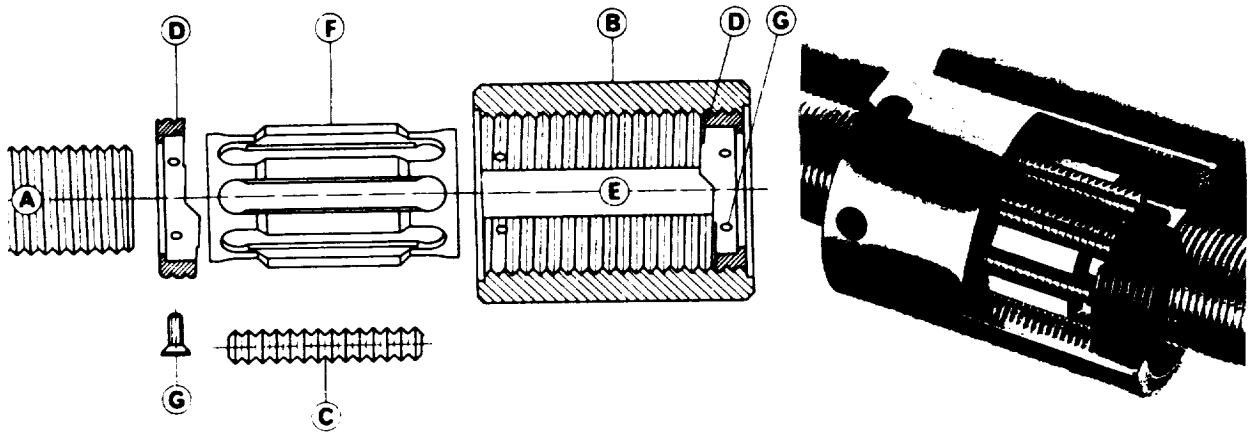

Figure 10: Transrol Spindel Type SV

The motor shaft bearing configuration consists of two radial ball bearings, one of which acts as axial fixation, while the inner ring of the second one can float on the motor shaft.

A cross section of the clamps actuator is shown in Fig. 11.

Ball bearings and spindle are lubricated with high vacuum synthetic oil Fomblin Z25 (Montedison). The motor brush ring consists of 40 - 61 percent silver, balance graphite.

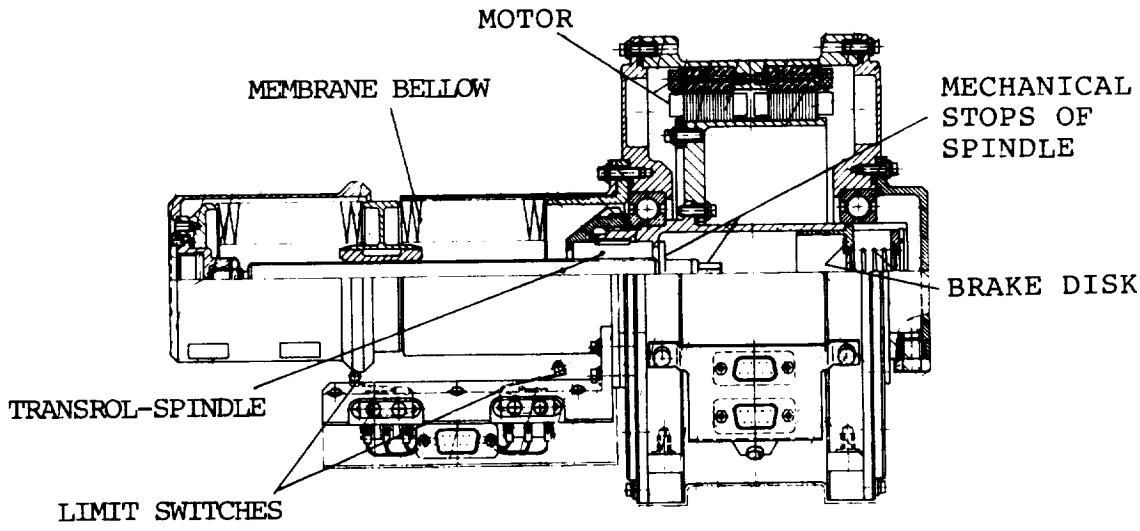

Figure 11: Cross Section of Clamps Actuator

TESTING

An extensive qualification test program was set up for the mechanisms to demonstrate the required performance for 50 missions.

The main tests are:

- TV test at +120°C and -80°C for clamps and actuator
- Guiding function test for the PAF in TV at +120°C and -80°C
- Vibration test for PAF, Clamp Unit and Actuator
- Static load test in a dummy pallet applying design limit loads, i.e., 230000 N acting in P/L center of gravity
- Damping test to demonstrate dynamic behaviour of clamp unit in connection with PAF

The test program is almost completed and was successful so far. A part of vibration testing has still to be performed.

The difficulties encountered were mainly associated with tribology. High loads and weight restrictions requiring light-weight high-strength material led to extensive use of Titanium Alloy which proved again its tendency to galling.

Sine vibration tests up to 3 g's in the range of 5 to 35 Hz on PAF-trunnion and spherical bearing at a pressure of approximately 3 N/mm^2 caused failure of MoS_2-films and titanium nitride coatings which were tried next failed also.

Investigations revealed that the reason for MoS_2 failure was a modification of MoS_2 into MoO_3 (abrasive material) at simultaneous presence of O_2, pressure and oscillation causing local high temperatures.

The present solution is electroless nickelplated maraging steel for the trunnion paired with a glass fibre reinforced teflonliner on the spherical bearing which gave good results.

At low sliding velocity (i.e., joints of levers of the clamp mechanism) carefully applied and polished MoS_2 films performed satisfactorily.

The damping test with a dummy P/L of about 1.5 tons revealed that the structural damping of the PCA is in the range of 10 to 15 percent, which will reduce considerably the dynamic forces on the clamp mechanism.

CONCLUSION

A payload clamp mechanism compatible with a wide range of payload configurations up to 3 tons mass has been developed. Low actuation power demand could be achieved by an arrangement of double toggle joint levers in connection with transrol spindle-actuator. A statically determined payload attachment necessitates floating bearings which on the one hand generate tribology problems but on the other hand provide high damping factors which helps to limit stress resulting from dynamic ascent/descent load environment.

SPACECRAFT AUTOMATIC UMBILICAL SYSTEM

R. W. Goldin
G. G. Jacquemin
Lockheed Missiles and Space Company

W. H. Johnson
George C. Marshall Space Flight Center

ABSTRACT

Space operations in the late 1980s and early 1990s will require semi-automatic docking and berthing mechanisms with supporting automatic umbilicals. Long life satellites and payloads, such as the 25 kW Power System, will require special services to be supplied across the interface umbilical to accommodate the various multiple, replaceable payloads. Required operational features of the umbilical are expected to be a remotely controlled mate/demate, a manual override as backup, numerous cycle connect/disconnect durability, and a continuous five-year operational life with on-orbit maintenance and repair capability utilizing current Orbiter Replacement Unit (ORU) technology.

In a specific application to the 25 kW Power System, the umbilical services will include transfer of nominal 25 kW of electrical power, heat rejection through a fluid transfer loop, various commands and signals for effecting control, data transfer, and communication services to any mated single or multiple payload which also enables extension of mission time.

The complex mission requirements resulted in selecting a total of 14 electrical connectors that included eight power connectors, four signal connectors, and 2 coax connectors. To meet fluid transfer requirements, two one-half inch diameter line connectors were selected to handle fluid pressures up to 3000 psi. These requirements led to a large platen (12 inches by 22 inches) with self-aligning devices, a free-floating, self-aligning ram system, manual and emergency release systems, and ORU capabilities. The orbital repair, replacement, and maintenance consideration strongly governed the design and led to a system configuration consisting of two major ORU assemblies.

To demonstrate the design capability, a prototype umbilical was built and a series of preliminary operational tests was performed and documented.

SPACECRAFT AUTOMATIC UMBILICAL SYSTEM

INTRODUCTION

Space operations in the late 1980s and early 1990s will require semiautomatic docking and berthing mechanisms with supporting automatic umbilicals. Long-life satellite and Space Shuttle payloads, such as the 25 kW Power System, will require special services to be supplied across the interface to accommodate the various multiple replaceable subsatellites. To provide the necessary capabilities, NASA-MSFC issued a set of requirements, and then awarded a study to Lockheed Missiles & Space Company, Inc. (LMSC), to first conceptually define an appropriate berthing technique and then to complete a prototype design of an automatic umbilical system suitable for use with payloads carried by the Space Shuttle.

After considering a variety of docking concepts, a four-element berthing system was selected, as is shown in Fig. 1. This concept consists of a set of four remote manipulator system (RMS)-type end-effector capture/tie-down devices on the power system and corresponding RMS-type grapple fittings on the payload. In operation, the RMS maneuvers the payload to a position where the four grapple fittings can be snared within the end-effectors and then secured to the power system. The concept takes advantage of mechanisms and operating techniques developed for attaching the RMS to a payload.

The umbilical installation is shown in Figs. 2 and 3. Although it is attached to the docking interface structure, its operation is independent,and it must comply with the following set of primary requirements specified by Marshall Space Flight Center (MSFC):

- The umbilical shall contain:
  - 2 12.7-mm self-sealing quick-disconnects for use with 3000-psi (gaseous nitrogen) fluid lines
  - 8 Four-pin electrical connectors, shell size 40
  - 4 Sixty-pin electrical connectors, shell size 36
  - 2 Sixty-pin electrical connectors, shell size 24
  - 2 Coaxial connectors, shell size 20
- Angular misalignment: ±3°, carrier-to-plate
- Maximum travel from retracted lock position to carrier plate: 6 inches
- Umbilical: floating, nonload carrying
- Mating: a separate function, but may be simultaneous with docking
- Mating and demating: by remote command, backed by extravehicular activity (EVA) and/or pyrotechnics

- Operating life: 100-cycle
- Repairable or orbital replaceable units (ORUs)

In the discussions which follow, the general characteristics of the umbilical system are described, followed by detailed descriptions of each individual mechanism.

UMBILICAL GENERAL CONCEPT

The required set of connectors is mounted on rigid platens in the configuration shown in Fig. 4. Two platens, facing each other, constitute a remotely controlled mating/demating interface. One platen is fixed rigidly to the spacecraft frame while the other is movable upon command. One side has its connectors in floating mounts to allow for manufacturing tolerances, differential thermal expansion, and misalignments. The overall installation includes the ORU provisions, which requires two more pair of secondary platens, and is shown in Fig. 5. The complete system thus consists of six platens. Two platens at the two ORU interfaces are passive: one mounted on the power system and the other on the payload. Their counterparts are, respectively, on the two on-orbit replaceable assemblies: the movable platen assembly and the slave platen assembly. These two sets of hand-connected platens provide the ORU interconnect capabilities of the umbilical system. These enable removal of either assembly one at a time or both assemblies as a unit, with the umbilical platen connected as shown in Fig. 5. A schematic of the system is given in Fig. 6 to clarify the geometry and identify the primary component nomenclature. The umbilical system thus consists of two assemblies incorporating two sets of secondary platens, a slave platen and a movable platen.

DETAILS OF MECHANISMS

Eighteen different mechanisms, as shown in Table I, are necessary to perform all the functions required for the operation of this automatic umbilical. Compliance with the ORU requirements dictates that all powered mechanisms must also be manually operable within the working capabilities of an astronaut in EVA. Additionally, the operation of the ram system, which connects the movable platen to the slave platen, must not apply a reaction/separation force to the docking system. An external ram system, as shown in Fig. 7(a), would transfer the insertion load via a long and elastic path through the docking system. Such an arrangement is obviously unsatisfactory inasmuch as it would be conducive to poor control of the umbilical operation and could lead to inadvertent separation of the connectors in case of spacecraft disturbances. A short rigid load path, independent of structure and docking interface, is shown in Fig. 7(b). It is the solution that has been adopted. Its mode of operation (shown in Fig. 8) requires driving the specially threaded end of the Saginaw ram screw into the securing nut with sufficient guidance so that cross-threading will not occur. Rotation of the Saginaw nut then completes the umbilical interconnect operation. Reversal of the sequence separates the umbilical and secures the movable platen in the stowed position with a suitable preload.

The ram mechanism is shown in Fig. 9. This device is based on the use of a Saginaw screw and ball bearing nut, each of which is driven separately by worm screw and gear arrangements. Two such units are mounted under the movable platen. One unit is motorized and drives the other by means of two standard chains

and sprockets. Operating the screw drive moves the screw with respect to the platen; operating the nut drive moves the platen along the screw. The two units are connected by chain guards designed to resist the chain loads and protect the umbilical cabling. These are shown in Fig. 10.

The movable platen is mounted in a frame as shown in Fig. 11. It is guided by rollers at each end and rests on four adjustable posts when stowed. When disconnected from the tie-down nuts, it is free to rise within the limits of the cabling and has ±6.4-mm clearance fore and aft, and laterally. These clearances also provide significant rotational freedom about the three axes so that a realistic range of docking position tolerances can be accommodated.

To prevent possible connector misalignments, one of each connector-socket pair is elastically mounted with 3 degrees of freedom: two translational and one rotational (Fig. 12). Centering is provided by springs or by strips of elastomers. The flange rests on a teflon pad to minimize friction forces. Typical installation of a size 40 connector is shown in Fig. 13. It should be noted that the two shells are designed to self-center before the pins contact their sockets. A guiding keyway (not shown) ensures proper indexing by forcing the socket-side shell to rotate against its centering springs. Figure 14 shows the centering precision that can be expected at various stages of umbilical connection. The precision drops from ±3 mm at docking to ±0.4 mm at shell insertion, and then to normal pin clearance at pin insertion. This design approach should ensure safe and repeatable pin insertion in the specified 100-cycle operations.

MISCELLANEOUS MECHANISMS

A number of secondary mechanisms are required to: (1) guide the movable platen, (2) secure the movable platen frame assembly and the slave assembly, (3) provide positioning guidance for ORU removal or insertion of these units, and (4) ensure positive locking of all removable components employing EVA astronaut capabilities aided by a standard 11.11-mm (7/16-in.) hexagonal socket driver.

Figure 15 shows the typical configuration of the movable platen guide system. It consists of aluminum channels used as tracks and sets of two delrin rollers having diameters 6.4 mm smaller than the track width. This system provides also a ±3.2-mm lateral freedom.

Figure 16 shows the general arrangement of the movable platen tie-down system. The system consists of a pair of angle tracks with centering ramps so that the EVA astronaut needs only to set the unit within the track and push it in place over the ram pin. The ram mechanism shown in Fig. 17 consists of a special centering pin and clamp with a high mechanical advantage linkage driven by a worm gear mechanism. Thus, with little effort, an EVA astronaut can connect the secondary platens; or conversely, safely disconnect them. A simple lock device is added at the corners of the frame for rigidity and to relieve possible loads on the secondary ram system. It is also designed for simple manual operation.

Figure 18 shows the tie-down arrangement of the slave platen. The platen ram system is identical to that of Fig. 17. The frame lock-pin is considered a necessity in this case to avoid having this unit cantilevered on the ram pin. Without the side lock-pin, it would be difficult to maintain the close platen alignment required for correct threading of the Saginaw screw ends of the main ram system.

Protective doors are used to guard against debris and to prevent accidental damage to the connectors when the umbilical is in the stowed position. These doors are required both on the movable and on the slave platen sides. The doors, mounted on telescopic tracks as shown in Fig. 19, are driven by electric motors. Only the movable-platen door is powered. The slave door has a catch by means of which it is pushed open by the other door. A spring device ensures its closure. This approach is taken because the payload may be passive with no access to its control system until the umbilical is connected.

Figure 20 shows the installation of the power drive units on the movable platen ram system. They are attached to the side of the chain guard and drive the worm gears through reduction drives. A typical power drive unit is shown in Fig. 21. It consists of two electric motors (for redundancy) driving a reducing gear train of specified ratio. The motors are mounted in spring-loaded sockets, with their pinions meshing the main gear. In case of failure, a motor can be partially withdrawn (out of mesh) or removed and replaced by a new one. Current would be supplied to these motors through the sockets so that an EVA astronaut can plug and unplug them when servicing the umbilical. The total umbilical system requires three to four power units (six to eight motors). [1]

ANCILLARY DESIGN FEATURES

The electric power cables specified for the large connectors are multistrand size "O." Their outer diameter is close to 12 mm, which necessitates special preforming to enable assembly of the platen cabling configuration as shown in Fig. 22. However, a more practical approach may be obtained using the configuration of Fig. 23, which will most likely be used for the flex fluid hoses. A total of 32 No. O cables is to be installed, plus 4 bundles of 61 small cables and 2 large coaxial cables.

In case of emergency, such as pin seizure, main power failure, or jettison of payload to protect the crew, it may be necessary to separate the umbilical platen forcibly and/or quickly. This can be achieved by using protechnic separation nuts for releasing the Saginaw rods and separation actuators as shown in Fig. 24. The pyrotechnic bellows motors have the advantage of providing a large force in a compact volume, and they do not release any contaminants. Because they are mounted on the slave platen, they will be accessible for replacement by an EVA astronaut.

The electrical system consists of power supply to the electric motors and wiring for a set of position sensors (microswitches) to provide for a status readout for each function. A typical setup suitable for ground testing is shown in Fig. 25. It requires four command switches: doors, screws, platen, and emergency release.

[1]Normally three power units. A fourth may be needed to provide proper door tracking.

RESULTS AND CONCLUSIONS

An umbilical system design has been completed that incorporates all the features specified for a power system-to-payload interconnect capability. A proof-of-concept prototype of the umbilical system has been built to determine experimentally the suitability of the threading characteristics of the ram mechanism and to verify freedom from cross-threading. It will also be used to measure connector insertion loads, first in an ambient laboratory environment and later in a space-simulated environment (thermal-vacuum chamber). Laboratory ambient testing is being performed by the engineering staff and students at San Jose State University.

The following highlight key conclusions derived from the study:

1. Berthing systems that utilize the RMS can be simplified by using RMS targets, closed-circuit TV cameras, tie into the RMS control system, and grapple-fixture and end-effector-like capture and secure mechanisms.

2. To effect a remotely controlled umbilical interconnect in proximity with a manned spacecraft and to provide for EVA backup and ORU maintenance capabilities, 18 different mechanisms are found to be necessary.

3. The weight impact of providing for ORU capability in a large multiple connector umbilical system was found to be in the order of +60 percent.

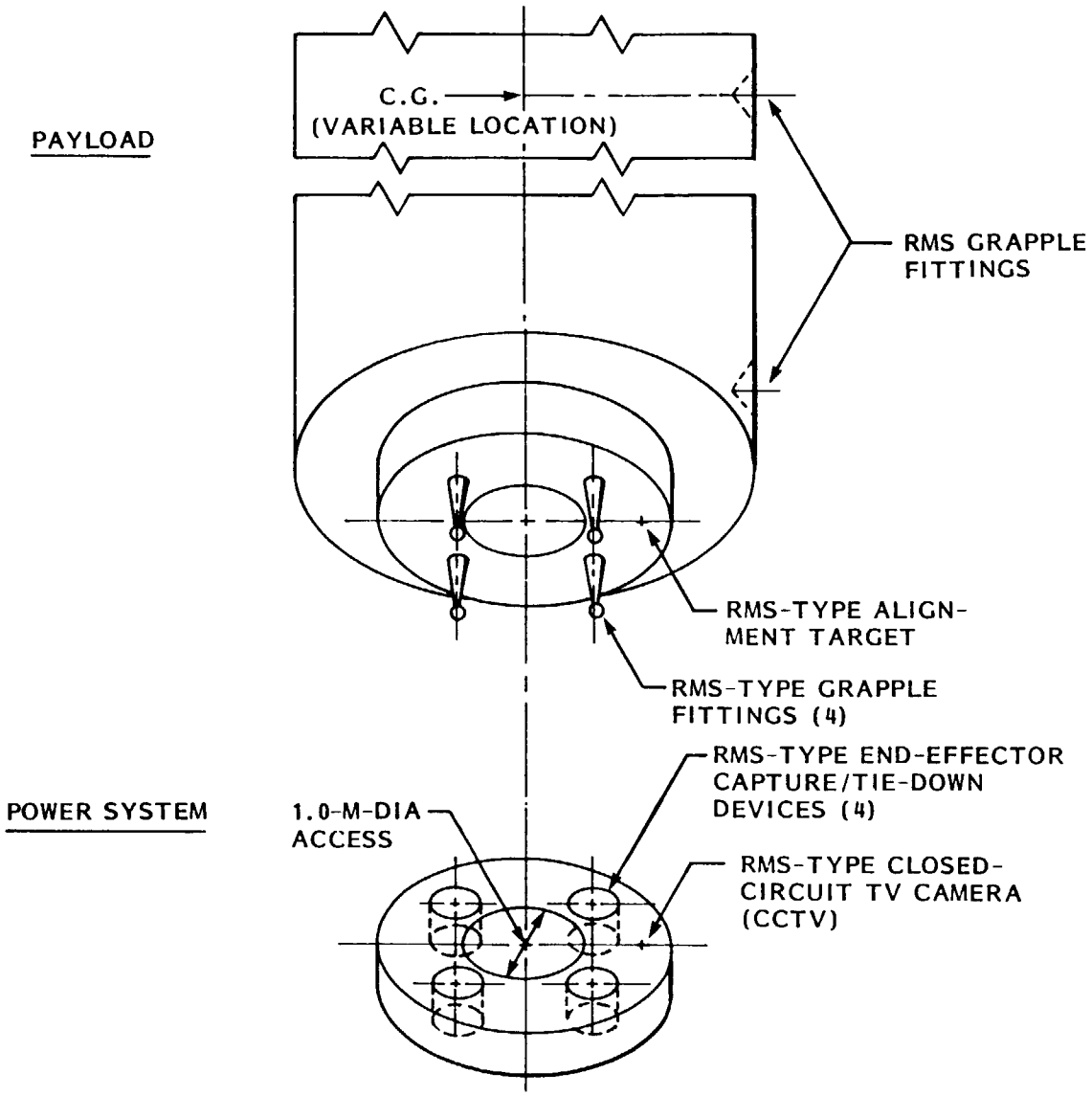

Figure 1. Berthing System Concept

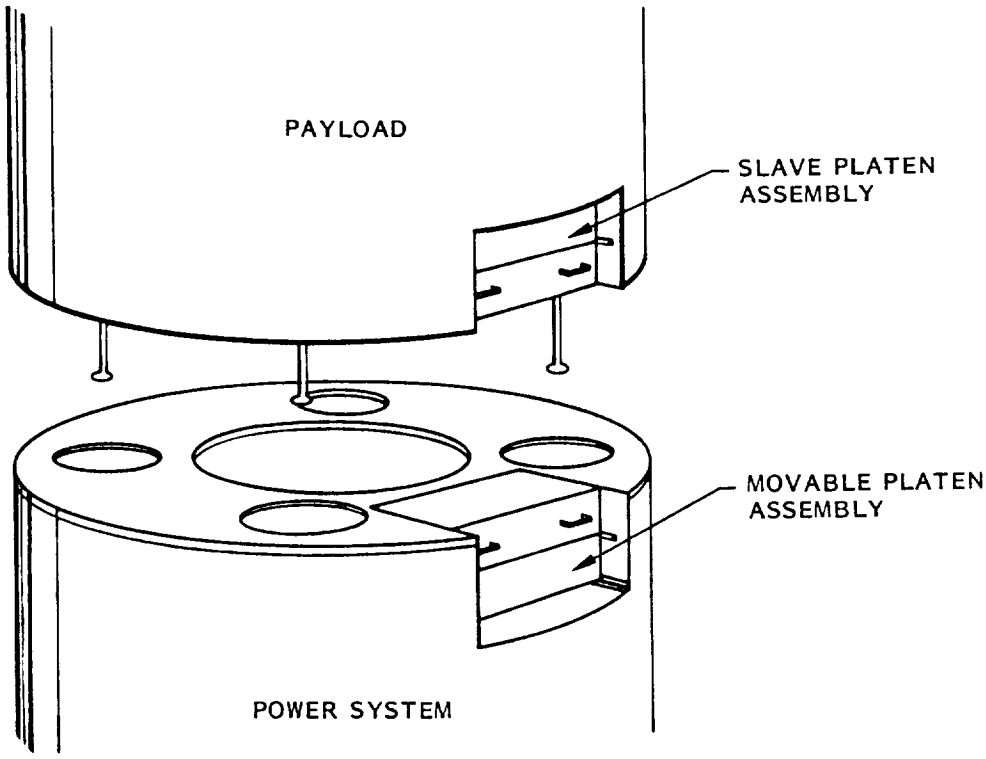

Figure 2. Berthing and Umbilical Installation

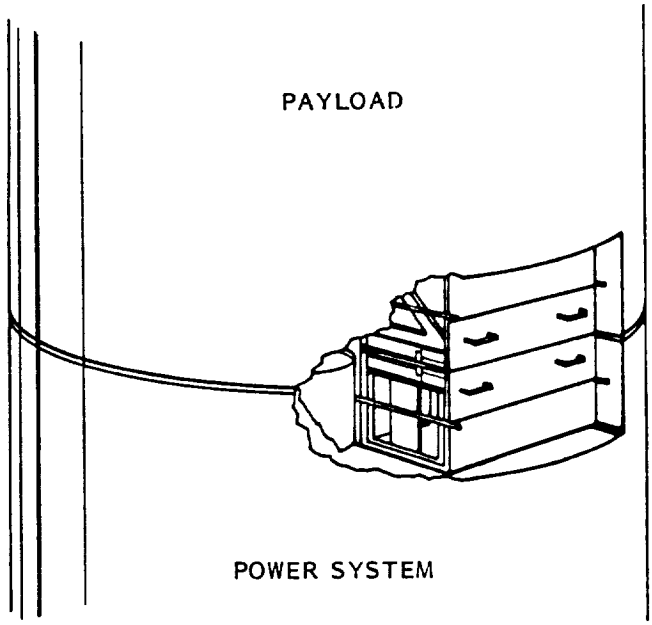

Figure 3. Umbilical Prior to Connection

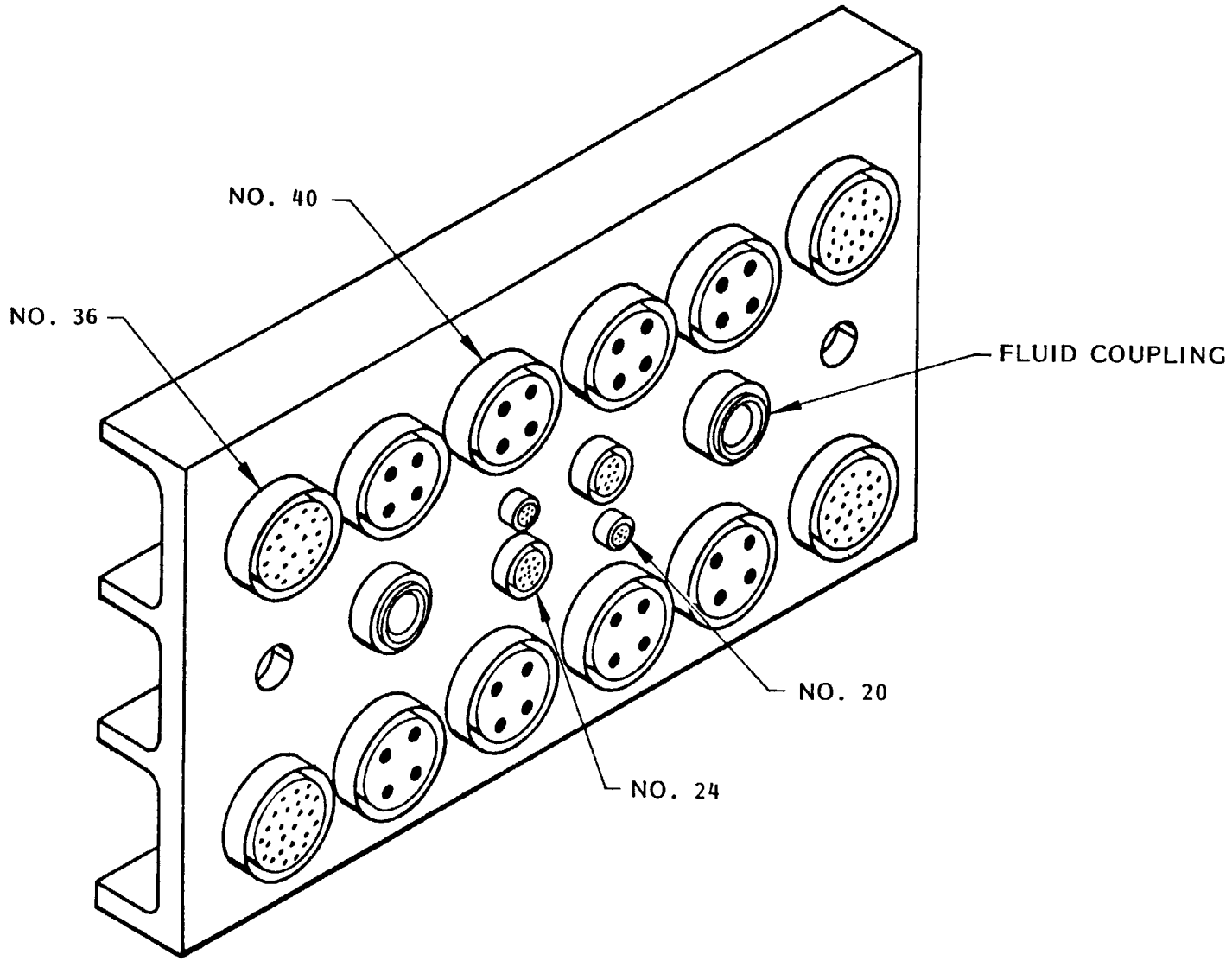

Figure 4. Typical Platen Connector Arrangement

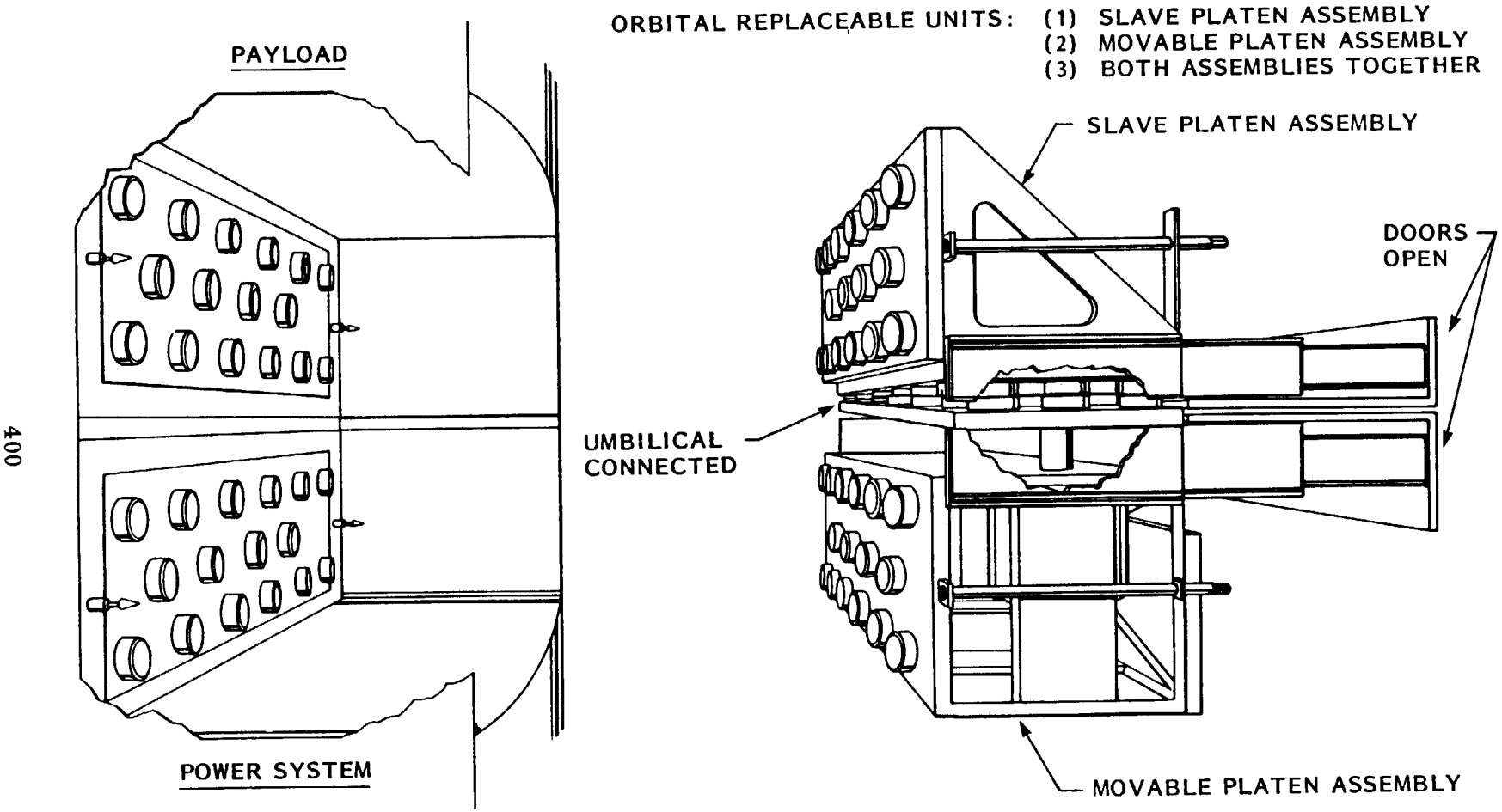

Figure 5. Orbital Replacement Unit

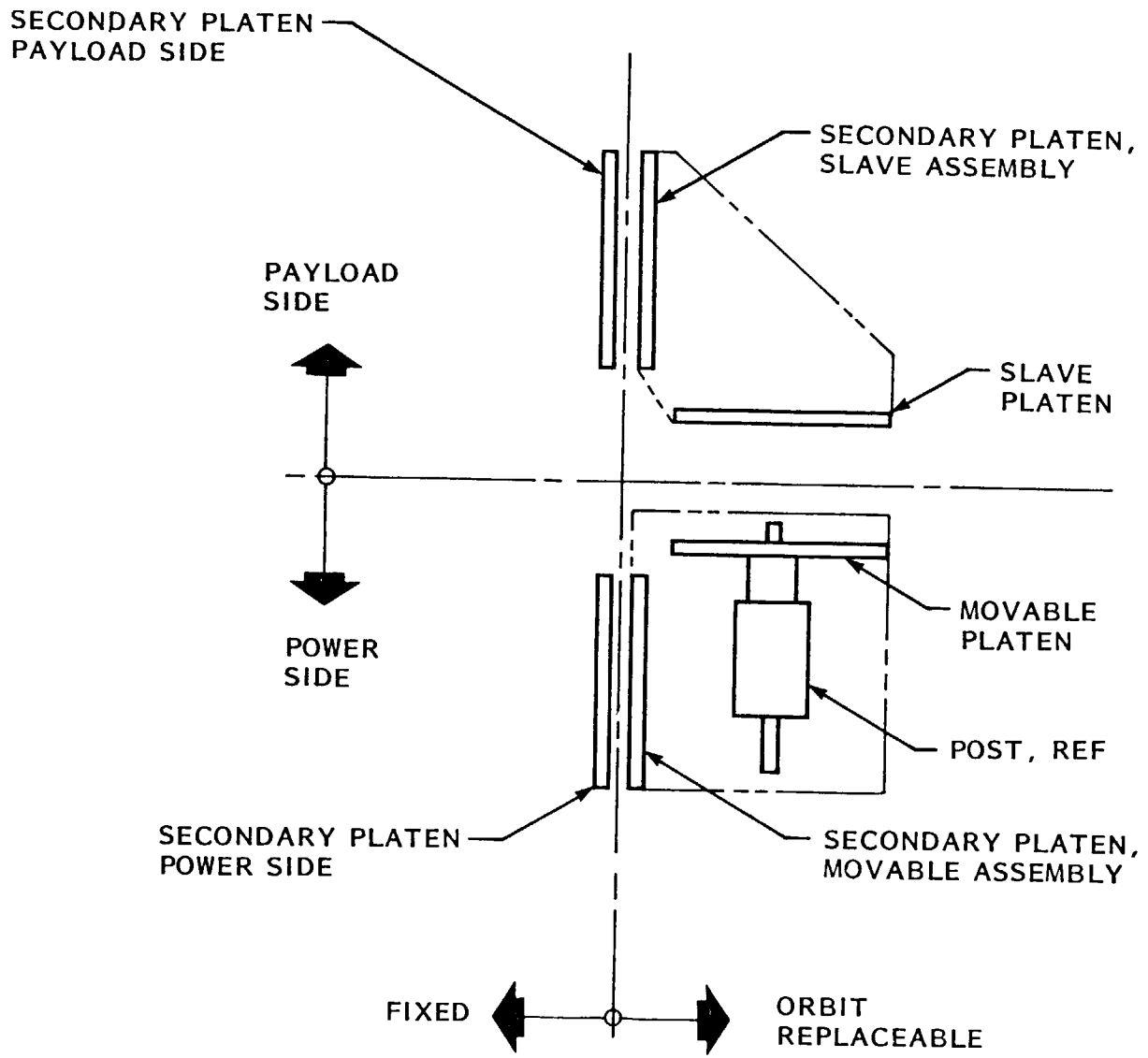

Figure 6. Schematic and Nomenclature

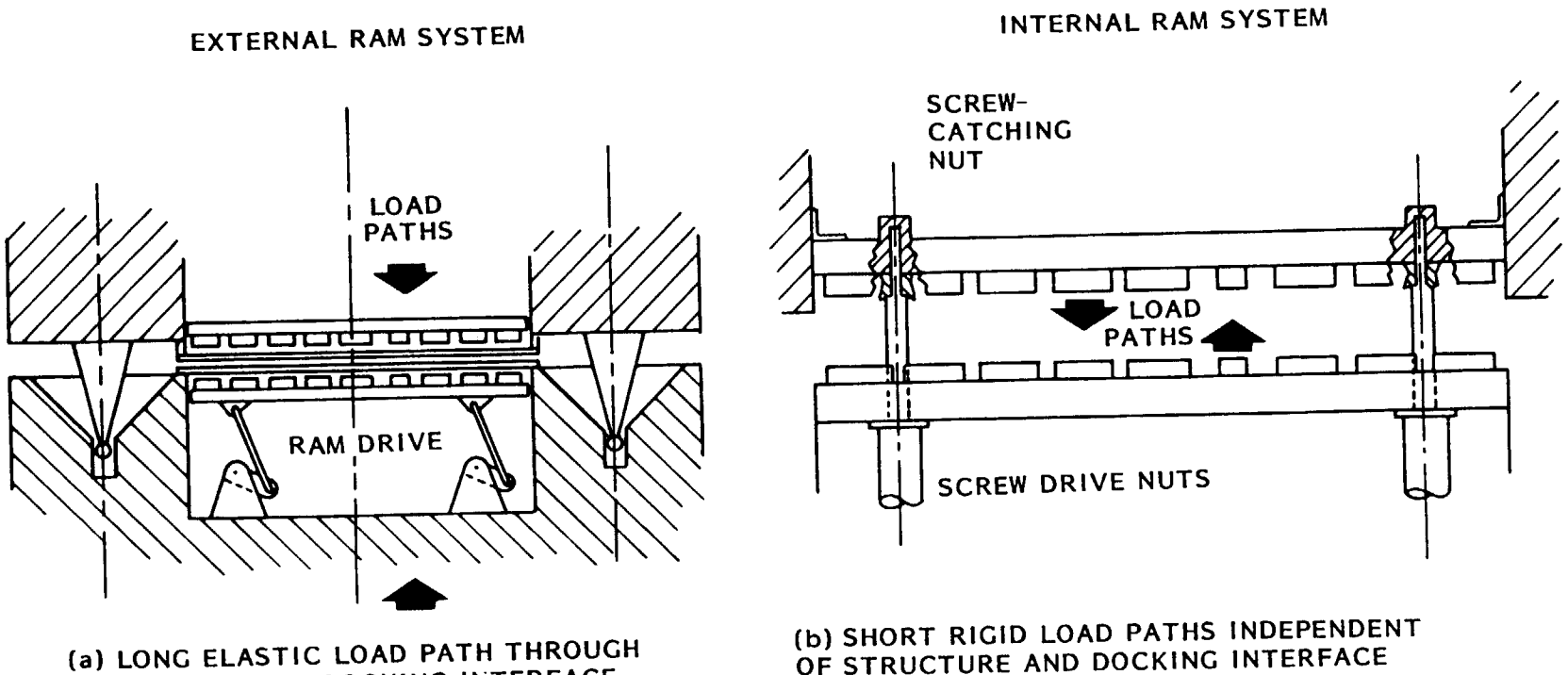

Figure 7. Umbilical Drive System

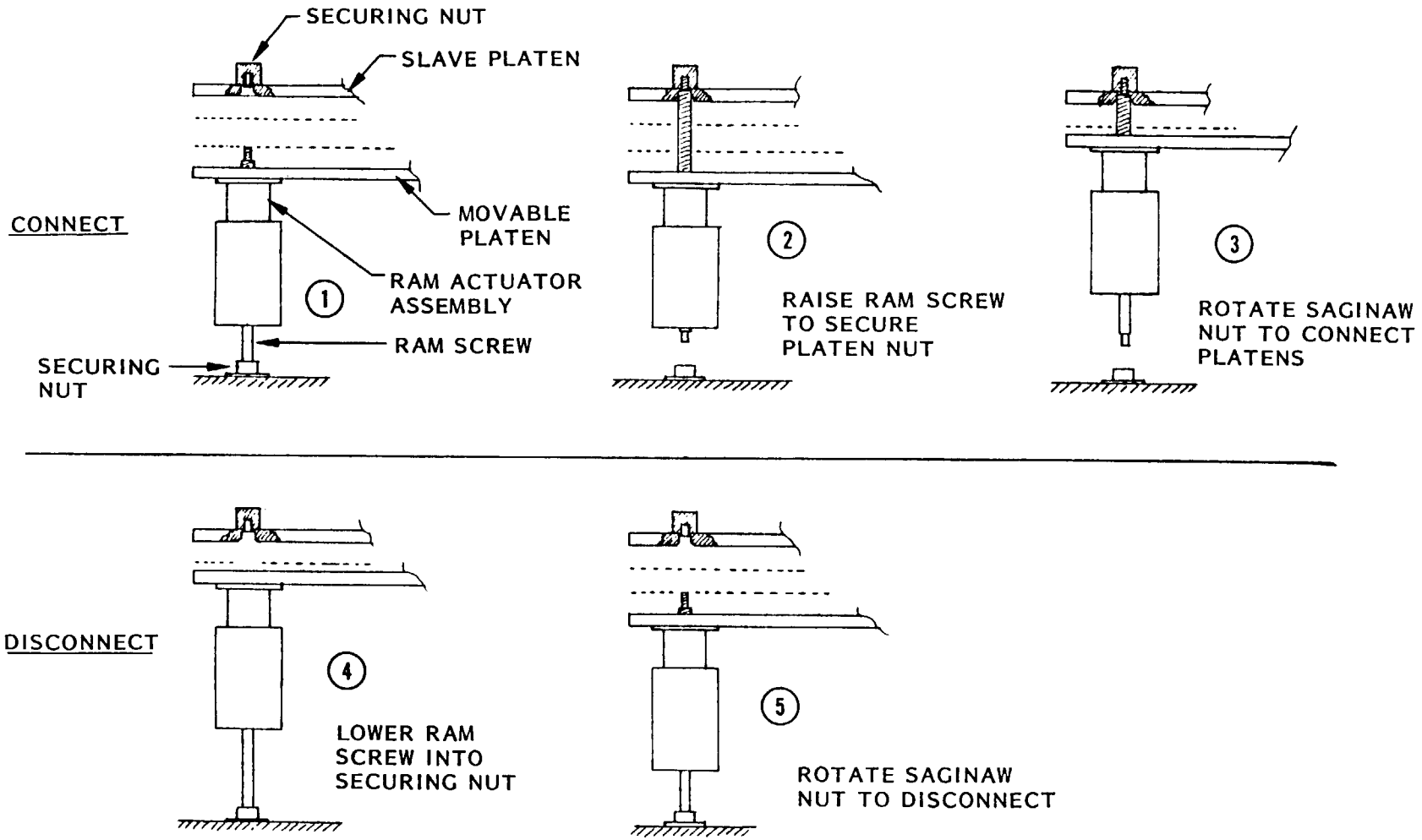

Figure 8. Operation of Selected Umbilical Drive System

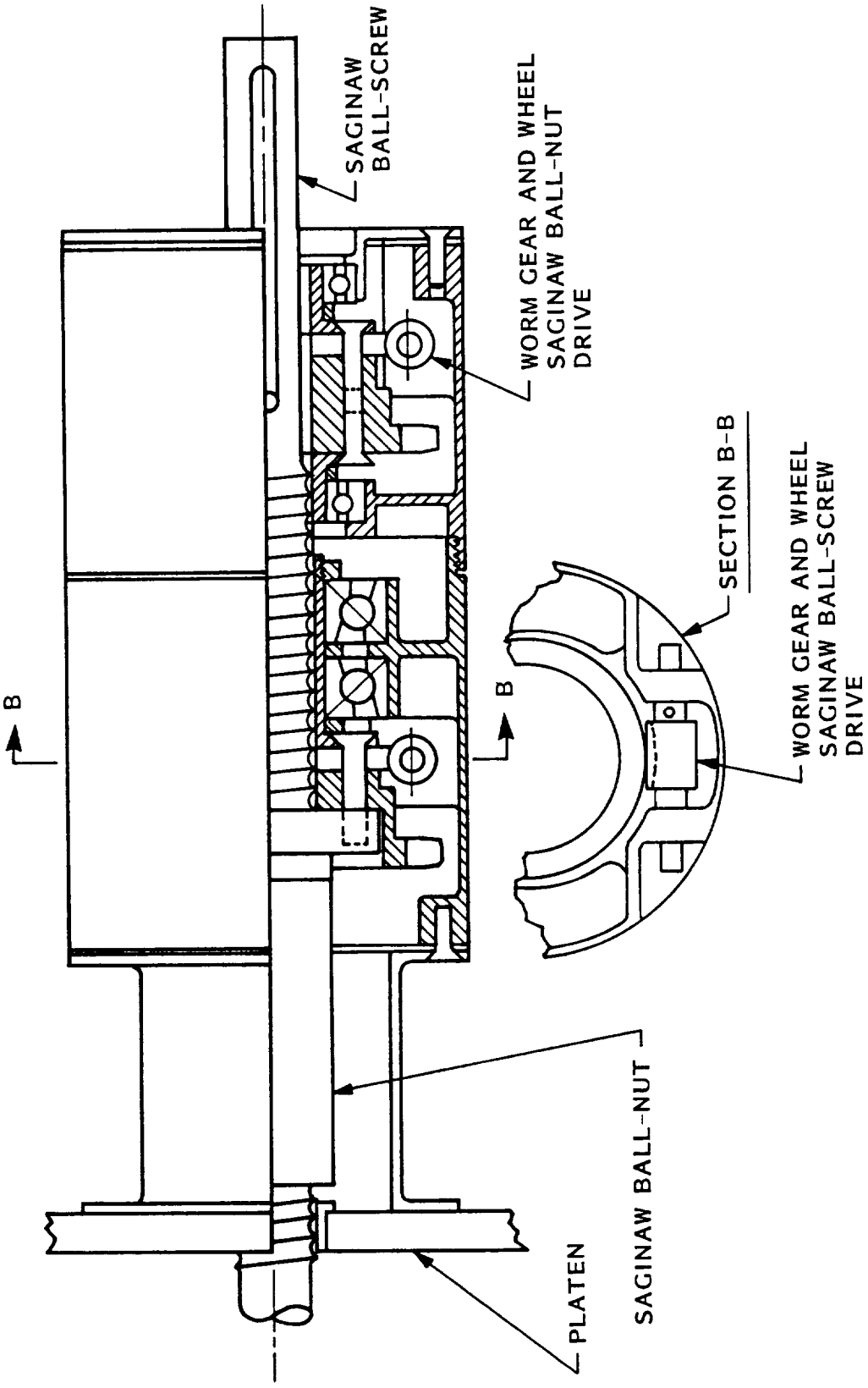

Figure 9. Ram Screw Drive System

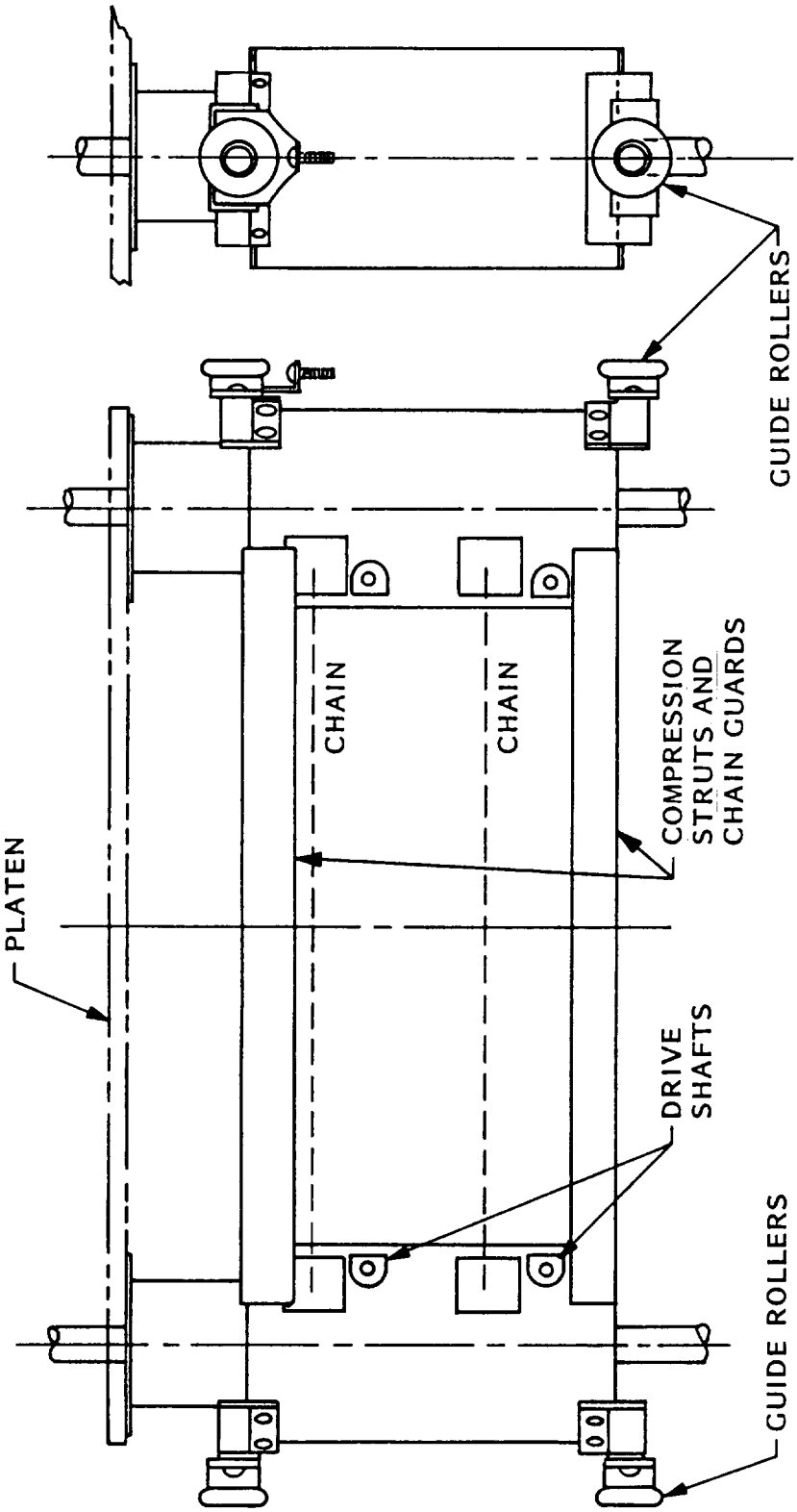

Figure 10. Details of Ram Drive Installation

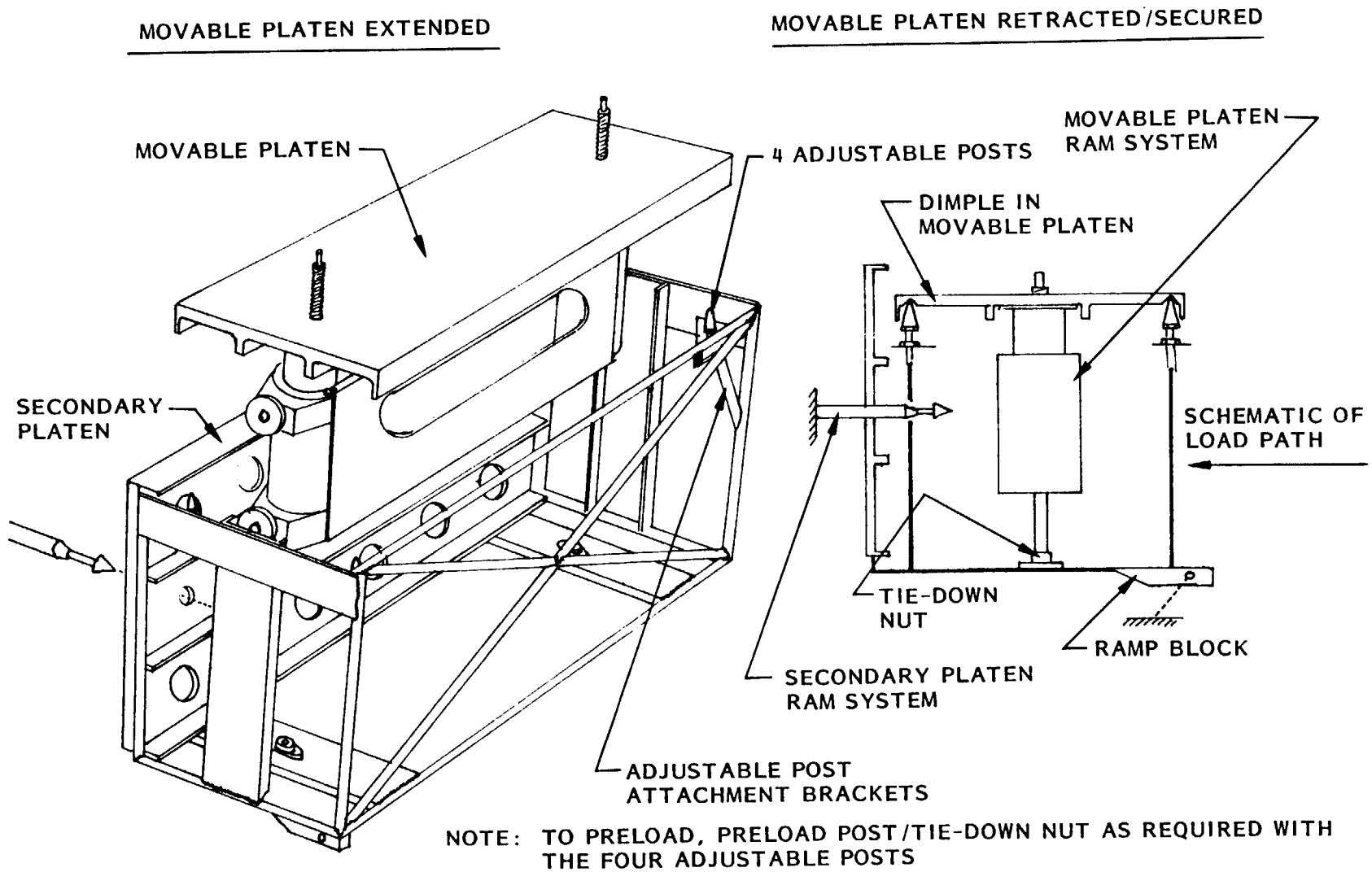

Figure 11. Movable Platen Tie-Down System

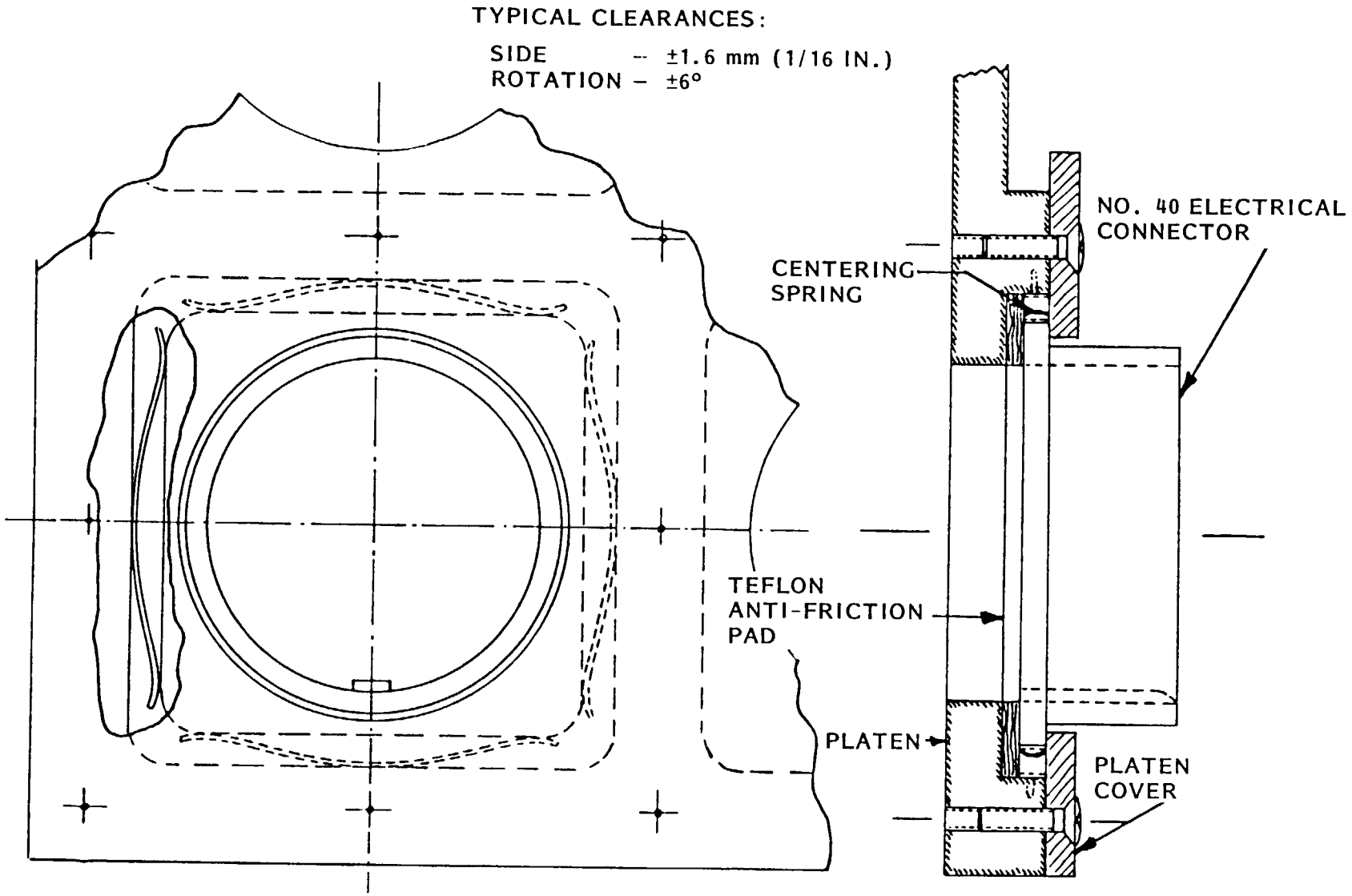

Figure 12. Floating Electric Connector/Platen Installation

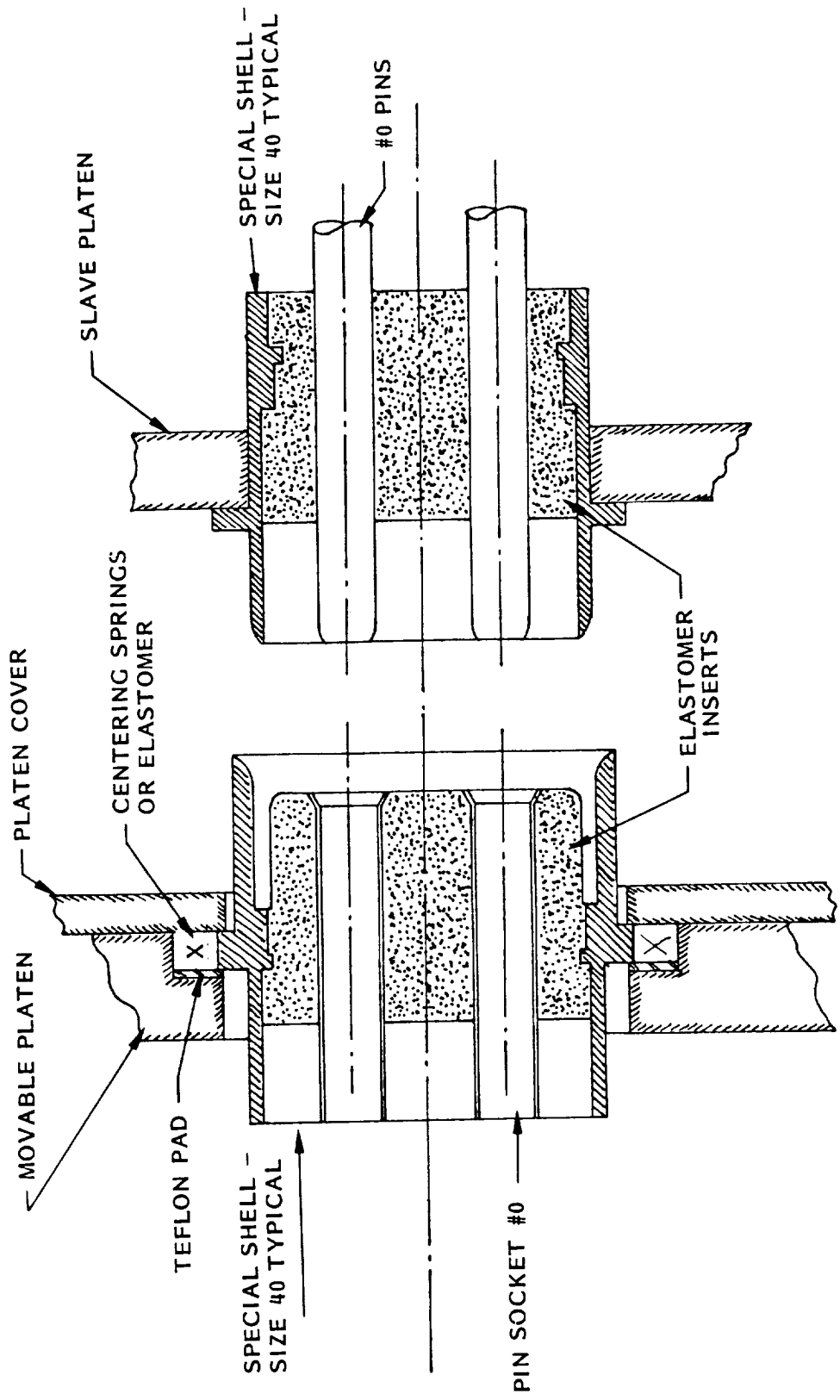

Figure 13. Typical Electric Connector Configuration

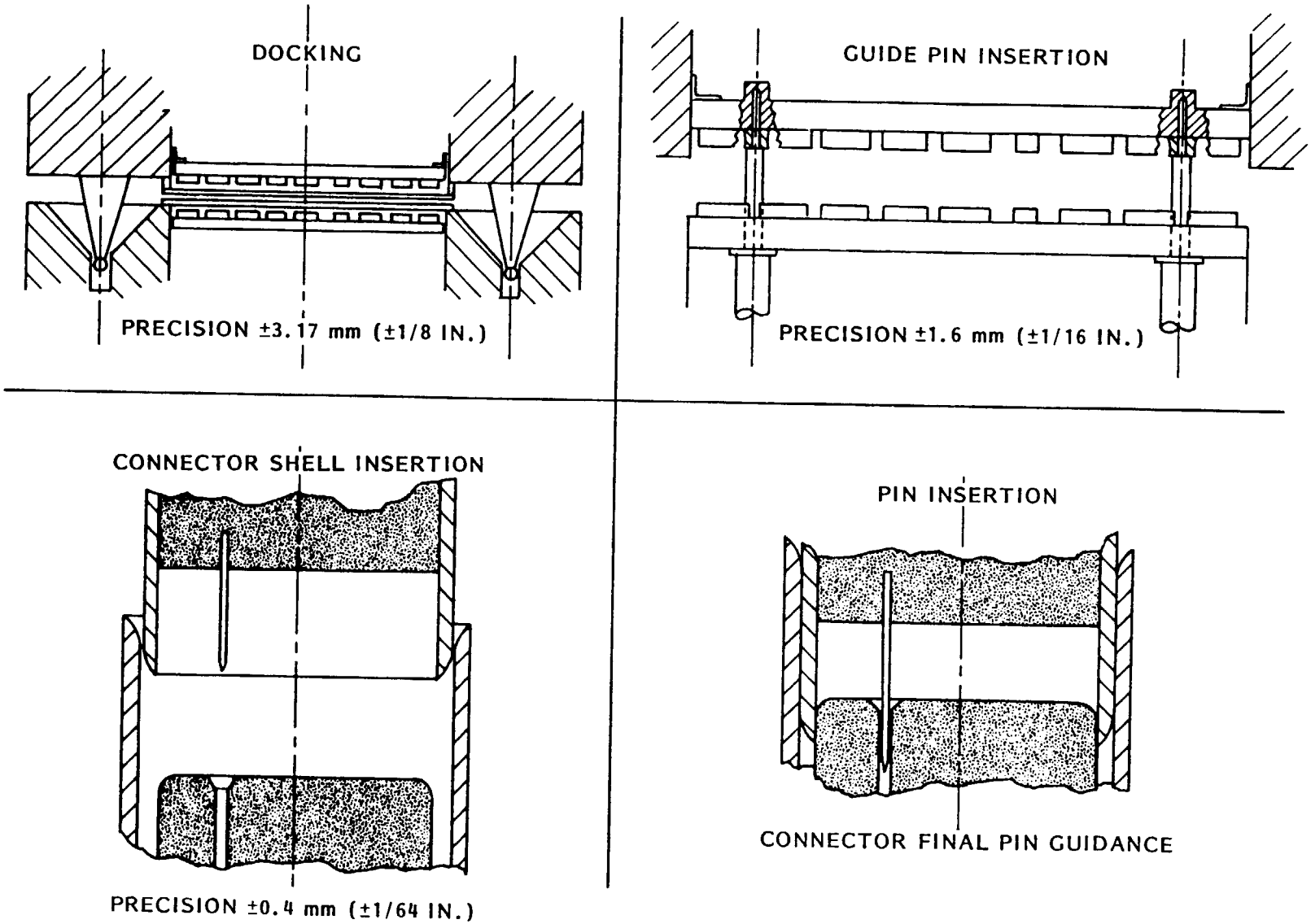

Figure 14. Precision of Connector Insertion

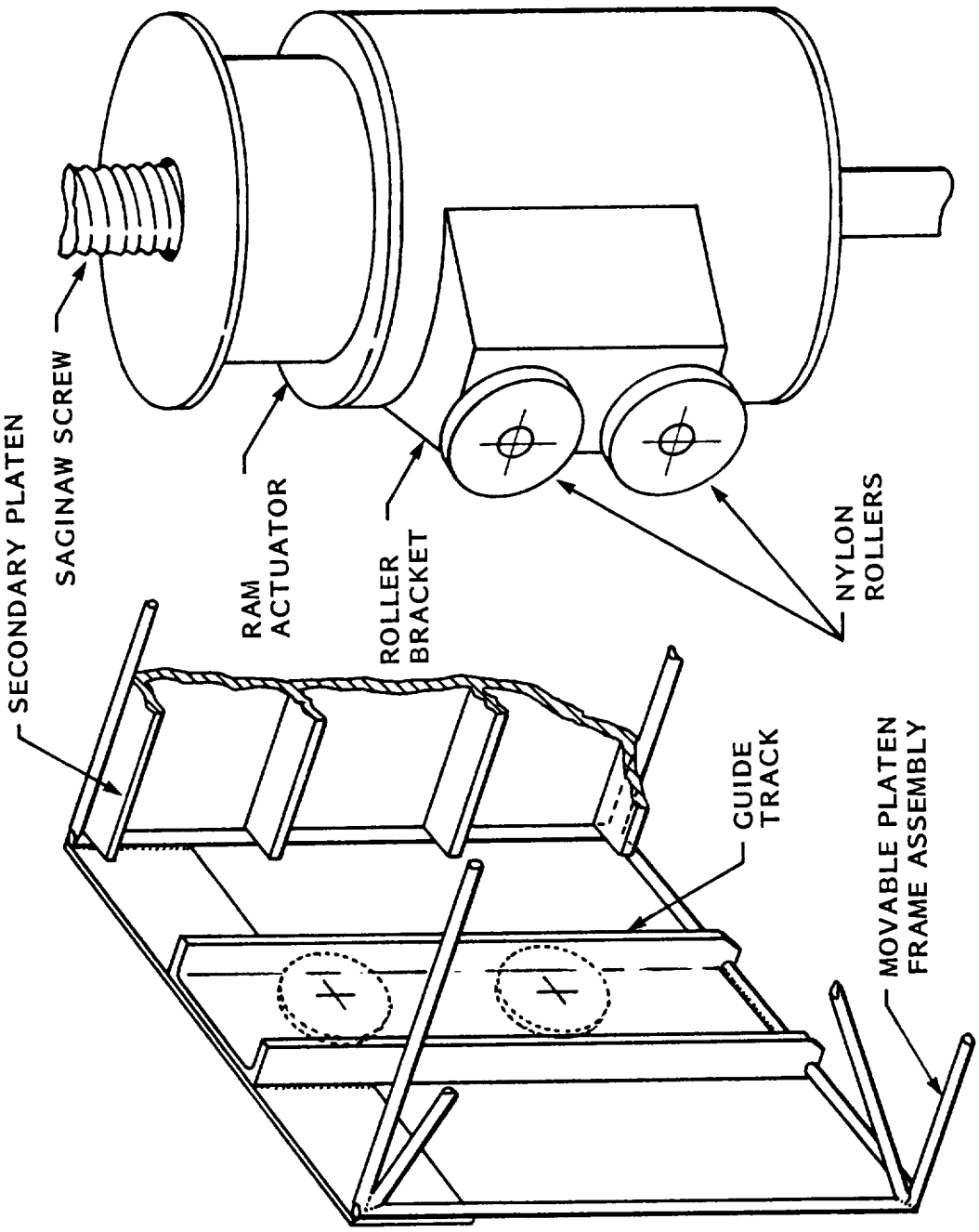

Figure 15. Detail of Guide Track

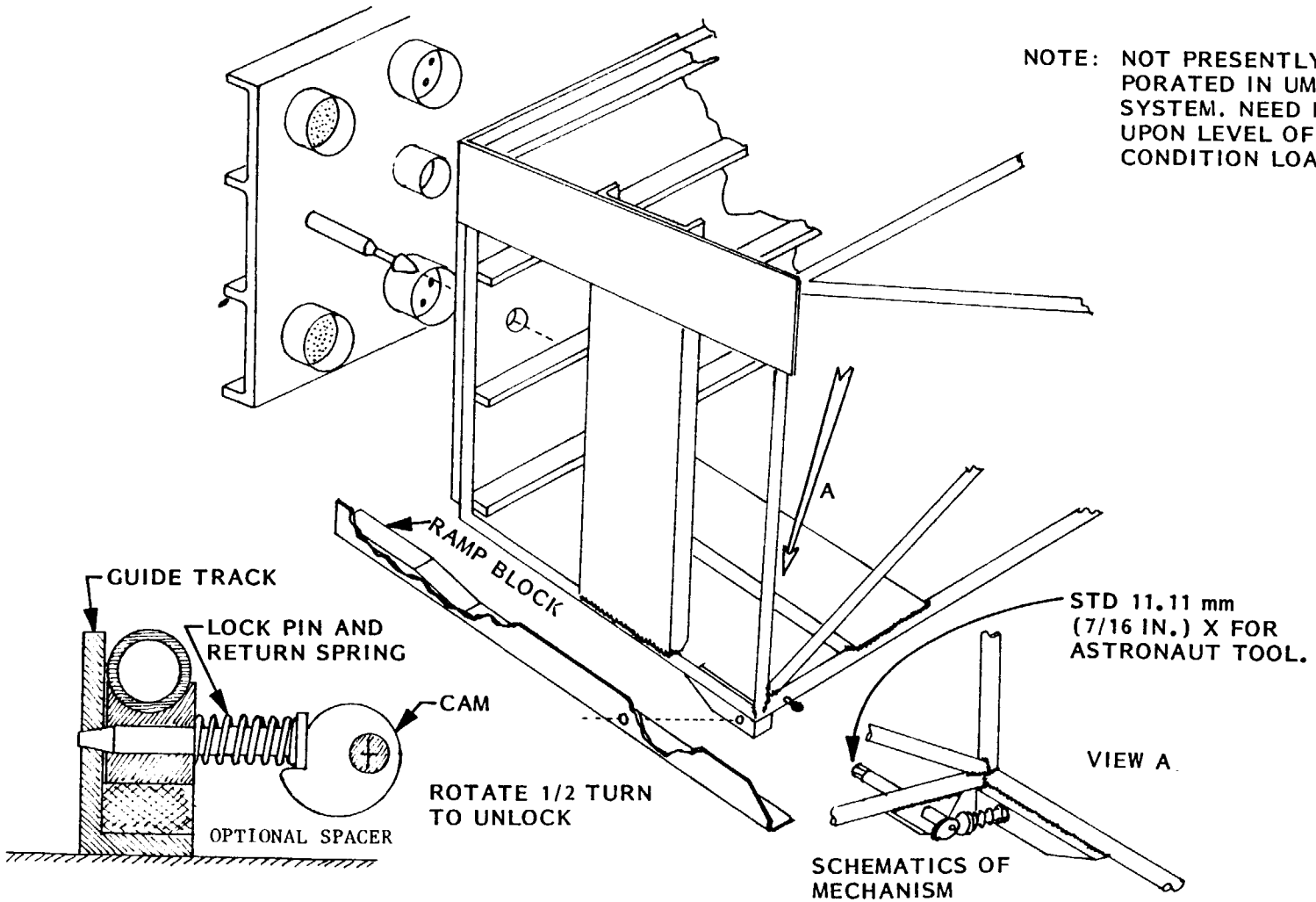

Figure 16. Frame Assembly Tie-Down Mechanism

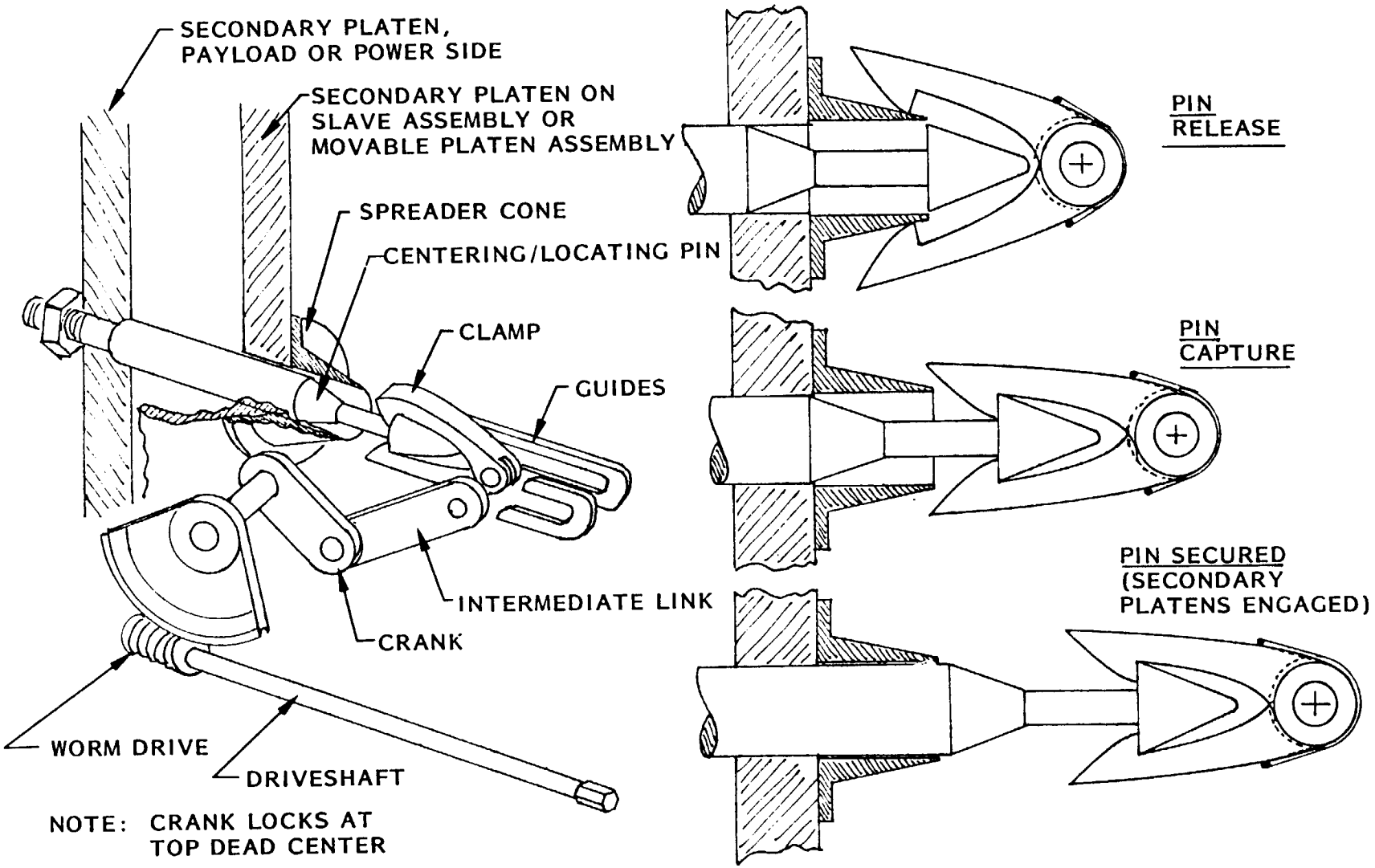

Figure 17. Secondary Platen Tie-Down Mechanism

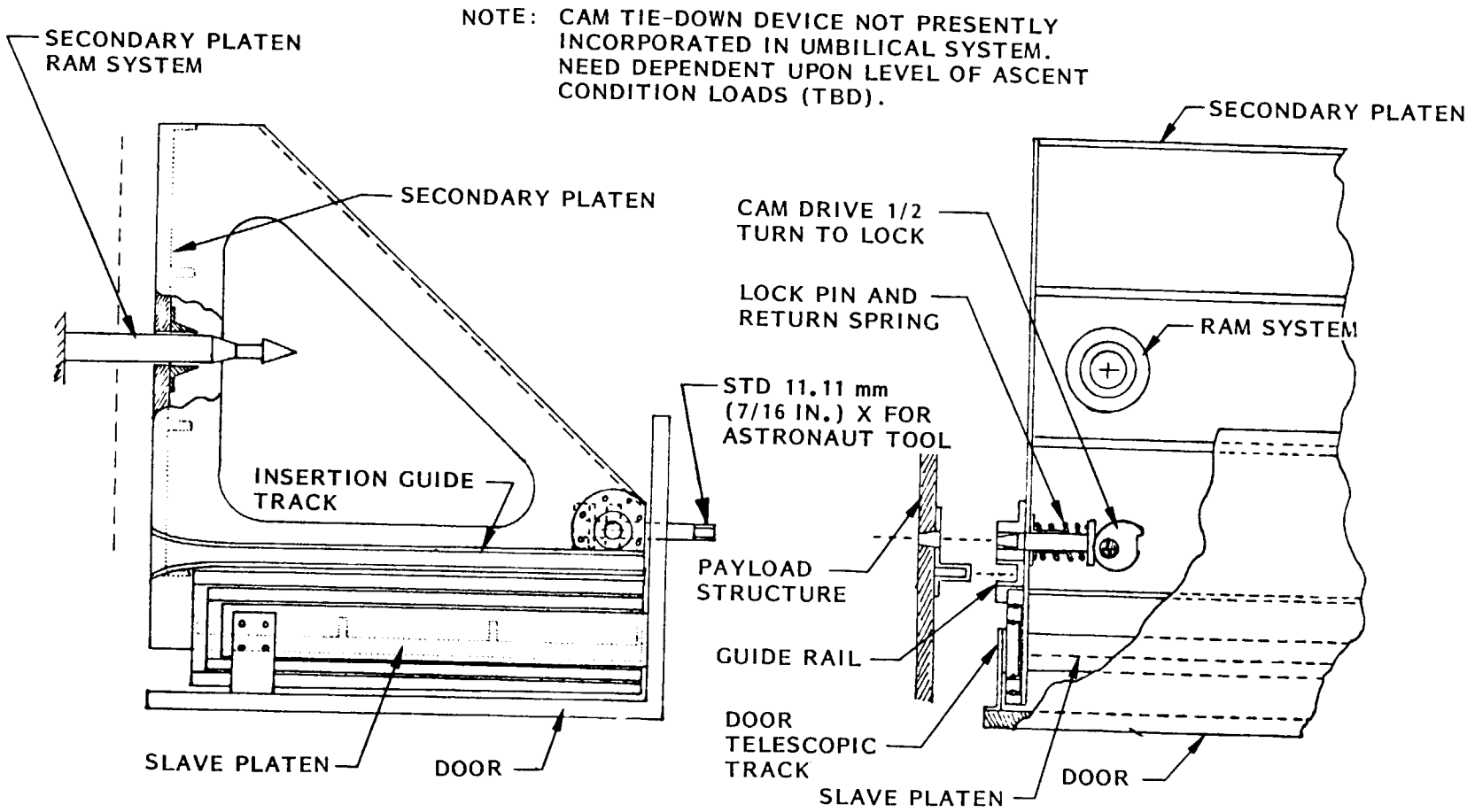

Figure 18. Slave Platen Assembly Tie-Down Mechanism

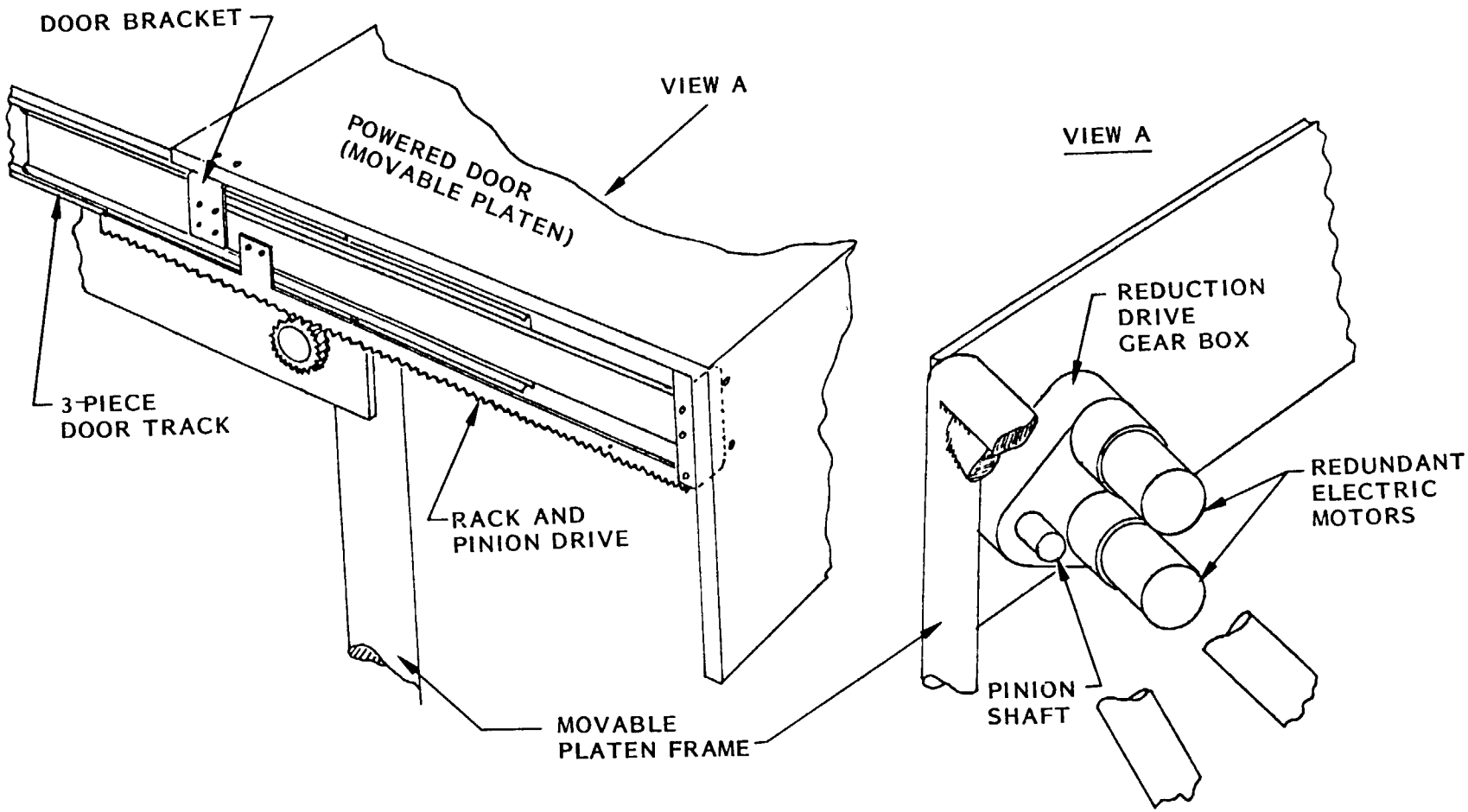

Figure 19. Powered Door Slide and Drive

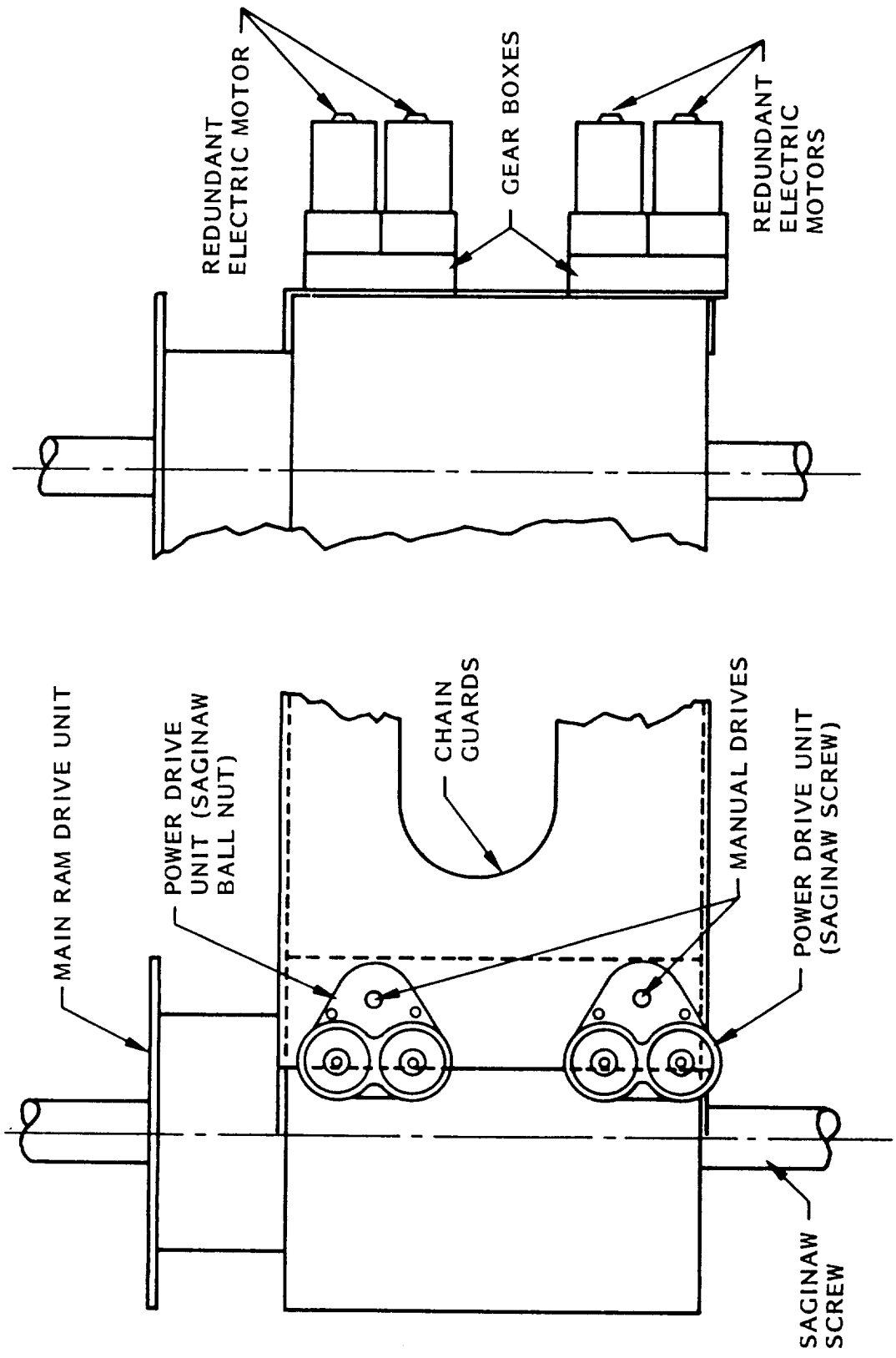

Figure 20. Power Drive Installation (Ram System)

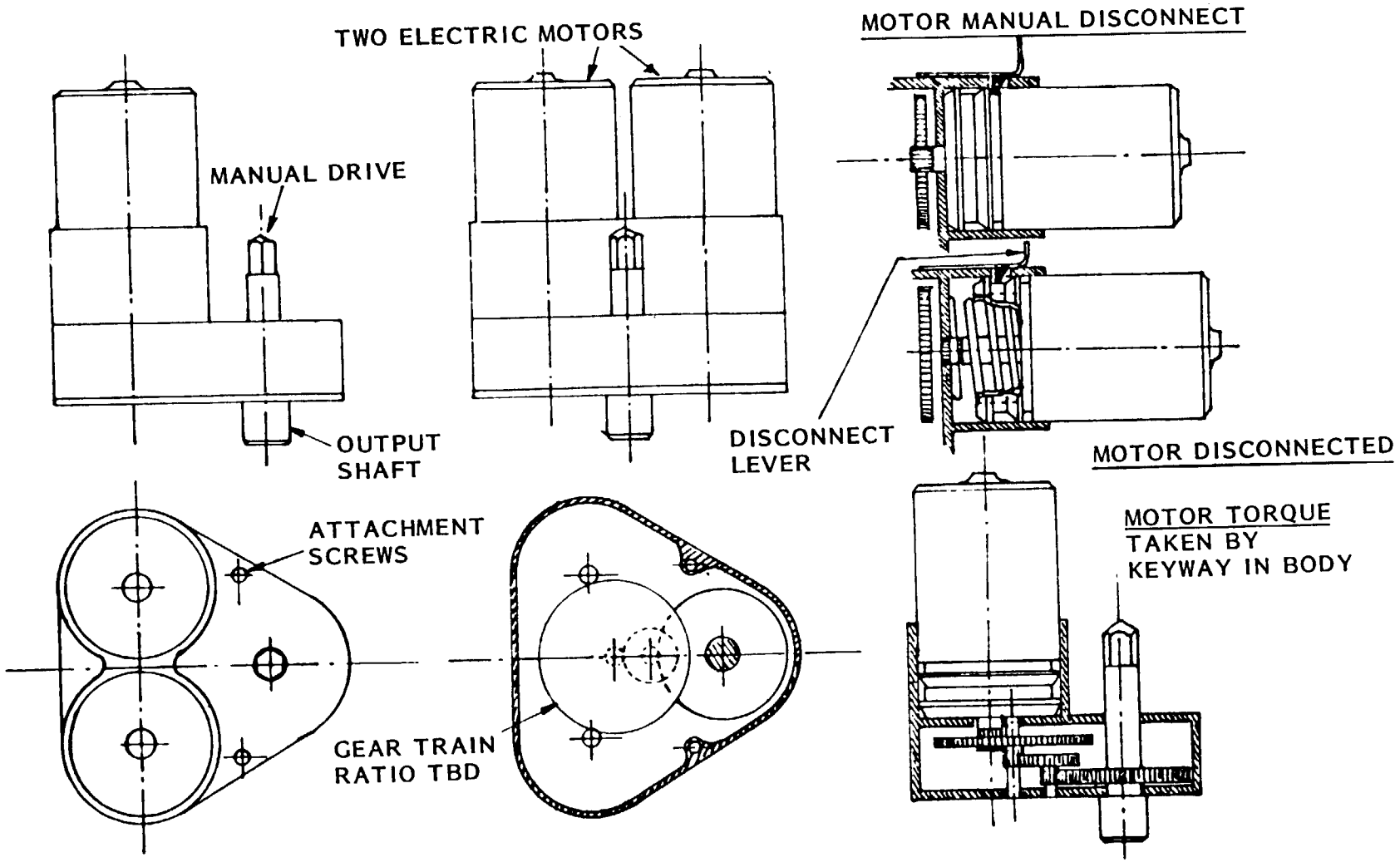

Figure 21. Redundant Power Drive System

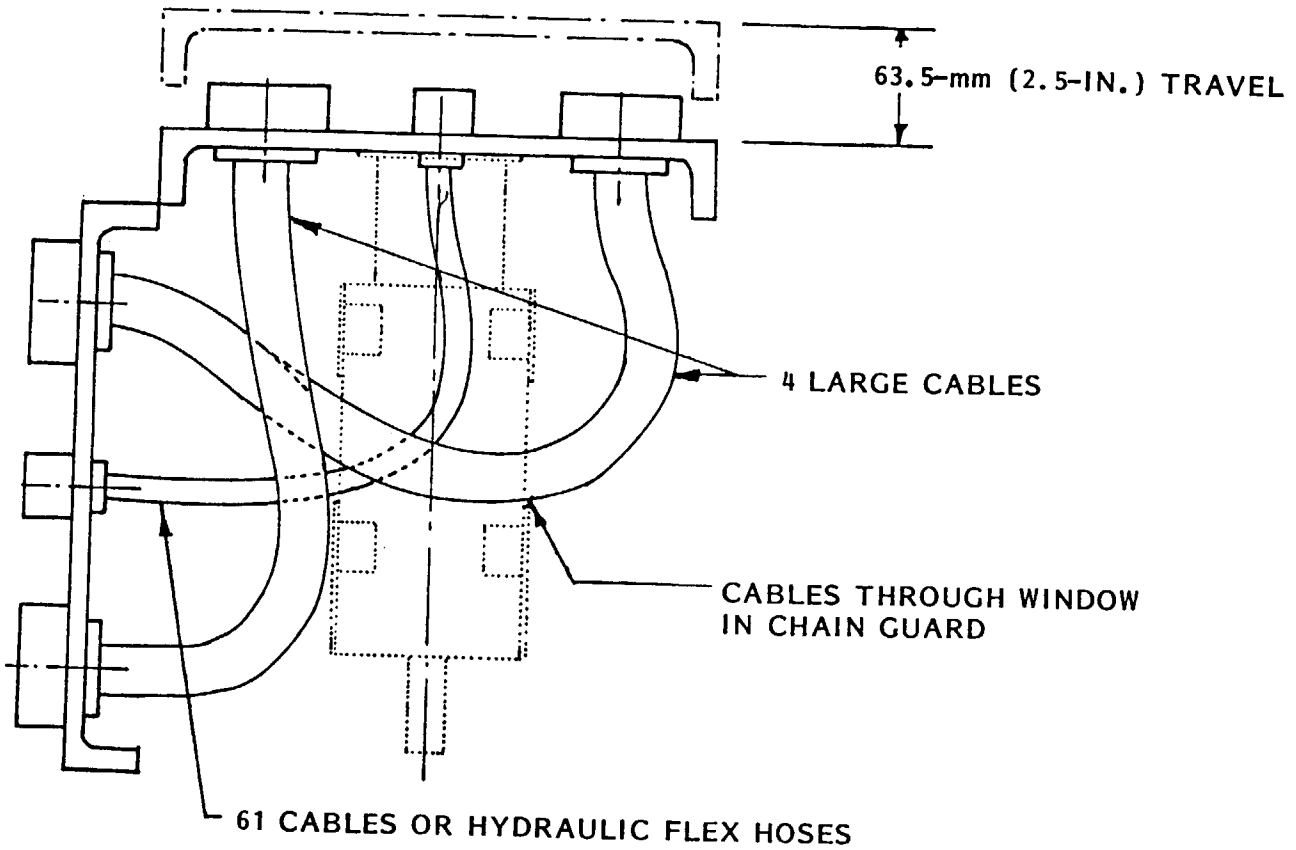

Figure 22. Preliminary Concept of Platen Cabling

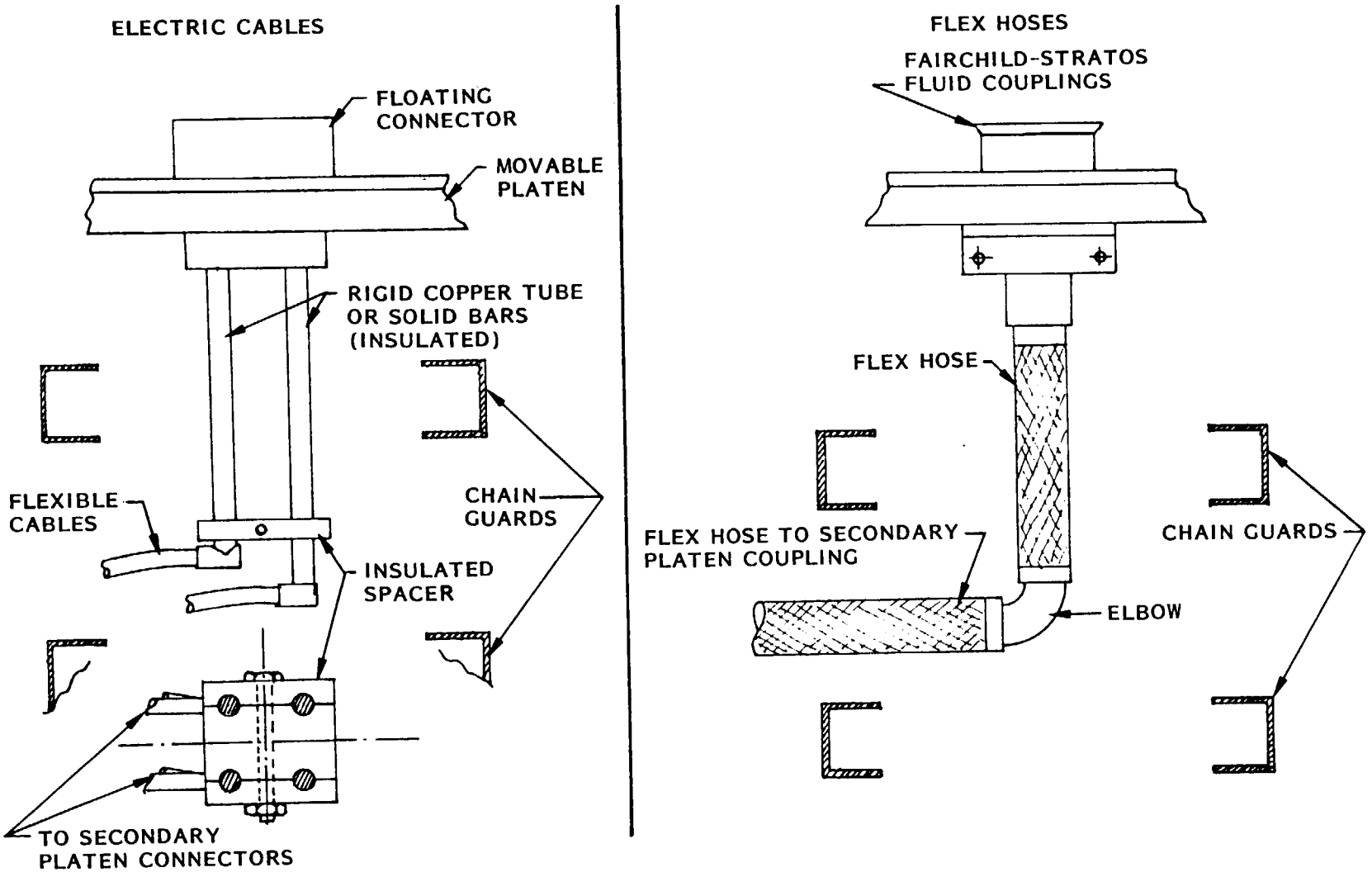

Figure 23. Electric Cables and Flex Hoses

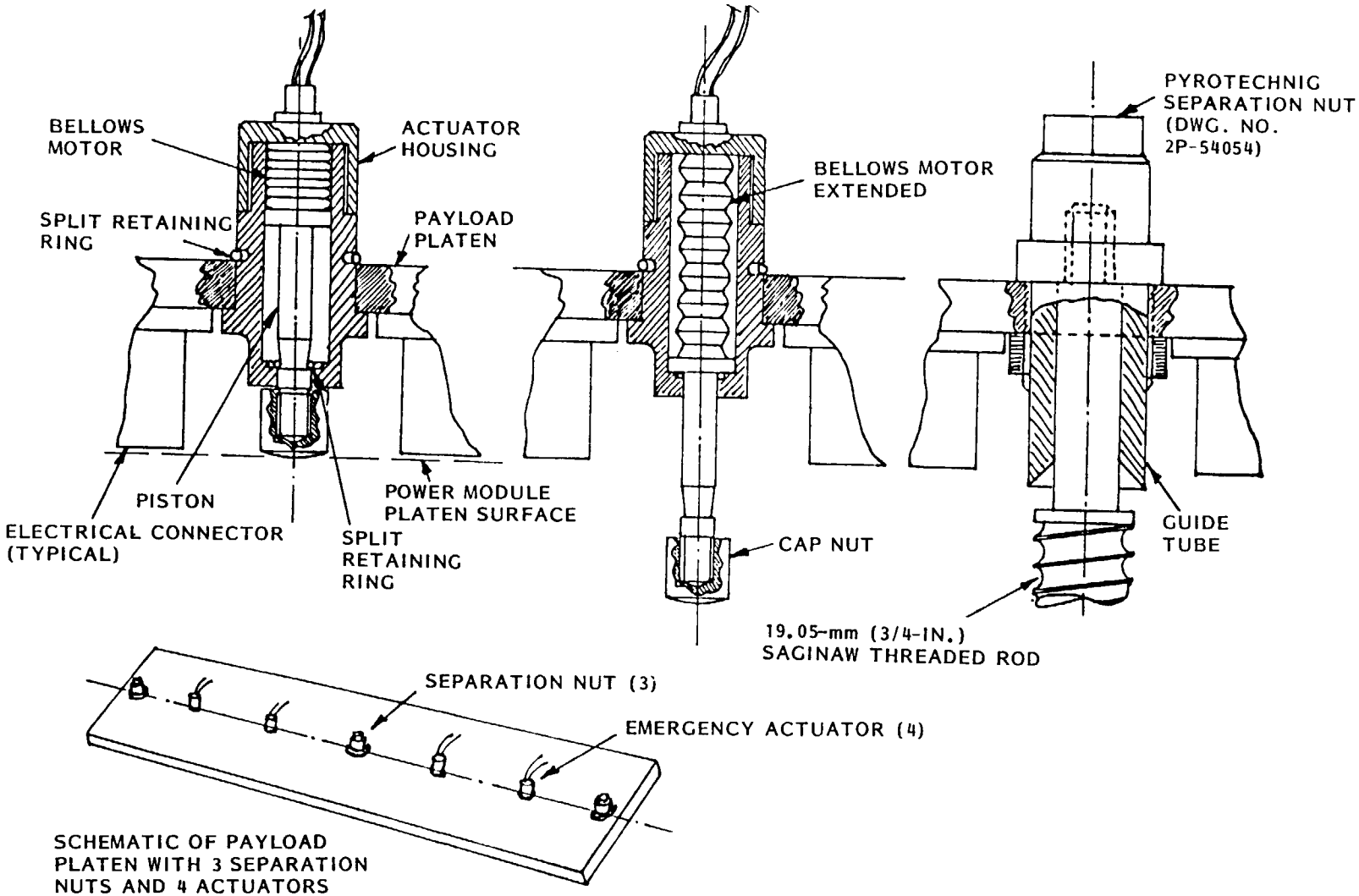

Figure 24. Emergency Release System

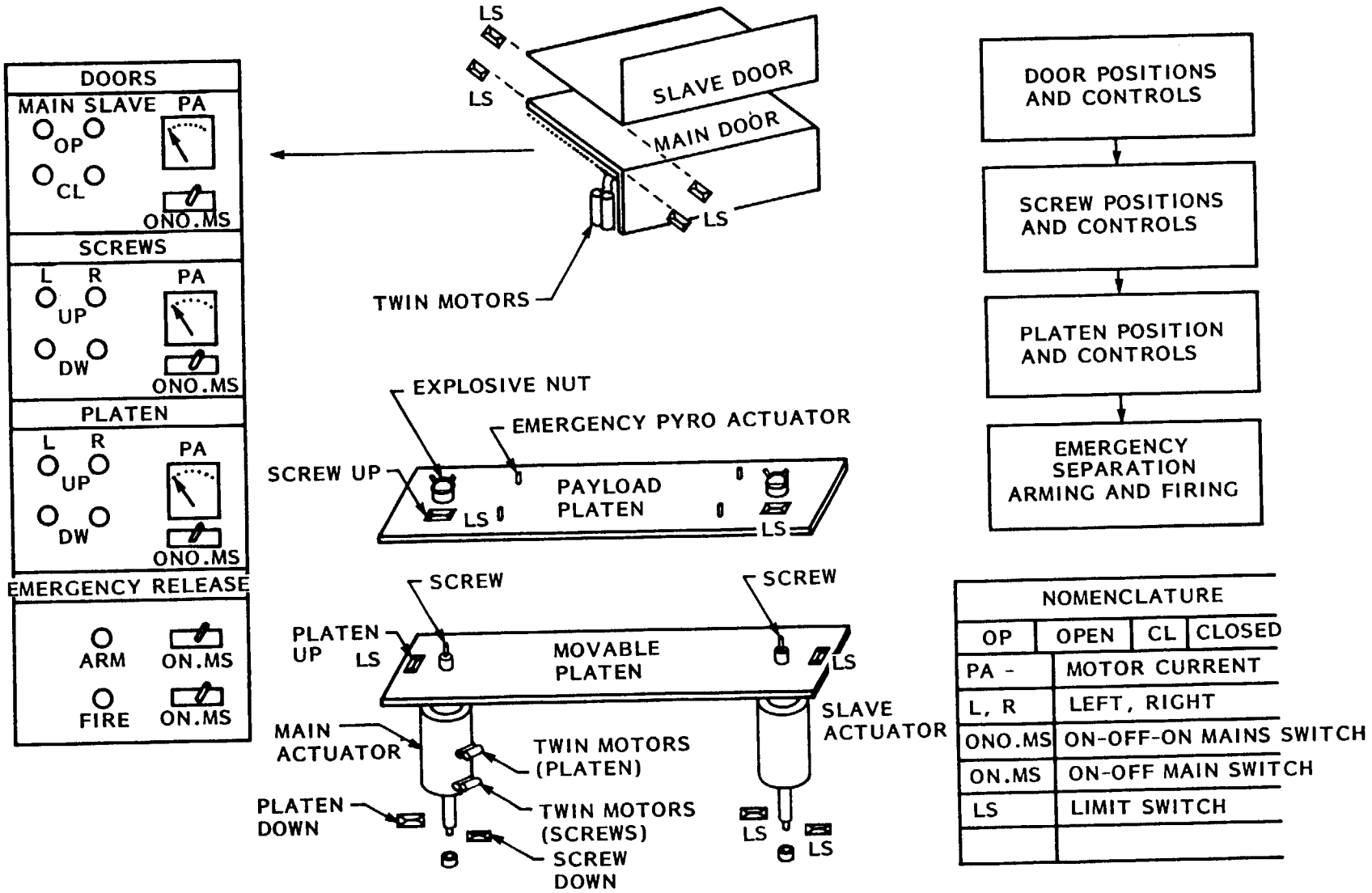

NOMENCLATURE			
OP	OPEN	CL	CLOSED
PA -	MOTOR CURRENT		
L, R	LEFT, RIGHT		
ONO.MS	ON-OFF-ON MAINS SWITCH		
ON.MS	ON-OFF MAIN SWITCH		
LS	LIMIT SWITCH		

Figure 25. Control System

TABLE I MECHANISMS

MOVABLE PLATEN ASSEMBLY

- CENTERING SCREW DRIVE
- RAM DRIVE
- FRAME ASSEMBLY ORU ROLLER/TRACKS
- MOVABLE PLATEN GUIDE TRACKS
- DOOR CLOSURE DRIVE SYSTEM
- UMBILICAL ASCENT AND RE-ENTRY SAFETY LOCKS
- DUAL ELECTRIC MOTORS INSTALLATION
- ELECTRIC MOTOR EMERGENCY SHAFT DISCONNECT
- SECONDARY PLATENS MANUAL DRIVE *
- DOOR TRACKS *
- DOOR OPEN TOGGLE LOCK*
- DOOR CLOSED TOGGLE LOCK *
- ELECTRIC CONNECTORS FLOATING MOUNTS*

SLAVE PLATEN ASSEMBLY

- ORU ROLLER/TRACKS
- DOOR CLOSURE SYSTEM
- SCREW-DRIVE EMERGENCY RELEASE NUT
- EMERGENCY SEPARATION PYRO MOTORS
- DOOR TRACKS *
- SECONDARY PLATENS MANUAL DRIVE *
- DOOR OPEN TOGGLE LOCK *
- DOOR CLOSED TOGGLE LOCK *
- ELECTRICAL CONNECTORS FLOATING MOUNTS *

MISCELLANEOUS

- FLUID COUPLING SELF-ALIGNING SYSTEM (ON ALL SIX PLATENS)

NOTE: ASTERISK * ITEMS ARE THE SAME ON BOTH MAIN ASSEMBLIES.

THE LONG DURATION EXPOSURE FACILITY STRUCTURAL INTERFACE

Moses J. Long
Langley Research Center

SUMMARY

The Long Duration Exposure Facility (LDEF) is one of the first large structures specifically designed for insertion into orbital free flight with later retrieval and return to Earth by the Space Transportation System (Shuttle). Thermal gradients and manufacturing tolerances restrict the number of retention points in the Shuttle to four with no more than three in one plane. Loads during the powered exit, high drag reentry, and landing are also critical factors in the location of retention poirts. The LDEF design meets all requirements while avoiding the structural weight penalties associated with an asymmetrical arrangement. The ground handling and assembly problems have also been resolved in an economical and effective manner.

INTRODUCTION

The LDEF is a large (4.4 meters dia. x 9.1 meters long) structure that will carry a number of experiments into Earth orbit. The experimental materials and devices will be mounted in shallow trays attached all around the LDEF outer surfaces. Exposure to the space environment for 6 months or longer will demonstrate their suitability for use on future space projects. Since the experimental arrays are mainly passive, they must be recovered for examination. The plan is to launch the LDEF into orbit in the Shuttle Orbiter Payload Bay, deploy it into free flight with the orbiter's Remote Manipulation System (see Figure 1), recover it with the same system on a later flight, and return to Earth. The experimental trays will then be demounted and returned to the individual investigators.

SHUTTLE RETENTION SYSTEM

The Shuttle payload integration instructions permit retention by statically determinate or statically indeterminate arrangements. However, the indeterminate option is applicable only to structures that are compliant enough to avoid overloading the retention clamps when forced into position. The determinate case is shown in Figure 2, which is an excerpt from JSC 07700, Volume XIV. Only four suspension points are allowed. The Primary fittings are on the bridges at the sides of the cargo bay (longerons) and are pinned to the bridge so that forces in the x-x and z-z directions are resisted. The Stabilizing fitting is also on the bridge but is not pinned so that it resists forces in the z-z direction only. The Auxiliary fitting is on the keel and resists loads in the y-y direction only. Trunnions free to move axially rest

in split spherical bearings at each fitting. It can be seen that the four-point suspension fixes the payload against all translations and rotations while having no more than three points touching the orbiter in one plane. A reasonable thermal distortion on insertion can thus be accommodated by rotating the plane defined by the three points into that defined by the fittings. It can also be seen that the single Stabilizing fitting cannot be placed so that a symmetric stucture will connect all four points.

STRUCTURAL TRADEOFFS

The LDEF basic framework geometry was largely defined by the requirements for mounting the experimental trays. Maximum outer surface area was desired so the diameter (actually a dodecagon) was made as large as permitted by the payload bay. Payload weight limitation imposed by the Shuttle were then used to determine the length. Candidate structural arrangements were modeled for finite element analysis on high speed computers. Placing the Primary fittings on opposite sides at one end and the Stabilizing fitting on either side at the other end was an obvious first cut (see Figure 3). This proved to be completely impractical from both a stress and deflection standpoint. Subsequent variations soon established that structural weight decreased as the Primary fittings moved toward the center of gravity and the optimum position was in the plane of the c.g. The Auxiliary keel fitting was then located in the same plane using the same logic. This allowed the three main load bearing fittings to be incorporated in a fairly massive welded center ring. The principal load remaining to be carried by the Stabilizing fitting is that caused by the overturning moment which occurs during longitudinal acceleration due to the bridge being above the centerline of the LDEF (see Figure 4). This misalinement is necessary if the LDEF peripheral area is to be maximized.

Although the loads at the Stabilizing fitting located as described above are relatively low compared to those at the primary fittings, the torsional input, due to the asymmetrical position, proved to be troublesome. Many structural variations were investigated, but all those with satisfactory stiffness characteristics exceeded the weight budget.

THE WALKING BEAM

During the tradeoff studies, it was apparent that the ideal position to react the stabilizing force was the longitudinal centerline at the forward or aft face (see Figure 5). It was finally decided to achieve this with a beam free to rotate about the center mounting point that would span the payload bay and attach to standard stabilizing fittings at both ends (see Figure 6). This structure has been alternately called the walking beam or the whiffle tree. As the LDEF is lowered into the payload bay, one end of the beam will contact a fitting and the beam will rotate until the other end is also in contact and both are clamped in place. Longitudinal location can be achieved either by the central pin sliding in its bearing or by movement of the Stabilizing fittings along the bridge rails. This arrangement is symmetrical,

statically determinate since the forces at the ends of the beam are one-half the center load, and does not require high clamping forces. It permits the transmission of loads from the end structure directly to the Primary fittings by tension/compression struts, thereby greatly reducing bending loads in the LDEF longerons.

If a standard, automatic clamping, Stabilizing fitting were mounted at the centerline, the beam could be retained in the orbiter after LDEF deployment and carried aloft again on the retrieval flight. However, this would restrict the deployable payload on the second mission, and for this reason, present plans are to have the beam remain with the LDEF. Mechanical stops prevent excessive rotation while deployed so the beam will have approximately the correct alinement at insertion and no additional manipulations will be required.

Suitable margins for both stress and deflection during the powered boost, reentry, normal landing, and emergency landing were thus achieved within the weight budget. Limited load and vibration testing subsequently verified the computer models. The LDEF basic structure has been placed in storage awaiting qualification of the experimental arrays and a flight opportunity, which is now tentatively scheduled for 1984.

ASSEMBLY AND TRANSPORTATION SYSTEM

It was apparent early in the program that a special vehicle would be needed for short distance ground movements of LDEF with and without experiment trays installed. Two slightly modified flat-bed trailers were welded together to form a single vehicle of sufficient width to mount the LDEF utilizing the Primary, Stabilizing, and Auxiliary attach points (see Figure 6). The assembly is much too wide for highway transport and will only be used on base at Langley Research Center and Kennedy Space Center. A barge will be used for travel between centers.

It was further realized that assembly and other flight preparations would be greatly facilitated if the entire LDEF structure could be rotated about the longitudinal centerline. Luckily, the centrally located pins at each end were available; and because of the structural arrangement, they were capable of supporting the weight of the fully-loaded spacecraft. An off-the-shelf welding positioner was purchased to furnish the necessary motive power (see Figure 7). The opposite end is supported by a commercial pillow-block bearing (see Figure 8). To convert from the transport mode to the rotational mode, the rear bearing is installed, the walking beam removed, and the welding positioner is attached. The special structures at the Primary and Auxiliary fittings are removed and the assembly is free to rotate. Portable work stands are then moved into place to provide a platform so that tray installation or removal operations may be carried out at a convenient working height and with complete accessibility for overhead crane-supported loads (see Figure 9).

GROUND SUPPORT EQUIPMENT

The two main items of ground support equipment are the Experiment Tray Shipping Container (Figure 10) and the Experiment Tray Lifting Rig (Figure 11). The shipping containers provide a shockproof, humidity-controlled, and dust-free environment for the worldwide movement of the individual experimental packages. The lifting rig is attached to a tray in the horizontal position. It is then hoisted by the overhead crane and the tray is rotated by the lifting rig for easy insertion into the recess of the LDEF frame (see Figure 12). The heavy framework largely counterbalances the weight of the experiment tray so that manual exertion is minimized.

ENVIRONMENTAL ENCLOSURE

The final major item of LDEF equipment is an easily-assembled, weatherproof, climate-controlled housing that encloses the complete spacecraft in the transport mode. External equipment will furnish conditioned air during barge operations. The environmental enclosure is designed to withstand hurricane force winds. It is shown being checked for leaks in Figure 13.

CONCLUSION

The Long Duration Exposure Facility has been designed, fabricated, and tested. An efficient structural interface between the spacecraft and the Space Transportation System Orbiter has been achieved. The unique "Walking Beam" concept resulted in substantial weight reduction compared to other potential solutions. Ground movements and assembly operations already carried out with mass simulation experimental trays have demonstrated the feasibility, efficiency, and economy of the proposed preflight and postflight procedures.

Figure 1. STS Deploying LDEF (Artist's Conception)

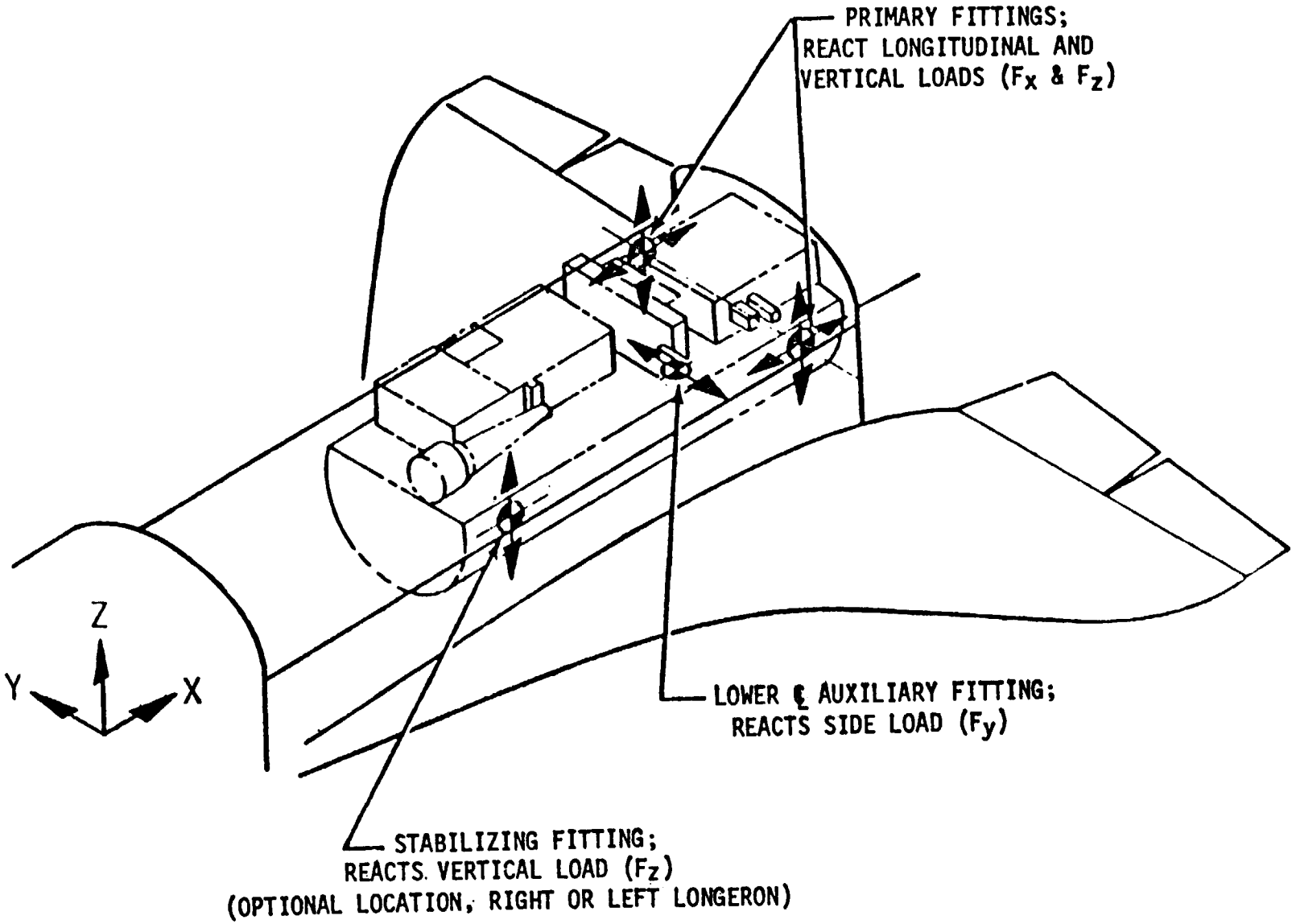

Figure 2. 4-Point Payload Retention System (Determinate)

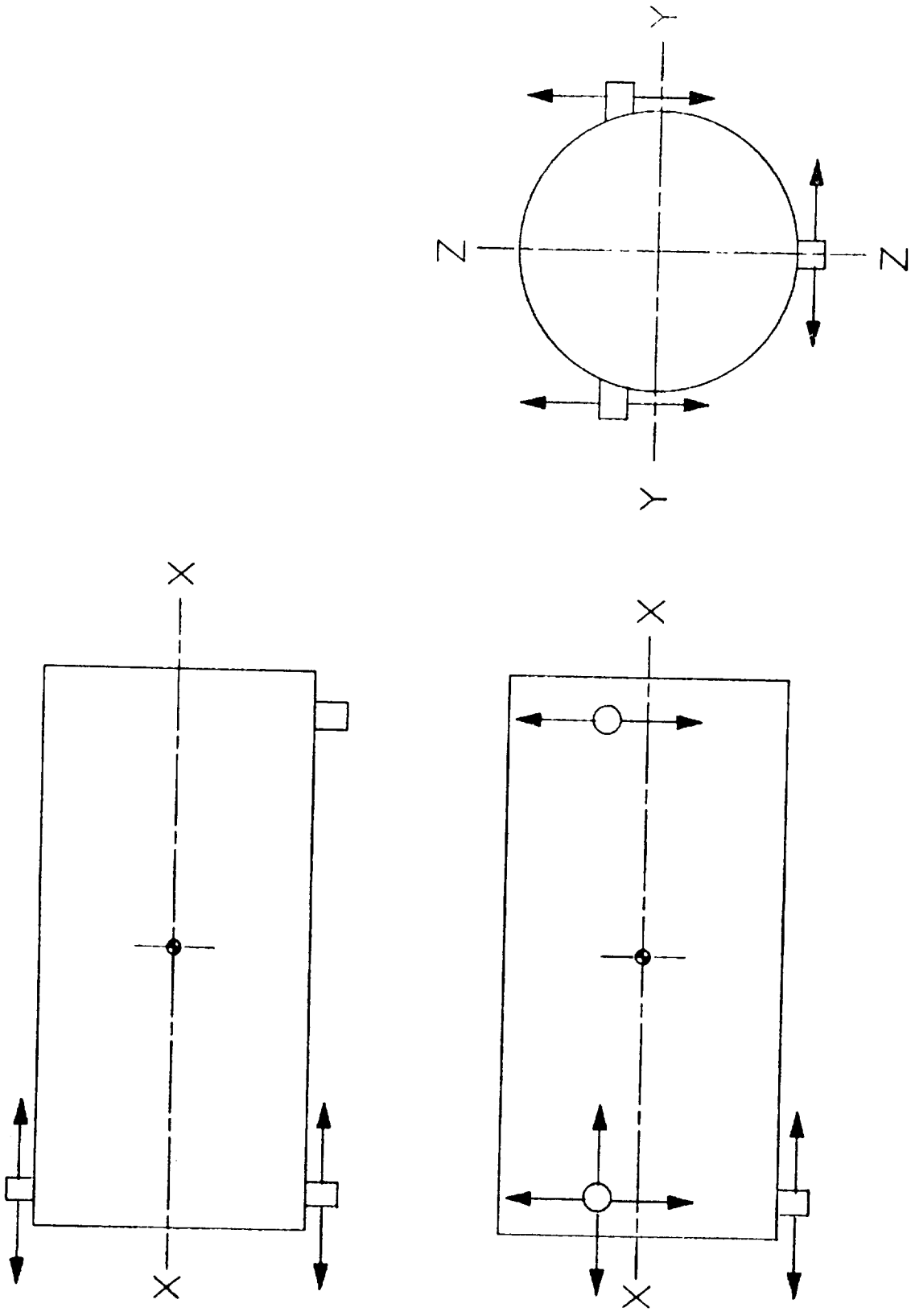

FIGURE 3

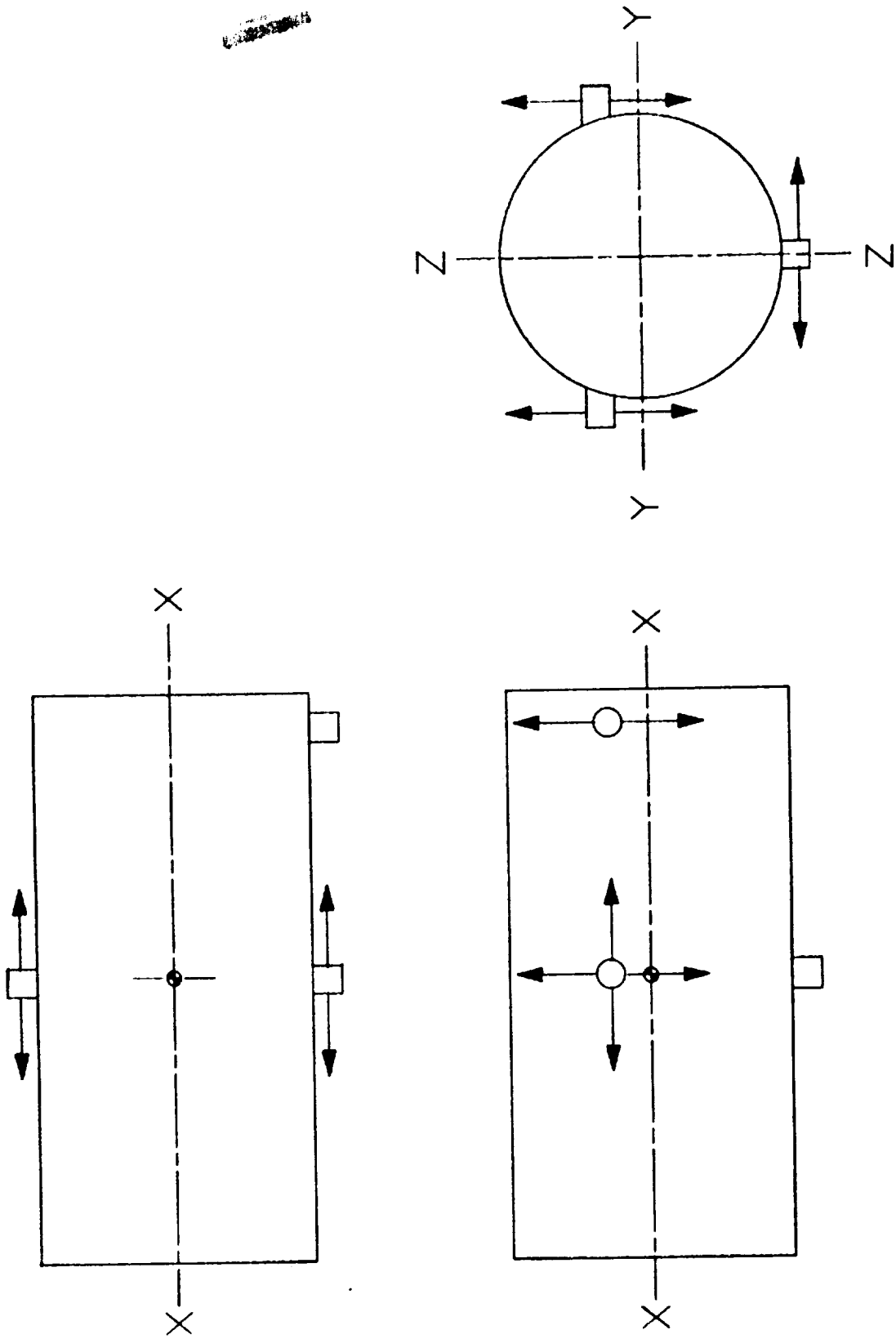

FIGURE 4

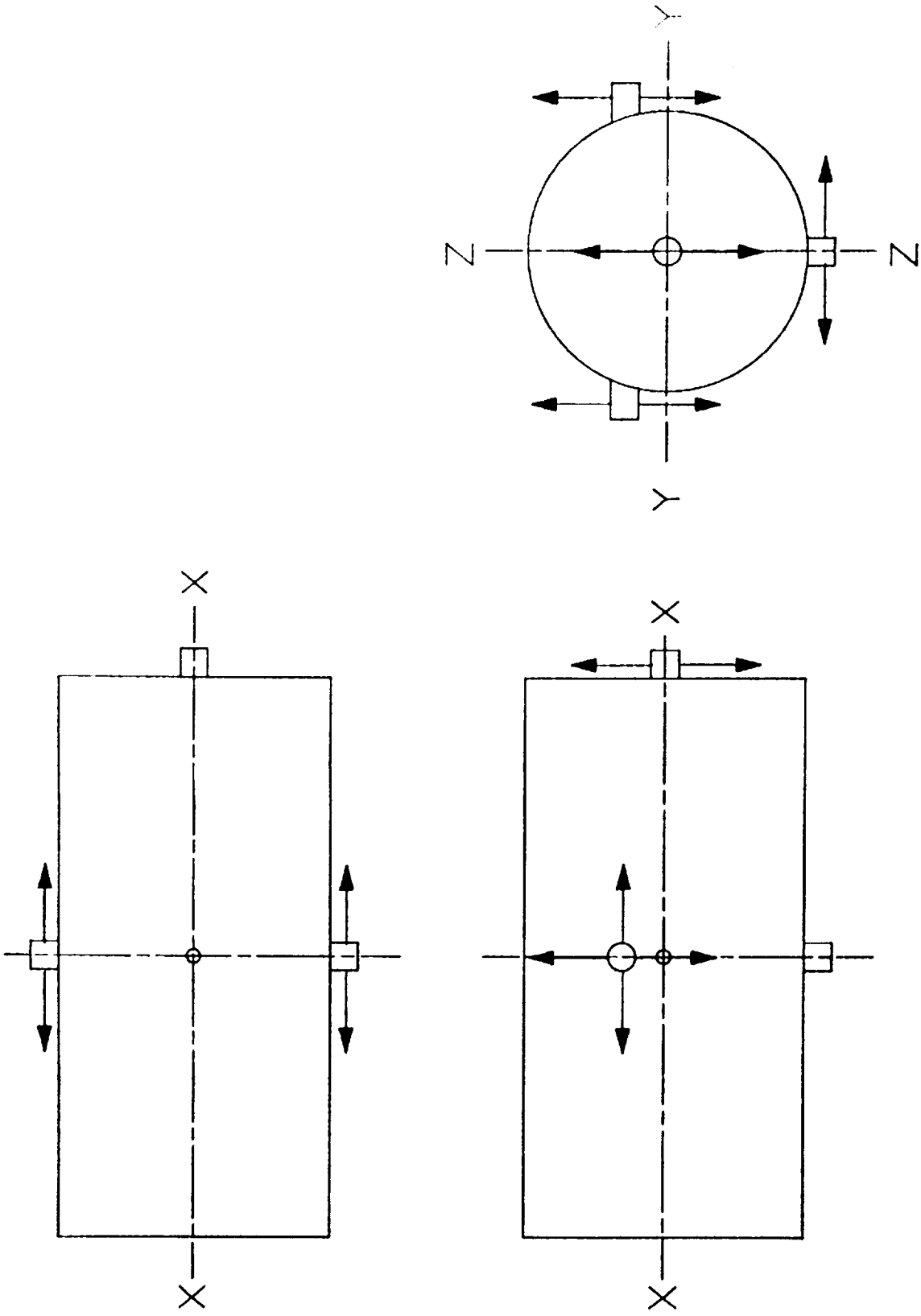

FIGURE 5

Figure 6. LDEF Structure on Transporter

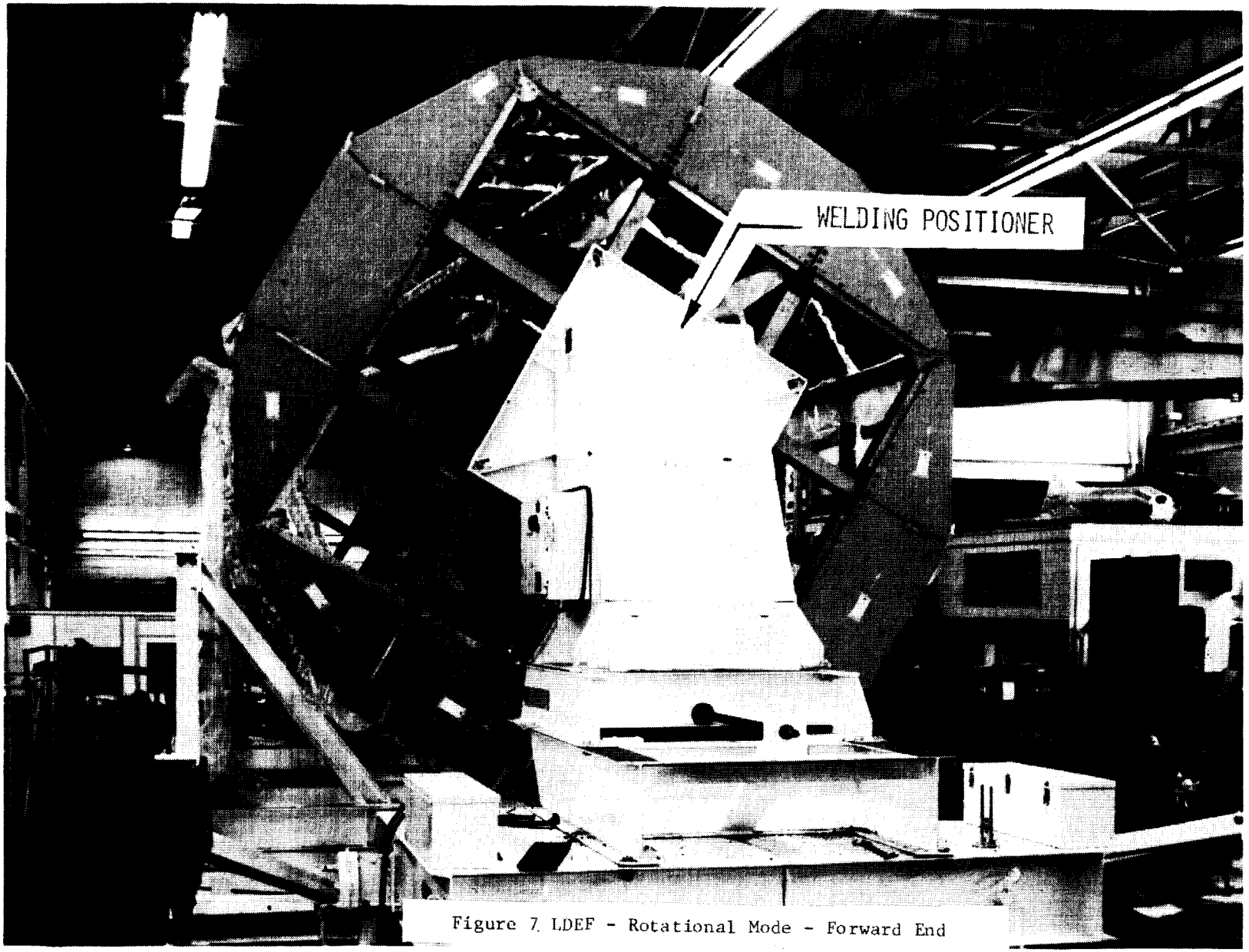

Figure 7. LDEF - Rotational Mode - Forward End

Figure 8. LDEF - Rotational Mode - Aft End

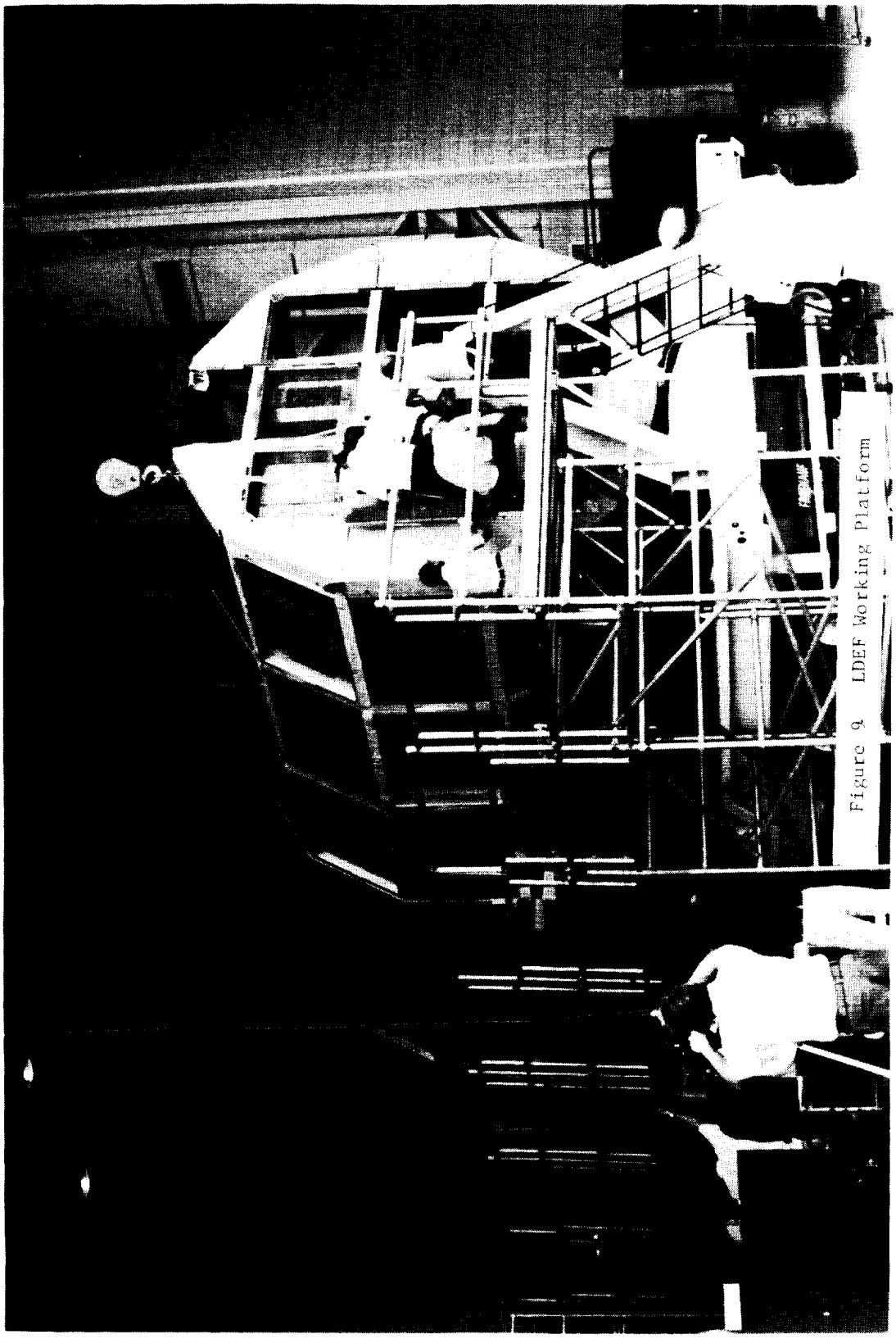

Figure 9 LDEF Working Platform

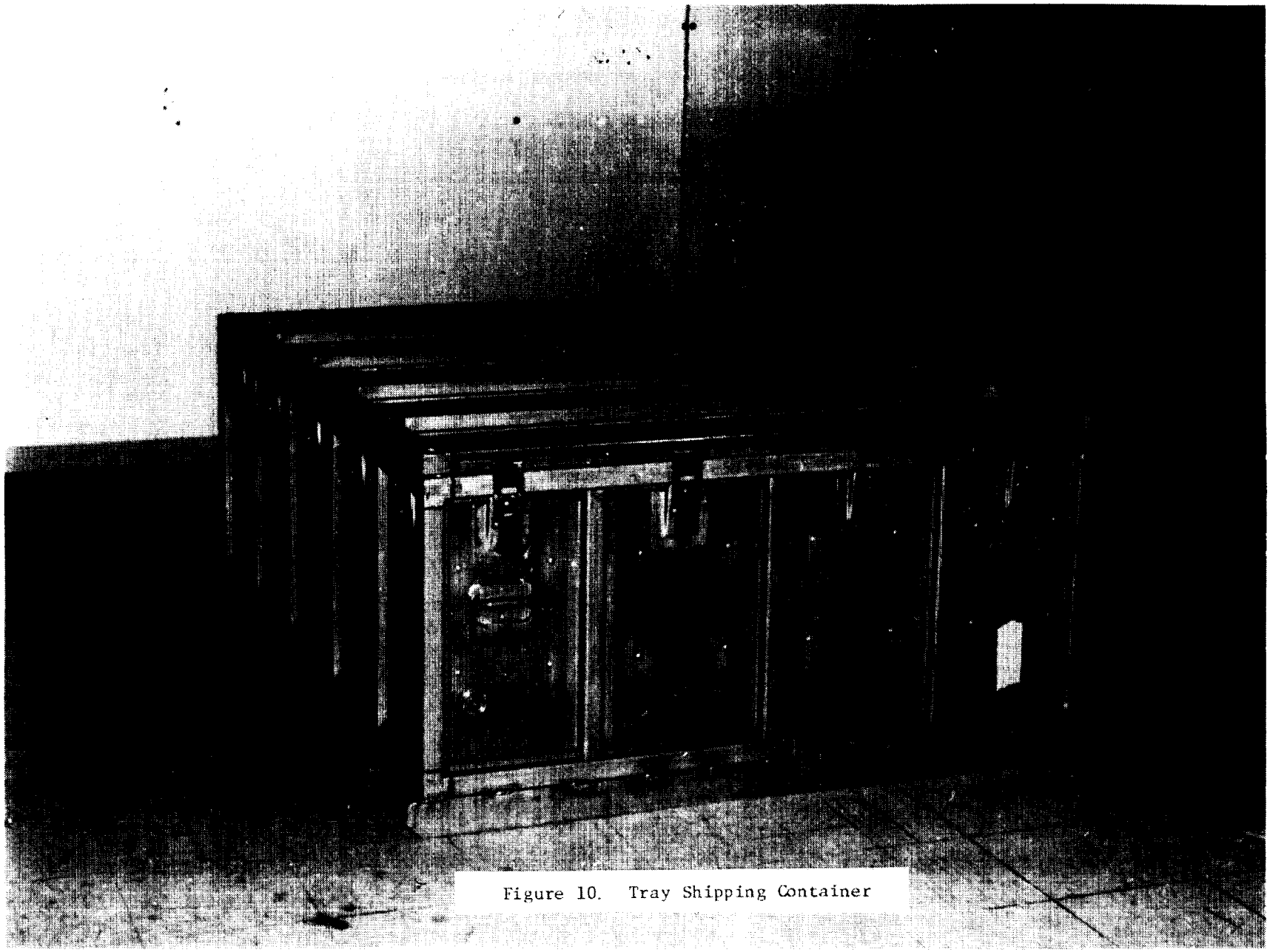

Figure 10. Tray Shipping Container

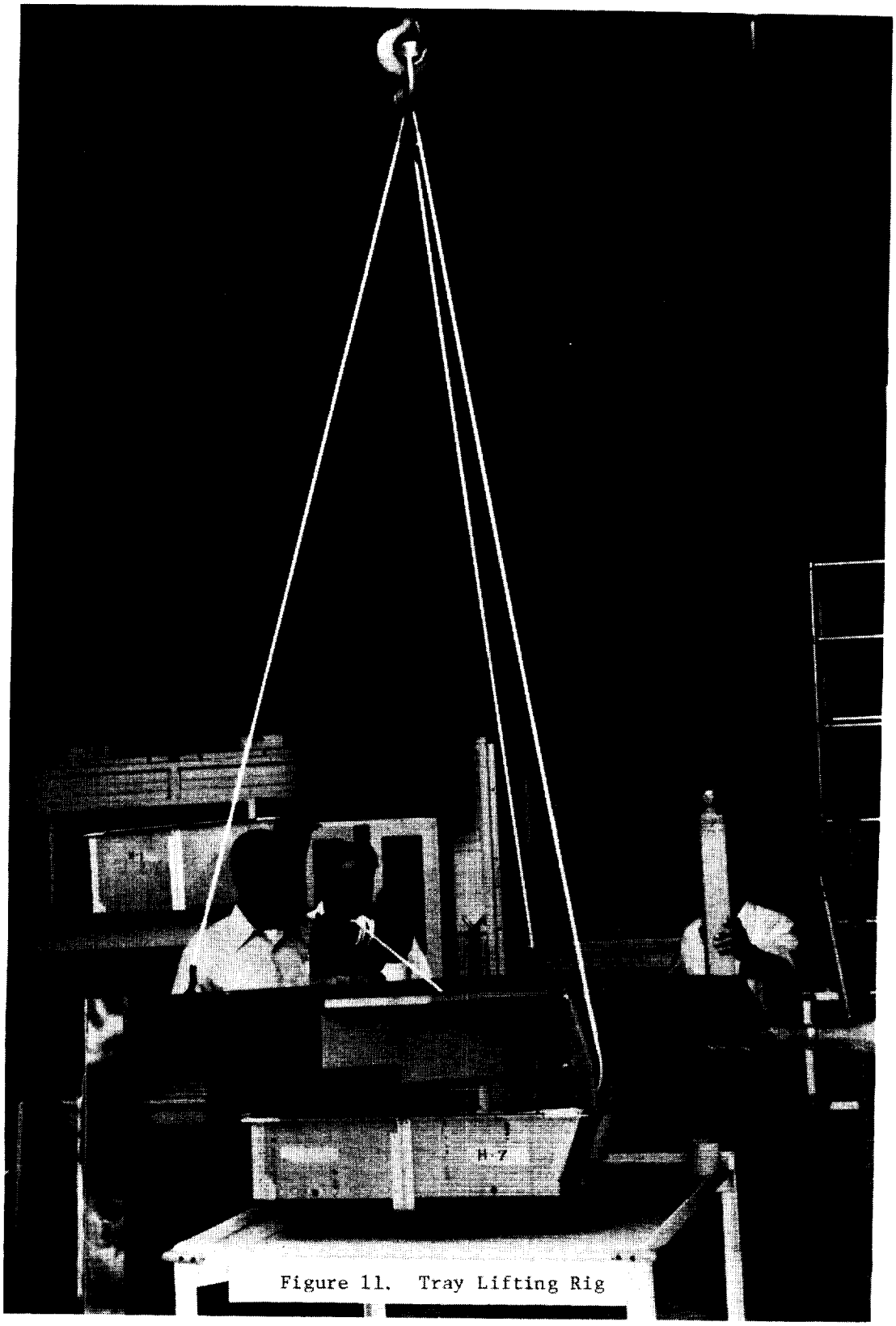

Figure 11. Tray Lifting Rig

Figure 12. Tray Installation

Figure 13. Environmental Enclosure

1. REPORT NO.	2. GOVERNMENT ACCESSION NO.	3. RECIPIENT'S CATALOG NO.
NASA CP-2181		

4. TITLE AND SUBTITLE	5. REPORT DATE
15th Aerospace Mechanisms Symposium	May 1981
	6. PERFORMING ORGANIZATION CODE
7. AUTHOR(S)	8. PERFORMING ORGANIZATION REPORT #
9. PERFORMING ORGANIZATION NAME AND ADDRESS George C. Marshall Space Flight Center Marshall Space Flight Center, Alabama 35812	10. WORK UNIT NO. M-349
	11. CONTRACT OR GRANT NO.
12. SPONSORING AGENCY NAME AND ADDRESS National Aeronautics and Space Administration, Wash, DC 20546 California Institute of Technology, Pasadena, CA 91109 Lockheed Missiles & Space Co., Inc, Sunnyvale, CA 94088	13. TYPE OF REPORT & PERIOD COVERED Conference Publication
	14. SPONSORING AGENCY CODE

15. SUPPLEMENTARY NOTES

16. ABSTRACT

The proceedings of the 15th Aerospace Mechanisms Symposium held at the George C. Marshall Space Flight Center on May 14-15, 1981, are reported in this NASA Conference Publication. Technological areas covered include aerospace propulsion, aerodynamic devices, and crew safety; space vehicle control; spacecraft deployment, positioning, and pointing; deployable antennas/reflectors; and large space structures. Devices for payload deployment, payload retention, and crew EVA on the Space Shuttle Orbiter are also described.

17. KEY WORDS		18. DISTRIBUTION STATEMENT
Actuators	Emergency escape	Unclassified - Unlimited
Latching devices	Umbilical connections	
Deployment devices	Shuttle orbiter	
Drive systems	Experiment protection	
Pointing systems	Alignment	
Experiment testing	Thrust vector control	Subject Category 39

19. SECURITY CLASSIF. (of this report)	20. SECURITY CLASSIF. (of this page)	21. NO. OF PAGES	22. PRICE
Unclassified	Unclassified	446	A19

For sale by National Technical Information Service, Springfield, Virginia 22161

NASA-Langley, 1981